21:51:28 OCA PAD AMENDMENT - PROJECT HEADER INFORMATION 01/13/92

Active

Project #: E-21-F53 Cost share #: E-21-338 Rev #: 3
Center # : 10/24-6-R6789-0A0 Center shr #: 10/22-1-F6789-0A0 OCA file #:
Work type : RES
Contract#: ECS-8909971 Mod #: AMENDMENT 1 Document : GRANT
Prime #: Contract entity: GTRC

Subprojects ? : N CFDA: 47.041
Main project #: PE #:

Project unit: ELEC ENGR Unit code: 02.010.118
Project director(s):
GLYTSIS E N ELEC ENGR (404)894-4813

Sponsor/division names: NATL SCIENCE FOUNDATION / GENERAL
Sponsor/division codes: 107 / 000

Award period: 890815 to 920731 (performance) 921031 (reports)

Sponsor amount	New this change	Total to date
Contract value	0.00	60,000.00
Funded	0.00	60,000.00
Cost sharing amount		20,235.00

Does subcontracting plan apply ?: N

Title: SEMICONDUCTOR QUANTUM WAVE DEVICES

PROJECT ADMINISTRATION DATA

OCA contact: Mildred S. Heyser 894-4820

Sponsor technical contact

LAWRENCE GOLBERG
(202)357-9618

NATIONAL SCIENCE FOUNDATION
1800 G STREET, N.W.
WASHINGTON, D.C.

Sponsor issuing office

MARTIN GEARY
(202)357-9602

NATIONAL SCIENCE FOUNDATION
1800 G STREET
WASHINGTON, D.C.

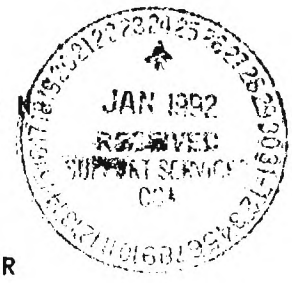

Security class (U,C,S,TS) : U ONR resident rep. is ACO (Y/N): N
Defense priority rating : N/A NSF supplemental sheet
Equipment title vests with: Sponsor GIT X
NONE PROPOSED
Administrative comments -
AMENDMENT 1 EXTENDS PERFORMANCE ENDING DATE TO JULY 31, 1992. ALL OTHER TERMS AND CONDITIONS REMAIN UNCHANGED.

GEORGIA INSTITUTE OF TECHNOLOGY
OFFICE OF CONTRACT ADMINISTRATION

NOTICE OF PROJECT CLOSEOUT

2-
SR, 437

Closeout Notice Date 11/18/92

Project No. E-21-F53 Center No. 10/24-6-R6789-0A0

Project Director GLYTSIS E N School/Lab ELEC ENGR

Sponsor NATL SCIENCE FOUNDATION/GENERAL

Contract/Grant No. ECS-8909971 Contract Entity GTRC

Prime Contract No.

Title SEMICONDUCTOR QUANTUM WAVE DEVICES

Effective Completion Date 920731 (Performance) 921031 (Reports)

Closeout Actions Required:	Y/N	Date Submitted
Final Invoice or Copy of Final Invoice	N	
Final Report of Inventions and/or Subcontracts	Y	
Government Property Inventory & Related Certificate	N	
Classified Material Certificate	N	
Release and Assignment	N	
Other	N	

Comments LETTER OF CREDIT APPLIES. EFFECTIVE DATE 8-15-89. CONTRACT VALUE $60,000.

Subproject Under Main Project No.

Continues Project No.

Distribution Required:

Project Director	Y
Administrative Network Representative	Y
GTRI Accounting/Grants and Contracts	Y
Procurement/Supply Services	Y
Research Property Managment	Y
Research Security Services	N
Reports Coordinator (OCA)	Y
GTRC	Y
Project File	Y
Other HARRY VANN-FMD	Y
FRED CAIN-OOD	Y

NOTE: Final Patent Questionnaire sent to PDPI.

SEMICONDUCTOR QUANTUM WAVE DEVICES

Project No. ECS-8909971

A RESEARCH INITIATION AWARD

ANNUAL PROGRESS REPORT (08-15-89/08-15-90)

SUBMITTED TO

NATIONAL SCIENCE FOUNDATION

WASHINGTON, D.C. 20550

BY

GEORGIA INSTITUTE OF TECHNOLOGY

ATLANTA, GEORGIA 30332

PRINCIPAL INVESTIGATOR

Elias N. Glytsis

Assistant Professor

School of Electrical Engineering

October 1990

I. INTRODUCTION

The efforts of the semiconductor industry to scale down the size of devices to achieve higher integration levels and higher speeds have been confronted by the major problem of the "troublesome" quantum-mechanical wave interference effects. These "troublesome" effects start to dominate device characteristics at dimensions of less than about one-quarter of a micron, thus, making further size reduction impossible. This limits the level of integration and the ultimate speed of integrated circuits. Further advances require fundamentally new device concepts and designs. The constructive use of the "troublesome" quantum effects was the basic premise of the proposed "Semiconductor Quantum Wave Optics" research. Using the quantitative analogies between electromagnetics and quantum mechanics [1], new electron wave superlattice structures can be designed that mimic corresponding devices in electromagnetic optics. Possible devices include narrow-band superlattice interference filters [2,3], filter/emitters [4,5], and negative-differential-resistivity devices [6]. These structures can potentially be utilized to produce terahertz bandwidth oscillators and switches. Impedance transformers between dissimilar materials can also be constructed [7]. Beyond improving the speed of existing devices, however, the totally new concept of "guided electron wave integrated circuits" has been proposed [8,9] to be investigated. In addition to the advantage of ultra-small size, these devices would have the advantages of optical-like processing – parallelism, interconnectivity, and bandwidth. Impressive experimental evidence of this optical-like electron behavior has recently been reported for gallium arsenide semiconductors.

II. WORK COMPLETED DURING THE 08-15-89/08-15-90 PERIOD

The work completed during the 08-15-89/08-15-90 period can be summarized into four categories: (a) theory and design of narrow-band semiconductor superlattice filter/emitters, (b) negative-differential-resistivity quantum interference devices, (c) theory and design of electron-wave impedance transformers, and (d) time-dependent characteristics of the electron-wave interference filters and filter/emitters.

A voltage-biased semiconductor superlattice structure has been designed to operate as a continuously voltage-tunable, electron-wave interference filter and as an electron emitter. Using the analogies between electromagnetic waves and electron-waves (de Broglie waves), a systematic procedure for designing the quantum wells and barriers comprising the electron-wave filter/emitter superlattice has been developed. A generalized procedure for analyzing the electron-current transmittance and reflectance spectral responses of these superlattice structures has also been developed. As an example, a practical continuously tunable filter/emitter consisting of multiple layers of $Ga_{1-x}Al_xAs$ (compositional superlattice) is designed to emit nearly monoenergetic 0.20eV electrons by appropriate selection of the layer compositions and thicknesses. The constraints required to have thicknesses that are integer multiples of the monolayer thickness and to minimize intervalley scattering (from Γ to L band) have also been included in the design. The filter/emitter has been shown to have a wide tunable energy range. The full width at half maximum (FWHM) of the filter/emitter has been shown to decrease as the number of the filter layers is increased. A sensitivity analysis of the device characteristics in the presence of fabrication errors has revealed a very stable device response. The narrow-band filter/emitters can be incorporated monolithically into transistor structures in order to increase their speed. Other possible applications include electroluminescent devices, photodetectors, and in future guided electron-wave integrated circuits. This part of the work has already been published in the *Journal of Applied Physics* [5] and part of it was presented in October 1989 at the *Annual Meeting of the Optical Society of America* in Orlando, Florida. In addition, a U.S. patent has already been allowed and will be issued within 1991.

In the case of the electron-wave quantum-interference filter/emitter semiconductor superlattice negative differential resistivity devices, the transmission and current-voltage characteristics have been analyzed with and without the self-consistency requirement. For the non-self-consistent calculation the single-band effective-mass time-independent Schroedinger equation has been solved. For the self-consistent calculation, Schroedinger and Poisson equations have been solved iteratively until a self-consistent electron poten-

tial energy and electron density were obtained. It has been shown that suitably designed electron-wave quantum-interference filter/emitters can exhibit strong negative differential resistance in the current-voltage characteristics, similar to those of resonant tunneling diodes. For low to moderate (2-30 meV) Fermi energies in the conduction band of $Ga_{1-x}Al_xAs$ (doping concentration less or equal to $2 \times 10^{18} cm^{-3}$), and temperatures near 30 K (in the ballistic transport regime), it has been shown that the space-charge effect was relatively small and resulted in a shift of the current-voltage and transmission characteristics toward higher bias voltages. In a fashion similar to that occurring in resonant tunneling diodes, the self-consistent field in electron-wave filter/emitter negative differential resistance devices effectively acts to screen the positive applied bias. Designs of $Ga_{1-x}Al_xAs$ devices have been analyzed. Resonant devices with current peak-to-valley ratios of $\sim$ 50 as well as nonresonant (not exhibiting negative differential resistance) devices have also been designed and analyzed. Importantly, in contrast to resonant tunneling diodes the valley current was lower and remained low over a larger voltage range ("flat valley"). The corresponding electron charge density distributions have also been calculated. Superlattice electron-wave filter/emitter negative differential resistance devices can be used as high-speed switches and oscillators and as monoenergetic emitters in electroluminescent devices and photodetectors. This part of the work has already been submitted for publication to the *Journal of Applied Physics.* Parts also of the above described work are going to be presented in the *Annual Meeting of the Optical Society of America* which will take place in November 1990 in Boston, Massachusetts.

In the construction of semiconductor quantum devices and guided electron-wave integrated circuits it will be necessary to connect semiconductor materials with differing electron energy-band structure. In such a configuration, detrimental reflections will occur at the energy-band discontinuity between materials. These reflections can be eliminated or minimized using impedance transformers. These type of impedance transformers for ballistic (collisionless) electron-waves traveling between dissimilar energy-gap semiconductors have been designed as a series of quarter (electron) wavelength layers in the form of a

compositional superlattice, using the quantitative analogies between electromagnetic and electron waves [1]. For the design energy, the electron-wave could be totally transmitted and the structure can be analogous to an antireflection coating in electromagnetic optics. Practical constraints on the impedance transformer that have been considered in the design were (a) that the compositions must be within the usable compositional range and (b) their thicknesses must be integer multiples of a monolayer thickness (similar to the design of filter/emitters). Procedures for designing narrow-band, maximally flat (Butterworth), and equal-ripple (Chebyshev) impedance transformers of arbitrary spectral bandwidth have been developed. Example practical single-layer and three-layer transformers for connecting GaAs and $Ga_{0.8}Al_{0.2}As$ have also been designed. This work has already been published in the *Journal of Applied Physics* [7].

The time-dependent characteristics of electron propagation in semiconductor superlattice interference filters and filter/emitters have also been studied. The transit time and the transmissivity across such structures have been determined by solving the time-dependent Schroedinger equation for Gaussian wavepackets. Ballistic transport has been assumed throughout the filter or filter/emitter region. It was shown that the transmissivity of the superlattice increases as the ratio of the energy width of the wavepacket divided by the full width at half maximum (FWHM) of the transmission coefficient increases. Transit times of the order of a few picoseconds are obtained for superlattices with total widths of 200Åwhen the average energy of the incident wavepacket is equal to the pass energy of the superlattice filter or filter/emitter. Part of this work was presented at the March 1990 meeting of the *Bulletin of the American Physical Society* [12].

III. CURRENT WORK

Additional work on *Semiconductor Quantum Wave Optics* is in progress. The areas that are being currently investigated can be summarized as follows: (a) investigation of the general similarities and differences between electromagnetic waves in lossless media and quantum-mechanical electron-waves semiconductors, (b) research on electron-wave slab

and channel waveguides with emphasis in practical configurations and current limitations, (c) analysis of the effects of the electron-electron and exchange interactions on semiconductor superlattice filters and filter/emitters, and (d) continuation of the analysis of the time-dependent effects of these devices.

Furthermore, the Microelectronics Research Center (MiRC) of Georgia Institute of Technology has the capabilities of fabricating these complicated ultra-small devices and collaboration with colleagues at this center has already been established for the simultaneous growth, fabrication, and testing of the designed quantum-wave devices.

IV. REFERENCES

1. T. K. Gaylord and K. F. Brennan, "Electron wave optics in semiconductors," *J. Appl. Phys.*, vol. 65, pp. 814–820, Jan. 15, 1989.
2. T. K. Gaylord and K. F. Brennan, "Semiconductor superlattice electron wave interference filters," *Appl. Phys. Lett.*, vol. 53, pp. 2047–2049, Nov. 21, 1988.
3. T. K. Gaylord, E. N. Glytsis, and K. F. Brennan, "Semiconductor superlattice interference filter design," *J. Appl. Phys.*, vol. 65, pp. 2535–2540, Mar. 15, 1989.
4. E. N. Glytsis, T. K. Gaylord, and K. F. Brennan, "Semiconductor biased superlattice tunable electron interference filter/emitter," *J. Appl. Phys.*, vol. 66, pp. 1494–1497, Aug. 1, 1989.
5. E. N. Glytsis, T. K. Gaylord, and K. F. Brennan, "Theory and design of semiconductor electron wave interference filter/emitters," *J. Appl. Phys.*, vol. 66, pp. 6158–6167, Dec. 15, 1989.
6. E. N. Glytsis, T. K. Gaylord, and K. F. Brennan, "Current-voltage characteristics of semiconductor superlattice electron-wave quantum-interference filter/emitter negative differential resistivity devices," *J. Appl. Phys.*, vol. 68, 1990. (submitted)
7. T. K. Gaylord, E. N. Glytsis, and K. F. Brennan, "Electron-wave quarter-wavelength impedance transformers between differing semiconductors," *J. Appl. Phys.*, vol. 67, pp. 2623–2630, Mar. 1, 1990.
8. T. K. Gaylord, E. N. Glytsis, and K. F. Brennan, "Semiconductor electron wave slab waveguides," *J. Appl. Phys.*, vol. 66, pp. 1483–1485, Aug. 1, 1989.
9. T. K. Gaylord, E. N. Glytsis, and K. F. Brennan, "Semiconductor quantum well electron waveguides," *J. Appl. Phys.*, vol. 66, pp. 1842–1848, Aug. 15, 1989.
10. J. Spector, H. L. Stormer, K. W. Baldwin, L. N. Pfeiffer, and K. W. West, "Electron focusing in two-dimensional systems by means of an electrostatic lens," *Appl. Phys. Lett.*, vol. 56, pp. 1290–1292, Mar. 26, 1990.
11. J. Spector, H. L. Stormer, K. W. Baldwin, L. N. Pfeiffer, and K. W. West, "Refractive switch for two-dimensional electrons," *Appl. Phys. Lett.*, vol. 56, pp. 2433–2435, June 11, 1990.
12. K. Diff, K. F. Brennan, T. K. Gaylord, and E. N. Glytsis, "Wavepacket propagation in semiconductor superlattice interference filters," *Bull. Amer. Phys. Soc.*, vol. 35, pg. 825, Mar. 1990.

V. PATENTS RELATED WITH THIS PROJECT

1. T. K. Gaylord, K. F. Brennan, and E. N. Glytsis, "Solid state quantum mechanical electron and hole wave devices," filed November 16, 1988, U.S. Patent Office application no. 07/272,175. Georgia Tech Record of Invention no. 1-88-13/1004. Patent Office notice of allowance September 1990.
2. T. K. Gaylord, E. N. Glytsis, and K. F. Brennan, "Semiconductor quantum well electron and hole waveguides," filed June 30, 1989, U.S. Patent Office application no. 07/374,437. Georgia Tech Record of Invention no. 1-88-14/1006A. Patent Office notice of allowance received July 19, 1990.
3. T. K. Gaylord, E. N. Glytsis, and K. F. Brennan, "Semiconductor biased superlattice tunable interference filter/emitter," filed June 30, 1989, U.S. Patent Office application no. 07/374,476. Georgia Tech Record of Invention no. 1-88-14/1006B. Patent Office notice of allowance September 1990.
4. T. K. Gaylord, K. F. Brennan, and E. N. Glytsis, "Solid state quantum mechanical electron and hole wave devices," international filing date of November 16, 1989, Patent Cooperative Treaty no. PCT/US89/05240. U. S. Patent Office serial nos. 07/272,175, 07/374,437, and 07/374,476. Georgia Tech Record of Invention nos. 1-88-13/1004, 1-88-14/1006A, 1-88- 14/1006B. Hurt, Richardson file no. 10733-066.
5. T. K. Gaylord, E. N. Glytsis, and K. F. Brennan, "Solid state quantum mechanical electron and hole wave devices," Chinise filing date of November 16, 1989, Patent Application no. 89108621.8. U. S. Patent Office serial nos. 07/272,175, 07/374,437, and 07/374,476. Georgia Tech Record of Invention nos. 1-88-13/1004, 1-88-14/1006A, 1-88- 14/1006B. Hurt, Richardson file no. 10733-063.
6. T. K. Gaylord, E. N. Glytsis, and K. F. Brennan, "Solid state quantum mechanical electron and hole wave devices," Canadian filing date of November 16, 1989, Patent File no. 2,003,134. U. S. Patent Office serial nos. 07/272,175, 07/374,437, and 07/374,476. Georgia Tech Record of Invention nos. 1-88-13/1004, 1-88-14/1006A, 1-88-14/1006B. Hurt, Richardson file no. 10733-065.

APPENDIX A

JOURNAL PAPERS PUBLISHED OR SUBMITTED DURING THE 08-15-89/08-15-90 PERIOD

- E. N. Glytsis, T. K. Gaylord, and K. F. Brennan, "Theory and design of semiconductor electron wave interference filter/emitters," *J. Appl. Phys.*, vol. 66, pp. 6158–6167, Dec. 15, 1989.

- T. K. Gaylord, E. N. Glytsis, and K. F. Brennan, "Electron-wave quarter-wavelength impedance transformers between differing semiconductors," *J. Appl. Phys.*, vol. 67, pp. 2623–2630, Mar. 1, 1990.

- E. N. Glytsis, T. K. Gaylord, and K. F. Brennan, "Current-voltage characteristics of semiconductor superlattice electron-wave quantum-interference filter/emitter negative diffrential resistivity devices," *J. Appl. Phys.*, vol. 68, 1990. (submitted)

Theory and design of semiconductor electron-wave interference filter/emitters

E. N. Glytsis, T. K. Gaylord, and K. F. Brennan
School of Electrical Engineering and Microelectronics Research Center, Georgia Institute of Technology, Atlanta, Georgia 30332-0250

(Received 15 June 1989; accepted for publication 30 August 1989)

A voltage-biased semiconductor superlattice structure is designed to operate simultaneously as a continuously voltage-tunable, electron interference filter and as an electron emitter. Using the analogies between electromagnetic waves and electron de Broglie waves, a systematic procedure for designing the quantum wells and barriers comprising the electron-wave filter/emitter superlattice is developed. A generalized procedure for analyzing the electron-current transmittance and reflectance spectral responses of these superlattice structures is then presented. A practical, continuously tunable filter/emitter consisting of multiple layers of $Ga_{1-x}Al_xAs$ (compositional superlattice) is designed to emit nearly monoenergetic 0.20-eV electrons by appropriate selection of the layer compositions and thicknesses. The constraints required to have thicknesses that are integer multiples of the monolayer thickness and to avoid phonon scattering of electrons into the L band are included. The filter/emitter is shown to have a wide tunable energy range. A sensitivity analysis of the device characteristics in the presence of fabrication errors reveals a very stable device response. Such quantum electron-wave devices could serve as continuously tunable hot-electron emitters in ballistic transistors and in future guided electron-wave integrated circuits.

I. INTRODUCTION

Quantum-mechanical interference effects have recently been observed in devices such as GaAs/AlGaAs and InGaAs/InAlAs single-well double-barrier structures.[1-4] This indicates that present-day semiconductor devices are rapidly approaching a fundamental size limitation.[5] At dimensions of less than about 0.3 μm, potentially "troublesome" quantum-wave effects start to dominate device characteristics, making further reduction in their sizes undesirable in some applications, thereby limiting the ultimate speed of the devices. This holds true regardless of the material (silicon, gallium arsenide, etc.). However, these quantum-wave effects may also potentially be used in the design of novel devices.

Starting from fundamental principles, quantitative analogies between quantum-mechanical electron waves in semiconductor materials and electromagnetic optical waves in dielectrics have recently been developed.[6] With these analogies, existing electromagnetic optical analysis and design techniques can be used for the analysis and design of new semiconductor quantum-wave devices. The possibility of realizing these device structures in practice has become more likely due to the rapid progress and relative maturity in semiconductor growth technologies such as molecular-beam epitaxy (MBE) and metalorganic chemical vapor deposition (MOCVD) that enable the fabrication of structures with precise monolayer compositional control. Possible devices include narrow-band superlattice interference filters[7,8] and filter/emitters[9] (present work). These structures could be incorporated into present-day ballistic transistors[10] to produce subpicosecond switching times. Beyond improving the speed of existing devices, however, the totally new concept of *guided electron-wave integrated circuits* has recently been proposed.[11] This next generation of integrated circuits would be comprised of many semiconductor quantum-wave devices interconnected by electron waveguides.[11-14]

In these ultrasmall superlattice interference filters or filter/emitters, electron waves can travel through the device maintaining their quantum-mechanical phase coherence. Thus these waves can interfere, reflect, refract, and diffract in a manner analogous to the electromagnetic plane waves in dielectric media. Even though quantum interference effects have been observed experimentally in single-well double-barrier structures, these effects can also occur in multiple-layer superlattices and at energies above the potential barriers. Furthermore, exploiting the electron-wave interference, novel electron-wave interference filter/emitters can be designed that are analogous to thin-film optical interference filters. These superlattice interference filter/emitters can exhibit very narrow electron kinetic energy passbands and can be integrated into solid-state devices for potential use as monoenergetic emitters for electroluminescent devices,[15,16] photodetectors,[15,17] and fast ballistic transistors.[15]

Although semiconductor superlattice interference filter designs can be visualized directly from the optical interference filters, their designs cannot simply be copies of thin-film optical designs. The reason for this is that due to the ultrasmall dimensions of each superlattice layer (on the order of a nanometer), the thickness quantization has to be taken into account (layer thicknesses must be an integer multiple of the monolayer thickness). Another constraint is the limited usable composition range that is available. Furthermore, in the case of an applied bias voltage, the potential energy along the undoped superlattice changes linearly with the device length. This is analogous to a varying optical refractive index in a thin-film filter. Presently, there are no available designs for this linearly varying index case. Another practical constraint is that the desired electron-energy states should be sufficiently below the L-band minimum in order to avoid phonon scattering which can reduce the electron coherence

 0021-8979/89/246158-10$02.40

length. The purpose of this paper is to present a systematic procedure for the design of continuously tunable semiconductor electron interference filter/emitters subject to the above constraints. An example design using the $Ga_{1-x}Al_xAs$ alloy system is presented, and the filter/emitter is shown to have a broad tunable range. Moreover, a sensitivity analysis of the device performance in the presence of fabrication variations indicates stable device characteristics.

II. SEMICONDUCTOR QUANTUM ELECTRON-WAVE OPTICS

Quantum-mechanical electron waves in semiconductors and electromagnetic optical waves in dielectrics exhibit transmission, reflection, interference, and diffraction characteristics that are analogous to each other since they satisfy analogous wave equations and boundary conditions. Quantum interference effects have been analyzed for single potential energy boundaries,[18] for normal incidence,[19] and for the general case of any number of boundaries and any angle of incidence.[6] From these results a quantitative mapping between electromagnetic optical waves and quantum electron waves has been established.[6] Thus, using these quantitative analogies, existing optical device designs can now have electron-wave device counterparts.

The plane-wave solutions of the Schrödinger's equation contain a wave-vector quantity k of magnitude $k = [2m^*(E - V)]^{1/2}/\hbar$, where m^* is the electron effective mass, E is the total electron energy, V is the electron potential energy, and $\hbar$ is Planck's constant divided by 2π. All plane-wave phase effects (for plane-wave interference) are described by the wave vector k. As a consequence, an electron-wave phase refractive index n_e(phase), can be introduced that is proportional to the square root of the product of the effective mass and the kinetic energy.[6] That is,

$$n_e(\text{phase}) \propto [m^*(E - V)]^{1/2}. \tag{1}$$

Furthermore, amplitude effects such as electron transmissivity and reflectivity may be described in terms of the wave-function amplitude for an electron wave or in terms of the electric field amplitude for TE-polarized optical wave incident upon a boundary. Continuity of the wave function across a potential energy boundary and conservation of electron probability current normal to a potential energy boundary are analogous to the continuity of the tangential component of the electric field across a boundary between dielectrics and to the conservation of power flow normal to a boundary between dielectrics, respectively. Using these analogies, an electron-wave amplitude refractive index n_e(amplitude) can be introduced[6] that makes the optical and electron-wave transmissivities and reflectivities equivalent. That is,

$$n_e(\text{amplitude}) \propto [(E - V)/m^*]^{1/2}. \tag{2}$$

Since the phase and amplitude effects are mathematically decoupled in the equations describing electromagnetic optical designs, the same designs have quantum electron-wave counterparts that are described by the two electron-wave refractive indices [Eqs. (1) and (2)]. Both types of these refractive indices exhibit normal dispersion; i.e., they increase with decreasing wavelength.

III. THIN-FILM OPTICAL INTERFERENCE FILTERS

Due to the analogies between the electromagnetic optical waves and the quantum-mechanical electron waves, the thin-film optical interference filters and the electron-wave interference superlattice filters have many common characteristics. For completeness some of the more relevant properties of thin-film optical filters[20–22] are summarized below.

A simple type of narrow-bandpass optical interference filter is the all-dielectric Fabry–Perot filter. It consists of a half-wavelength layer sandwiched between quarter-wavelength layers of high refractive index (designated H) and of low refractive index (designated L). The combination of quarter-wavelength layers constitutes a reflector. The electron-wave analog of this elementary type of interference optical filter is treated in this work. The full width at half maximum (FWHM) of the bandpass of this filter can be reduced by increasing the reflectivity of the reflectors, i.e., by increasing the ratio of high to low refractive indices. In the optical literature there are two basic types of all-dielectric Fabry–Perot interference filters which are symbolically represented as $[HL]^N HH[LH]^N$ and $H[LH]^N LL[HL]^N H$, where H and L represent quarter-wavelength layers of high and low refractive index, respectively, and N represents the number of repetitions of the layer-pair type indicated in brackets. Some other important characteristics of the all-dielectric Fabry–Perot interference filters, that are related with the electron-wave interference filter designs, are the following: (1) The maximum transmittance of the filter is 100%. (2) The maximum transmittance occurs at the wavelength for which the central layer is a half-wavelength thick (as measured in that material) and the surrounding layers are quarter-wavelength layers (as measured in those materials). (3) The FWHM decreases as the number of the surrounding layers increases (as N increases). (4) The transmittance characteristics are relatively insensitive to variations in the reflectivities and thicknesses of the layers. (5) The filter is effective only over a limited range since sidebands necessarily occur on either side of the passband.

IV. DESIGN OF SEMICONDUCTOR SUPERLATTICE INTERFERENCE FILTER/EMITTERS

A. Computation of the layer thicknesses and compositions for a given bias voltage and electron energy

When a voltage bias is applied to a superlattice structure, the resulting device can serve as an electron-wave interference filter and electron emitter. Using the previously presented analogies between the quantum electron waves and the electromagnetic optical waves, the quantum well and barrier widths and heights in the direction of emission can be systematically designed to comprise an interference filter which is embedded in the emitter. The optical analog of this device does not exist since the equivalent phase and amplitude refractive indices of the electron waves vary along the emission direction of the structure due to the applied bias potential energy. Thus the optical counterpart would be comprised of inhomogeneous regions where the correspond-

ing optical refractive indices would vary as functions of the propagation distance within the optical filter. However, the same concepts that are used for the design of homogeneous optical interference filters can be adopted in the case of the electron-wave interference filter/emitter. Moreover, the successive quantum wells and barriers can act as the high (H) and low (L) electron refractive index materials that comprise the reflectors of the interference filter/emitter.

The electron potential energy of a quantum-well superlattice interference filter/emitter with an applied bias voltage is shown in Fig. 1. The structure consists of M layers surrounded by bulk semiconductor material. The filter/emitter is designed to be a simple narrow-bandpass interference filter (the optical counterpart would be an all dielectric inhomogeneous Fabry–Perot interference filter). The filter/emitter consists of M layers, where M is an odd integer, and the central layer is a half-wavelength layer sandwiched between quarter-wavelength layers of high (H) and low (L) equivalent electron-wave refractive index. When the design voltage is applied, electrons in a narrow spectral band around the prespecified pass energy E_p (Fig. 1) traverse the filter/emitter and are emitted with an output energy $\mathrm{KE}_{\mathrm{out}}$. At the design voltage, with corresponding bias potential energy V_{bias}, each reflector layer [of high (H) or low (L) average electron-wave refractive index] is exactly a quarter of an electron wavelength (as measured in that layer) in the thickness, and the resonant central layer is exactly one-half of an electron wavelength (as measured in that layer). In the case of the biased filter/emitter, the kinetic electron energy varies linearly within each individual layer due to the applied voltage. Thus the electron wavelength changes continuously inside each layer. However, a quarter or a half of an electron wavelength is defined as the required layer thickness to produce a total phase shift of the traveling electron-wave function inside the layer of $\pi/2$ or π, respectively (or odd multiples of these phase shifts). Although only an average electron wavelength can be defined within each layer, the terminology of "quarter" or "half electron wavelength" are used in order to be analogous to the corresponding quantities appearing in the design of optical thin-film interference filters. The jth quantum well or barrier (Fig. 1) has a thickness d_j and at zero bias a potential energy of V_j. The layers surrounding the emitter/filter regions are taken to have the same zero-bias potential energy of V_0. The material system in which the filter/emitter can be implemented is taken to form a continuous set of alloys of the type $\mathrm{G}_{1-x}\mathrm{H}_x\mathrm{K}$ where G, H, and K are chemical elements, and x is the atomic percentage of the H chemical element. For example, a practical material system is $\mathrm{Ga}_{1-x}\mathrm{Al}_x\mathrm{As}$. Even if the range of values for the composition x can vary from zero to one, the range of usable compositions may be restricted to $0<x<x_{\max}$, where $x_{\max}<1$. For example, this can occur due to a possible transition at $x_{\max}$ from a direct to an indirect energy-gap material as in the case of $\mathrm{Ga}_{1-x}\mathrm{Al}_x\mathrm{As}$.

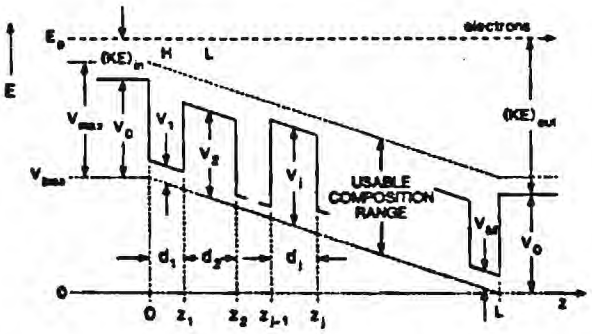

FIG. 1. Schematic representation of a biased semiconductor superlattice electron-wave interference filter/emitter. At the design potential energy bias V_{bias} and input kinetic energy $\mathrm{KE}_{\mathrm{in}}$, the layers have a thickness of a quarter (or a half for the resonant central layer) of an electron wavelength as measured in that layer.

The electron potential energy is given by

$$V_j \equiv \Delta E_c = Ax_j, \tag{3}$$

where ΔE_c is the change in the energy of the conduction-band edge, and A is a constant. Due to restrictions on usable composition range, the corresponding range of potential energies is $0<V_j<V_{\max}=Ax_{\max}$. The layers surrounding the filter/emitter regions have a composition of x_0. An additional design constraint for the electron-wave filter/emitter is that the layer thicknesses should be an integer multiple of the monolayer thickness. Thus the thickness of the jth layer d_j should be an integer multiple p_j of the monolayer thickness r_j. For the jth layer to be a quarter of an electron wavelength in thickness at the design pass energy E_p, the phase difference between the input boundary z_{j-1} and the output boundary z_j (Fig. 1) must be an odd integer multiple of $\pi/2$. That is,

$$\int_{z_{j-1}}^{z_j} k_j(z)\,dz = \int_{z_{j-1}}^{z_j} \left(\frac{1}{\hbar}\right)\{2m_j^*[E_p - V_j(z)]\}^{1/2}dz = (2q_j-1)\pi/2, \tag{4}$$

where the potential energy in the jth layer with bias applied is given by

$$V_j(z) = V_{\mathrm{bias}}\left(1-\frac{z}{L}\right) + V_j. \tag{5}$$

L is the total length of the superlattice (Fig. 1), and $q_j = 1,2,\ldots$. The electron pass energy may be expressed as $E_p = V_{\mathrm{bias}} + V_0 + \mathrm{KE}_{\mathrm{in}}$ where $\mathrm{KE}_{\mathrm{in}}$ is the pass kinetic energy in the input region (leftmost region in Fig. 1). The electron effective mass is given by $m_j^* = (B + Cx_j)m_0$ where m_0 is the free-electron mass, and B and C are material-system-dependent constants. Using Eqs. (3), (5), and the integral identity $\int (a+bz)^{1/2}dz \equiv (2/3b)(a+bz)^{3/2}$, Eq. (4) can be rewritten

$$\frac{2L\,[2m_0(B+Cx_j)]^{1/2}}{3\hbar V_{\mathrm{bias}}} \times \left[\left(V_0 + \mathrm{KE}_{\mathrm{in}} - Ax_j + V_{\mathrm{bias}}\frac{z_j}{L}\right)^{3/2} - \left(V_0 + \mathrm{KE}_{\mathrm{in}} - Ax_j + V_{\mathrm{bias}}\frac{z_{j-1}}{L}\right)^{3/2}\right] = (2q_j-1)\frac{\pi}{2}. \tag{6}$$

The above equation has to be solved for the composition x_j of the jth layer with V_{bias}, V_0, and $\mathrm{KE}_{\mathrm{in}}$ as design parameters. Equation (6) is valid for all the layers except the center reso-

nant layer. In this case the $\pi/2$ term of Eq. (6) is replaced by π. The monolayers of the device will be numbered with the index i. The rightmost monolayer of the jth region is i_j. The total number of monolayers in the emitter/filter is designated i_M. Therefore, the number of monolayers of the jth layer is $p_j = i_j - i_{j-1}$, and the corresponding thickness of this layer is $d_j = p_j r_j = z_j - z_{j-1}$. The total thickness of the structure is $L = \sum_{j=1}^{M} p_j r_j$ (if the monolayer thicknesses are the same in each layer, $r_1 = r_2 = \cdots r_M = r$, then $L = i_M r$). The boundaries between the various layers which are designated as z_j (Fig. 1) are given by $z_j = \sum_{l=1}^{j} p_l r_l$ [for equal monolayer thicknesses, $z_j = (i_j/i_M)L$]. It is worth mentioning that the solution of Eq. (6) is not trivial since Eq. (6) for the jth layer depends on the thicknesses of the other layers. Furthermore, Eq. (6) is valid only if $V_{bias} \neq 0$. In the case of zero applied bias, $V_{bias} = 0$, Eq. (4) leads to Eq. (11) of Ref. 8, which is much simpler to solve.

A systematic procedure for designing a biased continuously tunable superlattice interference filter/emitter for a given output kinetic energy ($KE_{out} = KE_{in} + V_{bias}$) and given compositions (x_0) of the surrounding filter/emitter regions, using Eq. (6), is now described. The design parameters V_0(or x_0), KE_{in}, and V_{bias} have to be specified at the beginning. Next the characteristics of the unbiased superlattice electron-wave interference filter[7,8] are used as a starting point in estimating the number of regions M and the number of monolayers p_j ($j = 1,2,\ldots,M$) to be used in the filter/emitter. The initial values of the number of monolayers in each layer are designed as p_j^0, the total initial thickness is designated as L^0, and the total number of monolayers is designated as i_M^0. It is important to keep the length of the structure as small as possible in order to be less than the electron coherence length. Consequently, it is more practical to set the parameters $q_j = 1$ in order to find the minimum thickness device. Starting from the first layer ($j = 1$), Eq. (6) is solved for x_j. Since an iterative scheme is used, the solution of Eq. (6) for x_j is designated as $x_j^{n_j}$, where n_j is a counting index for the iterations of the jth layer. In the next step it is determined if the solution $x_j^{n_j}$ lies within the range of usable composition values ($0 < x_j^{n_j} < x_{max}$). If $x_j^{n_j}$ is outside the usable range, then the number of monolayers is changed as $p_j^{n_j} = p_j^{n_j-1} + \Delta p_j^{n_j}$, where $\Delta p_j^{n_j}$ is the change in the number of monolayers of region j. The procedure is repeated until a value for $x_j^{n_j}$ is found within the usable range. For the filter to have a narrower response, it is important to increase the reflectivity between the low (L) and high (H) electron refractive index layers. For the low index layers the composition should be as close to x_{max} as possible. Similarly, for the high index layers the composition should be as close to zero as possible. As a result, some additional refining of the calculated solution for the jth layer can be found by changing the value of $p_j^{n_j}$ by ± 1 ($\Delta p_j^{n_j} = \pm 1$). This is continued until the solution $x_j^{n_j}$ is the maximum possible (within the usable composition range) for a low (L) index layer or the minimum possible (within the usable composition range) for a high (H) index layer. This procedure is repeated for all the layers ($j = 1,2,\ldots,M$). However, the solution for the last layer may result in a new value of i_M (or equivalently L) which differs from the initially estimated i_M^0 (or equivalently L^0). In this case the resultant value of L is set equal to L^0 and the design process is repeated until the final thickness L is consistent with the initially assumed thickness L^0, i.e., $L = L^0$. The design procedure is summarized in the algorithm presented in Fig. 2.

B. Computation of the designed filter/emitter response

In order to evaluate the response of the interference filter/emitter designed with the above-described procedure, the electron-wave function has to be calculated in the output region of the structure. Using the one-electron-wave function approximation, and neglecting the electron-electron and the exchange interaction which partially compensate one another, the electron-wave function in each layer satisfies the Schrödinger's equation. That is,

$$\frac{\hbar^2}{2m_j^*}\frac{d^2\psi_j(z)}{dz^2} + [E - V_j(z)]\psi_j(z) = 0, \tag{7}$$

where $\psi_j(z)$ is the electron-wave function in region j ($j = 1,2,\ldots,M$), and $V_j(z)$ is given by Eq. (5). The electron-wave function in any layer of the biased superlattice can be expressed as a linear combination of Airy functions $\mathrm{Ai}(\rho)$ and complimentary Airy functions $\mathrm{Bi}(\rho)$.[23–25] By defining within each layer a new variable $\rho_j = \rho_j(z) = (2m_j^* V_{bias}/\hbar^2 L)^{1/3}[z + (E - V_{bias} - V_j)L/V_{bias}]$, Eq. (7) can be transformed into the form $d^2\psi_j(\rho_j)/d\rho_j^2 + \rho_j\psi_j(\rho_j) = 0$, which has solution of the form

$$\psi_j(\rho_j) = \psi_j(z) = C_j\mathrm{Ai}[-\rho_j(z)] + D_j\mathrm{Bi}[-\rho_j(z)], \tag{8}$$

where C_j and D_j are unknown amplitude constants. The solution of Schrödinger's equation in the two external regions (leftmost and rightmost regions in Fig. 1) is straightforward since the potential energy does not vary in these regions. Specifically, the wave function in the input region is given by $\psi_0(z) = \exp(jk_0z) + r\exp(-jk_0z)$, while the wave function for the output region is given by $\psi_{M+1}(z) = t\exp[jk_{M+1}(z - z_M)]$. The k_0 and k_{M+1} are the electron-wave vectors in the input and output regions, respectively. Using the boundary condition for the wave function, $\psi_j(z_j) = \psi_{j+1}(z_j)$, and $(1/m_j^*)d\psi_j(z_j)/dz = (1/m_{j+1}^*)\,d\psi_{j+1}(z_j)/dz$, the reflected and transmitted amplitude of the wave function (r and t) may be expressed as

$$\begin{pmatrix}1\\r\end{pmatrix}=\frac{1}{2jK_1}\begin{pmatrix}jK_1 & -1\\ jK_1 & 1\end{pmatrix}[S_1(z_0)][S_1(z_1)]^{-1}[S_2(z_1)][S_2(z_2)]^{-1}[S_3(z_2)]\cdots[S_{M-1}(z_{M-1})]^{-1}$$
$$\times[S_M(z_{M-1})][S_M(z_M)]^{-1}\begin{pmatrix}1 & 1\\ -jK_2 & jK_2\end{pmatrix}\begin{pmatrix}t\\0\end{pmatrix}, \tag{9}$$

where

$$[S_j(z)]=\begin{pmatrix}\mathrm{Ai}[-\rho_j(z)] & \mathrm{Bi}[-\rho_j(z)]\\ (1/M_j^*)^{2/3}\mathrm{Ai}'[-\rho_j(z)] & (1/M_j^*)^{2/3}\mathrm{Bi}'[-\rho_j(z)]\end{pmatrix}, \tag{10}$$

and where $M_j^*=m_j^*/m_0$, $K_1=[(2m_0/\hbar^2)^{1/3}(E-V_0-V_{\mathrm{bias}})/M_0^*]^{1/2}(L/V_{\mathrm{bias}})^{1/3}$ and $K_2=[(2m_0/\hbar^2)^{1/3}(E-V_0)/M_{M+1}^*]^{1/2}(L/V_{\mathrm{bias}})^{1/3}$, and Ai′ and Bi′ are the first derivatives of the Airy and complimentary Airy functions, respectively. Equations (9) can be solved directly for the amplitude transmittance t and the amplitude reflectance r. The electron current transmittance T_e is given by

$$T_e=\frac{[(E-V_0)/M_{M+1}^*]^{1/2}}{[(E-V_0-V_{\mathrm{bias}})/M_0^*]^{1/2}}|t|^2. \tag{11}$$

Using Eq. (11), the response of the designed electron interference filter/emitter can be evaluated.

C. Design of a filter/emitter with *L*-valley electron potential energy constraint

If the electron energy is near the ⟨111⟩ L-valley minimum, then the resulting phonon scattering in the device may decrease the electron coherence length. As a result the phonon scattering can deteriorate the performance of an electron-wave interference filter/emitter. However, some additional constraints can be imposed in the design process of the device that can minimize the phonon scattering. The L-valley potential energy in the jth layer, V_{Lj}, is given by

$$V_{Lj}=D+Fx_j \tag{12}$$

where D and F are material-dependent constants, and x_j is the material composition (alloys of the type $G_{1-x}H_xK$ are being assumed). In the previously described design process, the composition of the input and the output regions of the device were taken to be the same (x_0). This assumption does not imply any restriction in the device design, but only reflects the symmetry of the electron Fabry–Perot. For positive energies, the electron pass energy must be larger than the electron potential energy V_0 in the input region (i.e., electron energy should be above the Γ-valley minimum). Furthermore, for practical devices, the input kinetic energy KE_{in} should be at least ΔE_1, where ΔE_1 is a design parameter that ensures sufficient input velocity. In addition, at the output layer the electron energy should be less than the L-valley minimum by at least ΔE_2, where ΔE_2 is a design parameter that ensures that there will be neither intervalley phonon emission nor absorption. The above-described constraints can be written as follows:

$$V_0+\Delta E_1<E<V_{L0}-\Delta E_2, \tag{13}$$

where V_{L0} is the L-valley electron potential energy in the output region ($V_{L0}=D+Fx_0$). It is implied that the bias potential energy is non-negative as shown in Fig. 1($V_{\mathrm{bias}}>0$). Inequalities (13) impose the following condition for the allowable bias potential energy:

$$V_{\mathrm{bias}}<D-(A-F)x_0-\Delta E_1-\Delta E_2 \tag{14}$$

Inequality (14) limits the maximum value of the applied bias potential energy to $(V_{\mathrm{bias}})_{\max}=D-(A-F)x_0-\Delta E_1-\Delta E_2$. The maximum applied bias potential energy depends on the compositions of the input and output regions. Constraints similar to inequality (13) can be applied for each layer inside the device. That is,

$$V_j(z)<E<V_{Lj},\quad \text{for } z_{j-1}<z<z_j, \tag{15}$$

which imposes on the composition x_j the following constraint:

$$\frac{1}{A}\left(Ax_0+\Delta E_1+V_{\mathrm{bias}}\frac{z_j}{L}-D\right)$$
$$<x_j<\frac{1}{F}\left(Ax_0+V_{\mathrm{bias}}\frac{z_{j-1}}{L}\right). \tag{16}$$

Inequality (15) can be even tighter if energy margins ΔE_{1j} and ΔE_{2j} are nearly equal to ΔE_1 and ΔE_2. However, for practical purposes the inequalities (13) and (15) can be considered sufficient.

The design procedure described in Sec. IV A remains basically the same with the exception that V_{bias} has to satisfy inequality (14) and the layer compositions should lie in the range expressed by inequality (16).

V. $Ga_{1-x}Al_xAs$ EXAMPLE CASES

A practical material system to be used in fabricating the above-described electron-wave interference filter/emitters is $Ga_{1-x}Al_xAs$. For this material system the maximum composition in Al is $x_{\max}=0.45$ in order to avoid the direct/indirect band-gap transition. Other parameters of this material system include $A=0.773$ eV, $B=0.067$, $C=0.083$, $D=0.284$ eV, and $F=0.168$. The ⟨100⟩ monolayer thickness for any usable composition remains the same $r_j=0.282\,665$ nm (lattice-matched material system).

At first, some designs that are not restricted by the L-valley energy are presented. For these filter/emitters the

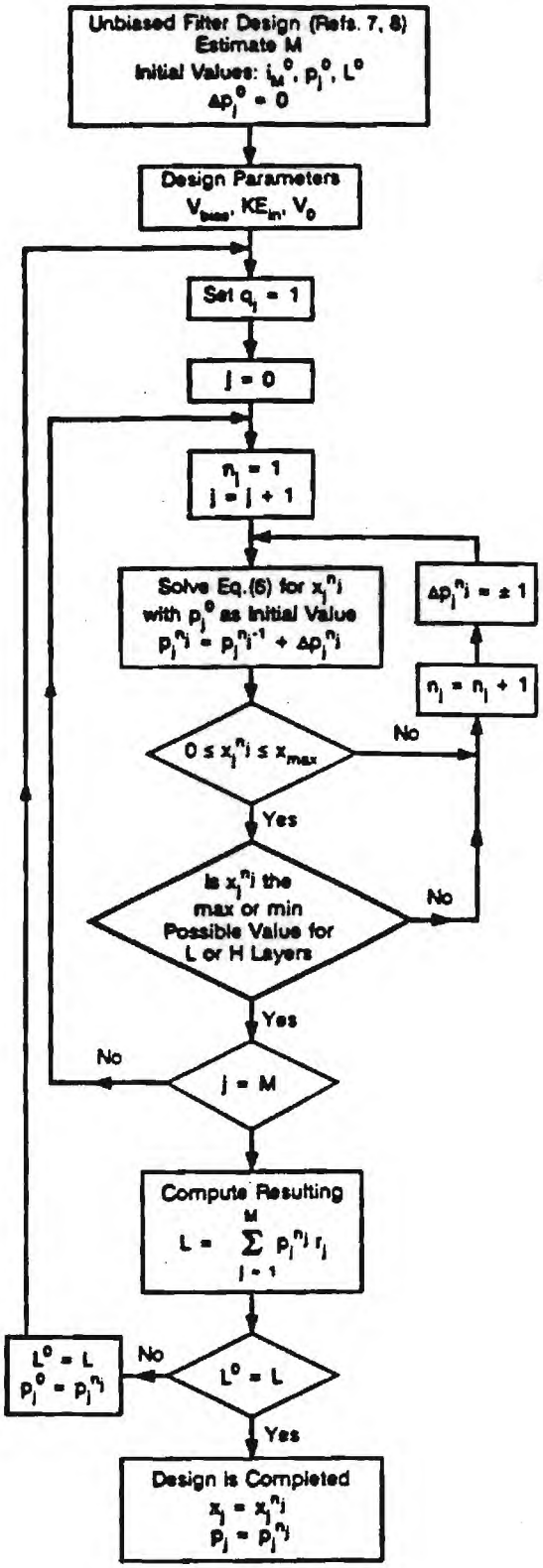

FIG. 2. Flow chart of the calculational procedure used for the computation of the filter/emitter layer compositions and thicknesses.

compositions of the surrounding regions (rightmost and leftmost regions in Fig. 1) are chosen to be $x_0 = 0.45$. The design parameters V_{bias} and KE_{in} are chosen both to be 0.10 eV each. Using the procedure described in Sec. IV A (algorithm of Fig. 2), the layer thicknesses (expressed in number of monolayers) and the layer compositions can be calculated. These results are summarized in Table I for various number of layers $M = 9$, 13, and 17. The total thickness of the design structures is 20.1 nm (71 monolayers), 28 nm (99 monolayers), and 36.2 nm (128 monolayers) for $M = 9$, 13, and 17, respectively, which is within the desired electron coherence length. Experimental measurements in ballistic hot-electron devices[10,26,27] (on GaAs/GaAlAs and InGaAs/InAlAs) indicate that the electron coherence length lies roughly between 10 and 100 nm. However, the electron coherence length is a statistical quantity. Therefore, the experimental data suggest that at least some measurable fraction of electrons exhibit a coherence length within the design for the filter/emitter requirements. The spectral response (transmittance versus output kinetic energy) of the designed structure can be computed using the analysis described in Sec. IV B. The electron-current transmittance T_e [Eq. (11)] is shown in Figs. 3(a), 3(b), and 3(c) as a function of the output kinetic energy KE_{out} for $M = 9$, 13, and 17, respectively, with the applied bias potential energy V_{bias} as a parameter. From these figures it is shown that for $V_{bias} = 0.10$ eV the filter/emitter has a peak in the electron-current transmittance (of about 100%) for the design output kinetic energy of 0.20 eV. The spectral response of the filter/emitter has a narrow passband around the designed output kinetic energy, and the FWHM decreases as the number of layers increases. For the cases shown in Figs. 3(a), 3(b), and 3(c), the FWHM values are 30.7, 13.4, and 5.9 meV for $M = 9$, 13, and 17, respectively. However, by increasing the number of the layers M, (1) the total thickness of the device increases (thickness should be less than the electron coherence length), and (2) some secondary peaks in the electron-current transmittance appear as is shown in Figs. 3(b) and 3(c) for $M = 13$ and 17, respectively. Thus there is a trade-off between the FWHM and the device thick-

TABLE I. Design parameters of an electron-wave interference filter/emitter with the $(HL)^N HH(LH)^N$ $[N = (M-1)/2]$ configuration. The surrounding input and output regions consist of $Ga_{0.55}Al_{0.45}As$, and the filter/emitter is designed to emit 0.20-eV electrons when biased at 0.10 eV.

Layer	$M = 9$		$M = 13$		$M = 17$	
j	p_j	x_j	p_j	x_j	p_j	x_j
1	7	0.2222	7	0.2194	7	0.2178
2	9	0.4151	9	0.4081	9	0.4041
3	7	0.2663	7	0.2513	7	0.2426
4	9	0.4493	9	0.4327	9	0.4231
5	12	0.0639	7	0.2823	7	0.2668
6	8	0.4364	8	0.3978	9	0.4421
7	6	0.1442	12	0.0639	7	0.2905
8	7	0.3748	8	0.4301	8	0.4020
9	6	0.1951	6	0.1237	12	0.0654
10			7	0.3582	8	0.4271
11			6	0.1626	6	0.1125
12			7	0.3815	7	0.3493
13			6	0.1982	6	0.1439
14					7	0.3674
15					6	0.1729
16					7	0.3853
17					6	0.1999

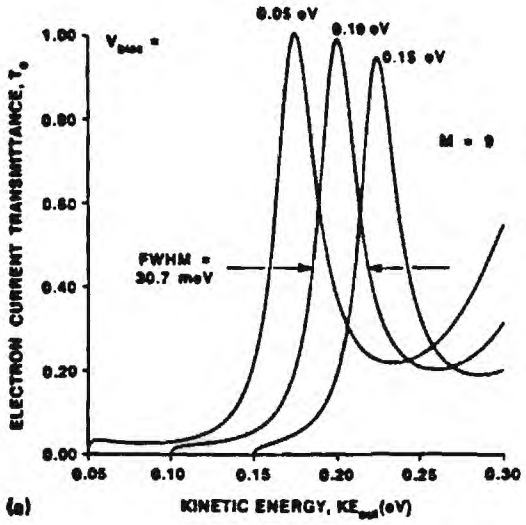

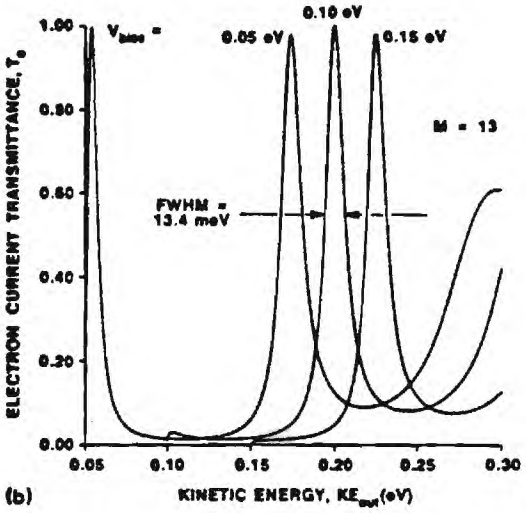

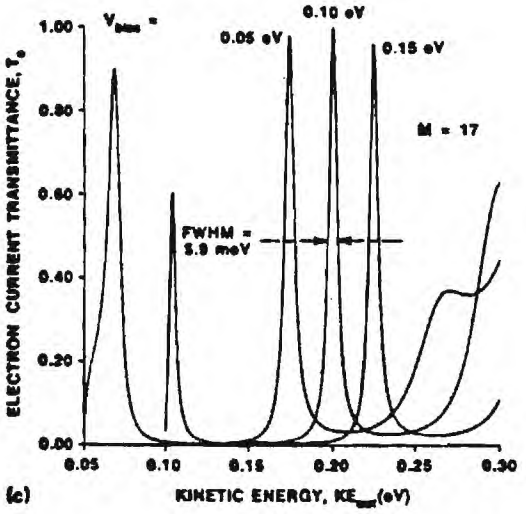

FIG. 3. Electron-current transmission of M-layer $Ga_{1-x}Al_xAs$ superlattice interference filter/emitter as a function of the electron output kinetic energy for V_{bias} = 0.05, 0.10, and 0.15 eV for (a) M = 9, (b) M = 13, and (c) M = 17. The spectral tuning with the bias is apparent. Furthermore, the spectral widths become narrower as the number of the layers M increases.

ness. Another important feature of the filter/emitter spectral response is that using the same design (of V_{bias} = 0.10 eV and KE_{in} = 0.10 eV), and applying other bias potential energies, the narrow-band characteristic of the filter/emitter remains almost unchanged, but shifted in output kinetic energy. For example, the spectral response of the designed filter/emitter is shown in Figs. 3(a), 3(b), and 3(c) for V_{bias} = 0.05, 0.10, and 0.15 eV. It is observed that there is no significant change in the electron-current transmittance peak and the FWHM, but there is a shift in the output kinetic energy for which the peak electron-current transmittance occurs. The change in the output kinetic energy ΔKE_{out} is approximately half of the change in the applied bias potential energy ΔV_{bias}. This can be explained by the fact that the resonant central layer (HH) is almost at the middle of the device and consequently experiences half of the change of the bias potential energy. Furthermore, due to this property of the filter/emitter, the device can be continuously tuned over a range of output kinetic energies, around the designed value, by varying the applied voltage. The tunability of the device is further illustrated in Fig. 4 (for M = 13) for a range of bias potential energies from 0.0 to 0.2 eV. It is observed that the output kinetic energy at the peak electron-current transmittance varies linearly with the applied bias potential energy in the range between −0.15 and −0.25 eV (the slope of the straight line in Fig. 4 is 0.496). Moreover, the peak of the electron-current transmittance, $T_{e,peak}$, varies smoothly around the design value of V_{bias} (0.10 eV) in the range between 92.1% and ~100%.

The electron-current transmittance of the filter/emitter as a function of the applied bias potential energy with the electron output kinetic energy KE_{out} as a parameter is shown in Fig. 5 for V_{bias} varying between 0.0 and 0.3 eV with KE_{out} = 0.10, 0.15, 0.20 (design value), 0.25, and 0.30 eV. The design parameters of this filter/emitter are given in Table I for M = 9. Figure 5 is equivalent to Fig. 3(a), but with the roles of KE_{out} and V_{bias} interchanged. It is observed that for KE_{out} = 0.15, 0.20, 0.25, and 0.30 eV there is a peak in the electron-current transmittance. For KE_{out} = 0.10 eV the transmittance is low as it can also be seen from Fig. 3(a).

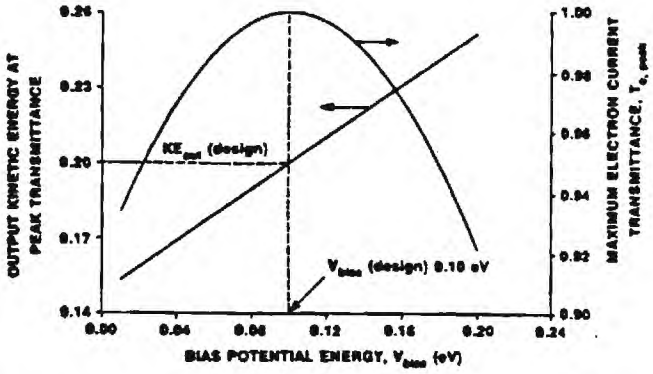

FIG. 4. Tunability characteristics of a filter/emitter for M = 13. The design values are V_{bias} = 0.10 eV and KE_{in} = 0.10 eV. The electron output kinetic energy at peak electron-current transmittance and the value of the peak electron-current transmittance are shown as functions of the bias potential energy V_{bias}.

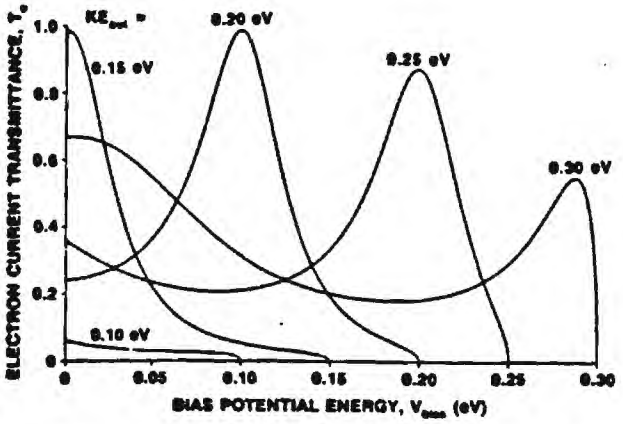

FIG. 5. Electron-current transmittance of a filter/emitter for $M = 9$, as a function of the applied bias potential energy V_{bias} with the output electron kinetic energy as a parameter. Design values are $V_{bias} = 0.10$ eV and $KE_{in} = 0.10$ eV.

The peak value of the transmittance decreases as the output kinetic energy deviates from the design value (of 0.20 eV at $V_{bias} = 0.10$ eV).

Another important practical factor is the sensitivity of the designed electron-wave interference filter/emitters to fabrication process variations. Since these devices are ultrasmall, the layer thicknesses should ideally be the design number of monolayers. Furthermore, the Al composition usually can be controlled to within 1%–2%. In order to evaluate the sensitivity of the electron-wave filter/emitter, the layer thicknesses and compositions were varied from the design values, and the spectral response of the resulting devices were calculated using Eq. (11). Three cases were considered along with the design case (case 1, $V_{bias} = 0.10$ eV, $KE_{in} = 0.10$ eV, and $M = 9$). These are summarized in Table II. Case 2 corresponds to fabrication variations of the Al compositions (x_j's), while cases 3a/3b and 4 correspond to fabrication variations of the central (resonant) layer thickness and of the surrounding layer thicknesses, respectively. The spectral responses that correspond to the filter/emitters of cases 1 and 2 are shown in Fig. 6(a). It is observed that

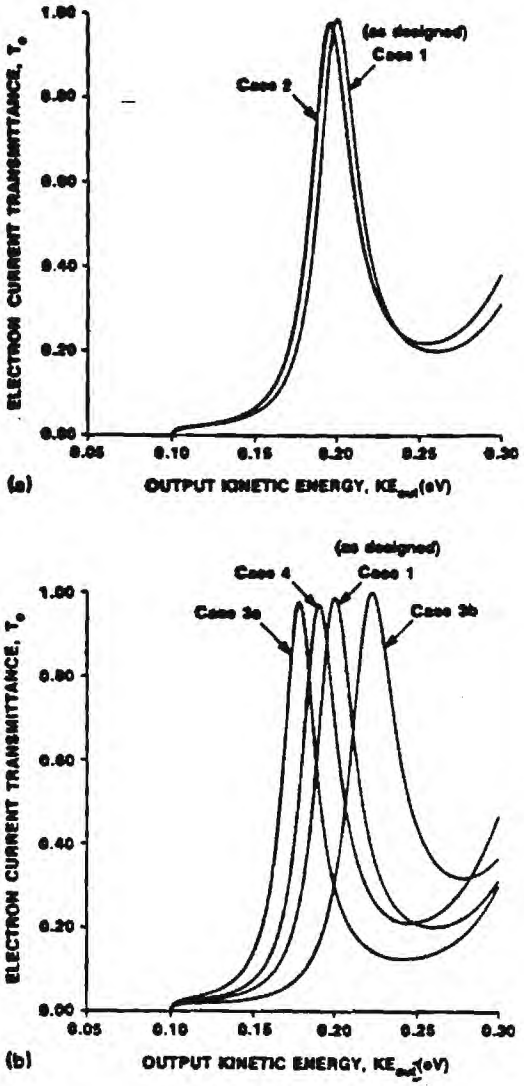

FIG. 6. Electron-current transmittance of a filter/emitter as a function of the electron output kinetic energy. Design values are $V_{bias} = 0.10$ eV, $KE_{in} = 0.10$ eV, and $M = 9$. (a) Cases 1 and 2 of Table II (fabrication variations in the layer compositions) and (b) cases 3a/3b and 4 of Table II (fabrication variations in the layer thicknesses).

TABLE II. Design parameters of an electron-wave interference filter/emitter with the $(HL)^N HH(LH)^N$ $[N = (M-1)/2]$ configuration (case 1), a suboptimal design with rounded-off composition values (case 2), and two suboptimal designs with incorrect monolayer thicknesses (cases 3a, 3b, and 4). The surrounding input and output regions consist of $Ga_{0.55}Al_{0.45}As$, and the filter/emitter is designed to emit 0.20-eV electrons when biased at 0.10 eV. In all the listed cases the number of the layers is $M = 9$.

Layer	Case 1		Case 2		Cases 3a/3b		Case 4	
j	p_j	x_j	p_j	x_j	p_j	x_j	p_j	x_j
1	7	0.2222	7	0.20	7	0.2222	7	0.2222
2	9	0.4151	9	0.40	9	0.4151	9	0.4151
3	7	0.2663	7	0.25	7	0.2663	6	0.2663
4	9	0.4493	9	0.43	9	0.4493	9	0.4493
5	12	0.0639	12	0.08	13/11	0.0639	12	0.0639
6	8	0.4364	8	0.43	8	0.4364	9	0.4364
7	6	0.1442	6	0.15	6	0.1442	7	0.1442
8	7	0.3748	7	0.36	7	0.3748	8	0.3748
9	6	0.1951	6	0.20	6	0.1951	6	0.1951

even if the layer compositions vary between 0.5%–2.2% (possible fabrication variation) from the design values the filter/emitter response is not substantially altered. When the thicknesses of the layers deviate from the optimal design values (cases 3a/3b and 4), the filter emitter response is shown in Fig. 6(b). From Figs. 6(a) and 6(b) it is observed that deviation from the design thicknesses is much more important than the deviation from the design compositions. Especially, the variation of the thickness of the resonant layer is most important. However, from the same figures [6(a) and 6(b)] it is shown that even though the designs that correspond to cases 2, 3a/3b, and 4 are nonoptimal, the filter/emitter characteristics remain basically unaffected. Shifts of the peak electron-current transmittance are observed, while the peak transmittance value and the corresponding FWHM remain approximately the same. Even if the filter/emitter response is shifted due to fabrication process variations, it is possible to shift the response back to its designed position by

changing the applied voltage.

Finally, an additional consideration in the design of electron-wave interference filter/emitters is the restriction that the design electron energy be sufficiently below the L-valley potential energy to minimize phonon scattering. Selecting $\Delta E_1 = \mathrm{KE}_{in} = \Delta E_2 = 0.05$ eV and the input/output regions compositions 0.10 and 0.20 ($x_0 = 0.10$ or 0.20), two additional filter/emitters were designed. As is described by inequalities (14) and (16), there is a restriction in the maximum applied bias potential energy and the layer compositions. For $x_0 = 0.10$ and 0.20 the corresponding maximum values of the applied bias potential energy are 0.124 and 0.063 eV, respectively. If the layer compositions are less than x_0 ($x_j < x_0$ for $j = 1,2,\ldots,M$), then inequality (16) is also satisfied. Using $V_{bias} = 0.12$ and 0.06 eV as the design parameters for $x_0 = 0.10$ and 0.20, respectively, and $M = 9$ layers, two additional designs were developed that take into account this electron-energy constraint. The characteristics of these two designs are summarized in Table III. The spectral (energy) response of the corresponding two filter/emitters is shown in Figs. 7(a) (for $x_0 = 0.10$, $V_{bias} = 0.12$ and 0.07 eV) and 7(b) (for $x_0 = 0.20$, $V_{bias} = 0.06$ and 0.03 eV). From these figures it is again observed that the electron-current transmittance has a peak at the design KE_{out} and V_{bias} values and, in addition, has the same tunability properties that were described previously. However, the design that corresponds to $x_0 = 0.10$ does not have a particularly good rejection band (since the transmittance value is not very small). This is due to the reduced reflectivity at layer boundaries. The reduced reflectivity is a result of the small differences in the layer compositions, which in turn correspond to small differences in the electron-wave refractive indices. Especially at larger electron energies, the corresponding electron-wave refractive indices become nearly equal and this degrades the performance of the filter/emitter at energies above the pass energy. However, when $x_0 = 0.20$ there is a significant variation of the electron-wave refractive index, which results in an increased reflectivity between the filter/emitter layers. For this reason the response that corresponds to $x_0 = 0.20$ has much narrower energy passband and lower rejection band transmittance.

TABLE III. Design parameters of an electron-wave interference filter/emitter with the $(HL)^N HH(LH)^N$ $[N = (M-1)/2]$ configuration ($N = 2$, $M = 9$), taking into account the L-valley constraint. The surrounding input and output regions consist of $Ga_{1-x}Al_xAs$. For both designs, $\mathrm{KE}_{in} = 0.05$ eV.

Layer j	$V_{bias} = 0.12$ eV, $x_0 = 0.10$ p_j	x_j	$V_{bias} = 0.06$ eV, $x_0 = 0.20$ p_j	x_j
1	12	0.0194	10	0.0561
2	13	0.0677	12	0.1429
3	11	0.0278	9	0.0070
4	12	0.0831	12	0.1617
5	20	0.0307	18	0.0365
6	10	0.0602	11	0.1589
7	9	0.0077	9	0.0635
8	10	0.0965	11	0.1772
9	9	0.0489	9	0.0852

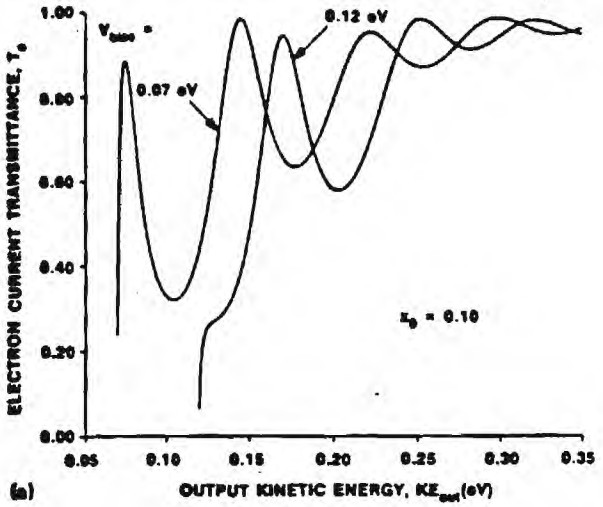

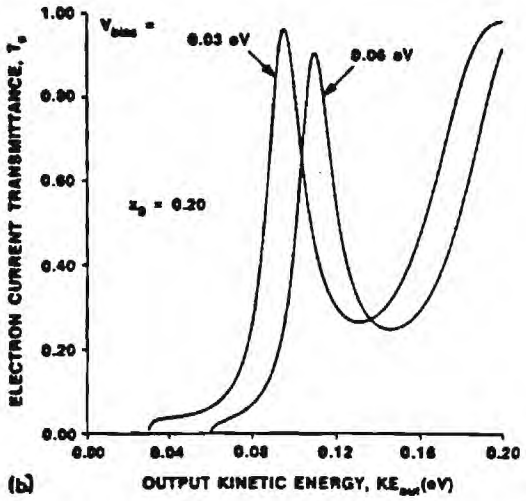

FIG. 7. Electron-current transmittance of a filter/emitter designed taking into account L-valley potential energy constraint for (a) design values $x_0 = 0.10$, $V_{bias} = 0.12$ eV, $\mathrm{KE}_{in} = 0.05$ eV, and $M = 9$, and (b) for design values $x_0 = 0.20$, $V_{bias} = 0.06$ eV, $\mathrm{KE}_{in} = 0.05$ eV, and $M = 9$.

VI. DISCUSSION AND SUMMARY

In all the electron-wave interference filter/emitters presented, the semiconductor materials had parabolic band structure. However, for sufficiently high electron energies, the band structure is more appropriately treated as nonparabolic. Futhermore, the band structure may vary with the direction of the electron-wave propagation. Both of these effects can be incorporated by using an energy-dependent anisotropic effective mass. In this case the solutions of Schrödinger's equation described in Sec. III B needs to be modified; however, the design procedure of the filter/emitter remains unchanged.

The response of the electron-wave Fabry–Perot filter/emitter has been shown to have a narrow passband around the design value of the output kinetic energy. However, additional passbands in kinetic energy exist beyond the rejection band. At large electron energies the corresponding electron-wave refractive indices of the filter/emitter layers become

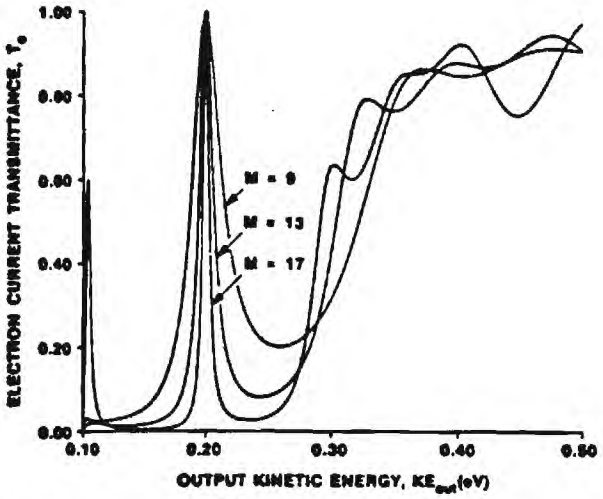

FIG. 8. Electron-current transmittance of a filter/emitter for $M = 9$, 13, and 17 as a function of the output electron kinetic energy. Design values are $V_{bias} = 0.10$ eV and $KE_m = 0.10$ eV.

nearly equal. This effect reduces the electron reflectivity at the layer boundaries and consequently degrades the filter/emitter performance. For example, the response characteristics of the filter/emitters, described in Table I, are shown in Fig. 8 for $V_{bias} = 0.10$ eV (design value) for $M = 9$, 13, and 17 layers, for output electron kinetic energies between 0.0 and 0.5 eV. It is observed that as the electron energy increases above 0.3 eV, the filter/emitter has an electron-current transmittance larger than 0.75, which reduces the width of the rejection band on the high-energy side of the peak value.

The design procedure described in Sec. III A may result in multiple designs differing by a few monolayers from the initial unbiased solution. In this case the best filter/emitter response is obtained by selecting the most symmetric solution for the electron-wave refractive indices.

In summary, a systematic procedure has been described for the design of biased semiconductor superlattices that can serve as narrow-band electron-energy filter/emitters. Various design constraints were identified and quantified. These filter/emitters are continously voltage tunable in electron energy. The FWHM of the filter/emitter decreases as the number of the filter layers increases. The characteristics of the filter/emitter are stable in the presence of variations in the layer compositions and thicknesses. These narrow-band filter/emitters can be incorporated monolithically into transistor structures in order to increase their speed. Other possible applications include electroluminescent devices, photodetectors, and in future guided electron-wave integrated circuits.

ACKNOWLEDGMENTS

This research was sponsored in part by a grant from the Joint Services Electronics Program under Contract No. DAAL-03-87-K-0059. One of us (K.F.B.) was supported in part by a Presidential Young Investigator award from the National Science Foundation and another (E.N.G.) by a Research Initiation award from the National Science Foundation.

[1]M. Heiblum, M. V. Fischetti, W. P. Dumke, D. J. Frank, I. M. Anderson, and C. M. Knoedler, Phys. Rev. Lett. 58, 816 (1987).
[2]S. Sen, F. Capasso, A. C. Gossard, and R. A. Spah, Appl. Phys. Lett. 51, 1428 (1987).
[3]R. C. Potter and A. A. Lakhani, Appl. Phys. Lett. 52, 1349 (1988).
[4]J. R. Hayes, P. England, and J. P. Harbison, Appl. Phys. Lett. 52, 1578 (1988).
[5]L. Esaki and R. Tsu, IBM J. Res. Dev. 13, 61 (1970).
[6]T. K. Gaylord and K. F. Brennan, J. Appl. Phys. 65, 814 (1989).
[7]T. K. Gaylord and K. F. Brennan, Appl. Phys. Lett. 53, 2047 (1988).
[8]T. K. Gaylord, E. N. Glytsis, and K. F. Brennan, J. Appl. Phys. 65, 2535(1989).
[9]E. N. Glytsis, T. K. Gaylord, and K. F. Brennan, J. Appl. Phys. 66, 1494 (1989).
[10]M. Heiblum, M. I. Nathan, D. C. Thomas, and C. M. Knoedler, Phys. Rev. Lett. 55, 2200 (1985).
[11]T. K. Gaylord, E. N. Glytsis, and K. F. Brennan, J. Appl. Phys. 66, 1842 (1989).
[12]T. K. Gaylord, E. N. Glytsis, and K. F. Brennan, J. Appl. Phys. 66, 1483 (1989).
[13]G. Nimtz and P. Marquardt, Appl. Phys. A 47, 317 (1988).
[14]A. Szafer and A. D. Stone, Phys. Rev. Lett. 62, 300 (1989).
[15]C. J. Summers and K. F. Brennan, Appl. Phys. Lett. 48, 806 (1986).
[16]K. F. Brennan and C. J. Summers, J. Appl. Phys. 61, 5410 (1987).
[17]K. F. Brennan and C. J. Summers, IEEE J. Quantum Electron. QE-23, 320 (1987).
[18]C. M. Wu and E. S. Yang, Solid-State Electron. 22, 241 (1979).
[19]A. N. Khondker, M. R. Khan, and A. F. M. Anwar, J. Appl. Phys. 63, 5191 (1988).
[20]O. S. Heavens, *Optical Properties of Thin Solid Films* (Butterworths, London, 1955).
[21]J. A. Dobrowolski, in *Handbook of Optics*, edited by W. G. Driscoll (McGraw-Hill, New York, 1978), Sec. 8.
[22]H. A. Macleod, *Thin-Film Optical Filters* (Macmillan, New York, 1986).
[23]E. J. Austin and M. Jaros, Phys. Rev. B 31, 5569 (1985).
[24]K. F. Brennan and C. J. Summers, J. Appl. Phys. 61, 614 (1987).
[25]C. J. Summers, K. F. Brennan, A. Torabi, and H. M. Harris, Appl. Phys. Lett. 52, 132 (1988).
[26]K. Imamura, S. Muto, N. Yokoyama, M. Sasa, H. Ohnishi, S. Hiyamizu, and H. Nishi, Surf. Sci. 174, 481 (1986).
[27]K. Seo, M. Heiblum, C. M. Knoedler, J. E. Oh, J. Pamulapati, and P. Bhattacharya, IEEE Electron. Device Lett. 2, 73 (1989).

Electron-wave quarter-wavelength quantum well impedance transformers between differing energy-gap semiconductors

T. K. Gaylord, E. N. Glytsis, and K. F. Brennan
School of Electrical Engineering and Microelectronics Research Center, Georgia Institute of Technology, Atlanta, Georgia 30332

(Received 21 July 1989; accepted for publication 13 November 1989)

Impedance transformers for ballistic (collisionless) electron waves traveling between dissimilar energy-gap semiconductors are designed as a series of quarter (electron) wavelength layers in the form of a compositional superlattice. The quantitative analogies that have been previously established [J. Appl. Phys. 65, 814 (1989)] between electron-wave propagation in semiconductors and electromagnetic-wave propagation in dielectrics are used. For the design energy, the electron wave would be totally transmitted and the structure is analogous to an antireflection coating in electromagnetic optics. Practical constraints on the impedance transformer layers are (1) their compositions must be within the usable compositional range and (2) their thicknesses must be integer multiples of a monolayer thickness. These constraints are included in the design process. Procedures for designing narrow-band, maximally flat (Butterworth), and equal-ripple (Chebyshev) impedance transformers of arbitrary spectral bandwidth are presented. Example practical single-layer and three-layer transformers for connecting GaAs and $Ga_{0.8}Al_{0.2}As$ are presented.

I. BACKGROUND

Molecular-beam epitaxy (MBE) and metalorganic chemical vapor deposition (MOCVD) have been developed and refined to the point where single monolayers can be grown with precise compositional control.[1] These technologies have allowed important multiple quantum well devices composed of wide and narrow band-gap semiconductors such as GaAs and $Ga_{1-x}Al_xAs$ to be produced. With further improvements in the quality of the materials grown, ballistic transport has been observed.[2,3] That is, electrons travel through the device without being scattered by deviations from crystalline perfection. Even with the addition of elastic scattering, the electrons exhibit clear quantum mechanical plane-wave behavior.[4,5] Since these coherent waves maintain their phase throughout the device, they can be refracted, reflected, interfered, guided, and diffracted in a manner quantitatively analogous to electromagnetic waves.[6] Quantum interference effects have been experimentally observed for electron energies below the potential energy barriers in resonant tunneling structures[7-10] and for electron energies above the barriers in negative differential resistance[11,12] and potential barrier[13] devices.

In the construction of semiconductor quantum devices and guided electron-wave integrated circuits[14] it will be necessary to connect semiconductor materials with differing electron energy-band structures. This occurs, for example, in the electron flow from the GaAs base of a bipolar junction transistor to the $Ga_{1-x}Al_xAs$ collector where $Ga_{1-x}Al_xAs$ is used to increase the breakdown voltage in the high electric field collector. In such a configuration, detrimental reflections will occur at the energy-band discontinuity between materials. However, for a given electron energy or a given band of electron energies, these reflections can be completely eliminated and total transmission achieved by fabricating an impedance transformer between the two materials. The type of impedance transformer directly amenable to semiconductor technology consists of a series of layers that are each a quarter of an electron wavelength thick. Transformers of arbitrary bandwidth can be designed using the quantitative analogies between electron-wave propagation in semiconductors and electromagnetic waves in dielectrics[6] and the theory of impedance transformers as developed for microwave transmission lines and waveguides.[15] In addition, practical constraints require that the impedance transformer layers have (1) compositions that are within the usable compositional range and (2) thicknesses that are an integer multiple of a monolayer thickness. The purpose of this paper is to present systematic design procedures for narrow-band, maximally flat (Butterworth), and equal-ripple (Chebyshev) impedance transformers subject to the above constraints and then apply these procedures to example impedance transformers between GaAs and $Ga_{0.8}Al_{0.2}As$.

II. SEMICONDUCTOR ELECTRON-WAVE OPTICS

The transmission and reflection characteristics of quantum mechanical electron waves in semiconductors have been analyzed for single potential energy boundaries,[16] for normal incidence,[17] and for the general case of any number of boundaries and any angle of incidence.[6] From these results, a mapping has been established between electromagnetic and quantum mechanical quantities.[6] As a consequence, existing electromagnetic optical device designs now have electron-wave device counterparts.

Electron-wave phase effects such as the phase thicknesses of the impedance transformer layers are described by the electron wave-vector magnitude which is

$$k = [2m^*(E - V)]^{1/2}/\hbar, \tag{1}$$

where m^* is the electron effective mass, E is the total electron energy, V is the electron potential energy, and $\hbar$ is Planck's constant divided by 2π. Thus, the electron-wave phase refractive index n_p is proportional to the square root of the

 0021-8979/90/052623-08$03.00

product of the effective mass and the kinetic energy.[6] That is,

$$n_p \propto [m^*(E-V)]^{1/2}. \quad (2)$$

Amplitude effects such as transmissivity and reflectivity may be described in terms of the wave-function amplitude for an electron wave or in terms of the electric field amplitude for a transverse electric (TE) electromagnetic optical wave incident upon a boundary between dielectrics. Continuity of the wave function across a potential energy boundary is analogous to the continuity of the tangential component of the electric field across a boundary between dielectrics. Similarly, conservation of electron probability current normal to a potential energy boundary is analogous to conservation of power flow normal to a boundary between dielectrics. Using these, the electron-wave and electromagnetic-wave reflectivities and transmissivities are made equivalent by introducing, in quantum mechanics, an analogous index of refraction or characteristic impedance.[6,17] Thus, the electron-wave amplitude refractive index n_a is proportional to the square root of the ratio of the kinetic energy to the effective mass,[6] and so

$$n_a \propto [(E-V)/m^*]^{1/2}. \quad (3)$$

The amplitude transmissivity t of an electron wave normally incident upon a boundary between semiconductors 1 and 2 is given by[6]

$$t = 2n_{a1}/(n_{a1}+n_{a2}). \quad (4)$$

The amplitude reflectivity r is similarly given by[6]

$$r = (n_{a1}-n_{a2})/(n_{a1}+n_{a2}). \quad (5)$$

The electron current density in quantum mechanics is analogous to Poynting vector power in electromagnetics. Thus, the electron current transmitted T is given by[6]

$$T = (n_{a2}/n_{a1})^2 t^2 \quad (6)$$

and the electron current reflected R is given by[6]

$$R = r^2. \quad (7)$$

In the above expressions, only dimensionless ratios of the electron-wave amplitude refractive indices occur. Both types of electron-wave refractive indices exhibit normal dispersion. That is, they increase with decreasing wavelength.

III. IMPEDANCE TRANSFORMERS

A. General

In microwave engineering, impedance transformation between transmission lines and waveguiding systems of differing characteristic impedance can be achieved with a variety of devices[15] including quarter-wave transformers, double-stub tuners, triple-stub tuners, slot lines, and E-plane–H-plane tuners. Quarter-wave transformers may also be used for unguided electromagnetic plane waves and unguided electron plane waves. In electromagnetic optics they are simply thin-film antireflection coatings. Each layer is a dielectric with a thickness of quarter of a wavelength (as measured in that material) at the pass frequency. In electron-wave optics in semiconductors, quarter-wave transformers are merely layers of semiconductor material with thicknesses that are a quarter of an electron wavelength (as measured in that material) at the pass energy. Such a semiconductor superlattice impedance transformer is depicted in Fig. 1 in terms of its conduction-band edge (labeled Γ for the case of the conduction-band minimum occurring at the center of the Brillouin zone). If impedance matching is required only over a narrow band of energies, then a single section (layer) impedance transformer may be used. In this situation the transformer acts as a narrow-band filter. If impedance matching is required over a broad range of energies, then multiple layers will be needed. The energy range covered increases with increasing number of layers.

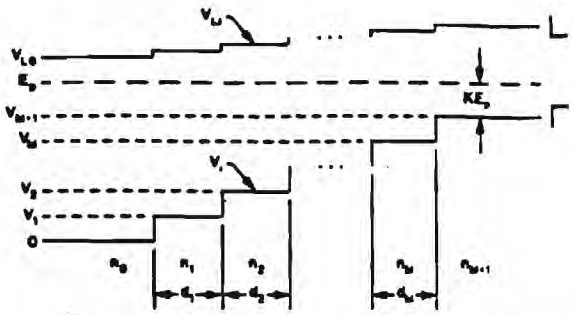

FIG. 1. Electron-wave quarter-wavelength impedance transformer shown by the spatial variation in the electron potential energy of the Γ [000] and L [111] conduction-band edges for a material system such as $Ga_{1-x}Al_xAs$. The M layers of the impedance transformer are labeled with the electron-wave amplitude refractive indices for those layers. The incident (0) and transmitted ($M+1$) regions are similarly labeled.

The impedance transformer of Fig. 1 is a general quarter-wave device consisting of M layers. The wave-function reflectivity of an electron wave in region 0 incident upon a boundary with a semi-infinite region 1 is designated r_0. Similarly the reflectivity of an electron wave in region i incident upon a boundary with a semi-infinite region $i+1$ is designated r_i. The physical thickness of the ith layer is denoted d_i. In practical impedance transformers, the reflectivities r_i are relatively small. In this situation, the total electron amplitude reflection coefficient r for the entire impedance transformer is given by the sum of the first-order reflected waves.[15] Thus

$$r = r_0 + r_1 \exp(-2jk_1d_1) + r_2 \exp(-4jk_2d_2) + \cdots + r_i \exp(-j2ik_id_i) + \cdots. \quad (8)$$

Since all sections (layers) have the same electron optical thicknesses, then $k_1d_1 = k_2d_2 = \cdots = k_Md_M = \theta$. For quarter-wavelength transformers, this means $\theta = \pi/2$ at the pass energy. Furthermore, for a symmetrical transformer $r_0 = r_M, r_1 = r_{M-1}$, etc. For this common case, Eq. (8) may be rewritten as

$$r = 2\exp(-jM\theta)\{r_0\cos(M\theta) + r_1\cos[(M-2)\theta] + \cdots + r_i\cos(M-2i)\theta + \cdots\}. \quad (9)$$

By appropriate selection of the reflectivities $r_0, r_1, \ldots, r_M$, a wide variety of passband characteristics can be obtained.

B. Maximally flat transformers

A maximally flat passband is characterized by the first $M-1$ derivatives of the total electron amplitude transmission coefficient t with respect to the electron energy being

zero at the pass energy. Maximally flat transformers are also called Butterworth or binomial transformers. The maximally flat characteristic is obtained when

$$r = 2^{-M}\frac{n_{a0}-n_{aM+1}}{n_{a0}+n_{aM+1}}\sum_{i=0}^{M} C_i^M \exp(-j2i\theta), \quad (10)$$

where C_i^M are the binomial coefficients given by

$$C_i^M = M!/[i!(M-i)!]. \quad (11)$$

Comparing Eq. (10) with Eq. (8) yields

$$r_i = 2^{-M}[(n_{a0}-n_{aM+1})/(n_{a0}+n_{aM+1})]C_i^M. \quad (12)$$

Since the reflectivities $r_i = (n_{ai}-n_{ai+1})/(n_{ai}+n_{ai+1})$ are small, then $\ln(n_{ai}/n_{ai+1}) \simeq 2r_i$. Thus

$$\ln(n_{ai}/n_{ai+1}) = 2^{-M}C_i^M \ln(n_{a0}/n_{aM+1}), \quad (13)$$

providing a relationship between the refractive indices of the various layers.

C. Equal-ripple transformer

In an equal-ripple impedance transformer, the electron amplitude reflectivity varies in an oscillatory fashion between 0 and r_m, where r_m is a specified maximum reflectivity in the passband. This is obtained when the reflection coefficient is given by

$$r = r_m \exp(-jM\theta)T_M(\sec\theta_m \cos\theta), \quad (14)$$

where $T_M(x)$ are Chebyshev polynomials and are given by $T_1(x) = x$, $T_2(x) = 2x^2 - 1$, $T_3(x) = 4x^3 - 3x$, $T_4(x) = 8x^4 - 8x^2 + 1$,..., $T_i(x) = 2xT_{i-1}(x) - T_{i-2}(x)$. The quantity θ_m is the normalized half-bandwidth parameter given by $\theta_m = (\pi/2)(E_m/E_p)$, where E_m is the lowest electron energy at which the reflectivity equals r_m and E_p is the pass energy (see Fig. 1). For a specified value of the maximum reflectivity r_m, the quantity θ_m may be determined by solving the polynomial equation[15]

$$T_M(\sec\theta_m) = (1/r_m)(n_{a0}-n_{aM+1})/(n_{a0}+n_{aM+1}). \quad (15)$$

The electron amplitude refractive indices may then be determined by equating Eqs. (9) and (14). This gives a series of equations by then equating like terms in $\cos(i\theta)$. Each of these equations gives one of the reflectivities $r_0, r_1,...$ and thus allows the amplitude refractive indices to be calculated as illustrated in Sec. IV.

IV. OPTIMUM SEMICONDUCTOR IMPEDANCE TRANSFORMERS

A. Configuration of semiconductors

The interconnection of GaAs and $Ga_{0.8}Al_{0.2}As$ with several types of impedance transformers will be treated for illustration. This might correspond to electron flow from the base (GaAs) to the collector ($Ga_{0.8}Al_{0.2}As$) in a bipolar junction transistor as mentioned previously. The $Ga_{1-x}Al_xAs$ material system is perhaps the most advanced of current semiconductor superlattice material systems. For these alloys, all compositions are lattice matched. The material is a direct gap semiconductor for $0<x<0.45$ with the conduction-band minimum occurring at the center of the Brillouin zone (Γ point). The electron potential energy of the conduction band V_i is given by

$$V_i = Ax_i, \quad i = 0,1,...,M+1, \quad (16)$$

and the electron mass is given by

$$m_i^* = (B + Cx_i)m_0, \quad i = 0,1,...,M+1, \quad (17)$$

where A, B, and C are constants and m_0 is the free-electron mass. For $Ga_{1-x}Al_xAs$, $A = 773.14$ meV (using a 62% conduction-band offset), $B = 0.067$, and $C = 0.083$.[18,19] In Fig. 1, region 0 would be GaAs and region $M+1$ would be $Ga_{0.8}Al_{0.2}As$. As also shown in Fig. 1, the conduction-band potential energy edge increases monotonically from GaAs to $Ga_{0.8}Al_{0.2}As$ through the transformer.

The next higher conduction-band minimum in $Ga_{1-x}Al_xAs$ for this range of compositions occurs along the [111] directions at the edge of the Brillouin zone (L point). The electron potential energy at the bottom of the L band, V_{Li}, is given by

$$V_{Li} = D + Fx_i, \quad i = 0,1,...,M+1, \quad (18)$$

relative to the Γ conduction-band edge for GaAs ($x = 0$). The quantities D and F are constants given by $D = 284$ meV and $F = 168.14$ meV for $Ga_{1-x}Al_xAs$.[18,19] The corresponding curve appears in Fig. 1 and is labeled L. To support ballistic transport by ensuring that intervalley scattering does not occur through phonon absorption, the pass electron energy will be arbitrarily set to be 50 meV below the L band of GaAs. The pass electron energy is thus $E_p = 234$ meV. As the aluminum concentration increases through the transformer, the energy separation $V_{Li} - E_p$ further increases until it is 83.6 meV in the $Ga_{0.8}Al_{0.2}As$ as depicted in Fig. 1.

Since the reference for the electron amplitude refractive index is arbitrary, it will be taken to be unity in the $Ga_{0.8}Al_{0.2}As$ since this is the low index side of the impedance transformer. That is $n_{aM+1} = 1$. The amplitude index of any other region is then given by

$$n_{ai} = [(E_p - V_i)m_{M+1}^*/(E_p - V_{M+1})m_i^*]^{1/2}n_{aM+1}. \quad (19)$$

Therefore in the $i = 0$ GaAs region, the amplitude index is $n_{a0} = 1.917\,962$.

The electron wavelength in any of the regions determines the electron optical phase thickness of that region. The electron wavelength for the pass energy in the ith region is given by

$$\lambda_{pi} = h/[2m_i^*(E_p - V_i)]^{1/2}, \quad (20)$$

where λ_{pi} is the pass wavelength as measured in the ith region and h is Planck's constant.

B. Optimum single-layer transformer

For the single-layer narrow-band impedance transformer, maximally flat and equal-ripple design procedures both

give the same result. It is the well-known single-layer antireflection coating result that the amplitude index should be

$$n_{a1} = (n_{a0} n_{aM+1})^{1/2}. \tag{21}$$

Thus, for the present case $n_{a1} = 1.384\,905$. The composition of this layer may be determined by substituting Eqs. (16) and (17) into Eq. (19) and solving for x_i. The result is

$$x_i = (E_p - BGm_0)/(A + CGm_0), \tag{22}$$

where $G \equiv [(E_p - V_{M+1})/m^*_{M+1}](n_{ai}/n_{aM+1})^2$. With the composition known, the potential energy V_i and the effective mass m_i^* are determined through Eqs. (16) and (17), respectively. The required physical thickness is then

$$d_i = \lambda_{pi}/4 = h/[32m_i^*(E_p - V_i)]^{1/2}, \tag{23}$$

to produce a quarter-wavelength thickness. For the present case, Eqs. (22), (16), (17), and (23) yield $x_1 = 0.121\,2$, $V_1 = 93.682$ meV, $m_1^* = 0.077\,06 m_0$, and $d_1 = 2.9482$ nm, respectively. The resulting overall electron current transmittance T for this optimum single-layer impedance transformer is shown in Fig. 2. The transmittance was calculated by the procedure described in Ref. 6. At the pass kinetic energy $KE_p = 79.372$ meV, the electron current transmittance is unity as it should be.

C. Optimum three-layer maximally flat transformer

The design of a three-layer maximally flat impedance transformer to connect GaAs and $Ga_{0.8}Al_{0.2}As$ for a broader range of electron energies near the passband is presented in this section. For a three-layer device, $M = 3$. For $M = 3$ and $i = 0$, Eq. (13) becomes $\ln(n_{a0}/n_{a1}) = \frac{1}{3}\ln(n_{a0}/n_{aM+1})$ and so

$$n_{a1} = n_{a0}^{7/8} n_{aM+1}^{1/8}. \tag{24}$$

For the present case $n_{a0} = 1.917\,962$ and $n_{aM+1} = 1$ and so $n_{a1} = 1.768\,011$. The required composition is obtained from Eq. (22) and is $x_1 = 0.0345$. Likewise the needed physical thickness is found from Eq. (23) and is $d_1 = 2.5472$ nm. For $M = 3$ and $i = 1$, Eq. (13) gives $n_{a2} = n_{a0}^{-3/8} n_{a1} n_{aM+1}^{3/8}$. Using Eq. (24) this may be rewritten as

$$n_{a2} = n_{a0}^{1/2} n_{aM+1}^{1/2}. \tag{25}$$

Thus the center section of a maximally flat transformer is the same as that for the single-layer transformer [see Eq. (21)]. Therefore $n_{a2} = 1.384\,905$, $x_2 = 0.1212$, and $d_2 = 2.9482$ nm. For $M = 3$ and $i = 2$, Eq. (13) gives $n_{a3} = n_{a0}^{-3/8} n_{a2} n_{aM+1}^{3/8}$. Using Eq. (25) this may be written as

$$n_{a3} = n_{a0}^{1/8} n_{aM+1}^{7/8}. \tag{26}$$

For the present case, $n_{a3} = 1.084\,813$. The required composition and physical thickness are $x_3 = 0.1838$ and $d_3 = 3.5259$ nm. A summary of the parameters of this impedance transformer is given in Table I. The overall electron current transmittance T for this optimum three-layer maximally flat impedance transformer is shown in Fig. 3. Again at the pass kinetic energy $KE_p = 79.372$ eV, the electron current transmittance T is unity. The passband, however, is much broader than that for the one-layer transformer (Fig. 2). The maximally flat character of the passband is also evident in the transmittance shown in Fig. 3.

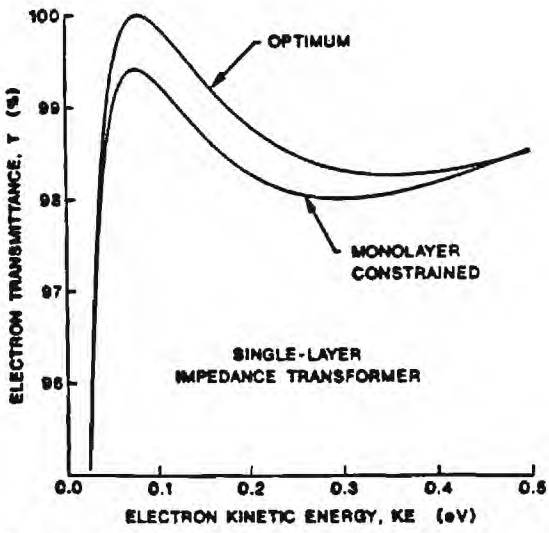

FIG. 2. The electron current transmittance as a function of electron kinetic energy as measured in the transmitted $(M + 1)$ region for a single-layer quarter-wavelength impedance transformer between GaAs and $Ga_{0.8}Al_{0.2}As$ of (a) optimum design (Sec. IV B) and of (b) monolayer-thickness-constrained design (Sec. V B).

TABLE I. Design parameters of optimum three-layer maximally flat and three-layer equal-ripple electron impedance transformers for connecting GaAs to $Ga_{0.8}Al_{0.2}As$. The design pass energy is $E_p = 234$ meV and the design output kinetic energy is $KE_p = 79.372$ meV.

Layer i	Amplitude refractive index n_{ai}	Aluminum composition x_i	Thickness d_i (nm)	Number of monolayers p_i
Maximally flat				
0	1.9180	0.0000	...	...
1	1.7680	0.0345	2.5472	9.0113
2	1.3849	0.1212	2.9482	10.4300
3	1.0848	0.1838	3.5259	12.4739
4	1.0000	0.2000	...	...
Equal ripple				
0	1.9180	0.0000	...	...
1	1.5738	0.0789	2.7180	9.6155
2	1.3992	0.1180	2.9280	10.3585
3	1.2440	0.1515	3.1786	11.2449
4	1.0000	0.2000	...	...

D. Optimum three-layer equal-ripple transformer

The design of a three-layer equal-ripple impedance transformer to connect GaAs and $Ga_{0.8}Al_{0.2}As$ is presented in this section. For a maximum electron current reflectivity within the passband of 2%, the amplitude reflectivity is $r_m = (0.02)^{1/2} = 0.141\,42$. For a three-section device $M = 3$. Using the polynomial representation for $T_3(x)$, Eq. (15) may be written as

$$4x^3 - 3x = (1/r_m)(n_{a0} - n_{aM+1})/(n_{a0} + n_{aM+1}) = 2.224\,488, \tag{27}$$

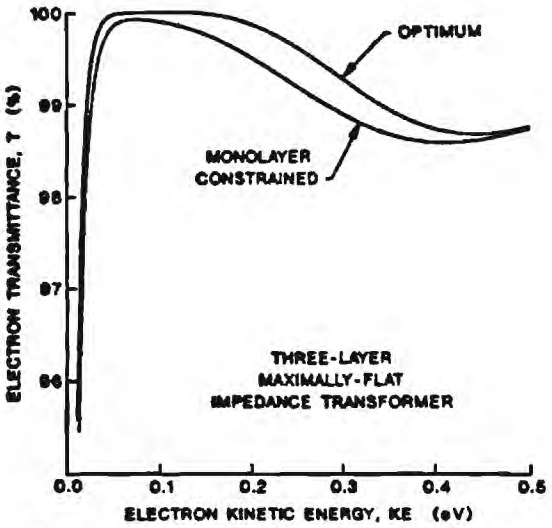

FIG. 3. The electron current transmittance as a function of electron kinetic energy as measured in the transmitted $(M+1)$ region for a three-layer maximally flat quarter-wavelength impedance transformer between GaAs and $Ga_{0.8}Al_{0.2}As$ of (a) optimum design (Sec. IV C and Table I) and of (b) monolayer-thickness-constrained design (Sec. V C and Table II).

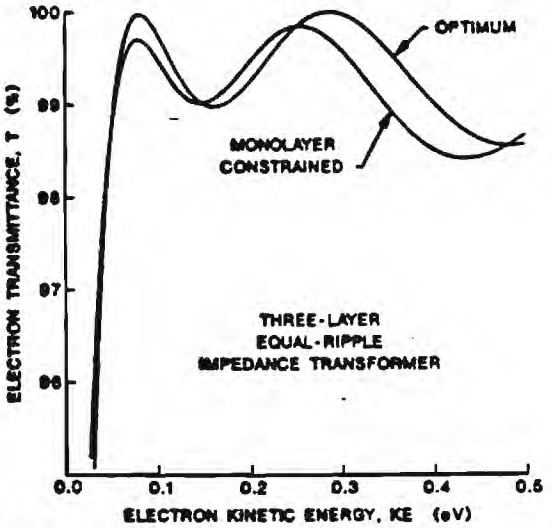

FIG. 4. The electron current transmittance as a function of electron kinetic energy as measured in the transmitted $(M+1)$ region for a three-layer equal-ripple quarter-wavelength impedance transformer between GaAs and $Ga_{0.8}Al_{0.2}As$ of (a) optimum design (Sec. IV D and Table I) and of (b) monolayer-thickness-constrained design (Sec. V D and Table II).

for a transformer between GaAs and $Ga_{0.8}Al_{0.2}As$, where $x \equiv \sec\theta_m$. Solving this cubic equation gives $x = 1.117\,068$ and $x = -0.558\,534 \pm j0.431\,139$. Only the real solution is meaningful in this design procedure. Equating Eqs. (9) and (14) for the case of $M = 3$ gives

$$2(r_0 \cos 3\theta + r_1 \cos\theta) = r_m[\sec^3\theta_m(\cos 3\theta + 3\cos\theta) - 3\sec\theta_m \cos\theta]. \quad (28)$$

Equating like terms in $\cos 3\theta$ produces $2r_0 = r_m \sec^3\theta_m$. Solving this gives $r_0 = 0.098\,565$. Equating like terms in $\cos\theta$ similarly produces $2r_1 = 3r_m(\sec^3\theta_m - \sec\theta_m)$ and solving this yields $r_1 = 0.058\,730$. From Eq. (5), the amplitude refractive index in region $i+1$ is

$$n_{ai+1} = [(1-r_i)/(1+r_i)]n_{ai}. \quad (29)$$

For the present configuration of materials, $n_{a0} = 1.917\,962$ and so for $i = 0$ Eq. (29) becomes $n_{a1} = [(1-r_0)/(1+r_0)]n_{a0} = 1.573\,796$. The required composition is obtained from Eq. (22) and is $x_1 = 0.0789$. The needed physical thickness is found from Eq. (23) and is $d_1 = 2.717\,966$ nm. For $i = 1$, Eq. (29) gives

$$n_{a2} = [(1-r_1)/(1+r_1)]n_{a1} = 1.399\,193.$$

The corresponding composition is $x_2 = 0.1180$ and the corresponding thickness is $d_2 = 2.9280$. Since the transformer is symmetrical, then $r_2 = r_1$ and thus the third layer has

$$n_{a3} = [(1-r_2)/(1+r_2)]n_{a2} = 1.243\,961.$$

The corresponding composition and thickness are $x_3 = 0.1515$ and $d_3 = 3.1786$ nm. A summary of the parameters of this impedance transformer is also given in Table I. The resulting electron current transmittance for this optimum Chebyshev impedance transformer is shown in Fig. 4. The equal-ripple character of the passband is evident. The passband of a multiple-section equal-ripple transformer is broader than that of the corresponding multiple-section maximally flat transformer. Furthermore, both multiple-layer transformers have much broader bandwidths than that of the narrow-band one-layer transformer (Fig. 2). Upon detailed inspection, the center layer in the Chebyshev transformer should have been $n_{a2} = (n_{a0}n_{aM+1})^{1/2}$. That is, it should have been 1.3849 rather than 1.3992 as calculated. This is due to minor approximations that are commonly made in the design of equal-ripple transformers. An exact, but more complicated, procedure is available[15] but the additional effort required to implement it produces only a negligible change in the resultant design.

V. MONOLAYER-CONSTRAINED SEMICONDUCTOR IMPEDANCE TRANSFORMER

A. Monolayer thickness constraint

The thicknesses of the layers in the optimum impedance transformers as designed in Sec. IV can have any of a continuum of values. In reality the thicknesses of all layers must be integer multiples of the monolayer thickness for that region. For lattice-matched $Ga_{1-x}Al_xAs$ the monolayer thickness s is the same for any composition x. For this material system $s = 0.282\,665$ nm.

To construct a quarter-wavelength impedance transformer, the thicknesses of the layers must also be an odd multiple of a quarter wavelength as measured in that layer for the pass energy E_p. That is

$$d_i = p_i s = (2q_i - 1)\lambda_{pi}/4, \quad i = 1,2,..., \quad (30)$$

where p_i is the integer number of monolayers for the ith region and q_i is a positive integer ($q_i = 1,2,3,...$). Substituting Eqs. (16) and (17) into Eq. (20) and then substituting the resulting λ_{pi} into Eq. (30) gives the following quadratic

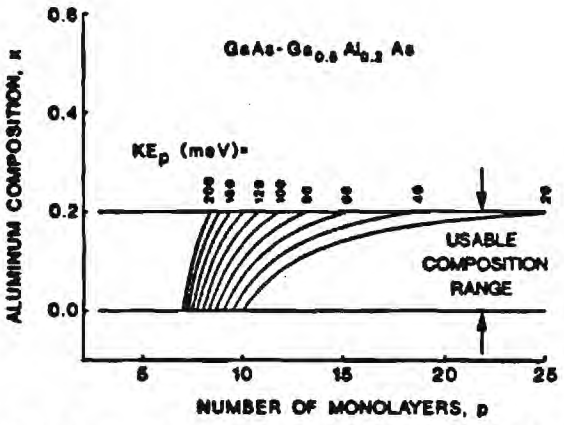

FIG. 5. Aluminum composition x $Ga_{1-x}Al_xAs$ that is needed to construct an impedance transformer for a transition from GaAs to $Ga_{0.8}Al_{0.2}As$. The pass kinetic energy KE_p in the $Ga_{0.8}Al_{0.2}As$ $(M+1)$ region is given as a parameter. Only integer values of the monolayer index correspond to realizable quarter-wavelength structures.

equation in the composition x_i

$$ACx_i^2 + (AB - CE_p)x_i + (h^2/32m_0) \times [(2q_i - 1)^2/p_i^2s^2] - BE_p = 0. \quad (31)$$

The solution for the composition x_i is

$$x_i = [-b \pm (b^2 - 4ac_i)^{1/2}]/2a, \quad (32)$$

where $a = AC$, $b = AB - CE_p$, and

$$c_i = (h^2/32m_0)[(2q_i - 1)^2/p_i^2s^2] - BE_p.$$

In order to design an impedance transformer, solutions x_i must be found in the usable composition range that correspond closely to the optimum values calculated by the procedures given in Sec. IV. To minimize the total thickness of the filter, q_i is initially set equal to unity. Then Eq. (32) is repetitively evaluated for $p_i = 1,2,3,...$ until all of the positive real roots in the range $0<x_i<x_{max}$ are found. Plots of aluminum composition x as a function of the number of monolayers

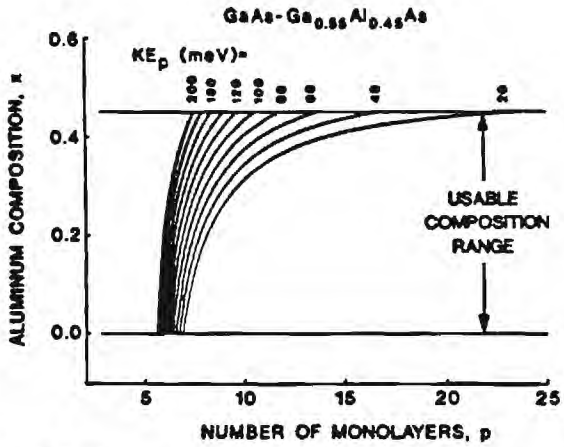

FIG. 6. Aluminum composition x in $Ga_{1-x}Al_xAs$ that is needed to construct an impedance transformer for a transition from GaAs to $Ga_{0.55}Al_{0.45}As$. The pass kinetic energy KE_p in the $Ga_{0.55}Al_{0.45}As$ $(M+1)$ region is given as a parameter. Only integer values of the monolayer index correspond to realizable quarter-wavelength structures.

thickness are shown for a transition from GaAs to $Ga_{0.8}Al_{0.2}As$ in Fig. 5 and for a transition from GaAs to $Ga_{0.55}Al_{0.45}As$ in Fig. 6. In each figure, multiple curves are shown for various values of the pass kinetic energy KE_p $(KE_p = E_p - V_{M+1})$. For large values of KE_p there are only a few values of composition that correspond to thicknesses that are integer multiples of the monolayers. For smaller values of KE_p there are a greater number of thicknesses available that simultaneously satisfy the quarter-wavelength and monolayer constraints.

B. Monolayer-constrained single-layer transformer

The monolayer thickness constraint is now applied to the design impedance transformers for a transition from GaAs to $Ga_{0.8}Al_{0.2}As$. Using $E_p = 234$ meV, setting $q_i = 1$, and repetitively evaluating Eq. (32) for integer values of p_i yields within the range $0<x_i<x_{max}$ the following aluminum concentrations: $x_i = 0.0335$ for $p_i = 9$, $x_i = 0.1008$ for $p_i = 10$, $x_i = 0.1433$ for $p_i = 11$, $x_i = 0.1728$ for $p_i = 12$, and $x_i = 0.1944$ for $p_i = 13$.

For a monolayer thickness constrained single-layer narrow-band impedance transformer, the middle value of aluminum composition may be used to approximate the optimum single-layer transformer. Therefore $x_1 = 0.1433$. With the composition x_i and number of monolayers p_i known, the potential energy V_i, effective mass m_i^*, the amplitude refractive index n_{ai}, the thickness of the layer d_i, and wavelength in the layer λ_i can be determined from Eqs. (16), (17), (19), (30), and (23), respectively. For the present monolayer-thickness-constrained $(p_1 = 11)$ single-layer impedance transformer, these quantities are $V_1 = 110.78$ meV, $m_1^* = 0.078\,89m_0$, $d_1 = 3.1093$ nm, $n_{a1} = 1.2826$, and $\lambda_1 = 12.437$ nm. The resulting overall electron current transmittance T for this monolayer thickness constrained impedance transformer is shown in Fig. 2 along with the transmittance for the optimum (without monolayer constraint) single-layer transformer. The passband characteristics have similar functional forms. However, at the pass kinetic energy $KE_p = 79.4$ meV, the electron current transmittance is reduced from the optimum 100% to 99.41%.

C. Monolayer-constrained three-layer maximally flat transformer

For an optimum three-layer maximally flat impedance transformer as described in Sec. IV C and summarized in Table I, the needed values of aluminum concentration are near the lower end, near the middle, and near the upper end of the range $0<x_i<x_{max}$. The optimum three-layer maximally flat impedance transformer may be approximated by selecting the aluminum compositions of $x_1 = 0.0335$ for $p_1 = 9$, $x_2 = 0.1433$ for $p_2 = 11$, and $x_3 = 0.1944$ for $p_3 = 13$. As before, a knowledge of the composition x_i and number of monolayers p_i allows the potential energy V_i, effective mass m_i^*, amplitude refractive index n_{ai}, thickness of the layer d_i, and wavelength in the layer λ_i to be calculated. For the present monolayer-thickness-constrained $(p_1 = 9$, $p_2 = 11$, $p_3 = 13)$ three-layer maximally flat impedance

TABLE II. Design parameters of monolayer-constrained three-layer maximally flat and three-layer equal-ripple electron impedance transformers for connecting GaAs to $Ga_{0.8}Al_{0.2}As$. The design pass energy is $E_p = 234$ meV and the design output kinetic energy is $KE_p = 79.372$ meV.

Layer i	Amplitude refractive index n_{ai}	Aluminum composition x_i	Thickness d_i (nm)	Number of monolayers p_i
Maximally flat				
0	1.9180	0.0000	...	...
1	1.7723	0.0335	2.5440	9
2	1.2826	0.1433	3.1093	11
3	1.0299	0.1944	3.6746	13
4	1.0000	0.2000	...	...
Equal ripple				
0	1.9180	0.0000	...	...
1	1.4769	0.1008	2.8267	10
2	1.2826	0.1433	3.1093	11
3	1.1403	0.1728	3.3920	12
4	1.0000	0.2000	...	...

transformer, these quantities are $V_1 = 25.90$ meV, $V_2 = 110.78$ meV, $V_3 = 150.28$ meV, $m_1^* = 0.069\,78m_0$, $m_2^* = 0.078\,89m_0$, $m_3^* = 0.083\,13m_0$, $n_{a1} = 1.7723$, $n_{a2} = 1.2826$, $n_{a3} = 1.0299$, $d_1 = 2.5440$ nm, $d_2 = 3.1093$ nm, $d_3 = 3.6746$ nm, and $\lambda_1 = 10.176$ nm, $\lambda_2 = 12.437$ nm, $\lambda_3 = 14.698$ nm. A summary of the primary design parameters is given in Table II. The resulting overall electron current transmittance T for this monolayer-thickness-constrained impedance transformer is shown in Fig. 3 along with the transmittance for the optimum (without monolayer constraint) three-layer maximally flat transformer. The passband characteristics have very similar flat-top forms. At the pass kinetic energy $KE_p = 79.4$ meV, the electron current transmittance is reduced from the optimum 100% to 99.93%.

D. Monolayer-constrained three-layer equal-ripple transformer

For an optimum three-layer equal-ripple impedance transformer as described in Sec. IV D and summarized in Table I, the needed values of aluminum concentration are closer to the middle of the range $0 < x_i < x_{max}$ than is the case for the maximally flat transformer. The optimum three-layer equal-ripple impedance transformer may be approximated by selecting the aluminum compositions of $x_1 = 0.1008$ for $p_1 = 10$, $x_2 = 0.1433$ for $p_2 = 11$, and $x_3 = 0.1728$ for $p_3 = 12$. As before, a knowledge of the composition x_i and number of monolayers p_i allows the potential energy V_i, effective mass m_i^*, amplitude refractive index n_{ai}, thickness of the layer d_i, and wavelength in the layer λ_i to be calculated. For the present monolayer-thickness-constrained ($p_1 = 10$, $p_2 = 11$, $p_3 = 12$) three-layer maximally flat impedance transformer, these quantities are $V_1 = 77.93$ meV, $V_2 = 110.78$ meV, $V_3 = 133.58$ meV, $m_1^* = 0.075\,37m_0$, $m_2^* = 0.078\,89m_0$, $m_3^* = 0.081\,34m_0$, $n_{a1} = 1.4769$, $n_{a2} = 1.2826$, $n_{a3} = 1.1403$, $d_1 = 2.8267$ nm $d_2 = 3.1093$ nm, $d_3 = 3.3920$ nm, and $\lambda_1 = 11.3068$ nm, $\lambda_2 = 12.437$ nm, $\lambda_3 = 13.5680$ nm. A summary of the primary design parameters is given in Table II. The resulting overall electron current transmittance T for this monolayer-thickness-constrained impedance transformer is shown in Fig. 3 along with the transmittance for the optimum (without monolayer constraint) three-layer equal-ripple transformer. The passband characteristics have very similar oscillating forms. At the pass kinetic energy $KE_p = 79.4$ meV, the electron current transmittance is reduced from the optimum 100% to 99.72%.

VI. SUMMARY AND DISCUSSION

The quantitative analogies that have been previously established[6] between electron-wave propagation in semiconductors and electromagnetic-wave propagation in dielectrics have been used to design impedance transformers for ballistic (collisionless) electron waves traveling between dissimilar energy-gap semiconductors. These devices have been designed as a series of quarter (electron) wavelength quantum well layers in the form of compositional superlattices. Procedures for designing maximally flat (Butterworth) and equal-ripple (Chebyshev) impedance transformers of arbitrary spectral bandwidth have been presented. An alternate method to design maximally flat and equal-ripple transformers is through the use of precalculated tables[20–22] of refractive indices *if* the tables contain the ratio of beginning and ending refractive indices that is needed.

Additional constraints on the impedance transformer quantum well layers in practice are that (1) their compositions must be within the usable compositional range and that (2) their thicknesses must be integer multiples of a monolayer thickness. These constraints have been incorporated into the design procedure producing designs that approximate the optimum designs. However, even with these additional constraints, it has been shown that the general characteristics of the optimum design can be retained. While the transmittances presented in Figs. 2–4 have been calculated for electrons moving perpendicular to the boundaries, these results accurately apply to electrons with angles of incidence beyond 10°. Thus the results presented are rather insensitive to the electron angle of incidence.

The electron potential energy shown in Fig. 1 is idealized and does not include the effects of space charge in these undoped layers. The space charge which is a function of the current, will alter the potential energy (as calculated by the Poisson equation). This new potential energy will, in turn, alter the wave function (as calculated by the Schrödinger equation). Thus, in general, a self-consistent solution of these equations is needed, particularly at high current levels.

The designs of practical single-layer and three-layer transformers for connecting GaAs and $Ga_{0.8}Al_{0.2}As$ have been presented. Although this well-developed, lattice-matched material system was used as an example, the procedures presented would also apply to other material systems. Dispersion effects in electromagnetic (e.g., microwave) impedance transformers are relatively small compared to the dispersion effects in semiconductor electron-wave devices. For the present case of impedance transformers this causes a decrease in the electron current transmittance at energies

below the pass energy and an increase in the transmittance at energies above the pass energy.

ACKNOWLEDGMENTS

This research was sponsored in part by a grant from the Joint Services Electronics Program under Contract No. DAAL-03-87-K-0059. One of us (K.F.B.) was supported in part by a Presidential Young Investigator award from the National Science Foundation and another (E.N.G.) by a Research Initiation award from the National Science Foundation.

[1] L. Esaki and R. Tsu, IBM J. Res. Dev. 13, 61 (1970).
[2] A. F. J. Levi, J. R. Hayes, P. M. Platzman, and W. Wiegmann, Phys. Rev. Lett. 55, 2071 (1985).
[3] M. Heiblum, M. I. Nathan, D. C. Thomas, and C. M. Knoedler, Phys. Rev. Lett. 55, 2200 (1985).
[4] S. Washburn and R. A. Webb, Adv. Phys. 35, 375 (1986).
[5] Y. Imry, in *Directions in Condensed Matter Physics*, edited by G. Grinstein and G. Mazenko (World Scientific, Singapore, 1986), pp. 101–163.
[6] T. K. Gaylord and K. F. Brennan, J. Appl. Phys. 65, 814 (1989).
[7] M. Heiblum, M. V. Fischetti, W. P. Dumke, D. J. Frank, I. M. Anderson, and C. M. Knoedler, Phys. Rev. Lett. 58, 816 (1987).
[8] S. Sen, F. Capasso, A. C. Gossard, and R. A. Spah, Appl. Phys. Lett. 51, 1428 (1987).
[9] R. C. Potter and A. A. Lakhani, Appl. Phys. Lett. 52, 1349 (1988).
[10] J. R. Hayes, P. England, and J. P. Harbison, Appl. Phys. Lett. 52, 1578 (1988).
[11] C. J. Summers and K. F. Brennan, Appl. Phys. Lett. 48, 806 (1986).
[12] K. F. Brennan and C. J. Summers, J. Appl. Phys. 61, 5410 (1987).
[13] K. F. Brennan and C. J. Summers, IEEE J. Quantum Electron. QE-23, 320 (1987).
[14] T. K. Gaylord, E. N. Glytsis, and K. F. Brennan, J. Appl. Phys. 65, 1842 (1989).
[15] R. E. Collin, *Foundations for Microwave Engineering* (McGraw-Hill, New York, 1966).
[16] C. M. Wu and E. S. Yang, Solid-State Electron. 22, 241 (1979).
[17] A. N. Khondker, M. R. Khan, and A. F. M. Anwar, J. Appl. Phys. 63, 5191 (1988).
[18] H. C. Casey and M. B. Panish, *Heterostructure Lasers Part A. Fundamental Principles* (Academic, New York, 1978), Chap. 4.
[19] R. C. Miller, D. A. Kleinman, and A. C. Gossard, Phys. Rev. B 29, 7085 (1984).
[20] L. Young, IRE Trans. Microwave Theory Tech. 7, 233 (1959).
[21] L. Young, IRE Trans. Microwave Theory Tech. 8, 243 (1960).
[22] L. Young, J. Opt. Soc. Am. 51, 967 (1961).

Current-Voltage Characteristics of Semiconductor Superlattice Electron-Wave Quantum-Interference Filter/Emitter Negative Differential Resistance Devices

Elias N. Glytsis, Thomas K. Gaylord, and Kevin F. Brennan
School of Electrical Engineering and Microelectronics Research Center
Georgia Institute of Technology, Atlanta, Georgia 30332–0250

Abstract

The transmission and current-voltage characteristics of semiconductor superlattice electron-wave quantum-interference filter/emitter negative differential resistance devices are analyzed with and without the self-consistency requirement. For the non-self-consistent calculation the single-band effective-mass time-independent Schroedinger equation is solved. For the self-consistent calculation, Schroedinger and Poisson equations are solved iteratively until a self-consistent electron potential energy and electron density are obtained. It is shown that suitably designed electron-wave quantum-interference filter/emitters can exhibit strong negative differential resistance in the current-voltage characteristics, similar to those of resonant tunneling diodes. For low to moderate (2-30 meV) Fermi energies in the conduction band of $Ga_{1-x}Al_xAs$ (doping concentration less or equal to $2 \times 10^{18} cm^{-3}$), and temperatures near 30 K (in the ballistic transport regime), it is shown that the space-charge effect is relatively small and results in a shift of the current-voltage and transmission characteristics toward higher bias voltages. In a fashion similar to that occuring in resonant tunneling diodes, the self-consistent field in electron-wave filter/emitter negative differential resistance devices effectively acts to screen the positive applied bias. Designs of $Ga_{1-x}Al_xAs$ devices are presented. Resonant devices with current peak-to-valley ratios of ~ 50 as well as nonresonant (not exhibiting negative differential resistance) devices are analyzed. The corresponding electron charge density distributions are also presented. Superlattice electron-wave filter/emitter negative differential resistance

devices can be used as high-speed switches and oscillators and as monoenergetic emitters in electroluminescent devices and photodetectors.

I. INTRODUCTION

Nanostructure devices like multiple quantum wells and superlattices have been rapidly developed due to recent advances of microfabrication technology, particularly metalorganic chemical vapor deposition (MOCVD) and molecular-beam epitaxy (MBE). These fabrication technologies have been refined to the point where single monolayers can be grown with precise compositional control.[1] At these spatial dimensions, quantization effects largely dominate device characteristics, making further reduction in their sizes undesirable in some applications, thereby limiting the ultimate speed of the devices. However, quantum interference effects may also potentially be used in an advantageous way in novel devices. Quantum-mechanical interference effects have been experimentally observed for electron energies below the potential energy barriers in double-barrier and multi-barrier resonant tunneling devices[2-6] and for electron energies above the barriers in single- and double-barrier structures.[7-9] With further improvements in the quality of the materials grown, ballistic transport has also been experimentally observed.[10,11] That is, electrons travel through the device without being scattered by deviations from crystalline perfection. Even with the addition of elastic scattering, the electrons exhibit clear quantum-mechanical plane-wave behavior.[12,13] These coherent waves maintain their phase throughout the device and thus can interfere, reflect, refract, and diffract in a manner analogous to the electromagnetic plane waves in dielectric media. Impressive experimental evidence of optical-like electron behavior in GaAs semiconductors has recently been reported.[14,15]

Quantitative analogies between quantum-mechanical electron waves in semiconductor materials and electromagnetic optical waves in dielectrics have already been developed.[16] With these analogies, existing electromagnetic optical analysis and design techniques can be used for the analysis and design of novel semiconductor quantum-

wave devices. Possible devices include narrow-band superlattice interference filters[17,18] and filter/emitters[19,20] which can exhibit very narrow electron kinetic energy passbands and can be integrated into solid-state devices for potential use as monoenergetic emitters for electroluminescent devices,[21,22] photodetectors,[21,23] and subpicosecond ballistic transistors.[11,21] Beyond improving the speed of existing devices, however, the totally new concept of *guided electron-wave integrated circuits* has been proposed.[24,25] This potentially next generation of integrated circuits could be comprised by many semiconductor quantum electron-wave devices interconnected by electron waveguides.[24-29]

Semiconductor superlattice interference filter and filter/emitter designs can be visualized from the optical interference filters counterparts but their designs cannot be simple copies of thin-film optical designs due to the constraints that are imposed by the ultra small dimensions, the usable composition range, and the applied bias voltage. The design of such quantum interference filters and filter/emitters has been presented in Refs. 17–20. In the present work the current-voltage (I-V) characteristics of these filter/emitters are calculated self-consistently. It is shown that these devices can exhibit negative differential resistivity similar to that occuring in resonant tunneling diodes. In addition, space-charge effects due to electron localization that have been shown to be very important in semiconductor device analysis and design, are quantified for these structures. Several analytical techniques have been used and can be classified into two major categories: the classical approaches that include the solution of the nonlinear Poisson equation using Boltzmann or Fermi-Dirac statistics for the electron and hole concentrations,[30-35] and the quantum-mechanical approaches in which both the Schroedinger and Poisson equations are solved self-consistently through an iterative algorithm until a self-consistent electrostatic potential and electron density are acheived.[35-47] Most of these analyses have been applied to the resonant tunneling diodes[37,39-41,44] in which the space-charge effects have been shown to be significant. In this paper, for the first time, a complete quantum-mechanical self-consistent analysis of the semiconductor superlattice filter/emitter is presented. These devices inherently differ

from the resonant tunneling diodes in that they are designed to operate at electron energies above all barriers and wells of the semiconductor superlattice. Thus, electron localization is purely due to the quantum-mechanical interference mechanism.

In this work, the effects of the self-consistent potential on quantum-interference filter/emitter negative differential resistance devices are isolated and analyzed. The details of the model used are described in Sec. II. Several example cases are presented in Sec. III for the GaAs/$Ga_{1-x}Al_xAs$ alloy system. Resonant (exhibiting negative differential resistance) and nonresonant (not exhibiting negative differential resistance) filter/emitter devices are analyzed. The effects of the Fermi energy (doping) and temperature on the filter/emitter transmittance and current-voltage characteristics are included. Electron densities in the superlattice are also presented for resonant and nonresonant filter/emitters. It is found that the space-charge effects on the transmission and I-V characteristics of the filter/emitter devices can be significant for relatively high Fermi energies (above 30 meV) and generally lead to shifting of the device characteristics toward higher bias voltages. Finally, in Sec. IV, a summary and some discussion are presented.

II. MODEL DESCRIPTION

A voltage biased semiconductor superlattice can serve simultaneously as an electron-wave interference filter and electron emitter. The theory and the design of such electron-wave filter/emitters have been presented in Refs. 19 and 20 using a non-self-consistent (linear electrostatic potential) model. The present self-consistent model is similar to the one used for the resonant tunneling devices.[36-45] The model formulation is based on the following given conditions:

(a) The semiconductor superlattice consists of an intrinsic region where quantum-mechanical analysis applies. Thus, the length of the device is smaller than the electron coherence length. Experimental measurements in ballistic hot-electron devices[10,11,14,15,48,49] (on GaAs/GaAlAs and InGaAs/InAlAs structures) indicate that the electron coherence

length lies roughly between 10 and 100nm. Of course, the electron coherence length depends strongly on the temperature (electron coherence length of the order of several microns was recently reported at very low temperatures[14,15]) and it is a statistical quantity. Therefore, the experimental data suggest that a measurable fraction of the electrons will exhibit a coherent behavior within the filter/emitter. The transport of electrons through the filter/emitter negative differential resistance device is assumed to be strictly collisionless.

(b) For the filter/emitter region, the one-electron single-band effective mass time-independent Schroedinger equation is used. This is a valid approximation for electron energies near the Γ-point in accordance with the filter/emitter design requirements.[20] The boundary conditions used at the heterojunction interfaces of the filter/emitter region (intrinsic region) are the continuity of the envelope wavefunction, ψ, and the continuity of the normal component of the probability current density or equivalently the continuity of the envelope wavefunction first derivative weighted by the inverse effective mass, $(1/m^*)\psi'$ (where ψ' denotes a first derivative). These two boundary conditions work sufficiently well for the III-V semiconductor family as long as the same band edge is considered on both sides of the discontinuity[50] (the conduction band direct gap minimum for the electron-wave filter/emitters).

(c) The applied voltage bias appears across the filter/emitter region. The voltage drop in the contacts is assumed negligible.

(d) The contact regions outside the filter/emitter are treated as having constant Fermi energy levels and equilibrium Fermi-Dirac statistics apply.

The electron potential energy of the electron-wave filter/emitter negative differential resistance device with an applied bias voltage is shown in Fig. 1. In this figure the electrostatic potential energy is assumed to be linear which is the first estimate used in order to start the iterative solution of the Schroedinger and Poisson equations. The filter/emitter consists of M layers, where M is an odd integer. The center layer is the resonant layer while

the surrounding layers are quarter electron-wavelength layers (for the design pass energy of the filter/emitter).[19,20] When the design voltage is applied, electrons in a narrow energy band around the prespecified pass energy, E_p (Fig. 1), traverse the filter/emitter and are emitted with an output kinetic energy KE_{out}. The applied bias potential energy is denoted by V_{bias}, while the potential energies of the different layers are denoted by V_j and their effective masses by m_j^* $(j = 1, 2, \cdots, M)$. For the solution of the self-consistent problem the filter/emitter region is divided into N subregions of equal width Δz as shown in Fig. 2. The potential energy of each subregion i $(i = 1, 2, \cdots, N)$ is $V_i' = [V(z_{i-1}') + V(z_i')]/2$, where $V(z)$ is the electrostatic potential energy (which is one of the unknowns of the self-consistent problem). An alternative to the stair-step approximation[51] would be a piecewise linear potential energy approximation.[20,52] In the limit of large N both approximations converge to the same solution. The one-electron envelope wavefunction in the i-th subregion is denoted by ψ_i, while the change in the conduction band edge, v_i, and the effective mass, m_i^*, are the change in the conduction band edge and the effective mass of the region j $(j = 1, 2, \cdots, M)$ to which the subregion i belongs. Thus, the one-electron envelope function time-independent Schroedinger equation for the i-th subregion can be written

$$\frac{\hbar^2}{2m_i^*}\frac{d^2\psi_i}{dz^2} + (E - V_i' - v_i)\psi_i = 0 \qquad z_{i-1}' \le z \le z_i', \tag{1}$$

where $\hbar$ is Planck's constant divided by 2π and E is the total electron energy. In order to solve Eq. (1) knowledge of the electrostatic potential energy $V(z)$ is required. Assuming that $V(z)$ is known, the solution for ψ_i can be written in the form

$$\psi_i(z) = C_i \exp[+jk_i(z - z_{i-1}')] + D_i \exp[-jk_i(z - z_{i-1}')], \tag{2}$$

for $z_{i-1}' \le z \le z_i'$ and with the electron wavevector $k_i = [2m_i^*(E - V_i' - v_i)/\hbar^2]^{1/2}$. The coefficients C_i and D_i of each subregion i can be found from the boundary conditions for the envelope wavefunctions and assuming that $\psi_0(z) = \exp(jk_0 z) + r_e \exp(-jk_0 z)$ and $\psi_{N+1}(z) = t_e \exp[jk_{N+1}(z - z_N')]$, where r_e and t_e are the amplitude reflection and transmission coefficients of the wavefunction. Using a transfer matrix approach[51] r_e and

t_e can be calculated first, and then all C_i and D_i can be computed recursively. Thus, once the overall transmission and reflection coefficients are found, the steady-state wavefunction $\psi(z) = \psi_\ell(z)$ for $z'_{\ell-1} \leq z \leq z'_\ell$ $(\ell = 1, 2, \cdots, N)$ can be determined at each incident energy E over the full range of interest.

After the wavefunction $\psi(z)$ is known throughout the entire structure, the electron density, $n(z)$, can be calculated by $n(z) = \langle \psi(z)\psi^*(z) \rangle$, where $\langle\ \rangle$ denotes summation (or equivalently integration) over all energies.[36] Furthermore, assuming Fermi-Dirac statistics the previous equation becomes

$$n(z) = \langle \psi(z)\psi^*(z) f(E, E_f) \rangle, \tag{3}$$

where $f(E, E_f)$ is the Fermi distribution function and E_f is the Fermi energy level. The distribution function is taken as being in equilibrium, despite of the fact that a current flows through the filter/emitter when a voltage bias is applied. However, the distribution function $f(E, E_f) = 1/\{1 + \exp[(E - E_f)/k_B T]\}$, where k_B is Boltzmann's constant and T is the absolute temperature, is reasonably accurate since the xy system is essentially decoupled from the quantization direction z, and can be considered in a quasi-equilibrium state.[37-43] Evaluation of Eq. (3) yields to following approximate expression for $n(z)$,

$$n(z) \simeq \frac{k_B T (m_0^*)^{3/2}}{2\sqrt{2}\pi^2 \hbar^3} \int_0^\infty |\psi(z)|^2 \ln[1 + \exp(E_f - E_z)/k_B T] \frac{dE_z}{\sqrt{E_z}}, \tag{4}$$

where E_z is the longitudinal component of the energy E. For the above computation parabolic band structure and independence of $|\psi(z)|^2$ on the transverse energy component (momentum) were assumed. None of the two previous assumptions is strictly valid, but for low energies near the bottom of the conduction band (Γ-valley) these are very good approximations and they greatly simplify the computational procedure for the evaluation of the electron density.[37-43] In addition, Eq. (4) accounts for only the left-to-right incident electrons. In order to be strictly correct, the electrons impinging from right-to-left should also be taken into account,[39-41] and the total electron density should be the sum of these two streams of electrons. However, the right-to-left incident stream of electrons

has a negligible effect on the current density of the device for the design values of the applied voltage and temperature. The charge density corresponding to the spatial electron distributions given by Eq. (4) can be calculated by $-en(z)$ (where e is the electron charge) and then substituted into the one-dimensional Poisson equation,

$$\frac{d}{dz}(\epsilon_0 \varepsilon_r(z)\frac{d\phi}{dz}) = -en(z), \tag{5}$$

where ϵ_0 is the permittivity of freespace, ε_r is the relative permittivity along the device, and $\phi(z)$ is the electrostatic potential. Defining the electrostatic potential energy as before by $V(z) = -e\phi(z)$, Eq. (5) can be written as

$$\frac{d^2V(z)}{dz^2} \simeq -\frac{e^2 n(z)}{\epsilon_0 \varepsilon_r}, \tag{6}$$

where ε_r is the relative permittivity of GaAs (assumed constant throughout the filter/emitter for simplicity). Solving Eq. (6) numerically, using the method of finite differences, the electrostatic potential energy $V(z)$ can be found and used in the Schroedinger equation [Eq. (1)].

The computation algorithm starts with the solution of Eq. (1) assuming linear electrostatic potential energy (Fig. 1). After computation of the wavefunction, the electron density can be calculated from Eq. (4). Then Eq. (6) can be solved for a new estimate of the electrostatic potential energy $V(z)$. This procedure is iterated until convergence of the electrostatic potential energy $V(z)$ is obtained. Then, the current density, J, can be calculated at each applied bias using the equation[51,53]

$$J \simeq \frac{em_0^* k_B T}{2\pi^2\hbar^3}\int_0^\infty T(E_z)\ln\left[\frac{1+\exp[(E_f - E_z)/k_B T]}{1+\exp[(E_f - E_z - V_{bias})/k_B T]}\right]dE_z, \tag{7}$$

where $T(E_z)$ is the transmission coefficient of the device, calculated using the self-consistent electrostatic potential, and is given by

$$T(E_z) = \left[\frac{(E - V_0)/m^*_{M+1}}{(E - V_0 - V_{bias})/m_0^*}\right]^{1/2}|t_e|^2. \tag{8}$$

For the derivation of Eq. (7), parabolic band structure and independence of $T(E_z)$ on transverse energy component were assumed, similarly to the assumptions for the validity of Eq. (4). In the following section several results of resonant (exhibiting negative differential resistance) and nonresonant (not exhibiting negative differential resistance) devices in the $Ga_{1-x}Al_xAs$ alloy family are presented.

III. RESULTS OF THE CALCULATIONS FOR $Ga_{1-x}Al_xAs$ ALLOYS

A practical material system to be used in fabricating electron-wave interference devices is $Ga_{1-x}Al_xAs$. For this material system the maximum allowable composition in aluminum is $x_{max} = 0.45$, in order to avoid the direct/indirect band-gap transition. The electron potential energy of the j-th layer is given by $V_j = Ax_j$ ($A = 0.773$eV), using the $\sim 60/40$ rule conduction-to-valence band-edge discontinuity,[54,55] and its effective mass is given by $m_j^* = (B + Cx_j)m_0$ ($B = 0.067$, $C = 0.083$), where m_0 is the free electron mass. The $\langle 100 \rangle$ monolayer thickness for any usable composition remains the same and equals 0.2827 nm (lattice-matched material system). Two resonant and one nonresonant example designs will be presented. These designs will take into account the minimization of the intervalley scattering (Γ-L band transition) according to the analysis presented in Ref. 20. The two resonant devices will be referred to as resonant filter/emitters A and B respectively.

A. Resonant Filter/Emitter A Design Criteria

Resonant filter/emitter A was designed with the algorithm of Ref. 20 for a bias potential energy $V_{bias} = 0.10$eV and an output kinetic energy at resonance $KE_{out} = 0.13$eV, assuming a Fermi energy level at the input region of 30meV (measured from the bottom of the conduction band). The phonon energy was assumed to be 35meV for the Γ-L intervalley transition. In order to reduce intervalley transitions for the applied resonance bias and kinetic energy, the maximum allowable aluminum composition had to be reduced[20] to 0.2 which was also selected to be the input and output region compositions

(Fig. 1). The operating temperature was assumed to be 25 K. The characteristics of the nine layer ($M = 9$) resonant filter/emitter A (exact design) are given in Table I. In this table, the thickness of each layer in monolayers, the aluminum composition x_j, the unbiased electron potential energy V_j, and the normalized effective mass m_j^*/m_0, are given. The total thickness of the filter/emitter A is 100 monolayers (28.3 nm), which is within the electron coherence length [assumption (a) of Sec. II] at 25 K. An alternate design which takes into account the practical constraint of having a finite number of composition levels is also shown in Table I (constrained-composition design). This version of resonant filter/emitter A restricts the aluminum compositions to four distinct levels (0.0, 0.07, 0.13, and 0.20 as is required by typical MBE fabrication systems). The transmission characteristics, (calculated using a non-self-consistent analysis) of these exact and the constrained-composition designs, are shown in Fig. 3a as functions of the output kinetic energy KE_{out} (Fig. 1) for an applied bias potential energy of 0.10eV (resonance design value). The constrained-composition design has its peak electron transmission at $KE_{out} =$ 0.125eV instead of the 0.13eV design value, due to the four distinct aluminum composition levels. Interestingly, the transmission (transmission of 99.8% at 0.125eV) peak of the constrained-composition design is larger than the peak of the exact design (transmission of 94.4% at 0.13eV). This is due to the more symmetric configuration of the constrained composition design. However, the exact design remains the optimal design for $KE_{out} =$ 0.13eV and for $V_{bias} = 0.10$eV.

B. Resonant Filter/Emitter B Design Criteria

Resonant filter/emitter B was designed using the same procedure[19] as resonant filter/emitter A. The Fermi energy level of resonant filter/emitter B was calculated to be $E_f = 2.26$meV using a donor concentration of $N_D = 2 \times 10^{18}\text{cm}^{-3}$, a donor ionization energy of 5.8meV (for silicon dopant), and an operating temperature of 25 K. The calculational procedure was based on the numerical solution of the charge neutrality equation at flatband equilibrium using Fermi-Dirac statistics.[56] This is a conservative calculation

which does not take into account the broadening of the donor ionization energies and the band-tailing due to the heavy doping.[57] To restrict intervalley scattering the maximum allowable aluminum composition was chosen again to be 0.2 which is also equal to the compositions of the input and output regions. In this design, due to the lower Fermi energy level, the design bias potential energy had to be chosen lower than previously and was selected to be 0.05eV. The output kinetic energy of resonant filter/emitter B at its resonance was selected to be 0.052eV in order to be near the Fermi level of the input region. The design characteristics of the nine layer ($M = 9$) resonant filter/emitter B (exact design) are shown in Table II. For this design the total thickness of the filter/emitter is 136 monolayers (38.4 nm) which is again within the electron coherence length at 25 K. The thickness of resonant filter/emitter B is larger than that of resonant filter/emitter A due to the lower resonance energy and applied voltage bias. A constrained-composition design is also included in Table II with three only aluminum composition levels (the 0.13 composition level is not necessary in this case). In this constrained-composition design the center layer thickness was increased by one monolayer (21 instead of 20) to shift the transmission peak closer to the design transmission peak and at lower output kinetic energies (which is desirable due to the low Fermi energy level). The transmission characteristics of the exact and the constrained composition designs are shown in Fig. 3b as function of the output kinetic energy for a bias potential energy of 0.05eV (non-self-consistent calculation). For both of the resonant filter/emitter B designs the peak transmissions are smaller than those of resonant filter/emitter A (37.9% for the exact design and 34.4% for the constrained-composition design) for the corresponding design energy and bias potential. The smaller peak transmission is due to the lower input kinetic energies and applied resonant bias voltages. In the remainder of this paper, the constrained-composition designs for both resonant filter/emitters A and B will be analyzed, since these designs are practical from a fabrication point of view.

C. Self-Consistent and Non-Self-Consistent Analyses

Using the algorithm presented in Sec. II, constrained-composition resonant filter/emitters A and B were analyzed with both the non-self-consistent (linear electrostatic potential) and the self-consistent approach. The stair-step representation used for the self-consistent computation consisted of steps of monolayer thickness, i.e. $\Delta z = 0.2827$ nm and $N = 100$ for resonant filter/emitter A and $N = 137$ for resonant filter/emitter B. Comparing the stair-step results with these of the exact analysis (using Airy and complimentary Airy functions[20,52] for non-self-consistent potential) excellent agreement was found (error was smaller than $\pm 10^{-5}$ for the wavefunction amplitude). Thus, the above selection of Δz was also considered more than adequate for the self-consistent analysis.

The electron potential energy across the filter/emitter is shown as a function of the longitudinal distance (z) for the non-self-consistent (linear) and the self-consistent electrostatic potential in Figs. 4a (resonant filter/emitter A for $V_{bias} = 0.10$eV) and 4b (resonant filter/emitter B for $V_{bias} = 0.05$eV). It is observed that the difference between the self-consistent and the linear potential is larger for resonant filter/emitter A (with a Fermi energy $E_f = 30$ meV) than for filter/emitter B (with a Fermi energy $E_f = 2.26$ meV). This difference is at least an order of magnitude smaller for resonant filter/emitter B. The difference between the self-consistent and the linear electrostatic potential energy, $\Delta V = V_{SC}(z) - V_L(z)$ [where $V_{SC}(z)$ and $V_L(z)$ are the self-consistent and linear electrostatic potential energies], is shown in Figs. 5a (resonant filter/emitter A for $V_{bias} = 0.10$eV) and 5b (resonant filter/emitter B for $V_{bias} = 0.05$eV). Since resonant filter/emitter A has more carriers available and larger transmission peak at the resonant energy, stronger electron localization is expected, which raises the potential energy profile for the transmitted electrons higher than that of filter/emitter B.

The wavefunction square amplitude, $|\psi(z)|^2$, as function of the longitudinal (z) direction, is shown for both the non-self-consistent and the self-consistent approaches in Figs. 6a (resonant filter/emitter A) and 6b (resonant filter/emitter B). In both cases the square amplitude of the wavefunction was calculated at the resonant energy of the non-

self-consistent design. Consequently for resonant filter/emitter A the wavefunction was computed for $KE_{out} = 0.0125$eV (or total electron energy $E = V_0 + KE_{out} = 0.28$eV) and $V_{bias} = 0.10$eV, while for filter/emitter B it is computed for $KE_{out} = 0.0536$eV (or $E = 0.21$eV) and $V_{bias} = 0.05$eV. From Fig. 6a it is observed that the square of the wavefunction amplitude peaks at the boundaries between layers of differing compositions. In addition, the highest peaks appear at the boundaries of the central (resonant) layer. The square of the wavefunction amplitude is not exactly symmetric around the central (resonant) layer due to the asymmetry of the filter/emitter in layer thicknesses. For the self-consistent calculation it can be seen from Figs. 6a and 6b that the wavefunctions corresponding to the self-consistent potentials have lower and slightly shifted peaks (Fig. 6a) since the self-consistent electrostatic potential is expected to shift the filter/emitter characteristics to higher applied voltages. The self-consistent effect is more pronounced in the case of resonant filter/emitter A since for this design a higher Fermi energy level ($E_f = 30$ meV) was assumed, and consequently, the screening effect was stronger. Comparing the square of the wavefunction amplitudes of these filter/emitters with those of resonant tunneling diodes,[43] a fundamental difference is observed. The peaks of the square of the wavefunction amplitude in the resonant tunneling diodes occur inside the well region (resonant layer), while in the resonant filter/emitter cases the peaks occur at the boundaries of the central (resonant) layer with the surrounding layers. Thus, electron localization is expected near and at the interfaces between differing aluminum composition layers and especially near the interfaces of the central layer. This may be due to higher electron velocities inside the well regions than inside the barrier regions resulting in an electron localization near the interfaces between the differing electron velocity regions.

The electron-wave transmission characteristics of the resonant filter/emitters can be calculated using Eqs. (1), (2), and (8) for both the non-self-consistent and the self-consistent electrostatic potential. The results of the calculation are shown in Figs. 7a (resonant filter/emitter A for $V_{bias} = 0.10$eV) and 7b (resonant filter/emitter B for $V_{bias} =$

0.05eV). In both self-consistent electrostatic potential cases there is a slight shift of the transmittance curve toward higher output kinetic energies (or equivalently input kinetic energies) from its corresponding linear electrostatic potential case. This was expected due to the increased electron potential energy. The effect is again more pronounced for resonant filter/emitter A due to its higher Fermi energy.

The electron density, $n(z)$, can be calculated from Eq. (4) using the self-consistent electrostatic potential. The electron densities of the two resonant filter/emitters are shown in Figs. 8a (resonant filter/emitter A for $V_{bias} = 0.10$eV) and 8b (resonant filter/emitter B for $V_{bias} = 0.05$eV), as functions of the longitudinal distance (z). Comparisons of Figs. 6 and 8 reveal some similarity between the $|\psi(z)|^2$ and $n(z)$. This is expected since $n(z)$ is an energy average over all electrons using Fermi-Dirac statistics [Eq. (3)], and to this average, electrons with energies near the resonant energy (Figs. 6) mainly contribute.

Finally the current-voltage characteristics of the resonant filter/emitters can be calculated using Eq. (7), with either a linear or a self-consistent electrostatic potential. The I-V characteristics of resonant filter/emitters A and B are shown in Figs. 9a and 9b, respectively. The effect of the self-consistent electrostatic potential is again stronger for resonant filter/emitter A. In both cases the self-consistent characteristics are shifted (in the case of resonant filter/emitter B this shift is small) to higher applied bias voltages. This is in agreement with the I-V characteristics of the resonant tunneling diodes.[37-43] From the I-V characteristics a negative differential resistivity (NDR) is clearly observed. For resonant filter/emitter A the peak-to-valley ratio is 5.74 (with peak current density $J = 3.22 \times 10^6\,\mathrm{A/cm^2}$ at 0.155 volts) for the self-consistent calculation, and 5.78 for the non-self-consistent calculation (with peak current density $J = 3.20 \times 10^6\,\mathrm{A/cm^2}$ at 0.135 volts). For resonant filter/emitter B the peak-to-valley ratio is 46.1 (with peak current density $J = 1.09 \times 10^3\,\mathrm{A/cm^2}$ at ~0.0525 volts) for the self-consistent calculation, and 47.2 (with peak current density $J = 1.11 \times 10^3\,\mathrm{A/cm^2}$ at 0.0525 volts) for the non-self-consistent calculation. It is observed that filter/emitter B has about 3 orders of magnitude

smaller current density even if its Fermi energy is only one order of magnitude smaller than that of resonant filter/emitter A. However, resonant filter/emitter B exhibits an order of magnitude larger peak-to-valley ratio. All the above calculations were performed for $T = 25$ K and for a relative dielectric permittivity of GaAs of 13.18.

D. Effects of Temperature Variation

The temperature dependence of resonant filter/emitter B current-voltage characteristics is shown in Fig. 10 for $T = 25, 35$, and 50 K. The Fermi energy levels were computed[56] as described previously for resonant filter/emitter B and are $E_f = 2.26, 3.63$, and 5.26 meV respectively. The self-consistent as well as the non-self-consistent I-V characteristics are shown for the three selected temperatures. For higher temperatures the electron coherence length is expected to be smaller than the dimensions of the filter/emitter, thus, significantly degrading the quantum interference behavior of the device due to scattering mechanisms.

E. Analysis of Nonresonant Filter/Emitters

The two resonant filter/emitters A and B described previously have been designed to exhibit electron transmission peaks for a specified input (or output) kinetic energy and applied bias potential. A question that now arises is how a nonresonant filter/emitter would perform. In order to answer this question, resonant filter/emitter B is redesigned so that the central layer is a quarter electron wavelength layer instead of a half electron wavelength layer. The resulting nonresonant filter/emitter C (Table III) has a 10 monolayer thick central layer (instead of 21 monolayer thick central layer for the resonant filter/emitter B). Consequently, the nonresonant filter/emitter C is not expected to exhibit any negative differential resistance behavior. The rest of the layers of nonresonant filter/emitter C have the characteristics shown in Table II for the resonant filter/emitter B. The electron potential energy profile of the nonresonant filter/emitter C is shown in Fig. 11a for both the non-self-consistent and self-consistent computation. The difference ΔV between the self-consistent and the linear electrostatic potential energy is shown in Fig. 11b. It is

observed that this difference is approximately two orders of magnitude smaller than that of the resonant filter/emitter B. Thus, the space-charge effects are much less significant in the nonresonant design. The square of the wavefunction amplitude, $|\psi(z)|^2$, for an output kinetic energy of 0.0536eV (resonant energy of the resonant filter/emitter B) and for an applied bias potential energy of 0.05eV (resonant bias potential energy of the resonant filter/emitter B) is shown in Fig. 11c. Comparing Fig. 11c with Fig. 6b a significant difference can be observed. In the nonresonant filter/emitter C the wavefunction square amplitude drops fast along the longitudinal direction of the device revealing very small electron localization inside the nonresonant filter/emitter. The difference between the self-consistent and the non-self-consistent calculation is insignificant for the nonresonant device. The electron transmission characteristics of the nonresonant filter/emitter C are presented in Fig. 11d for $V_{bias} = 0.05$eV. No peak in the transmission is observed between 0.05-0.08eV as was expected (compare with Fig. 7b for the resonant filter/emitter B). The electron density distribution, $n(z)$, is shown in Fig. 11e. This distribution resembles the $|\psi(z)|^2$ distribution since for all the electron energies near the Fermi level the filter/emitter exhibits the same nonresonant electron transmission response. Finally, the I-V characteristics of the nonresonant filter/emitter C are shown in Fig. 11f. No negative differential resistance is observed in this case as was expected (compare with Fig. 9b of the resonant filter/emitter B). In addition, the current density is much smaller (2-3 orders of magnitude) for voltages up to 0.10 volts since most of the incident electrons are reflected due to the nonresonant behavior of the filter/emitter. All the computations for the nonresonant filter/emitter C were performed again for a temperature of 25 K.

IV. DISCUSSION AND SUMMARY

In all the example cases presented for both the resonant and the nonresonant filter/emitters, the step size Δz of the stair-step approximation was selected to be one monolayer. Smaller step sizes (fraction of a monolayer) have also been tested but the final results were almost unaffected (observed changes were smaller than $\pm 10^{-6}$). Therefore

the one monolayer thickness was retained for savings and efficiency of computer time. The number of energy points (in momentum space), for the integral computation [Eqs. (4) and (7)], was varied between 400 to 1000 points depending on the electron transmission characteristics of the filter/emitter. For example resonant filter/emitter B needed more energy points than resonant filter/emitter A due to its sharper energy (momentum) space characteristics. Convergence of the algorithm was obtained within 3-25 iterations for resonant filter/emitter A, and 2-6 iterations for resonant filter/emitter B. The convergence criterion selected was that the maximum absolute difference of the electrostatic potential energy between two successive iterations should be less than a pre-selected value. This value for the examples presented was set equal to 10^{-4}. All computations were performed in a CDC-Cyber 855 or 990 mainframe computer with CPU times varying between 400-45,000 seconds, with the most time consuming cases being the I-V characteristics computations (using 80 voltage values).

In all the examples analyzed, it was assumed that the semiconductor materials had parabolic band structure. This was a good approximation since both filter/emitters have been designed to resonate at low electron energies. However, for sufficiently high applied bias voltages, the electron energies exceed the parabolic band structure regime, and the band structure is more appropriately treated as nonparabolic. Furthermore, the band structure may vary with the direction of the electron-wave propagation (anisotropy). Both of these effects can be incorporated by using an energy dependent anisotropic effective mass. In the latter case the solutions of the Schroedinger equation have to be modified but the remainder of the analysis is still valid. The anisotropic case could be used when the lowest energy band consisted of ellipsoidal X minima energy surfaces (Si, AlAs, etc.) or ellipsoidal L minima energy surfaces (Ge) rather than the spherical Γ minimum energy surface associated with the direct gap $Ga_{1-x}Al_xAs$.

Finally, in the analysis and the examples presented, the effect of the space-charge field due to the contact-filter/emitter junctions was not taken into account. The present

analysis has focussed on the filter/emitter region design and function. The impinging electrons (from the left side of Fig. 1) were assumed to originate from the quasi-equilibrium contact regions and are incident on the filter/emitter. The self-consistent potential will not be significantly altered by the contacts in shape or relative magnitude. However, the contacts will cause an elevation of the electron potential energy profile of the whole filter/emitter structure due to the inevitable alignment of the Fermi energy levels at equilibrium. For this reason a specialized transit region between the contacts and the filter/emitter will be required for the designed operation of the device. The design and fabrication of this specialized region and its effect in the function of the filter/emitter is under investigation.

In summary, for the first time to our knowledge, the transmission and the current-voltage characteristics of electron-wave quantum interference resonant filter/emitters were studied using a non-self-consistent and a self-consistent analysis. It was shown that the resonant filter/emitters can exhibit negative differential resistivity similar to that in resonant tunneling diodes. Several example designs on $Ga_{1-x}Al_xAs$ alloys were presented including both resonant and nonresonant filter/emitters. For low temperatures (in the ballistic transport regime) it was shown that the effect of the space-charge fields is insignificant for nonresonant filter/emitters while it can be quite significant for resonant filter/emitters at high Fermi energy levels. The I-V characteristics of the resonant filter/emitters are shifted to higher applied voltages due to the screening effect of the electron localization. However, the peak-to-valley ratios remained almost the same as those from the non-self-consistent computation. Importantly, in contrast to resonant tunneling diodes the valley current is lower and remains low over a larger voltage range ("flat valley"). The square of the wavefunction amplitude distributions, electron potential energy profiles, and electron density profiles were also presented. Semiconductor superlattice electron-wave quantum-interference resonant filter/emitters have potential use as high-speed switches and oscillators and as monoenergetic emitters in electroluminescent devices and photodetectors.

This research was supported in part by a grant from the Joint Services Electronics

Program under Contract No. DAAL-03-90-C-0004. One of us (K. F. B.) was supported in part by a Presidential Young Investigator award from the National Science Foundation and another (E. N. G.) by a Research Initiation award from the National Science Foundation.

REFERENCES

1. L. Esaki and R. Tsu, *IBM J. Res. Dev.* **13**, 61 (1970).

2. L. L. Chang, L. Esaki, and R. Tsu, *Appl. Phys. Lett.* **24**, 593 (1974).

3. T. C. L. G. Sollner, W. D. Goodhue, P. E. Tannenwald, C. D. Parker, and D. D. Peck, *Appl. Phys. Lett.* **43**, 588 (1983).

4. T. Nakagawa, H. Imamoto, T. Kojima, and K. Ohta, *Appl. Phys. Lett.* **49**, 73 (1986).

5. C. J. Summers, K. F. Brennan, A. Torabi, and H. M. Harris, *Appl. Phys. Lett.* **52**, 132 (1988).

6. S. Sen, F. Capasso, A. C. Gossard, R. A. Spah, A. L. Hutchinson, and S. N. G. Chu, *Appl. Phys. Lett.* **51**, 1428 (1987).

7. M. Heiblum, M. V. Fischetti, W. P. Dumke, D. J. Frank, I. M. Anderson, and C. M. Knoedler, *Phys. Rev. Lett.* **58**, 816 (1987).

8. R. C. Potter and A. A. Lakhani, *Appl. Phys. Lett.* **52**, 1349 (1988).

9. J. R. Hayes, P. England, and J. P. Harbison, *Appl. Phys. Lett.* **52**, 1578 (1988).

10. A. F. J. Levi, J. R. Hayes, P. M. Platzman, and W. Wiegmann, *Phys. Rev. Lett.* **55**, 2071 (1985).

11. M. Heiblum, M. I. Nathan, D. C. Thomas, and C. M. Knoedler, *Phys. Rev. Lett.* **55**, 2200 (1985).

12. S. Washburn and R. A.Webb, *Adv. Phys.* **35**, 375 (1986).

13. Y. Imry, in *Directions in Condensed Matter Physics*, edited by G. Grinstein and G. Mazenko (World Scientific, Singapore, 1986), pp. 101–163.

14. J. Spector, H. L. Stormer, K. W. Baldwin, L. N. Pfeiffer, and K. W. West, *Appl. Phys. Lett.* **56**, 1290 (1990).

15. J. Spector, H. L. Stormer, K. W. Baldwin, L. N. Pfeiffer, and K. W. West, *Appl. Phys. Lett.* **56**, 2433 (1990).

16. T. K. Gaylord and K. F. Brennan, *J. Appl. Phys.* **65**, 814 (1989).

17. T. K. Gaylord and K. F. Brennan, *Appl. Phys. Lett.* **53**, 2047 (1988).

18. T. K. Gaylord, E. N. Glytsis, and K. F. Brennan, *J. Appl. Phys.* **65**, 2535 (1989).

19. E. N. Glytsis, T. K. Gaylord, and K. F. Brennan, *J. Appl. Phys.* **66**, 1494 (1989).

20. E. N. Glytsis, T. K. Gaylord, and K. F. Brennan, *J. Appl. Phys.* **66**, 6158 (1989).

21. C. J. Summers and K. F. Brennan, *Appl. Phys. Lett.* **48**, 806 (1986).

22. K. F. Brennan and C. J. Summers, *J. Appl. Phys.* **61**, 5410 (1987).

23. K. F. Brennan and C. J. Summers, *IEEE J. Quantum Electron.* **QE-23**, 320 (1987).

24. T. K. Gaylord, E. N. Glytsis, and K. F. Brennan, *J. Appl. Phys.* **66**, 1483 (1989).

25. T. K. Gaylord, E. N. Glytsis, and K. F. Brennan, *J. Appl. Phys.* **66**, 1842 (1989).

26. G. Nimtz and P. Marquardt, *Appl. Phys. A* **47**, 317 (1988).

27. A. Szafer and A. D. Stone, *Phys. Rev. Lett.* **62**, 300 (1989).

28. S. Datta, M. R. Melloch, S. Bandyopadhyay, R. Noren, M. Vaziri, M. Miller, and R. Reinfenberger, *Phys. Rev. Lett.* **55**, 2344 (1985).

29. H. R. Frohne, M. J. McLennan, and S. Datta, *J. Appl. Phys.* **66**, 2699 (1989).

30. D. J. BenDaniel and C. B. Duke, *Phys. Rev* **152**, 683 (1966).

31. J. L. Blue and C. L. Wilson, *IEEE Trans. Electron Devices* **30**, 1056 (1983).

32. M. S. Lundstrom and R. J. Schuelke, *IEEE Trans. Electron Devices* **30**, 1151 (1983).

33. I. D. Mayergoyz, *J. Appl. Phys.* **59**, 195 (1986).

34. C. M. Snowden, *Semiconductor Device Modelling* (Peter Peregrinus Ltd., London, United Kingdom, 1988).

35. S. Selberherr, *Analysis and Simulation of Semiconductor Devices* (Springer-Verlag, New York, 1984).

36. S. Datta, *Quantum Phenomena* (vol. VIII in Modular Series on Solid-State Devices, Addison-Wesley, Reading Mass., 1989).

37. H. Ohnishi, T. Inata, S. Muto, N. Yokoyama, and A. Shibatomi, *Appl. Phys. Lett.* **49**, 1248 (1986).

38. H. Ohnishi, N. Yokoyama, and A. Shibatomi, *IEEE Trans. Electron Devices* **36**, 2335 (1989).

39. M. Cahay, M. McLennan, S. Datta, and M. S. Lundstrom, *Appl. Phys. Lett.* **50**, 612 (1987).

40. M. Cahay, M. A. Osman, H. L. Grubin, and M. McLennan, in *Nanostructure Physics and Fabrication* (Academic Press, 1989), pp. 495–499.

41. M. Cahay, M. McLennan, S. Datta, and M. S. Lundstrom, in *Fundamental Research on the Numerical Modelling of Semiconductor Devices and Processes* (edited by J. J. H. Miller, Boole Press Ltd., Dublin, Ireland, 1987), pp. 53–57.

42. W. Pötz, *Superlattices and Microstructures* **6**, 187 (1989).

43. K. F. Brennan, *J. Appl. Phys.* **62**, 2392 (1987).

44. C. M. Wu and E. S. Yang, *Solid-State Electronics* **22**, 241 (1979).

45. H. L. Berkowitz and R. A. Lux, *J. Vac. Sci. Technol. B* **5**, 967 (1987).

46. N. C. Kluksdahl, A. M. Kriman, and D. K. Ferry, *Phys. Rev. B* **39**, 7720 (1989).

47. R. K. Mains, J. P. Sun, and G. I. Haddad, *Appl. Phys. Lett.* **55**, 371 (1989).

48. K. Imamura, S. Muto, N. Yokoyama, M. Sasa, H. Ohnishi, S. Hiyamizu, and H. Nishi, *Surf. Sci.* **174**, 481 (1986).

49. K. Seo, M. Heiblum, C. M. Knoedler, J. E. Oh, J. Pamulapati, and P. Bhattacharya, *IEEE Electron. Device Lett.* **2**, 73 (1989).

50. M. Altarelli, in *Heterojunctions and Semiconductor Superlattices* (Eds. G. Allan, G. Bastard, N. Boccra, M. Lannoo, and M. Voos, Springer-Verlag, New York, 1986) pp. 12–37.

51. M. O. Vassell, Johnson Lee, and H. F. Lockwood, *J. Appl. Phys.* **54**, 5206 (1983).

52. K. F. Brennan and C. J. Summers, *J. Appl. Phys.* **61**, 614 (1986).

53. R. Tsu and L. Esaki, *Appl. Phys. Lett.* **22**, 562 (1973).

54. H. C. Casey and M. B. Panish, *Heterostructure Lasers Part A. Fundamental Principles* (Academic Press, New York 1978) Chap. 4.

55. R. C. Miller, D. A. Kleinman, and A. C. Gossard, *Phys. Rev. B* **29**, 7085 (1984).

56. T. K. Gaylord and J. N. Linxwiler, Jr., *Am. J. of Phys.* **44**, 353 (1976).

57. R. F. Pierret, *Advanced Semiconductor Fundamentals* (vol. VI in Modular Series on Solid-State Devices, Addison-Wesley, Reading Mass., 1987).

Table I: Design parameters of an electron wave interference resonant filter/emitter consisting of nine layers surrounded by $Ga_{0.8}Al_{0.2}As$ and designed to emit 0.13eV electrons for the exact design, and 0.125eV electrons for the constrained-composition design when biased at 0.10eV.

RESONANT FILTER/EMITTER A DESIGN

	Exact Design				Constrained-Composition Design			
Layer Number j	Number Monolayers Thick	Aluminum Composition x_j	Unbiased Electron Potential Energy V_j (eV)	Normalized Effective Mass m_j^*/m_0	Number Monolayers Thick	Aluminum Composition x_j	Unbiased Electron Potential Energy V_j (eV)	Normalized Effective Mass m_j^*/m_0
1	10	0.0249	0.0193	0.0691	10	0.00	0.0000	0.0670
2	12	0.1225	0.0947	0.0772	12	0.13	0.1005	0.0778
3	10	0.0630	0.0487	0.0722	10	0.07	0.0541	0.0728
4	12	0.1557	0.1204	0.0799	12	0.13	0.1005	0.0778
5	18	0.0402	0.0311	0.0703	18	0.00	0.0000	0.0670
6	11	0.1712	0.1324	0.0812	11	0.20	0.1546	0.0836
7	9	0.0855	0.0661	0.0741	9	0.07	0.0541	0.0728
8	10	0.1622	0.1254	0.0805	10	0.20	0.1546	0.0836
9	8	0.0142	0.0109	0.0682	8	0.00	0.0000	0.0670

Table II: Design parameters of an electron wave interference resonant filter/emitter consisting of nine layers surrounded by $Ga_{0.8}Al_{0.2}As$ and designed to emit 0.0520eV electrons for the exact design, and 0.0536eV electrons for the constrained-composition design when biased at 0.05eV.

RESONANT FILTER/EMITTER B DESIGN								
	Exact Design				Constrained Composition Design			
Layer Number j	Number Monolayers Thick	Aluminum Composition x_j	Unbiased Electron Potential Energy V_j (eV)	Normalized Effective Mass m_j^*/m_0	Number Monolayers Thick	Aluminum Composition x_j	Unbiased Electron Potential Energy V_j (eV)	Normalized Effective Mass m_j^*/m_0
1	11	0.0226	0.0175	0.0689	11	0.00	0.0000	0.0670
2	21	0.1702	0.1316	0.0811	21	0.20	0.1546	0.0836
3	11	0.0419	0.0324	0.0705	11	0.07	0.0541	0.0728
4	20	0.1814	0.1402	0.0821	20	0.20	0.1546	0.0836
5	20	0.0140	0.0109	0.0682	21	0.00	0.0000	0.0670
6	17	0.1819	0.1407	0.0821	17	0.20	0.1546	0.0836
7	10	0.0348	0.0269	0.0699	10	0.07	0.0541	0.0728
8	16	0.1866	0.1443	0.0825	16	0.20	0.1546	0.0836
9	10	0.0513	0.0397	0.0712	10	0.00	0.0000	0.0670

Table III: Design parameters of an electron wave interference nonresonant filter/emitter consisting of nine layers surrounded by $Ga_{0.8}Al_{0.2}As$ and designed to emit 0.0536eV electrons for the constrained-composition design when biased at 0.05eV.

NONRESONANT FILTER/EMITTER C DESIGN				
Constrained-Composition Design				
Layer Number j	Number Monolayers Thick	Aluminum Composition x_j	Unbiased Electron Potential Energy V_j (eV)	Normalized Effective Mass m_j^*/m_0
1	11	0.00	0.0000	0.0670
2	21	0.20	0.1546	0.0836
3	11	0.07	0.0541	0.0728
4	20	0.20	0.1546	0.0836
5	10	0.00	0.0000	0.0670
6	17	0.20	0.1546	0.0836
7	10	0.07	0.0541	0.0728
8	16	0.20	0.1546	0.0836
9	10	0.00	0.0000	0.0670

FIGURE CAPTIONS

1. Schematic representation of a biased semiconductor superlattice electron wave interference resonance filter/emitter. At the design potential energy bias, V_{bias}, and input kinetic energy, KE_{in}, the layers have a thickness of a quarter (or a half for the resonant central layer) of an electron wavelength as measured in that layer. In this figure a linear (non-self-consistent) electrostatic potential is assumed.

2. Part of the resonant filter/emitter region between points z'_{i-1} and z'_i where the stair-step representation is used for the self-consistent potential $V(z)$.

3. Electron transmission characteristics of the nine layer resonant filter/emitters as a function of the output kinetic energy for an applied bias potential energy of V_{bias}. The characteristics of the exact design (dashed line) and of the constrained composition design (solid line) are shown. (a) Resonant filter/emitter A for V_{bias} = 0.10eV, and (b) Resonant filter/emitter B for V_{bias} = 0.05eV.

4. Electron potential energy profile along the filter/emitter region. Both the self-consistent (solid line) and the non-self-consistent (dotted line) potential energy profiles are shown. (a) Resonant filter/emitter A for V_{bias} = 0.10eV, and (b) resonant filter/emitter B for V_{bias} = 0.05eV.

5. The difference ΔV between the self-consistent and the linear electrostatic potential energy along the filter/emitter region. (a) resonant filter/emitter A for V_{bias} = 0.10eV, and (b) resonant filter/emitter B for V_{bias} = 0.05eV.

6. The square of the wavefunction amplitude, $|\psi(z)|^2$, along the filter/emitter region. Both the self-consistent (solid line) and the non-self-consistent wavefunction (dotted line) are shown. The dashed lines represent boundaries between different aluminum composition layers of the filter/emitter. (a) Resonant filter/emitter A for V_{bias} =

0.10eV, and (b) resonant filter/emitter B for $V_{bias} = 0.05$eV.

7. Electron transmission characteristics of the nine layer filter/emitters as a function of the output kinetic energy for an applied bias potential energy of V_{bias}. The characteristics of the non-self-consistent (dotted line) and of the self-consistent electron potential energy (solid line) are shown. (a) Resonant filter/emitter A for $V_{bias} = 0.10$eV, and (b) resonant filter/emitter B for $V_{bias} = 0.05$eV.

8. Electron density distribution along the filter/emitter region using the self-consistent electron potential energy profile. The dashed lines represent boundaries between different aluminum composition layers of the filter/emitter. (a) Resonant filter/emitter A for $V_{bias} = 0.10$eV and $KE_{out} = 0.125$eV (resonant values), and (b) resonant filter/emitter B for $V_{bias} = 0.05$eV and $K_{out} = 0.0536$eV.

9. Current-voltage characteristics of the filter/emitters using the self-consistent (solid line) and the non-self-consistent electron potential energy profile (dotted line). (a) Resonant filter/emitter A, and (b) resonant filter/emitter B.

10. Temperature dependence of the I-V characteristics of resonant filter/emitter B for $T = 25$, 35, and 50 K. Both self-consistent (solid lines) and non-self-consistent (dotted lines) characteristics are included.

11. Characteristics of the nonresonant filter/emitter C. (a) The electron potential energy profile; self-consistent potential (solid line) and non-self-consistent (dotted line) potential energy profile along the filter/emitter region for $V_{bias} = 0.05$eV. (b) The difference ΔV between the self-consistent and non-self-consistent (linear) electron potential energy profiles along the filter/emitter region for $V_{bias} = 0.05$eV. (c) The square of the wavefunction amplitude distribution for $V_{bias} = 0.05$eV and $KE_{out} = 0.0536$eV. The dashed lines represent boundaries between the layers of differing aluminum composition of the filter/emitter. (d) The electron transmission

characteristics for both the self-consistent (solid line) and the non-self-consistent (dotted line) electron potential energy profile for $V_{bias} = 0.05$eV. (e) The self-consistent electron density distribution along the nonresonant filter/emitter for $V_{bias} = 0.05$eV. The dashed lines represent boundaries between different aluminum composition layers of the filter/emitter. (e) Current-voltage characteristics of the nonresonant filter/emitter using the self-consistent (solid line) and the non-self-consistent (dotted line) electron potential energy profile.

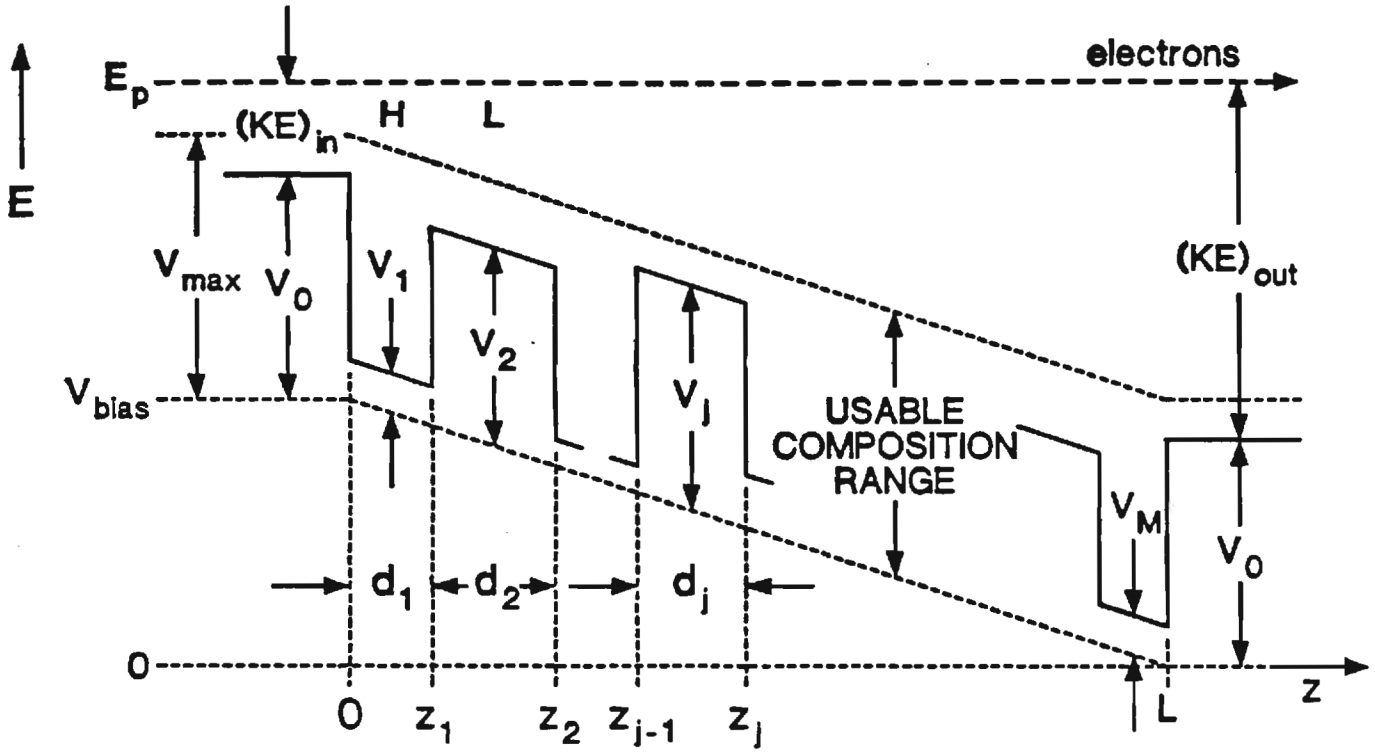
E
E_p
electrons
H
L
$(KE)_{in}$
V_{max}
V_0
V_1
V_2
V_j
V_{bias}
USABLE
COMPOSITION
RANGE
V_M
V_0
$(KE)_{out}$
d_1
d_2
d_j
0
0
z_1
z_2
z_{j-1}
z_j
L
z

Fig. 1

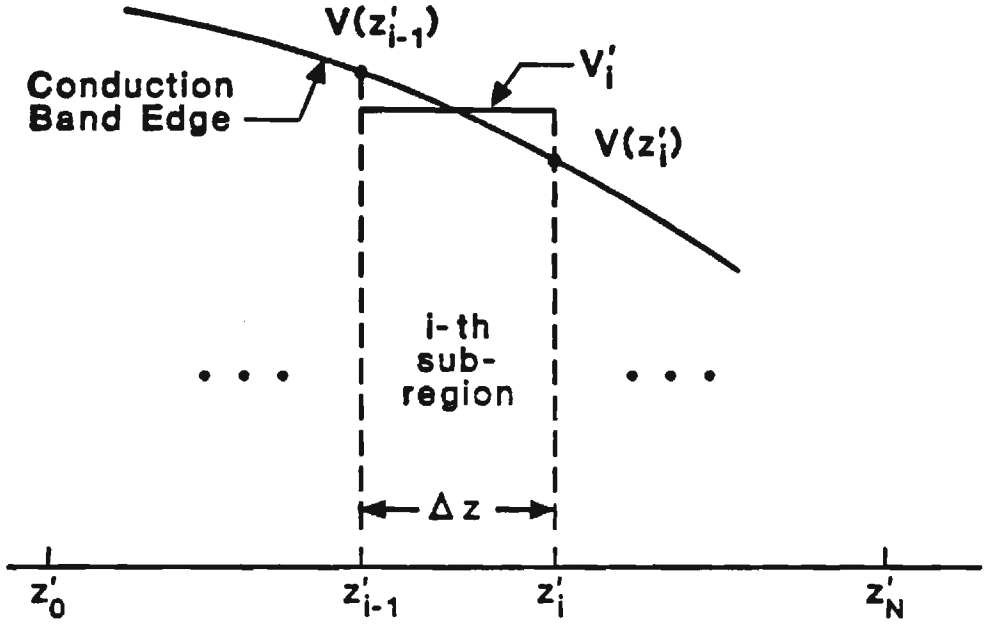
$V(z'_{i-1})$
V'_i
Conduction Band Edge
$V(z'_i)$
i-th sub-region
Δz
z'_0
z'_{i-1}
z'_i
z'_N

Fig. 2

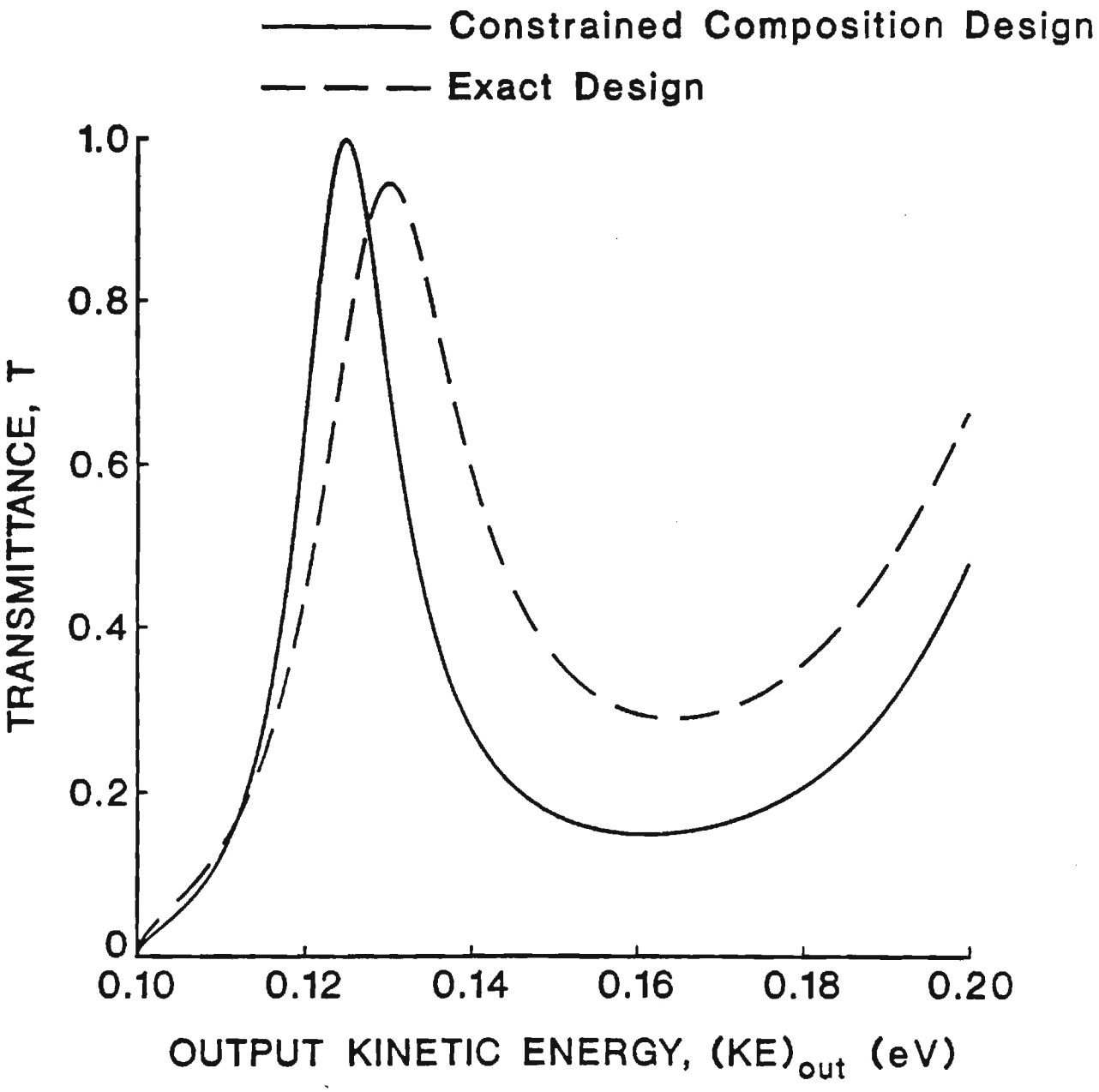
Constrained Composition Design
Exact Design
1.0
0.8
0.6
0.4
0.2
0
TRANSMITTANCE, T
0.10
0.12
0.14
0.16
0.18
0.20
OUTPUT KINETIC ENERGY, (KE)out (eV)

Fig. 3a

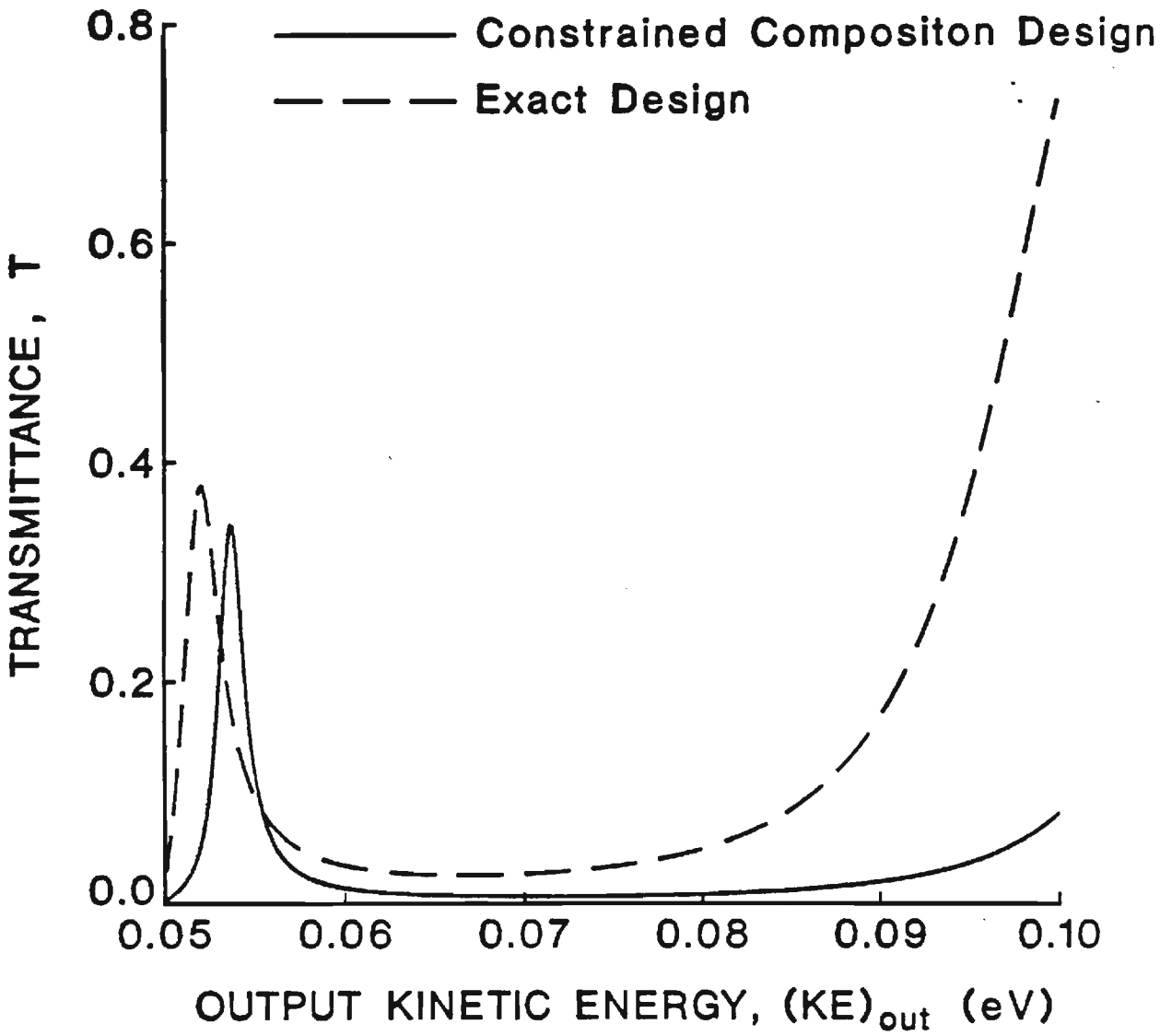
Constrained Compositon Design
Exact Design
TRANSMITTANCE, T
0.8
0.6
0.4
0.2
0.0
0.05
0.06
0.07
0.08
0.09
0.10
OUTPUT KINETIC ENERGY, (KE)out (eV)

Fig. 3b

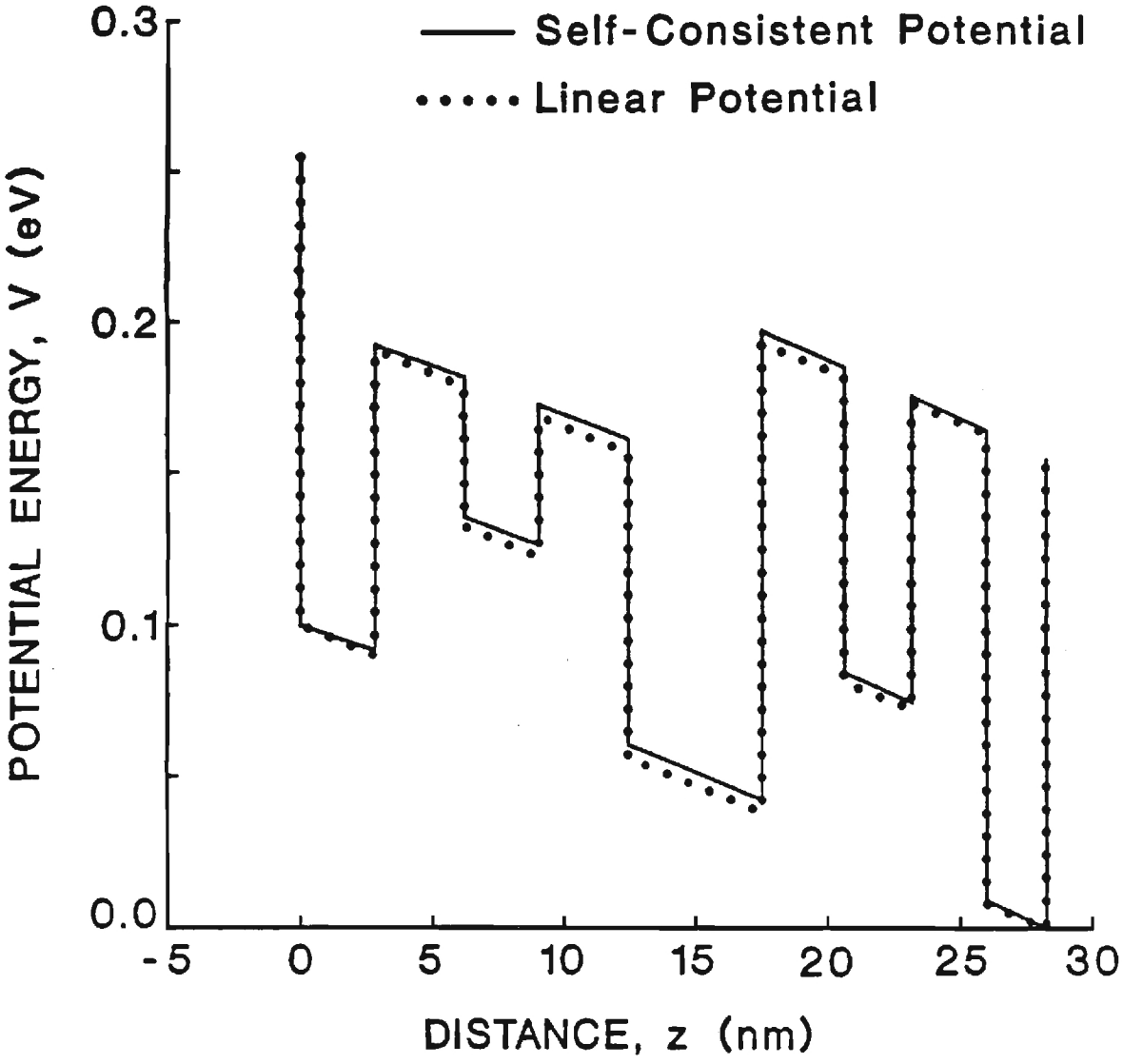
Self-Consistent Potential
Linear Potential
POTENTIAL ENERGY, V (eV)
0.3
0.2
0.1
0.0
-5
0
5
10
15
20
25
30
DISTANCE, z (nm)

Fig. 4a

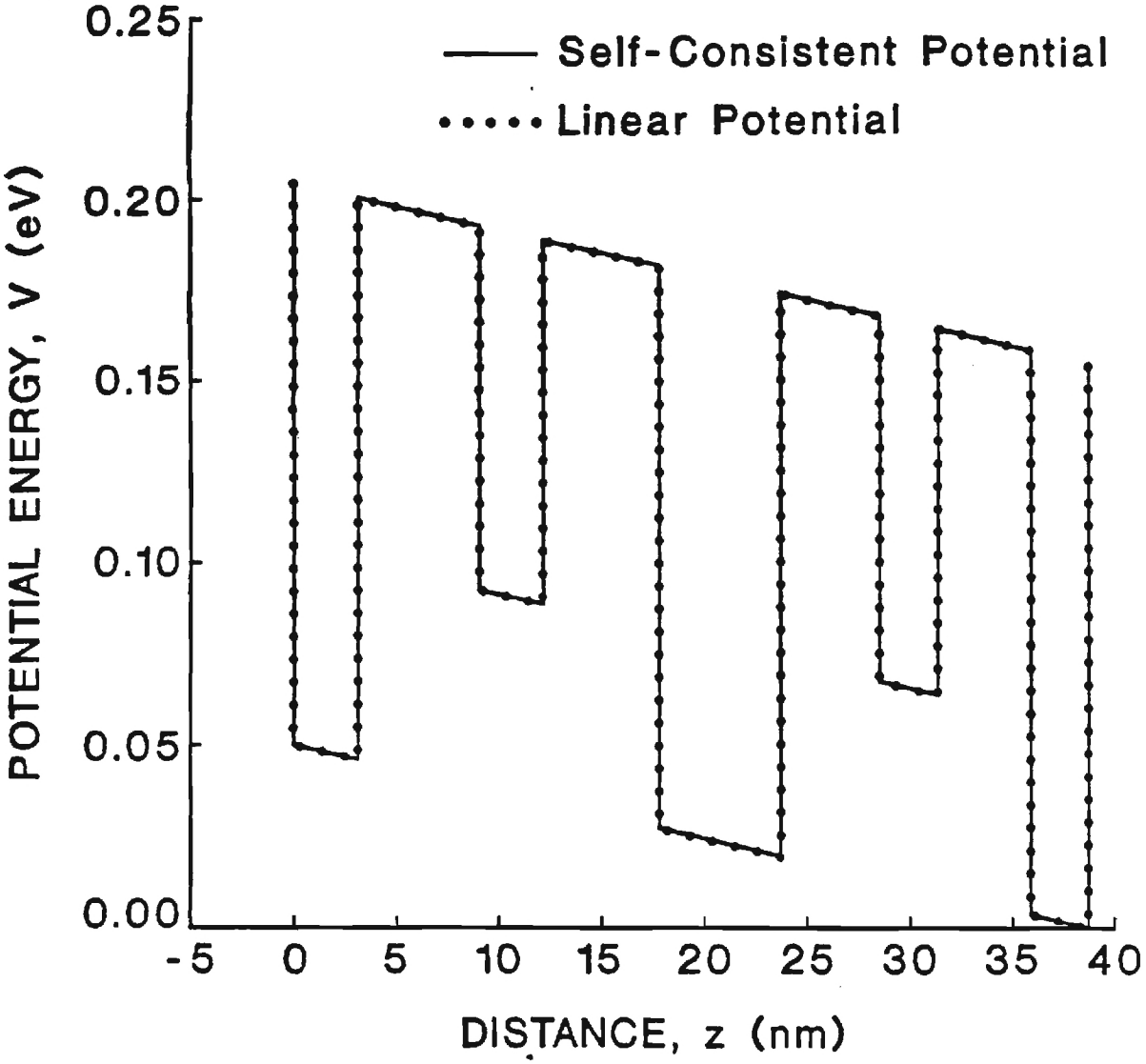
Self-Consistent Potential
Linear Potential
POTENTIAL ENERGY, V (eV)
0.25
0.20
0.15
0.10
0.05
0.00
-5
0
5
10
15
20
25
30
35
40
DISTANCE, z (nm)

Fig. 4b

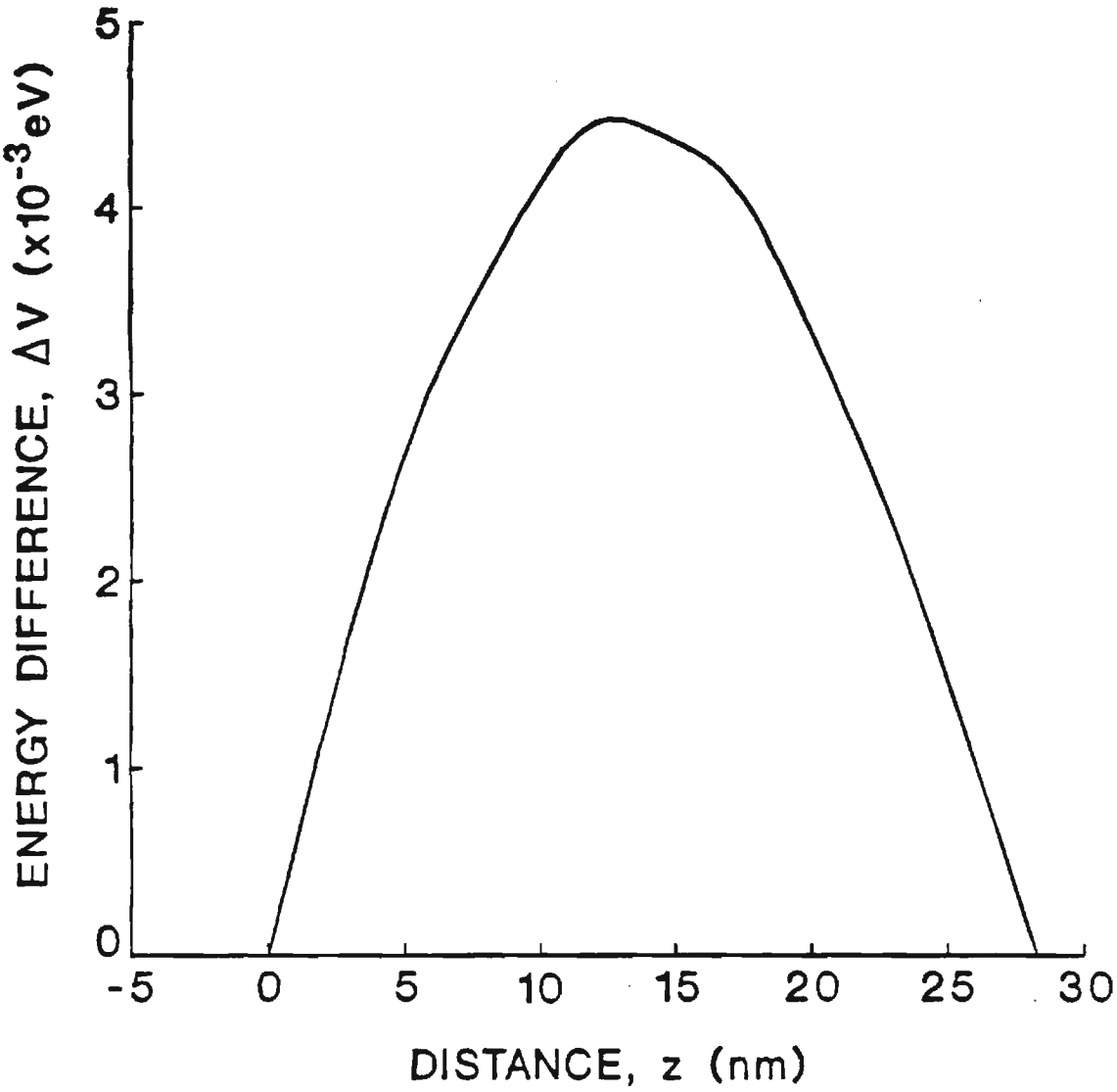
ENERGY DIFFERENCE, ΔV (x10^{-3}eV)
5
4
3
2
1
0
-5
0
5
10
15
20
25
30
DISTANCE, z (nm)

Fig. 5a

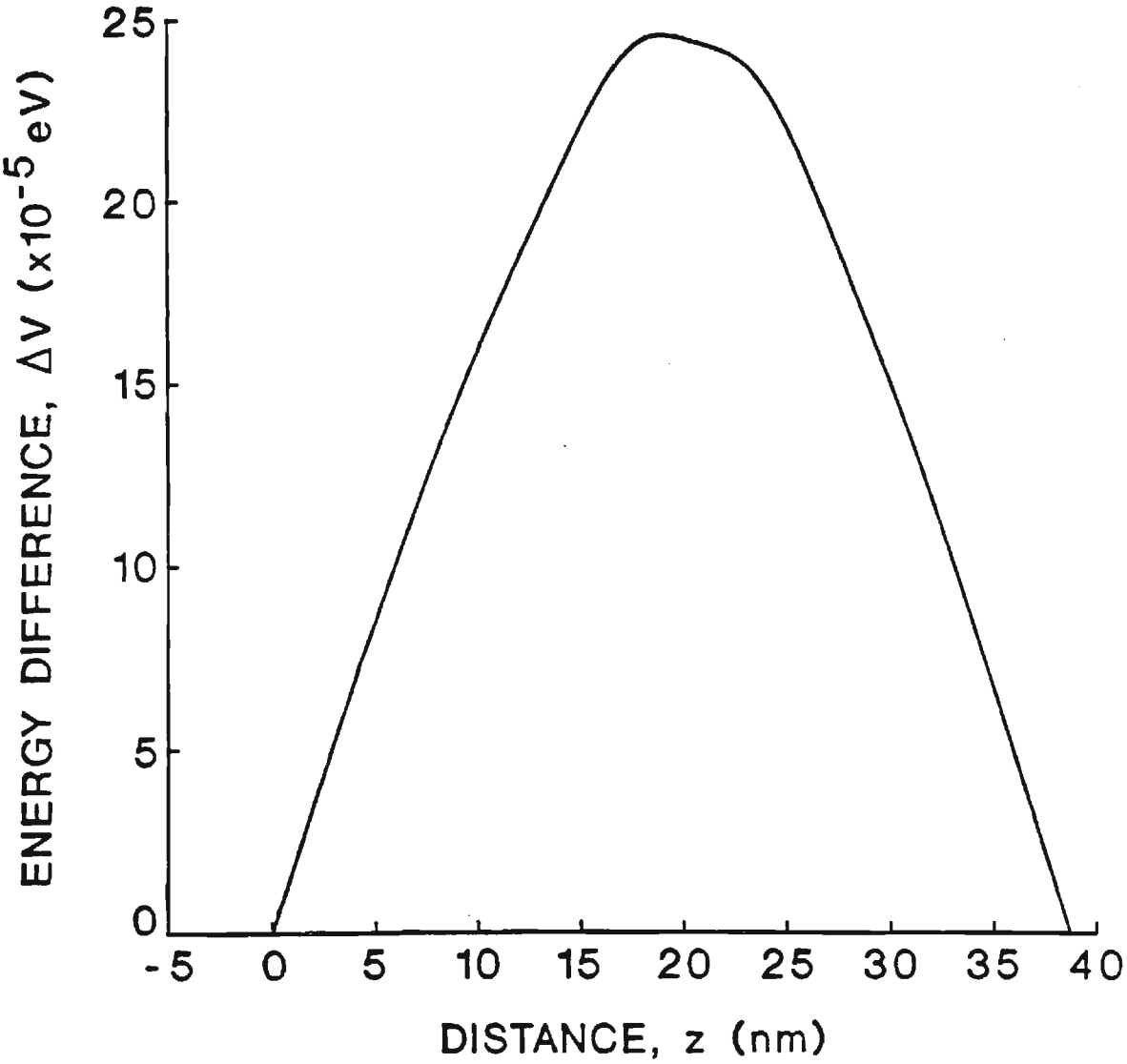
ENERGY DIFFERENCE, ΔV (x10^{-5} eV)
25
20
15
10
5
0
-5
0
5
10
15
20
25
30
35
40
DISTANCE, z (nm)

Fig. 5b

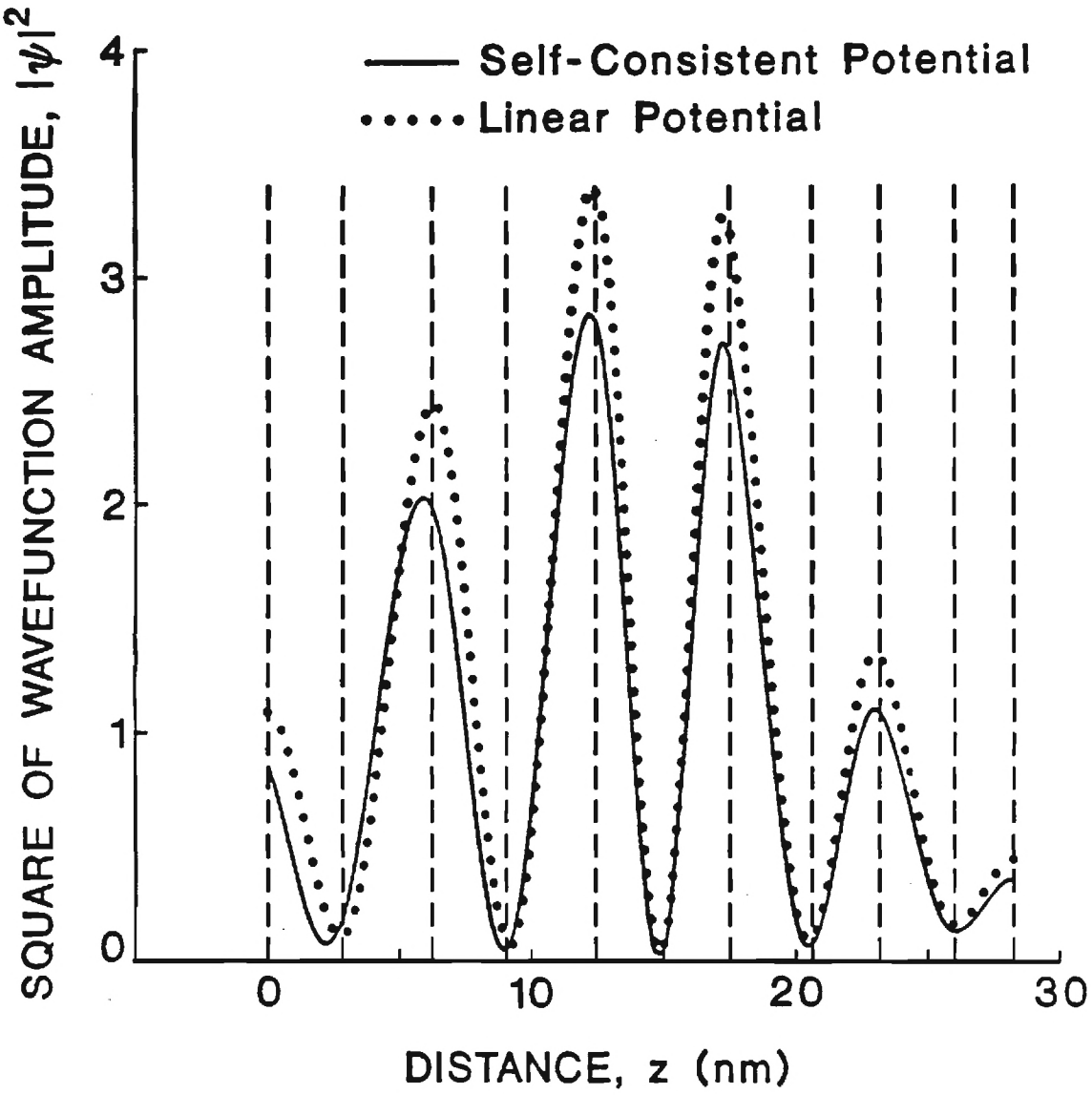
SQUARE OF WAVEFUNCTION AMPLITUDE, $|\psi|^2$
Self-Consistent Potential
Linear Potential
4
3
2
1
0
0
10
20
30
DISTANCE, z (nm)

Fig. 6a

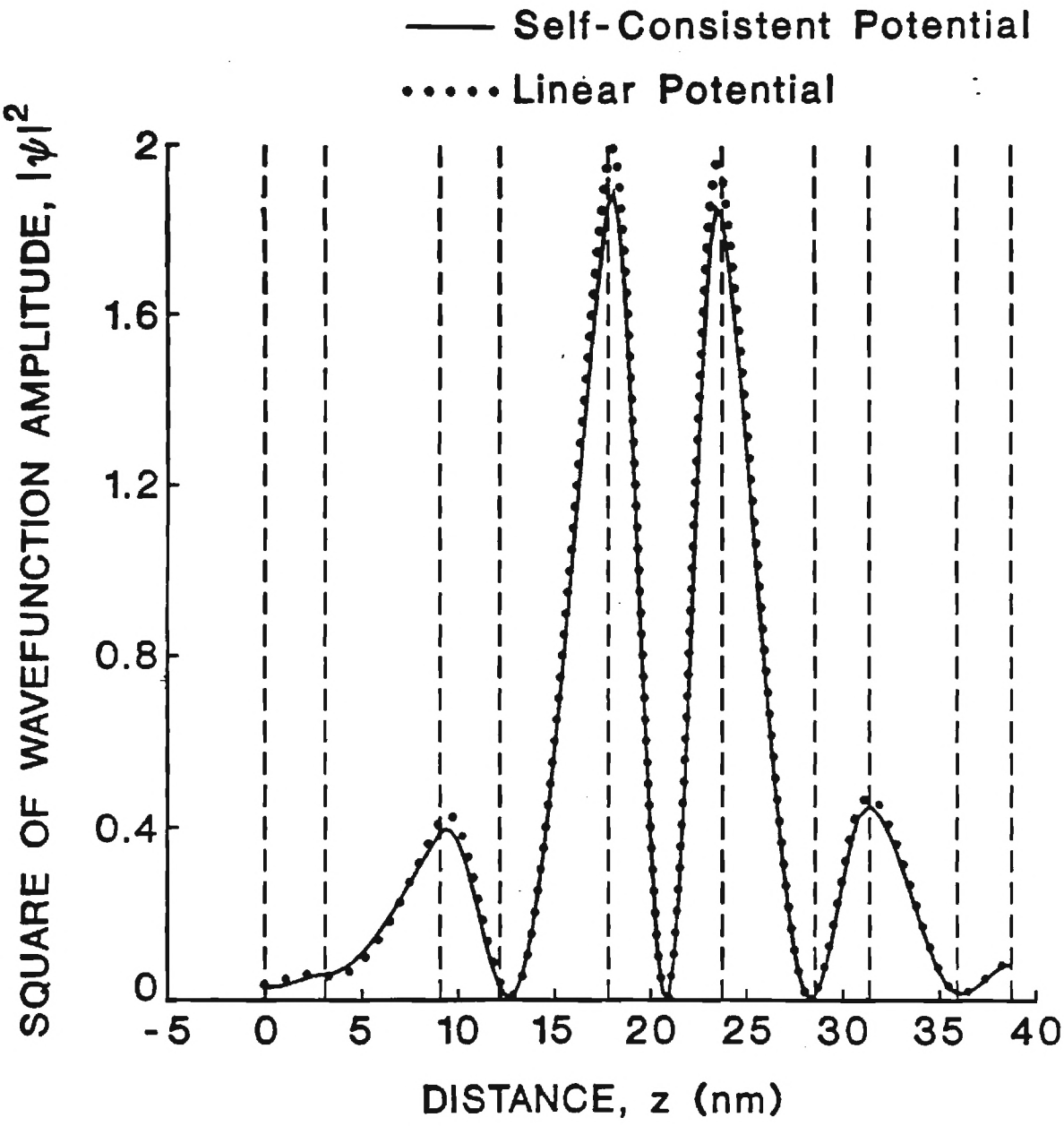
Self-Consistent Potential
Linear Potential
SQUARE OF WAVEFUNCTION AMPLITUDE, $|\psi|^2$
2
1.6
1.2
0.8
0.4
0
-5
0
5
10
15
20
25
30
35
40
DISTANCE, z (nm)

Fig. 6b

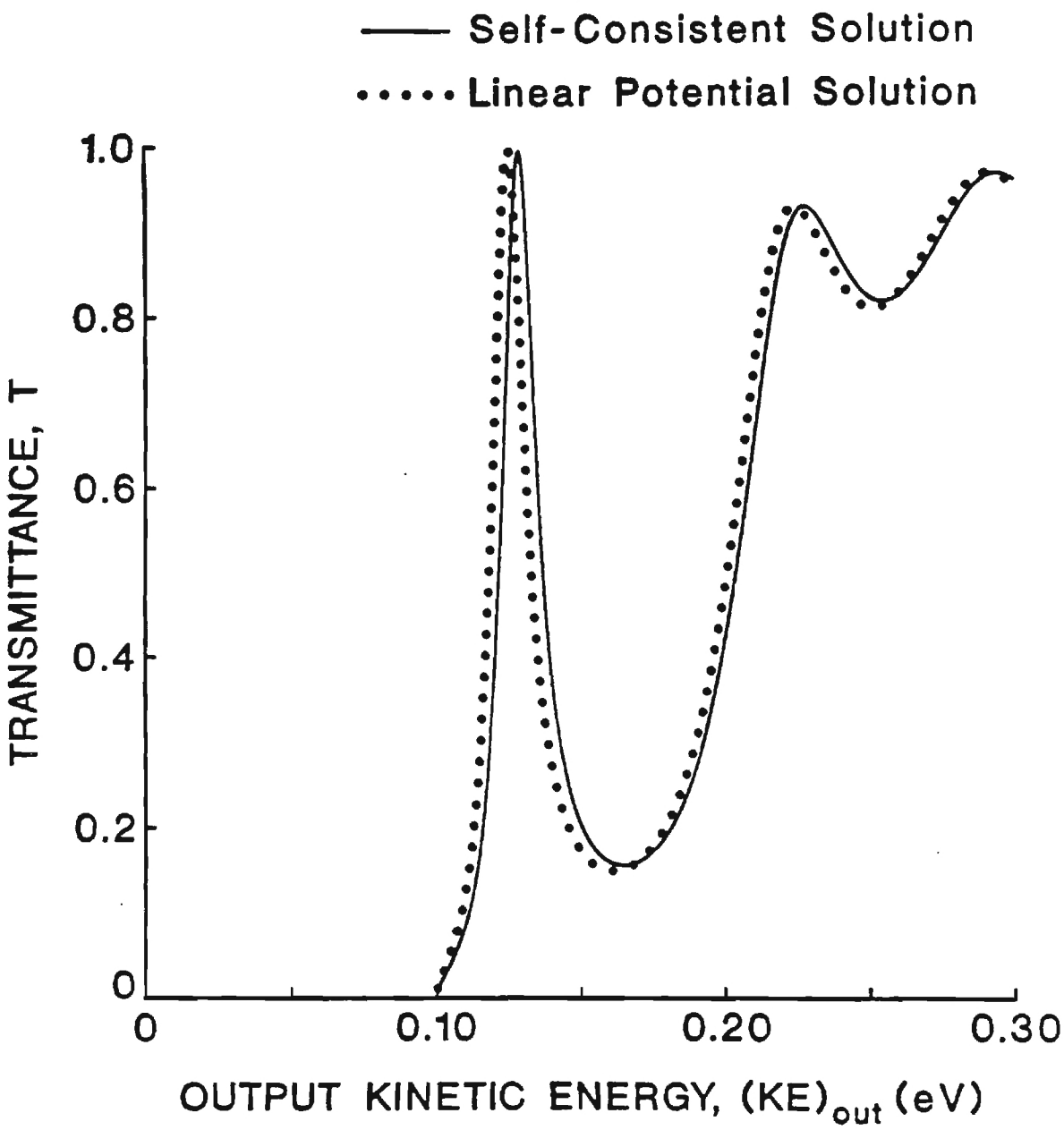
Self-Consistent Solution
Linear Potential Solution
1.0
0.8
0.6
0.4
0.2
0
TRANSMITTANCE, T
0
0.10
0.20
0.30
OUTPUT KINETIC ENERGY, (KE)out (eV)

Fig. 7a

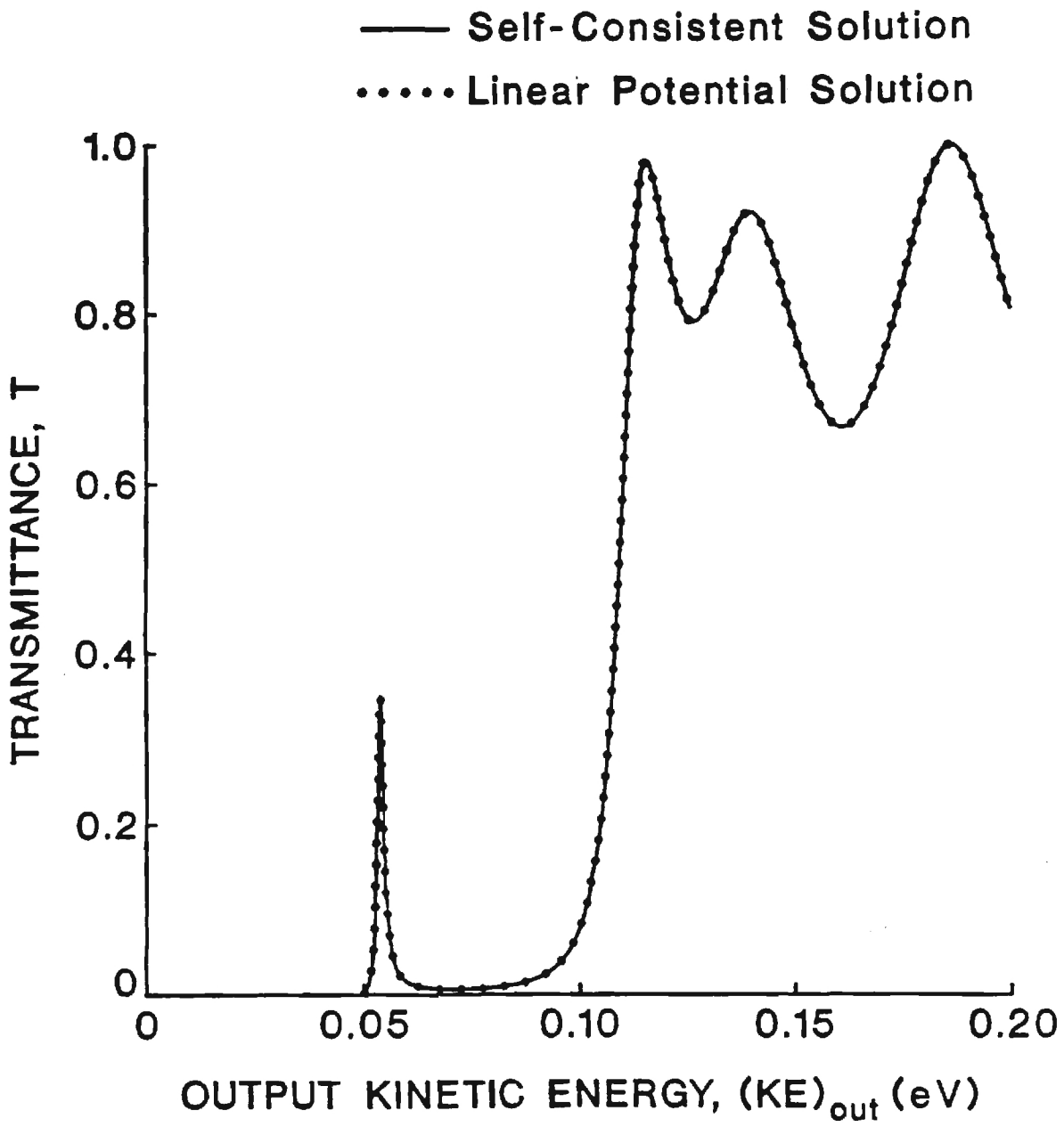
Self-Consistent Solution
Linear Potential Solution
1.0
0.8
0.6
0.4
0.2
0
TRANSMITTANCE, T
0
0.05
0.10
0.15
0.20
OUTPUT KINETIC ENERGY, (KE)out (eV)

Fig. 7b

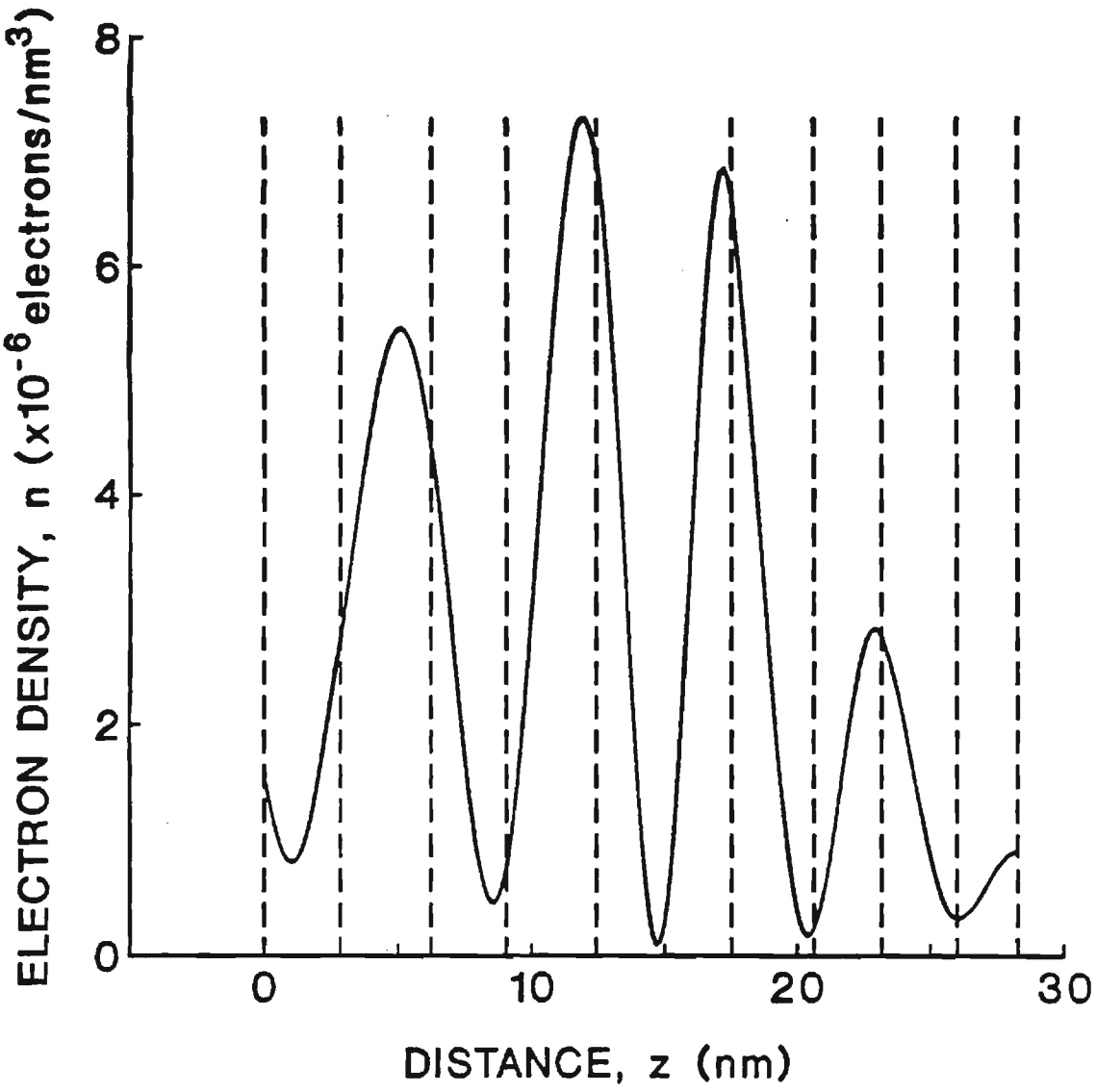
ELECTRON DENSITY, n (x10^{-6}electrons/nm^3)
8
6
4
2
0
0
10
20
30
DISTANCE, z (nm)

Fig. 8a

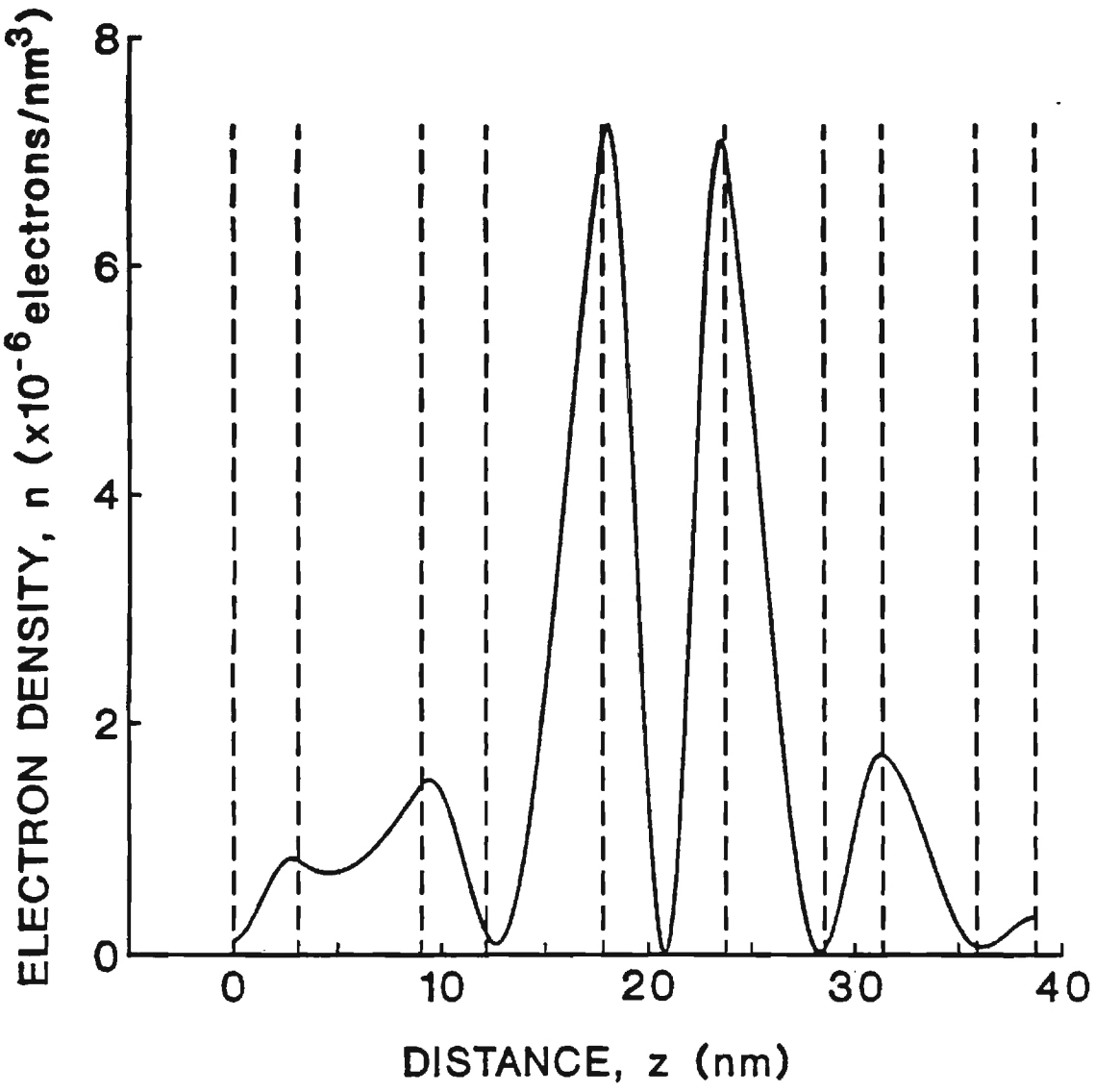
ELECTRON DENSITY, n (x10^{-6}electrons/nm^3)
8
6
4
2
0
0
10
20
30
40
DISTANCE, z (nm)

Fig. 8b

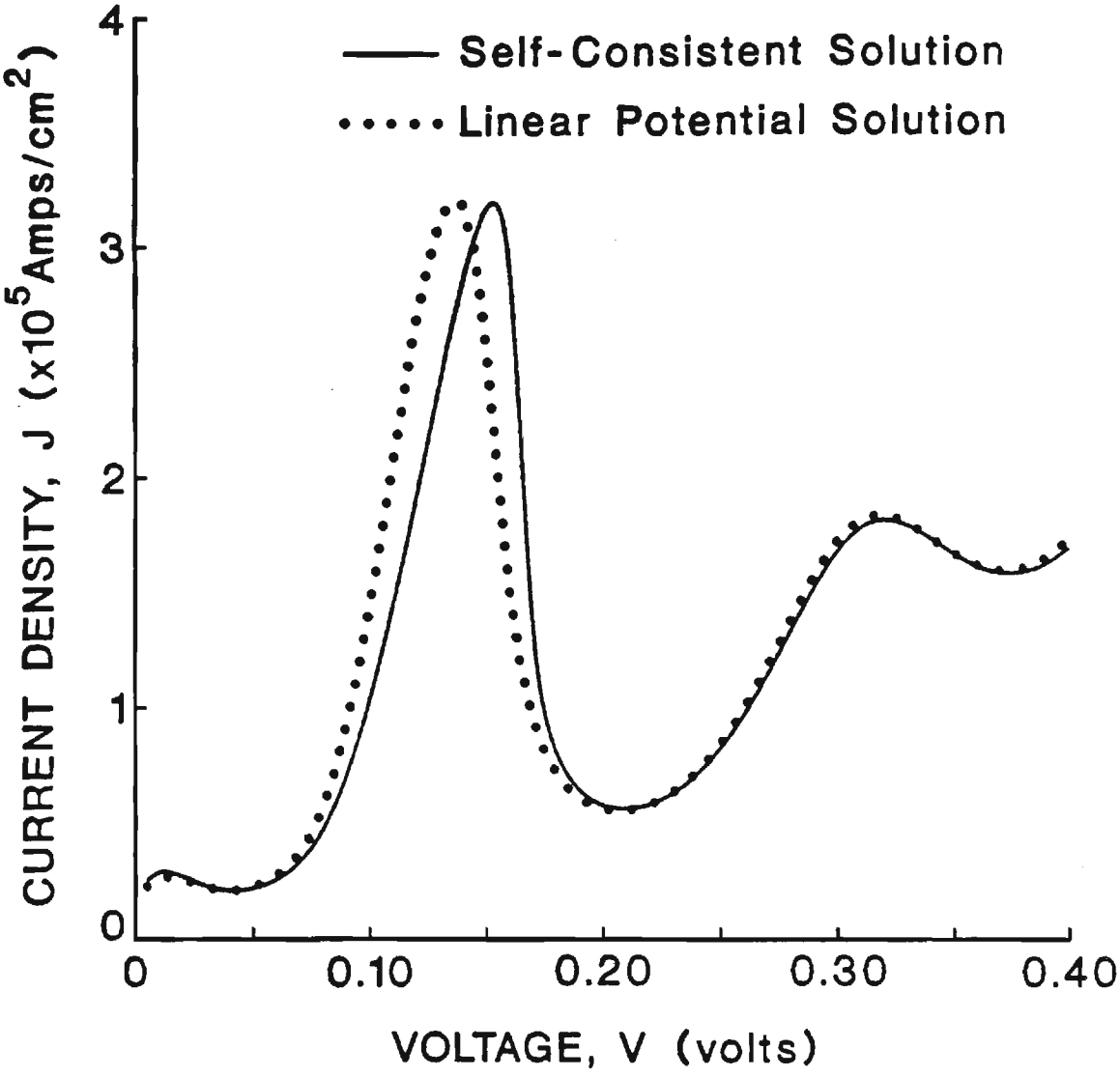
Self-Consistent Solution
Linear Potential Solution
CURRENT DENSITY, J (x10^5 Amps/cm^2)
4
3
2
1
0
0
0.10
0.20
0.30
0.40
VOLTAGE, V (volts)

Fig. 9a

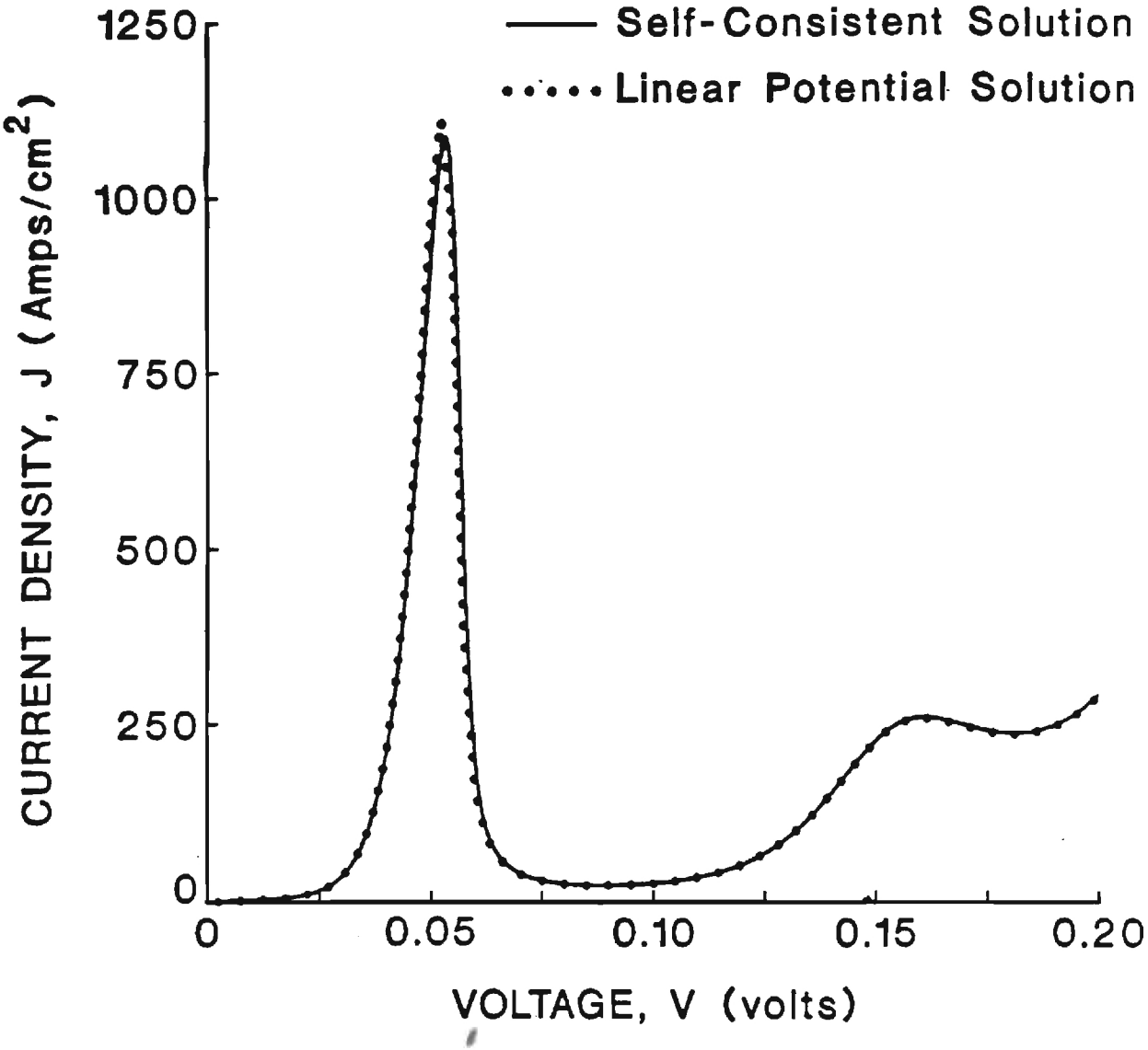
Self-Consistent Solution
Linear Potential Solution
CURRENT DENSITY, J (Amps/cm²)
1250
1000
750
500
250
0
0
0.05
0.10
0.15
0.20
VOLTAGE, V (volts)

Fig. 9b

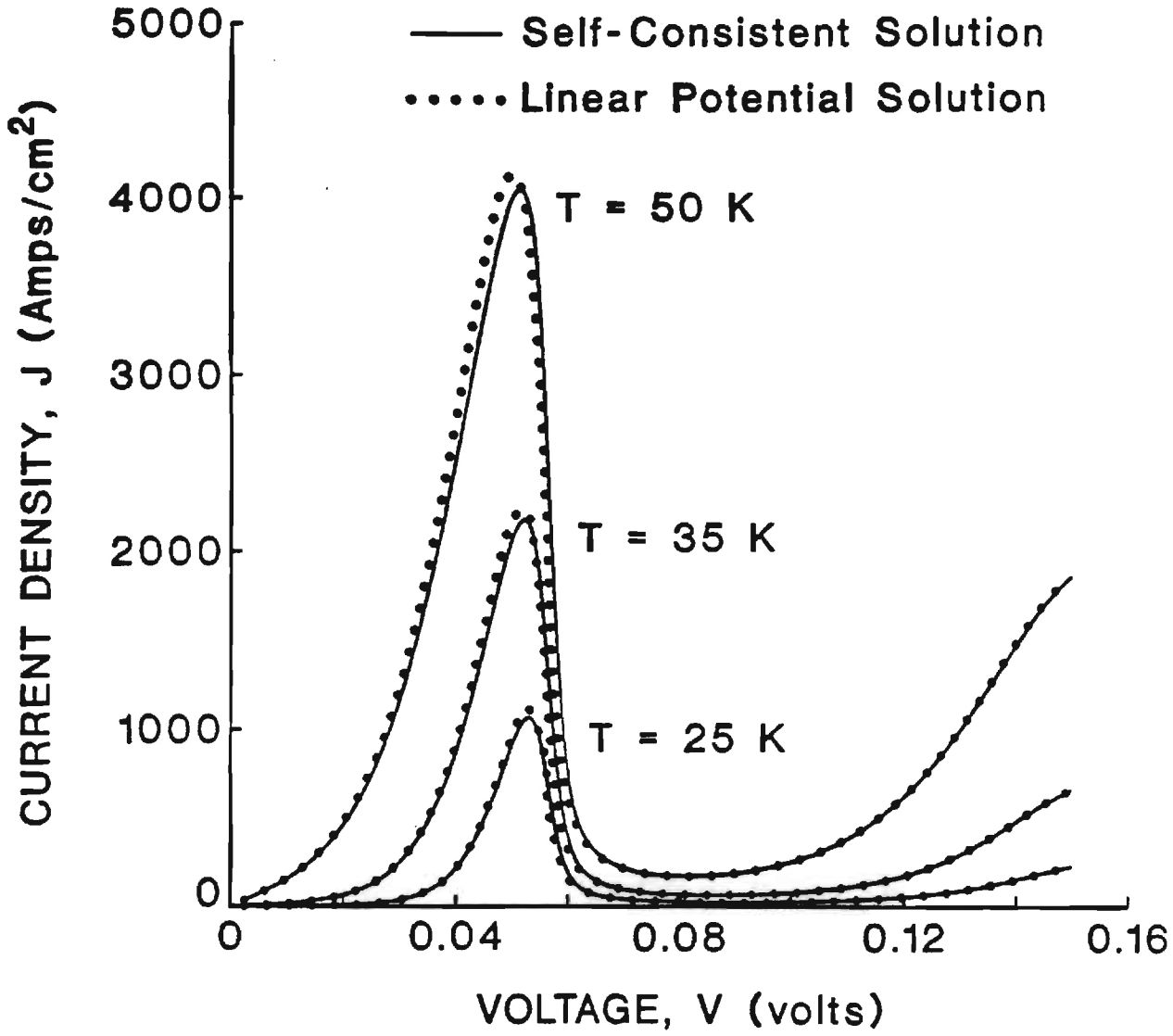
5000
4000
3000
2000
1000
0
CURRENT DENSITY, J (Amps/cm²)
Self-Consistent Solution
Linear Potential Solution
T = 50 K
T = 35 K
T = 25 K
0
0.04
0.08
0.12
0.16
VOLTAGE, V (volts)

Fig. 10

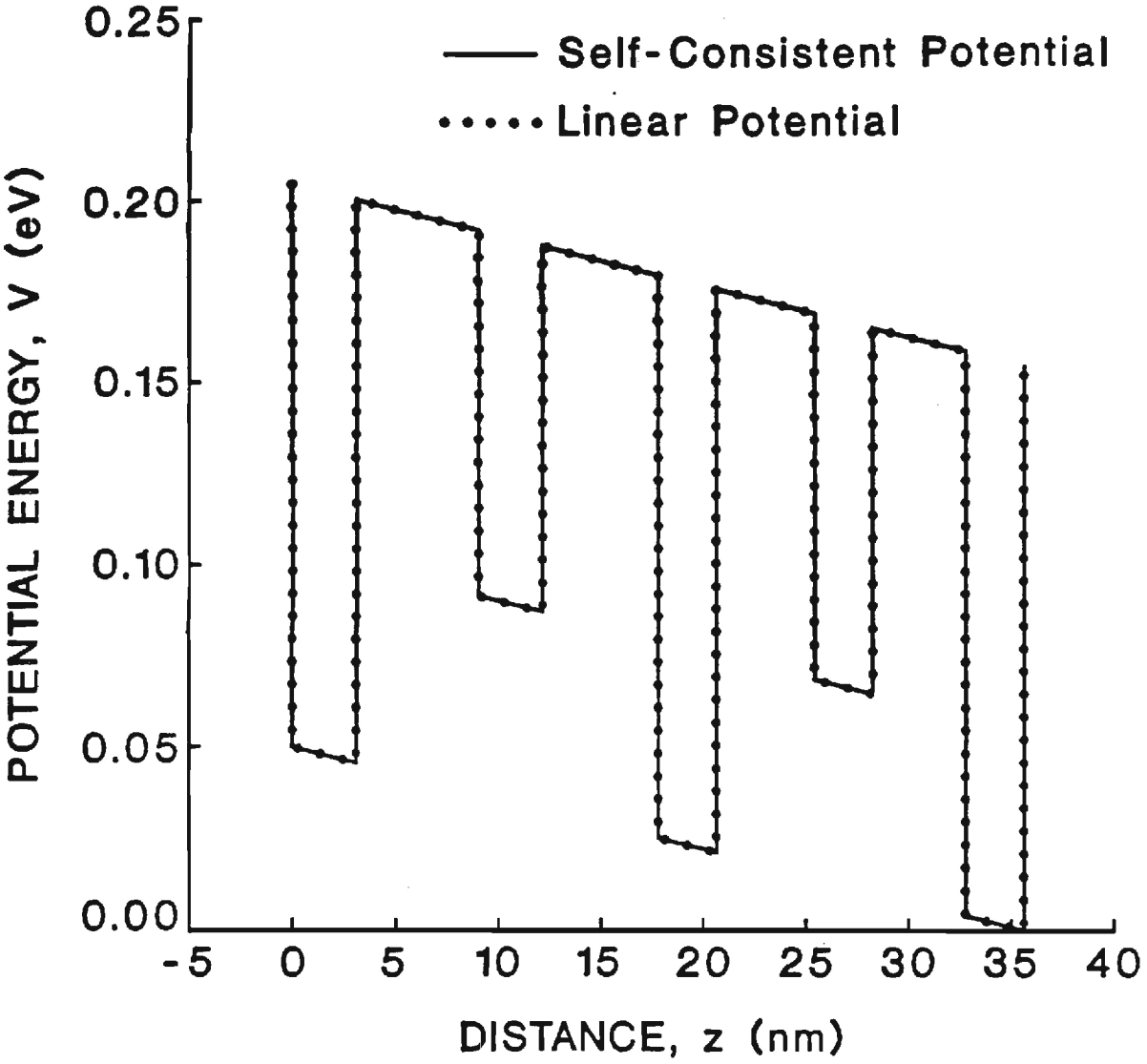
Self-Consistent Potential
Linear Potential
POTENTIAL ENERGY, V (eV)
0.25
0.20
0.15
0.10
0.05
0.00
-5
0
5
10
15
20
25
30
35
40
DISTANCE, z (nm)

Fig. 11a

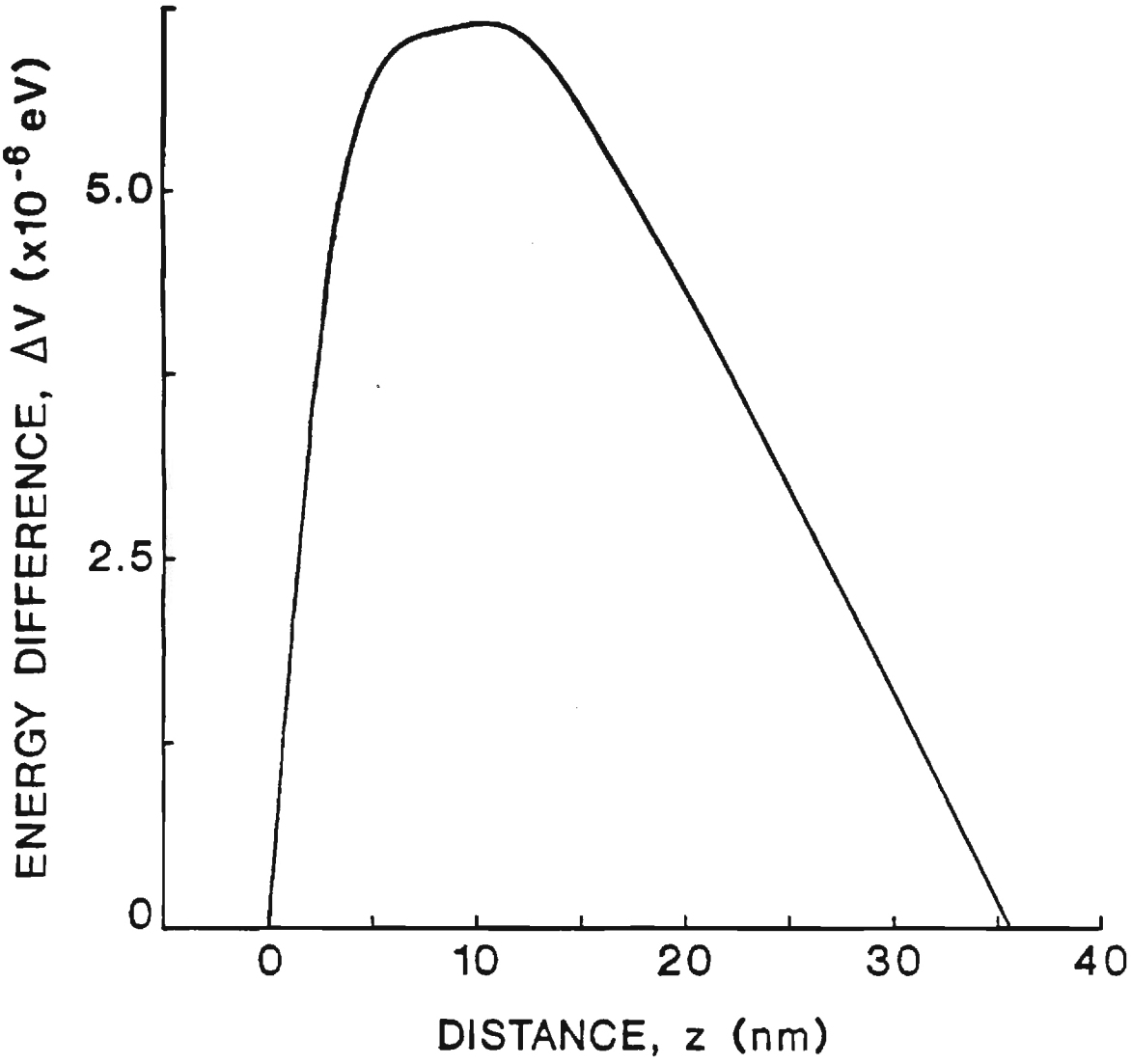

Fig. 11 b

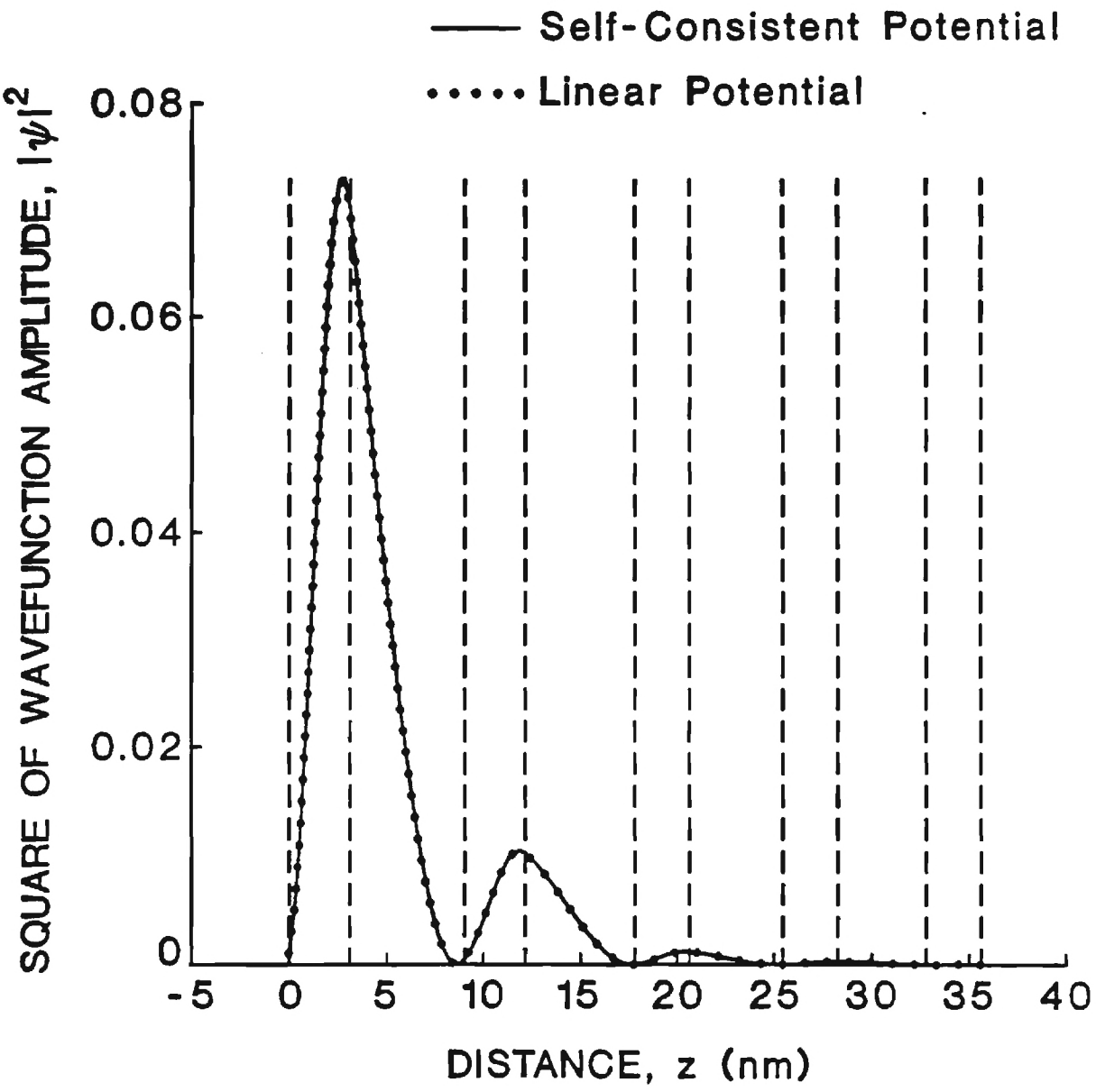
Self-Consistent Potential
Linear Potential
SQUARE OF WAVEFUNCTION AMPLITUDE, $|\psi|^2$
0.08
0.06
0.04
0.02
0
-5
0
5
10
15
20
25
30
35
40
DISTANCE, z (nm)

Fig. 11c

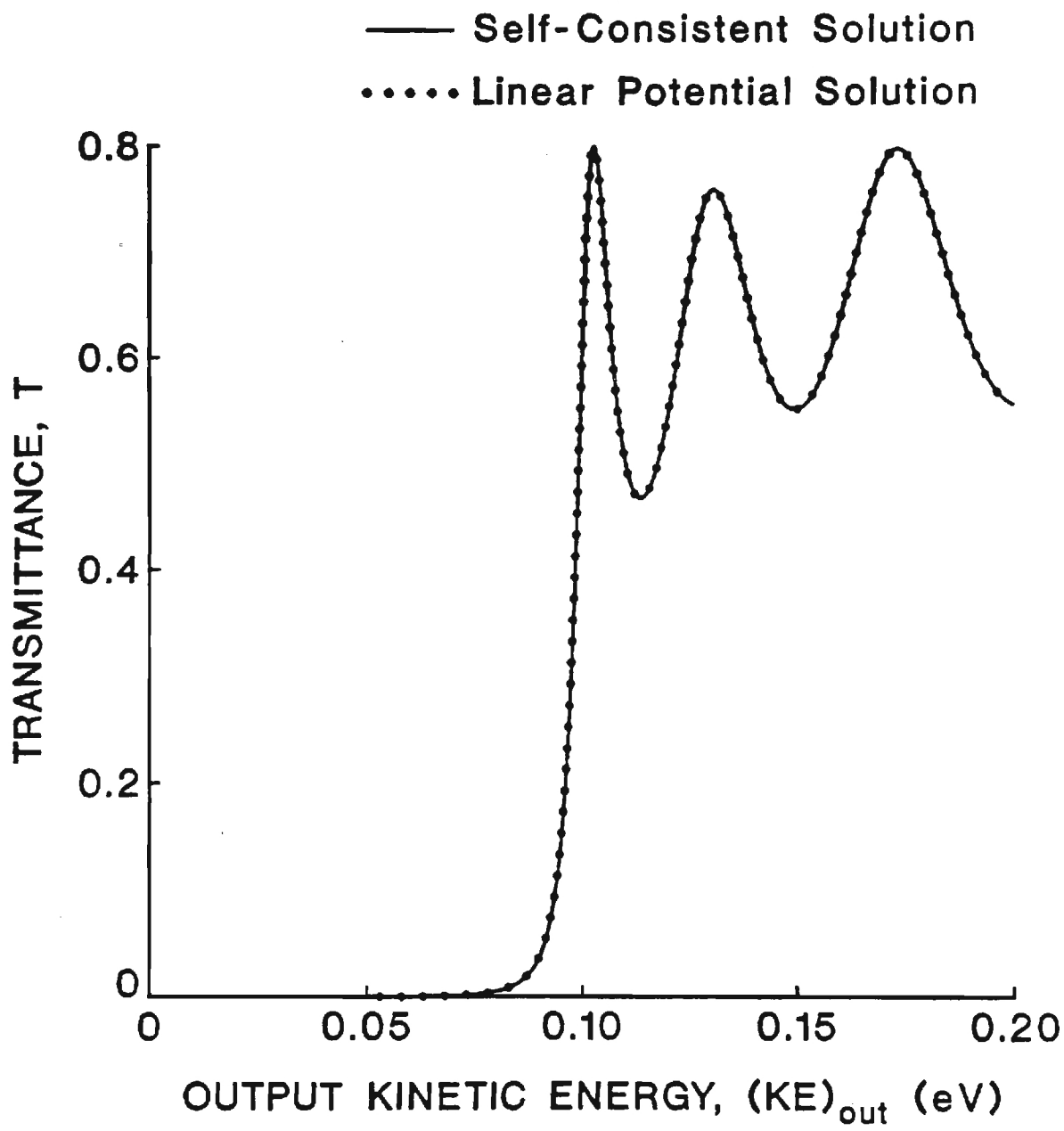
Self-Consistent Solution
Linear Potential Solution
TRANSMITTANCE, T
0.8
0.6
0.4
0.2
0
0
0.05
0.10
0.15
0.20
OUTPUT KINETIC ENERGY, (KE)out (eV)

Fig. 11d

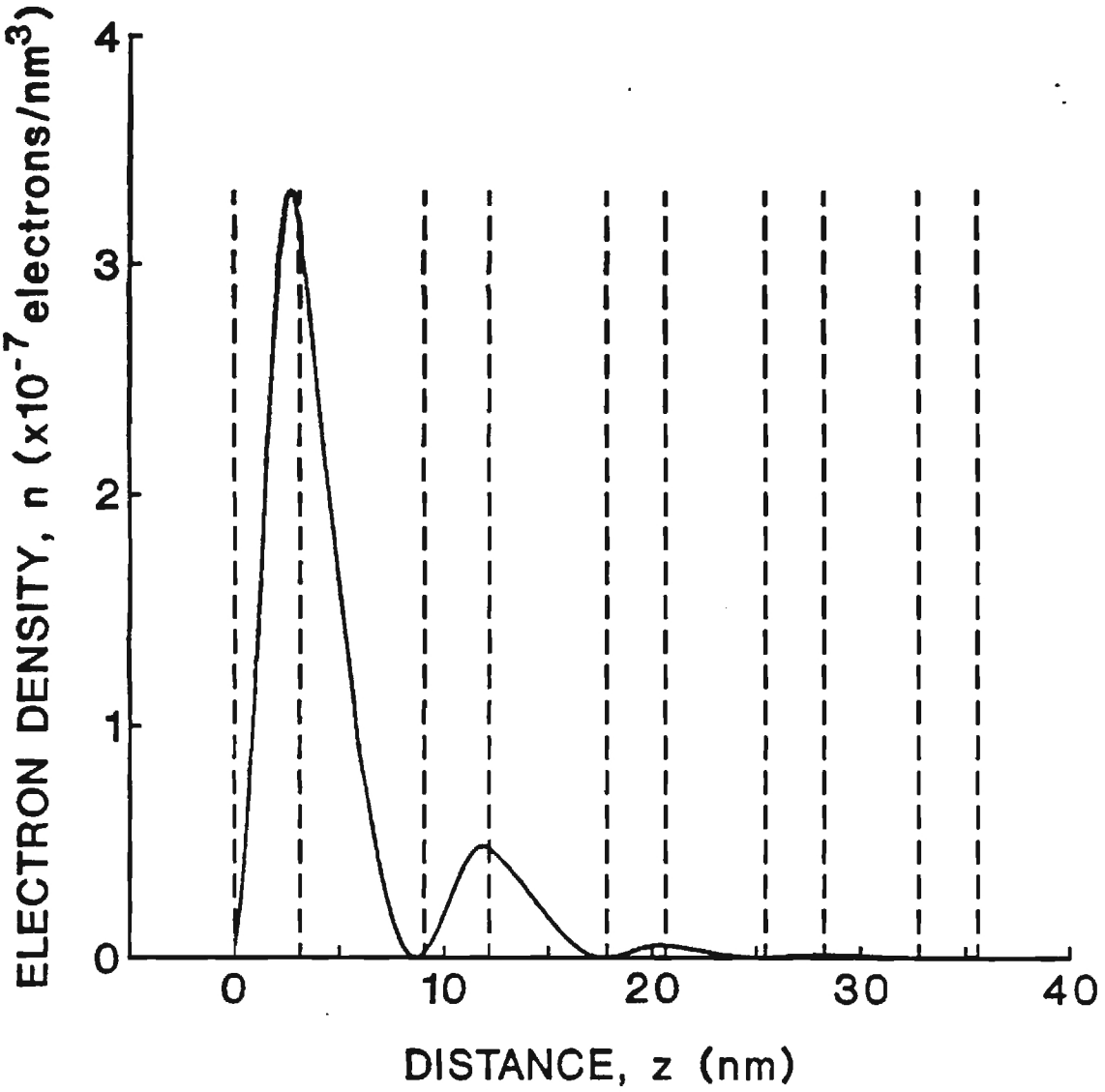
ELECTRON DENSITY, n (x10^{-7} electrons/nm^3)
4
3
2
1
0
0
10
20
30
40
DISTANCE, z (nm)

Fig. 11e

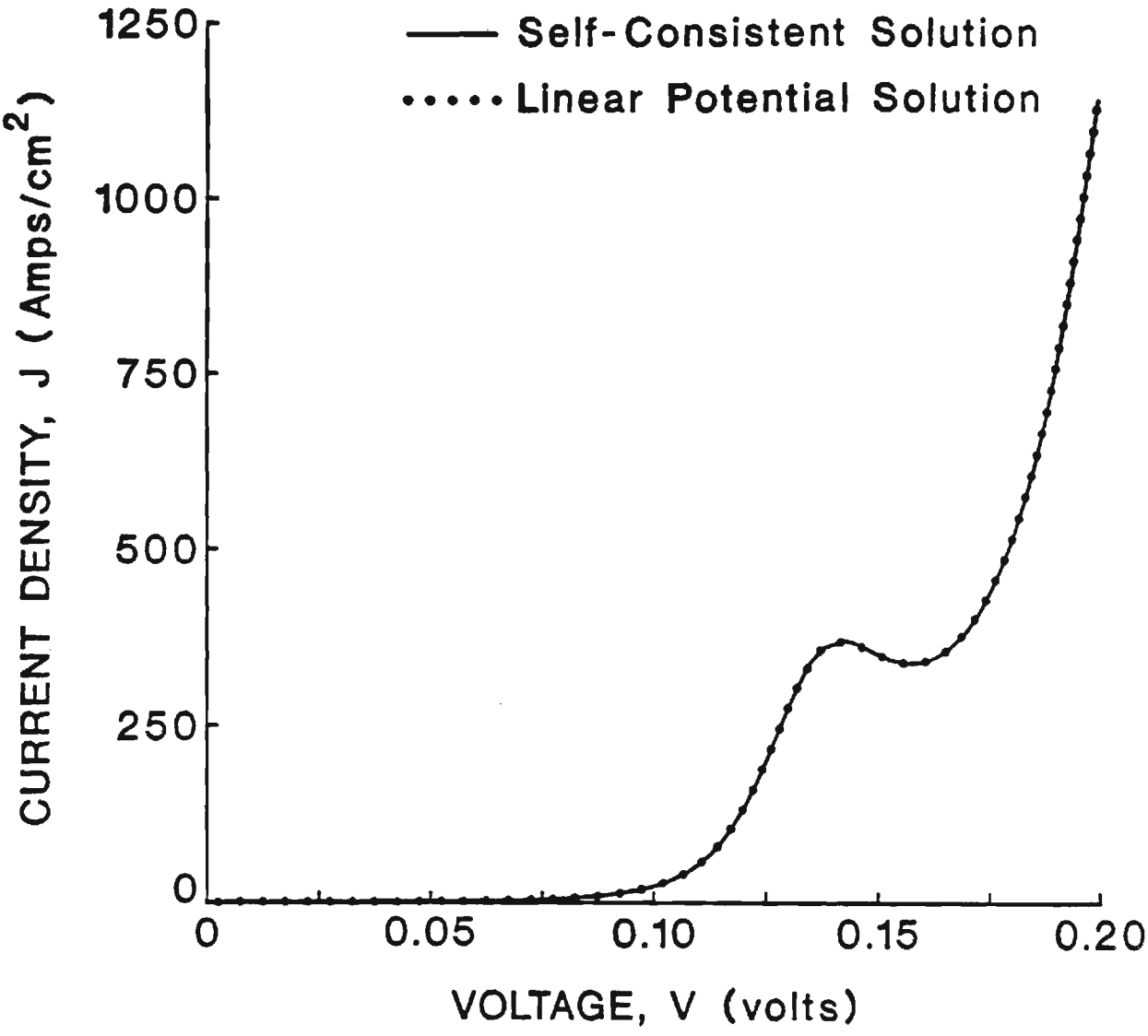
Self-Consistent Solution
Linear Potential Solution
CURRENT DENSITY, J (Amps/cm^2)
1250
1000
750
500
250
0
0
0.05
0.10
0.15
0.20
VOLTAGE, V (volts)

Fig. 11f

APPENDIX B

CONFERENCE PAPERS PUBLISHED AND PRESENTED DURING THE 08-15-89/08-15-90 PERIOD

- E. N. Glytsis, T. K. Gaylord, and K. F. Brennan, "Semiconductor biased superlattices as electron wave interference filter/emitters," at Annual Meeting of the Optical Society of America, Orlando, FL, Oct. 15–20, 1989, and (Abstract) *J. Opt. Soc. Am. A*, vol. 6, no. 13, pg. 32, Dec. 1989.

- T. K. Gaylord, E. N. Glytsis, and K. F. Brennan, "Guided electron waves in semiconductor quantum wells," at Annual Meeting of the Optical Society of America, Orlando, FL, Oct. 15–20, 1989, and (Abstract) *J. Opt. Soc. Am. A*, vol. 6, no. 13, pg. 21, Dec. 1989.

- K. Diff, K. F. Brennan, T. K. Gaylord, and E. N. Glytsis, "Wavepacket propagation in semiconductor superlattice interference filters," *Bull. Amer. Phys. Soc.*, vol. 35, pg. 825, Mar. 1990.

SEMICONDUCTOR BIASED SUPERLATTICES AS ELECTRON WAVE INTERFERENCE FILTER/EMITTERS

E. N. Glytsis, T. K. Gaylord, and K. F. Brennan
School of Electrical Engineering
and Microelectronics Research Center
Georgia Institute of Technology

OUTLINE

1. Introduction

2. Previous Work

3. Quantum Wave Optics

4. Theory and Design

5. Example Cases

6. Summary

INTRODUCTION

1. Ultra-Small Devices

2. Quantum Interference

3. Electron Wave Optics

UNBIASED SUPERLATTICE ELECTRON WAVE INTERFERENCE FILTER

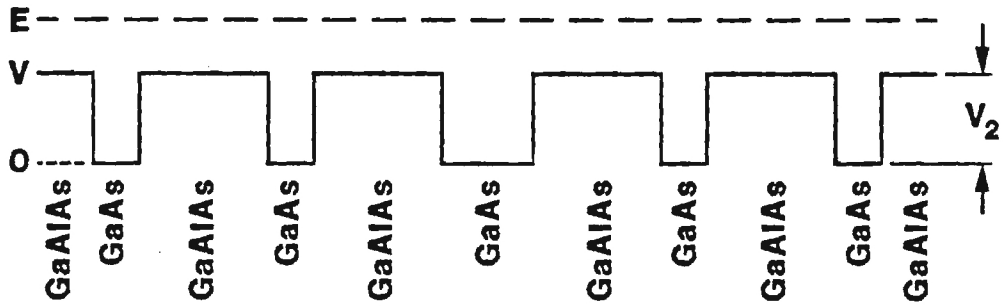

T. K. Gaylord, E. N. Glytsis, and K. F. Brennan, J. Appl. Phys., 65, 2535 (1989).

QUANTUM WAVE OPTICS

1. Electron Wave Phase Refractive Index

$$n_e(\text{phase}) \propto [m^* (E - V)]^{1/2}$$

2. Electron Wave Amplitude Refractive Index

$$n_e(\text{amplitude}) \propto [(E - V)/m^*]^{1/2}$$

3. Optical Designs Mapped into Electron Wave Designs

T. K. Gaylord and K. F. Brennan, Appl. Phys. Lett., 53, 2047 (1988).

T. K. Gaylord and K. F. Brennan, J. Appl. Phys., 65, 814 (1989).

THEORY AND DESIGN OF SEMICONDUCTOR ELECTRON WAVE FILTER/EMITTERS

1. Thin Film Optical Interference Filters

2. Objectives
   - Fabry-Perot type filter
   - Calculation of layer thicknesses
   - Calculation of layer compositions

3. Given Parameters
   - Bias voltage
   - Electron Energy

4. Constraints
   - Layer thicknesses integer number of monolayers
   - Restricted usable composition range
   - Device length of the order of electron coherence length
   - Phonon Scattering

SEMICONDUCTOR ELECTRON WAVE FILTER/EMITTER

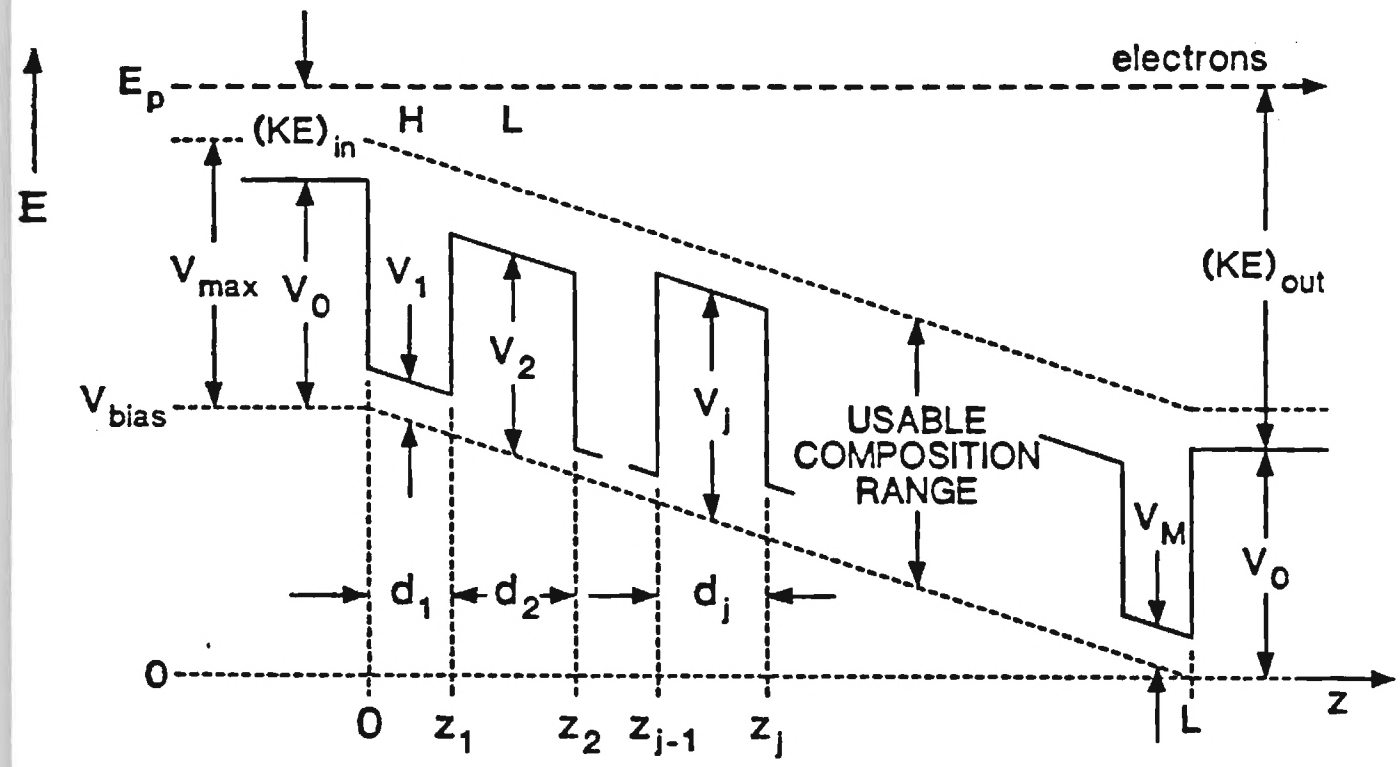

E. N. Glytsis, T. K. Gaylord, and K. F. Brennan, J. Appl. Phys., 66, 1494 (1989).

DESIGN PROCEDURE

1. Estimate layer thicknesses and compositions using unbiased filter design[a]

2. Use an iterative technique[b] to determine final layer thicknesses and compositions

a. T. K. Gaylord, E. N. Glytsis, and K. F. Brennan, J. Appl. Phys., 65, 2535 (1989).

b. E. N. Glytsis, T. K. Gaylord, and K. F. Brennan, J. Appl. Phys., (1989) (accepted).

BIAS FILTER/EMITTER DESIGNS

($Ga_{1-x}Al_xAs$)

Surrounding Material $Ga_{0.55}Al_{0.45}As$

Design Filter/Emitter Electron Energy = 0.20eV

Design Bias Potential Energy = 0.10eV

Layer	$M = 9$		$M = 13$		$M = 17$	
j	p_j	x_j	p_j	x_j	p_j	x_j
1	7	0.2222	7	0.2194	7	0.2178
2	9	0.4151	9	0.4081	9	0.4041
3	7	0.2663	7	0.2513	7	0.2426
4	9	0.4493	9	0.4327	9	0.4231
5	12	0.0639	7	0.2823	7	0.2668
6	8	0.4364	8	0.3978	9	0.4421
7	6	0.1442	12	0.0639	7	0.2905
8	7	0.3748	8	0.4301	8	0.4020
9	6	0.1951	6	0.1237	12	0.0654
10			7	0.3582	8	0.4271
11			6	0.1626	6	0.1125
12			7	0.3815	7	0.3493
13			6	0.1982	6	0.1439
14					7	0.3674
15					6	0.1729
16					7	0.3853
17					6	0.1999

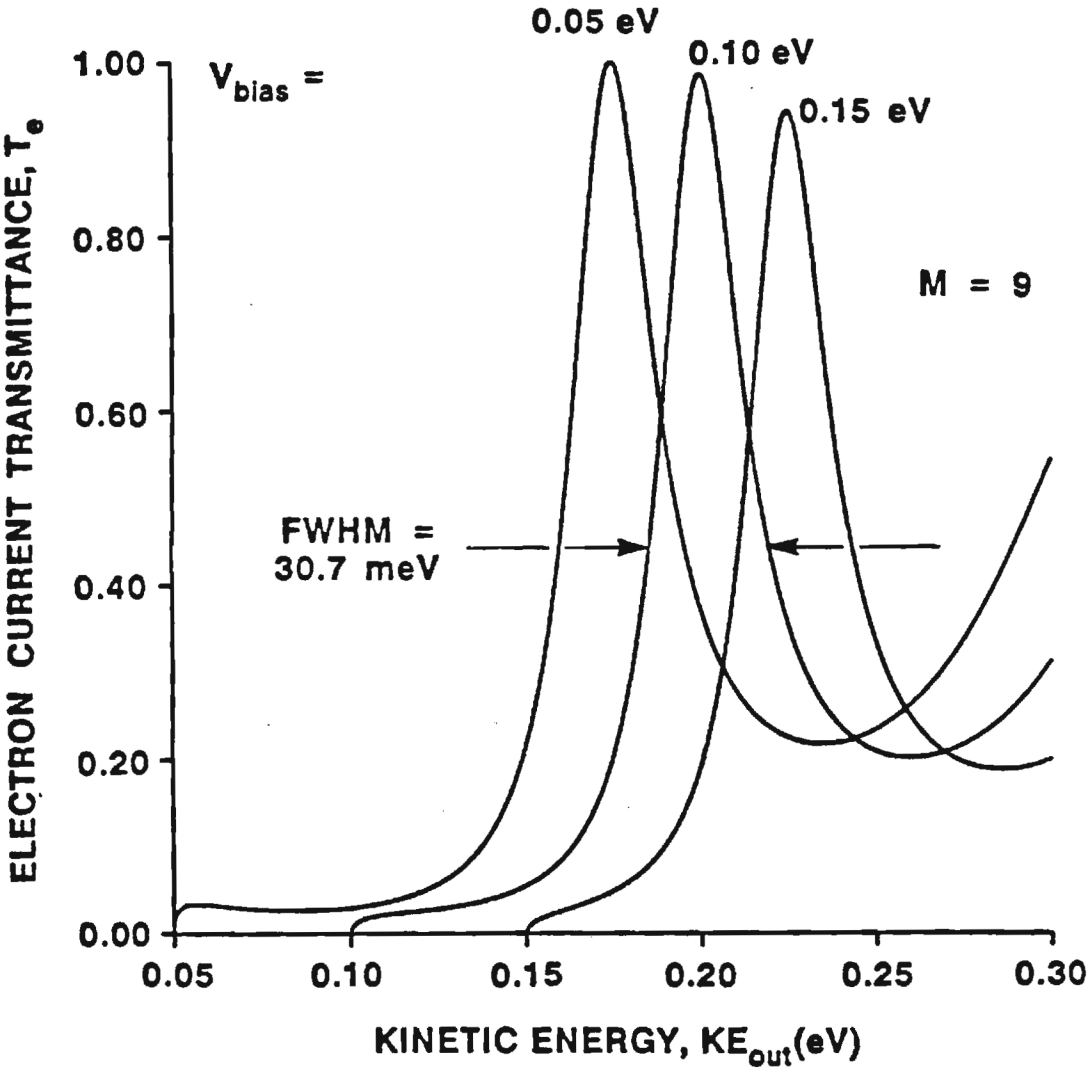
0.05 eV
0.10 eV
0.15 eV
V_{bias} =
1.00
0.80
0.60
0.40
0.20
0.00
M = 9
FWHM =
30.7 meV
0.05
0.10
0.15
0.20
0.25
0.30
ELECTRON CURRENT TRANSMITTANCE, T_e
KINETIC ENERGY, KE_{out}(eV)

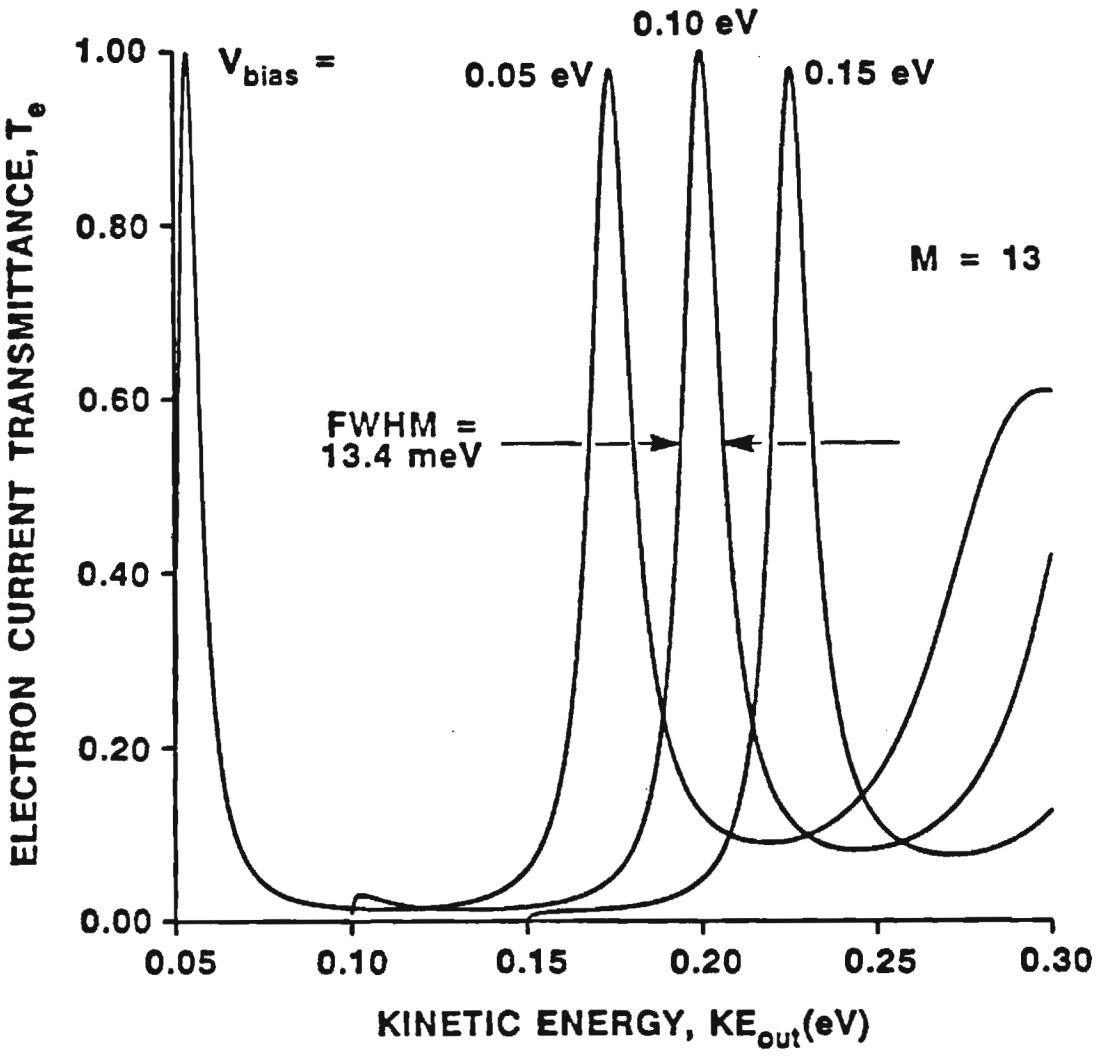
ELECTRON CURRENT TRANSMITTANCE, T_e
1.00
0.80
0.60
0.40
0.20
0.00
V_{bias} =
0.05 eV
0.10 eV
0.15 eV
M = 13
FWHM =
13.4 meV
0.05
0.10
0.15
0.20
0.25
0.30
KINETIC ENERGY, KE_{out}(eV)

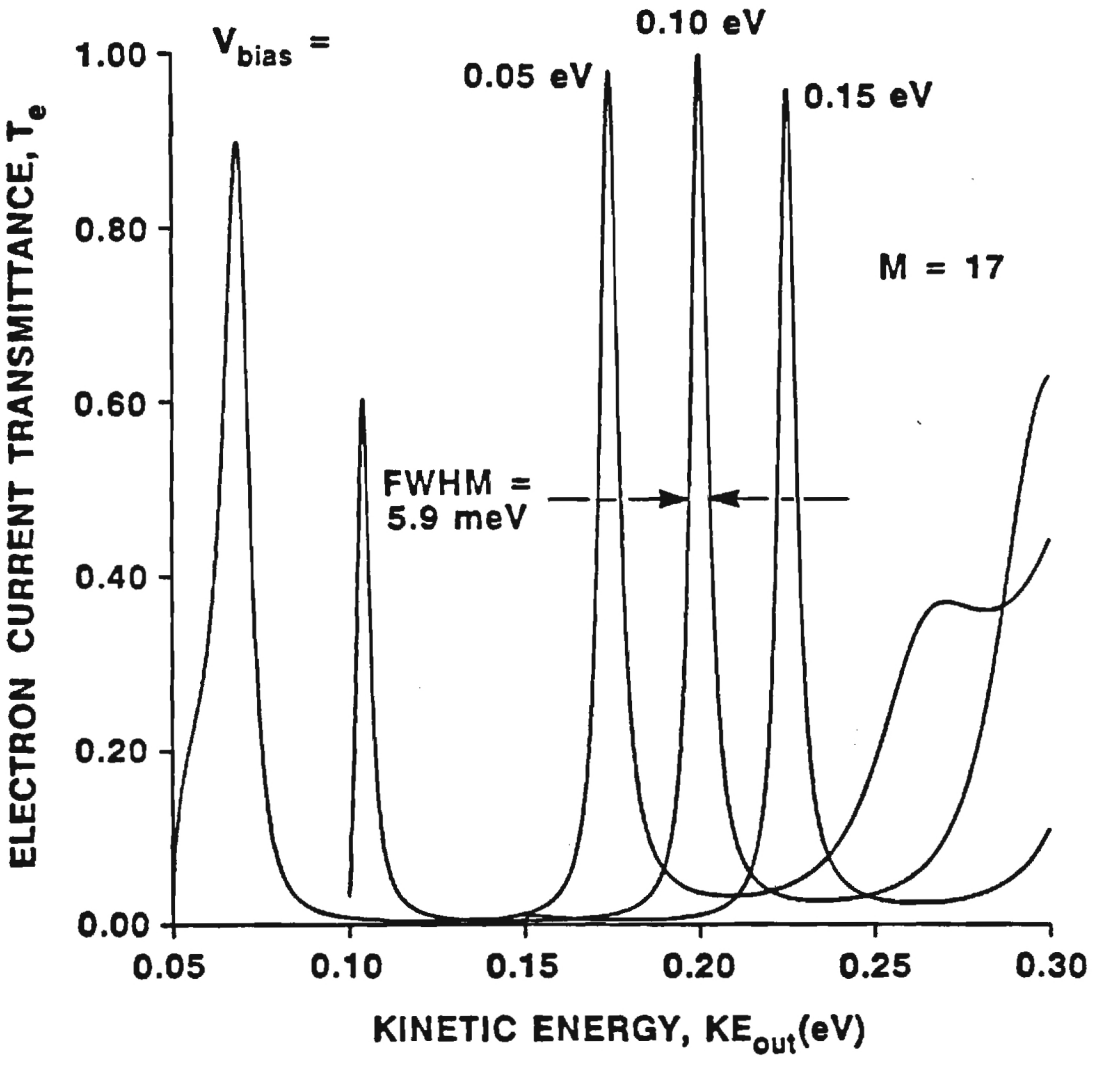
V_{bias} =
0.05 eV
0.10 eV
0.15 eV
M = 17
FWHM = 5.9 meV
1.00
0.80
0.60
0.40
0.20
0.00
0.05
0.10
0.15
0.20
0.25
0.30
ELECTRON CURRENT TRANSMITTANCE, T_e
KINETIC ENERGY, KE_{out}(eV)

TUNABILITY OF THE FILTER/EMITTER

1. Linear variation of output kinetic energy at peak transmittance with applied bias

2. Corresponding electron current transmittance remains within 90 - 100%

VARIATION IN LAYER THICKNESSES

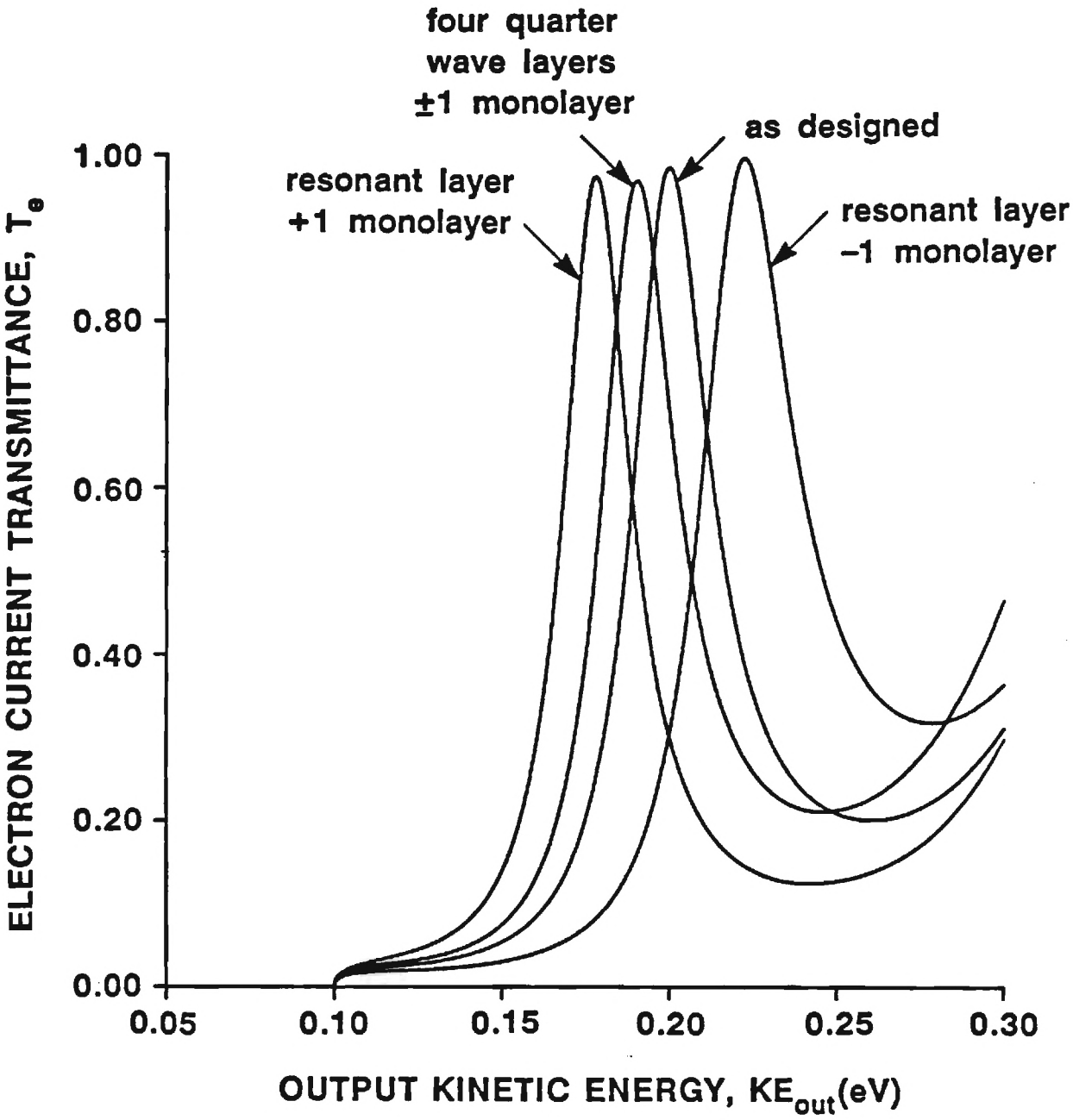

VARIATION IN LAYER COMPOSITIONS

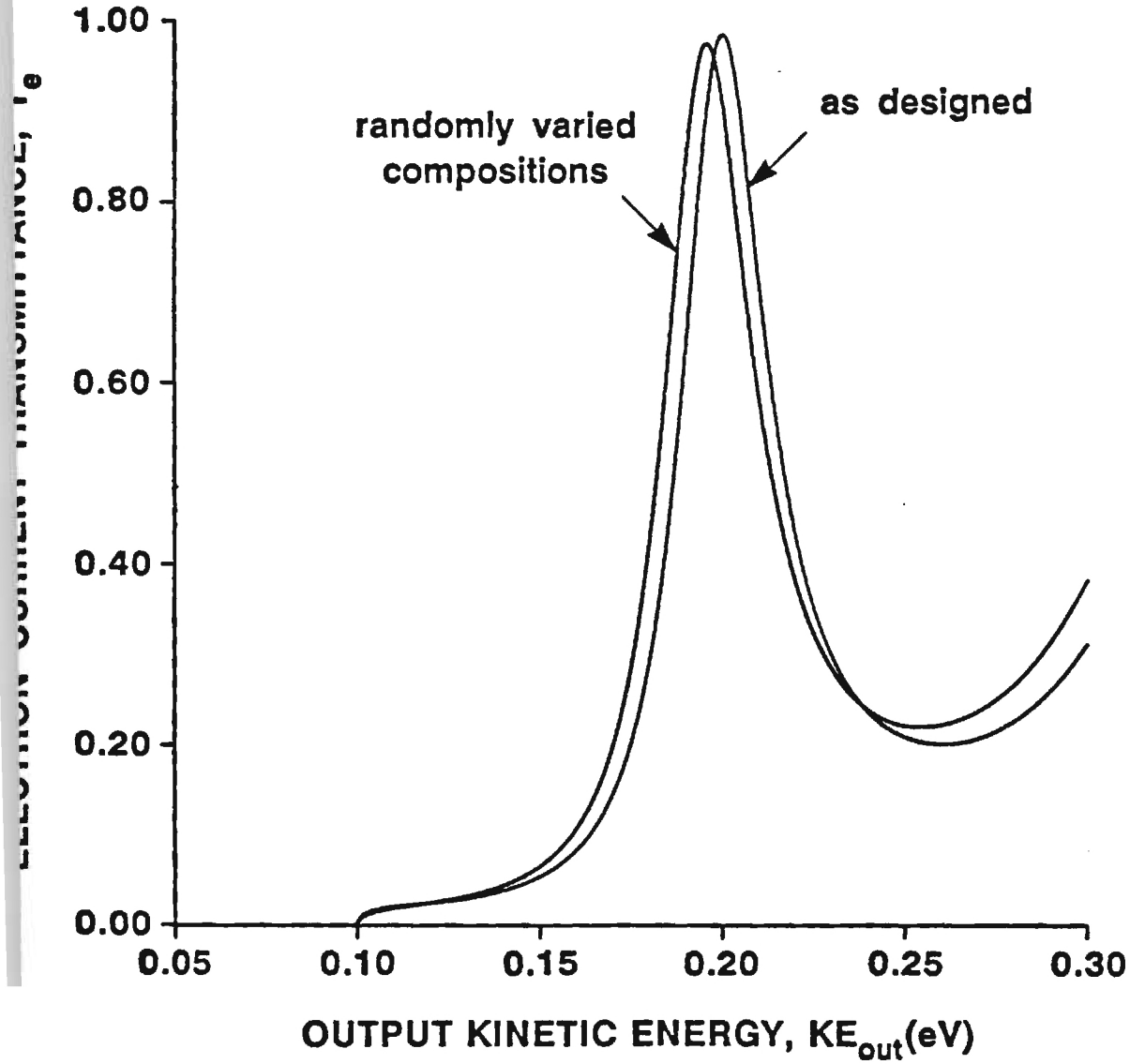

SUMMARY

1. Design of Semiconductor Electron Wave Filter/Emitters
   - Tunability
   - Insensitivity to fabrication variations
   - Designs for reduced phonon scattering

2. First-Order Model Theoretical Verification

3. Example Cases

4. Further Research
   - Higher-order models
   - Time dependence
   - Experimental verification

5. Applications
   - Electroluminescent devices
   - Fast ballistic transistors
   - Photodetectors
   - Quantum transistors
   - Quantum logic devices
   - Electron wave integrated circuits

Wavepacket propagation in semiconductor superlattice interference filters.

K. Diff. K. Brennan, T. Gaylord, E.N. Glytsis

School of Electrical Engineering
and
Microelectronics Research Center

Georgia Institute of Technology

Outline

1. Structure geometry

2. Time-*Independent* characteristics

3. Time-*Dependent* characteristics

4. Conclusion

Superlattice interference filter structure

- Structure originally proposed by Gaylord and Brennan [1]
- Analogous to optical transmission line with quarter-wavelength and half-wavelength layers
- Transport **ABOVE** the barriers. No tunneling

[1] T.K. Gaylord and K.F. Brennan, Appl. Phys. Lett., **53**, 2047 (1988)

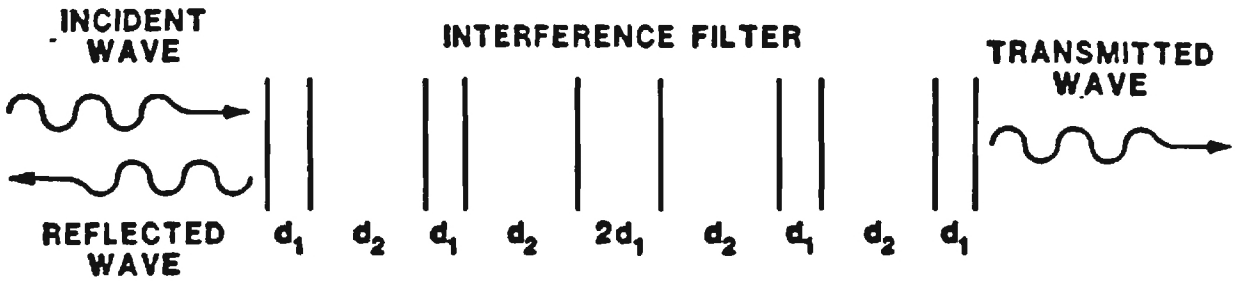

OPTICAL THIN FILM INTERFERENCE FILTER

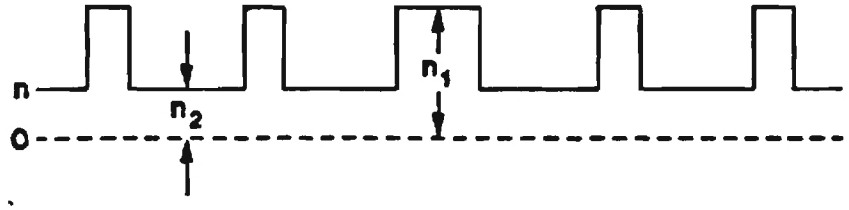

ELECTRON SUPERLATTICE INTERFERENCE FILTER

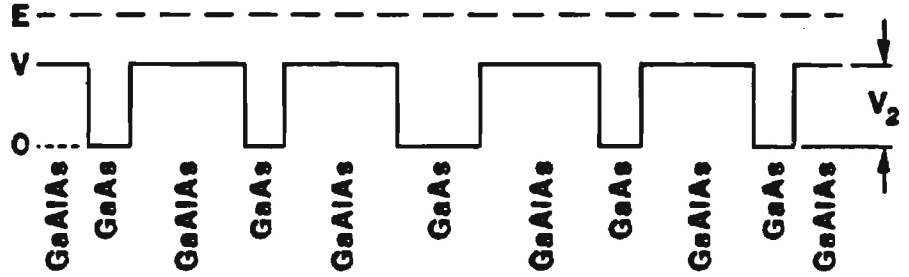

Time-independent study

1. Solve the Time-independent Schrodinger equation

2. Use effective mass approximation

3. Consider specular case for simplicity: Zero energy in direction parallel to interfaces. Can be generalized to arbitrary angles of incidence.

4. Compute transmissivity of the structure

5. Compute I-V curve

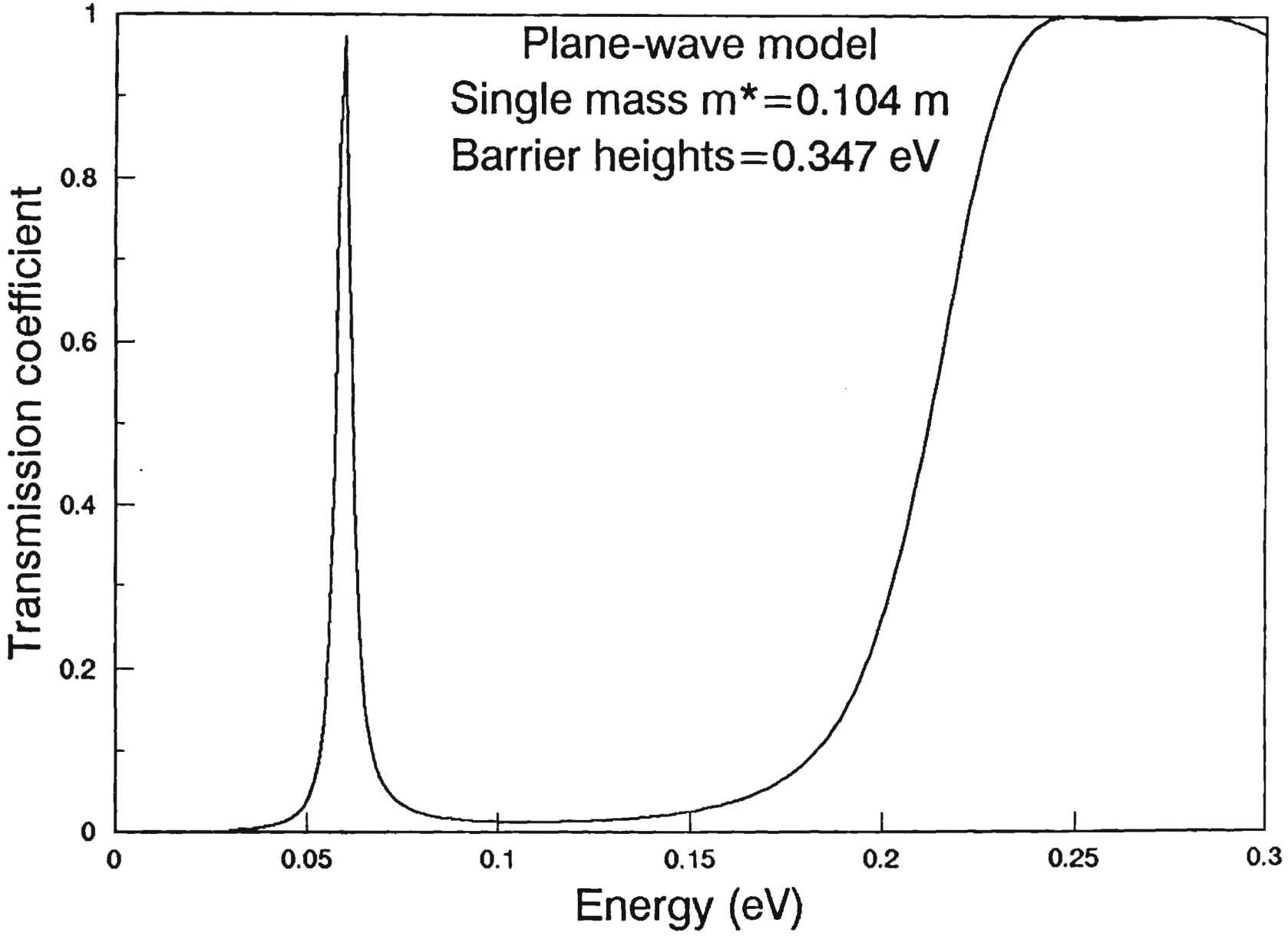
Plane-wave model
Single mass m*=0.104 m
Barrier heights=0.347 eV
Transmission coefficient
Energy (eV)
0
0.2
0.4
0.6
0.8
1
0
0.05
0.1
0.15
0.2
0.25
0.3

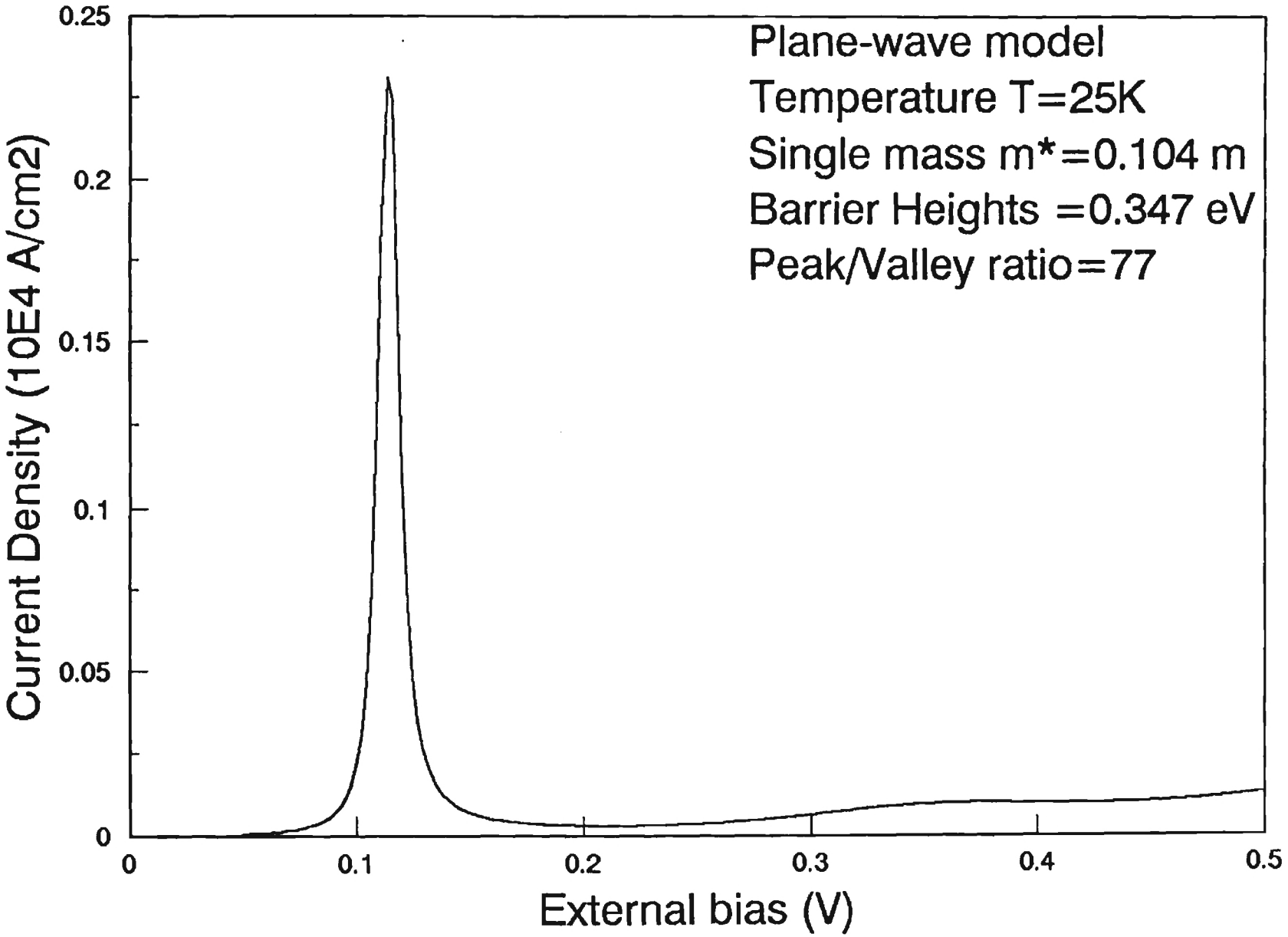
Plane-wave model
Temperature T=25K
Single mass m*=0.104 m
Barrier Heights =0.347 eV
Peak/Valley ratio=77
Current Density (10E4 A/cm2)
External bias (V)
0.25
0.2
0.15
0.1
0.05
0
0
0.1
0.2
0.3
0.4
0.5

Results for time-independent study

1. Sharp and narrow peak at Er=0.06 eV with width $\Gamma = 0.004eV$

2. Peak current density J=0.23 $10^4 A/cm^2$ at V=0.11 V

3. Peak-to-Valley ratio =77 at T=25K

Time-dependent study

1. Solve the Time-dependent Schrodinger equation

2. Use Gaussian wavepackets

3. Use Crank-Nicholson algorithm

4. Use large mesh to avoid problems with reflections

5. Compute the probability of finding electron in each region as a function of time

6. Compute the position of the center of gravity of the incident, reflected and transmitted wavepackets as a function of time

7. Compute the time-delay across the structure using the asymptotic positions of the incident and transmitted packets

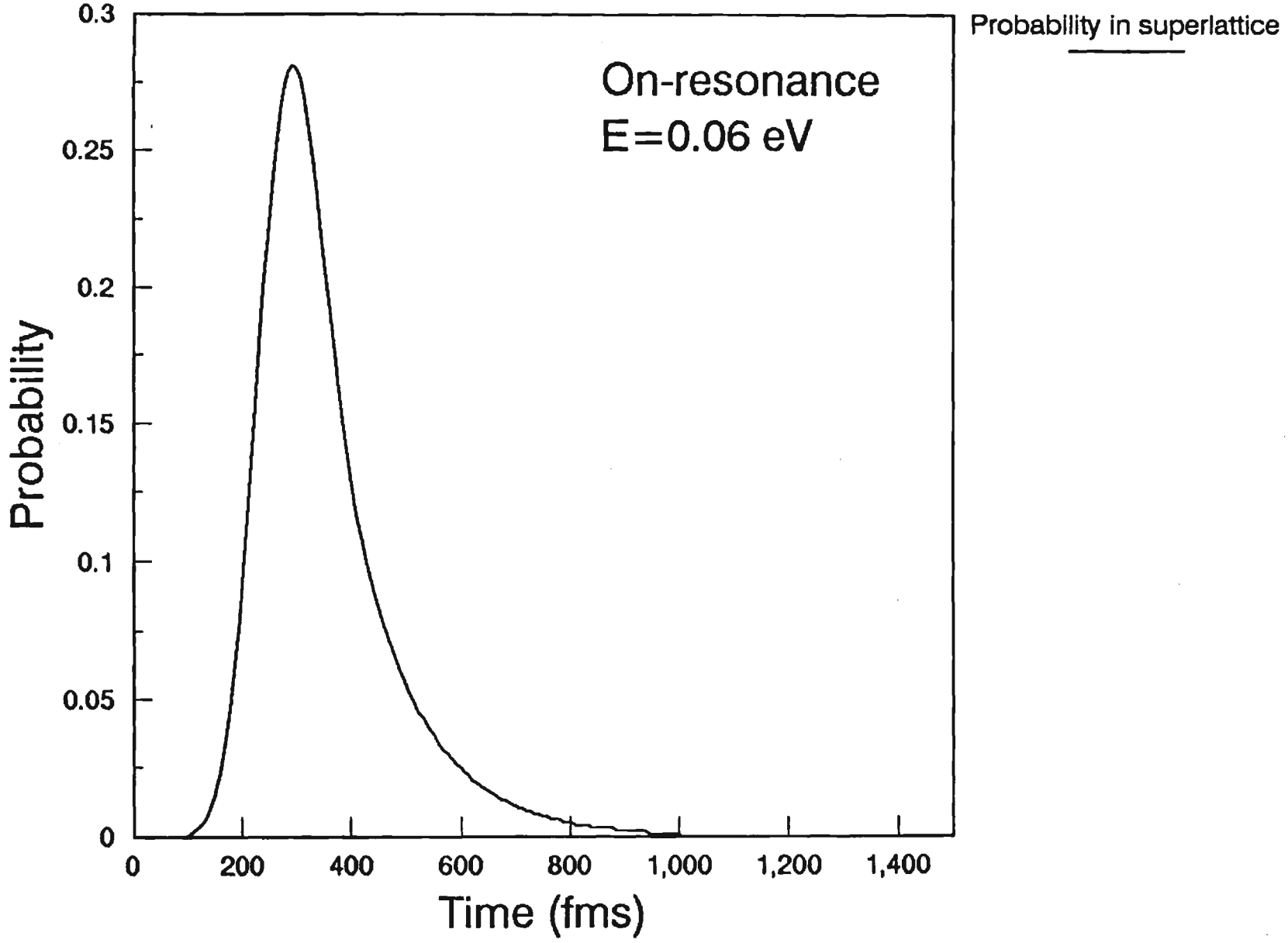
Probability in superlattice
On-resonance
E=0.06 eV
Probability
0.3
0.25
0.2
0.15
0.1
0.05
0
0
200
400
600
800
1,000
1,200
1,400
Time (fms)

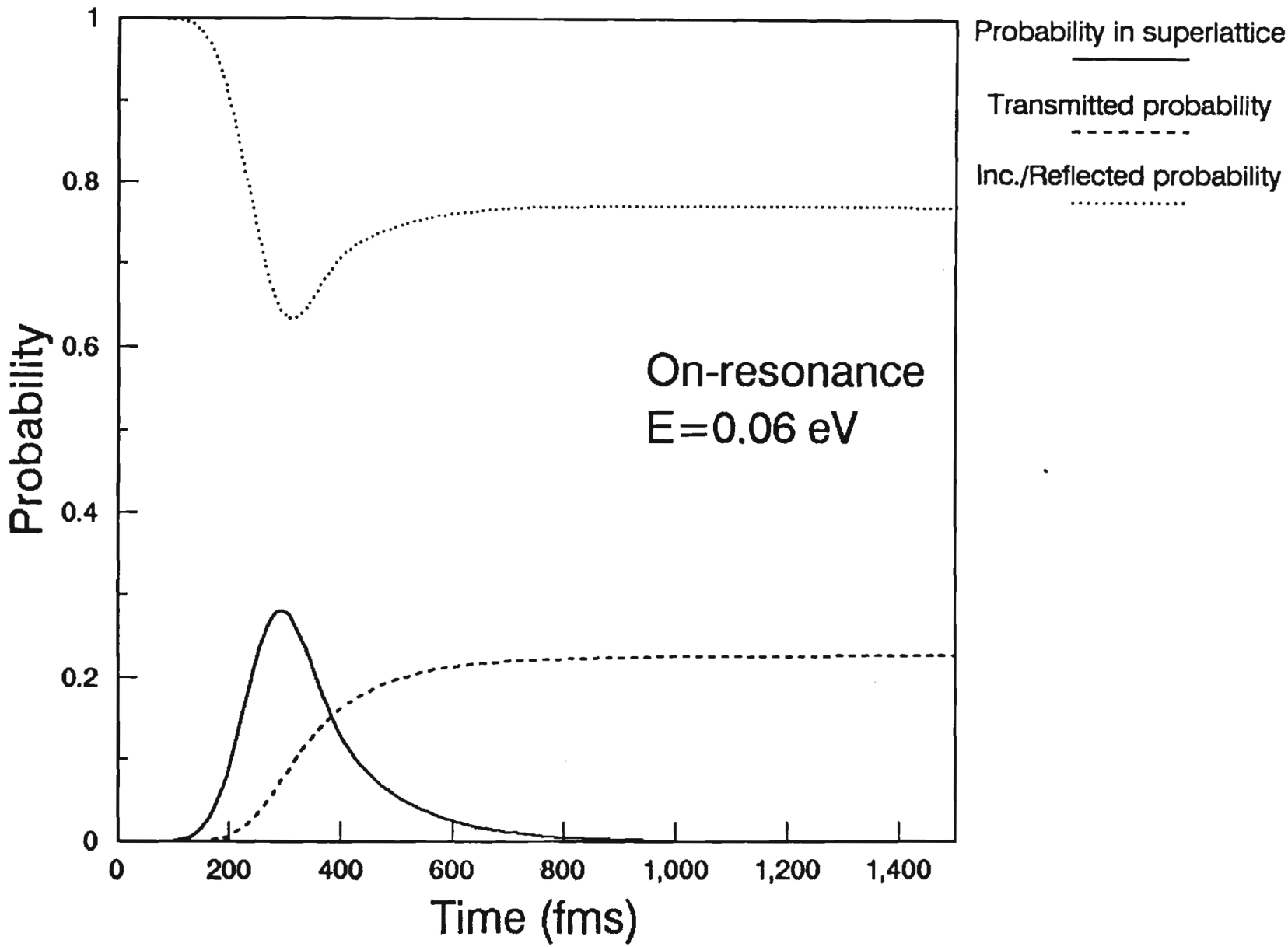
Probability in superlattice
Transmitted probability
Inc./Reflected probability
On-resonance
E=0.06 eV
Probability
1
0.8
0.6
0.4
0.2
0
0
200
400
600
800
1,000
1,200
1,400
Time (fms)

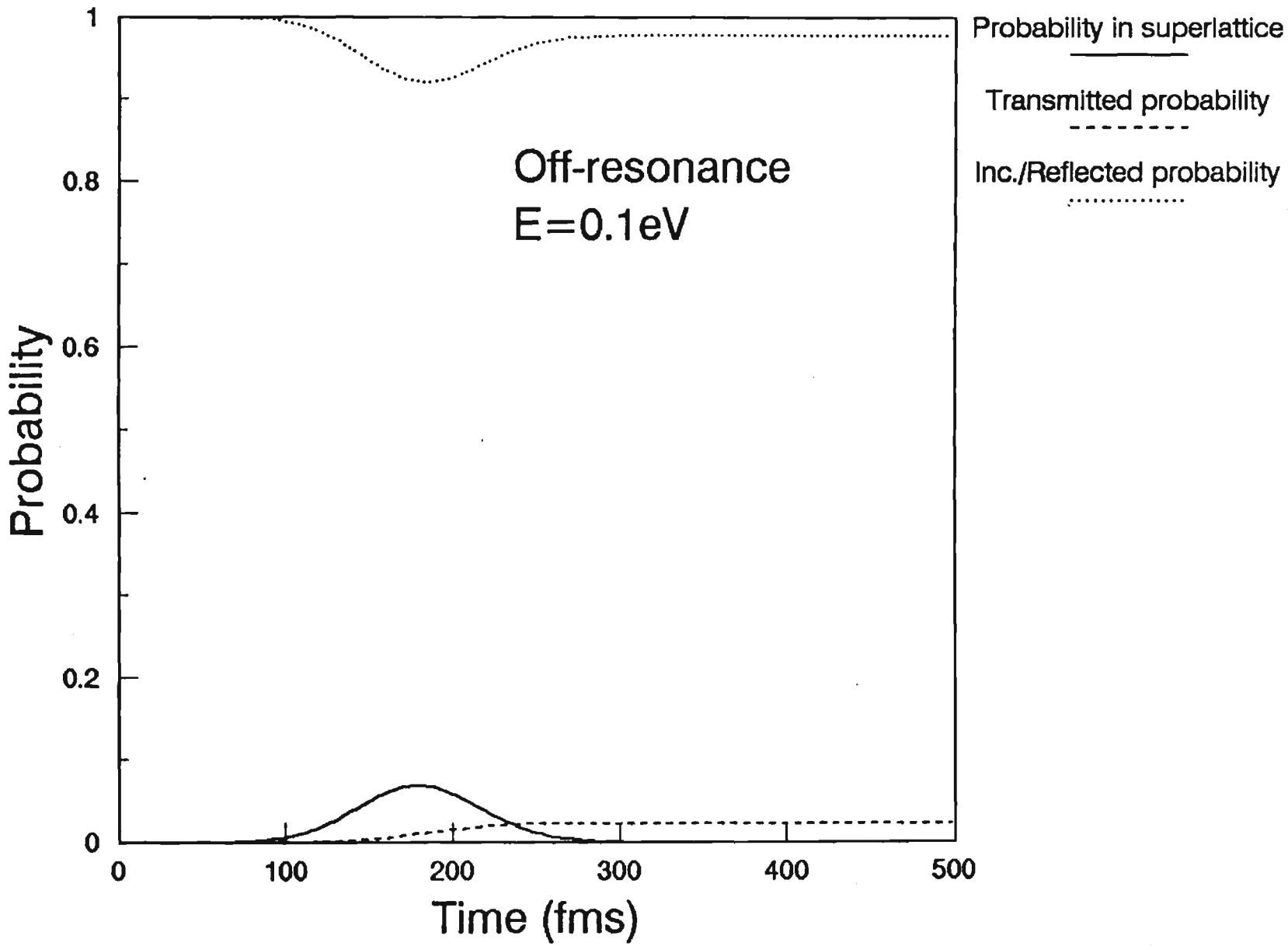
Off-resonance
E=0.1eV
Probability in superlattice
Transmitted probability
Inc./Reflected probability
Probability
Time (fms)
0
0.2
0.4
0.6
0.8
1
0
100
200
300
400
500

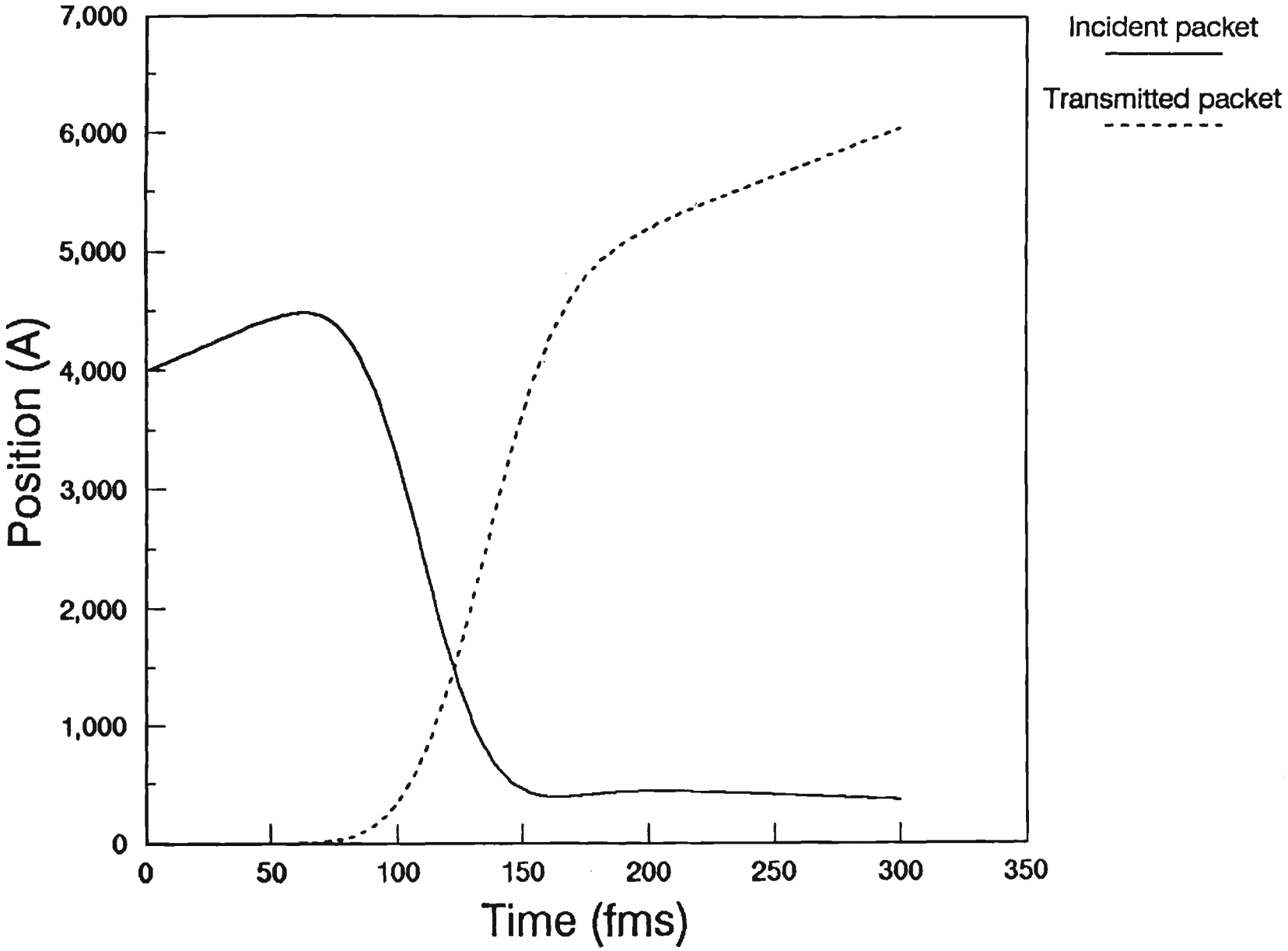
7,000
6,000
5,000
4,000
3,000
2,000
1,000
0
Position (A)
0
50
100
150
200
250
300
350
Time (fms)
Incident packet
Transmitted packet

Results for time-dependent study

1. Transmissivity depends on ratio of packet width to the level width

2. Maximum transmissivity (T=1) only for plane waves

3. Time-delay of the order of 100 fms

Conclusions

1. Behavior similar to resonant tunneling diode, without tunneling

2. Direct analogy with optics

3. Characteristics offer many potential applications

4. Future work will include self-consistent analysis in time-dependent formalism

5. Fabrication currently underway

GUIDED ELECTRON WAVES IN

SEMICONDUCTOR QUANTUM WELLS

Thomas K. Gaylord
Elias N. Glytsis
Kevin F. Brennan

School of Electrical Engineering
and
Microelectronics Research Center
Georgia Institute of Technology

QUANTUM WELL TECHNOLOGY

Molecular Beam Epitaxy (M B E)

Metal Organic Chemical Vapor Deposition (M O C V D)

QUANTUM WELLS

Electronic Applications

- Microwave Oscillators

Electromagnetic Optical Applications

- Electroluminescent Devices
- Photodetectors
- Lasers
- Switching Devices
- Modulators

Electron Wave Optical Applications

- Ballistic Transistors
- Emitter / Filters
- Diffraction Gratings
- Logic Gates
- Electron Waveguides

PREVIOUS WORK

Ballistic Transport:

A. F. J. Levi, J. R. Hayes, P. M. Platzman, and W. Weigmann, Phys. Rev. Lett. 55, 2071 (1985).

M. Heiblum, M. I. Nathan, D. C. Thomas, and C. M. Knoedler, Phys. Rev. Lett. 55, 2200 (1985).

Electron Waveguiding:

G. Timp, A. M. Chang, P. Mankiewich, R. Behringer, J. E. Cunningham, T. Y. Chang, and R. E. Howard, Phys. Rev. Lett. 59, 732 (1987).

M. L. Roukes, A. Scherer, S. J. Allen, H. G. Craighead, R. M. Ruthen, E. D. Beebe, and J. P. Harbison, Phys. Rev. Lett. 59, 3011 (1987).

B. J. van Wees, H. van Houten, C. W. J. Beenakker, J. G. Williamson, L. P. Kouwenhoven, D. van der Marel, and C. T. Foxon, Phys. Rev. Lett. 60, 848 (1988).

ELECTRON INCIDENT ON BARRIER

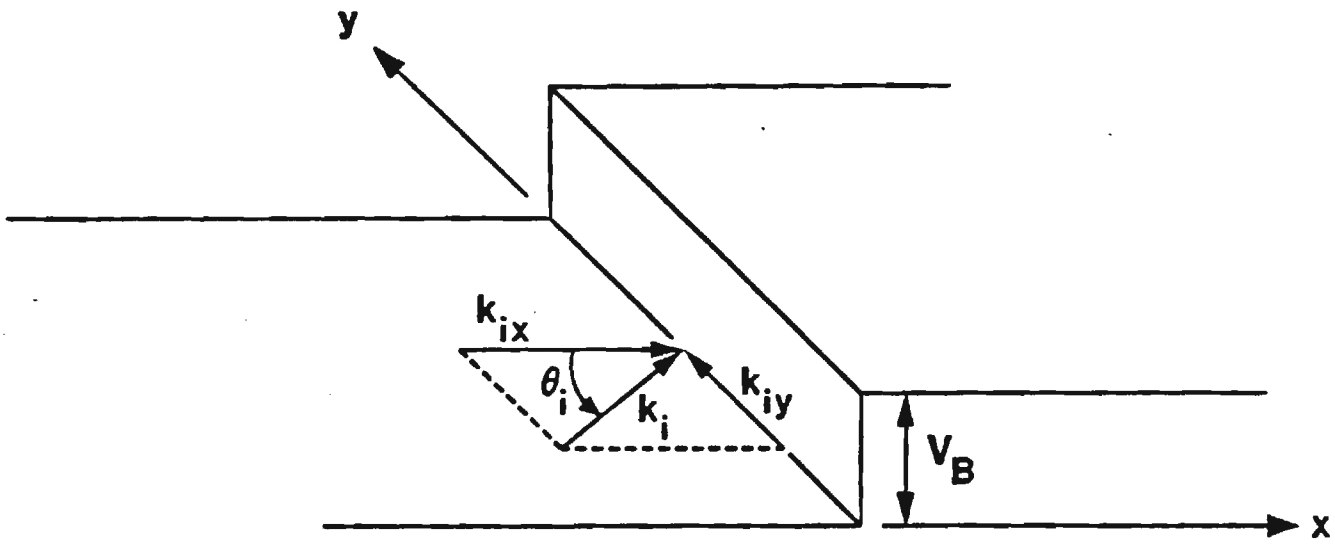

Region 1 Region 2

ALLOWED WAVEVECTORS

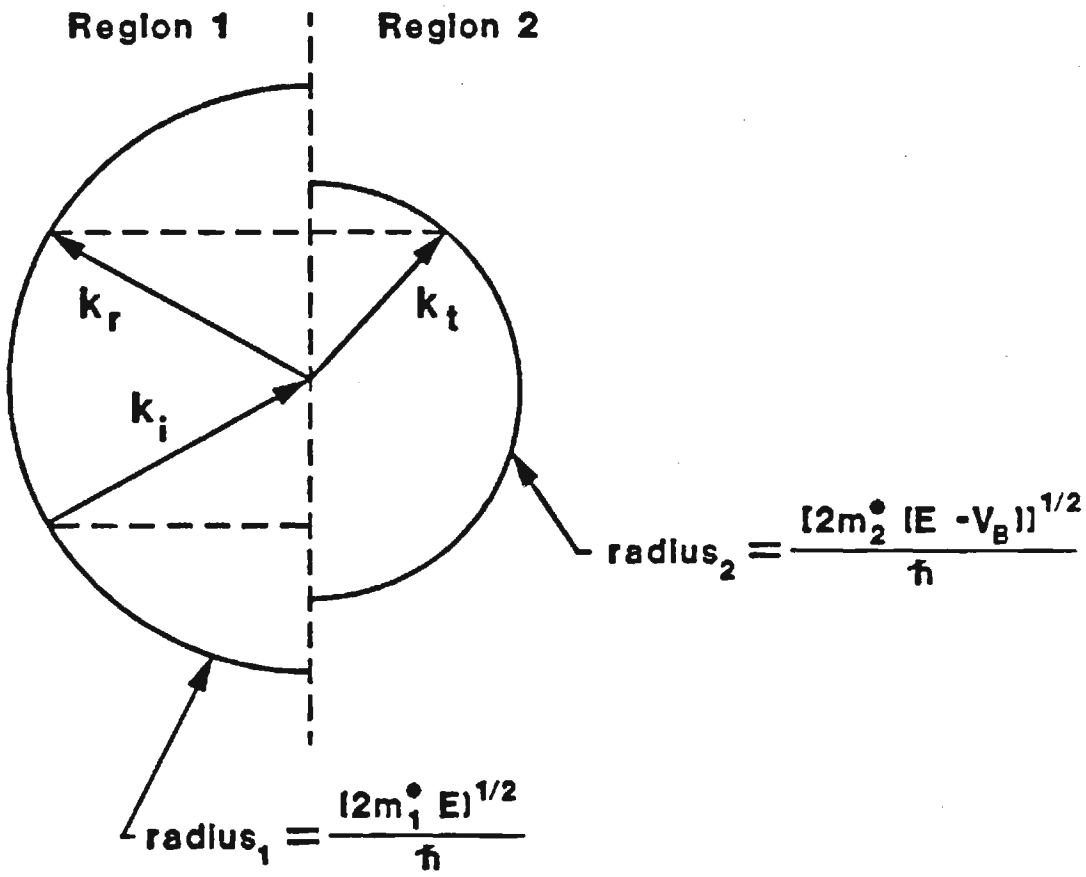

Critical Angle for Total Internal Reflection

$$\theta_{ic} = \begin{cases} \sin^{-1}\left[\dfrac{m_2^*(E-V_B)}{m_1^* E}\right]^{\frac{1}{2}} & \text{for } E - V_B > 0 \\ 0 & \text{for } E - V_B \leq 0 \end{cases}$$

QUANTUM WELL

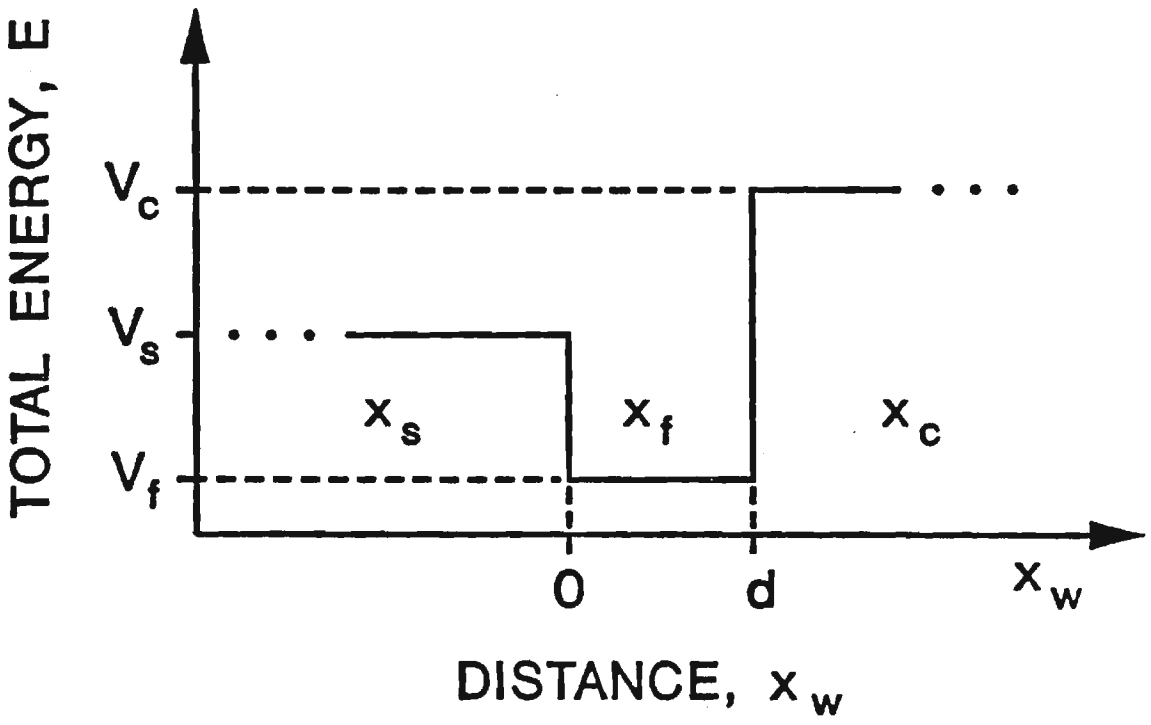

QUANTUM WELL WAVEGUIDE

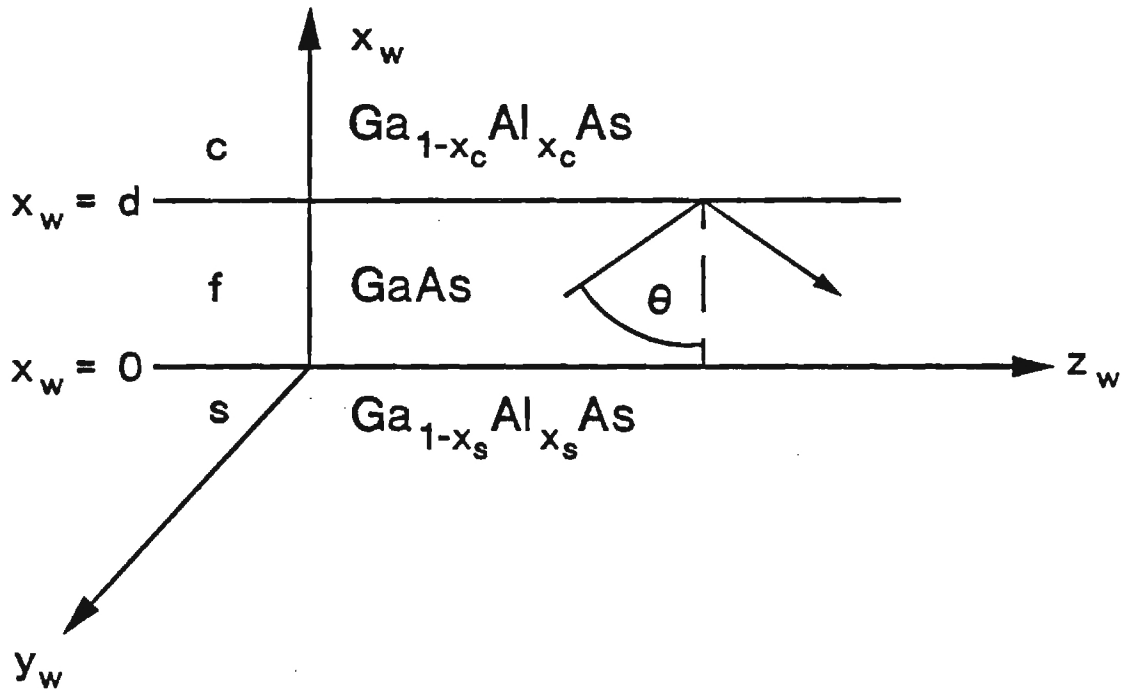

Guided Mode Wavefunction

$$\psi_\nu(x_w, z_w) \;=\; \psi_\nu(x_w)\exp(+j\beta_\nu z_w)$$

GUIDED MODE REGION

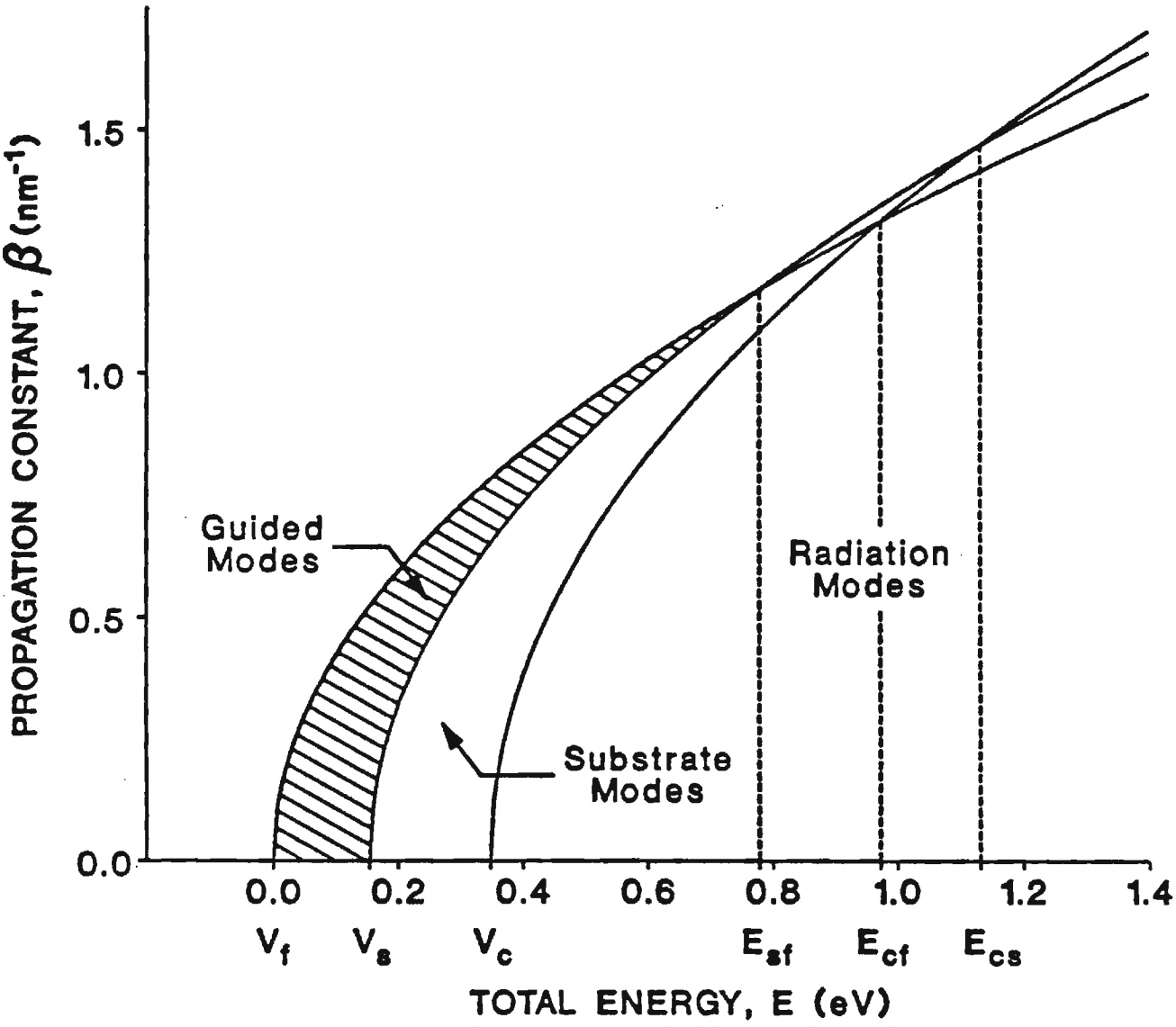

Schroedinger Time-Independent Wave Equation

$$\frac{d\psi_\nu^2(x_w)}{dx_w^2} + \{\frac{2m^*}{\hbar^2}[E_\nu - V(x_w)] - \beta_\nu^2\}\psi_\nu(x_w) = 0$$

Cover

$$\psi_{\nu c}(x_w) = A_c \exp[-\gamma_c(x_w - d)]$$

Film

$$\psi_{\nu f}(x_w) = A_{f1} \exp(j\kappa_f x_w) + A_{f2} \exp(-j\kappa_f x_w)$$

Substrate

$$\psi_{\nu s}(x_w) = A_s \exp(\gamma_s x_w)$$

$$\begin{aligned} \text{where } \gamma_s^2 &= \beta_\nu^2 - [\frac{2m_s^*}{\hbar^2}(E_\nu - V_s)] \\ \kappa_f^2 &= [\frac{2m_f^*}{\hbar^2}(E_\nu - V_f)] - \beta_\nu^2 \\ \gamma_c^2 &= \beta_\nu^2 - [\frac{2m_c^*}{\hbar^2}(E_\nu - V_c)] \end{aligned}$$

GUIDED MODE REPRESENTATIONS

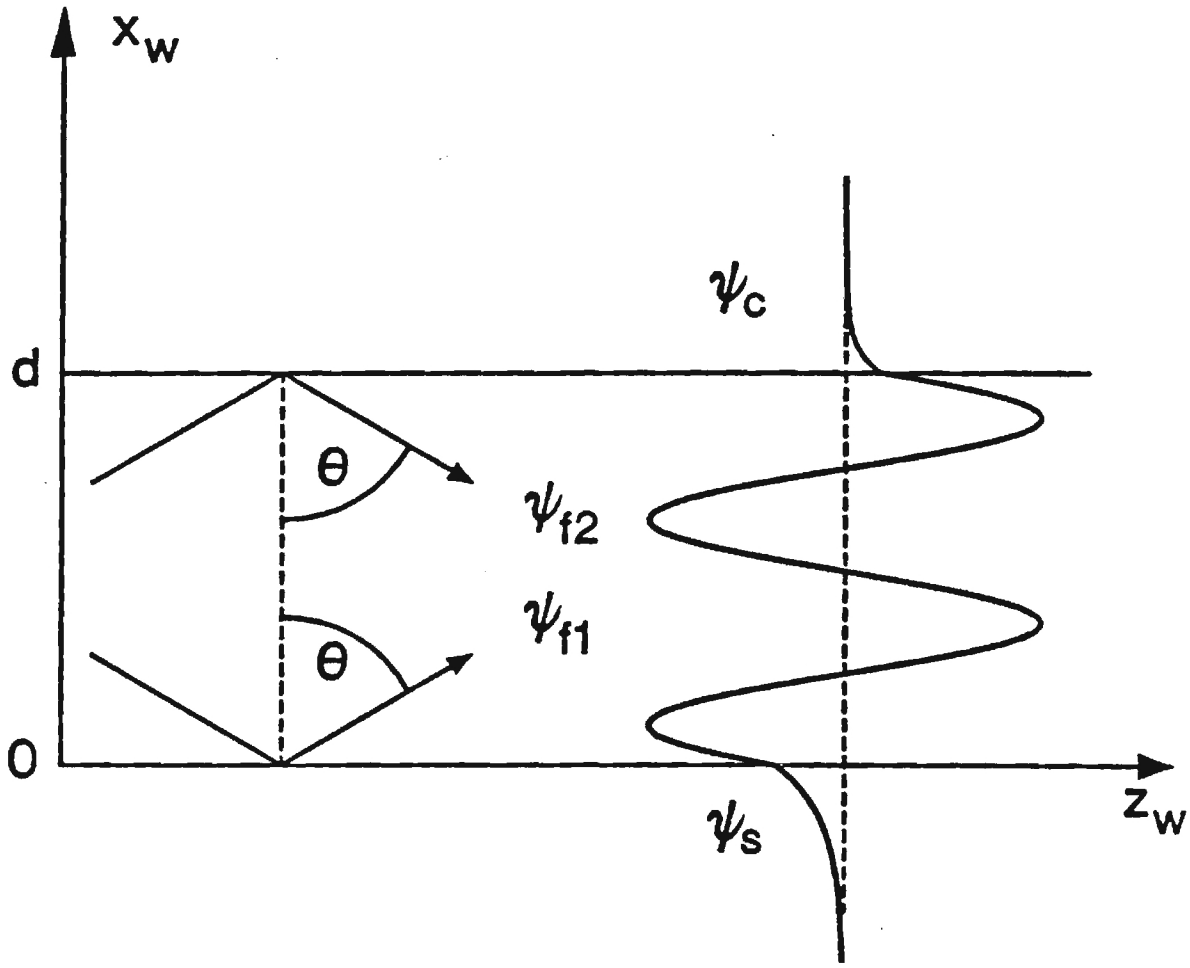

Boundary Conditions

$$\psi_\nu \text{ and } \frac{1}{m^*}\,\frac{d\psi_\nu}{dx} \text{ are continuous.}$$

Dispersion Equation

$$\kappa_f d - \tan^{-1}\left[\frac{\gamma_s/m_s^*}{\kappa_f/m_f^*}\right] - \tan^{-1}\left[\frac{\gamma_c/m_c^*}{\kappa_f/m_f^*}\right] = \nu\pi$$

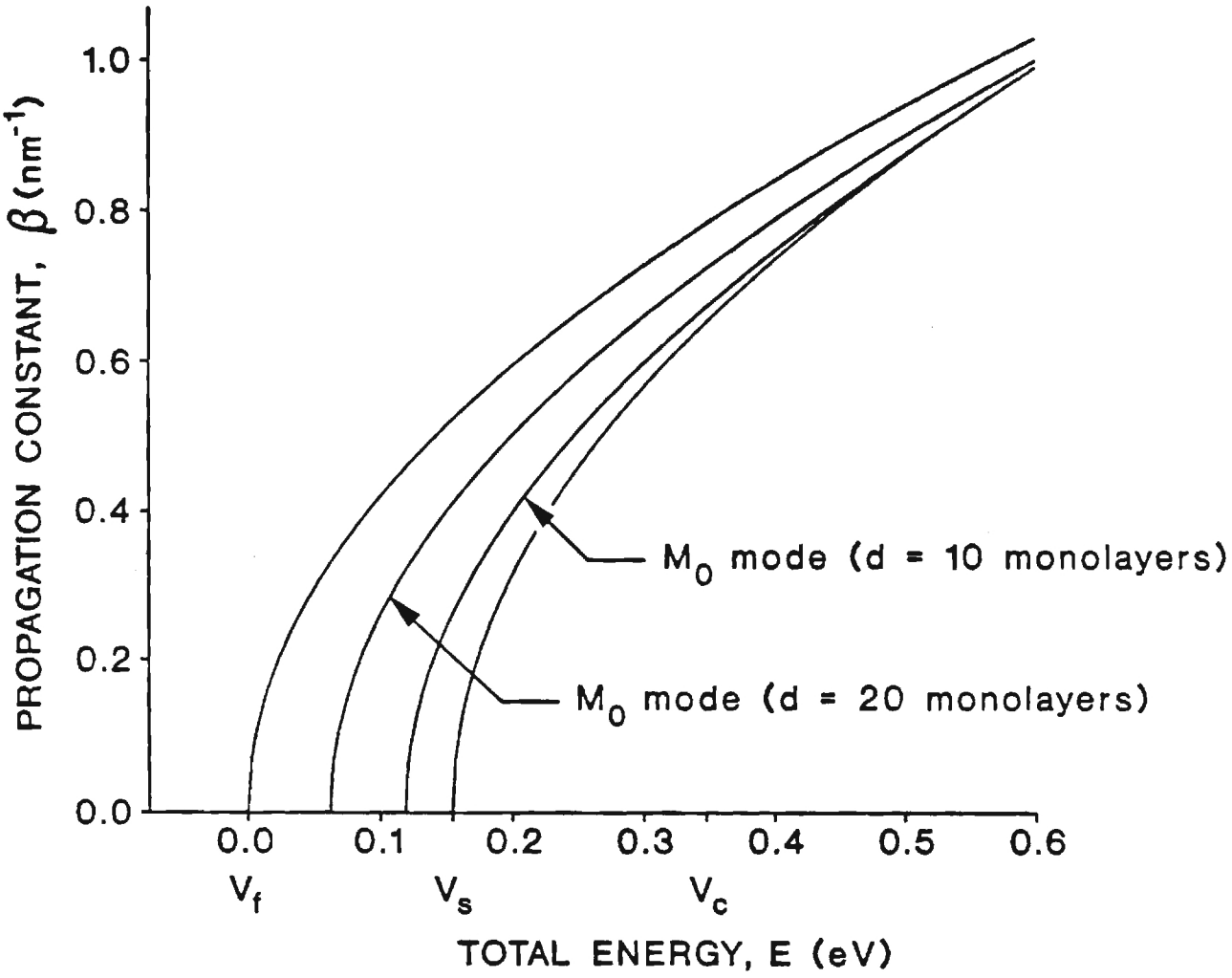
PROPAGATION CONSTANT, β (nm⁻¹)
1.0
0.8
0.6
0.4
0.2
0.0
0.0
0.1
0.2
0.3
0.4
0.5
0.6
V_f
V_s
V_c
TOTAL ENERGY, E (eV)
M_0 mode (d = 10 monolayers)
M_0 mode (d = 20 monolayers)

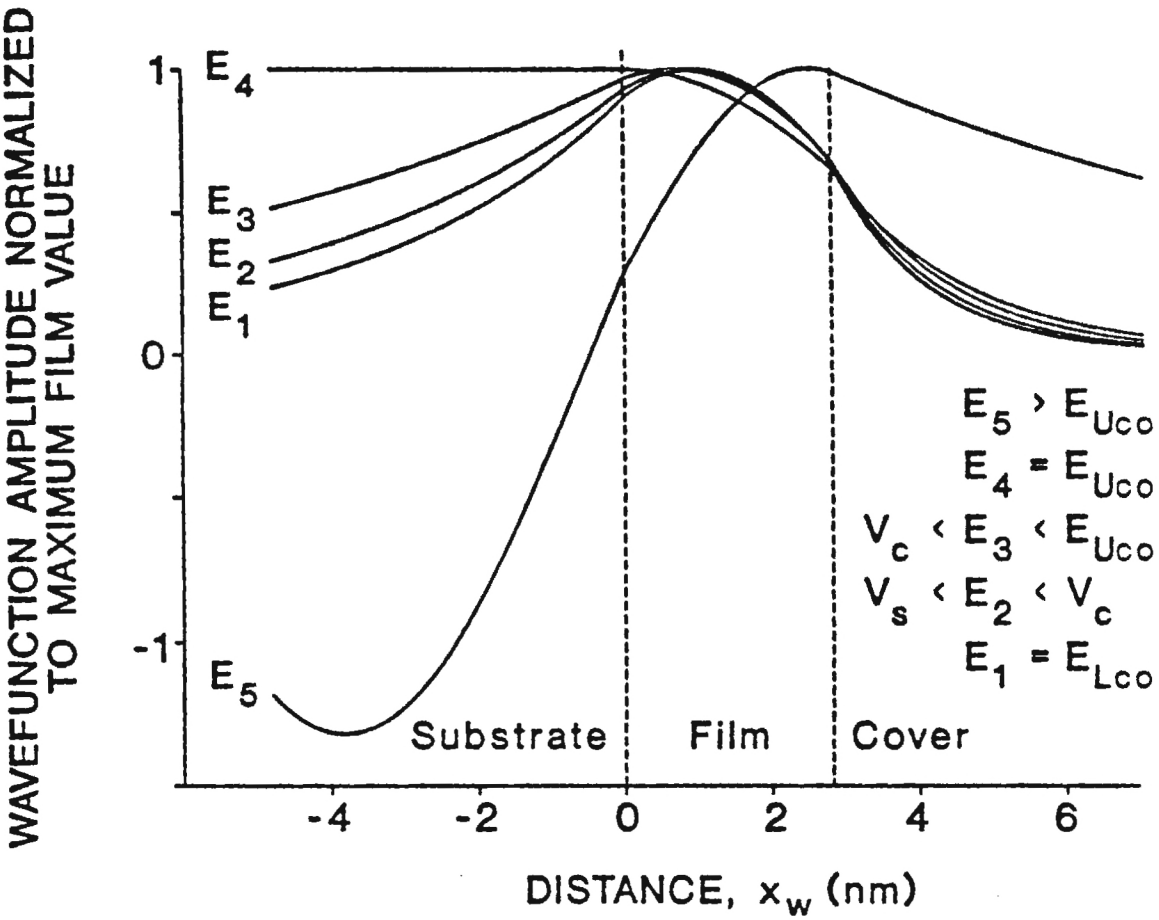
WAVEFUNCTION AMPLITUDE NORMALIZED TO MAXIMUM FILM VALUE
1
0
-1
E4
E3
E2
E1
E5
Substrate
Film
Cover
E5 > ELco
E4 = ELco
Vc < E3 < ELco
Vs < E2 < Vc
E1 = ELco
-4
-2
0
2
4
6
DISTANCE, xw (nm)

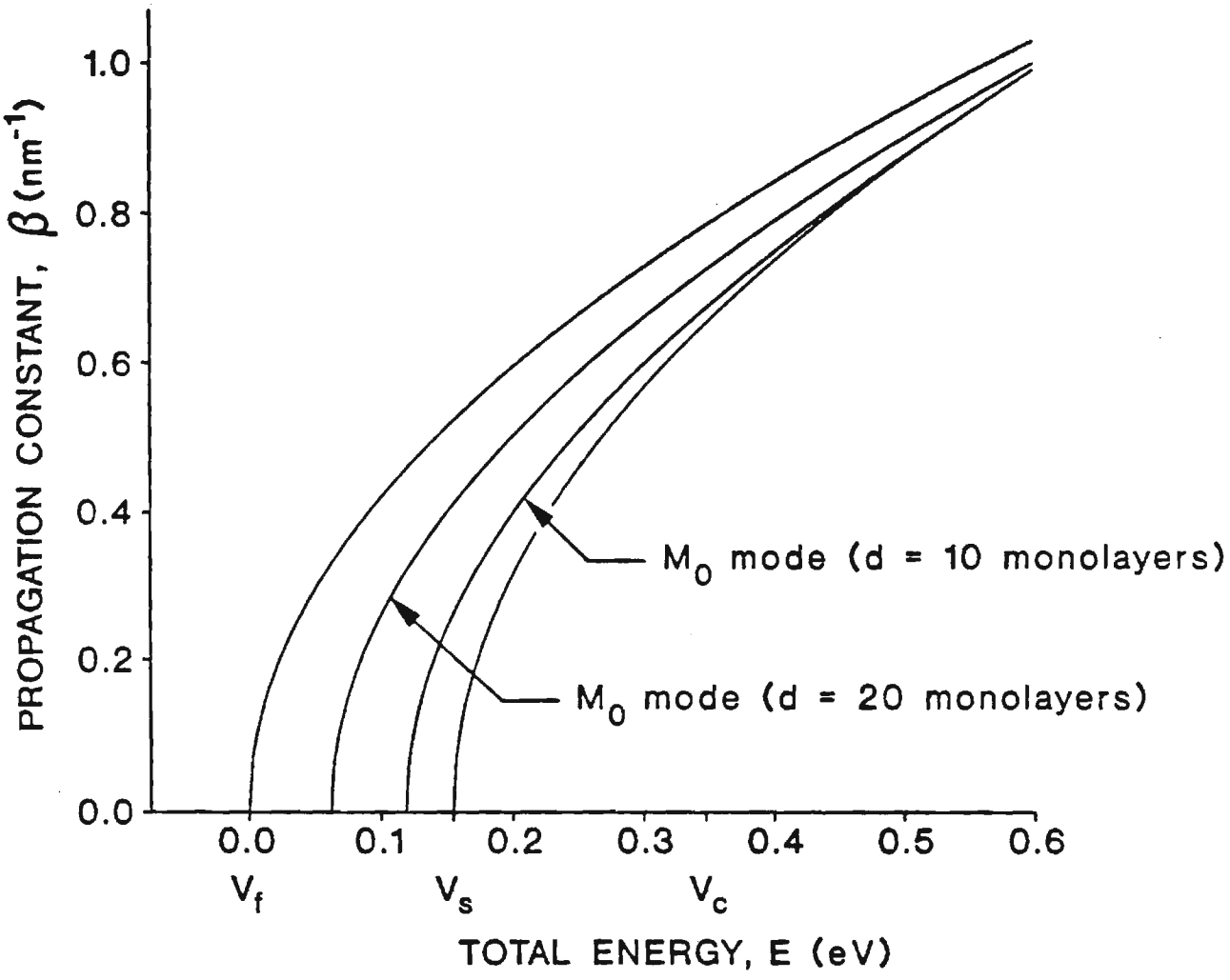
PROPAGATION CONSTANT, β (nm⁻¹)
1.0
0.8
0.6
0.4
0.2
0.0
0.0
0.1
0.2
0.3
0.4
0.5
0.6
V_f
V_s
V_c
TOTAL ENERGY, E (eV)
M0 mode (d = 10 monolayers)
M0 mode (d = 20 monolayers)

Lower-Energy Cutoff

$$[2m_f^*(E_{Lco}-V_f)]^{\frac{1}{2}} - \tan^{-1}[\frac{m_f^*(V_s-E_{Lco})}{m_s^*(E_{Lco}-V_f)}]^{\frac{1}{2}} - \tan^{-1}[\frac{m_f^*(V_c-E_{Lco})}{m_c^*(E_{Lco}-V_f)}]^{\frac{1}{2}} = \nu\pi$$

Upper-Energy Cutoff

$$\{2[(m_s^*V_s - m_f^*V_f - (m_s^*-m_f^*)E_{Uco}]\}^{\frac{1}{2}}d/\hbar - \tan^{-1}\{[\frac{m_c^*V_c - m_s^*V_s - (m_c^*-m_s^*)E_{Uco}m_f^{*2}}{m_s^*V_s - m_f^*V_f - (m_s^*-m_f^*)E_{Uco}m_c^{*2}}\}^{\frac{1}{2}} = \nu\pi$$

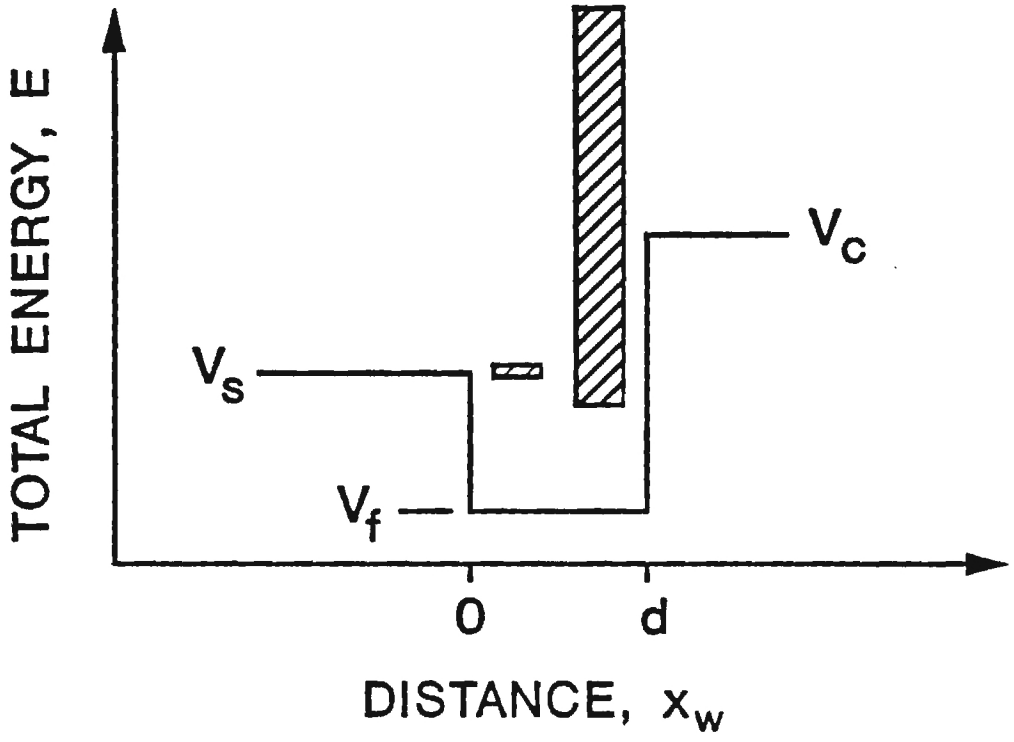
TOTAL ENERGY, E
V_c
V_s
V_f
0
d
DISTANCE, x_w

ELECTRON WAVE DEVICES AND CIRCUITS

Electron Wave Devices

- Spectral Filters
- Impedance Transformers
- Modulators
- Switches
- Deflectors
- Tunable Sources
- Tunable Filters
- Negative Resistance Devices
- Quantum Logic Gates
- Quantum Transistors
- Multiplexers - Demultiplexers
- Lenses
- Diffraction Gratings

Guided Electron Wave Integrated Circuits

- Devices Connected with
  - Electron Waveguides

REFERENCES

T. K. Gaylord and K. F. Brennan, "Electron wave optics in semiconductors," Journal of Applied Physics, vol. 65, pp. 814 - 820, Jan. 15, 1989.

T. K. Gaylord, E. N. Glytsis, and K. F. Brennan, "Semiconductor electron wave slab waveguides," Journal of Applied Physics, vol. 65, pp. 1483 - 1485, Aug. 1, 1989.

T. K. Gaylord, E. N. Glytsis, and K. F. Brennan, "Semiconductor quantum wells as electron slab waveguides," Journal of Applied Physics, vol. 65, pp. 1842 - 1848, Aug. 15, 1989.

OMB Number 345-0058

NATIONAL SCIENCE FOUNDATION
1800 G STREET, NW
WASHINGTON, DC 20550

BULK RATE
POSTAGE & FEES PAID
National Science Foundation
Permit No. G-69

PI/PD Name and Address

Elias N. Glytsis
Electrical Engineering
Georgia Institute of Tech
Atlanta GA 30332

NATIONAL SCIENCE FOUNDATION
FINAL PROJECT REPORT

PART I - PROJECT IDENTIFICATION INFORMATION

1. Program Official/Org. Lawrence S. Goldberg - ECS

2. Program Name QUANTUM ELECTRONICS, WAVES & BEAMS PROG

3. Award Dates (MM/YY) From: 08/89 To: 07/92

4. Institution and Address
GA Tech Res Corp - GTRI
Atlanta GA 30332

5. Award Number 8909971

6. Project Title
(IA: Semiconductor Quantum Wave Devices

This Packet Contains
NSF Form 98A
And 1 Return Envelope

PART IV — FINAL PROJECT REPORT — SUMMARY DATA ON PROJECT PERSONNEL

(To be submitted to cognizant Program Officer upon completion of project)

The data requested below are important for the development of a statistical profile on the personnel supported by Federal grants. The information on this part is solicited in response to Public Law 99-383 and 42 USC 1885C. All information provided will be treated as confidential and will be safeguarded in accordance with the provisions of the Privacy Act of 1974. You should submit a single copy of this part with each final project report. However, submission of the requested information is not mandatory and is not a precondition of future award(s). Check the "Decline to Provide Information" box below if you do not wish to provide the information.

Please enter the numbers of individuals supported under this grant.
Do not enter information for individuals working less than 40 hours in any calendar year.

	Senior Staff		Post-Doctorals		Graduate Students		Under-Graduates		Other Participants[1]	
	Male	Fem.	Male	Fem.	Male	Fem.	Male	Fem.	Male	Fem.
A. Total, U.S. Citizens										
B. Total, Permanent Residents			1		3		1	1		
U.S. Citizens or Permanent Residents[2]:										
American Indian or Alaskan Native ...										
Asian			X							
Black, Not of Hispanic Origin										
Hispanic										
Pacific Islander										
White, Not of Hispanic Origin					3		1	1		
C. Total, Other Non-U.S. Citizens										
Specify Country 1.										
2.										
3.										
D. Total, All participants (A + B + C)			1		3		1	1		
Disabled[3]										

☐ Decline to Provide Information: Check box if you do not wish to provide this information (you are still required to return this page along with Parts I-III).

[1]Category includes, for example, college and precollege teachers, conference and workshop participants.

[2]Use the category that best describes the ethnic/racial status for all U.S. Citizens and Non-citizens with Permanent Residency. *(If more than one category applies, use the one category that most closely reflects the person's recognition in the community.)*

[3]A person having a physical or mental impairment that substantially limits one or more major life activities; who has a record of such impairment; or who is regarded as having such impairment. *(Disabled individuals also should be counted under the appropriate ethnic/racial group unless they are classified as "Other Non-U.S. Citizens.")*

AMERICAN INDIAN OR ALASKAN NATIVE: A person having origins in any of the original peoples of North America, and who maintain cultural identification through tribal affiliation or community recognition.

ASIAN: A person having origins in any of the original peoples of East Asia, Southeast Asia and the Indian subcontinent. This area includes, for example, China, India, Indonesia, Japan, Korea and Vietnam.

BLACK, NOT OF HISPANIC ORIGIN: A person having origins in any of the black racial groups of Africa.

HISPANIC: A person of Mexican, Puerto Rican, Cuban, Central or South American or other Spanish culture or origin, regardless of race.

PACIFIC ISLANDER: A person having origins in any of the original peoples of Hawaii; the U.S. Pacific Territories of Guam, American Samoa, or the Northern Marianas; the U.S. Trust Territory of Palau; the islands of Micronesia or Melanesia; or the Philippines.

WHITE, NOT OF HISPANIC ORIGIN: A person having origins in any of the original peoples of Europe, North Africa, or the Middle East.

ELIAS N. GLYTSIS

SEMICONDUCTOR QUANTUM WAVE DEVICES – ECS 8909971

SUMMARY

The efforts of the semiconductor industry to scale down the size of devices to achieve higher integration levels and higher speeds have been confronted by the major problem of the "troublesome" quantum-mechanical wave interference effects. These "troublesome" effects start to dominate device characteristics at dimensions of less than about one-quarter of a micron, thus, making further size reduction impossible. This limits the level of integration and the ultimate speed of integrated circuits. Further advances require fundamentally new device concepts and designs. The constructive use of the "troublesome" quantum effects was the basic premise of the proposed "Semiconductor Quantum Wave Optics" research. The long-term scientific objective of the completed research was to generate the necessary knowledge of nanometer-scale semiconductor quantum wave devices that would allow the practical development and use of these structures. Utilization of these quantum devices would be both for ultra-small high-speed versions of present-day devices (such as higher speed switches, oscillators, et.) and for future guided electron wave integrated circuits. This objective of this activity was to bring together understanding of the underlying physics, device modeling, development of software tools, device design methodology, evaluation of existing quantum interference experiments, crystal growth, device fabrication, and device testing. The work completed during the period of the award can be summarized into eight categories: (a) generalization of the analogies between electromagnetic waves in general dielectrics and electron waves in semiconductors, (including analogies with a generalized Hamiltonian) (b) theory and design of narrow-band semiconductor superlattice filter/emitters, (c) negative-differential-resistivity quantum interference devices, (d) theory and design of electron-wave impedance transformers, (e) space-charge effects in quantum wave devices, (f) time-dependent characteristics of the electron-wave interference filters and filter/emitters, (g) electron wave slab waveguides, (h) electron wave quantum interference grating devices, (i) a quantum interference effects in semiconductors bibliography, (j) a proposed innovative testing technique of quantum interference structures using ballistic electron emission microscopy, and (k) three related patents and four patent applications. The aforementioned research results are summarized in the final technical report.

JOURNAL PUBLICATIONS RESULTING FROM THE NSF AWARD

1. T. K. Gaylord, E. N. Glytsis, and K. F. Brennan, "Semiconductor Superlattice Interference Filter Design," *J. of Appl. Phys.*, vol.65, pp. 2535-2540, Mar. 15, 1989.

2. E. N. Glytsis, T. K. Gaylord, and K. F. Brennan, "Semiconductor Biased Superlattice Tunable Electron Interference Filter/Emitter," *J. Appl. Phys.*, vol. 66, pp. 1494-1497, Aug. 1, 1989.

3. T. K. Gaylord, E. N. Glytsis, and K. F. Brennan, "Semiconductor Electron Wave Slab Waveguides," *J. Appl. Phys.*, vol. 66, pp. 1483-1485, Aug. 1, 1989.

4. T. K. Gaylord, E. N. Glytsis, and K. F. Brennan, "Semiconductor Quantum Well Electron Waveguides," *J. Appl. Phys.*, vol. 66, pp. 1842-1848, Aug. 15, 1989.

5. E. N. Glytsis, T. K. Gaylord, and K. F. Brennan, "Theory and Design of Semiconductor Electron-Wave Interference Filter/Emitters," *J. Appl. Phys.*, vol. 66, pp. 6158-6167, Dec. 15, 1989.

6. T. K. Gaylord, E. N. Glytsis, and K. F. Brennan, "Electron-Wave Quarter-Wavelength Impedance Transformers Between Differing Semiconductors," *J. Appl. Phys.*, vol. 67, pp. 2623-2630, Mar. 1, 1990.

7. G. N. Henderson, E. N. Glytsis, and T. K. Gaylord, "Electron Wave Diffraction by Semiconductor Gratings: Rigorous Analysis and Design Parameters," *Appl. Phys. Lett.*, vol. 59, pp. 440-442, July 22, 1991.

8. T. K. Gaylord, E. N. Glytsis, G. N. Henderson, K. P. Martin, D. B. Walker, D. W. Wilson, and K. F. Brennan, "Quantum Interference Effects in Semiconductors: A Bibliography," (invited) *Proc. IEEE*, vol. 79, pp. 1159-1180, Aug. 1991.

9. E. N. Glytsis, T. K. Gaylord, and K. F. Brennan, " Ballistic Current- Voltage Characteristics of Semiconductor Superlattice Electron-Wave Quantum-Interference Filter/Emitter Negative Differential Resistivity Devices," *J. Appl. Phys.*, vol. 70, pp. 3920-3933, Oct. 1, 1991.

10. D. W. Wilson, E. N. Glytsis, and T. K. Gaylord, "Quantum Well, Voltage- Induced Quantum Well, and Quantum Barrier Electron Waveguides: Modes, Cutoffs, and Maximum Current," *Appl. Phys. Lett.*, vol. 59, pp. 1855-1857, Oct. 7, 1991.

11. G. N. Henderson, T. K. Gaylord, and E. N. Glytsis, "Ballistic Electron Transport in Semiconductor Heterostructures and its Analogies in Electromagnetic Propagation in General Dielectrics," *Proc. IEEE*, vol. 79, pp. 1643-1659, Nov. 1991.

12. G. N. Henderson, T. K. Gaylord, E. N. Glytsis, P. N. First, and W. J. Kaiser, "Ballistic Electron Emission Microscopy Testing of Quantum Electron Wave Heterostructures," *Solid State Comm.*, vol. 80, no. 8, pp. 591-596, Nov. 1991.

13. G. N. Henderson, T. K. Gaylord, and E. N. Glytsis, "Electromagnetic Analogies to General-Hamiltonian Effective-mass Electron-Wave Propagation in Semiconductors," *Physical Rev. B (Condensed Matter)*, vol. 45, pp. 8404-8407, Apr. 15, 1992.

14. G. N. Henderson, T. K. Gaylord, and E. N. Glytsis, "Diffraction of Ballistic Electrons by Semiconductor Gratings: Rigorous Analysis, Approximate Analyses, and Device Design," *IEEE J. Quantum Electron.*, QE-XX, 1992. (submitted)

15. D. W. Wilson, E. N. Glytsis, and T. K. Gaylord, "Electron Waveguiding Characteristics and Ballistic Current Capacity of Semiconductor Quantum Slabs," *IEEE J. Quantum Electron.*, 1992. (submitted)

16. T. K. Gaylord, G. N. Henderson, and E. N. Glytsis, "Application of Electromagnetic Formalism to Quantum Mechanical Electron Wave Propagation in Semiconductors," *J. Opt. Soc. Am. B*, 1992. (submitted)

CONFERENCE PAPERS RESULTING FROM THE NSF AWARD

1. E. N. Glytsis, T. K. Gaylord, and K. F. Brennan, "Semiconductor Biased Superlattices as Electron Wave Interference Filter/Emitters," at Annual Meeting of the Optical Society of America, Orlando, FL, Oct. 15 - 20, 1989, and (Abstract) *J. Opt. Soc. Am. A*, vol. 6, no. 13, pg. 32, Dec. 1989.

2. T. K. Gaylord, E. N. Glytsis, and K. F. Brennan, "Guided Electron Waves in Semiconductor Quantum Wells," at Annual Meeting of the Optical Society of America, Orlando, FL, Oct. 15 - 20, 1989, and (Abstract) *J. Opt. Soc. Am. A*, vol. 6, no. 13, pg. 21, Dec. 1989.

3. K. Diff, K. F. Brennan, T. K. Gaylord, and E. N. Glytsis, "Wavepacket Propagation in Semiconductor Superlattice Interference Filters," *Bull. Amer. Phys. Soc.*, vol. 35,

pg. 825, Mar. 1990.

4. E. N. Glytsis, T. K. Gaylord, and K. F. Brennan, "Current-Voltage Characteristics and Space-Charge Effects in Semiconductor Electron/Wave Filter/Emitters," (Abstract) *Optical Society of America Annual Meeting Technical Digest Series*, vol. 15, pg. 261, Nov. 1990.

5. D. W. Wilson, E. N. Glytsis, and T. K. Gaylord, "Analysis of Ballistic Electron Transport in Semiconductor Quantum-Well Waveguides," (Abstract) *Optical Society of America Annual Meeting Technical Digest Series*, vol. 15, pg. 261, Nov. 1990.

6. G. N. Henderson, E. N. Glytsis, and T. K. Gaylord, "Relationship of Electromagnetic Reflection and Refraction to Quantum-Mechanical Transport in Semiconductor Superlattices," (Abstract) *Optical Society of America Annual Meeting Technical Digest Series*, vol. 15, pg. 261, Nov. 1990.

7. G. N. Henderson, T. K. Gaylord, E. N. Glytsis, P. N. First, and W. J. Kaiser, "Testing of Multilayer Semiconductor Electron Wave Devices Using Ballistic Electron Emission Microscopy," (Abstract) *Optical Society of America Annual Meeting Technical Digest Series*, vol. 17, pg. 143, Nov. 1991.

8. D. B. Walker, E. N. Glytsis, and T. K. Gaylord, "Time-Dependent Characteristics, of Semiconductor Resonant Structures," (Abstract) *Optical Society of America Annual Meeting Technical Digest Series*, vol. 17, pp. 32-33, Nov. 1991.

9. D. W. Wilson, E. N. Glytsis, and T. K. Gaylord, "Electron Waveguiding in Quantum Wells, Voltage-Induced Wells, and Quantum Barriers," (Abstract) *Optical Society of America Annual Meeting Technical Digest Series*, vol. 17, pg. 144, Nov. 1991.

10. G. N. Henderson, E. N. Glytsis, and T. K. Gaylord, "Ballistic Electron Diffraction by Semiconductor Gratings: Analysis, Design, and Analogies to Electromagnetic Diffraction," (Abstract) *Optical Society of America Annual Meeting Technical Digest Series*, vol. 16, pg. 143, Nov. 1991.

11. G. N. Henderson, P. N. First, T. K. Gaylord, E. N. Glytsis, and W. J. Kaiser, "Low-Temperature Beem Testing of Quantum Semiconductor Heterostructures," *Ballistic Electron Emission Microscopy Workshop 1992 Abstracts*, January 27, 1992, Furnace Creek Inn and Ranch Resort, Death Valley, California.

12. T. K. Gaylord, G. N. Henderson, E. N. Glytsis, D. W. Wilson, P. N. First, and D. B. Walker, "Semiconductor Ballistic Electron Reflection, Refraction, and Diffraction Effects: Modeling and Quantum Device Applications," (invited), *Integrated Photonics Research Topical Meeting*, April 13-15, 1992, New Orleans, Louisiana.

13. G. N. Henderson, T. K. Gaylord, and E. N. Glytsis, "Ballistic Electron Diffractive Switches: Design and Performance Analysis," *Integrated Photonics Research Topical Meeting*, April 13-15, 1992, New Orleans, Louisiana.

PATENTS AND PATENT APPLICATIONS RESULTING FROM THE NSF AWARD

1. T. K. Gaylord, K. F. Brennan, and E. N. Glytsis, "Semiconductor quantum well electron and hole waveguides," U.S. Patent No. 4,970,563, assigned to Georgia Research Corporation, issued Nov. 13, 1990.

2. T. K. Gaylord, K. F. Brennan, and E. N. Glytsis, "Solid state quantum mechanical electron and hole wave devices," U.S. Patent No. 4,985,737, assigned to Georgia tech Research Corporation, issued Jan. 15, 1991.

3. T. K. Gaylord, E. N. Glytsis, and K. F. Brennan, "Semiconductor biased superlattice tunable interference filter/emitter," U.S. Patent, No. 4,987,458, assigned to Georgia Tech Research Corporation, issued Jan. 22, 1991.

4. T. K. Gaylord, K. F. Brennan, and E. N. Glytsis, "Solid state quantum mechanical electron and hole wave devices," international filing date of November 16, 1989, Patent Cooperative Treaty no. PCT/US89/05240. U. S. Patent Office serial nos. 07/272,175, 07/374,437, and 07/374,476. Georgia Tech Record of Invention nos. 1-88-13/1004, 1-88-14/1006A, 1-88- 14/1006B. Hurt, Richardson file no. 10733-066.

5. T. K. Gaylord, E. N. Glytsis, and K. F. Brennan, "Solid state quantum mechanical electron and hole wave devices," Chinise filing date of November 16, 1989, Patent Application no. 89108621.8. U. S. Patent Office serial nos. 07/272,175, 07/374,437, and 07/374,476. Georgia Tech Record of Invention nos. 1-88-13/1004, 1-88-14/1006A, 1-88- 14/1006B. Hurt, Richardson file no. 10733-063.

7. T. K. Gaylord, E. N. Glytsis, and K. F. Brennan, "Solid state quantum mechanical electron and hole wave devices," Canadian filing date of November 16, 1989, Patent File

no. 2,003,134. U. S. Patent Office serial nos. 07/272,175, 07/374,437, and 07/374,476. Georgia Tech Record of Invention nos. 1-88-13/1004, 1-88-14/1006A, 1-88-14/1006B. Hurt, Richardson file no. 10733-065.

8. G. N. Henderson, T. K. Gaylord, and E. N. Glytsis, "Quantum-mechanical semiconductor device with electron/hole diffractive grating." U. S. filing date of July 18, 1991. U. S. Patent Office serial no. 07/734,300. Georgia Tech Record of Invention no. ROI 1194. Hurt, Richardson file no. 10733-109.

FINAL REPORT OF THE

NSF RESEARCH INITIATION AWARD ENTITLED:

SEMICONDUCTOR QUANTUM WAVE DEVICES

ECS-8909971

Award Dates: August 1989 — July 1992

Submitted to

the National Science Foundation

by the Georgia Institute of Technology

PRINCIPAL INVESTIGATOR

Elias N. Glytsis

School of Electrical Engineering and

Microelectronics Research Center

November 1992

SUMMARY

The efforts of the semiconductor industry to scale down the size of devices to achieve higher integration levels and higher speeds have been confronted by the major problem of the "troublesome" quantum-mechanical wave interference effects. These "troublesome" effects start to dominate device characteristics at dimensions of less than about one-quarter of a micron, thus, making further size reduction impossible. This limits the level of integration and the ultimate speed of integrated circuits. Further advances require fundamentally new device concepts and designs. The constructive use of the "troublesome" quantum effects was the basic premise of the proposed "Semiconductor Quantum Wave Optics" research. The long-term scientific objective of the completed research was to generate the necessary knowledge of nanometer-scale semiconductor quantum wave devices that would allow the practical development and use of these structures. Utilization of these quantum devices would be both for ultra-small high-speed versions of present-day devices (such as higher speed switches, oscillators, et.) and for future guided electron wave integrated circuits. This objective of this activity was to bring together understanding of the underlying physics, device modeling, development of software tools, device design methodology, evaluation of existing quantum interference experiments, crystal growth, device fabrication, and device testing. The work completed during the period of the award can be summarized into eight categories: (a) generalization of the analogies between electromagnetic waves in general dielectrics and electron waves in semiconductors, (including analogies with a generalized Hamiltonian) (b) theory and design of narrow-band semiconductor superlattice filter/emitters, (c) negative-differential-resistivity quantum interference devices, (d) theory and design of electron-wave impedance transformers, (e) space-charge effects in quantum wave devices, (f) time-dependent characteristics of the electron-wave interference filters and filter/emitters, (g) electron wave slab waveguides, (h) electron wave quantum interference grating devices, (i) a quantum interference effects in semiconductors bibliography, (j) a proposed innovative testing technique of quantum interference structures using ballistic electron emission microscopy, and (k) three related patents and four patent applications. The aforementioned research results are summarized in the following report.

MAIN RESULTS DURING THE AWARD PERIOD

1. Ballistic Electron Transport in Semiconductor Heterostructures and its Analogies in Electromagnetic Propagation in General Dielectrics

A comprehensive set of analogies was established between electromagnetic propagation in general isotropic dielectrics (differing permeability and permittivity) and electron wave propagation in semiconductors. First, the electromagnetic results for propagation in non-magnetic dielectrics were generalized to describe propagation, reflection, and refraction in general dielectrics through the definition of separate phase and amplitude refractive indices. Through the analogous definition of electron wave phase and amplitude refractive indices, the expressions for electron wave propagation, reflection, and refraction were shown to have the same functional form as the electromagnetic results. Using these results, the reflectivity characteristics such as total internal reflection (critical angle) and zero reflectivity (Brewster angle) were analyzed as a function of material parameters for both general dielectrics and semiconductor materials. The critical angle and Brewster angle results were then applied to electron wave propagation in the $Ga_{1-x}Al_xAs$ material system, where it is shown that all interfaces in this material will have both a critical angle and a Brewster angle. This was the first prediction of an electron wave Brewster angle in semiconductors.

2. Electromagnetic Analogies to General-Hamiltonian Single-Band Effective-Mass Electron Wave Propagation in Semiconductors with Spatially Varying Effective Mass and Potential Energy

It was shown that exact, quantitative electromagnetic analogies exist for all forms of the general Hamiltonian of Morrow and Brownstein [Phys. Rev. B 30, 678 (1984)] which applies to single-band effective-mass electron wave propagation in semiconductors. It was further shown that these analogies are valid for propagation in the bulk, propagation past abrupt interfaces between materials, and propagation within two-dimensionally inhomogeneous materials. These results indicate that the correct form of the single-band effective-mass Hamiltonian can be determined through appropriate wavefunction-amplitude-sensitive experiments. Wavefunction- phase-sensitive experiments (such as the measurement of electron wave refraction directions) are not adequate to specify completely the Hamiltonian.

3. Theory and design of narrow-band semiconductor superlattice filter/emitters

A voltage-biased semiconductor superlattice structure was designed to operate as a continuously voltage-tunable, electron-wave interference filter and as an electron emitter. Using the analogies between electromagnetic waves and electron-waves, a systematic procedure was developed for designing the quantum wells and barriers comprising the electron-wave filter/emitter superlattice. A generalized procedure was also developed for analyzing the electron-current transmittance and reflectance spectral responses of these superlattice structures. The constraints required to have thicknesses that are integer multiples of the monolayer thickness and to minimize intervalley scattering were also included in the design. The filter/emitter was shown to operate over a wide tunable energy range. The full width at half maximum (FWHM) of the filter/emitter was shown to decrease as the number of the filter layers was increased. A sensitivity analysis of the device characteristics in the presence of fabrication errors revealed a very stable device response.

4. Ballistic Current-Voltage Characteristics of Semiconductor Superlattice Electron Wave Quantum Interference Filter/Emitter Negative Differential Resistance Devices

The transmission and current-voltage characteristics of semiconductor superlattice electron-wave quantum-interference filter/emitter negative differential resistance devices were analyzed with and without the self-consistency requirement. For the non-self-consistent calculation the single-band effective-mass time-independent Schroedinger equation was solved. For the self-consistent calculation, Schroedinger and Poisson equations were solved iteratively until a self-consistent electron potential energy and electron density were obtained. It was shown that suitably designed electron- wave quantum-interference filter/emitters can exhibit strong negative differential resistance in the current-voltage characteristics, similar to those of resonant tunneling diodes. For low to moderate (2-30 meV) Fermi energies in the conduction band of $Ga_{1-x}Al_xAs$ (doping concentration less or equal to 2×10^{18} cm^3), and temperatures near 30 K (in the ballistic transport regime), it was shown that the space-charge effect is relatively small and results in a shift of the current-voltage and transmission characteristics toward higher bias voltages. In a fashion similar to that occurring in resonant tunneling diodes, the self-consistent field in electron-wave filter/emitter negative differential resistance devices effectively acts to screen the

positive applied bias. Designs of $Ga_{1-x}Al_xAs$ devices were presented. Resonant devices with current peak-to-valley ratios of 50 as well as nonresonant (not exhibiting negative differential resistance) devices were analyzed. The corresponding electron charge density distributions were also presented. Superlattice electron-wave filter/emitter negative differential resistance devices can be used as high-speed switches and oscillators and as monoenergetic emitters in electroluminescent devices and photodetectors.

5. Theory and design of electron wave impedance transformers

In the construction of semiconductor quantum devices and guided electron-wave integrated circuits it will be necessary to connect semiconductor materials with differing electron energy-band structure. In such a configuration, detrimental reflections will occur at the energy-band discontinuity between materials. These reflections can be eliminated or minimized using impedance transformers. These type of impedance transformers for ballistic (collisionless) electron-waves traveling between dissimilar energy-gap semiconductors were designed as a series of quarter (electron) wavelength layers in the form of a compositional superlattice, using the quantitative analogies between electromagnetic and electron waves. For the design energy, the electron-wave could be totally transmitted and the structure can be analogous to an antireflection coating in electromagnetic optics. Procedures for designing narrow-band, maximally flat (Butterworth), and equal-ripple (Chebyshev) impedance transformers of arbitrary spectral bandwidth were developed.

6. Space Charge Effects in Quantum Wave Devices

Theoretical techniques for studying the properties of electron wave superlattice structures have been developed. Specifically, we have included self-consistent effects in the design of superlattice electron-wave filters through the simultaneous solution of the Poisson and Schroedinger Equations. It was found that at doping concentrations less than or equal to 2×10^{18} cm^3 and temperatures near 30 K (ballistic regime) that space-charge effects are relatively small in superlattice electron-wave filters. Nevertheless, self-consistent effects act in a similar manner as in resonant tunneling diodes; the current-voltage shifts towards higher voltages. In addition, we have solved the time-dependent Schroedinger Equation in order to determine the temporal response of electron-wave superlattice filters. It was found that the frequency response is much greater in these devices than in existing resonant tunneling devices offering the possibility of a new ultra-high frequency (THz) oscillator.

7. Time-Dependent Characteristics of Semiconductor Resonant Structures

Double-barrier tunneling structures operate based on quantum mechanical tunneling through two barriers. Quantum electron wave structures operate based on traveling-wave propagation above all conduction band edges. These are the fundamental structures proposed to realize ballistic electron transport devices in semiconductors. The time-dependent behavior of resonant tunneling structures has been discussed extensively in the literature, but no such analysis has been performed on quantum wave structures. A numerical solution of the time-dependent effective mass equation was used to calculate the traversal time of a Gaussian packet and the percentage of the packet transmitted for resonant tunneling and quantum wave structures.

8. Electron Waveguiding in Quantum Wells, Voltage-Induced Quantum Wells, and Quantum Barriers

Recent experiments have produced ballistic electron transport over micron lengths in semiconductor two-dimensional electron gas (2DEG) systems. This has made possible the demonstration of electron devices that exhibit impressive optical-like behavior. In these devices, the quantum well at the 2DEG interface acts as a slab waveguide for ballistic electron waves. In this work, we showed how finite-potential heterostructure wells, homostructure voltage-induced wells, and heterostructure barriers can act as electron slab waveguides. We found that the waveguiding in all of these structures is described by a single dispersion relation and can occur at energies above all band edges. The guided mode cutoffs, electron velocity, effective mass, density of states, and ballistic current density were determined. A multiple layer theory was developed to analyze wells and barriers with arbitrary potential energy profiles. The maximum ballistic guided current flowing in a given direction for a 10 monolayer $Ga_{0.75}Al_{0.25}As/GaAs/\text{-}Ga_{0.9}Al_{0.1}As$ waveguide was found to be 2.3 mA per micron of waveguide width. This relatively large value suggests that interconnecting multiple ballistic electron devices through a single slab waveguide may be feasible.

9. Ballistic Electron Diffraction by Semiconductor Gratings: Analysis, Design, and Analogies to Electromagnetic Diffraction

Due to recent advances in the growth and fabrication of nanostructure electronic devices, it has been demonstrated that ballistic electron waves can be reflected, refracted,

interfered, waveguided, and diffracted in a manner analogous to electromagnetic optics. This has provided a surge of interest in the new field of semiconductor electron wave optics. In this paper, ballistic electron grating diffraction by a grating with an arbitrary effective mass and/or potential energy profile was analyzed using a rigorous coupled-wave analysis (RCWA). These results are related to electromagnetic diffraction by a permittivity grating. It was shown that electron diffraction by a kinetic energy grating was exactly analogous to TE electromagnetic diffraction and that electron diffraction by an effective mass grating was exactly analogous to TM electromagnetic diffraction. Approximate solutions to the RCWA equations were derived that are equivalent to Bragg regime and Raman-Nath diffraction. Using these results, sample electron wave diffractive switches and multiplexers were designed using achievable device configurations. The angular and energy selectivity of these devices were examined.

10. Quantum Interference Effects in Semiconductors: A Bibliography

Refinements in growth techniques such as molecular beam epitaxy (MBE) have produced materials with ballistic (collisionless) electron transport lengths of over a micron. Coupled with nanolithography it is now possible to fabricate structures with both lateral and vertical dimensions on the order of the deBroglie wavelength of a ballistic electron. In these structures quantum interference effects can dominate the electronic behavior. In view of the rapidly expanding interest and activity in this area, the following bibliography has been compiled as an introduction and study guide to this field. The papers listed describe the extensive theoretical and experimental results that have been obtained on quantum interference effects as well as discuss possible application areas. Works of a fundamental nature concerning phenomena that are basic to all semiconductor behavior have not been included. Articles on the properties and band structure of semiconductors, which are essential to a complete understanding of quantum interference effects, have not been included. Conference papers, though frequently very important, have not been included to conserve space. The papers are listed alphabetically according to the first author's surname. As in the compilation of any bibliography, numerous valuable and pertinent articles have probably been inadvertently omitted.

11. Testing Multilayer Semiconductor Electron Wave Devices Using Ballistic Electron Emission Microscopy

Ballistic electron emission microscopy (BEEM) has recently been developed to study

the electrical properties of buried interfaces where ballistic electrons are injected into a sample using a scanning tunneling microscope (STM). In this paper, a method was proposed that uses the BEEM technique to observe electron wave optical properties of ballistic transport in semiconductors. This method provides a three-terminal configuration for characterizing electron wave devices that overcomes many of the problems encountered in traditional two- and three-terminal techniques. Specifically, the method provides a highly collimated beam of ballistic carriers with a precisely controlled energy distribution. These carriers probe the quantum transmittance of a voltage-tunable electron wave interference device with minimal impurity scattering. A general procedure was presented for analyzing this experimental configuration based on a combination of the models used to describe BEEM and ballistic electron transport in semiconductors.

Using this procedure, a BEEM analysis of an electron wave energy filter was modeled, showing clear electron wave interference effects. This BEEM configuration allows for the precise characterization of a wide range of ballistic electron transport effects, such as quantum reflections from interfaces and electron wave interference effects, that are currently of wide interest.

12. Solid State Quantum Mechanical Electron and Hole Wave Devices Patents and Patent Applications

Solid state quantum mechanical electron or hole wave devices which are analogous to optical thin-film devices provide among other things, energy selectivity for substantially ballistic electron or hole wave propagation in superlattice structures at energies above the superlattice potential energy barriers. Further, in accordance with this patent, the inventive devices may be designed by transforming existing optical thin-film design methods and existing optical interference filter designs into inventive semiconductor devices. This transformation from existing optical design methods and existing optical interference filter designs into semiconductor devices is performed for electron devices by mapping the optical phase index of refraction into a first solid state index of refraction for phase quantities which is proportional to the square root of the product of the electron kinetic energy and the electron effective mass and by mapping the optical amplitude index of refraction into a second solid state index of refraction for amplitude quantities which is proportional to the square root of the electron kinetic energy divided by the electron effective mass.

This patent pertains to solid state quantum mechanical electron and hole wave devices

and method for fabricating them and, in particular, to solid state quantum mechanical electron and hole wave devices such as, without limitation, low pass filters, high pass filters, narrow band and wide band notch filters, narrow band and wide band bandpass filters, impedance transformers, resonant electron and hole emitters, and so forth and method for fabricating them.

Recent progress in semiconductor growth technologies, particularly in molecular beam epitaxy (MBE) and metal organic chemical vapor deposition (MOCVD), enable the growth of multilayered superlattice structures with precise monolayer compositional control. For example, successively grown layers of narrow and wide band gap semiconductor materials such as GaAs and $Ga_{1-x}Al_xAs$ have been produced and widely used to provide multiple quantum well structures. In fact, there are many references in the prior art which are concerned with the use of these superlattice structures in resonant tunneling superlattice/multiple quantum well devices. Specifically, in such devices, a superlattice is formed by growing successive layers of narrow and wide band gap semiconductor material epitaxially and the materials and the widths of the layers in these devices are chosen so that quantum states which arise from spatial quantization effects in adjacent wells become coupled. Further, in such devices, the interaction of these coupled states leads to the formation of minibands of allowed energies through which carriers can tunnel.

The first embodiments of the inventive solid state electron wave devices comprise solid state analogs of Fabry-Perot optical interference filters which may be fabricated from alloys of GaAlAs and GaAs.

13. Semiconductor Quantum Well Electron and Hole Waveguides Patent and Patent Applications

Semiconductor, quantum well, electron and hole slab waveguides include a substrate, semiconductor layer, a film semiconductor layer, and a cover semiconductor layer, wherein the semiconductor layers provide substantially ballistic transport for electrons and wherein the thicknesses and compositions of the semiconductor layers are determined in accordance with this patent to provide a waveguide.

Embodiments of the patent solve the above-identified need in the art by providing semiconductor, quantum well, electron and hole slab waveguides. Specifically, an electron slab waveguide is comprised of a substrate semiconductor layer, a film semiconductor layer,

and a cover semiconductor layer, wherein the semiconductor layers provide substantially ballistic transport for electrons and wherein the thicknesses and compositions of the semiconductor layers are determined in accordance with the inventive method which is set forth in detail below to provide a potential well.

In particular, in accordance with this patent, electron waveguide modes exist for electron energies in the well and for electron energies above one or both of the potential energy barriers of the substrate layer and the cover layer, respectively. Further, in contrast to the behavior of electromagnetic guided waves which only have a lower-energy cutoff due to dispersion, each electron waveguide mode also has an upper-energy cutoff wherein an electron wave is refracted into the substrate layer and/or the cover layer.

Doping of semiconductors is not required for embodiments of the present invention, however, it is preferred that doping not be done within the active region of the device in order to avoid scattering within the materials. This provides a further advantage for the inventive waveguide devices because the absence of doping makes them easier to fabricate.

Note that semiconductor electron slab waveguides can perform as described provided that ballistic transport can be achieved over sufficient distances and that the density of electrons is small enough to make electron-electron interactions negligible.

The inventive electron waveguides should be useful in high-speed electronic circuitry and as a central component in electron guided wave integrated circuits.

14. Solid State Quantum Mechanical Electron and Hole Wave Devices Patents and Patent Applications

Continuously tunable, biased, semiconductor superlattice electron interference filter/emitter which can serve, for example, as a hot electron emitter in a ballistic transistor, provides energy selectivity for substantially ballistic electron wave propagation at electron energies above the superlattice potential barriers. The layers of the biased superlattice have alternatively high and low electron refractive indices wherein each layer is a quarter or half of an electron wavelength in thickness and wherein the quantum well barrier widths are adjusted in the direction of emission to provide the desired energy selectivity.

Embodiments of this patent solve the above-identified need in the art by providing biased, semiconductor superlattice tunable electron interference filters/emitters which can

serve,for example, as a hot electron emitter in a ballistic transistor. In particular, embodiments of the present invention comprise biased superlattice filter/emitters which provide energy selectivity for substantially ballistic electron wave propagation at electron energies above the superlattice potential barriers. Further, the layers of the biased superlattice comprise alternately high and low electron refractive indices wherein each layer is a multiple of a quarter or half of an electron wavelength in thickness and wherein the quantum well barrier widths are adjusted in the direction of emission to provide the desired energy selectivity.

Specifically, embodiments of the present invention comprise biased, semiconductor superlattice filter/emitters which are designed, in accordance with the inventive method, by transforming optical, thin-film interference filter designs which are designed in accordance with existing optical interference filter design methods into inventive semiconductor devices. In particular, the transformation from an optical interference filter design is performed by mapping the optical phase index of refraction into a solid state index of refraction for phase quantities which is proportional to the square root of the product of electron kinetic energy and electron effective mass and by mapping the optical amplitude index of refraction into a solid state index of refraction for amplitude quantities which is proportional to the square root of the electron kinetic energy divided by the electron effective mass. That is, the mapping makes an exact analogy between an electromagnetic optical wave and a quantum mechanical electron wave by using the electron wavevector above in place of the electromagnetic optical wavevector and by using the electron wave amplitude refractive index in expressions for reflectivity and transmissivity at a boundary, which expressions are well known from electromagnetic design.

The efficacy of the above-defined mapping between electromagnetic optical waves and quantum mechanical electron waves depends on the existence of ballistic electron transport in the solid state materials, i.e., where electrons travel through the solid state materials without being scattered by deviations from crystalline perfection. In the inventive filter/emitter devices, the ballistic electrons have energies above the potential barriers in the solid state materials and exhibit quantum mechanical plane wave behavior. Further, since these plane waves maintain their phase through the device, these coherent waves will refract, reflect, interfere, and diffract in a manner which is analogous to the behavior of electromagnetic waves traveling through dielectrics.

15. Quantum Mechanical Semiconductor Device with Electron/Hole Diffraction Grating Patent Application

A solid state, quantum mechanical electron/hole wave device in the form of a switch or a multiplexor includes a layer of semiconductor material supporting substantially ballistic electron/hole transport and a periodic grating structure formed in the layer of semiconductor material, with the grating structure comprising a modulation in electron/hole potential energy and/or effective mass. Preferably, means are provided for applying and varying the grating modulation. By constructing the device to divide the input substantially completely into two output beams (0 and +1) (to Operate in the Bragg regime), a useful switch is provided. Likewise, by constructing the device to divide the input into a selected number of three or more output beams (± 1, 0, ± 2) (to operate in the Raman-Nath regime), a useful multiplexor (broadcasting device) is provided.

HUMAN RESOURCES DEVELOPMENT

Three graduate students have been involved in the research work described previously. These are: (a) Mr. Gregory N. Henderson (Ph.D. expected December 1992) who has been working on analogies between electron wave and electromagnetic wave propagation, electron wave grating interference devices, and ballistic electron emission testing of quantum heterostructures; (b) Mr. Daniel W. Wilson (Ph.D. candidate) who has been working on electron wave slab waveguides as part of his thesis work; (c) Mr. David B. Walker (Ph.D. candidate) who has been working on time-dependent simulations of vertical transport devices. In addition, a post doctoral fellow, Dr. Karim Diff, was partially supported for a six month period working also on time-dependent solutions of the Schrödinger equation. Two undergraduate students have recently been involved in this research work. Mr. Daniel Guthrie (EE senior) has been working on simulations of quantum interference vertical transport biased and unbiased structures and calculations of density of states, and Ms. Patricia Dantzscher (EE senior) who has been working on software and hardware development for the scanning tunneling microscope.

JOURNAL PUBLICATIONS RESULTING FROM THE NSF AWARD

1. T. K. Gaylord, E. N. Glytsis, and K. F. Brennan, "Semiconductor Superlattice Interference Filter Design," *J. of Appl. Phys.*, vol.65, pp. 2535-2540, Mar. 15, 1989.

2. E. N. Glytsis, T. K. Gaylord, and K. F. Brennan, "Semiconductor Biased Superlattice

Tunable Electron Interference Filter/Emitter," *J. Appl. Phys.*, vol. 66, pp. 1494-1497, Aug. 1, 1989.

3. T. K. Gaylord, E. N. Glytsis, and K. F. Brennan, "Semiconductor Electron Wave Slab Waveguides," *J. Appl. Phys.*, vol. 66, pp. 1483-1485, Aug. 1, 1989.

4. T. K. Gaylord, E. N. Glytsis, and K. F. Brennan, "Semiconductor Quantum Well Electron Waveguides," *J. Appl. Phys.*, vol. 66, pp. 1842-1848, Aug. 15, 1989.

5. E. N. Glytsis, T. K. Gaylord, and K. F. Brennan, "Theory and Design of Semiconductor Electron-Wave Interference Filter/Emitters," *J. Appl. Phys.*, vol. 66, pp. 6158-6167, Dec. 15, 1989.

6. T. K. Gaylord, E. N. Glytsis, and K. F. Brennan, "Electron-Wave Quarter-Wavelength Impedance Transformers Between Differing Semiconductors," *J. Appl. Phys.*, vol. 67, pp. 2623-2630, Mar. 1, 1990.

7. G. N. Henderson, E. N. Glytsis, and T. K. Gaylord, "Electron Wave Diffraction by Semiconductor Gratings: Rigorous Analysis and Design Parameters," *Appl. Phys. Lett.*, vol. 59, pp. 440-442, July 22, 1991.

8. T. K. Gaylord, E. N. Glytsis, G. N. Henderson, K. P. Martin, D. B. Walker, D. W. Wilson, and K. F. Brennan, "Quantum Interference Effects in Semiconductors: A Bibliography," (invited) *Proc. IEEE*, vol. 79, pp. 1159-1180, Aug. 1991.

9. E. N. Glytsis, T. K. Gaylord, and K. F. Brennan, " Ballistic Current- Voltage Characteristics of Semiconductor Superlattice Electron-Wave Quantum-Interference Filter/Emitter Negative Differential Resistivity Devices," *J. Appl. Phys.*, vol. 70, pp. 3920-3933, Oct. 1, 1991.

10. D. W. Wilson, E. N. Glytsis, and T. K. Gaylord, "Quantum Well, Voltage- Induced Quantum Well, and Quantum Barrier Electron Waveguides: Modes, Cutoffs, and Maximum Current," *Appl. Phys. Lett.*, vol. 59, pp. 1855-1857, Oct. 7, 1991.

11. G. N. Henderson, T. K. Gaylord, and E. N. Glytsis, "Ballistic Electron Transport in Semiconductor Heterostructures and its Analogies in Electromagnetic Propagation in General Dielectrics," *Proc. IEEE*, vol. 79, pp. 1643-1659, Nov. 1991.

12. G. N. Henderson, T. K. Gaylord, E. N. Glytsis, P. N. First, and W. J. Kaiser, "Ballistic

Electron Emission Microscopy Testing of Quantum Electron Wave Heterostructures," *Solid State Comm.*, vol. 80, no. 8, pp. 591-596, Nov. 1991.

13. G. N. Henderson, T. K. Gaylord, and E. N. Glytsis, "Electromagnetic Analogies to General-Hamiltonian Effective-mass Electron-Wave Propagation in Semiconductors," *Physical Rev. B (Condensed Matter)*, vol. 45, pp. 8404-8407, Apr. 15, 1992.

14. G. N. Henderson, T. K. Gaylord, and E. N. Glytsis, "Diffraction of Ballistic Electrons by Semiconductor Gratings: Rigorous Analysis, Approximate Analyses, and Device Design," *IEEE J. Quantum Electron.*, QE-XX, 1992. (submitted)

15. D. W. Wilson, E. N. Glytsis, and T. K. Gaylord, "Electron Waveguiding Characteristics and Ballistic Current Capacity of Semiconductor Quantum Slabs," *IEEE J. Quantum Electron.*, 1992. (submitted)

16. T. K. Gaylord, G. N. Henderson, and E. N. Glytsis, "Application of Electromagnetic Formalism to Quantum Mechanical Electron Wave Propagation in Semiconductors," *J. Opt. Soc. Am. B*, 1992. (submitted)

CONFERENCE PAPERS RESULTING FROM THE NSF AWARD

1. E. N. Glytsis, T. K. Gaylord, and K. F. Brennan, "Semiconductor Biased Superlattices as Electron Wave Interference Filter/Emitters," at Annual Meeting of the Optical Society of America, Orlando, FL, Oct. 15 - 20, 1989, and (Abstract) *J. Opt. Soc. Am. A*, vol. 6, no. 13, pg. 32, Dec. 1989.

2. T. K. Gaylord, E. N. Glytsis, and K. F. Brennan, "Guided Electron Waves in Semiconductor Quantum Wells," at Annual Meeting of the Optical Society of America, Orlando, FL, Oct. 15 - 20, 1989, and (Abstract) *J. Opt. Soc. Am. A*, vol. 6, no. 13, pg. 21, Dec. 1989.

3. K. Diff, K. F. Brennan, T. K. Gaylord, and E. N. Glytsis, "Wavepacket Propagation in Semiconductor Superlattice Interference Filters," *Bull. Amer. Phys. Soc.*, vol. 35, pg. 825, Mar. 1990.

4. E. N. Glytsis, T. K. Gaylord, and K. F. Brennan, "Current-Voltage Characteristics and Space-Charge Effects in Semiconductor Electron/Wave Filter/Emitters," (Abstract) *Optical Society of America Annual Meeting Technical Digest Series*, vol. 15, pg. 261,

Nov. 1990.

5. D. W. Wilson, E. N. Glytsis, and T. K. Gaylord, "Analysis of Ballistic Electron Transport in Semiconductor Quantum-Well Waveguides," (Abstract) *Optical Society of America Annual Meeting Technical Digest Series*, vol. 15, pg. 261, Nov. 1990.

6. G. N. Henderson, E. N. Glytsis, and T. K. Gaylord, "Relationship of Electromagnetic Reflection and Refraction to Quantum-Mechanical Transport in Semiconductor Superlattices," (Abstract) *Optical Society of America Annual Meeting Technical Digest Series*, vol. 15, pg. 261, Nov. 1990.

7. G. N. Henderson, T. K. Gaylord, E. N. Glytsis, P. N. First, and W. J. Kaiser, "Testing of Multilayer Semiconductor Electron Wave Devices Using Ballistic Electron Emission Microscopy," (Abstract) *Optical Society of America Annual Meeting Technical Digest Series*, vol. 17, pg. 143, Nov. 1991.

8. D. B. Walker, E. N. Glytsis, and T. K. Gaylord, "Time-Dependent Characteristics, of Semiconductor Resonant Structures," (Abstract) *Optical Society of America Annual Meeting Technical Digest Series*, vol. 17, pp. 32-33, Nov. 1991.

9. D. W. Wilson, E. N. Glytsis, and T. K. Gaylord, "Electron Waveguiding in Quantum Wells, Voltage-Induced Wells, and Quantum Barriers," (Abstract) *Optical Society of America Annual Meeting Technical Digest Series*, vol. 17, pg. 144, Nov. 1991.

10. G. N. Henderson, E. N. Glytsis, and T. K. Gaylord, "Ballistic Electron Diffraction by Semiconductor Gratings: Analysis, Design, and Analogies to Electromagnetic Diffraction," (Abstract) *Optical Society of America Annual Meeting Technical Digest Series*, vol. 16, pg. 143, Nov. 1991.

11. G. N. Henderson, P. N. First, T. K. Gaylord, E. N. Glytsis, and W. J. Kaiser, "Low-Temperature Beem Testing of Quantum Semiconductor Heterostructures," *Ballistic Electron Emission Microscopy Workshop 1992 Abstracts*, January 27, 1992, Furnace Creek Inn and Ranch Resort, Death Valley, California.

12. T. K. Gaylord, G. N. Henderson, E. N. Glytsis, D. W. Wilson, P. N. First, and D. B. Walker, "Semiconductor Ballistic Electron Reflection, Refraction, and Diffraction Effects: Modeling and Quantum Device Applications," (invited), *Integrated Photonics Research Topical Meeting*, April 13-15, 1992, New Orleans, Louisiana.

13. G. N. Henderson, T. K. Gaylord, and E. N. Glytsis, "Ballistic Electron Diffractive Switches: Design and Performance Analysis," *Integrated Photonics Research Topical Meeting*, April 13-15, 1992, New Orleans, Louisiana.

PATENTS AND PATENT APPLICATIONS RESULTING FROM THE NSF AWARD

1. T. K. Gaylord, K. F. Brennan, and E. N. Glytsis, "Semiconductor quantum well electron and hole waveguides," U.S. Patent No. 4,970,563, assigned to Georgia Research Corporation, issued Nov. 13, 1990.

2. T. K. Gaylord, K. F. Brennan, and E. N. Glytsis, "Solid state quantum mechanical electron and hole wave devices," U.S. Patent No. 4,985,737, assigned to Georgia tech Research Corporation, issued Jan. 15, 1991.

3. T. K. Gaylord, E. N. Glytsis, and K. F. Brennan, "Semiconductor biased superlattice tunable interference filter/emitter," U.S. Patent, No. 4,987,458, assigned to Georgia Tech Research Corporation, issued Jan. 22, 1991.

4. T. K. Gaylord, K. F. Brennan, and E. N. Glytsis, "Solid state quantum mechanical electron and hole wave devices," international filing date of November 16, 1989, Patent Cooperative Treaty no. PCT/US89/05240. U. S. Patent Office serial nos. 07/272,175, 07/374,437, and 07/374,476. Georgia Tech Record of Invention nos. 1-88-13/1004, 1-88-14/1006A, 1-88- 14/1006B. Hurt, Richardson file no. 10733-066.

5. T. K. Gaylord, E. N. Glytsis, and K. F. Brennan, "Solid state quantum mechanical electron and hole wave devices," Chinise filing date of November 16, 1989, Patent Application no. 89108621.8. U. S. Patent Office serial nos. 07/272,175, 07/374,437, and 07/374,476. Georgia Tech Record of Invention nos. 1-88-13/1004, 1-88-14/1006A, 1-88- 14/1006B. Hurt, Richardson file no. 10733-063.

7. T. K. Gaylord, E. N. Glytsis, and K. F. Brennan, "Solid state quantum mechanical electron and hole wave devices," Canadian filing date of November 16, 1989, Patent File no. 2,003,134. U. S. Patent Office serial nos. 07/272,175, 07/374,437, and 07/374,476. Georgia Tech Record of Invention nos. 1-88-13/1004, 1-88-14/1006A, 1-88-14/1006B. Hurt, Richardson file no. 10733-065.

8. G. N. Henderson, T. K. Gaylord, and E. N. Glytsis, "Quantum-mechanical semicon-

ductor device with electron/hole diffractive grating." U. S. filing date of July 18, 1991. U. S. Patent Office serial no. 07/734,300. Georgia Tech Record of Invention no. ROI 1194. Hurt, Richardson file no. 10733-109.

APPENDIX

Copies of most important Journal Publications

Semiconductor superlattice interference filter design

T. K. Gaylord, E. N. Glytsis, and K. F. Brennan
School of Electrical Engineering and Microelectronics Research Center, Georgia Institute of Technology, Atlanta, Georgia 30332

(Received 25 October 1988; accepted for publication 21 November 1988)

The quantitative analogies that have been previously established [J. Appl. Phys. 65, 814 (1989)] between electron wave propagation in semiconductors and optical wave propagation in dielectrics may be used to translate thin-film optical device designs into semiconductor superlattice device designs. The procedure for this direct mapping is also described in the above reference. The resulting designs, however, have compositions that are not constrained to be within a usable compositional range and they have layer thicknesses that are not constrained to be integer multiples of a monolayer thickness. In the present work, a systematic design procedure is presented that includes these required practical constraints. This procedure is then applied to the design of $Ga_{1-x}Al_xAs$ superlattice narrow interference filters. For pass kinetic energies in the range of 0.14–0.20 eV, compositions (values of x) and numbers of monolayer thicknesses needed to produce quarter-wavelength layers are calculated. The detailed design of an example narrow bandpass (15.4 meV) filter with a pass electron energy of 0.20 eV is presented.

I. BACKGROUND AND MOTIVATION

The development and refinement of molecular-beam epitaxy (MBE) and metalorganic chemical vapor deposition (MOCVD) has enabled semiconductor multilayered superlattices to be grown with precise monolayer compositional control.[1] Successively grown layers of narrow and wide band-gap semiconductor materials such as GaAs and $Ga_{1-x}Al_xAs$ have produced the well-known and widely used multiple quantum-well structures. Furthermore, improvements in the quality of materials grown have simultaneously produced ballistic electron transport.[2-4] That is, electrons travel through the device without being scattered (by deviations from crystalline perfection). The resulting ballistic electrons exhibit clear quantum mechanical plane-wave behavior. Since they maintain their phase throughout the device, these coherent waves will refract, reflect, interfere, and diffract in a manner analogous to electromagnetic waves.[5] Quantum interference effects have been observed experimentally in single-well double-barrier $GaAs/Ga_{1-x}Al_xAs$ and $In_{1-x}Ga_xAs/In_{1-y}Al_yAs$ potential barrier structures.[6-9] These measurements were made for single-well, double-barrier structures. Of course, electron interference effects are not limited to these single-well structures. In fact, the use of multilayer superlattices and electron energies above the potential barriers allows generalized semiconductor superlattice interference filters to be designed that are directly analogous to thin-film optical interference filters. These superlattice interference filters may exhibit very narrow passbands with full widths at half maximum (FWHM) on the order of only several meV.[10] Monolithically integrated into solid-state devices, these structures have potential use as monoenergetic emitters for electroluminescent devices,[11,12] photodetectors,[11,13] and fast ballistic transistors.[11,14] In addition, these devices could assist in the control of free-space electron beams in fields such as electron spectroscopy, electron beam lithography, and electron diffraction analysis of crystals.[15,16]

Electron wave propagation at energies above the potential barriers can be described by the analogies that exist between electron waves in semiconductors and electromagnetic waves in dielectrics.[5] However, semiconductor superlattice interference filter designs cannot simply be copies of thin-film optical filter designs. In the design of semiconductor superlattice interference filters, the thicknesses of the layers are restricted to be integer multiples of the monolayer thickness. In addition, there is typically only a limited usable composition range available. The purpose of this paper is to present a systematic design procedure for semiconductor superlattice interference energy filters subject to these constraints and then to apply this procedure to the example case of designing $Ga_{1-x}Al_xAs$ superlattice filters.

II. SEMICONDUCTOR ELECTRON WAVE OPTICS

Quantum mechanical electron waves in semiconductors and electromagnetic optical waves in dielectrics exhibit transmission, reflection, interference, and diffraction characteristics that are analogous to each other. At an infinitely thick potential energy barrier, for example, an electron wave with energy above the barrier will be total internally reflected if the angle of incidence is greater than the electron wave critical angle.[5] Likewise, in semiconductor superlattices, an electron wave may be totally transmitted or totally reflected depending on its energy and angle of incidence. These characteristics are analogous to the corresponding optical thin-film devices (an antireflection coating and a dielectric coated mirror). Quantum interference effects have been analyzed for single potential energy boundaries,[17] for normal incidence,[18] and for the general case of any number of boundaries and any angle of incidence.[5] From these results, a mapping has been established between electromagnetic and quantum mechanical quantities.[5] As a consequence, existing optical device designs now have electron wave device counterparts.

To describe phase effects such as in wave interference

 0021-8979/89/062535-06$02.40

for either electron or optical waves, the corresponding wave vector is used. For an electron wave, the wave-vector magnitude is

$$k = [2m^*(E - V)]^{1/2}/\hbar, \tag{1}$$

where m^* is the electron effective mass, E is the total electron energy, V is the electron potential energy, and $\hbar$ is Planck's constant divided by 2π. Thus, the electron wave phase refractive index, n_e (phase), is proportional to the square root of the product of the effective mass and the kinetic energy.[5] That is,

$$n_e(\text{phase}) \propto [m^*(E - V)]^{1/2}. \tag{2}$$

Amplitude effects such as transmissivity and reflectivity may be described in terms of the wave-function amplitude for an electron wave or in terms of the electric field amplitude for an optical wave incident upon a boundary. Continuity of the wave function across a potential energy boundary is analogous to the continuity of the tangential component of the electric field across a boundary between dielectrics. Similarly, conservation of electron probability current normal to a potential energy boundary is analogous to conservation of power flow normal to a boundary between dielectrics. Using these, the electron wave and optical wave reflectivities and transmissivities are made equivalent by introducing, in quantum mechanics, an analogous index of refraction or characteristic impedance.[5,18] Thus, the electron wave amplitude refractive index n_e (amplitude) is proportional to the square root of the ratio of the kinetic energy to the effective mass,[5] and so

$$n_e(\text{amplitude}) \propto [(E - V)/m^*]^{1/2}. \tag{3}$$

In the expressions for transmissivity and reflectivity, only dimensionless ratios of the electron wave amplitude refractive indices occur. Both types of electron wave refractive indices exhibit normal dispersion. That is, they increase with decreasing wavelength.

III. THIN-FILM OPTICAL INTERFERENCE FILTERS

Superlattice electron wave interference filters share common characteristics with thin-film optical interference filters. Therefore it is useful initially to review some of the primary properties of these optical filters.[19-22] This is particularly appropriate since the procedure for designing superlattice electron wave filters is an extension of that used for thin-film optical filters.

The simplest type of narrow bandpass optical interference filter is the Fabry–Perot filter. It consists of a half-wavelength layer (frequently called a "spacer" in optical literature) sandwiched between reflectors. In the case of an all-dielectric Fabry–Perot filter, the reflectors are stacks of high index (designated H) and low index (designated L) quarter-wavelength layers. Only this elementary type of interference filter will be treated in this paper. The FWHM of the bandpass in this type of filter can be reduced by increasing the reflectivity at the boundaries between the layers. This may be accomplished by increasing the ratio of the high index (n_H) to the low index (n_L). Furthermore, for a given number of layers, the higher reflectance occurs with high index (H) layers on the outside boundaries of the filter. The half-wavelength (resonant) layer at the center of the filter may be of high index (n_H) or low index (n_L) material. Thus there are two basic types of all-dielectric Fabry–Perot interference filters. In the optical literature, these are symbolically represented as $[HL]^N HH[LH]^N$ and $H[LH]^N LL[HL]^N H$ where H and L represent quarter-wavelength layers of high and low index materials, respectively, and N represents the number of repetitions of the layer-pair type indicated in square brackets.

Other important characteristics of the all-dielectric Fabry–Perot interference filters are as follows: (1) The maximum transmittance of the filter is 100%. (2) The maximum transmittance occurs at the wavelength for which the spacer layer is a half-wavelength thick (as measured in that material) and the reflector layers are a quarter-wavelength thick (as measured in those materials). This wavelength will be called the pass wavelength in this paper. (3) The FWHM decreases as the number of quarter-wavelength layers is increased. (4) The transmittance characteristic is symmetric about the pass wavelength when the characteristic is plotted as a function of the reciprocal of the wavelength (as measured in the material surrounding the filter). (5) A proportional change in the thicknesses of all the layers produces a simple displacement of the transmittance characteristic plotted as a function of the reciprocal wavelength. (6) If the thicknesses of all layers are increased by an odd integer factor (the parameter q_i in Sec. V), a passband will occur at the original pass wavelength and it will have a decreased FWHM. (7) As the angle of incidence upon the filter is increased, the pass wavelength is tuned to shorter wavelengths. (8) The transmittance characteristics are relatively insensitive to variations in the reflectivities and thicknesses of the layers. (9) Normal dispersion causes a narrowing of the FWHM. (10) The filter is effective over only a limited range since sidebands necessarily occur on either side of the passband. The wavelength range around the pass wavelength over which the transmission is low is called the rejection range. The range from the nearest passband peak below the pass wavelength to the nearest passband peak above the pass wavelength is called the free spectral range (FSR). Other terminology commonly employed in describing these filters include the finesse (= FSR/FWHM) and the resolving power (pass wavelength/$\frac{1}{2}$FWHM).

IV. SEMICONDUCTOR SUPERLATTICE INTERFERENCE FILTERS

Using the above electron wave refractive indices established from considering a single potential energy boundary, the characteristics of a many-boundary semiconductor superlattice system can be found.[5] This may be done by applying the chain matrix approach commonly employed in electromagnetics[23,24] but substituting the electron wave vector as given by Eq. (1) for the optical wavevector and using the electron wave amplitude refractive index as given by Eq. (3) in the expressions for the reflectivity and transmissivity at a boundary.[5]

In layer $m-1$ the amplitude of the electron wave incident (traveling in the positive direction) upon layer m is designated $\psi_{i,m}$. In layer $m-1$ the amplitude of the electron wave reflected (traveling in the negative direction) from layer m is designated $\psi_{r,m}$. These complex amplitudes may be expressed in terms of the corresponding amplitudes ($\psi_{i,m+1}$ and $\psi_{r,m+1}$) incident upon and reflected from the boundary between layer m and layer $m+1$ as

$$\begin{bmatrix}\psi_{i,m}\\ \psi_{r,m}\end{bmatrix}=\frac{1}{t_{e,m}}\begin{bmatrix}1 & r_{e,m}\\ r_{e,m} & 1\end{bmatrix}\begin{bmatrix}\exp(jk_{e,m}d_m\cos\theta_m) & 0\\ 0 & \exp(-jk_{e,m}d_m\cos\theta_m)\end{bmatrix}\begin{bmatrix}\psi_{i,m+1}\\ \psi_{r,m+1}\end{bmatrix}, \tag{4}$$

where $t_{e,m}$ is the amplitude transmissivity of the interface between layer $m-1$ and layer m, $r_{e,m}$ is the amplitude reflectivity at the same interface, $k_{e,m}$ is the magnitude of the electron wavevector in layer m as given by Eq. (1), d_m is the thickness of layer m, and θ_m is the angle of the wavevector direction in layer m. For a stack of M layers, the total normalized transmitted electron wave amplitude $\psi_{i,M+1}$ (in region $M+1$) and the total normalized reflected electron wave amplitude $\psi_{r,0}$ (in region 0) are obtained by chain multiplying a total of $M+1$ versions of Eq. (4) together, one for each of the M layers and one for the output region. The result is

$$\begin{bmatrix}1\\ \psi_{r,0}\end{bmatrix}=\prod_{m=1}^{M}\frac{1}{t_{e,m}}\begin{bmatrix}1 & r_{e,m}\\ r_{e,m} & 1\end{bmatrix}\begin{bmatrix}\exp(jk_{e,m}d_m\cos\theta_m) & 0\\ 0 & \exp(-jk_{e,m}d_m\cos\theta_m)\end{bmatrix}\frac{1}{t_{e,M+1}}\begin{bmatrix}1 & r_{e,M+1}\\ r_{e,M+1} & 1\end{bmatrix}\begin{bmatrix}\psi_{i,M+1}\\ 0\end{bmatrix}, \tag{5}$$

and this can be solved directly for the amplitude transmissivity $\psi_{i,M+1}$ and the amplitude reflectivity $\psi_{r,0}$.

The procedure for directly translating a thin-film optical filter design into a superlattice electron filter design has been described in Ref. 5. In that reference, the procedure was applied to translate an 11-layer thin-film optical filter into a corresponding superlattice filter. The resulting design, however, has compositions that are not constrained to fit a usable compositional range and it has layer thicknesses that are not integer multiples of a monolayer thickness. In the next section, a systematic design procedure that includes these practical constraints is presented.

V. SEMICONDUCTOR SUPERLATTICE INTERFERENCE FILTER DESIGN

A semiconductor compositional superlattice is depicted in Fig. 1. The given material system is taken to form a continuous set of alloys of the type $F_{1-x}G_xH$. The range of usable compositions is $0\leqslant x\leqslant x_{\max}$ (for example, due to a possible transition at $x_{\max}$ from a direct to an indirect energy gap as in the case of $Ga_{1-x}Al_xAs$). The materials surrounding the filter ($i=0$ regions) have compositions x_0. The superlattice itself consists of two compositions of material. The composition in the high (electron wave amplitude) refractive index regions is x_1 ($i=1$ regions). The composition in the low (electron wave amplitude) refractive index regions is x_2 ($i=2$ regions). The monolayer thicknesses are r_1 ($i=1$ region) and r_2 ($i=2$ regions). The electron potential energy in the three types of regions is given by[25]

$$V_i\equiv\Delta E_c=Ax_i,\quad i=0,1,2, \tag{6}$$

where ΔE_c is the change in the energy of the conduction-band edge and A is a constant. The electron effective mass in the three types of regions is given by[26]

$$m_i^*=(B+Cx_i)m_0,\quad i=0,1,2, \tag{7}$$

where B and C are constants and m_0 is the free-electron mass. The electron kinetic energy in the ith region is $E-V_i=h^2/2m_i^*\lambda_i^2$. The total electron energy to be passed by the filter is designated E_p. The pass kinetic energy as measured in the various regions is thus

$$E_p-V_i=h^2/2m_i^*(\lambda_p)_i^2,\quad i=0,1,2, \tag{8}$$

where $(\lambda_p)_i$ is the pass wavelength as measured in the ith region. The overall pass kinetic energy of the filter (as measured in the material surrounding the filter) is simply E_p-V_0. This is the pass kinetic energy that will be specified by the user and is thus the starting point in the design procedure. Substituting Eqs. (6) and (7) into Eq. (8) and solving

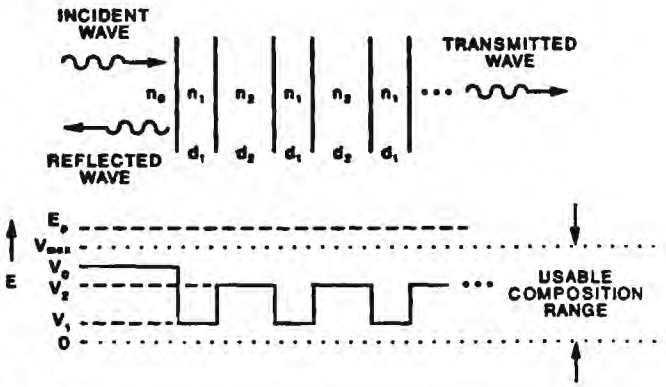

FIG. 1. Schematic representation of a semiconductor compositional (variable band gap) superlattice. The interference filter equivalent of this structure is shown in the upper diagram and the conduction-band energy is shown in the lower diagram.

for the pass wavelength gives

$$(\lambda_p)_i = h/\{2m_0[-ACx_i^2 + (CE_p - AB)x_i + BE_p]\}^{1/2}, \quad i = 0, 1, 2. \tag{9}$$

The thicknesses of the superlattice layers are designated d_i ($i = 1, 2$). These thicknesses must be integer multiples of the monolayer thicknesses r_i. Furthermore, these thicknesses must also be odd multiples of a quarter wavelength as measured in these regions. These constraints may be expressed as

$$d_i = p_i r_i = (2q_i - 1)(\lambda_p)_i/4, \quad i = 1, 2, \tag{10}$$

where p_i is the integer number of monolayers for the ith region and q_i is a positive integer ($q_i = 1, 2, 3, \ldots$). Eliminating $(\lambda_p)_i$ between Eqs. (9) and (10) gives the following quadratic equation in the composition x_i:

$$ACx_i^2 + (AB - CE_p)x_i + (h^2/32m_0) \times [(2q_i - 1)^2/p_i^2 r_i^2] - BE_p = 0. \tag{11}$$

The solution for the composition x_i is

$$x_i = [-b \pm (b^2 - 4ac_i)^{1/2}]/2a, \tag{12}$$

where

$$a = AC, \quad b = AB - CE_p,$$

and

$$c_i = (h^2/32m_0)[(2q_i - 1)^2/p_i^2 r_i^2] - BE_p.$$

In order to design a superlattice interference filter, at least two solutions for x_i must be found in the range $0 < x_i < x_{max}$. The smallest value of x_i within this range will become x_1, the composition of the high index material. The value of p_i that produces x_1 becomes p_1, the number of monolayers of type 1 material used to make a quarter-wavelength layer. Similarly, the largest value of x_i within this range will become x_2, the composition of the low index material. The value of p_i that produces x_2 becomes p_2, the number of monolayers of type 2 material used to make a quarter-wavelength layer.

To allow the broadest range of solutions, V_0 is set equal to V_{max}. For a specified pass kinetic energy ($E_p - V_0$), the value of E_p is then determined. Furthermore, to minimize the total thickness of the filter, q_i is initially set equal to unity. Then Eq. (12) is repetitively evaluated for $p_i = 1, 2, 3, \ldots$ until all of the positive real roots in the range $0 < x_i < x_{max}$ are found. If only one root or no roots are found, then the procedure must be started over with changed parameters. The quantities that can be varied are the integer q_i, the surrounding material composition x_0 (changes E_p), and the crystallographic direction of growth (changes r_i).

After x_1, p_1, x_2, and p_2 have been determined as described above, the other parameters of the filter can be calculated. The potential energies V_i and the effective masses m_i^* are calculated using Eqs. (6) and (7), respectively. Then the electron wave amplitude refractive index for each type of region can be calculated from

$$n_e(\text{amplitude})_i \propto [(E - V_i)/m_i^*]^{1/2}, \tag{13}$$

for the pass energy E_p or for any other energy. Similarly, the electron wave-vector magnitude in the ith region is

$$k_i = [2m_i^*(E - V_i)]^{1/2}/\hbar. \tag{14}$$

VI. EXAMPLE $Ga_{1-x}Al_xAs$ SUPERLATTICE INTERFERENCE FILTER DESIGNS

To illustrate the design procedure of the previous section, superlattice interference filters fabricated from the $Ga_{1-x}Al_xAs$ material system will be treated here. This system is perhaps the most technologically advanced of current semiconductor superlattice material systems. For these alloys, all compositions are lattice matched. For growth along the [100] direction, the monolayer thickness is $r = r_1 = r_2 = 2.826\,65$ Å. The material is a direct gap semiconductor for $0 < x < 0.45$ and this represents the usable composition range. Furthermore, for $Ga_{1-x}Al_xAs$, $A = 0.773\,14$ eV, $B = 0.067$, and $C = 0.083$.

As an example, to design a $Ga_{1-x}Al_xAs$ superlattice interference filter with a pass kinetic energy of 0.20 eV (such as for an emitter in a high-speed ballistic transistor), the following calculations are performed. Let $x_0 = x_{max} = 0.45$. Thus $V_0 = 0.347\,913$ eV from Eq. (6). Since $E_p - V_0 = 0.20$ eV, then $E_p = 0.547\,913$ eV. Letting $q_i = 1$, the composition x_i is evaluated for $p_i = 1, 2, 3, \ldots$ using Eq. (12) until all of the positive real roots are found in the range $0 < x < 0.45$. For the present case there are two roots. They are $x_1 = 0.2063$ (corresponding to $p_1 = 6$) and $x_2 = 0.3984$ (corresponding to $p_2 = 7$). The smaller value of x_i is designated x_1 and the larger value x_2. A plot of the positive real root from Eq. (12) is shown as a function of p (taken as a continuous variable) in Fig. 2. The thickness of the $Ga_{0.79}Al_{0.21}As$ quarter-wavelength layer is $d_1 = p_1 r = 16.9599$ Å (6 monolayers). The thickness of the $Ga_{0.60}Al_{0.40}As$ quarter-wavelength layer is $d_2 = p_2 r = 19.7866$ Å (7 monolayers). The electron effective masses in the three regions are calculated from Eq. (7) and are $m_0^* = 0.104\,35m_0$, $m_1^* = 0.084\,123m_0$, $m_2^* = 0.100\,07m_0$. The pass kinetic energies in the three regions are calculated from Eq. (8) and are $E_p - V_0 = 0.2000$ eV, $E_p - V_1 = 0.3884$ eV, $E_p - V_2 = 0.2399$ eV. The electron wave amplitude refractive indices normalized to the surrounding [$(i = 0)$ regions] are calculated from Eq. (13) and are $n_e(\text{amplitude})_0 = 1.000\,000$, $n_e(\text{amplitude})_1 = 1.552\,027$, $n_e(\text{amplitude})_2 = 1.118\,372$. For an

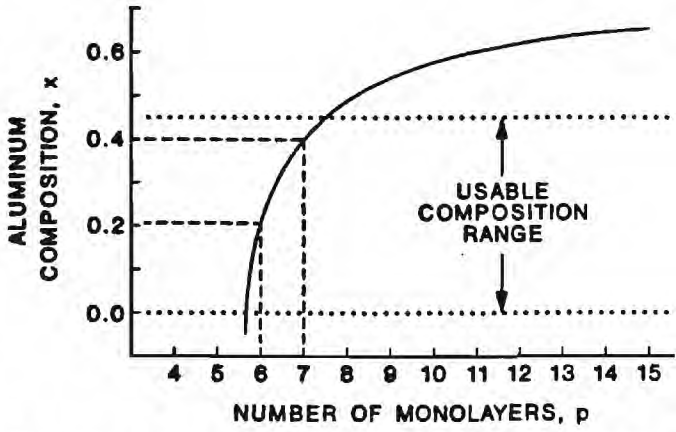

FIG. 2. The required aluminum composition (value of x) to produce a quarter-wavelength layer as a function of the number of monolayers for pass kinetic energy of 0.20 eV.

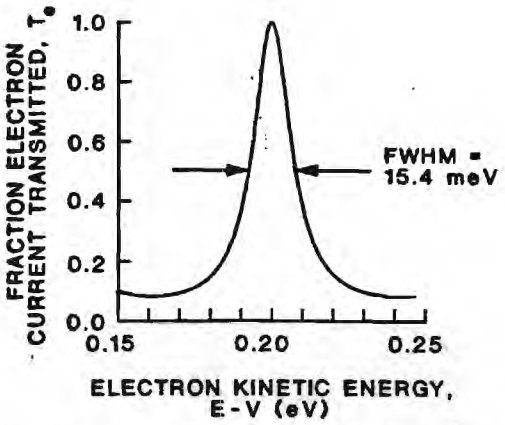

FIG. 3. Transmission characteristic of 13-layer $Ga_{1-x}Al_xAs$ superlattice Fabry–Perot interference filter of the form $[HL]^3HH[LH]^3$ designed to have a pass kinetic energy of 0.20 eV. Parameters of the filter are detailed in Sec. VI.

elementary 13-layer Fabry–Perot interference filter of the form $[HL]^3HH[LH]^3$, these calculated material characteristics produce the transmission characteristic shown in Fig. 3. The pass energy is indeed 0.20 eV and the FWHM of the filter is 15.4 meV.

Repeating the above procedure, $Ga_{1-x}Al_xAs$ superlattice interference filters were designed for pass kinetic energies from 0.14 eV up through 0.20 eV, the range of energies potentially most useful in ballistic transistors. The positive real roots as given by Eq. (12) are shown in Table I for 6–10 monolayer thicknesses. Roots, of course, must be in the range $0<x<0.45$. At the 0.14 eV low end of this energy range, there are essentially four roots. At the 0.20 eV high end of the energy range, there are two roots. The $Ga_{1-x}Al_xAs$ superlattice interference filter described in Ref. 10 (quarter-wavelength layers produced by 6 monolayers of GaAs and by 9 monolayers of $Ga_{0.55}Al_{0.45}As$) essentially corresponds to the 0.14-eV pass energy case given in Table I.

TABLE I. Calculated compositions (values of x in $Ga_{1-x}Al_xAs$) that produce one ($q_i = 1$) quarter-wavelength layers for the kinetic energies and number of monolayers indicated. In all cases, the surrounding material is $Ga_{0.55}Al_{0.45}As$ and the monolayers are crystalline (100) planes. Only compositions in the range $0<x<0.45$ represent usable values.

Pass kinetic energy (eV)	Number of monolayers				
	6	7	8	9	10
0.140	0.0015	0.2902	0.3923	0.4513	0.4898
0.145	0.0278	0.2996	0.4004	0.4588	0.4970
0.150	0.0502	0.3088	0.4084	0.4663	0.5042
0.155	0.0702	0.3180	0.4164	0.4738	0.5115
0.160	0.0885	0.3272	0.4244	0.4813	0.5187
0.165	0.1057	0.3363	0.4324	0.4888	0.5259
0.170	0.1219	0.3453	0.4403	0.4963	0.5331
0.175	0.1373	0.3543	0.4482	0.5037	0.5403
0.180	0.1520	0.3632	0.4561	0.5112	0.5475
0.185	0.1662	0.3721	0.4640	0.5186	0.5547
0.190	0.1800	0.3809	0.4718	0.5260	0.5619
0.195	0.1933	0.3897	0.4797	0.5334	0.5690
0.200	0.2063	0.3984	0.4875	0.5408	0.5762

VII. SUMMARY

The quantitative analogies that have been established between electron wave propagation in semiconductors and optical wave propagation in dielectrics may be used to translate thin-film optical device designs into semiconductor superlattice device designs. The procedure for this direct mapping has previously been described and applied to the case of semiconductor superlattice narrow bandpass interference filters in Ref. 5. The resulting designs, however, have compositions that are not constrained to be within a usable compositional range and have layer thicknesses that are not integer multiples of a monolayer thickness. In the present work, a systematic design procedure that includes these practical constraints is presented. This method is applicable to any material system. For illustration, this procedure is applied to the case of designing $Ga_{1-x}Al_xAs$ superlattice interference filters. For pass kinetic energies in the range investigated (0.14–0.20 eV), compositions and numbers of monolayer thicknesses needed to produce one ($q_i = 1$) quarter-wavelength layers are presented (Table I). Like their thin-film optical counterparts, semiconductor superlattice interference filters would be relatively insensitive to variations about the design composition values. Furthermore, the effects of nonparabolic and anisotropic energy band structure, if present, may be incorporated into the design process by using an energy-dependent anisotropic effective mass.

There is considerable flexibility in the design of semiconductor superlattice interference filters. For example, other odd multiples of a quarter wavelength may be used ($q_i = 2, 3, 4, \ldots$), the surrounding material can be changed (alters V_0), and other crystallographic growth directions may be used (alters r_i). Beyond the simple Fabry–Perot interference filters treated here, there is a wide variety of more sophisticated thin-film designs that incorporate two or more half-wavelength resonant layers ("spacers") that have been developed for optical applications. For example, the superlattice filter described in Ref. 5 contains two half-wavelength layers.

A wide variety of semiconductor superlattice electron wave filters are possible by analogy to thin-film optical filters. These include low-pass filters, high-pass filters, notch filters (narrow band and wide band),.bandpass filters (narrow band and wide band), impedance transformers (antireflection coatings), and high reflectance surfaces (dielectric mirrors). In addition to being incorporated in semiconductor devices such as ballistic transistors, semiconductor superlattice filters could be used to control freespace electron beams in applications such as electron spectroscopy, electron diffraction analysis of materials, and electron-beam lithography. Active devices that have electrically tunable characteristics are also possible.

ACKNOWLEDGMENTS

This research was sponsored in part by a grant from the Joint Services Electronics Program under Contract No DAAL-03-87-K-0059. One of us (K.F.B.) was supported ir

part by a Presidential Young Investigator award from the National Science Foundation.

[1]L. Esaki and R. Tsu, IBM J. Res. Dev. **13**, 61 (1970).
[2]M. Heiblum, M. I. Nathan, D. C. Thomas, and C. M. Knoedler, Phys. Rev. Lett. **55**, 2200 (1983).
[3]M. Heiblum and L. F. Eastman, Sci. Am. **255**, 103 (1987).
[4]M. Heiblum, Opt. News **14**, 13 (1988).
[5]T. K. Gaylord and K. F. Brennan, J. Appl. Phys. **65**, 814 (1989).
[6]M. Heiblum, M. V. Fischetti, W. P. Dumke, D. J. Frank, I. M. Anderson, and C. M. Knoedler, Phys. Rev. Lett. **58**, 816 (1987).
[7]S. Sen, F. Capasso, A. C. Gossard, R. A. Spah, A. L. Hutchinson, and S. N. G. Chu, Appl. Phys. Lett. **51**, 1428 (1987).
[8]R. C. Potter and A. A. Lakhani, Appl. Phys. Lett. **52**, 1349 (1988).
[9]J. R. Hayes, P. England, and J. P. Harbison, Appl. Phys. Lett. **52**, 1578 (1988).
[10]T. K. Gaylord and K. F. Brennan, Appl. Phys. Lett. **53**, 2047 (1988).
[11]C. J. Summers and K. F. Brennan, Appl. Phys. Lett. **48**, 806 (1986).
[12]K. F. Brennan and C. J. Summers, J. Appl. Phys. **61**, 5410 (1987).
[13]K. F. Brennan and C. J. Summers, IEEE J. Quantum Electron. **QE-23**, 320 (1987).
[14]M. I. Nathan and M. Heiblum, IEEE Spectrum **23**, 45 (1986).
[15]G. A. Nagy and M. Szilágyi, *Introduction to the Theory of Space-Charge Optics* (Halsted, New York, 1974).
[16]P. Dahl, *Introduction to Electron and Ion Optics* (Academic, New York, 1973).
[17]C. M. Wu and E. S. Yang, Solid-State Electron. **22**, 241 (1979).
[18]A. N. Khondker, M. R. Khan, and A. F. M. Anwar, J. Appl. Phys. **63**, 5191 (1988).
[19]O. S. Heavens, *Optical Properties of Thin Solid Films* (Butterworths, London, 1955).
[20]A. Thelen, *Physics of Thin Films*, edited by G. Hass and R. E. Thun (Academic, New York, 1969), Vol. 5, p. 47.
[21]J. A. Dobrowolski, *Handbook of Optics*, edited by W. G. Driscoll (McGraw-Hill, New York, 1978), Sec. 8.
[22]H. A. Macleod, *Thin-Film Optical Filters* (Macmillan, New York, 1986).
[23]M. Born and E. Wolf, *Principles of Optics*, 6th ed. (Pergamon, Oxford, 1980), p. 55.
[24]R. E. Collin, *Field Theory of Guided Waves* (McGraw-Hill, New York, 1960), p. 79.
[25]H. C. Casey, Jr. and M. B. Panish, J. Appl. Phys. **40**, 4910 (1969).
[26]S. Adachi, J. Appl. Phys. **58**, R1 (1985).

Semiconductor biased superlattice tunable electron interference filter/emitter

E. N. Glytsis, T. K. Gaylord, and K. F. Brennan
School of Electrical Engineering and Microelectronics Research Center, Georgia Institute of Technology, Atlanta, Georgia 30332

(Received 13 January 1989, accepted for publication 25 March 1989)

It is shown that a voltage-biased semiconductor superlattice structure can serve simultaneously as a tunable electron-wave interference filter and electron emitter. A systematic design procedure for selecting the quantum well and barrier widths to be alternately high and low electron refractive indices and a quarter (or a half) of an electron wavelength in thickness is developed. A practical narrow-band filter/emitter consisting of layers of $Ga_{1-x}Al_xAs$ and designed to emit 0.20-eV electrons is presented and analyzed. Such a structure would serve well as a tunable hot-electron emitter in ballistic transistors, and in future guided electron-wave integrated circuits.

Molecular-beam epitaxy and metalorganic chemical vapor deposition have allowed semiconductor multilayered superlattices to be grown with precise monolayer compositional control.[1] Refinement of these methods have produced devices in which ballistic (collisionless) electron transport has been observed.[2–4] Ballistic electrons are quantum mechanical deBroglie waves, and thus they can be refracted, reflected, diffracted, guided, and interfered[5,6] in a manner analogous to electromagnetic waves.[7] Quantum interference effects have been observed experimentally in single-well double-barrier $GaAs/Ga_{1-x}Al_xAs$ and $In_{1-x}Ga_xAs/In_{1-y}Al_yAs$ potential barrier structures.[8–11]

Phase effects such as path differences and wave interference for electron waves may be described using the wave-vector magnitude $k = [2m^*(E - V)]^{1/2}/\hbar$, where m^* is the electron effective mass, E is the total electron energy, V is the electron potential energy, and $\hbar$ is Planck's constant divided by 2π. Thus, the electron wave phase refractive index n_e (phase) is proportional to the square root of the product of the effective mass and the kinetic energy.[7] Amplitude effects

 0021-8979/89/151494-04$02.40

such as transmissivity and reflectivity may be described in terms of the electron wave amplitude refractive index n_e (amplitude) which is proportional to the square root of the ratio of the kinetic energy to the effective mass.[7] Using these electron wave refractive indices, the characteristics of an unbiased[6] or biased (this work) many boundary semiconductor superlattice system can be found. The simplest type of narrow bandpass interference filter consists of a half-wavelength layer sandwiched between reflectors which are stacks of high index (designated H) and low index (designated L) quarter-wavelength layers. The full width at half maximum (FWHM) of the bandpass in this type of filter is reduced by increasing the reflectivity at the boundaries between the layers. This is accomplished by increasing the ratio of the high index to the low index of the bounding materials. In this work, an electron emitter that incorporates a narrow-band interference filter is designed.

The electron potential energy of a quantum-well superlattice emitter/filter with a voltage bias applied is shown in Fig. 1. It consists of M layers surrounded by bulk semiconductor material. When the design value of voltage is applied, electrons in a narrow spectral band around the pass energy E_p traverse the device and are emitted with an output kinetic energy of $(\mathrm{KE})_{\mathrm{out}}$. The jth quantum well or barrier has a thickness of d_j, and at zero bias a potential energy of V_j. The surrounding regions are taken to have the same zero-bias potential energy of V_0. The layers have alternately low potential energy (high electron refractive index) and high potential energy (low refractive index). When the design value of the bias potential energy V_{bias} (product of electronic charge and design voltage) is applied, each reflector layer is exactly a quarter of an electron wavelength (as measured in that layer) in thickness, and the resonant layer is exactly one half of an electron wavelength. The given material system is taken to form a continuous set of alloys of the type $F_{1-x}G_xH$. The range of usable compositions is $0 \leq x \leq x_{\max}$ (for example, due to a possible transition at $x_{\max}$ from a direct to an indirect energy gap as in the case of $\mathrm{Ga}_{1-x}\mathrm{Al}_x\mathrm{As}$). The materials surrounding the filter have compositions x_0. The electron potential energy is given by $V_j \equiv \Delta E_c = Ax_j$, where ΔE_c is the change in the energy of the conduction-band edge and A is a constant. Thus, the corresponding range of potential energies is $0 \leq V \leq V_{\max}$. In addition, for an electron emitter/filter to be realizable, the

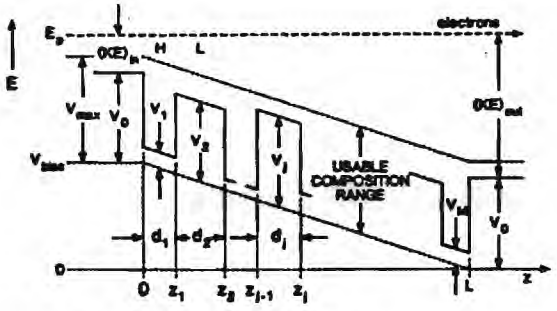

FIG. 1. Schematic representation of a biased semiconductor superlattice interference filter/emitter. At the design potential energy bias V_{bias}, all layers have a thickness of a quarter (or a half) of an electron wavelength as measured in that layer.

thickness d_j of each layer must be an integer multiple p_j of the monolayer thickness r. For the jth layer to be a quarter of an electron wavelength in thickness at the pass energy E_p, the phase difference between the input boundary at z_{j-1}, and the output boundary at z_j, must be an odd multiple of $\pi/2$. That is,

$$\int_{z_{j-1}}^{z_j} k_j\,dz = \int_{z_{j-1}}^{z_j} (1/\hbar)\{2m_j^* \times [E_p - V_j(z)]\}^{1/2}\,dz = (2q_j - 1)(\pi/2), \tag{1}$$

where the potential energy in the jth layer with bias applied is given by $V_j(z) = V_{\mathrm{bias}}(1 - z/L) + V_j$, L is the total length of the superlattice, and q_j is a positive integer. The pass energy may be expressed as $E_p = V_{\mathrm{bias}} + V_0 + (\mathrm{KE})_{\mathrm{in}}$, where $(\mathrm{KE})_{\mathrm{in}}$ is the pass kinetic energy in the leftmost (input) region. The electron effective mass is given by $m_j^* = (B + Cx_j)m_0$, where B and C are constants and m_0 is the free-electron mass. Using $V_j = Ax_j$ and the integral identity $\int (a+bz)^{1/2}\,dz \equiv (2/3b)(a+bz)^{3/2}$, the quarter electron wavelength condition may be expressed as

$$\{2L\,[2m_0(B + Cx_j)]^{1/2}/3\hbar V_{\mathrm{bias}}\}\{[V_0 + (\mathrm{KE})_{\mathrm{in}} - Ax_j + V_{\mathrm{bias}}z_j/L\,]^{3/2} - [V_0 + (\mathrm{KE})_{\mathrm{in}} - Ax_j + V_{\mathrm{bias}}z_{j-1}/L\,]^{3/2}\} = (2q_j - 1)\pi/2. \tag{2}$$

This equation will be solved for the composition x_j in the jth layer following the procedure described below. For the half-wavelength resonant section in the center of the filter, the phase difference in Eqs. (1) and (2) should be π rather than $\pi/2$. The monolayers of the device will be numbered with the index i. The rightmost monolayer in the jth region is i_j. The total number of monolayers in the emitter/filter is designated i_M. Therefore, $z_{j-1} = (i_{j-1}/i_M)L$, $z_j = (i_j/i_M)L$, the total thickness is $L = i_M r$, and the thickness of the jth layer is $d_j = p_j r$, where $p_j = i_j - i_{j-1}$ is the number of monolayers in the jth region.

A systematic procedure for designing a biased superlattice emitter/filter for a given output kinetic energy $[(\mathrm{KE})_{\mathrm{out}} = V_{\mathrm{bias}} + (\mathrm{KE})_{\mathrm{in}}]$ using Eq. (2) is now described. The material system of the superlattice is taken to be $\mathrm{Ga}_{1-x}\mathrm{Al}_x\mathrm{As}$ with the surrounding regions being the same and having $V_0 = V_{\max} = 0.3479$ eV, corresponding to an aluminum composition of $x_0 = 0.45$. The characteristics of (unbiased) superlattice electron wave interference filters[5,6] may be used as a starting point in estimating the number of regions M and the number of monolayers i_M to be used in the emitter/filter. Following the example presented in Ref. 5, a nine-layer filter ($M = 9$) will be designed. The estimated number of monolayers needed is $i_M = 72$ (from Ref. 5). The device is to emit electrons with a kinetic energy of 0.20 eV $[(\mathrm{KE})_{\mathrm{out}} = 0.20$ eV$]$. The input kinetic energy is taken to be $(\mathrm{KE})_{\mathrm{in}} = 0.10$ eV, and thus the bias potential energy $V_{\mathrm{bias}} = (\mathrm{KE})_{\mathrm{out}} - (\mathrm{KE})_{\mathrm{in}} = 0.10$ eV. The parameters q_j are set equal to unity. Starting with the first layer, $i_{j-1} = 0$, the value of the monolayer index i_j is incremented 1, 2, 3,..., and Eq. (2) solved for x_j for each value of i_j. Since the $j = 1$ layer is to be a high electron refractive index layer, the resulting positive real value of x_j closest to zero is selected. The corre-

sponding value of i_j then becomes the value of i_{j-1} for the next layer. Equation (2) is then solved again as i_j is further incremented. Since the $j=2$ the layer is to be a low refractive index layer, the resulting real value of x_j closest to, but less than 0.45 is selected. This process is continued for all layers. For the half-wavelength layer, $\pi/2$ in Eq. (2) is replaced by π. For the last ($j=M$) layer, the number of monolayers left may be too few or too many. The value of i_M must then be revised, and the design process restarted at the first ($j=1$) layer. This process is then repeated until the optimum thickness (corresponding to the value of x_M closest to zero) of the last region produces a total thickness in a self-consistent agreement with the value of i_M used. The results for this nine-layer emitter/filter are shown in Table I. The total thickness is 71 monolayers ($L=20.0692$ nm).

The electron wave function in any layer of the biased superlattice may be expressed as a linear combination of Airy functions $\mathrm{Ai}(\rho)$ and complementary Airy functions $\mathrm{Bi}(\rho)$.[12,13] Within the jth layer the new variable is defined as

$$\rho_j \equiv (2m_j^* V_{\mathrm{bias}}/\hbar^2 L)^{1/3}[z+(E-V_{\mathrm{bias}}-V_j)L/V_{\mathrm{bias}}].$$

For a stack of M layers as shown in Fig. 1, the total normalized transmitted electron wave amplitude $\psi_{t,M+1}$ (in region $M+1$) and the total normalized reflected electron wave amplitude $\psi_{r,0}$ (in region 0) may be expressed as

$$\begin{aligned}\begin{pmatrix}1\\ \psi_{r,0}\end{pmatrix} = \frac{1}{2jK_1}\begin{pmatrix} jK_1 & -1\\ jK_1 & 1\end{pmatrix}[S_1(z_0)][S_1(z_1)]^{-1}\\ \times[S_2(z_1)][S_2(z_2)]^{-1}[S_3(z_2)]\\ \cdots[S_{M-1}(z_{M-1})]^{-1}[S_M(z_{M-1})]\\ \times[S_M(z_M)]^{-1}\begin{pmatrix}1 & 1\\ -jK_2 & jK_2\end{pmatrix}\begin{pmatrix}\psi_{t,M+1}\\ 0\end{pmatrix},\end{aligned} \quad (3)$$

where

$$[S_j(z)] = \begin{pmatrix}\mathrm{Ai}(-\rho_j) & \mathrm{Bi}(-\rho_j)\\ (1/M_j^*)^{2/3}\,\mathrm{Ai}'(-\rho_j) & (1/M_j^*)^{2/3}\,\mathrm{Bi}'(-\rho_j)\end{pmatrix}, \quad (4)$$

and where

$$M_j^* = m_j^*/m_0,$$

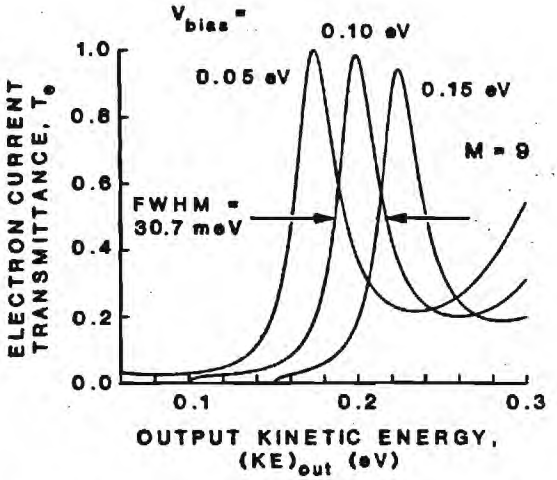

FIG. 2. Transmission characteristic of a nine-layer $Ga_{1-x}Al_xAs$ superlattice interference filter/emitter as a function of the output kinetic energy for $V_{bias}=0.05$, 0.10, and 0.15 eV. The tuning with bias is apparent.

$$K_1 = [(2m_0/\hbar^2)^{1/3}(E-V_0-V_{\mathrm{bias}})/M_0^*]^{1/2}(L/V_{\mathrm{bias}})^{1/3},$$

$$K_2 = [(2m_0/\hbar^2)^{1/3}(E-V_0)/M_{M+1}^*]^{1/2}(L/V_{\mathrm{bias}})^{1/3},$$

and $'$ indicates a derivative. These equations can be solved directly for the amplitude transmittance $\psi_{t,M+1}$ and the amplitude reflectance $\psi_{r,0}$. The electron current transmittance is $T_e = R|\psi_{t,M+1}|^2$, where $R=[(E-V_0)/M_{M+1}^*]^{1/2}/[(E-V_0-V_{\mathrm{bias}})/M_0^*]^{1/2}$, and this is shown in Fig. 2 for the biased superlattice design described in Table I. At the design bias of $V_{\mathrm{bias}}=0.10$ eV, the device emits $(\mathrm{KE})_{\mathrm{out}}=0.20$ eV electrons into the output region. The full width at half maximum (FWHM) is 30.7 meV or 15.4% of the center energy. Furthermore, the output kinetic energy is tunable by changing the bias potential energy. Since the *HH* resonant layer is at the center (as measured in electron optical path length) of the device, the change in the output kinetic energy $\Delta(\mathrm{KE})_{\mathrm{out}}$ is one half of the change in the bias potential energy ΔV_{bias}. Thus, as shown in Fig. 2, for $\Delta V_{\mathrm{bias}}=\pm 50$ meV, the output kinetic energy is changed by $\Delta(\mathrm{KE})_{\mathrm{out}}=\pm 25$ meV. Furthermore, the FWHM of the electron current transmittance can be decreased as required by incorporating additional quarter-wavelength thick super-

TABLE I. Design parameters of electron interference filters/emitters consisting of nine layers in (*H L H L HH L H L H*) configuration surrounded by $Ga_{0.55}Al_{0.45}As$, and designed to emit 0.200-eV electrons when biased at 0.100 V.

Layer number (j)	Layer type	Starting monolayer number (i_{j-1})	Ending monolayer number (i_j)	Number monolayers thick (ρ_j)	Aluminum composition (x_j)	Unbiased electron potential energy (V_j)	Normalized effective mass (m_j^*/m_0)
1	*H*	0	7	7	0.2222	0.1718	0.0854
2	*L*	7	16	9	0.4151	0.3209	0.1015
3	*H*	16	23	7	0.2663	0.2059	0.0891
4	*L*	23	32	9	0.4493	0.3473	0.1043
5	*HH*	32	44	12	0.0639	0.0494	0.0723
6	*L*	44	52	8	0.4364	0.3374	0.1032
7	*H*	52	58	6	0.1442	0.1115	0.0790
8	*L*	58	65	7	0.3748	0.2898	0.0981
9	*H*	65	71	6	0.1951	0.1508	0.0832

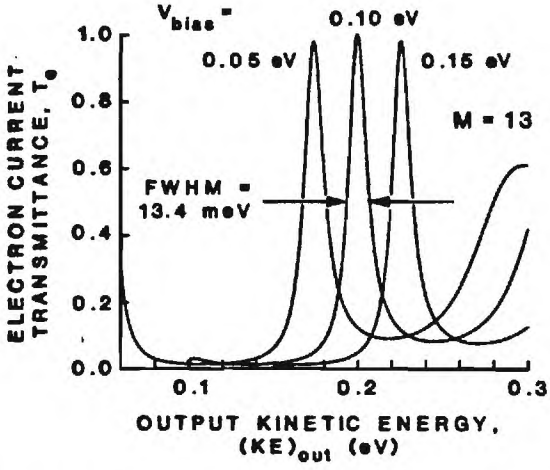

FIG. 3. Transmission characteristic of the corresponding 13-layer $Ga_{1-x}Al_xAs$ superlattice interference filter/emitter as a function of the output kinetic energy. The spectral widths are correspondingly narrower than those for the nine-layer filter/emitter (Fig. 2).

lattice layers. The transmittance of the corresponding 13-layer filter/emitter is shown in Fig. 3. The overall characteristics are the same as those of the nine-layer filter/emitter of Fig. 2, except that the FWHM is reduced to 13.4 meV (6.7% of center energy).

The procedures for designing and analyzing narrow-band semiconductor superlattice interference filter/emitters have been presented in this communication. Such structures may be used as hot-electron emitters in ballistic transistors, electroluminescent devices, and photodetectors. They could also be used as tunable electron sources in the emerging new area of guided electron wave integrated circuits. Such tunable narrow-band emitters could provide numerous simultaneously energy multiplexed data channels in the same guided electron wave integrated circuit in a manner analogous to that used in electromagnetic optical integrated circuits. However, the corresponding electron wavelengths would be typically 100 times smaller.

This research was sponsored in part by a grant from the Joint Services Electronics Program under Contract No. DAAL-03-87-K-0059. One of us (K.F.B.) was supported in part by a Presidential Young Investigator Award from the National Science Foundation.

[1]L. Esaki and R. Tsu, IBM J. Res. Dev. 13, 61 (1970).
[2]M. Heiblum, M. I. Nathan, D. C. Thomas, and C. M. Knoedler, Phys. Rev. Lett. 55, 2200 (1983).
[3]M. Heiblum and L. F. Eastman, Sci. Am. 255, 103 (Feb. 1987).
[4]M. Heiblum, Opt. News 14, 13 (1988).
[5]T. K. Gaylord and K. F. Brennan, Appl. Phys. Lett. 53, 2047 (1988).
[6]T. K. Gaylord, E. N. Glytsis, and K. F. Brennan, J. Appl. Phys. 65, 2535 (1989).
[7]T. K. Gaylord and K. F. Brennan, J. Appl. Phys. 65, 814 (1989).
[8]M. Heiblum, M. V. Fischetti, W. P. Dumke, D. J. Frank, I. M. Anderson, and C. M. Knoedler, Phys. Rev. Lett. 58, 816 (1987).
[9]S. Sen, F. Capasso, A. C. Gossard, R. A. Spah, A. L. Hutchinson, and S. N. G. Chu, Appl. Phys. Lett. 51, 1428 (1987).
[10]R. C. Potter and A. A. Lakhani, Appl. Phys. Lett. 52, 1349 (1988).
[11]J. R. Hayes, P. England, and J. P. Harbison, Appl. Phys. Lett. 52, 1578 (1988).
[12]K. F. Brennan and C. J. Summers, J. Appl. Phys. 61, 614 (1987).
[13]C. J. Summers, K. F. Brennan, A. Torabi, and H. M. Harris, Appl. Phys. Lett. 52, 132 (1988).

Semiconductor electron-wave slab waveguides

T. K. Gaylord, E. N. Glytsis, and K. F. Brennan
School of Electrical Engineering and Microelectronics Research Center, Georgia Institute of Technology, Atlanta, Georgia 30332

(Received 14 December 1988; accepted for publication 11 April 1989)

A one-dimensional semiconductor quantum well can act as a waveguide for ballistic electrons owing to the quantum mechanical wave behavior of these electrons. The allowed modes in an asymmetric quantum well slab waveguide are quantified. Electron waveguiding can occur for energies above one or both of the potential barriers. Due to dispersion, each electron waveguide mode has an upper-energy cutoff as well as a lower-energy cutoff. An example waveguide consisting of $Ga_{0.85}Al_{0.15}As$ (substrate), GaAs (film), and $Ga_{0.70}Al_{0.30}As$ (cover) is treated. This structure is a single-mode electron waveguide for [100] GaAs thicknesses of from 6 through 31 monolayers.

Semiconductor growth technologies such as molecular-beam epitaxy have enabled structures to be fabricated with precise monolayer compositional control.[1] Improvements in these techniques have produced devices in which ballistic (collisionless) electron transport has been observed.[2–4] Ballistic electrons are quantum mechanical deBroglie waves and thus they can be refracted, reflected, diffracted, interfered, and guided in a manner analogous to electromagnetic waves.[5–6]

An asymmetric potential energy well is shown in Fig. 1. Using waveguide terminology,[7] the three regions are denoted substrate (s), film (f), and cover (c), and the direction perpendicular to the waveguide surfaces is x_w. The electron potential energy at the bottom of the quantum well (film) is V_f. The potential energy barrier heights associated with the substrate and cover are V_s and V_c, respectively. This quantum well can act as an asymmetric slab waveguide. The angle of incidence of the two plane-wave components that constitute the guided wave is the zigzag angle θ.

The magnitude of the electron wave vector in any of the three regions is $k_i = [2m_i^*(E - V_i)]^{1/2}/\hbar$, where $i = c, f, s$ and m_i^* is the electron effective mass, E is the total electron energy, and V_i is the electron potential energy. Thus, the electron-wave phase refractive index n_e (phase) is proportional to the square root of the product of the effective mass and the kinetic energy.[6] The onset of total internal reflection occurs when θ is equal to the critical angle θ' given by[6]

$$\theta'_{if} = \sin^{-1}[m_i^*(E - V_i)/m_f^*(E - V_f)]^{1/2}, \quad V_i < E < E_{if}, \tag{1}$$

where $i = c$ for the cover-film critical angle, $i = s$ for the substrate-film critical angle, and $E_{if} = (m_i^* V_i - m_f^* V_f)/(m_i^* - m_f^*)$. For an electron wave incident at an angle greater than θ'_{if}, the wave is totally internally reflected for an infinitely thick barrier. At steady state, all of the electron current is reflected back into the film. The electron-wave function decays exponentially into the cover. If the kinetic energy $E - V_i < 0$, then total internal reflection occurs for any angle of incidence including normal incidence. For a guided mode, the zigzag angle θ shown in Fig. 1 must be greater than both θ'_{cf} and θ'_{sf}. That is, $\theta > \max(\theta'_{cf}, \theta'_{sf})$ is a necessary condition for a guided mode.

A representation of the electron propagation constant versus total electron energy for the $Ga_{0.85}Al_{0.15}As/GaAs/Ga_{0.70}Al_{0.30}As$ example is given in Fig. 2. For an infinite medium, the electron propagation constant is $\beta_i = [2m_i^*(E - V_i)]^{1/2}/\hbar$, where $i = c, f, s$. These three propagation constants are plotted in Fig. 2. For a given energy E, the propagation constant of a guided mode can be no longer than β_f. The region to the left of this curve corresponds to evanescent (nonphysical) modes. Thus the allowed guided modes must lie to the right of this curve in Fig. 2. However, in order to satisfy the $\theta > \max(\theta'_{cf}, \theta'_{sf})$ condition, the guided modes must also lie left of β_s.

An electron-guided wave mode can become cutoff by decreasing the electron energy to the lower-energy cutoff. The zigzag angle decreases with decreasing energy and this cutoff occurs when $\theta = 0$. The propagation constants β_ν of the νth guided mode M_ν, where $\nu = 0,1,2,...$, is given by

$$\beta_\nu = [2m_f^*(E - V_f)/\hbar^2]^{1/2} \sin\theta, \tag{2}$$

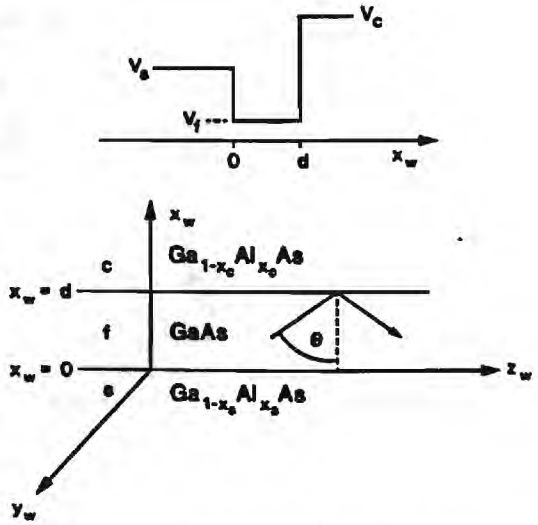

FIG. 1. Asymmetric quantum well showing electron potential energy in the three regions that in waveguide terminology are denoted substrate (s), film (f), and cover (c) and the three-dimensional waveguide coordinate system (x_w, y_w, z_w). A guided mode propagates in the z_w direction and is composed of two plane-wave components each making an angle of incidence θ with respect to the waveguide walls ($x_w = 0, d$).

 0021-8979/89/151483-03$02.40

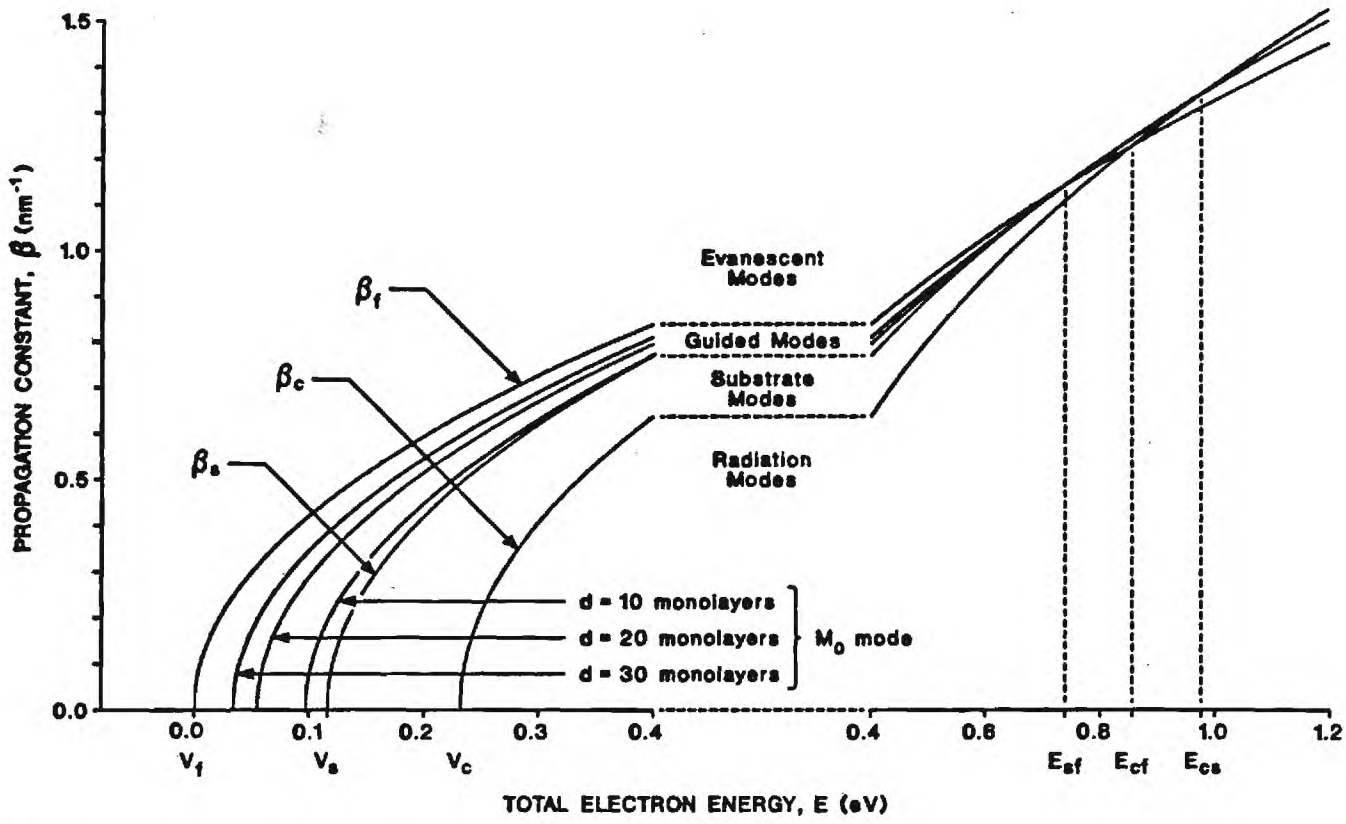

FIG. 2. Electron-guided-mode propagation constant as a function of total electron energy showing the regions of evanescent modes, guided modes, substrate modes, and radiation modes for the example quantum well waveguide composed of $Ga_{0.85}Al_{0.15}As$ (substrate), GaAs (film), and $Ga_{0.70}Al_{0.30}As$ (cover). The mode dispersion curves for the fundamental mode M_0 are shown for film thicknesses of 10, 20, and 30 monolayers.

and so $\beta_\nu = 0$ at the lower-energy cutoff. The wave function is sinusoidal in the film and exponentially decaying in the substrate and cover. In this sense, the lower-energy cutoff is like the cutoff in an electromagnetic hollow metallic waveguide with finite conductivity walls.

As the electron energy of a guided mode is increased, an upper-energy cutoff will also occur. The upper-energy cutoff can be of three types: (1) cutoff to a substrate mode which is like the cutoff in an electromagnetic asymmetric dielectric waveguide with the substrate index higher than the cover index; (2) cutoff to a radiation mode which is like the cutoff in an electromagnetic symmetric dielectric waveguide (equal substrate and cover indices); and (3) cutoff to a cover mode which is like the cutoff in an electromagnetic asymmetric dielectric waveguide with the cover index higher than the substrate index. The type of upper-energy cutoff that occurs depends on the material parameters. For the example case depicted in Fig. 2, the upper-energy cutoff will be to substrate modes since β_s occurs at lower energy, in general, than does β_c.

For a two-dimensional (x_w, z_w) quantum-well-guided electron wave, the wave function has a sinusoidal dependence in the z_w direction and can be expressed as $\psi_\nu(x_w, z_w) = \psi_\nu(x_w)\exp(j\beta_\nu z_w)$, where β_ν is the guided mode propagation constant. Using this, the Schrödinger time-independent wave equation becomes

$$d\psi_\nu^2(x_w)/dx_w^2 + \{(2m^*/\hbar^2)[E - V(x_w)] - \beta_\nu^2\}\psi_\nu(x_w) = 0.$$

Thus for a guided mode, the wave-function amplitude in the substrate may be expressed as

$$\psi_{\nu s}(x_w) = A_s \exp(\gamma_s x_w),$$

and in the film as

$$\psi_{\nu f}(x_w) = A_{f1}\exp(j\kappa_f x_w) + A_{f2}\exp(-j\kappa_f x_w),$$

and in the cover as

$$\psi_{\nu c}(x_w) = A_c \exp[-\gamma_c(x_w - d)],$$

where

$$\gamma_s^2 = \beta_\nu^2 - [(2m_s^*/\hbar^2)(E - V_s)],$$

$$\kappa_f^2 = [(2m_f^*/\hbar^2)(E - V_f)] - \beta_\nu^2,$$

and

$$\gamma_c^2 = \beta_\nu^2 - [(2m_c^*/\hbar^2)(E - V_c)].$$

By applying the boundary conditions that ψ and $(1/m^*)(d\psi/dx)$ must be continuous across the cover-film and substrate-film boundaries, the dispersion equation is found to be

$$\kappa_f d - \tan^{-1}[(\gamma_s/m_s^*)/(\kappa_f/m_f^*)] - \tan^{-1}[(\gamma_c/m_c^*)/(\kappa_f/m_f^*)] = \nu\pi. \quad (3)$$

For $V_f = 0$ and normal incidence ($\beta_\nu = 0$), this dispersion equation predicts, in the limit as V_c and V_s approach infinity, that

$$E = E_\nu = (\nu + 1)\hbar^2\pi^2/2m_f^* d^2,$$

in agreement with the well-known one-dimensional infinite potential well results.

Cutoff for the guided M_ν modes can occur as the electron energy is decreased and the guided wave propagation constant goes to zero. The electron energy at which the lower-energy cutoff occurs is designated E_{Lco}. The condition for this type of cutoff is obtained by substituting $\beta_\nu = 0$ into the dispersion equation (3). The cutoff condition is

$$[2m_f^*(E_{Lco} - V_f)]^{1/2} d/\hbar - \tan^{-1}[m_f^*(V_s - E_{Lco})/m_s^*(E_{Lco} - V_f)]^{1/2} - \tan^{-1}[m_f^*(V_c - E_{Lco})/m_c^*(E_{Lco} - V_f)]^{1/2} = \nu\pi. \quad (4)$$

For given substrate, film, and cover materials, thickness, and integer mode number ν, this transcendental equation may be solved for the lower cutoff energy E_{Lco} corresponding to that mode. Cutoff for the guided M_ν modes can also occur as the electron energy is increased and total internal reflection no longer occurs at the substrate-film boundary. The electron energy at which the upper-energy cutoff occurs is designated E_{Uco}. The condition for the occurrence of this type of cutoff is $\gamma_s = 0$, and thus the mode "leaks" into the substrate. This is analogous to the cutoff of an electromagnetic guided mode in an asymmetric dielectric slab waveguide. This type of cutoff occurs when the zigzag angle is equal to the substrate-film critical angle. Substituting $\gamma_s = 0$ into the dispersion equation (3), the condition for cutoff to substrate modes is thus

$$\{2[m_s^* V_s - m_f^* V_f - (m_s^* - m_f^*)E_{Uco}]\}^{1/2} d/\hbar - \tan^{-1}\{[m_c^* V_c - m_s^* V_s - (m_c^* - m_s^*)E_{Uco}]m_f^{*2}/[m_s^* V_s - m_f^* V_f - (m_s^* - m_f^*)E_{Uco}]m_c^{*2}\}^{1/2} = \nu\pi. \quad (5)$$

For a given set of material parameters, as the waveguide thickness is increased, a guided mode M_ν first starts to propagate at an energy $E = V_s$. This corresponds to the highest possible value of the cutoff energy for the lower-energy type cutoff as well as the lowest possible value of the cutoff energy for the higher-energy type cutoff. Substituting $E = V_s$ into Eq. (3) gives the thickness at which the M_ν mode starts to propagate as

$$d = \{\hbar/[2m_f^*(V_s - V_f)]^{1/2}\} \times \{\tan^{-1}[m_f^*(V_c - V_s)/m_c^*(V_s - V_f)]^{1/2} + \nu\pi\}. \quad (6)$$

For the quantum well waveguide consisting of $Ga_{0.85}Al_{0.15}As$ (substrate), GaAs (film), and $Ga_{0.70}Al_{0.30}As$ (cover), the potential energies are $V_s = 0.115\,971$ eV, $V_f = 0.000\,00$ eV, and $V_c = 0.231\,942$ eV. The electron effective masses are $m_s^* = 0.079\,45\ m_0$, $m_f^* = 0.067\ m_0$, and $m_c^* = 0.0919\ m_0$. Growth is taken to be along the [100] direction and thus each monolayer corresponds to a thickness of 0.2827 nm. The fundamental mode M_0 starts propagating at a thickness of 6 monolayers. The next mode, M_1, starts propagating at a thickness of 31 monolayers. The dispersion curves for the M_0 mode are shown in Fig. 2 for thicknesses of $d = 2.826\,65$ nm (10 monolayers), $d = 5.6533$ nm (20 monolayers), and $d = 8.479\,95$ nm (30 monolayers). A summary of the upper cutoff energies E_{Uco}, the lower cutoff energies E_{Lco}, and the range of allowed energies ΔE for these thicknesses is given in Table I.

TABLE I. Upper and lower cutoff energies and range of energies for the lowest-order waveguide mode M_0 for various film thicknesses in a $Ga_{0.85}Al_{0.15}As$ (substrate), GaAs (film), and $Ga_{0.70}Al_{0.30}As$ (cover) quantum well waveguide.

	Waveguide film (GaAs) thickness		
d (nm)	2.8267	5.6533	8.4800
d (monolayers)	10	20	30
Upper cutoff energy E_{Uco} (eV)	0.4979	0.6536	0.6926
Lower cutoff energy E_{Lco} (eV)	0.0973	0.0551	0.0341
Propagation energy range ΔE (eV)	0.4006	0.5985	0.6585

Semiconductor electron-wave slab waveguides can perform as described here provided that ballistic transport can be achieved over sufficient distances and that the density of electrons is small enough to make electron-electron interactions negligible. Electron waveguides are potentially useful in high-speed electronic circuitry. They could also be a central component in future electron guided-wave integrated circuits. In these circuits, electron waveguides could be used to interconnect a wide variety of quantum devices. These circuits could perform "optical-like" processing functions similar to those of present-day integrated optical circuits.

This research was sponsored in part by a grant from the Joint Services Electronics Program under contract No. DAAL-03-87-K-0059. One of us (K.F.B.) was supported in part by a Presidential Young Investigator award from the National Science Foundation.

[1] L. Esaki and R. Tsu, IBM J. Res. Dev. 13, 61 (1970).
[2] M. Heiblum, M. I. Nathan, D. C. Thomas, and C. M. Knoedler, Phys. Rev. Lett. 55, 2200 (1985).
[3] M. Heiblum and L. F. Eastman, Sci. Am. 255, 103 (Feb. 1987).
[4] M. Heiblum, Opt. News 14, 13 (1988).
[5] T. K. Gaylord and K. F. Brennan, Appl. Phys. Lett. 53, 2047 (1988).
[6] T. K. Gaylord and K. F. Brennan, J. Appl. Phys. 65, 814 (1989).
[7] H. Kogelnik, *Integrated Optics*, edited by T. Tamir (Springer, New York, 1975), p. 13.

Semiconductor quantum wells as electron wave slab waveguides

T. K. Gaylord, E. N. Glytsis, and K. F. Brennan
School of Electrical Engineering and Microelectronics Research Center, Georgia Institute of Technology, Atlanta, Georgia 30332

(Received 6 December 1988; accepted for publication 21 April 1989)

A quantum well in a semiconductor can act as a slab waveguide for electron waves in a manner analogous to the way a layered dielectric can act as a slab waveguide for electromagnetic waves (e.g., as commonly employed in integrated optics). In this work, the case of a general electron asymmetric slab waveguide (a quantum well comprised of three materials each with a different potential energy and a different effective mass) is analyzed and the conditions for electron waveguiding are quantified. Electron waveguide modes exist for electron energies in the well and for electron energies above one or both of the potential energy barriers. Furthermore, due to dispersion, each electron waveguide mode has an upper-energy cutoff as well as a lower-energy cutoff. This is in contrast to electromagnetic guided modes which typically have only lower-energy (low-frequency) cutoffs. At the upper-energy cutoff the electron wave is refracted into the substrate and/or cover. An example quantum well waveguide consisting of $Ga_{0.80}Al_{0.20}As$ (substrate), GaAs (film), $Ga_{0.55}Al_{0.45}As$ (cover) is analyzed. This structure is a single-mode electron waveguide for GaAs thicknesses of from 5 (1.413 nm) to 26 monolayers (7.349 nm).

I. BACKGROUND AND MOTIVATION

Interest in quantum well devices has increased in recent years owing to progress in semiconductor growth technologies such as molecular beam epitaxy (MBE) and metal organic chemical vapor deposition (MOCVD) that enable the fabrication of structures with precise monolayer compositional control.[1] Furthermore, improvements in the crystalline quality of these grown materials have simultaneously produced devices in which ballistic electron transport has been observed.[2,3] That is, conduction electrons move through the material without being scattered and behave like waves (quantum mechanical deBroglie waves). Even in the presence of elastic scattering, electrons retain their phase coherence[4] and can thus refract, reflect, diffract, and interfere in a manner analogous to electromagnetic waves.[5] Also, electron waves may be guided by structures having characteristic dimensions on the order of an electron wavelength[6-8] in a manner analogous to electromagnetic waves in a dielectric waveguide.[9] Furthermore, the analogies[5] between electron waves in semiconductors and electromagnetic waves in dielectrics provide a basis for designing semiconductor quantum wave devices such as electron waveguides.

The behavior of an electron in a single quantum well has been understood since the beginning of quantum mechanics. In the usual situation, the electron is normally incident upon the two potential energy barriers. This corresponds to a zigzag angle of $\theta = 0$ in the waveguide terminology used in subsequent sections. Furthermore, as shown in this paper, these solutions correspond to the lower-energy cutoff that occurs for guided modes of energies within the quantum well. For $\theta \neq 0$, a quantum well is shown to act like a waveguide. Electron waveguide modes exist for electron energies in the well and for electron energies above one or both of the potential energy barriers.

The purposes of this paper are as follows: (1) Present the conditions under which a quantum well acts like an electron waveguide; (2) quantify and label as M_ν (M_0, M_1, M_2, ...) the guided modes; (3) describe the lower-energy cutoff (at which the propagation constant $\beta_\nu = 0$) in which the electron waveguide is analogous to an electromagnetic hollow metallic waveguide with finite conductivity walls; (4) describe the upper-energy cutoff which may be a transition from a guided mode to a substrate "mode" or a radiation "mode" or a cover "mode"; (5) develop the dispersion relation governing electron guided modes; (6) derive the cutoff

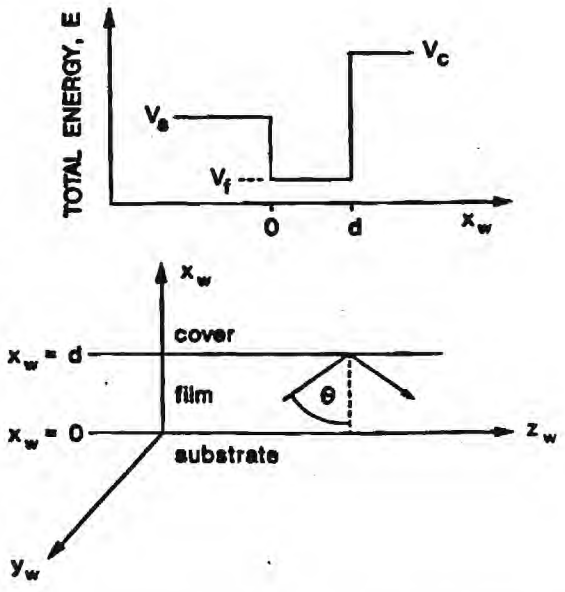

FIG. 1. Asymmetric quantum well showing electron potential energy in the three regions that in waveguide terminology are denoted substrate (s), film (f), and cover (c) and the corresponding three-dimensional waveguide coordinate system. A guided electron wave is composed of two plane-wave components each making an angle of incidence θ with respect to the waveguide walls ($x_w = 0, d$). The electron guided mode propagation direction is z_w.

 0021-8979/89/161842-07$02.40

conditions for the lower-energy cutoff and the upper-energy cutoff; and (7) present a practical example of a quantum well waveguide consisting of $Ga_{0.80}Al_{0.20}As$ (substrate), GaAs (film), $Ga_{0.55}Al_{0.45}As$ (cover), and quantify its modes as a function of the GaAs thickness.

II. ELECTRON WAVEGUIDING IN QUANTUM WELLS

A. Configuration

An asymmetric potential energy well and its depiction as a slab waveguide are shown in Fig. 1. Using standard waveguide terminology,[9] the three regions are denoted substrate (s), film (f), and cover (c), and the direction perpendicular to the waveguide surfaces is x_w. The electron potential energy at the bottom of the quantum well (film) is V_f. The potential energy barrier heights associated with the substrate and cover are V_s and V_c, respectively. Given a material system of the type $F_{1-x}G_xH$, the compositions of the substrate, film, and cover are x_s, x_f, and x_c, respectively. This quantum well can act as an asymmetric slab waveguide. The waveguide coordinate system is also shown in Fig. 1. The direction of guided mode propagation is z_w. The thickness of the waveguide is d. The angle of incidence of the two plane-wave components that constitute the guided wave is the zig-zag angle θ.

B. Critical angles

The magnitude of the electron wave vector in any of the three regions may be expressed as

$$k = [2m^*(E - V)]^{1/2}/\hbar, \tag{1}$$

where m^* is the electron effective mass, E is the total electron energy, and V is the electron potential energy. Thus, the electron wave phase refractive index, n_e (phase), is proportional to the square root of the product of the effective mass and the kinetic energy.[5] The phase of the transmitted and reflected electron waves along the boundary must be identical to that of the incident electron wave. This phase-matching requirement means that the component of the wave vector parallel to the boundary must be the same before and after reflection and refraction. This gives rise to the equivalent of Snell's law for electrons. For incidence upon the film-cover interface, as shown in Fig. 1, it may be written as

$$\frac{\sin\theta_c}{\sin\theta_f} = \left(\frac{m_f^*(E - V_f)}{m_c^*(E - V_c)}\right)^{1/2}. \tag{2}$$

The onset of total internal reflection occurs when $\theta_c = 90°$. This happens when the angle of incidence is equal to the critical angle θ'. Thus from Eq. (2), the cover-film critical angle is

$$\theta'_{cf} = \sin^{-1}[m_c^*(E - V_c)/m_f^*(E - V_f)]^{1/2},$$
$$V_c < E < E_{cf}, \tag{3}$$

where E_{cf} is defined in Sec. II C. For an electron wave incident at an angle greater than θ'_{cf}, the wave is totally internally reflected for an infinitely thick barrier. At steady state, all of the electron current is reflected back into the film. The electron wave function decays exponentially into the cover. If the kinetic energy $E - V_c < 0$, then total internal reflection occurs for any angle of incidence including normal incidence. This is in contrast to the electromagnetic case where total internal reflection can never occur at normal incidence due to the nonzero value of the refractive index. Similarly, the substrate-film critical angle is

$$\theta'_{sf} = \sin^{-1}[m_s^*(E - V_s)/m_f^*(E - V_f)]^{1/2},$$
$$V_s < E < E_{sf}, \tag{4}$$

where E_{sf} is defined in Sec. II C. For a guided mode, the zig-zag angle θ shown in Fig. 1 must be greater than both θ'_{cf} and θ'_{sf}. That is,

$$\theta > \max(\theta'_{cf}, \theta'_{sf}) \tag{5}$$

are necessary conditions for a guided mode. For the example quantum well waveguide of $Ga_{0.80}Al_{0.20}As$ (substrate), GaAs (film), $Ga_{0.55}Al_{0.45}As$ (cover) treated in this paper, the critical angles θ'_{cf} and θ'_{sf} are shown in Fig. 2 on a plot of zig-zag angle versus total energy.

C. Types of guided modes and unguided "modes"

The range of zig-zag angles and total energies in Fig. 2 that satisfy (5) corresponds to the region of allowed guided modes. As the energy increases in a guided mode, the zig-zag angle θ also increases. When θ reaches θ'_{sf}, the guided wave starts to refract into the substrate (rather than exponentially decaying). For energies greater than this energy, the electron wave is propagating in the substrate as well as in the film. This is called a substrate "mode." Quotation marks are used to emphasize that this is not a true guided mode. As the energy is further increased, θ reaches θ'_{cf}, and the electron wave starts to refract into the cover as well as into the substrate. The electron wave is now a propagating wave in all three regions, and this is called a radiation "mode." For a different set of material parameters, as the electron energy is increased, it is possible for the electron wave to be refracted into the cover. This situation is similarly called a cover "mode."

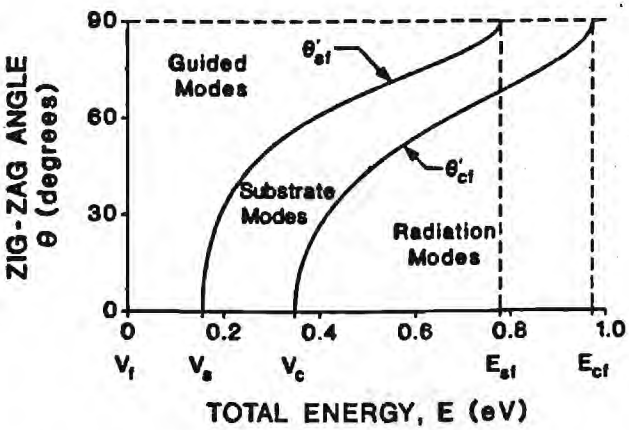

FIG. 2. The critical angles of θ'_{sf} and θ'_{cf} on a plot of zig-zag angle vs total energy for the example quantum well waveguide composed of $Ga_{0.80}Al_{0.20}As$ (substrate), GaAs (film), $Ga_{0.55}Al_{0.45}As$ (cover). The regions of guided modes, substrate modes, and radiation modes are shown.

D. Types of cutoff

An electron guided wave mode can become cutoff by decreasing the electron energy. This will be called the lower-energy cutoff. The zig-zag angle decreases with decreasing energy and this cutoff occurs when $\theta = 0$. The guided wave may be decomposed into two plane-wave components each having an angle of incidence of θ with respect to the waveguide walls. The propagation constant, β_ν, of the νth guided mode, where ν is an integer is

$$\beta_\nu = 2\pi/\Lambda_\nu, \tag{6}$$

where Λ_ν is the period of the interference pattern produced by the two plane waves that constitute the νth guided mode as measured in the guided mode direction of propagation (z_w). The propagation constant β_ν is the same as the component of the wave vector parallel to the boundary. In conventional solid state notation, $\beta_\nu \equiv k_{\parallel\nu}$. Therefore it is given by

$$\beta_\nu = [2m_f^*(E - V_f)/\hbar^2]^{1/2} \sin\theta, \tag{7}$$

and so $\beta_\nu = 0$ at the lower-energy cutoff. The wave function is sinusoidal in the film and exponentially decaying in the substrate and cover. In this sense, the lower-energy cutoff is like the cutoff in an electromagnetic hollow metallic waveguide with finite conductivity walls.

A representation of the electron propagation constant versus total electron energy for the $Ga_{0.80}Al_{0.20}As/GaAs/Ga_{0.55}Al_{0.45}As$ example is given in Fig. 3. For an infinite medium having the properties of the substrate, the electron propagation constant is

$$\beta_s = [2m_s^*(E - V_s)]^{1/2}/\hbar. \tag{8}$$

Similarly, for an infinite medium having the properties of the film, it is

$$\beta_f = [2m_f^*(E - V_f)]^{1/2}/\hbar, \tag{9}$$

and for an infinite cover medium, it is

$$\beta_c = [2m_c^*(E - V_c)]^{1/2}/\hbar. \tag{10}$$

These three propagation constant relationships are plotted in Fig. 3. For a given energy E, the propagation constant of a guided mode can be no larger than that given by Eq. (9). The region to the left of this curve corresponds to evanescent (nonphysical) modes. Thus the allowed guided modes must lie to the right of this curve in Fig. 3.

As the electron energy of a guided mode is increased, an upper-energy cutoff will occur. The upper-energy cutoff can be of three types: (1) cutoff to a substrate "mode" which is like the cutoff in an electromagnetic asymmetric dielectric waveguide with the substrate index higher than the cover index, (2) cutoff to a radiation "mode" which is like the cutoff in an electromagnetic symmetric dielectric waveguide (equal substrate and cover indices), (3) cutoff to a cover "mode" which is like the cutoff in an electromagnetic asymmetric dielectric waveguide with the cover index higher than the substrate index. The type of upper-energy cutoff that occurs depends on the material parameters. For the example case depicted in Fig. 4, the upper-energy cutoff will be to substrate "modes" since β_s occurs at lower energy, in general, than does β_c.

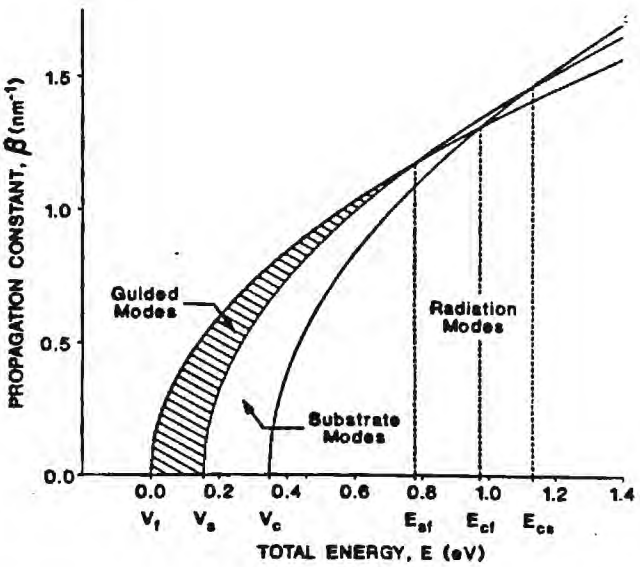

FIG. 3. Electron guided mode propagation constant as a function of total electron energy showing the regions of guided modes, substrate modes, and radiation modes for the example quantum well waveguide composed of $Ga_{0.80}Al_{0.20}As$ (substrate), GaAs (film), $Ga_{0.55}Al_{0.45}As$ (cover).

The intersection of β_f and β_s occurs at an energy E_{sf} which is given by

$$E_{sf} = (m_s^* V_s - m_f^* V_f)/(m_s^* - m_f^*). \tag{11}$$

At this energy, the electron wave phase refractive indices for the film and the substrate are equal. When this energy is reached, the waveguide can no longer guide an electron wave even if it is at grazing incidence along the walls of the waveguide. Thus this energy is equivalent to the substrate-film critical angle $\theta'_{sf} = 90°$. Similarly, the intersection of β_f and β_c occurs at an energy E_{cf} and this energy is given by

$$E_{cf} = (m_c^* V_c - m_f^* V_f)/(m_c^* - m_f^*). \tag{12}$$

At this energy, the electron wave phase refractive indices for the film and the cover are equal. This energy is equivalent to the cover-film critical angle $\theta'_{cf} = 90°$. Similarly, the intersection of β_s and β_c occurs at an energy E_{cs} and this energy is given by

$$E_{cs} = (m_c^* V_c - m_s^* V_s)/(m_c^* - m_s^*). \tag{13}$$

At this energy, the electron wave phase refractive indices for the substrate and the cover are equal.

III. QUANTUM WELL ELECTRON SLAB WAVEGUIDES

A. Dispersion relation for guided modes

The analysis of a two-dimensional (x_w, z_w) quantum well guided electron wave is similar to the conventional one-dimensional (x_w) quantum well but with the addition of the guided mode dependence in the z_w direction and differing effective masses in the three regions. The wave function has a sinusoidal dependence in the z_w direction and can be expressed in the form

$$\psi_\nu(x_w, z_w) = \psi_\nu(x_w)\exp(+j\beta_\nu z_w), \tag{14}$$

where β_ν is the guided mode propagation constant. The Schroedinger time-independent wave equation becomes

$$\frac{d^2\psi_\nu(x_w)}{dx_w^2}+\left(\frac{2m^*}{\hbar^2}[E_\nu - V(x_w)] - \beta_\nu^2\right)\psi_\nu(x_w)=0. \tag{15}$$

For a guided mode, the wave function amplitude in the substrate may now be expressed as $\psi_{\nu s}(x_w) = A_s \exp(\gamma_s x_w)$, in the film as

$$\psi_{\nu f}(x_w) = A_{f1}\exp(j\kappa_f x_w) + A_{f2}\exp(-j\kappa_f x_w),$$

and in the cover as

$$\psi_{\nu c}(x_w) = A_c \exp[-\gamma_c(x_w - d)],$$

where

$$\gamma_c^2 = \beta_\nu^2 - [(2m_c^*/\hbar^2)(E_\nu - V_c)],$$
$$\kappa_f^2 = [(2m_f^*/\hbar^2)(E_\nu - V_f)] - \beta_\nu^2,$$

and

$$\gamma_s^2 = \beta_\nu^2 - [(2m_s^*/\hbar^2)(E_\nu - V_s)].$$

Applying the boundary condition that the wave function amplitude ψ_ν and $(1/m^*)(d\psi_\nu/dx)$ be continuous at the substrate film and at the cover-film boundaries gives a set of four linear homogeneous equations in the four unknowns $(A_s, A_{f1}, A_{f2}, A_c)$. For nontrivial solutions, the determinant of coefficients must vanish. This gives

$$\tan(\kappa_f d) = \frac{(\kappa_f/m_f^*)[(\gamma_s/m_s^*) + (\gamma_c/m_c^*)]}{(\kappa_f^2/m_f^{*2}) - (\gamma_s/m_s^*)(\gamma_c/m_c^*)}. \tag{16}$$

Using the identity

$$\tan(x+y) \equiv [(\tan x + \tan y)/(1 - \tan x \tan y)]$$

and then taking the arctangent of both sides of this equation gives

$$\kappa_f d - \tan^{-1}\left(\frac{\gamma_s/m_s^*}{\kappa_f/m_f^*}\right) - \tan^{-1}\left(\frac{\gamma_c/m_c^*}{\kappa_f/m_f^*}\right) = \nu\pi. \tag{17}$$

For $V_f = 0$ and normal incidence ($\beta_\nu = 0$), this dispersion equation predicts, in the limit as V_c and V_s approach infinity, that

$$E_\nu = (\nu+1)^2\hbar^2\pi^2/2m_f^* d^2$$

in agreement with the quantum mechanical one-dimensional infinite potential well results.

B. Lower-energy cutoff (cutoff at normal incidence)

Cutoff for the guided M_ν modes can occur as the electron energy is decreased and the guided wave propagation constant goes to zero. This can occur only for an electron energy below the lower barrier energy ($E < V_s$). When $\beta_\nu = 0$, the mode is no longer propagating. This is analogous to the cutoff of an electromagnetic guided mode in a hollow metallic waveguide with finite conductivity walls. The plane-wave components of the guided wave are reflecting back and forth at normal incidence to the waveguide boundaries. The electron energy at which the lower-energy cutoff occurs is designated E_{Lco}. The condition for this type of cutoff is obtained by substituting $\beta_\nu = 0$ into the dispersion Eq. (17). The cutoff condition is

$$[2m_f^*(E_{Lco} - V_f)]^{1/2} d/\hbar - \tan^{-1}\left(\frac{m_f^*(V_s - E_{Lco})}{m_s^*(E_{Lco} - V_f)}\right)^{1/2} - \tan^{-1}\left(\frac{m_f^*(V_c - E_{Lco})}{m_c^*(E_{Lco} - V_f)}\right)^{1/2} = \nu\pi. \tag{18}$$

For given substrate, film, and cover materials, thickness, and integer mode number ν, this transcendental equation may be solved for the $\beta_\nu = 0$ cutoff energy E_{Lco} corresponding to that mode.

C. Upper-energy cutoff (cutoff to substrate "mode")

Cutoff for the guided M_ν modes can occur as the electron energy is *increased* and total internal reflection no longer occurs at the substrate-film boundary. In electromagnetic waveguides there is typically only a lower-energy (lower-frequency) cutoff, and no higher-energy cutoff exists. In the present situation, however, as the electron energy is increased, the electron wave is refracted into the substrate. As the energy is increased through this cutoff transition, the electron wave function amplitude in the substrate changes from being evanescent (exponentially decaying) to propagating (sinusoidal). This can occur only for an electron energy above the lower barrier energy ($E > V_s$). The electron energy at which the upper-energy cutoff occurs is designated E_{Uco}. The condition for the occurrence of this type of cutoff is $\gamma_s = 0$, and thus the mode "leaks" into the substrate. This is analogous to the cutoff of an electromagnetic guided mode in an asymmetric dielectric slab waveguide. This type of cutoff occurs when the zig-zag angle is equal to the substrate-film critical angle. The condition for this type of cutoff is obtained by substituting $\gamma_s = 0$ into the dispersion Eq. (17). The condition for cutoff to substrate "modes" is thus

$$\{2[(m_s^* V_s - m_f^* V_f - (m_s^* - m_f^*)E_{Uco}]\}^{1/2} d/\hbar - \tan^{-1}\left(\frac{[m_c^* V_c - m_s^* V_s - (m_c^* - m_s^*)E_{Uco}]m_f^{*2}}{[m_s^* V_s - m_f^* V_f - (m_s^* - m_f^*)E_{Uco}]m_c^{*2}}\right)^{1/2} = \nu\pi. \tag{19}$$

This transcendental equation may be solved for the cutoff to substrate "mode" energy E_{Uco} corresponding to the M_ν mode.

D. Energy of first appearance of modes

For a given set of material parameters, as the waveguide thickness is increased, a guided mode M_ν first starts to propagate at an energy $E = V_s$. This corresponds to the highest possible value of the cutoff energy for the lower-energy type cutoff as well as the lowest possible value of the cutoff energy for the higher-energy type cutoff. For $E = V_s$, Eqs. (18) and (19) are the same. Namely,

$$\frac{[2m_f^*(V_s - V_f)]^{1/2} d}{\hbar} - \tan^{-1}\left(\frac{m_f^*(V_c - V_s)}{m_c^*(V_s - V_f)}\right)^{1/2} = \nu\pi. \tag{20}$$

From Eq. (20), the M_ν first starts propagating as the thickness is increased to the value

$$d=\left(\frac{\hbar}{[2m_f^*(V_s-V_f)]^{1/2}}\right)\times\left[\tan^{-1}\left(\frac{m_f^*(V_c-V_s)}{m_c^*(V_s-V_f)}\right)^{1/2}+\nu\pi\right]. \quad (21)$$

Also from Eq. (20), the range of thicknesses that will produce a waveguide that supports only the lowest-order ($\nu=0$) mode (M_0) is obtained and is

$$\left(\frac{\hbar}{[2m_f^*(V_s-V_f)]^{1/2}}\right)\tan^{-1}\left(\frac{m_f^*(V_c-V_s)}{m_c^*(V_s-V_f)}\right)^{1/2}<d<\left(\frac{\hbar}{[2m_f^*(V_s-V_f)]^{1/2}}\right)\times\left[\tan^{-1}\left(\frac{m_f^*(V_c-V_s)}{m_c^*(V_s-V_f)}\right)^{1/2}+\pi\right]. \quad (22)$$

As with electromagnetic asymmetric slab waveguides, there is a minimum thickness required for any modes to propagate.

E. Symmetric waveguides

If the waveguide is symmetric, $V_c=V_s$ and the substrate and cover dispersion curves coincide. In this situation the lower-energy cutoff again occurs as the energy is decreased and the propagation constant goes to zero ($\beta_\nu=0$). This can occur only for an electron energy below the lower barrier energy ($E<V_s=V_c$). When $\beta_\nu=0$, also $\theta=0$ and the plane-wave components of the guided wave are reflecting back and forth at normal incidence to the waveguide boundaries.

For a symmetric waveguide, the upper-energy cutoff occurs as the energy is increased and the guided mode becomes a radiation "mode." At the cutoff energy, total internal reflection occurs *neither* at the substrate-film boundary *nor* at the cover-film boundary. The electron wave is then refracted both into the substrate and the cover. As the electron energy is increased through this cutoff transition, the electron wave function amplitude in the substrate and cover change from being evanescent to propagating. This can occur only for an electron energy above the barrier energy ($E>V_s=V_c$). When $\gamma_s=\gamma_c=0$, the mode "leaks" into the substrate and cover. This is analogous to the cutoff of an electromagnetic guided mode in a symmetric dielectric slab waveguide. This type of cutoff occurs when the zig-zag angle becomes simultaneously equal to the substrate-film critical angle and the cover-film critical angle.

The first appearance of the M_ν again occurs when the electron energy $E=V_s$ ($=V_c$). The M_ν first starts propagating as the thickness is increased to the value $d=\nu\hbar\pi/[2m_f^*(V_s-V_f)]^{1/2}$. Also from Eq. (20), the range of thicknesses that will produce a waveguide that supports only the lowest-order ($\nu=0$) mode (M_0) is obtained and is $0<d<\hbar\pi/[2m_f^*(V_s-V_f)]^{1/2}$. As with electromagnetic symmetric slab waveguides, there is a no minimum thickness required for the lowest-order mode to propagate. Any thickness will support the M_0 mode. However, for very thin waveguides, the exponentially decaying tails of the wave function may extend very far into the substrate and cover.

IV. EXAMPLE $Ga_{1-x}Al_xAs$ ELECTRON WAVEGUIDE

To illustrate the analysis presented in Sec. III, the example quantum well waveguide consisting of a substrate of $Ga_{0.80}Al_{0.20}As$, a film of GaAs, and a cover of $Ga_{0.55}Al_{0.45}As$ is further treated in this section. The electron potential energies in the three regions of the quantum well are given by the conduction band edge as

$$V_i=Ax_i, \quad i=s,f,c, \quad (23)$$

where $x_s=0.2$ for the substrate, $x_f=0$ for the film, $x_c=0.45$ for the cover, and $A=0.7731$ eV (in which the conduction band discontinuity has been taken to be 60% of the energy gap change). Therefore $V_s=0.1546$ eV, $V_f=0.0000$ eV, and $V_c=0.3479$ eV. The electron effective mass in the three regions is given by

$$m_i^*=(B+Cx_i)m_0, \quad i=s,f,c, \quad (24)$$

where m_0 is the free electron mass, $B=0.067$, and $C=0.083$. Therefore $m_s^*=0.0836\,m_0$, $m_f^*=0.067\,m_0$, and $m_c^*=0.10435\,m_0$.

Numerically solving the waveguide dispersion Eq. (17), the waveguide modes were quantified as a function of the GaAs waveguide (film) thickness. Growth is taken to be along the [100] direction and thus each monolayer corresponds to a thickness of 0.28267 nm. Mode dispersion curves for the lowest-order mode, M_0, are shown in Fig. 4 for thicknesses of 10 monolayers ($d=2.8267$ nm) and 20 monolayers ($d=5.6533$ nm). The modes first appear at $E=V_s$ and $\beta=0$, the lower-right-hand corner of the guided mode region in a β vs E plot such as Fig. 4. As the thickness is further increased, the mode dispersion curves move to the left and upward. In the limit of very large thickness the mode lines approach the left-hand β_f curve given by Eq. (9). For the composition treated, there are no modes at all for a thick-

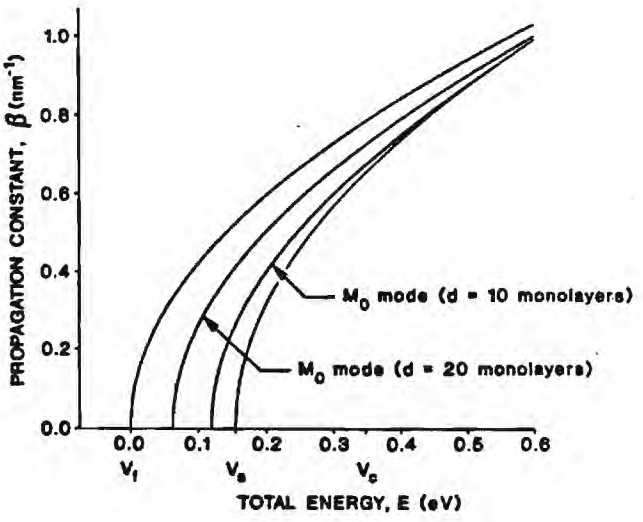

FIG. 4. Propagation constant of the M_0 electron guided mode as a function of total electron energy (mode dispersion curve) for the example quantum well waveguide composed of $Ga_{0.80}Al_{0.20}As$ (substrate), GaAs (film), $Ga_{0.55}Al_{0.45}As$ (cover) with film thicknesses of 10 monolayers and 20 monolayers. The lower-energy cutoffs ($\beta=0$) and upper-energy cutoffs are apparent.

TABLE I. Upper- and lower-cutoff energies and range of energies for the allowed waveguide modes for various film thicknesses in a $Ga_{0.80}Al_{0.20}As$ (substrate), GaAs (film), $Ga_{0.55}Al_{0.45}As$ (cover) quantum well waveguide.

	Waveguide film (GaAs) thickness					
(nm)	1.1307	1.4133	2.8267	5.6533	7.3493	7.6320
(monolayers)	4	5	10	20	26	27
M_0 mode						
Propagating or cutoff	cutoff	prop.	prop.	prop.	prop.	prop.
Upper-cutoff energy, E_{Uco} (eV)	···	0.1635	0.5657	0.7017	0.7268	0.7297
Lower-cutoff energy, E_{Lco} (eV)	···	0.1546	0.1190	0.0623	0.0451	0.0430
Propagation energy range, ΔE (eV)	···	0.0089	0.4467	0.6394	0.6817	0.6867
M_1 mode						
Propagating or cutoff	cutoff	cutoff	cutoff	cutoff	cutoff	prop.
Upper-cutoff energy, E_{Uco} (eV)	···	···	···	···	···	0.1866
Lower-cutoff energy, E_{Lco} (eV)	···	···	···	···	···	0.1532
Propagation energy range ΔE (eV)	···	···	···	···	···	0.0334

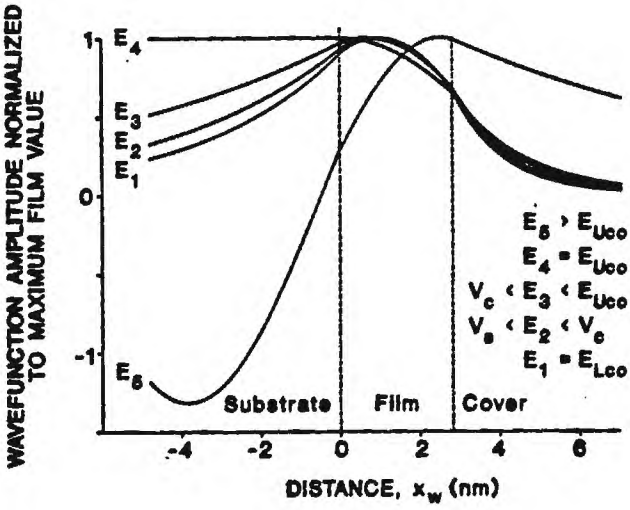

FIG. 5. The wave function amplitude (normalized to the maximum value in the film region) as a function of position for various energies for a quantum well waveguide with thickness of 10 monolayers ($d = 2.82665$ nm). The wave function is shown for an electron energy at the lower-energy cutoff ($E_1 = 0.1190$ eV), for an energy above the substrate barrier but below the cover barrier ($E_2 = 0.25$ eV), for an energy above both barriers ($E_3 = 0.40$ eV), for an energy at the upper-energy cutoff ($E_4 = 0.5657$ eV), and for a substrate "mode" at an energy above the upper-energy cutoff ($E_5 = 0.70$ eV).

ness of four monolayers ($d = 1.1307$ nm). For a thickness of five monolayers ($d = 1.4133$ nm), the M_0 mode has just started to propagate. The energy difference, ΔE, between the upper-cutoff energy (cutoff to substrate mode) and the lower-cutoff energy (cutoff at $\beta = 0$), is only $\Delta E = 0.0089$ eV. For a thickness of 10 monolayers ($d = 2.8267$ nm) as shown in Fig. 4, the propagation energy range has increased to $\Delta E = 0.4466$ eV. As the thickness increases, the lower-cutoff energy decreases and the upper-cutoff energy increases as depicted in Fig. 4. Notice that even at a thickness of 10 monolayers, the guided mode can propagate at energies above both potential barriers ($E > V_s, E > V_c$). At a thickness of 27 monolayers ($d = 7.6320$ nm), the M_1 mode starts to propagate. Thus for this combination of materials, this structure operates as a single mode waveguide for GaAs thicknesses from five (1.4133 nm) through 26 monolayers (7.3493 nm). A summary of the upper- and lower-cutoff energies and the range of allowed energies for these waveguide modes is given in Table I.

Plots of the wave function ψ_v for the M_0 mode for GaAs thickness of 10 monolayers are given in Fig. 5 for electron energies of $E = E_{Lco}$ ($\beta = 0$ cutoff), $V_s < E < V_c$, $V_c < E < E_{Uco}$, and $E = E_{Uco}$ to illustrate guided mode behavior in these ranges of electron energy. The wave function is also shown for an energy above the upper-cutoff energy ($E > E_{Uco}$) to illustrate substrate "mode" behavior.

V. SUMMARY AND DISCUSSION

The use of a semiconductor quantum well as an electron slab waveguide has been analyzed. The dispersion relation, Eq. (17), governing the guided modes has been developed. The guided modes have been labeled M_ν where ν is the integer mode number ($\nu = 0, 1, 2, \ldots$). A lower-energy cutoff ($\beta_\nu = 0$) has been quantified in which the electron waveguide is analogous to an electromagnetic hollow metallic waveguide with finite conductivity walls. This cutoff simply corresponds to the allowed energies of the one-dimensional potential energy well. Unlike electromagnetic waveguides, an upper-energy cutoff is also found to be present. The upper-energy cutoff may be a transition to a substrate "mode," a transition to a radiation "mode," or a transition to a cover "mode." These cutoffs are due to dispersion effects. The effective electron phase refractive indices become more nearly equal at higher electron energies (see Fig. 3) and thus the index of the film is not sufficiently large with respect to the substrate and/or cover to support a guided mode. That is, electron total internal reflection [Eqs. (3) and (4)] no longer occurs. The upper cutoff energies occur above the potential barriers and thus electron waveguiding has been shown to be possible at energies well above the potential energy barriers.

Electron waveguides are potentially useful in high-speed electronic circuitry and as a central component in future electron guided-wave integrated circuits which could perform "optical-like" processing that is analogous to present-day electromagnetic optical processing that is done with guided-wave integrated optical circuits.

ACKNOWLEDGMENTS

This research was sponsored in part by a grant from the Joint Services Electronics Program under Contract No. DAAL-03-87-K-0059. One of us (K.F.B) was supported in part by a Presidential Young Investigator award from the National Science Foundation.

[1] L. Esaki and R. Tsu, IBM J. Res. Dev. **13**, 61 (1970).
[2] A. F. J. Levi, J. R. Hayes, P. M. Platzman, and W. Wiegmann, Phys. Rev. Lett. **55**, 2071 (1985).
[3] M. Heiblum, M. I. Nathan, D. C. Thomas, and C. M. Knoedler, Phys. Rev. Lett. **55**, 2200 (1985).
[4] S. Washburn and R. A. Webb, Adv. Phys. **35**, 375 (1986).
[5] T. K. Gaylord and K. F. Brennan, J. Appl. Phys. **65**, 814 (1989).
[6] G. Timp, A. M. Chang, P. Mankiewich, R. Behringer, J. E. Cunningham, T. Y. Chang, and R. E. Howard, Phys. Rev. Lett. **59**, 732 (1987).
[7] M. L. Roukes, A. Scherer, S. J. Allen, H. G. Craighead, R. M. Ruthen, E. D. Beebe, and J. P. Harbison, Phys. Rev. Lett. **59**, 3011 (1987).
[8] B. J. van Wees, H. van Houten, C. W. J. Beenakker, J. G. Williamson, L. P. Kouwenhoven, D. van der Marel, and C. T. Foxon, Phys. Rev. Lett. **60**, 848 (1988).
[9] H. Kogelnik, *Integrated Optics*, edited by T. Tamir (Springer, New York, 1975), p. 13.

Theory and design of semiconductor electron-wave interference filter/emitters

E. N. Glytsis, T. K. Gaylord, and K. F. Brennan
School of Electrical Engineering and Microelectronics Research Center, Georgia Institute of Technology, Atlanta, Georgia 30332-0250

(Received 15 June 1989; accepted for publication 30 August 1989)

A voltage-biased semiconductor superlattice structure is designed to operate simultaneously as a continuously voltage-tunable, electron interference filter and as an electron emitter. Using the analogies between electromagnetic waves and electron de Broglie waves, a systematic procedure for designing the quantum wells and barriers comprising the electron-wave filter/emitter superlattice is developed. A generalized procedure for analyzing the electron-current transmittance and reflectance spectral responses of these superlattice structures is then presented. A practical, continuously tunable filter/emitter consisting of multiple layers of $Ga_{1-x}Al_xAs$ (compositional superlattice) is designed to emit nearly monoenergetic 0.20-eV electrons by appropriate selection of the layer compositions and thicknesses. The constraints required to have thicknesses that are integer multiples of the monolayer thickness and to avoid phonon scattering of electrons into the L band are included. The filter/emitter is shown to have a wide tunable energy range. A sensitivity analysis of the device characteristics in the presence of fabrication errors reveals a very stable device response. Such quantum electron-wave devices could serve as continuously tunable hot-electron emitters in ballistic transistors and in future guided electron-wave integrated circuits.

I. INTRODUCTION

Quantum-mechanical interference effects have recently been observed in devices such as GaAs/AlGaAs and InGaAs/InAlAs single-well double-barrier structures.[1–4] This indicates that present-day semiconductor devices are rapidly approaching a fundamental size limitation.[5] At dimensions of less than about 0.3 μm, potentially "troublesome" quantum-wave effects start to dominate device characteristics, making further reduction in their sizes undesirable in some applications, thereby limiting the ultimate speed of the devices. This holds true regardless of the material (silicon, gallium arsenide, etc.). However, these quantum-wave effects may also potentially be used in the design of novel devices.

Starting from fundamental principles, quantitative analogies between quantum-mechanical electron waves in semiconductor materials and electromagnetic optical waves in dielectrics have recently been developed.[6] With these analogies, existing electromagnetic optical analysis and design techniques can be used for the analysis and design of new semiconductor quantum-wave devices. The possibility of realizing these device structures in practice has become more likely due to the rapid progress and relative maturity in semiconductor growth technologies such as molecular-beam epitaxy (MBE) and metalorganic chemical vapor deposition (MOCVD) that enable the fabrication of structures with precise monolayer compositional control. Possible devices include narrow-band superlattice interference filters[7,8] and filter/emitters[9] (present work). These structures could be incorporated into present-day ballistic transistors[10] to produce subpicosecond switching times. Beyond improving the speed of existing devices, however, the totally new concept of *guided electron-wave integrated circuits* has recently been proposed.[11] This next generation of integrated circuits would be comprised of many semiconductor quantum-wave devices interconnected by electron waveguides.[11–14]

In these ultrasmall superlattice interference filters or filter/emitters, electron waves can travel through the device maintaining their quantum-mechanical phase coherence. Thus these waves can interfere, reflect, refract, and diffract in a manner analogous to the electromagnetic plane waves in dielectric media. Even though quantum interference effects have been observed experimentally in single-well double-barrier structures, these effects can also occur in multiple-layer superlattices and at energies above the potential barriers. Furthermore, exploiting the electron-wave interference, novel electron-wave interference filter/emitters can be designed that are analogous to thin-film optical interference filters. These superlattice interference filter/emitters can exhibit very narrow electron kinetic energy passbands and can be integrated into solid-state devices for potential use as monoenergetic emitters for electroluminescent devices,[15,16] photodetectors,[15,17] and fast ballistic transistors.[15]

Although semiconductor superlattice interference filter designs can be visualized directly from the optical interference filters, their designs cannot simply be copies of thin-film optical designs. The reason for this is that due to the ultrasmall dimensions of each superlattice layer (on the order of a nanometer), the thickness quantization has to be taken into account (layer thicknesses must be an integer multiple of the monolayer thickness). Another constraint is the limited usable composition range that is available. Furthermore, in the case of an applied bias voltage, the potential energy along the undoped superlattice changes linearly with the device length. This is analogous to a varying optical refractive index in a thin-film filter. Presently, there are no available designs for this linearly varying index case. Another practical constraint is that the desired electron-energy states should be sufficiently below the L-band minimum in order to avoid phonon scattering which can reduce the electron coherence

 0021-8979/89/246158-10$02.40

length. The purpose of this paper is to present a systematic procedure for the design of continuously tunable semiconductor electron interference filter/emitters subject to the above constraints. An example design using the $Ga_{1-x}Al_xAs$ alloy system is presented, and the filter/emitter is shown to have a broad tunable range. Moreover, a sensitivity analysis of the device performance in the presence of fabrication variations indicates stable device characteristics.

II. SEMICONDUCTOR QUANTUM ELECTRON-WAVE OPTICS

Quantum-mechanical electron waves in semiconductors and electromagnetic optical waves in dielectrics exhibit transmission, reflection, interference, and diffraction characteristics that are analogous to each other since they satisfy analogous wave equations and boundary conditions. Quantum interference effects have been analyzed for single potential energy boundaries,[18] for normal incidence,[19] and for the general case of any number of boundaries and any angle of incidence.[6] From these results a quantitative mapping between electromagnetic optical waves and quantum electron waves has been established.[6] Thus, using these quantitative analogies, existing optical device designs can now have electron-wave device counterparts.

The plane-wave solutions of the Schrödinger's equation contain a wave-vector quantity k of magnitude $k = [2m^*(E - V)]^{1/2}/\hbar$, where m^* is the electron effective mass, E is the total electron energy, V is the electron potential energy, and $\hbar$ is Planck's constant divided by 2π. All plane-wave phase effects (for plane-wave interference) are described by the wave vector k. As a consequence, an electron-wave phase refractive index n_e(phase), can be introduced that is proportional to the square root of the product of the effective mass and the kinetic energy.[6] That is,

$$n_e(\text{phase}) \propto [m^*(E - V)]^{1/2}. \tag{1}$$

Furthermore, amplitude effects such as electron transmissivity and reflectivity may be described in terms of the wavefunction amplitude for an electron wave or in terms of the electric field amplitude for TE-polarized optical wave incident upon a boundary. Continuity of the wave function across a potential energy boundary and conservation of electron probability current normal to a potential energy boundary are analogous to the continuity of the tangential component of the electric field across a boundary between dielectrics and to the conservation of power flow normal to a boundary between dielectrics, respectively. Using these analogies, an electron-wave amplitude refractive index n_e(amplitude) can be introduced[6] that makes the optical and electron-wave transmissivities and reflectivities equivalent. That is,

$$n_e(\text{amplitude}) \propto [(E - V)/m^*]^{1/2}. \tag{2}$$

Since the phase and amplitude effects are mathematically decoupled in the equations describing electromagnetic optical designs, the same designs have quantum electron-wave counterparts that are described by the two electron-wave refractive indices [Eqs. (1) and (2)]. Both types of these refractive indices exhibit normal dispersion; i.e., they increase with decreasing wavelength.

III. THIN-FILM OPTICAL INTERFERENCE FILTERS

Due to the analogies between the electromagnetic optical waves and the quantum-mechanical electron waves, the thin-film optical interference filters and the electron-wave interference superlattice filters have many common characteristics. For completeness some of the more relevant properties of thin-film optical filters[20–22] are summarized below.

A simple type of narrow-bandpass optical interference filter is the all-dielectric Fabry–Perot filter. It consists of a half-wavelength layer sandwiched between quarter-wavelength layers of high refractive index (designated H) and of low refractive index (designated L). The combination of quarter-wavelength layers constitutes a reflector. The electron-wave analog of this elementary type of interference optical filter is treated in this work. The full width at half maximum (FWHM) of the bandpass of this filter can be reduced by increasing the reflectivity of the reflectors, i.e., by increasing the ratio of high to low refractive indices. In the optical literature there are two basic types of all-dielectric Fabry–Perot interference filters which are symbolically represented as $[HL]^N HH[LH]^N$ and $H[LH]^N LL[HL]^N H$, where H and L represent quarter-wavelength layers of high and low refractive index, respectively, and N represents the number of repetitions of the layer-pair type indicated in brackets. Some other important characteristics of the all-dielectric Fabry–Perot interference filters, that are related with the electron-wave interference filter designs, are the following: (1) The maximum transmittance of the filter is 100%. (2) The maximum transmittance occurs at the wavelength for which the central layer is a half-wavelength thick (as measured in that material) and the surrounding layers are quarter-wavelength layers (as measured in those materials). (3) The FWHM decreases as the number of the surrounding layers increases (as N increases). (4) The transmittance characteristics are relatively insensitive to variations in the reflectivities and thicknesses of the layers. (5) The filter is effective only over a limited range since sidebands necessarily occur on either side of the passband.

IV. DESIGN OF SEMICONDUCTOR SUPERLATTICE INTERFERENCE FILTER/EMITTERS

A. Computation of the layer thicknesses and compositions for a given bias voltage and electron energy

When a voltage bias is applied to a superlattice structure, the resulting device can serve as an electron-wave interference filter and electron emitter. Using the previously presented analogies between the quantum electron waves and the electromagnetic optical waves, the quantum well and barrier widths and heights in the direction of emission can be systematically designed to comprise an interference filter which is embedded in the emitter. The optical analog of this device does not exist since the equivalent phase and amplitude refractive indices of the electron waves vary along the emission direction of the structure due to the applied bias potential energy. Thus the optical counterpart would be comprised of inhomogeneous regions where the correspond-

ing optical refractive indices would vary as functions of the propagation distance within the optical filter. However, the same concepts that are used for the design of homogeneous optical interference filters can be adopted in the case of the electron-wave interference filter/emitter. Moreover, the successive quantum wells and barriers can act as the high (H) and low (L) electron refractive index materials that comprise the reflectors of the interference filter/emitter.

The electron potential energy of a quantum-well superlattice interference filter/emitter with an applied bias voltage is shown in Fig. 1. The structure consists of M layers surrounded by bulk semiconductor material. The filter/emitter is designed to be a simple narrow-bandpass interference filter (the optical counterpart would be an all dielectric inhomogeneous Fabry–Perot interference filter). The filter/emitter consists of M layers, where M is an odd integer, and the central layer is a half-wavelength layer sandwiched between quarter-wavelength layers of high (H) and low (L) equivalent electron-wave refractive index. When the design voltage is applied, electrons in a narrow spectral band around the prespecified pass energy E_p (Fig. 1) traverse the filter/emitter and are emitted with an output energy $\mathrm{KE}_{\mathrm{out}}$. At the design voltage, with corresponding bias potential energy V_{bias}, each reflector layer [of high (H) or low (L) average electron-wave refractive index] is exactly a quarter of an electron wavelength (as measured in that layer) in the thickness, and the resonant central layer is exactly one-half of an electron wavelength (as measured in that layer). In the case of the biased filter/emitter, the kinetic electron energy varies linearly within each individual layer due to the applied voltage. Thus the electron wavelength changes continuously inside each layer. However, a quarter or a half of an electron wavelength is defined as the required layer thickness to produce a total phase shift of the traveling electron-wave function inside the layer of $\pi/2$ or π, respectively (or odd multiples of these phase shifts). Although only an average electron wavelength can be defined within each layer, the terminology of "quarter" or "half electron wavelength" are used in order to be analogous to the corresponding quantities appearing in the design of optical thin-film interference filters. The jth quantum well or barrier (Fig. 1) has a thickness d_j and at zero bias a potential energy of V_j. The layers surrounding the emitter/filter regions are taken to have the same zero-bias potential energy of V_0. The material system in which the filter/emitter can be implemented is taken to form a continuous set of alloys of the type $\mathrm{G}_{1-x}\mathrm{H}_x\mathrm{K}$ where G, H, and K are chemical elements, and x is the atomic percentage of the H chemical element. For example, a practical material system is $\mathrm{Ga}_{1-x}\mathrm{Al}_x\mathrm{As}$. Even if the range of values for the composition x can vary from zero to one, the range of usable compositions may be restricted to $0<x<x_{\max}$, where $x_{\max}<1$. For example, this can occur due to a possible transition at $x_{\max}$ from a direct to an indirect energy-gap material as in the case of $\mathrm{Ga}_{1-x}\mathrm{Al}_x\mathrm{As}$.

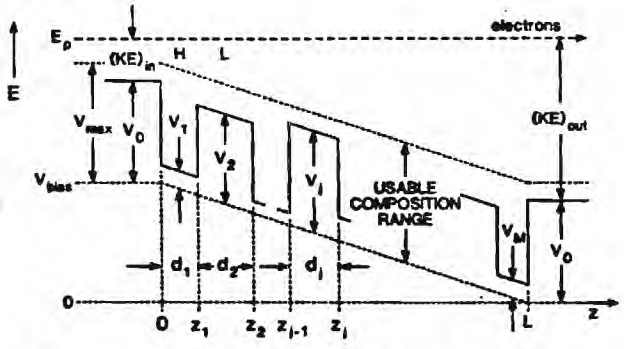

FIG. 1. Schematic representation of a biased semiconductor superlattice electron-wave interference filter/emitter. At the design potential energy bias V_{bias} and input kinetic energy $\mathrm{KE}_{\mathrm{in}}$, the layers have a thickness of a quarter (or a half for the resonant central layer) of an electron wavelength as measured in that layer.

The electron potential energy is given by

$$V_j \equiv \Delta E_c = Ax_j, \tag{3}$$

where ΔE_c is the change in the energy of the conduction-band edge, and A is a constant. Due to restrictions on usable composition range, the corresponding range of potential energies is $0<V_j<V_{\max}=Ax_{\max}$. The layers surrounding the filter/emitter regions have a composition of x_0. An additional design constraint for the electron-wave filter/emitter is that the layer thicknesses should be an integer multiple of the monolayer thickness. Thus the thickness of the jth layer d_j should be an integer multiple p_j of the monolayer thickness r_j. For the jth layer to be a quarter of an electron wavelength in thickness at the design pass energy E_p, the phase difference between the input boundary z_{j-1} and the output boundary z_j (Fig. 1) must be an odd integer multiple of $\pi/2$. That is,

$$\int_{z_{j-1}}^{z_j} k_j(z)dz = \int_{z_{j-1}}^{z_j} \left(\frac{1}{\hbar}\right)\{2m_j^*[E_p - V_j(z)]\}^{1/2}dz = (2q_j-1)\pi/2, \tag{4}$$

where the potential energy in the jth layer with bias applied is given by

$$V_j(z) = V_{\mathrm{bias}}\left(1-\frac{z}{L}\right)+V_j. \tag{5}$$

L is the total length of the superlattice (Fig. 1), and $q_j = 1,2,\ldots$. The electron pass energy may be expressed as $E_p = V_{\mathrm{bias}} + V_0 + \mathrm{KE}_{\mathrm{in}}$ where $\mathrm{KE}_{\mathrm{in}}$ is the pass kinetic energy in the input region (leftmost region in Fig. 1). The electron effective mass is given by $m_j^* = (B+Cx_j)m_0$ where m_0 is the free-electron mass, and B and C are material-system-dependent constants. Using Eqs. (3), (5), and the integral identity $\int(a+bz)^{1/2}dz \equiv (2/3b)(a+bz)^{3/2}$, Eq. (4) can be rewritten

$$\frac{2L\,[2m_0(B+Cx_j)]^{1/2}}{3\hbar V_{\mathrm{bias}}} \times\left[\left(V_0+\mathrm{KE}_{\mathrm{in}}-Ax_j+V_{\mathrm{bias}}\frac{z_j}{L}\right)^{3/2} -\left(V_0+\mathrm{KE}_{\mathrm{in}}-Ax_j+V_{\mathrm{bias}}\frac{z_{j-1}}{L}\right)^{3/2}\right] = (2q_j-1)\frac{\pi}{2}. \tag{6}$$

The above equation has to be solved for the composition x_j of the jth layer with V_{bias}, V_0, and $\mathrm{KE}_{\mathrm{in}}$ as design parameters. Equation (6) is valid for all the layers except the center reso-

nant layer. In this case the $\pi/2$ term of Eq. (6) is replaced by π. The monolayers of the device will be numbered with the index i. The rightmost monolayer of the jth region is i_j. The total number of monolayers in the emitter/filter is designated i_M. Therefore, the number of monolayers of the jth layer is $p_j = i_j - i_{j-1}$, and the corresponding thickness of this layer is $d_j = p_j r_j = z_j - z_{j-1}$. The total thickness of the structure is $L = \sum_{j=1}^{M} p_j r_j$ (if the monolayer thicknesses are the same in each layer, $r_1 = r_2 = \cdots r_M = r$, then $L = i_M r$). The boundaries between the various layers which are designated as z_j (Fig. 1) are given by $z_j = \sum_{l=1}^{j} p_l r_l$ [for equal monolayer thicknesses, $z_j = (i_j/i_M)L$]. It is worth mentioning that the solution of Eq. (6) is not trivial since Eq. (6) for the jth layer depends on the thicknesses of the other layers. Furthermore, Eq. (6) is valid only if $V_{\text{bias}} \neq 0$. In the case of zero applied bias, $V_{\text{bias}} = 0$, Eq. (4) leads to Eq. (11) of Ref. 8, which is much simpler to solve.

A systematic procedure for designing a biased continuously tunable superlattice interference filter/emitter for a given output kinetic energy ($\text{KE}_{\text{out}} = \text{KE}_{\text{in}} + V_{\text{bias}}$) and given compositions (x_0) of the surrounding filter/emitter regions, using Eq. (6), is now described. The design parameters V_0(or x_0), KE_{in}, and V_{bias} have to be specified at the beginning. Next the characteristics of the unbiased superlattice electron-wave interference filter[7,8] are used as a starting point in estimating the number of regions M and the number of monolayers p_j ($j = 1,2,...,M$) to be used in the filter/emitter. The initial values of the number of monolayers in each layer are designed as p_j^0, the total initial thickness is designated as L^0, and the total number of monolayers is designated as i_M^0. It is important to keep the length of the structure as small as possible in order to be less than the electron coherence length. Consequently, it is more practical to set the parameters $q_j = 1$ in order to find the minimum thickness device. Starting from the first layer ($j = 1$), Eq. (6) is solved for x_j. Since an iterative scheme is used, the solution of Eq. (6) for x_j is designated as $x_j^{n_j}$, where n_j is a counting index for the iterations of the jth layer. In the next step it is determined if the solution $x_j^{n_j}$ lies within the range of usable composition values ($0 < x_j^{n_j} < x_{\max}$). If $x_j^{n_j}$ is outside the usable range, then the number of monolayers is changed as $p_j^{n_j} = p_j^{n_j-1} + \Delta p_j^{n_j}$, where $\Delta p_j^{n_j}$ is the change in the number of monolayers of region j. The procedure is repeated until a value for $x_j^{n_j}$ is found within the usable range. For the filter to have a narrower response, it is important to increase the reflectivity between the low (L) and high (H) electron refractive index layers. For the low index layers the composition should be as close to $x_{\max}$ as possible. Similarly, for the high index layers the composition should be as close to zero as possible. As a result, some additional refining of the calculated solution for the jth layer can be found by changing the value of $p_j^{n_j}$ by ± 1 ($\Delta p_j^{n_j} = \pm 1$). This is continued until the solution $x_j^{n_j}$ is the maximum possible (within the usable composition range) for a low (L) index layer or the minimum possible (within the usable composition range) for a high (H) index layer. This procedure is repeated for all the layers ($j = 1,2,...,M$). However, the solution for the last layer may result in a new value of i_M (or equivalently L) which differs from the initially estimated i_M^0 (or equivalently L^0). In this case the resultant value of L is set equal to L^0 and the design process is repeated until the final thickness L is consistent with the initially assumed thickness L^0, i.e., $L = L^0$. The design procedure is summarized in the algorithm presented in Fig. 2.

B. Computation of the designed filter/emitter response

In order to evaluate the response of the interference filter/emitter designed with the above-described procedure, the electron-wave function has to be calculated in the output region of the structure. Using the one-electron-wave function approximation, and neglecting the electron-electron and the exchange interaction which partially compensate one another, the electron-wave function in each layer satisfies the Schrödinger's equation. That is,

$$\frac{\hbar^2}{2m_j^*}\frac{d^2\psi_j(z)}{dz^2} + [E - V_j(z)]\psi_j(z) = 0, \tag{7}$$

where $\psi_j(z)$ is the electron-wave function in region j ($j = 1,2,...,M$), and $V_j(z)$ is given by Eq. (5). The electron-wave function in any layer of the biased superlattice can be expressed as a linear combination of Airy functions $\text{Ai}(\rho)$ and complimentary Airy functions $\text{Bi}(\rho)$.[23–25] By defining within each layer a new variable $\rho_j = \rho_j(z) = (2m_j^* V_{\text{bias}}/\hbar^2 L)^{1/3}[z + (E - V_{\text{bias}} - V_j)L/V_{\text{bias}}]$, Eq. (7) can be transformed into the form $d^2\psi_j(\rho_j)/d\rho_j^2 + \rho_j\psi_j(\rho_j) = 0$, which has solution of the form

$$\psi_j(\rho_j) = \psi_j(z) = C_j\text{Ai}[-\rho_j(z)] + D_j\text{Bi}[-\rho_j(z)], \tag{8}$$

where C_j and D_j are unknown amplitude constants. The solution of Schrödinger's equation in the two external regions (leftmost and rightmost regions in Fig. 1) is straightforward since the potential energy does not vary in these regions. Specifically, the wave function in the input region is given by $\psi_0(z) = \exp(jk_0 z) + r\exp(-jk_0 z)$, while the wave function for the output region is given by $\psi_{M+1}(z) = t\exp[jk_{M+1}(z - z_M)]$. The k_0 and k_{M+1} are the electron-wave vectors in the input and output regions, respectively. Using the boundary condition for the wave function, $\psi_j(z_j) = \psi_{j+1}(z_j)$, and $(1/m_j^*)d\psi_j(z_j)/dz = (1/m_{j+1}^*)\,d\psi_{j+1}(z_j)/dz$, the reflected and transmitted amplitude of the wave function (r and t) may be expressed as

$$\begin{pmatrix}1\\r\end{pmatrix}=\frac{1}{2jK_1}\begin{pmatrix}jK_1 & -1\\ jK_1 & 1\end{pmatrix}[S_1(z_0)][S_1(z_1)]^{-1}[S_2(z_1)][S_2(z_2)]^{-1}[S_3(z_2)]\cdots[S_{M-1}(z_{M-1})]^{-1}$$
$$\times[S_M(z_{M-1})][S_M(z_M)]^{-1}\begin{pmatrix}1 & 1\\ -jK_2 & jK_2\end{pmatrix}\begin{pmatrix}t\\0\end{pmatrix}, \tag{9}$$

where

$$[S_j(z)]=\begin{pmatrix}\mathrm{Ai}[-\rho_j(z)] & \mathrm{Bi}[-\rho_j(z)]\\ (1/M_j^*)^{2/3}\mathrm{Ai}'[-\rho_j(z)] & (1/M_j^*)^{2/3}\mathrm{Bi}'[-\rho_j(z)]\end{pmatrix}, \tag{10}$$

and where $M_j^*=m_j^*/m_0$, $K_1=[(2m_0/\hbar^2)^{1/3}(E-V_0-V_{\text{bias}})/M_0^*]^{1/2}$ $(L/V_{\text{bias}})^{1/3}$ and $K_2=[(2m_0/\hbar^2)^{1/3}(E-V_0)/M_{M+1}^*]^{1/2}$ $(L/V_{\text{bias}})^{1/3}$, and Ai′ and Bi′ are the first derivatives of the Airy and complimentary Airy functions, respectively. Equations (9) can be solved directly for the amplitude transmittance t and the amplitude reflectance r. The electron current transmittance T_e is given by

$$T_e=\frac{[(E-V_0)/M_{M+1}^*]^{1/2}}{[(E-V_0-V_{\text{bias}})/M_0^*]^{1/2}}|r|^2. \tag{11}$$

Using Eq. (11), the response of the designed electron interference filter/emitter can be evaluated.

C. Design of a filter/emitter with L-valley electron potential energy constraint

If the electron energy is near the ⟨111⟩ L-valley minimum, then the resulting phonon scattering in the device may decrease the electron coherence length. As a result the phonon scattering can deteriorate the performance of an electron-wave interference filter/emitter. However, some additional constraints can be imposed in the design process of the device that can minimize the phonon scattering. The L-valley potential energy in the jth layer, V_{Lj}, is given by

$$V_{Lj}=D+Fx_j \tag{12}$$

where D and F are material-dependent constants, and x_j is the material composition (alloys of the type $G_{1-x}H_xK$ are being assumed). In the previously described design process, the composition of the input and the output regions of the device were taken to be the same (x_0). This assumption does not imply any restriction in the device design, but only reflects the symmetry of the electron Fabry–Perot. For positive energies, the electron pass energy must be larger than the electron potential energy V_0 in the input region (i.e., electron energy should be above the Γ-valley minimum). Furthermore, for practical devices, the input kinetic energy KE_{in} should be at least ΔE_1, where ΔE_1 is a design parameter that ensures sufficient input velocity. In addition, at the output layer the electron energy should be less than the L-valley minimum by at least ΔE_2, where ΔE_2 is a design parameter that ensures that there will be neither intervalley phonon emission nor absorption. The above-described constraints can be written as follows:

$$V_0+\Delta E_1<E<V_{L0}-\Delta E_2, \tag{13}$$

where V_{L0} is the L-valley electron potential energy in the output region ($V_{L0}=D+Fx_0$). It is implied that the bias potential energy is non-negative as shown in Fig. 1($V_{\text{bias}}>0$). Inequalities (13) impose the following condition for the allowable bias potential energy:

$$V_{\text{bias}}<D-(A-F)x_0-\Delta E_1-\Delta E_2 \tag{14}$$

Inequality (14) limits the maximum value of the applied bias potential energy to $(V_{\text{bias}})_{\max}=D-(A-F)x_0-\Delta E_1-\Delta E_2$. The maximum applied bias potential energy depends on the compositions of the input and output regions. Constraints similar to inequality (13) can be applied for each layer inside the device. That is,

$$V_j(z)<E<V_{Lj}, \quad \text{for } z_{j-1}<z<z_j, \tag{15}$$

which imposes on the composition x_j the following constraint:

$$\frac{1}{A}\left(Ax_0+\Delta E_1+V_{\text{bias}}\frac{z_j}{L}-D\right)$$
$$<x_j<\frac{1}{F}\left(Ax_0+V_{\text{bias}}\frac{z_{j-1}}{L}\right). \tag{16}$$

Inequality (15) can be even tighter if energy margins ΔE_{1j} and ΔE_{2j} are nearly equal to ΔE_1 and ΔE_2. However, for practical purposes the inequalities (13) and (15) can be considered sufficient.

The design procedure described in Sec. IV A remains basically the same with the exception that V_{bias} has to satisfy inequality (14) and the layer compositions should lie in the range expressed by inequality (16).

V. $Ga_{1-x}Al_xAs$ EXAMPLE CASES

A practical material system to be used in fabricating the above-described electron-wave interference filter/emitters is $Ga_{1-x}Al_xAs$. For this material system the maximum composition in Al is $x_{\max}=0.45$ in order to avoid the direct/indirect band-gap transition. Other parameters of this material system include $A=0.773$ eV, $B=0.067$, $C=0.083$, $D=0.284$ eV, and $F=0.168$. The ⟨100⟩ monolayer thickness for any usable composition remains the same $r_j=0.282\,665$ nm (lattice-matched material system).

At first, some designs that are not restricted by the L-valley energy are presented. For these filter/emitters the

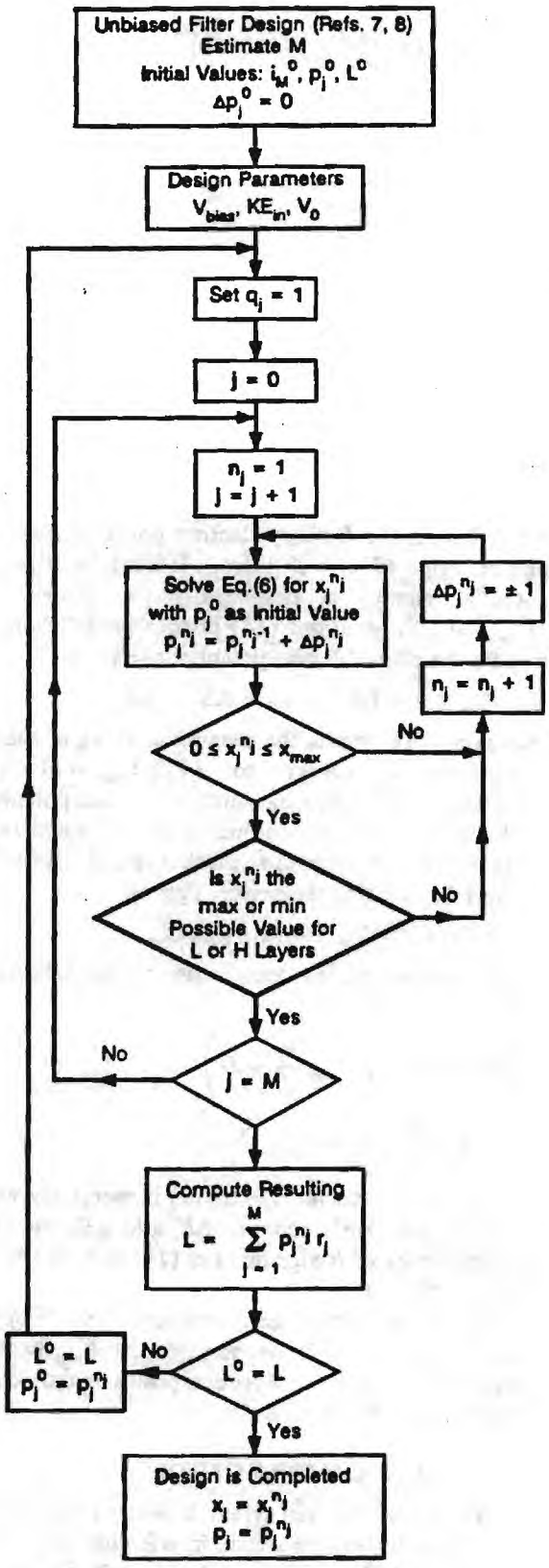

FIG. 2. Flow chart of the calculational procedure used for the computation of the filter/emitter layer compositions and thicknesses.

compositions of the surrounding regions (rightmost and leftmost regions in Fig. 1) are chosen to be $x_0 = 0.45$. The design parameters V_{bias} and KE_{in} are chosen both to be 0.10 eV each. Using the procedure described in Sec. IV A (algorithm of Fig. 2), the layer thicknesses (expressed in number of monolayers) and the layer compositions can be calculated. These results are summarized in Table I for various number of layers $M = 9$, 13, and 17. The total thickness of the design structures is 20.1 nm (71 monolayers), 28 nm (99 monolayers), and 36.2 nm (128 monolayers) for $M = 9$, 13, and 17, respectively, which is within the desired electron coherence length. Experimental measurements in ballistic hot-electron deviced[10,26,27] (on GaAs/GaAlAs and InGaAs/InAlAs) indicate that the electron coherence length lies roughly between 10 and 100 nm. However, the electron coherence length is a statistical quantity. Therefore, the experimental data suggest that at least some measurable fraction of electrons exhibit a coherence length within the design for the filter/emitter requirements. The spectral response (transmittance versus output kinetic energy) of the designed structure can be computed using the analysis described in Sec. IV B. The electron-current transmittance T_e [Eq. (11)] is shown in Figs. 3(a), 3(b), and 3(c) as a function of the output kinetic energy KE_{out} for $M = 9$, 13, and 17, respectively, with the applied bias potential energy V_{bias} as a parameter. From these figures it is shown that for $V_{bias} = 0.10$ eV the filter/emitter has a peak in the electron-current transmittance (of about 100%) for the design output kinetic energy of 0.20 eV. The spectral response of the filter/emitter has a narrow passband around the designed output kinetic energy, and the FWHM decreases as the number of layers increases. For the cases shown in Figs. 3(a), 3(b), and 3(c), the FWHM values are 30.7, 13.4, and 5.9 meV for $M = 9$, 13, and 17, respectively. However, by increasing the number of the layers M, (1) the total thickness of the device increases (thickness should be less than the electron coherence length), and (2) some secondary peaks in the electron-current transmittance appear as is shown in Figs. 3(b) and 3(c) for $M = 13$ and 17, respectively. Thus there is a trade-off between the FWHM and the device thick-

TABLE I. Design parameters of an electron-wave interference filter/emitter with the $(HL)^N HH(LH)^N$ $[N = (M-1)/2]$ configuration. The surrounding input and output regions consist of $Ga_{0.55}Al_{0.45}As$, and the filter/emitter is designed to emit 0.20-eV electrons when biased at 0.10 eV.

Layer	$M = 9$		$M = 13$		$M = 17$	
j	p_j	x_j	p_j	x_j	p_j	x_j
1	7	0.2222	7	0.2194	7	0.2178
2	9	0.4151	9	0.4081	9	0.4041
3	7	0.2663	7	0.2513	7	0.2426
4	9	0.4493	9	0.4327	9	0.4231
5	12	0.0639	7	0.2823	7	0.2668
6	8	0.4364	8	0.3978	9	0.4421
7	6	0.1442	12	0.0639	7	0.2905
8	7	0.3748	8	0.4301	8	0.4020
9	6	0.1951	6	0.1237	12	0.0654
10			7	0.3582	8	0.4271
11			6	0.1626	6	0.1125
12			7	0.3815	7	0.3493
13			6	0.1982	6	0.1439
14					7	0.3674
15					6	0.1729
16					7	0.3853
17					6	0.1999

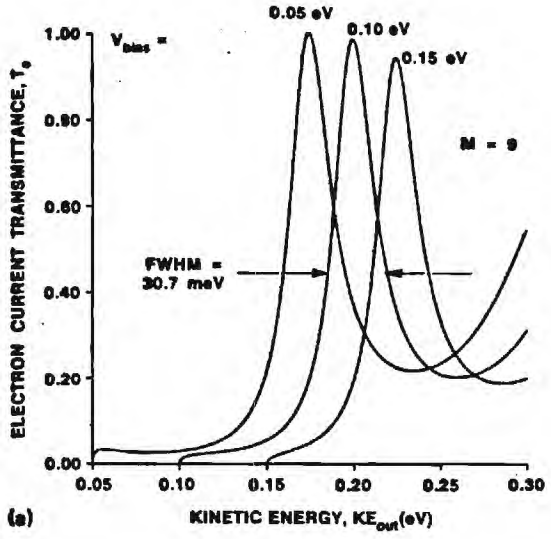

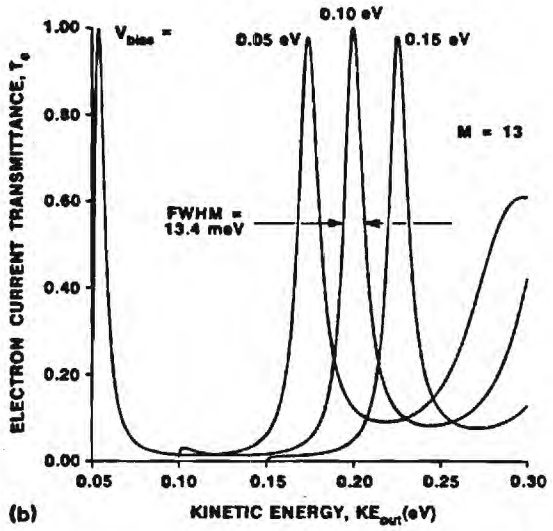

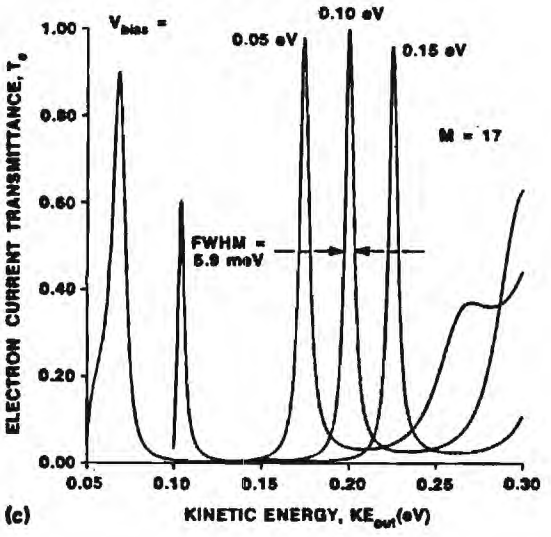

FIG. 3. Electron-current transmission of M-layer $Ga_{1-x}Al_xAs$ superlattice interference filter/emitter as a function of the electron output kinetic energy for $V_{bias} = 0.05$, 0.10, and 0.15 eV for (a) $M = 9$, (b) $M = 13$, and (c) $M = 17$. The spectral tuning with the bias is apparent. Furthermore, the spectral widths become narrower as the number of the layers M increases.

ness. Another important feature of the filter/emitter spectral response is that using the same design (of $V_{bias} = 0.10$ eV and $KE_{in} = 0.10$ eV), and applying other bias potential energies, the narrow-band characteristic of the filter/emitter remains almost unchanged, but shifted in output kinetic energy. For example, the spectral response of the designed filter/emitter is shown in Figs. 3(a), 3(b), and 3(c) for $V_{bias} = 0.05$, 0.10, and 0.15 eV. It is observed that there is no significant change in the electron-current transmittance peak and the FWHM, but there is a shift in the output kinetic energy for which the peak electron-current transmittance occurs. The change in the output kinetic energy ΔKE_{out} is approximately half of the change in the applied bias potential energy ΔV_{bias}. This can be explained by the fact that the resonant central layer (HH) is almost at the middle of the device and consequently experiences half of the change of the bias potential energy. Furthermore, due to this property of the filter/emitter, the device can be continuously tuned over a range of output kinetic energies, around the designed value, by varying the applied voltage. The tunability of the device is further illustrated in Fig. 4 (for $M = 13$) for a range of bias potential energies from 0.0 to 0.2 eV. It is observed that the output kinetic energy at the peak electron-current transmittance varies linearly with the applied bias potential energy in the range between -0.15 and -0.25 eV (the slope of the straight line in Fig. 4 is 0.496). Moreover, the peak of the electron-current transmittance, $T_{e,peak}$, varies smoothly around the design value of V_{bias} (0.10 eV) in the range between 92.1% and ~100%.

The electron-current transmittance of the filter/emitter as a function of the applied bias potential energy with the electron output kinetic energy KE_{out} as a parameter is shown in Fig. 5 for V_{bias} varying between 0.0 and 0.3 eV with $KE_{out} = 0.10$, 0.15, 0.20 (design value), 0.25, and 0.30 eV. The design parameters of this filter/emitter are given in Table I for $M = 9$. Figure 5 is equivalent to Fig. 3(a), but with the roles of KE_{out} and V_{bias} interchanged. It is observed that for $KE_{out} = 0.15$, 0.20, 0.25, and 0.30 eV there is a peak in the electron-current transmittance. For $KE_{out} = 0.10$ eV the transmittance is low as it can also be seen from Fig. 3(a).

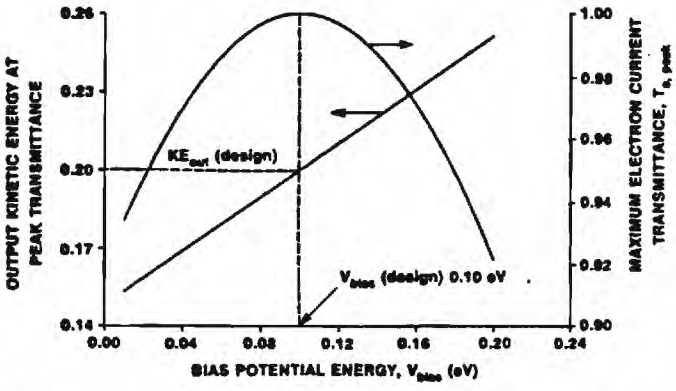

FIG. 4. Tunability characteristics of a filter/emitter for $M = 13$. The design values are $V_{bias} = 0.10$ eV and $KE_{in} = 0.10$ eV. The electron output kinetic energy at peak electron-current transmittance and the value of the peak electron-current transmittance are shown as functions of the bias potential energy V_{bias}.

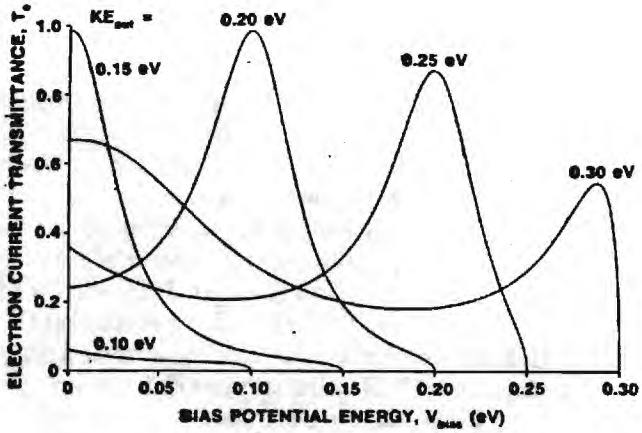

FIG. 5. Electron-current transmittance of a filter/emitter for $M = 9$, as a function of the applied bias potential energy V_{bias} with the output electron kinetic energy as a parameter. Design values are $V_{bias} = 0.10$ eV and $KE_{in} = 0.10$ eV.

The peak value of the transmittance decreases as the output kinetic energy deviates from the design value (of 0.20 eV at $V_{bias} = 0.10$ eV).

Another important practical factor is the sensitivity of the designed electron-wave interference filter/emitters to fabrication process variations. Since these devices are ultrasmall, the layer thicknesses should ideally be the design number of monolayers. Furthermore, the Al composition usually can be controlled to within 1%–2%. In order to evaluate the sensitivity of the electron-wave filter/emitter, the layer thicknesses and compositions were varied from the design values, and the spectral response of the resulting devices were calculated using Eq. (11). Three cases were considered along with the design case (case 1, $V_{bias} = 0.10$ eV, $KE_{in} = 0.10$ eV, and $M = 9$). These are summarized in Table II. Case 2 corresponds to fabrication variations of the Al compositions (x_j's), while cases 3a/3b and 4 correspond to fabrication variations of the central (resonant) layer thickness and of the surrounding layer thicknesses, respectively. The spectral responses that correspond to the filter/emitters of cases 1 and 2 are shown in Fig. 6(a). It is observed that

TABLE II. Design parameters of an electron-wave interference filter/emitter with the $(HL)^N HH(LH)^N$ $[N = (M-1)/2]$ configuration (case 1), a suboptimal design with rounded-off composition values (case 2), and two suboptimal designs with incorrect monolayer thicknesses (cases 3a, 3b, and 4). The surrounding input and output regions consist of $Ga_{0.55}Al_{0.45}As$, and the filter/emitter is designed to emit 0.20-eV electrons when biased at 0.10 eV. In all the listed cases the number of the layers is $M = 9$.

Layer	Case 1		Case 2		Cases 3a/3b		Case 4	
j	p_j	x_j	p_j	x_j	p_j	x_j	p_j	x_j
1	7	0.2222	7	0.20	7	0.2222	7	0.2222
2	9	0.4151	9	0.40	9	0.4151	9	0.4151
3	7	0.2663	7	0.25	7	0.2663	6	0.2663
4	9	0.4493	9	0.43	9	0.4493	9	0.4493
5	12	0.0639	12	0.08	13/11	0.0639	12	0.0639
6	8	0.4364	8	0.43	8	0.4364	9	0.4364
7	6	0.1442	6	0.15	6	0.1442	7	0.1442
8	7	0.3748	7	0.36	7	0.3748	8	0.3748
9	6	0.1951	6	0.20	6	0.1951	6	0.1951

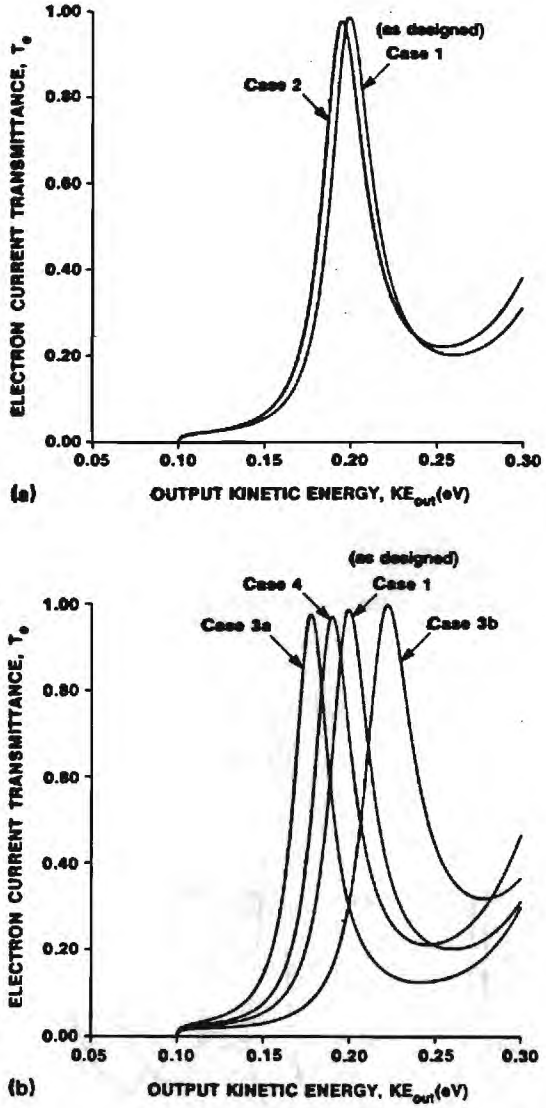

FIG. 6. Electron-current transmittance of a filter/emitter as a function of the electron output kinetic energy. Design values are $V_{bias} = 0.10$ eV, $KE_{in} = 0.10$ eV, and $M = 9$. (a) Cases 1 and 2 of Table II (fabrication variations in the layer compositions) and (b) cases 3a/3b and 4 of Table II (fabrication variations in the layer thicknesses).

even if the layer compositions vary between 0.5%–2.2% (possible fabrication variation) from the design values the filter/emitter response is not substantially altered. When the thicknesses of the layers deviate from the optimal design values (cases 3a/3b and 4), the filter emitter response is shown in Fig. 6(b). From Figs. 6(a) and 6(b) it is observed that deviation from the design thicknesses is much more important than the deviation from the design compositions. Especially, the variation of the thickness of the resonant layer is most important. However, from the same figures [6(a) and 6(b)] it is shown that even though the designs that correspond to cases 2, 3a/3b, and 4 are nonoptimal, the filter/emitter characteristics remain basically unaffected. Shifts of the peak electron-current transmittance are observed, while the peak transmittance value and the corresponding FWHM remain approximately the same. Even if the filter/emitter response is shifted due to fabrication process variations, it is possible to shift the response back to its designed position by

changing the applied voltage.

Finally, an additional consideration in the design of electron-wave interference filter/emitters is the restriction that the design electron energy be sufficiently below the L-valley potential energy to minimize phonon scattering. Selecting $\Delta E_1 = \mathrm{KE}_{in} = \Delta E_2 = 0.05$ eV and the input/output regions compositions 0.10 and 0.20 ($x_0 = 0.10$ or 0.20), two additional filter/emitters were designed. As is described by inequalities (14) and (16), there is a restriction in the maximum applied bias potential energy and the layer compositions. For $x_0 = 0.10$ and 0.20 the corresponding maximum values of the applied bias potential energy are 0.124 and 0.063 eV, respectively. If the layer compositions are less than x_0 ($x_j < x_0$ for $j = 1,2,...,M$), then inequality (16) is also satisfied. Using $V_{\mathrm{bias}} = 0.12$ and 0.06 eV as the design parameters for $x_0 = 0.10$ and 0.20, respectively, and $M = 9$ layers, two additional designs were developed that take into account this electron-energy constraint. The characteristics of these two designs are summarized in Table III. The spectral (energy) response of the corresponding two filter/emitters is shown in Figs. 7(a) (for $x_0 = 0.10$, $V_{\mathrm{bias}} = 0.12$ and 0.07 eV) and 7(b) (for $x_0 = 0.20$, $V_{\mathrm{bias}} = 0.06$ and 0.03 eV). From these figures it is again observed that the electron-current transmittance has a peak at the design $\mathrm{KE}_{\mathrm{out}}$ and V_{bias} values and, in addition, has the same tunability properties that were described previously. However, the design that corresponds to $x_0 = 0.10$ does not have a particularly good rejection band (since the transmittance value is not very small). This is due to the reduced reflectivity at layer boundaries. The reduced reflectivity is a result of the small differences in the layer compositions, which in turn correspond to small differences in the electron-wave refractive indices. Especially at larger electron energies, the corresponding electron-wave refractive indices become nearly equal, and this degrades the performance of the filter/emitter at energies above the pass energy. However, when $x_0 = 0.20$ there is a significant variation of the electron-wave refractive index, which results in an increased reflectivity between the filter/emitter layers. For this reason the response that corresponds to $x_0 = 0.20$ has much narrower energy passband and lower rejection band transmittance.

TABLE III. Design parameters of an electron-wave interference filter/emitter with the $(HL)^N HH(LH)^N$ $[N = (M-1)/2]$ configuration ($N = 2$, $M = 9$), taking into account the L-valley constraint. The surrounding input and output regions consist of $Ga_{1-x_0}Al_{x_0}As$. For both designs, $\mathrm{KE}_{in} = 0.05$ eV.

Layer j	$V_{\mathrm{bias}} = 0.12$ eV, $x_0 = 0.10$		$V_{\mathrm{bias}} = 0.06$ eV, $x_0 = 0.20$	
	p_j	x_j	p_j	x_j
1	12	0.0194	10	0.0561
2	13	0.0677	12	0.1429
3	11	0.0278	9	0.0070
4	12	0.0831	12	0.1617
5	20	0.0307	18	0.0365
6	10	0.0602	11	0.1589
7	9	0.0077	9	0.0635
8	10	0.0965	11	0.1772
9	9	0.0489	9	0.0852

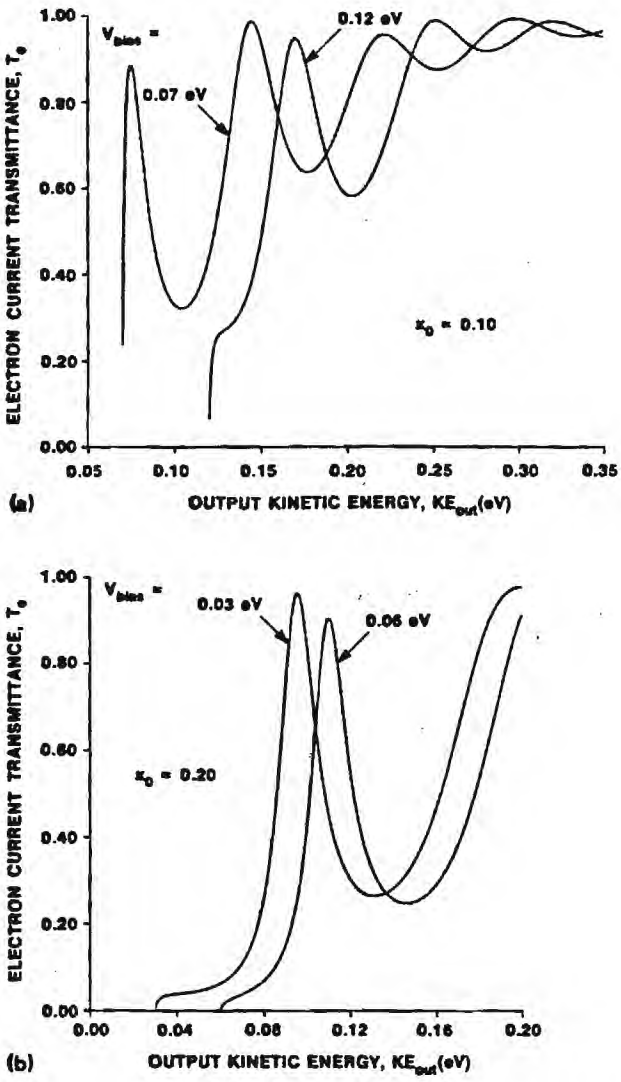

FIG. 7. Electron-current transmittance of a filter/emitter designed taking into account L-valley potential energy constraint for (a) design values $x_0 = 0.10$, $V_{\mathrm{bias}} = 0.12$ eV, $\mathrm{KE}_{in} = 0.05$ eV, and $M = 9$, and (b) for design values $x_0 = 0.20$, $V_{\mathrm{bias}} = 0.06$ eV, $\mathrm{KE}_{in} = 0.05$ eV, and $M = 9$.

VI. DISCUSSION AND SUMMARY

In all the electron-wave interference filter/emitters presented, the semiconductor materials had parabolic band structure. However, for sufficiently high electron energies, the band structure is more appropriately treated as nonparabolic. Futhermore, the band structure may vary with the direction of the electron-wave propagation. Both of these effects can be incorporated by using an energy-dependent anisotropic effective mass. In this case the solutions of Schrödinger's equation described in Sec. III B needs to be modified; however, the design procedure of the filter/emitter remains unchanged.

The response of the electron-wave Fabry–Perot filter/emitter has been shown to have a narrow passband around the design value of the output kinetic energy. However, additional passbands in kinetic energy exist beyond the rejection band. At large electron energies the corresponding electron-wave refractive indices of the filter/emitter layers become

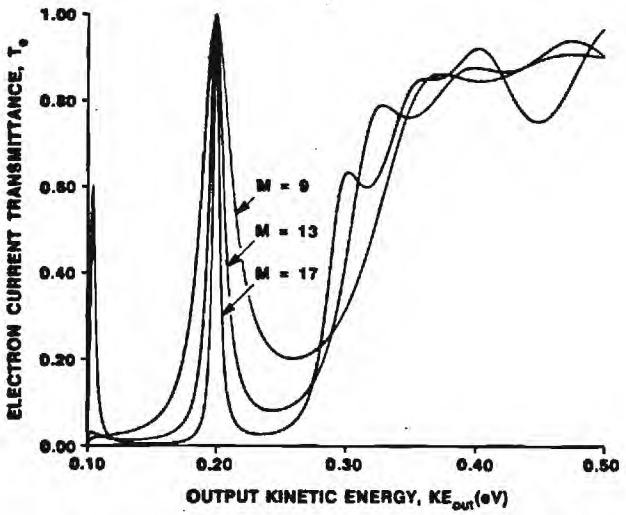

FIG. 8. Electron-current transmittance of a filter/emitter for $M = 9$, 13, and 17 as a function of the output electron kinetic energy. Design values are $V_{bias} = 0.10$ eV and $KE_{in} = 0.10$ eV.

nearly equal. This effect reduces the electron reflectivity at the layer boundaries and consequently degrades the filter/emitter performance. For example, the response characteristics of the filter/emitters, described in Table I, are shown in Fig. 8 for $V_{bias} = 0.10$ eV (design value) for $M = 9$, 13, and 17 layers, for output electron kinetic energies between 0.0 and 0.5 eV. It is observed that as the electron energy increases above 0.3 eV, the filter/emitter has an electron-current transmittance larger than 0.75, which reduces the width of the rejection band on the high-energy side of the peak value.

The design procedure described in Sec. III A may result in multiple designs differing by a few monolayers from the initial unbiased solution. In this case the best filter/emitter response is obtained by selecting the most symmetric solution for the electron-wave refractive indices.

In summary, a systematic procedure has been described for the design of biased semiconductor superlattices that can serve as narrow-band electron-energy filter/emitters. Various design constraints were identified and quantified. These filter/emitters are continously voltage tunable in electron energy. The FWHM of the filter/emitter decreases as the number of the filter layers increases. The characteristics of the filter/emitter are stable in the presence of variations in the layer compositions and thicknesses. These narrow-band filter/emitters can be incorporated monolithically into transistor structures in order to increase their speed. Other possible applications include electroluminescent devices, photodetectors, and in future guided electron-wave integrated circuits.

ACKNOWLEDGMENTS

This research was sponsored in part by a grant from the Joint Services Electronics Program under Contract No. DAAL-03-87-K-0059. One of us (K.F.B.) was supported in part by a Presidential Young Investigator award from the National Science Foundation and another (E.N.G.) by a Research Initiation award from the National Science Foundation.

[1]M. Heiblum, M. V. Fischetti, W. P. Dumke, D. J. Frank, I. M. Anderson, and C. M. Knoedler, Phys. Rev. Lett. 58, 816 (1987).
[2]S. Sen, F. Capasso, A. C. Gossard, and R. A. Spah, Appl. Phys. Lett. 51, 1428 (1987).
[3]R. C. Potter and A. A. Lakhani, Appl. Phys. Lett. 52, 1349 (1988).
[4]J. R. Hayes, P. England, and J. P. Harbison, Appl. Phys. Lett. 52, 1578 (1988).
[5]L. Esaki and R. Tsu, IBM J. Res. Dev. 13, 61 (1970).
[6]T. K. Gaylord and K. F. Brennan, J. Appl. Phys. 65, 814 (1989).
[7]T. K. Gaylord and K. F. Brennan, Appl. Phys. Lett. 53, 2047 (1988).
[8]T. K. Gaylord, E. N. Glytsis, and K. F. Brennan, J. Appl. Phys. 65, 2535(1989).
[9]E. N. Glytsis, T. K. Gaylord, and K. F. Brennan, J. Appl. Phys. 66, 1494 (1989).
[10]M. Heiblum, M. I. Nathan, D. C. Thomas, and C. M. Knoedler, Phys. Rev. Lett. 55, 2200 (1985).
[11]T. K. Gaylord, E. N. Glytsis, and K. F. Brennan, J. Appl. Phys. 66, 1842 (1989).
[12]T. K. Gaylord, E. N. Glytsis, and K. F. Brennan, J. Appl. Phys. 66, 1483 (1989).
[13]G. Nimtz and P. Marquardt, Appl. Phys. A 47, 317 (1988).
[14]A. Szafer and A. D. Stone, Phys. Rev. Lett. 62, 300 (1989).
[15]C. J. Summers and K. F. Brennan, Appl. Phys. Lett. 48, 806 (1986).
[16]K. F. Brennan and C. J. Summers, J. Appl. Phys. 61, 5410 (1987).
[17]K. F. Brennan and C. J. Summers, IEEE J. Quantum Electron. QE-23, 320 (1987).
[18]C. M. Wu and E. S. Yang, Solid-State Electron. 22, 241 (1979).
[19]A. N. Khondker, M. R. Khan, and A. F. M. Anwar, J. Appl. Phys. 63, 5191 (1988).
[20]O. S. Heavens, *Optical Properties of Thin Solid Films* (Butterworths, London, 1955).
[21]J. A. Dobrowolski, in *Handbook of Optics*, edited by W. G. Driscoll (McGraw-Hill, New York, 1978), Sec. 8.
[22]H. A. Macleod, *Thin-Film Optical Filters* (Macmillan, New York, 1986).
[23]E. J. Austin and M. Jaros, Phys. Rev. B 31, 5569 (1985).
[24]K. F. Brennan and C. J. Summers, J. Appl. Phys. 61, 614 (1987).
[25]C. J. Summers, K. F. Brennan, A. Torabi, and H. M. Harris, Appl. Phys. Lett. 52, 132 (1988).
[26]K. Imamura, S. Muto, N. Yokoyama, M. Sasa, H. Ohnishi, S. Hiyamizu, and H. Nishi, Surf. Sci. 174, 481 (1986).
[27]K. Seo, M. Heiblum, C. M. Knoedler, J. E. Oh, J. Pamulapati, and P. Bhattacharya, IEEE Electron. Device Lett. 2, 73 (1989).

Electron-wave quarter-wavelength quantum well impedance transformers between differing energy-gap semiconductors

T. K. Gaylord, E. N. Glytsis, and K. F. Brennan
School of Electrical Engineering and Microelectronics Research Center, Georgia Institute of Technology, Atlanta, Georgia 30332

(Received 21 July 1989; accepted for publication 13 November 1989)

Impedance transformers for ballistic (collisionless) electron waves traveling between dissimilar energy-gap semiconductors are designed as a series of quarter (electron) wavelength layers in the form of a compositional superlattice. The quantitative analogies that have been previously established [J. Appl. Phys. 65, 814 (1989)] between electron-wave propagation in semiconductors and electromagnetic-wave propagation in dielectrics are used. For the design energy, the electron wave would be totally transmitted and the structure is analogous to an antireflection coating in electromagnetic optics. Practical constraints on the impedance transformer layers are (1) their compositions must be within the usable compositional range and (2) their thicknesses must be integer multiples of a monolayer thickness. These constraints are included in the design process. Procedures for designing narrow-band, maximally flat (Butterworth), and equal-ripple (Chebyshev) impedance transformers of arbitrary spectral bandwidth are presented. Example practical single-layer and three-layer transformers for connecting GaAs and $Ga_{0.8}Al_{0.2}As$ are presented.

I. BACKGROUND

Molecular-beam epitaxy (MBE) and metalorganic chemical vapor deposition (MOCVD) have been developed and refined to the point where single monolayers can be grown with precise compositional control.[1] These technologies have allowed important multiple quantum well devices composed of wide and narrow band-gap semiconductors such as GaAs and $Ga_{1-x}Al_xAs$ to be produced. With further improvements in the quality of the materials grown, ballistic transport has been observed.[2,3] That is, electrons travel through the device without being scattered by deviations from crystalline perfection. Even with the addition of elastic scattering, the electrons exhibit clear quantum mechanical plane-wave behavior.[4,5] Since these coherent waves maintain their phase throughout the device, they can be refracted, reflected, interfered, guided, and diffracted in a manner quantitatively analogous to electromagnetic waves.[6] Quantum interference effects have been experimentally observed for electron energies below the potential energy barriers in resonant tunneling structures[7–10] and for electron energies above the barriers in negative differential resistance[11,12] and potential barrier[13] devices.

In the construction of semiconductor quantum devices and guided electron-wave integrated circuits[14] it will be necessary to connect semiconductor materials with differing electron energy-band structures. This occurs, for example, in the electron flow from the GaAs base of a bipolar junction transistor to the $Ga_{1-x}Al_xAs$ collector where $Ga_{1-x}Al_xAs$ is used to increase the breakdown voltage in the high electric field collector. In such a configuration, detrimental reflections will occur at the energy-band discontinuity between materials. However, for a given electron energy or a given band of electron energies, these reflections can be completely eliminated and total transmission achieved by fabricating an impedance transformer between the two materials. The type of impedance transformer directly amenable to semiconductor technology consists of a series of layers that are each a quarter of an electron wavelength thick. Transformers of arbitrary bandwidth can be designed using the quantitative analogies between electron-wave propagation in semiconductors and electromagnetic waves in dielectrics[6] and the theory of impedance transformers as developed for microwave transmission lines and waveguides.[15] In addition, practical constraints require that the impedance transformer layers have (1) compositions that are within the usable compositional range and (2) thicknesses that are an integer multiple of a monolayer thickness. The purpose of this paper is to present systematic design procedures for narrow-band, maximally flat (Butterworth), and equal-ripple (Chebyshev) impedance transformers subject to the above constraints and then apply these procedures to example impedance transformers between GaAs and $Ga_{0.8}Al_{0.2}As$.

II. SEMICONDUCTOR ELECTRON-WAVE OPTICS

The transmission and reflection characteristics of quantum mechanical electron waves in semiconductors have been analyzed for single potential energy boundaries,[16] for normal incidence,[17] and for the general case of any number of boundaries and any angle of incidence.[6] From these results, a mapping has been established between electromagnetic and quantum mechanical quantities.[6] As a consequence, existing electromagnetic optical device designs now have electron-wave device counterparts.

Electron-wave phase effects such as the phase thicknesses of the impedance transformer layers are described by the electron wave-vector magnitude which is

$$k = [2m^*(E - V)]^{1/2}/\hbar, \tag{1}$$

where m^* is the electron effective mass, E is the total electron energy, V is the electron potential energy, and $\hbar$ is Planck's constant divided by 2π. Thus, the electron-wave phase refractive index n_p is proportional to the square root of the

 0021-8979/90/052623-08$03.00

product of the effective mass and the kinetic energy.[6] That is,

$$n_p \propto [m^*(E-V)]^{1/2}. \tag{2}$$

Amplitude effects such as transmissivity and reflectivity may be described in terms of the wave-function amplitude for an electron wave or in terms of the electric field amplitude for a transverse electric (TE) electromagnetic optical wave incident upon a boundary between dielectrics. Continuity of the wave function across a potential energy boundary is analogous to the continuity of the tangential component of the electric field across a boundary between dielectrics. Similarly, conservation of electron probability current normal to a potential energy boundary is analogous to conservation of power flow normal to a boundary between dielectrics. Using these, the electron-wave and electromagnetic-wave reflectivities and transmissivities are made equivalent by introducing, in quantum mechanics, an analogous index of refraction or characteristic impedance.[6,17] Thus, the electron-wave amplitude refractive index n_a is proportional to the square root of the ratio of the kinetic energy to the effective mass,[6] and so

$$n_a \propto [(E-V)/m^*]^{1/2}. \tag{3}$$

The amplitude transmissivity t of an electron wave normally incident upon a boundary between semiconductors 1 and 2 is given by[6]

$$t = 2n_{a1}/(n_{a1}+n_{a2}). \tag{4}$$

The amplitude reflectivity r is similarly given by[6]

$$r = (n_{a1}-n_{a2})/(n_{a1}+n_{a2}). \tag{5}$$

The electron current density in quantum mechanics is analogous to Poynting vector power in electromagnetics. Thus, the electron current transmitted T is given by[6]

$$T = (n_{a2}/n_{a1})^2 t^2 \tag{6}$$

and the electron current reflected R is given by[6]

$$R = r^2. \tag{7}$$

In the above expressions, only dimensionless ratios of the electron-wave amplitude refractive indices occur. Both types of electron-wave refractive indices exhibit normal dispersion. That is, they increase with decreasing wavelength.

III. IMPEDANCE TRANSFORMERS

A. General

In microwave engineering, impedance transformation between transmission lines and waveguiding systems of differing characteristic impedance can be achieved with a variety of devices[15] including quarter-wave transformers, double-stub tuners, triple-stub tuners, slot lines, and E-plane–H-plane tuners. Quarter-wave transformers may also be used for unguided electromagnetic plane waves and unguided electron plane waves. In electromagnetic optics they are simply thin-film antireflection coatings. Each layer is a dielectric with a thickness of quarter of a wavelength (as measured in that material) at the pass frequency. In electron-wave optics in semiconductors, quarter-wave transformers are merely layers of semiconductor material with thicknesses that are a quarter of an electron wavelength (as measured in that material) at the pass energy. Such a semiconductor superlattice impedance transformer is depicted in Fig. 1 in terms of its conduction-band edge (labeled Γ for the case of the conduction-band minimum occurring at the center of the Brillouin zone). If impedance matching is required only over a narrow band of energies, then a single section (layer) impedance transformer may be used. In this situation the transformer acts as a narrow-band filter. If impedance matching is required over a broad range of energies then multiple layers will be needed. The energy range covered increases with increasing number of layers.

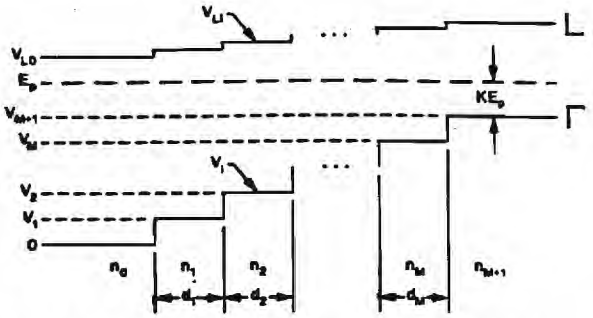

FIG. 1. Electron-wave quarter-wavelength impedance transformer shown by the spatial variation in the electron potential energy of the Γ[000] and L[111] conduction-band edges for a material system such as $Ga_{1-x}Al_xAs$. The M layers of the impedance transformer are labeled with the electron-wave amplitude refractive indices for those layers. The incident (0) and transmitted $(M+1)$ regions are similarly labeled.

The impedance transformer of Fig. 1 is a general quarter-wave device consisting of M layers. The wave-function reflectivity of an electron wave in region 0 incident upon a boundary with a semi-infinite region 1 is designated r_0. Similarly the reflectivity of an electron wave in region i incident upon a boundary with a semi-infinite region $i+1$ is designated r_i. The physical thickness of the ith layer is denoted d_i. In practical impedance transformers, the reflectivities r_i are relatively small. In this situation, the total electron amplitude reflection coefficient r for the entire impedance transformer is given by the sum of the first-order reflected waves.[15] Thus

$$r = r_0 + r_1 \exp(-2jk_1d_1) + r_2 \exp(-4jk_2d_2) + \cdots + r_i \exp(-j2ik_id_i) + \cdots. \tag{8}$$

Since all sections (layers) have the same electron optical thicknesses, then $k_1d_1 = k_2d_2 = \cdots = k_Md_M = \theta$. For quarter-wavelength transformers, this means $\theta = \pi/2$ at the pass energy. Furthermore, for a symmetrical transformer $r_0 = r_M, r_1 = r_{M-1}$, etc. For this common case, Eq. (8) may be rewritten as

$$r = 2\exp(-jM\theta)\{r_0\cos(M\theta) + r_1\cos[(M-2)\theta] + \cdots + r_i\cos(M-2i)\theta + \cdots\}. \tag{9}$$

By appropriate selection of the reflectivities $r_0, r_1, \ldots, r_M$, a wide variety of passband characteristics can be obtained.

B. Maximally flat transformers

A maximally flat passband is characterized by the first $M-1$ derivatives of the total electron amplitude transmission coefficient t with respect to the electron energy being

zero at the pass energy. Maximally flat transformers are also called Butterworth or binomial transformers. The maximally flat characteristic is obtained when

$$r = 2^{-M}\frac{n_{a0} - n_{aM+1}}{n_{a0} + n_{aM+1}} \sum_{i=0}^{M} C_i^M \exp(-j2i\theta), \quad (10)$$

where C_i^M are the binomial coefficients given by

$$C_i^M = M!/[i!(M-i)!]. \quad (11)$$

Comparing Eq. (10) with Eq. (8) yields

$$r_i = 2^{-M}[(n_{a0} - n_{aM+1})/(n_{a0} + n_{aM+1})]C_i^M. \quad (12)$$

Since the reflectivities $r_i = (n_{ai} - n_{ai+1})/(n_{ai} + n_{ai+1})$ are small, then $\ln(n_{ai}/n_{ai+1}) \simeq 2r_i$. Thus

$$\ln(n_{ai}/n_{ai+1}) = 2^{-M}C_i^M \ln(n_{a0}/n_{aM+1}), \quad (13)$$

providing a relationship between the refractive indices of the various layers.

C. Equal-ripple transformer

In an equal-ripple impedance transformer, the electron amplitude reflectivity varies in an oscillatory fashion between 0 and r_m, where r_m is a specified maximum reflectivity in the passband. This is obtained when the reflection coefficient is given by

$$r = r_m \exp(-jM\theta) T_M(\sec\theta_m \cos\theta), \quad (14)$$

where $T_M(x)$ are Chebyshev polynomials and are given by $T_1(x) = x$, $T_2(x) = 2x^2 - 1$, $T_3(x) = 4x^3 - 3x$, $T_4(x) = 8x^4 - 8x^2 + 1$,..., $T_i(x) = 2xT_{i-1}(x) - T_{i-2}(x)$. The quantity θ_m is the normalized half-bandwidth parameter given by $\theta_m = (\pi/2)(E_m/E_p)$, where E_m is the lowest electron energy at which the reflectivity equals r_m and E_p is the pass energy (see Fig. 1). For a specified value of the maximum reflectivity r_m, the quantity θ_m may be determined by solving the polynomial equation[15]

$$T_M(\sec\theta_m) = (1/r_m)(n_{a0} - n_{aM+1})/(n_{a0} + n_{aM+1}). \quad (15)$$

The electron amplitude refractive indices may then be determined by equating Eqs. (9) and (14). This gives a series of equations by then equating like terms in $\cos(i\theta)$. Each of these equations gives one of the reflectivities r_0, r_1,... and thus allows the amplitude refractive indices to be calculated as illustrated in Sec. IV.

IV. OPTIMUM SEMICONDUCTOR IMPEDANCE TRANSFORMERS

A. Configuration of semiconductors

The interconnection of GaAs and $Ga_{0.8}Al_{0.2}As$ with several types of impedance transformers will be treated for illustration. This might correspond to electron flow from the base (GaAs) to the collector ($Ga_{0.8}Al_{0.2}As$) in a bipolar junction transistor as mentioned previously. The $Ga_{1-x}Al_xAs$ material system is perhaps the most advanced of current semiconductor superlattice material systems. For these alloys, all compositions are lattice matched. The material is a direct gap semiconductor for $0 < x < 0.45$ with the conduction-band minimum occurring at the center of the Brillouin zone (Γ point). The electron potential energy of the conduction band V_i is given by

$$V_i = Ax_i, \quad i = 0,1,...,M+1, \quad (16)$$

and the electron mass is given by

$$m_i^* = (B + Cx_i)m_0, \quad i = 0,1,...,M+1, \quad (17)$$

where A, B, and C are constants and m_0 is the free-electron mass. For $Ga_{1-x}Al_xAs$, $A = 773.14$ meV (using a 62% conduction-band offset), $B = 0.067$, and $C = 0.083$.[18,19] In Fig. 1, region 0 would be GaAs and region $M+1$ would be $Ga_{0.8}Al_{0.2}As$. As also shown in Fig. 1, the conduction-band potential energy edge increases monotonically from GaAs to $Ga_{0.8}Al_{0.2}As$ through the transformer.

The next higher conduction-band minimum in $Ga_{1-x}Al_xAs$ for this range of compositions occurs along the [111] directions at the edge of the Brillouin zone (L point). The electron potential energy at the bottom of the L band, V_{Li}, is given by

$$V_{Li} = D + Fx_i, \quad i = 0,1,...,M+1, \quad (18)$$

relative to the Γ conduction-band edge for GaAs ($x = 0$). The quantities D and F are constants given by $D = 284$ meV and $F = 168.14$ meV for $Ga_{1-x}Al_xAs$.[18,19] The corresponding curve appears in Fig. 1 and is labeled L. To support ballistic transport by ensuring that intervalley scattering does not occur through phonon absorption, the pass electron energy will be arbitrarily set to be 50 meV below the L band of GaAs. The pass electron energy is thus $E_p = 234$ meV. As the aluminum concentration increases through the transformer, the energy separation $V_{Li} - E_p$ further increases until it is 83.6 meV in the $Ga_{0.8}Al_{0.2}As$ as depicted in Fig. 1.

Since the reference for the electron amplitude refractive index is arbitrary, it will be taken to be unity in the $Ga_{0.8}Al_{0.2}As$ since this is the low index side of the impedance transformer. That is $n_{aM+1} = 1$. The amplitude index of any other region is then given by

$$n_{ai} = [(E_p - V_i)m_{M+1}^*/(E_p - V_{M+1})m_i^*]^{1/2} n_{aM+1}. \quad (19)$$

Therefore in the $i = 0$ GaAs region, the amplitude index is $n_{a0} = 1.917\,962$.

The electron wavelength in any of the regions determines the electron optical phase thickness of that region. The electron wavelength for the pass energy in the ith region is given by

$$\lambda_{pi} = h/[2m_i^*(E_p - V_i)]^{1/2}, \quad (20)$$

where λ_{pi} is the pass wavelength as measured in the ith region and h is Planck's constant.

B. Optimum single-layer transformer

For the single-layer narrow-band impedance transformer, maximally flat and equal-ripple design procedures both

give the same result. It is the well-known single-layer antireflection coating result that the amplitude index should be

$$n_{a1} = (n_{a0} n_{aM+1})^{1/2}. \tag{21}$$

Thus, for the present case $n_{a1} = 1.384\,905$. The composition of this layer may be determined by substituting Eqs. (16) and (17) into Eq. (19) and solving for x_i. The result is

$$x_i = (E_p - BGm_0)/(A + CGm_0), \tag{22}$$

where $G \equiv [(E_p - V_{M+1})/m^*_{M+1}](n_{a1}/n_{aM+1})^2$. With the composition known, the potential energy V_i and the effective mass m_i^* are determined through Eqs. (16) and (17), respectively. The required physical thickness is then

$$d_i = \lambda_{pi}/4 = h/[32m_i^*(E_p - V_i)]^{1/2}, \tag{23}$$

to produce a quarter-wavelength thickness. For the present case, Eqs. (22), (16), (17), and (23) yield $x_1 = 0.121\,2$, $V_1 = 93.682$ meV, $m_1^* = 0.077\,06m_0$, and $d_1 = 2.9482$ nm, respectively. The resulting overall electron current transmittance T for this optimum single-layer impedance transformer is shown in Fig. 2. The transmittance was calculated by the procedure described in Ref. 6. At the pass kinetic energy $KE_p = 79.372$ meV, the electron current transmittance is unity as it should be.

C. Optimum three-layer maximally flat transformer

The design of a three-layer maximally flat impedance transformer to connect GaAs and $Ga_{0.8}Al_{0.2}As$ for a broader range of electron energies near the passband is presented in this section. For a three-layer device, $M = 3$. For $M = 3$ and $i = 0$, Eq. (13) becomes $\ln(n_{a0}/n_{a1}) = \frac{1}{8}\ln(n_{a0}/n_{aM+1})$ and so

$$n_{a1} = n_{a0}^{7/8} n_{aM+1}^{1/8}. \tag{24}$$

For the present case $n_{a0} = 1.917\,962$ and $n_{aM+1} = 1$ and so $n_{a1} = 1.768\,011$. The required composition is obtained from Eq. (22) and is $x_1 = 0.0345$. Likewise the needed physical thickness is found from Eq. (23) and is $d_1 = 2.5472$ nm. For $M = 3$ and $i = 1$, Eq. (13) gives $n_{a2} = n_{a0}^{-3/8} n_{a1} n_{aM+1}^{3/8}$. Using Eq. (24) this may be rewritten as

$$n_{a2} = n_{a0}^{1/2} n_{aM+1}^{1/2}. \tag{25}$$

Thus the center section of a maximally flat transformer is the same as that for the single-layer transformer [see Eq. (21)]. Therefore $n_{a2} = 1.384\,905$, $x_2 = 0.1212$, and $d_2 = 2.9482$ nm. For $M = 3$ and $i = 2$, Eq. (13) gives $n_{a3} = n_{a0}^{-3/8} n_{a2} n_{aM+1}^{3/8}$. Using Eq. (25) this may be written as

$$n_{a3} = n_{a0}^{1/8} n_{aM+1}^{7/8}. \tag{26}$$

For the present case, $n_{a3} = 1.084\,813$. The required composition and physical thickness are $x_3 = 0.1838$ and $d_3 = 3.5259$ nm. A summary of the parameters of this impedance transformer is given in Table I. The overall electron current transmittance T for this optimum three-layer maximally flat impedance transformer is shown in Fig. 3. Again at the pass kinetic energy $KE_p = 79.372$ eV, the electron current transmittance T is unity. The passband, however, is much broader than that for the one-layer transformer (Fig. 2). The maximally flat character of the passband is also evident in the transmittance shown in Fig. 3.

TABLE I. Design parameters of optimum three-layer maximally flat and three-layer equal-ripple electron impedance transformers for connecting GaAs to $Ga_{0.8}Al_{0.2}As$. The design pass energy is $E_p = 234$ meV and the design output kinetic energy is $KE_p = 79.372$ meV.

Layer i	Amplitude refractive index n_{ai}	Aluminum composition x_i	Thickness d_i (nm)	Number of monolayers p_i
Maximally flat				
0	1.9180	0.0000	...	...
1	1.7680	0.0345	2.5472	9.0113
2	1.3849	0.1212	2.9482	10.4300
3	1.0848	0.1838	3.5259	12.4739
4	1.0000	0.2000	...	...
Equal ripple				
0	1.9180	0.0000	...	...
1	1.5738	0.0789	2.7180	9.6155
2	1.3992	0.1180	2.9280	10.3585
3	1.2440	0.1515	3.1786	11.2449
4	1.0000	0.2000	...	...

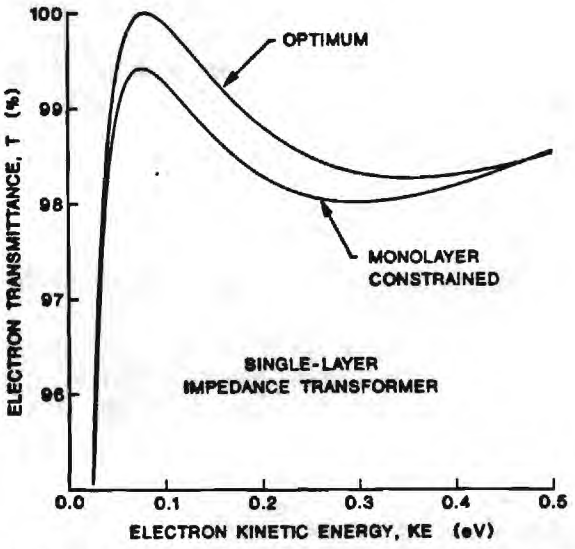

FIG. 2. The electron current transmittance as a function of electron kinetic energy as measured in the transmitted $(M + 1)$ region for a single-layer quarter-wavelength impedance transformer between GaAs and $Ga_{0.8}Al_{0.2}As$ of (a) optimum design (Sec. IV B) and of (b) monolayer-thickness-constrained design (Sec. V B).

D. Optimum three-layer equal-ripple transformer

The design of a three-layer equal-ripple impedance transformer to connect GaAs and $Ga_{0.8}Al_{0.2}As$ is presented in this section. For a maximum electron current reflectivity within the passband of 2%, the amplitude reflectivity is $r_m = (0.02)^{1/2} = 0.141\,42$. For a three-section device $M = 3$. Using the polynomial representation for $T_3(x)$, Eq. (15) may be written as

$$4x^3 - 3x = (1/r_m)(n_{a0} - n_{aM+1})/(n_{a0} + n_{aM+1}) = 2.224\,488, \tag{27}$$

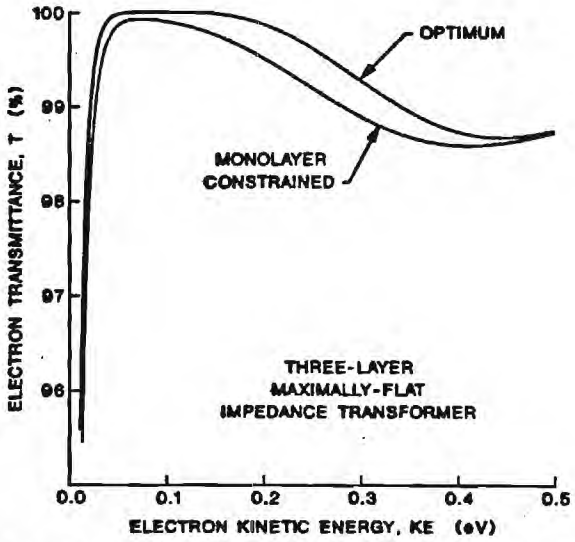

FIG. 3. The electron current transmittance as a function of electron kinetic energy as measured in the transmitted $(M+1)$ region for a three-layer maximally flat quarter-wavelength impedance transformer between GaAs and $Ga_{0.8}Al_{0.2}As$ of (a) optimum design (Sec. IV C and Table I) and of (b) monolayer-thickness-constrained design (Sec. V C and Table II).

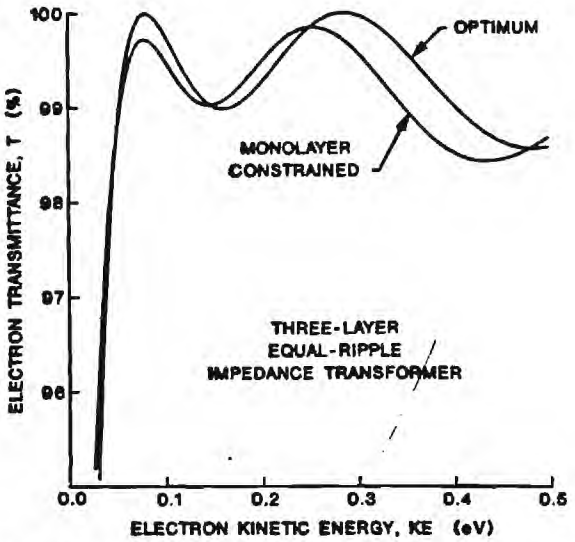

FIG. 4. The electron current transmittance as a function of electron kinetic energy as measured in the transmitted $(M+1)$ region for a three-layer equal-ripple quarter-wavelength impedance transformer between GaAs and $Ga_{0.8}Al_{0.2}As$ of (a) optimum design (Sec. IV D and Table I) and of (b) monolayer-thickness-constrained design (Sec. V D and Table II).

for a transformer between GaAs and $Ga_{0.8}Al_{0.2}As$, where $x \equiv \sec\theta_m$. Solving this cubic equation gives $x = 1.117\,068$ and $x = -0.558\,534 \pm j0.431\,139$. Only the real solution is meaningful in this design procedure. Equating Eqs. (9) and (14) for the case of $M = 3$ gives

$$2(r_0 \cos 3\theta + r_1 \cos\theta) = r_m[\sec^3\theta_m(\cos 3\theta + 3\cos\theta) - 3\sec\theta_m \cos\theta]. \quad (28)$$

Equating like terms in $\cos 3\theta$ produces $2r_0 = r_m \sec^3\theta_m$. Solving this gives $r_0 = 0.098\,565$. Equating like terms in $\cos\theta$ similarly produces $2r_1 = 3r_m(\sec^3\theta_m - \sec\theta_m)$ and solving this yields $r_1 = 0.058\,730$. From Eq. (5), the amplitude refractive index in region $i+1$ is

$$n_{ai+1} = [(1-r_i)/(1+r_i)]n_{ai}. \quad (29)$$

For the present configuration of materials, $n_{a0} = 1.917\,962$ and so for $i = 0$ Eq. (29) becomes $n_{a1} = [(1-r_0)/(1+r_0)]n_{a0} = 1.573\,796$. The required composition is obtained from Eq. (22) and is $x_1 = 0.0789$. The needed physical thickness is found from Eq. (23) and is $d_1 = 2.717\,966$ nm. For $i = 1$, Eq. (29) gives

$$n_{a2} = [(1-r_1)/(1+r_1)]n_{a1} = 1.399\,193.$$

The corresponding composition is $x_2 = 0.1180$ and the corresponding thickness is $d_2 = 2.9280$. Since the transformer is symmetrical, then $r_2 = r_1$ and thus the third layer has

$$n_{a3} = [(1-r_2)/(1+r_2)]n_{a2} = 1.243\,961.$$

The corresponding composition and thickness are $x_3 = 0.1515$ and $d_3 = 3.1786$ nm. A summary of the parameters of this impedance transformer is also given in Table I. The resulting electron current transmittance for this optimum Chebyshev impedance transformer is shown in Fig. 4. The equal-ripple character of the passband is evident. The passband of a multiple-section equal-ripple transformer is broader than that of the corresponding multiple-section maximally flat transformer. Furthermore, both multiple-layer transformers have much broader bandwidths than that of the narrow-band one-layer transformer (Fig. 2). Upon detailed inspection, the center layer in the Chebyshev transformer should have been $n_{a2} = (n_{a0}n_{aM+1})^{1/2}$. That is, it should have been 1.3849 rather than 1.3992 as calculated. This is due to minor approximations that are commonly made in the design of equal-ripple transformers. An exact, but more complicated, procedure is available[15] but the additional effort required to implement it produces only a negligible change in the resultant design.

V. MONOLAYER-CONSTRAINED SEMICONDUCTOR IMPEDANCE TRANSFORMER

A. Monolayer thickness constraint

The thicknesses of the layers in the optimum impedance transformers as designed in Sec. IV can have any of a continuum of values. In reality the thicknesses of all layers must be integer multiples of the monolayer thickness for that region. For lattice-matched $Ga_{1-x}Al_xAs$ the monolayer thickness s is the same for any composition x. For this material system $s = 0.282\,665$ nm.

To construct a quarter-wavelength impedance transformer, the thicknesses of the layers must also be an odd multiple of a quarter wavelength as measured in that layer for the pass energy E_p. That is

$$d_i = p_i s = (2q_i - 1)\lambda_{pi}/4, \quad i = 1,2,..., \quad (30)$$

where p_i is the integer number of monolayers for the ith region and q_i is a positive integer ($q_i = 1,2,3,...$). Substituting Eqs. (16) and (17) into Eq. (20) and then substituting the resulting λ_{pi} into Eq. (30) gives the following quadratic

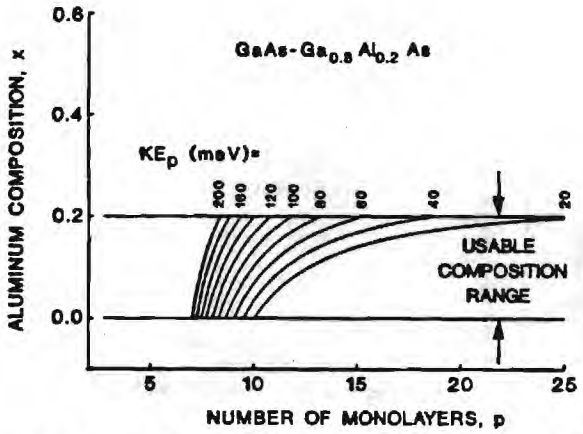

FIG. 5. Aluminum composition x $Ga_{1-x}Al_xAs$ that is needed to construct an impedance transformer for a transition from GaAs to $Ga_{0.8}Al_{0.2}As$. The pass kinetic energy KE_p in the $Ga_{0.8}Al_{0.2}As$ $(M+1)$ region is given as a parameter. Only integer values of the monolayer index correspond to realizable quarter-wavelength structures.

equation in the composition x_i

$$ACx_i^2 + (AB - CE_p)x_i + (h^2/32m_0) \times [(2q_i - 1)^2/p_i^2 s^2] - BE_p = 0. \quad (31)$$

The solution for the composition x_i is

$$x_i = [-b \pm (b^2 - 4ac_i)^{1/2}]/2a, \quad (32)$$

where $a = AC$, $b = AB - CE_p$, and

$$c_i = (h^2/32m_0)[(2q_i - 1)^2/p_i^2 s^2] - BE_p.$$

In order to design an impedance transformer, solutions x_i must be found in the usable composition range that correspond closely to the optimum values calculated by the procedures given in Sec. IV. To minimize the total thickness of the filter, q_i is initially set equal to unity. Then Eq. (32) is repetitively evaluated for $p_i = 1,2,3,...$ until all of the positive real roots in the range $0 < x_i < x_{max}$ are found. Plots of aluminum composition x as a function of the number of monolayers

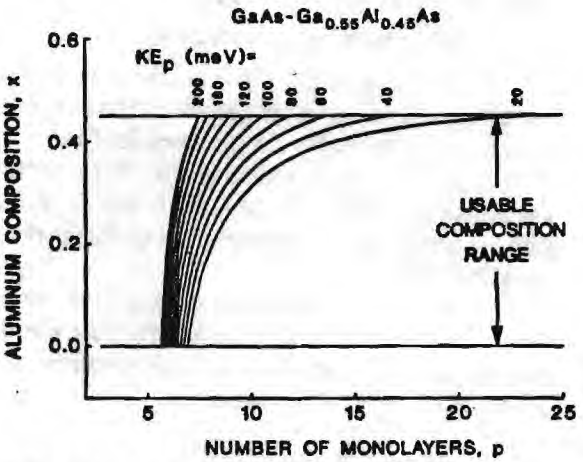

FIG. 6. Aluminum composition x in $Ga_{1-x}Al_xAs$ that is needed to construct an impedance transformer for a transition from GaAs to $Ga_{0.55}Al_{0.45}As$. The pass kinetic energy KE_p in the $Ga_{0.55}Al_{0.45}As$ $(M+1)$ region is given as a parameter. Only integer values of the monolayer index correspond to realizable quarter-wavelength structures.

thickness are shown for a transition from GaAs to $Ga_{0.8}Al_{0.2}As$ in Fig. 5 and for a transition from GaAs to $Ga_{0.55}Al_{0.45}As$ in Fig. 6. In each figure, multiple curves are shown for various values of the pass kinetic energy KE_p ($KE_p = E_p - V_{M+1}$). For large values of KE_p there are only a few values of composition that correspond to thicknesses that are integer multiples of the monolayers. For smaller values of KE_p there are a greater number of thicknesses available that simultaneously satisfy the quarter-wavelength and monolayer constraints.

B. Monolayer-constrained single-layer transformer

The monolayer thickness constraint is now applied to the design impedance transformers for a transition from GaAs to $Ga_{0.8}Al_{0.2}As$. Using $E_p = 234$ meV, setting $q_i = 1$, and repetitively evaluating Eq. (32) for integer values of p_i yields within the range $0 < x_i < x_{max}$ the following aluminum concentrations: $x_i = 0.0335$ for $p_i = 9$, $x_i = 0.1008$ for $p_i = 10$, $x_i = 0.1433$ for $p_i = 11$, $x_i = 0.1728$ for $p_i = 12$, and $x_i = 0.1944$ for $p_i = 13$.

For a monolayer thickness constrained single-layer narrow-band impedance transformer, the middle value of aluminum composition may be used to approximate the optimum single-layer transformer. Therefore $x_1 = 0.1433$. With the composition x_i and number of monolayers p_i known, the potential energy V_i, effective mass m_i^*, the amplitude refractive index n_{ai}, the thickness of the layer d_i, and wavelength in the layer λ_i can be determined from Eqs. (16), (17), (19), (30), and (23), respectively. For the present monolayer-thickness-constrained ($p_1 = 11$) single-layer impedance transformer, these quantities are $V_1 = 110.78$ meV, $m_1^* = 0.078\,89m_0$, $d_1 = 3.1093$ nm, $n_{a1} = 1.2826$, and $\lambda_1 = 12.437$ nm. The resulting overall electron current transmittance T for this monolayer thickness constrained impedance transformer is shown in Fig. 2 along with the transmittance for the optimum (without monolayer constraint) single-layer transformer. The passband characteristics have similar functional forms. However, at the pass kinetic energy $KE_p = 79.4$ meV, the electron current transmittance is reduced from the optimum 100% to 99.41%.

C. Monolayer-constrained three-layer maximally flat transformer

For an optimum three-layer maximally flat impedance transformer as described in Sec. IV C and summarized in Table I, the needed values of aluminum concentration are near the lower end, near the middle, and near the upper end of the range $0 < x_i < x_{max}$. The optimum three-layer maximally flat impedance transformer may be approximated by selecting the aluminum compositions of $x_1 = 0.0335$ for $p_1 = 9$, $x_2 = 0.1433$ for $p_2 = 11$, and $x_3 = 0.1944$ for $p_3 = 13$. As before, a knowledge of the composition x_i and number of monolayers p_i allows the potential energy V_i, effective mass m_i^*, amplitude refractive index n_{ai}, thickness of the layer d_i, and wavelength in the layer λ_i to be calculated. For the present monolayer-thickness-constrained ($p_1 = 9$, $p_2 = 11$, $p_3 = 13$) three-layer maximally flat impedance

TABLE II. Design parameters of monolayer-constrained three-layer maximally flat and three-layer equal-ripple electron impedance transformers for connecting GaAs to $Ga_{0.8}Al_{0.2}As$. The design pass energy is $E_p = 234$ meV and the design output kinetic energy is $KE_p = 79.372$ meV.

Layer i	Amplitude refractive index n_{ai}	Aluminum composition x_i	Thickness d_i (nm)	Number of monolayers p_i
Maximally flat				
0	1.9180	0.0000	...	...
1	1.7723	0.0335	2.5440	9
2	1.2826	0.1433	3.1093	11
3	1.0299	0.1944	3.6746	13
4	1.0000	0.2000	...	...
Equal ripple				
0	1.9180	0.0000	...	...
1	1.4769	0.1008	2.8267	10
2	1.2826	0.1433	3.1093	11
3	1.1403	0.1728	3.3920	12
4	1.0000	0.2000	...	...

transformer, these quantities are $V_1 = 25.90$ meV, $V_2 = 110.78$ meV, $V_3 = 150.28$ meV, $m_1^* = 0.069\,78 m_0$, $m_2^* = 0.078\,89 m_0$, $m_3^* = 0.083\,13 m_0$, $n_{a1} = 1.7723$, $n_{a2} = 1.2826$, $n_{a3} = 1.0299$, $d_1 = 2.5440$ nm, $d_2 = 3.1093$ nm, $d_3 = 3.6746$ nm, and $\lambda_1 = 10.176$ nm, $\lambda_2 = 12.437$ nm, $\lambda_3 = 14.698$ nm. A summary of the primary design parameters is given in Table II. The resulting overall electron current transmittance T for this monolayer-thickness-constrained impedance transformer is shown in Fig. 3 along with the transmittance for the optimum (without monolayer constraint) three-layer maximally flat transformer. The passband characteristics have very similar flat-top forms. At the pass kinetic energy $KE_p = 79.4$ meV, the electron current transmittance is reduced from the optimum 100% to 99.93%.

D. Monolayer-constrained three-layer equal-ripple transformer

For an optimum three-layer equal-ripple impedance transformer as described in Sec. IV D and summarized in Table I, the needed values of aluminum concentration are closer to the middle of the range $0 < x_i < x_{max}$ than is the case for the maximally flat transformer. The optimum three-layer equal-ripple impedance transformer may be approximated by selecting the aluminum compositions of $x_1 = 0.1008$ for $p_1 = 10$, $x_2 = 0.1433$ for $p_2 = 11$, and $x_3 = 0.1728$ for $p_3 = 12$. As before, a knowledge of the composition x_i and number of monolayers p_i allows the potential energy V_i, effective mass m_i^*, amplitude refractive index n_{ai}, thickness of the layer d_i, and wavelength in the layer λ_i to be calculated. For the present monolayer-thickness-constrained ($p_1 = 10$, $p_2 = 11$, $p_3 = 12$) three-layer maximally flat impedance transformer, these quantities are $V_1 = 77.93$ meV, $V_2 = 110.78$ meV, $V_3 = 133.58$ meV, $m_1^* = 0.075\,37 m_0$, $m_2^* = 0.078\,89 m_0$, $m_3^* = 0.081\,34 m_0$, $n_{a1} = 1.4769$, $n_{a2} = 1.2826$, $n_{a3} = 1.1403$, $d_1 = 2.8267$ nm $d_2 = 3.1093$ nm, $d_3 = 3.3920$ nm, and $\lambda_1 = 11.3068$ nm, $\lambda_2 = 12.437$ nm, $\lambda_3 = 13.5680$ nm, A summary of the primary design parameters is given in Table II. The resulting overall electron current transmittance T for this monolayer-thickness-constrained impedance transformer is shown in Fig. 3 along with the transmittance for the optimum (without monolayer constraint) three-layer equal-ripple transformer. The passband characteristics have very similar oscillating forms. At the pass kinetic energy $KE_p = 79.4$ meV, the electron current transmittance is reduced from the optimum 100% to 99.72%.

VI. SUMMARY AND DISCUSSION

The quantitative analogies that have been previously established[6] between electron-wave propagation in semiconductors and electromagnetic-wave propagation in dielectrics have been used to design impedance transformers for ballistic (collisionless) electron waves traveling between dissimilar energy-gap semiconductors. These devices have been designed as a series of quarter (electron) wavelength quantum well layers in the form of compositional superlattices. Procedures for designing maximally flat (Butterworth) and equal-ripple (Chebyshev) impedance transformers of arbitrary spectral bandwidth have been presented. An alternate method to design maximally flat and equal-ripple transformers is through the use of precalculated tables[20–22] of refractive indices *if* the tables contain the ratio of beginning and ending refractive indices that is needed.

Additional constraints on the impedance transformer quantum well layers in practice are that (1) their compositions must be within the usable compositional range and that (2) their thicknesses must be integer multiples of a monolayer thickness. These constraints have been incorporated into the design procedure producing designs that approximate the optimum designs. However, even with these additional constraints, it has been shown that the general characteristics of the optimum design can be retained. While the transmittances presented in Figs. 2–4 have been calculated for electrons moving perpendicular to the boundaries, these results accurately apply to electrons with angles of incidence beyond 10°. Thus the results presented are rather insensitive to the electron angle of incidence.

The electron potential energy shown in Fig. 1 is idealized and does not include the effects of space charge in these undoped layers. The space charge which is a function of the current, will alter the potential energy (as calculated by the Poisson equation). This new potential energy will, in turn, alter the wave function (as calculated by the Schrödinger equation). Thus, in general, a self-consistent solution of these equations is needed, particularly at high current levels.

The designs of practical single-layer and three-layer transformers for connecting GaAs and $Ga_{0.8}Al_{0.2}As$ have been presented. Although this well-developed, lattice-matched material system was used as an example, the procedures presented would also apply to other material systems. Dispersion effects in electromagnetic (e.g., microwave) impedance transformers are relatively small compared to the dispersion effects in semiconductor electron-wave devices. For the present case of impedance transformers this causes a decrease in the electron current transmittance at energies

below the pass energy and an increase in the transmittance at energies above the pass energy.

ACKNOWLEDGMENTS

This research was sponsored in part by a grant from the Joint Services Electronics Program under Contract No. DAAL-03-87-K-0059. One of us (K.F.B.) was supported in part by a Presidential Young Investigator award from the National Science Foundation and another (E.N.G.) by a Research Initiation award from the National Science Foundation.

[1]L. Esaki and R. Tsu, IBM J. Res. Dev. 13, 61 (1970).
[2]A. F. J. Levi, J. R. Hayes, P. M. Platzman, and W. Wiegmann, Phys. Rev. Lett. 55, 2071 (1985).
[3]M. Heiblum, M. I. Nathan, D. C. Thomas, and C. M. Knoedler, Phys. Rev. Lett. 55, 2200 (1985).
[4]S. Washburn and R. A. Webb, Adv. Phys. 35, 375 (1986).
[5]Y. Imry, in *Directions in Condensed Matter Physics*, edited by G. Grinstein and G. Mazenko (World Scientific, Singapore, 1986), pp. 101–163.
[6]T. K. Gaylord and K. F. Brennan, J. Appl. Phys. 65, 814 (1989).
[7]M. Heiblum, M. V. Fischetti, W. P. Dumke, D. J. Frank, I. M. Anderson, and C. M. Knoedler, Phys. Rev. Lett. 58, 816 (1987).
[8]S. Sen, F. Capasso, A. C. Gossard, and R. A. Spah, Appl. Phys. Lett. 51, 1428 (1987).
[9]R. C. Potter and A. A. Lakhani, Appl. Phys. Lett. 52, 1349 (1988).
[10]J. R. Hayes, P. England, and J. P. Harbison, Appl. Phys. Lett. 52, 1578 (1988).
[11]C. J. Summers and K. F. Brennan, Appl. Phys. Lett. 48, 806 (1986).
[12]K. F. Brennan and C. J. Summers, J. Appl. Phys. 61, 5410 (1987).
[13]K. F. Brennan and C. J. Summers, IEEE J. Quantum Electron. QE-23, 320 (1987).
[14]T. K. Gaylord, E. N. Glytsis, and K. F. Brennan, J. Appl. Phys. 65, 1842 (1989).
[15]R. E. Collin, *Foundations for Microwave Engineering* (McGraw-Hill, New York, 1966).
[16]C. M. Wu and E. S. Yang, Solid-State Electron. 22, 241 (1979).
[17]A. N. Khondker, M. R. Khan, and A. F. M. Anwar, J. Appl. Phys. 63, 5191 (1988).
[18]H. C. Casey and M. B. Panish, *Heterostructure Lasers Part A. Fundamental Principles* (Academic, New York, 1978), Chap. 4.
[19]R. C. Miller, D. A. Kleinman, and A. C. Gossard, Phys. Rev. B 29, 7085 (1984).
[20]L. Young, IRE Trans. Microwave Theory Tech. 7, 233 (1959).
[21]L. Young, IRE Trans. Microwave Theory Tech. 8, 243 (1960).
[22]L. Young, J. Opt. Soc. Am. 51, 967 (1961).

Electron wave diffraction by semiconductor gratings: Rigorous analysis and design parameters

Gregory N. Henderson, Elias N. Glytsis, and Thomas K. Gaylord
School of Electrical Engineering and Microelectronics Research Center, Georgia Institute of Technology, Atlanta, Georgia 30332-0250

(Received 21 March 1991; accepted for publication 22 April 1991)

An exact rigorous coupled-wave analysis has been developed to model ballistic electron wave diffraction by gratings with periodic effective mass and/or potential energy variations. Design expressions have been derived to calculate diffracted angles, to identify evanescent orders, and to identify the Bragg condition. Design expressions for Bragg regime (up to 100% diffraction efficiency in a single order) and Raman–Nath regime (high diffraction efficiency divided among multiple orders) diffraction are presented along with example $Ga_{1-x}Al_xAs$ grating designs. Design procedures for ballistic electron switches, multiplexers, spectrometers, and electron waveguide couplers are described.

Semiconductor growth techniques such as molecular beam epitaxy and metalorganic chemical vapor deposition together with nanolithography have been refined so that semiconductor structures can be fabricated with device dimensions on the order of electron wavelengths.[1] Using these techniques, devices exhibiting ballistic (collisionless) electron transport have been fabricated.[2,3] These ballistic electrons are quantum-mechanical deBroglie waves and can be reflected, refracted, diffracted, guided, and interfered like optical waves in dielectrics.[4]

The growth procedures mentioned above have been used to produce periodic structures such as superlattices,[1] arrays of quantum wires,[5] and periodic gate structures,[6] whose periods are on the order of electron wavelengths in semiconductors. These periodic structures can be used as ballistic electron wave diffractive devices analogous to gratings used in integrated optics.[7] Previous analyses of electron wave diffraction in semiconductors have been limited to the use of a two-mode amplitude transmittance analysis (to model diffraction from a symmetric rectangular potential-energy grating),[8] and a Fraunhoufer analysis (to model single-slit diffraction).[9] The rigorous coupled-wave analysis (RCWA) presented in this letter can model ballistic electron wave diffraction from a general effective mass and/or potential energy grating to an arbitrary level of accuracy. In addition, simple design expressions are presented to determine the angles of propagation for the diffracted waves and to identify the evanescent orders. The design constraints required to achieve Bragg and Raman–Nath regime diffraction are identified.

An electron wave diffraction grating is shown in Fig. 1 with grating vector $\mathbf{K}$, period Λ ($|\mathbf{K}| = 2\pi/\Lambda$), slant angle ϕ, and thickness d. The input and output regions are described by effective masses m_I^* and m_{III}^* and potential energies V_I and V_{III}, respectively. An electron wave of energy E and wave vector $\mathbf{k}'$ is incident from the input region at an angle θ' and is diffracted into forward- and backward-diffracted orders. The Hamiltonian used for the electron wave inside the grating is given as[10]

$$\frac{-\hbar^2}{2}\nabla\cdot\left(\frac{\nabla\psi}{m^*(\mathbf{r})}\right)=[E-V(\mathbf{r})]\psi, \tag{1}$$

where ψ is the electron wave amplitude, $\hbar$ is Planck's constant divided by 2π, and m^* and V are the periodic effective mass and potential energy in the grating (periodic in the grating vector $\mathbf{K}$). The Floquet theorem (Bloch theorem) for waves in a periodic medium[11] states that the electron wave inside the grating can be described as $\psi = \sum_{i=-\infty}^{\infty} U_i(z) \times \exp(-j\sigma_i\cdot\mathbf{r})$, where $\sigma_i = \mathbf{k} - i\mathbf{K}$, $\mathbf{k}$ is the incident wave vector refracted into the grating, i is the integer diffracted order, and $j = (-1)^{1/2}$. Likewise, the electron wave in the input region is given as $\psi = \exp(j\mathbf{k}'\cdot\mathbf{r}) + \sum_{i=-\infty}^{\infty} R_i \exp(j\mathbf{k}_i'\cdot\mathbf{r})$, where $\mathbf{k}_i'$ and R_i are the wave vector and amplitude of the ith backward-diffracted order, respectively. The electron wave in the output region is $\psi = \sum_{i=-\infty}^{\infty} T_i \exp(j\mathbf{k}_i''\cdot\mathbf{r})$, where $\mathbf{k}_i''$ and T_i are the wave vector and amplitude of the ith forward-diffracted order, respectively.

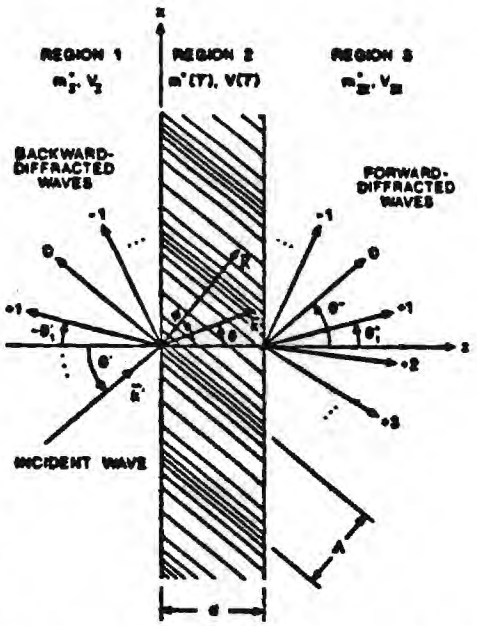

FIG. 1. Schematic diagram of an electron wave grating. A ballistic electron wave is incident upon the grating from region 1 and is diffracted into backward- and forward-diffracted orders in regions 1 and 3, respectively.

 0003-6951/91/290440-03$02.00

By employing phase matching of the input and output waves to the space harmonics in the grating region $[U_i(z)]$, one finds the grating equations to be

$$[2m_I^*(E-V_I)]^{1/2}\sin\theta' - (2\pi i\hbar/\Lambda)\sin\phi = r_n[2m_n^*(E-V_n)]^{1/2}\sin\theta_i'', \quad (2)$$

where $n = \mathrm{I}, \mathrm{III}$, $r_{\mathrm{I}} = -1$, $r_{\mathrm{III}} = 1$, and $\theta_i^{\mathrm{I}} = \theta_i'$ and $\theta_i^{\mathrm{III}} = \theta_i''$ are the angles of propagation of the ith backward- and forward-diffracted orders, respectively. Those space harmonics that cannot phase match to propagating orders are evanescent (k_i and θ_i are imaginary) or "cutoff" orders. The directions of the propagating diffracted orders are shown schematically in Fig. 1.

To calculate the amplitudes of the diffracted waves, a RCWA similar to that employed in electromagnetics[11] is used. The effective mass and potential energy in the grating region are expanded as Fourier series in K and substituted into Eq. (1). In order to allow for discontinuities in the effective mass (as in $Ga_{1-x}Al_xAs$ superlattice) Eq. (1) is separated into two first-order vector equations where the derivatives of the effective mass have been eliminated. These equations are solved using the state-variable approach.[11] The number of orders is chosen to ensure convergence of the diffraction efficiencies. Through the application of the boundary conditions (continuity of ψ and $\nabla\psi\cdot\hat{z}/m^*$), the R_i's and T_i's are calculated. By analogy to electromagnetics,[4] the diffraction efficiency for electron wave gratings is defined as the ratio of the z component of the probability current carried by the ith diffracted order to the z component of the probability current of the incident wave. Using the probability current $J = j\hbar(\psi\nabla\psi^* - \psi^*\nabla\psi)/2m^*$, one finds the diffraction efficiencies in regions I and III to be $DE_i^{\mathrm{I}} = (\cos\theta_i'/\cos\theta')|R_i|^2$ and $DE_i^{\mathrm{III}} = (\sqrt{m_I^*(E-V_{\mathrm{III}})}\cos\theta_i''/\sqrt{m_{\mathrm{III}}^*(E-V_I)}\cos\theta')|T_i|^2$, respectively.

The RCWA is a robust procedure that can be applied to arbitrary grating profiles. For design, however, it is useful to have analytical expressions that describe the diffraction efficiencies in terms of the grating parameters. In electromagnetics, the Bragg regime and the Raman–Nath regime are often used for grating design.[12] In the Bragg regime, the angle of incidence is adjusted so that the first diffracted wave vector inside the grating (σ_1) lies on the allowed wave vector surface inside the grating,[11] yielding

$$\sqrt{2m_{\mathrm{II}}^*(E-V_{\mathrm{II}})} = \pi\hbar/\Lambda\cos(\theta-\phi), \quad (3)$$

where m_{II}^* and V_{II} are the average effective mass and average potential energy inside the grating, and θ is the refracted wave vector angle inside the grating.[11] When an electron wave is incident at the Bragg condition [i.e., it satisfies Eq. (3)], the diffraction is in the Bragg regime if the grating thickness parameter Q' and the grating strength parameter γ satisfy the relation $\rho_B = Q'/2\gamma > 1$, where ρ_B is the Bragg regime parameter.[12] Q' is the effective thickness of the grating given by $Q' = 4\pi^2\hbar d/\sqrt{2m_{\mathrm{II}}^*(E-V_{\mathrm{II}})}\Lambda^2\cos\theta$.[12] γ is the coefficient that couples the power between the $i = 0$ and the $i = +1$ order when only two waves are included in the coupled-wave analysis. For a sinusoidal effective mass variation $\gamma = [m_{\mathrm{II}}^*(E-V_{\mathrm{I}}) + m_{\mathrm{I}}^*(E-V_{\mathrm{II}})\cos(2\theta)]d/\sqrt{2m_{\mathrm{II}}^*(E-V_{\mathrm{II}})}\,\hbar\cos\theta$, where m_{I}^* and V_{I} are the amplitudes of the sinusoidal effective mass and potential energy variation. The diffraction efficiency of the first diffracted order for a sinusoidal grating in the Bragg regime is found to be $DE_1^{\mathrm{III}} = \sin^2(\gamma)$. From this expression for DE_1^{III}, it is apparent that 100% diffraction efficiency is possible in the Bragg regime. Figure 2(a) shows both the approximate analysis and the RCWA for a Bragg regime grating constructed from a periodic aluminum composition variation in $Ga_{1-x}Al_xAs$. For this grating, $\rho_B = 2.60$. As ρ_B increases, the approximate analysis approaches the exact analysis, becoming indistinguishable around $\rho_B = 20.0$.

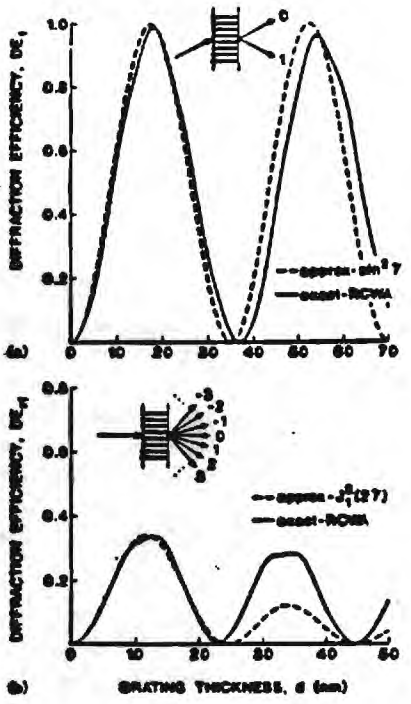

FIG. 2. RCWA and approximate solutions for diffraction from a sinusoidal $Al_xGa_{1-x}As$ grating with $E - V_I = 0.05$ eV, $x_I = x_{II} = x_{III} = 0.1$, and $x_1 = 0.03$, where x_I and x_{III} are the aluminum composition in regions 1 and 3, respectively, and x_{II} and x_1 are the average and modulating aluminum composition (in region 2) respectively. (a) Bragg regime grating with $\Lambda = 18$ nm. (b) Raman–Nath regime grating with $\Lambda = 60$ nm.

In the Raman–Nath regime, power is diffracted into multiple orders, and can be distributed almost evenly among many orders. This occurs when the Raman–Nath regime parameter $\rho_{RN} = Q'\gamma < 1$.[12] In this regime, the approximate solution to the coupled-wave equations is $DE_i^{\mathrm{III}} = J_i^2(2\gamma)$, where J_i is an ith order ordinary Bessel function of the first kind. Figure 2(b) shows the approximate analysis and the RCWA (for $i = \pm 1$) for a Raman–Nath regime grating. This grating leaves the Raman–Nath regime at $d \simeq 18$ nm, which explains the failure of the approximate analysis for $d > 20$ nm.

The electrons incident upon the grating will have a

distribution in both angle of incidence and energy. Therefore, it is important to understand the factors that affect the angular and energy selectivity of gratings. The angular (energy) selectivity describes the variation in the diffraction efficiency as the angle of incidence (energy) is changed. Strong angular (energy) selectivity refers to the case when the diffraction efficiency is appreciable for only a narrow corridor of angles of incidence (energies). It has been shown in electromagnetics that the angular and energy selectivity of a grating is a function of the ratio d/Λ.[12] A "thick" grating ($d/\Lambda > 10$) exhibits strong angular and energy selectivity. As a grating becomes "thinner" (d/Λ is decreased), the grating angular and energy selectivity become weaker. This behavior is demonstrated in Figs. 3(a) and 3(b) for three grating thicknesses. The suppression of the angular selectivity side lobes for angles less than 6.4° [Fig. 3(a)] is due to the fact that the $i = +1$ order becomes evanescent or "cutoff" at this angle of incidence [see Eq. (2)]. Similarly, the rapid drop in diffraction efficiency for kinetic energies around $E - V_1 = 0.025$ eV [Fig. 3(b)] is due to the fact that the $i = +1$ order becomes evanescent at this energy. The sharp discontinuity in the diffraction efficiency for $E - V_1 = 0.102$ eV [Fig. 3(b)] is analogous to a Wood's anomaly in electromagnetic optics and is due to the "cutting on" of the $i = +2$ order at this energy.

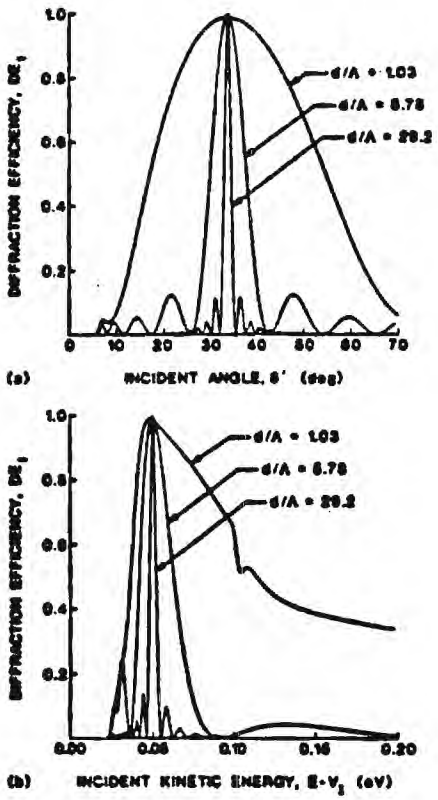

FIG. 3. (a) Angular and (b) energy selectivity of Bragg regime grating of Fig. 2(a) with combinations of thicknesses and aluminum modulations of $d/\Lambda = 1.03$ and $x_1 = 0.03$, $d/\Lambda = 5.78$ and $x_1 = 0.005$, and $d/\Lambda = 29.2$ and $x_1 = 0.001$.

With this information, one can design electron wave gratings for many applications such as switches, energy multiplexers, energy spectrometers, and electron waveguide couplers.[9] These devices could be invaluable in the development of future guided-wave electron devices.[4] If one desires a device with nearly 100% diffraction efficiency in a given order (e.g., a 1×1 switch) then the following design steps should be followed. First, the grating should be designed such that the electron wave is incident at the Bragg condition [Eq. (3)]. Then, the grating parameters should be chosen such that $\rho_B \gg 1$. Finally, the thickness and grating modulation should be chosen such that γ is a half-integer multiple of π so that $DE_1 \approx 100\%$. For this case, the grating parameters can also be adjusted such that all orders other than $i = 0$ and $i = +1$ are cutoff [as in Fig. 2(b)]. If one desires a grating with a large diffraction efficiency divided among multiple orders (e.g., a $1\times N$ switch), the following design steps should be followed. First, the grating should be designed [Eq. (2)] to have many propagating forward-diffracted orders. Then, the grating parameters should be chosen such that $\rho_{RN} \ll 1$. Finally, the argument of the Bessel functions (2γ) should be chosen to allow for a large diffraction efficiency in the desired orders. If one desires a grating with a large angular and energy selectivity (e.g., an energy multiplexer), then d/Λ should be made large (> 10). If one desires a grating with a low angular and energy selectivity (e.g., a 1×1 switch with high diffracted current) then d/Λ should be made small (< 1). After the grating has been designed using the above procedures, the diffraction can be determined using the RCWA to test the performance and finetune the grating design.

This research was supported in part by a grant from the Joint Services Electronics Program under contract No. DAAL-03-90-C-0004. One of us (G.N.H.) was supported by an Office of Naval Research Graduate Research Fellowship, and one of us (E.N.G.) was supported by a Research Initiation Award from the National Science Foundation.

[1] F. Capasso, ed., *Physics of Quantum Electron Devices* (Springer, New York, 1990), Chaps. 1–2.
[2] A. F. J. Levi, J. R. Hayes, P. M. Platzman, and W. Wiegman, Phys. Rev. Lett. 55, 2071 (1985).
[3] M. Heiblum, M. I. Nathan, D. C. Thomas, and C. M. Knoedler, Phys. Rev. Lett. 55, 2200 (1985).
[4] T. K. Gaylord and K. F. Brennan, J. Appl. Phys. 65, 814 (1989).
[5] M. Tsuchiya, P. M. Petroff, and L. A. Coldren, IEEE Trans. Electron. Devices 36, 2612 (1989).
[6] K. Ismail, W. Chu, D. A. Antoniadis, and H. I. Smith, Appl. Phys. Lett. 52, 1071 (1988).
[7] T. Tamir, in *Integrated Optics*, edited by T. Tamir (Springer, New York, 1979), p. 83.
[8] K. Furuya and K. Kurishima, IEEE J. Quantum Electron. 24, 1652 (1988).
[9] A. M. Kriman, G. H. Bernstein, B. S. Haukness, and D. K. Ferry, Superlatt. Microstruct. 6, 381 (1989).
[10] M. Altarelli, *Heterojunctions and Semiconductor Superlattices*, edited by G. Allan, G. Bastard, N. Boccara, M. Lannoo, and M. Voos (Springer, New York, 1986), p. 12.
[11] T. K. Gaylord and M. G. Moharam, Proc. IEEE 73, 894 (1985).
[12] T. K. Gaylord and M. G. Moharam, Appl. Opt. 20, 3271 (1981).

Ballistic Electron Transport in Semiconductor Heterostructures and Its Analogies in Electromagnetic Propagation in General Dielectrics

GREGORY N. HENDERSON, STUDENT MEMBER, IEEE, THOMAS K. GAYLORD, FELLOW, IEEE, AND ELIAS N. GLYTSIS, SENIOR MEMBER, IEEE

Developments in growth and fabrication technology have produced semiconductor structures with ballistic (collisionless) transport lengths of over a micron. In this paper, a comprehensive set of analogies is established between ballistic electron wave propagation in semiconductors (arbitrary kinetic energy and effective mass) and electromagnetic propagation in general dielectrics (arbitrary permittivity and permeability.) First, electromagnetic results for propagation in nonmagnetic dielectrics are generalized to describe propagation, reflection, and refraction in general dielectrics through the definition of separate phase and amplitude refractive indexes. The expressions for electron wave propagation, reflection, and refraction are then developed and are shown to have the same functional form as in electromagnetics, if analogous definitions of electron wave phase and amplitude refractive indexes are used. The reflectivity characteristics such as total internal reflection (critical angle) and zero reflectivity (Brewster angle) are analyzed as a function of material parameters for both general dielectrics and semiconductor materials. The critical angle and Brewster angle results are then applied to electron wave propagation in $Ga_{1-x}Al_xAs$ where it is shown that all interfaces in this material will have both a critical angle and a Brewster angle due to differing effective masses across the interface. This is the first prediction of an electron wave Brewster angle in semiconductors.

I. Introduction

Semiconductor growth techniques such as molecular beam epitaxy (MBE) and metalorganic chemical vapor deposition (MOCVD) have been refined so that semiconductor structures can be grown with precise monolayer and compositional control [1]. This has produced semiconductor materials in which ballistic electron transport has been observed [2]–[4]. That is, the electrons traverse the sample as quantum mechanical plane waves experiencing no elastic or inelastic scattering events. Ballistic electrons can account for more than 50% of the current in small devices [3] and have been shown to be prominent even in the presence of elastic scattering [5]. Since ballistic electrons are quantum mechanical deBroglie waves, they can be reflected, refracted, diffracted, and interfered in a manner analogous to optical waves in dielectrics [6], [7]. Electron wave interference effects have been observed experimentally for electron energies below the barriers in double-barrier and multibarrier resonant tunneling devices [8]–[12] and for electron energies above the conduction band edges in $GaAs/Ga_{1-x}Al_xAs$ and $In_{1-x}Ga_xAs/In_{1-y}Al_yAs$ heterostructures [13]–[16]. In addition, electron wave refraction has been experimentally demonstrated through the fabrication of electrostatic lenses [17], [18] and prisms [19] in a two-dimensional $GaAs/Ga_{1-x}Al_xAs$ electron gas.

In recent years, there has been a surge of interest in the development of analogies between electron wave (EW) propagation in semiconductors and electromagnetic wave (EMW) propagation in dielectrics [20]. Due to the fundamental differences between electrons and photons, however, it would seem difficult to draw quantitative, exact analogies between them. Specifically, as indicated in Fig. 1, electrons and photons differ in rest mass, charge, spin, particle specie (Fermion or Boson), and velocity. However, in the propagation of an EW in a charge-neutral crystal, where the electron is either in a single nondegenerate conduction band or in a degenerate conduction band with no zero-field spin splitting, the EW propagation is well described by the single-electron effective mass equation [21]. This equation is analogous to the Helmholtz equation for EMW propagation in dielectrics. Under these conditions, often referred to as the envelope-function approximation or the effective-mass approximation, exact, quantitative analogies can be drawn between EW and EMW propaga-

Manuscript received November 14, 1990; revised August 2, 1991. This work was supported by the Joint Services Electronics Program under Grant DAAL-03-90-C-0004 by the National Science Foundation under Grant ECS-9111866.

The authors are with the School of Electrical Engineering and Microelectronics Research Center, Georgia Institute of Technology, Atlanta, GA 30332.

IEEE Log Number 9104135.

tion. A number of conceptual and quantitative analogies have previously been developed. An analogy has been established between the nonmagnetic-dielectric Helmholtz equation and the time-independent Schrödinger equation for constant effective-mass conduction electrons [21], [22]. In addition, optical ray tracing methods for dielectrics have been used to describe ballistic electron refraction [17]–[19] and a Schrödinger equation has been derived for photons to relate constant effective-mass EW propagation to EMW propagation [23]. All of these analogies have been drawn to EMW propagation in nonmagnetic dielectrics. Such analogies are equivalent to neglecting effective mass changes across material interfaces. Separate EW phase and amplitude refractive indexes have previously been defined and used with the electromagnetic chain matrix method to describe EW propagation in semiconductor heterostructures with effective mass differences [6]. It is shown in the present work that the requirement of two EW refractive indexes is exactly analogous to EMW propagation in general dielectrics. Furthermore, recent experimental work has demonstrated that effective mass differences can have dramatic effects on the propagation of electrons across material interfaces [24]–[26]. Ohno, Mendez, and Wang [24] have demonstrated that effective mass differences between the emitter and well of a resonant tunneling diode have dramatic effects on the resulting current-voltage characteristic of the diode. These effects were well explained by the authors as being due to variations in the number of electrons that can phase match to the state in the well as a function of the effective masses. Similar results have been demonstrated through the ultrahigh resolution of Ballistic-Electron-Emission Microscopy (BEEM) [25], [26] of surfaces. In these experiments, ballistic electrons tunnel through an air gap and probe the electrical properties of a metal-semiconductor interface. Bell and Kaiser have explained the ultrahigh resolution in these experiments (on the order of 1 nm [25]) in terms of the total internal reflection of the nonnormal incidence electrons at the metal-semiconductor interface [26]. The existence of such a small critical angle ($\approx$ 3 deg for GaAs [26]) is due to the large effective mass difference between the metal and the semiconductor. It is straightforward to show that without the effective mass difference, the critical angle would be $\approx$ 52 deg and the resolution would be about 25 nm. These experimental results of Ohno *et al.* [24] and Bell *et al.* [25] are verification of the importance of including effective mass effects in the representation of ballistic electron transport.

In order to include these important effective mass effects, analogies in this paper are drawn to propagation in general dielectrics with arbitrary permittivity and permeability. A comprehensive set of analogies is established between EW propagation in semiconductor heterostructures and EMW propagation in general dielectrics. First, starting with Maxwell's equations, the expressions for EMW reflection and refraction in lossless nonmagnetic dielectrics are generalized to include lossless magnetic materials (with arbitrary permittivity and permeability). It is shown that the inclusion of lossless magnetic materials (general dielectrics) requires the definition of separate electromagnetic phase and amplitude refractive indexes. The phase refractive index is required to describe phase effects such as phase matching and total internal reflection at an interface between dielectrics. The amplitude refractive index is required to describe amplitude effects such as the reflectivity at an interface and the Brewster angle. In addition, by considering the reflectivity at interfaces between these general dielectrics, inherent analogies between the reflectivity of TE and TM polarizations are clarified. Then, starting with the single-electron effective-mass equation for conduction electrons, EW propagation in a semiconductor is treated. An EW phase refractive index is defined analogously to the electromagnetic phase refractive index. The EW phase refractive index describes phase matching at an interface between two semiconductor materials (with differing potential energy and effective mass) and total internal reflection from a semiconductor interface. By considering the reflectivity of an EW incident upon an interface between semiconductor materials an EW amplitude refractive index is defined analogously to the electromagnetic amplitude refractive index. Through the appropriate definition of these EW refractive indexes, it is shown that the electromagnetic expressions for calculating the critical angle, the reflectivity and transmissivity at an interface, and the Brewster angle can be used to calculate analogous quantities for EW propagation at interfaces between differing semiconductor materials. These analogies allow for the design of novel EW heterostructure devices (such as monoenergetic electron filters [27], [28]) using standard optical design techniques. The ranges of material parameters that allow for the existence of total internal reflection and for a Brewster angle are investigated for both optical and semiconductor materials. These results are applied to a boundary between two semiconductors in the $Ga_{1-x}Al_xAs$ material system to investigate the reflectivity characteristics as a function of material composition. These analogies lead to a number of new results about reflection and refraction.

	Electron	Photon
Mass	m_0	0
Charge	e	0
Spin	1/2	1
Pauli Exclusion Principle	Yes	No
Velocity	$< c/n$	c/n

Fig. 1. Comparison of electrons and photons in terms of rest mass, charge, particle specie (Fermion or Boson), spin, and velocity. In spite of their differences, a quantitative set of exact analogies can be drawn between EMW propagation and EW propagation for the propagation of an EW in a charge-neutral crystal, where the electron is either in a single nondegenerate conduction band or in a degenerate conduction band with no zero-field spin splitting.

First, by defining appropriate reference regions for the EW phase refractive index, inherent analogies are drawn between the electromagnetic constituitive parameters (permittivity and permeability) and the electron wave propagation parameters (kinetic energy and effective mass). These analogies allow the direct application of phase matching results from electromagnetics to the phase matching of electron waves. These analogies are used to calculate the angles of reflection and refraction at an interface between semiconductors and the conditions for total internal reflection at the interface.

Second, by considering the reflectivity of a dielectric interface between general dielectrics, an inherent analogy is developed between the reflectivity and transmissivity for TE polarized EMW's, for TM polarized EMW's, and for EW's. In the electromagnetic case, by defining a separate amplitude refractive index for both TE and TM polarizations, it is shown that a single set of expressions can be used to describe the reflectivity and transmissivity for both polarizations. Through the definition of analogous amplitude refractive indexes for an EW incident upon a boundary between two semiconductor materials, the reflectivity and transmissivity of the EW are shown to have the same form as the reflectivity of the polarization component of the EMW parallel to the interface (the electric field for TE polarization and the magnetic field for TM polarization). Thus a single set of reflectivity equations can be used for all three cases. In general dielectrics, the EMW phase (amplitude) refractive index is proportional to the square root of the product (ratio) of the relative permittivity and permeability of the material. In semiconductor materials, the EW phase (amplitude) refractive index is proportional to the square root of the product (ratio) of the kinetic energy and effective mass of the EW.

Third, an investigation of the material parameters that satisfy the total internal reflection condition shows that for both general dielectrics and semiconductor materials, there are a wide range of material parameters that can produce a given critical angle. In general dielectrics, the critical angle can be adjusted by varying the relative permittivity and permeability of the materials adjoining the interface. In semiconductors, the critical angle can be adjusted by varying the effective mass and the band offset of the semiconductor materials adjoining the interface. It is shown that for a $Ga_{1-x1}Al_{x1}As/Ga_{1-x2}Al_{x2}As$ interface the aluminum compositions x_1 and x_2 can be adjusted to achieve a given critical angle. By including these effective mass contributions it is shown that an EW at a $Ga_{1-x1}Al_{x1}As/Ga_{1-x2}Al_{x2}$ As interface can experience total internal reflection from both a potential rise and a potential drop.

Fourth, it is shown that since the reflectivity has the same form for TE and TM polarized EMW's, then one, both, or neither of the polarizations can have a Brewster angle. This result is not found in the standard nonmagnetic optical case (in which TM polarization always has a Brewster angle and TE polarization never has a Brewster angle). These results for the electromagnetic Brewster angle in general dielectrics are applied to the EW case. It is shown that when the kinetic energy and effective mass differ on the two sides of the interface, the EW will have a Brewster angle. If the effective mass difference were not included in the analysis, the EW results would follow the TE nonmagnetic case and a Brewster angle would not occur. It is shown that a Brewster angle will occur for a $Ga_{1-x1}Al_{x1}As/Ga_{1-x2}Al_{x2}$ As interface for all compositional combinations that maintain direct gap semiconductors. This is the first prediction of a Brewster angle for ballistic electron transport in semiconductors.

II. Phase Refractive Index

A. Electromagnetic Phase Refractive Index

Sinusoidal steady-state propagation of electromagnetic radiation in a lossless source-free medium is described by the sinusoidal steady-state form of Maxwell's equations where the time variation of the fields is taken to be $\exp(-j\omega t)$. A minus sign is used in the exponent in order to be consistent with the quantum mechanical formulation (see Section II-B). For an isotropic, homogeneous medium, Maxwell's equations reduce to Helmholtz equations for wave propagation,

$$\nabla^2\vec{E} = -\omega^2\mu\epsilon\vec{E}, \quad \nabla^2\vec{H} = -\omega^2\mu\epsilon\vec{H}, \tag{1}$$

where $\vec{E}$ and $\vec{H}$ are the complex electric and magnetic fields, ω is the radian frequency of the wave, and ϵ and μ are permittivity and permeability of the medium, respectively. The forward propagating solution to (1) is a plane wave of the form: $\vec{E} = \vec{E}_o\exp(+j\vec{k}^{EM}\cdot\vec{r})$ or $\vec{H} = \vec{H}_o\exp(+j\vec{k}^{EM}\cdot\vec{r})$ where $\vec{k}^{EM}$ is the wavevector for the forward propagating wave (which has a positive sign due to the choice of $\exp(-j\omega t)$), $\vec{E}_o$ and $\vec{H}_o$ are the vector wave amplitudes, and $j = \sqrt{-1}$. The isotropic dispersion relation for the wavevector of the forward propagating wave is found by inserting the plane wave solution into the Helmholtz equation, yielding the dispersion equation $|\vec{k}^{EM}| = \omega\sqrt{\mu\epsilon}$.

In electromagnetics, a phase refractive index is commonly defined to relate the magnitude of the wavevector in the medium of propagation, $|\vec{k}^{EM}|$, to the magnitude of the wavevector of the same frequency wave propagating in a reference medium, $|\vec{k}^{EM}_{ref}|$, by

$$n^{EM}_{ph} \triangleq \frac{|\vec{k}^{EM}|}{|\vec{k}^{EM}_{ref}|} = \frac{\sqrt{\mu\epsilon}}{\sqrt{\mu_{ref}\epsilon_{ref}}}, \tag{2}$$

where the wavevector of the reference region is related to the reference permittivity, ϵ_{ref}, and permeability, μ_{ref}, through the isotropic dispersion relationship: $|\vec{k}^{EM}_{ref}| = \omega\sqrt{\mu_{ref}\epsilon_{ref}}$. This definition of the phase refractive index given in (2) is a function of the material parameters of both the region of propagation and the reference region. It would be useful to normalize the refractive index such that it is only a function of quantities in the region of propagation This normalization can be performed if the reference region

is dispersionless. That is, ϵ_{ref} and μ_{ref} are not functions of the frequency of the EMW.

With a dispersionless reference region the phase refractive index can be defined in terms of the relative permittivity $\epsilon_r \triangleq \epsilon/\epsilon_{ref}$ and relative permeability $\mu_r \triangleq \mu/\mu_{ref}$, yielding

$$n_{ph}^{EM} = \sqrt{\mu_r \epsilon_r}. \tag{3}$$

In electromagnetics, the reference region is usually taken to be the vacuum. Using the vacuum as a reference region, (3) gives the definition of the electromagnetic phase refractive index that is commonly found in optics textbooks [29], [30]. In this case, the relative permittivity and permeability are normalized with respect to the vacuum quantities: $\epsilon_{ref} = \epsilon_o = 8.85 \times 10^{-12} F/m$ and $\mu_{ref} = \mu_o = 4\pi \times 10^{-7} H/m$.

B. Electron Wave Phase Refractive Index

The propagation of single parabolic-band conduction electrons in a semiconductor crystal is described by the time-dependent effective-mass Schrödinger equation [21]. If the energy of the electron is constant (not a function of time or position) and if the propagation is limited to a region of constant potential energy, the time-dependent effective-mass equation reduces to the time-independent effective-mass Schrödinger equation for constant potential energy given as

$$\nabla^2 \psi = \frac{-2m^*(\mathcal{E} - V)}{\hbar^2}\psi = \frac{-2m^*(KE)}{\hbar^2}\psi \tag{4}$$

where ψ is the EW amplitude, $\mathcal{E}$ is the total EW energy, V is the EW potential energy (band edge), (KE) is the EW kinetic energy, m^* is the electron effective mass, and $\hbar$ is Planck's constant divided by 2π. This constant energy formulation of the Schrödinger equation is analogous to the constant frequency (steady-state) formulation of Maxwell's equations where ω is replaced by the quantum mechanical radian frequency $\omega = \mathcal{E}/\hbar$. From this construction, it is apparent that the differential equation describing propagation of an EW in a region of constant potential energy (see (4)) is analogous to the Helmholtz equation describing propagation of an EMW in a homogeneous general dielectric (see (1)), where the EW amplitude is analogous to either the electric or the magnetic field. The solution to the EW propagation equation (see (4)) is also a plane wave of the form $\psi = \psi_o \exp(+j\vec{k}^{EW} \cdot \vec{r})$, where, in the EW case, the dispersion equation for the wavevector is $|\vec{k}^{EW}| = \sqrt{2m^*(KE)/\hbar^2}$.

As in electromagnetics, one can define a phase refractive index as the ratio of the magnitude of the wavevector in the region of propagation, $|\vec{k}^{EW}|$, to the magnitude of the wavevector of the same total energy $(\mathcal{E})$ wave propagating in a reference medium, $|\vec{k}_{ref}^{EW}|$, yielding

$$n_{ph}^{EW} \triangleq \frac{|\vec{k}^{EW}|}{|\vec{k}_{ref}^{EW}|} = \frac{\sqrt{m^*(KE)}}{\sqrt{m_{ref}^*(KE)_{ref}}} \tag{5}$$

where $|\vec{k}_{ref}^{EW}| = \sqrt{2m_{ref}^*(KE)_{ref}/\hbar^2}$. This is analogous to the definition of the phase refractive index in the electromagnetic case (see (2)).

As in the electromagnetic case, the dispersion in the EW phase refractive index needs to be proportional to the dispersion of the medium of propagation. This requires the use of a dispersionless EW reference region where the kinetic energy $(KE)_{ref}$ and effective mass m_{ref}^* are not functions of the total energy of the EW. The fact that this region may not exist in a real semiconductor is of no consequence. All physical calculations use ratios of refractive indexes and $(KE)_{ref}$ and m_{ref}^* will cancel.

Using a dispersionless reference region, the EW phase refractive index can be written in terms of a relative kinetic energy, $(KE)_r \triangleq (KE)/(KE)_{ref}$, and a relative effective mass, $m_r^* \triangleq m^*/m_{ref}^*$, as

$$n_{ph}^{EW} = \sqrt{m_r^*(KE)_r}. \tag{6}$$

Since the choice of a dispersionless reference region does not affect the physical calculations, m_{ref} and $(KE)_{ref}$ will be defined to be unity such that the relative kinetic energies and effective masses are equal to the actual values in the region of propagation.

Equation (6) is the expression for the EW phase refractive index given a dispersionless reference region. It is interesting to note that the EW phase refractive index is expressed as the square root of the product of two material parameters, the same form as is the EMW phase refractive index. In real semiconductor material systems, such as $Ga_{1-x}Al_xAs$, the kinetic energy and effective mass differ for each composition. Thus it is important that effects described by the EW phase refractive index, such as phase matching (Section III) and total internal reflection (Section V), be analyzed with respect to the variation of both material parameters. It is for this reason that the analogies in this paper are drawn between EMW propagation in general dielectrics and EW propagation in semiconductors. An analogy to electromagnetic propagation in nonmagnetic dielectrics ($\mu_r = 1$) is not complete since the EMW phase refractive index is expressed as the square root of one parameter, the relative permittivity of the medium.

III. Phase Matching Upon Reflection and Refraction

When an EMW is incident upon a lossless dielectric boundary, Maxwell's equations must be satisfied on both sides of the boundary, and the solutions must match at the boundary. By applying the appropriate boundary conditions, the angles of the reflected and transmitted waves can be calculated. An EW incident upon a boundary between two semiconductor materials will obey the same type of relationships. In the EW case, the EW must satisfy the time-independent Schrödinger equation on both sides of the boundary, and the solutions must match at the boundary.

A. Electromagnetic Phase Matching

Consider an electromagnetic plane wave incident upon a boundary between two charge-free general dielectric materials as shown in Fig. 2. The incident, reflected, and transmitted waves are propagating in the $x - z$ plane, and

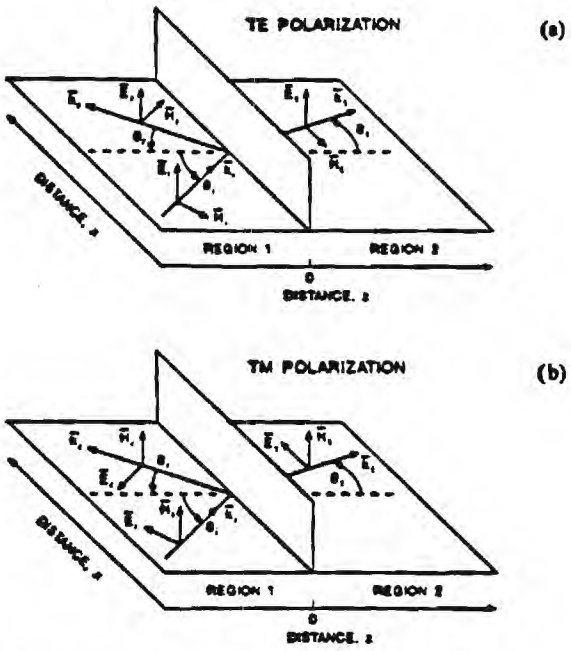

Fig. 2. Electromagnetic reflection and transmission from a general dielectric boundary for (a) TE and (b) TM polarizations.

the interface is located at $z = 0$. The dielectric to the left (right) of the interface, region 1 (2), is described by the relative permittivity ϵ_1 (ϵ_2) and the relative permeability μ_1 (μ_2) . The expressions for the incident ($\bar{E}_i$, $\bar{H}_i$), reflected ($\bar{E}_r$, $\bar{H}_r$), and transmitted ($\bar{E}_t$, $\bar{H}_t$) electric and magnetic fields are given as

$$\begin{aligned}\bar{W}_i &= \bar{W}_{oi}\exp(+j\bar{k}_{1,i}^{EM}\cdot\bar{r})\\ \bar{W}_r &= \bar{W}_{or}\exp(+j\bar{k}_{1,r}^{EM}\cdot\bar{r})\\ \bar{W}_t &= \bar{W}_{ot}\exp(+j\bar{k}_{2,t}^{EM}\cdot\bar{r})\end{aligned} \tag{7}$$

where $\bar{W} = \bar{E}$ or $\bar{H}$, $\bar{W}_{oi}$, $\bar{W}_{or}$, and $\bar{W}_{ot}$ are complex vector amplitudes, and $\bar{k}_{1,i}^{EM}$, $\bar{k}_{1,r}^{EM}$, and $\bar{k}_{2,t}^{EM}$ are the corresponding wavevectors that satisfy the isotropic dispersion relationship in regions 1 (for i and r) and 2 (for t). Maxwell's equations require the continuity of tangential component of the electric field, $\bar{E}\cdot\hat{x}|_{z=0}$, and the tangential component of the magnetic field, $\bar{H}\cdot\hat{x}|_{z=0}$, across the boundary. By substituting the field expressions (see (7)) into either of these two boundary conditions, it is found that the boundary conditions can be satisfied only if two phase matching conditions are satisfied, namely,

$$\theta_i = \theta_r = \theta_1, \quad \text{and} \quad n_{ph,1}^{EM}\sin\theta_1 = n_{ph,2}^{EM}\sin\theta_2 \tag{8}$$

where θ_1 and $\theta_2 = \theta_t$ are the angles between the incident (reflected) and transmitted wavevectors and the surface normal, measured counterclockwise as is shown in Fig. 2. The second expression of (8) is commonly referred to as Snell's law. If the transmitted wave cannot satisfy the phase matching condition, total internal reflection occurs, which is described in Section V.

B. Electron Wave Phase Matching

The reflection and refraction of an EW inciden upon an interface between two semiconductor materials can be analyzed in a manner analogous to the reflection and refraction of an EMW at an interface between dielectrics. As was the case in electromagnetics, expressions for the reflected and transmitted angles can be calculated by considering phase matching across the interface.

Consider an EW incident upon a boundary between two semiconductor materials as shown in Fig. 3. The EW propagation in region 1 (2) is characterized by the relative kinetic energy, $(KE)_1$ $[(KE)_2]$, and the relative effective mass, m_1^* (m_2^*). For the interface shown in Fig. 3, the material in region 2 has a higher potential energy (a larger band gap) than the material in region 1. The results, however, are equally applicable to propagation into a region of lower potential energy. The expression for the incident, ψ_i, reflected, ψ_r, and transmitted, ψ_t, EW's are given as

$$\begin{aligned}\psi_i &= \psi_{oi}\exp(+j\bar{k}_{1,i}^{EW}\cdot\bar{r})\\ \psi_r &= \psi_{or}\exp(+j\bar{k}_{1,r}^{EW}\cdot\bar{r})\\ \psi_t &= \psi_{ot}\exp(+j\bar{k}_{2,t}^{EW}\cdot\bar{r})\end{aligned} \tag{9}$$

where ψ_{oi}, ψ_{or}, and ψ_{ot} are complex wave amplitudes and $\bar{k}_{1,i}^{EW}$, $\bar{k}_{1,r}^{EW}$, $\bar{k}_{2,t}^{EW}$ are the wavevectors that satisfy the EW isotropic dispersion relationship in regions 1 (for i and r) and 2 (for t). In a manner analogous to the EMW, the EW amplitude, ψ, and the transmitted component of the product of the reciprocal of the effective mass and the gradient of the EW amplitude, $(1/m^*)\nabla\psi\cdot\hat{z}$, must be continuous across the boundary.

These EW boundary conditions have a direct analogy in the boundary conditions given above for an EMW incident upon a general dielectric interface. The electromagnetic boundary conditions are the matching of the tangential components of vector fields ($\bar{E}$ and $\bar{H}$). The EW boundary conditions involve the matching of a scalar field and the transmitted component of the gradient of the scalar field. In order to investigate the form of the analogies between the EMW boundary conditions and the EW boundary conditions, an analogy must be drawn between the EW amplitude and one of the electromagnetic field components E or H. The choice of field component will not affect the form of the results. For this analysis, an analogy will be drawn between the EW amplitude and the electric field amplitude. The same results would be obtained if an analogy were drawn between the magnetic field amplitude and the EW amplitude.

Using the analogy between the electric field E and the electron wave amplitude ψ, the EMW boundary condition matching the continuity of the tangential component of the electric field has the same functional form as the EW boundary condition matching the continuity of the wave amplitude across the boundary. The EMW boundary condition matching the continuity of the magnetic field should then have the same form as the EW boundary condition matching the continuity of the gradient of the wave amplitude. This analogy between the magnetic field

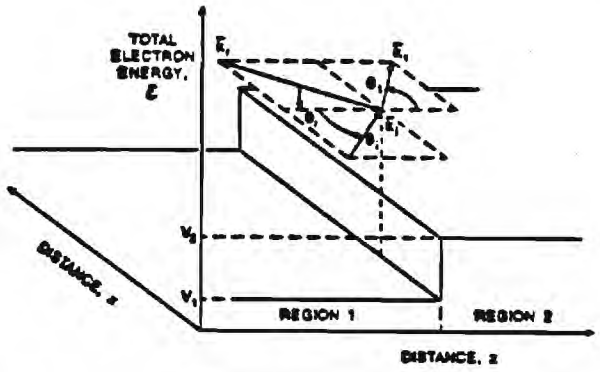

Fig. 3. Electron wave reflection and transmission across a semiconductor interface. The angles of reflection (θ_r) and transmission (θ_t) are calculated from phase matching considerations, and the amplitudes of the reflected and transmitted waves are calculated from the boundary conditions: the continuity of the wavevector and the continuity of the transmitted component of the probability current.

and the gradient of the electron wavefunction can be seen if the magnetic field is rewritten in terms of the electric field using Maxwell's curl relation, yielding $\vec{H} = (1/j\omega\mu_1\mu_{ref})(\vec{\nabla} \times \vec{E})$. Hence, the EMW boundary condition matching the continuity of the magnetic field can be expressed as a boundary condition matching the continuity of the tangential component of the curl (a vector derivative) of the electric field. The two electromagnetic boundary conditions are the matching of the tangential component of a vector field and the tangential component of its vector derivative. The EW boundary conditions involve the matching of a scalar field and the transmitted component of its vector derivative (gradient).

Since the boundary conditions and field expressions are similar for the EMW and the EW, it would be expected that the EW phase matching conditions have the same form as the EMW phase matching conditions. By substituting the EW amplitude expressions (see (9)) into either of the two electron wave boundary conditions, the EW phase matching conditions are found to be identical to the EMW phase matching conditions given in (8), where the EW phase refractive index, n_{ph}^{EW}, is used in place of the EMW phase refractive index, n_{ph}^{EM}. Since these equations describing the directions of propagation of the reflected and transmitted EW's are identical to the EMW results, standard electromagnetic results for describing phase propagation effects in general dielectrics, such as reflection, refraction, and total internal reflection (Section V) can be used to describe ballistic electron propagation in semiconductor heterostructures.

IV. Amplitude Refractive Index

A. Electromagnetic Amplitude Refractive Index

Phase matching of the boundary conditions for an EMW incident upon a dielectric boundary was used to calculate expressions for the propagation directions of the reflected and transmitted waves. The relative amplitudes of the reflected and transmitted waves can be calculated by considering the conditions placed on the field amplitudes by the boundary conditions. The reflectivity and transmissivity can be calculated by considering any two of the following three boundary conditions: continuity of the tangential component of the electric field, continuity of the tangential component of the magnetic field, and conservation of normal power flow across the boundary, where the power flow is given as 1/2 Re $(\vec{E} \times \vec{H}^*)$ and * denotes complex conjugate. Since any arbitrary wave polarization can be decomposed into a sum of the eigenmodes of the interface (TE and TM), and since the TE and TM modes are uncoupled (isotropic media), one can analyze TE and TM polarizations separately. Then, the reflection of any arbitrary polarization can be calculated from a vector superposition of the results for TE and TM polarizations.

1) TE Polarization: For a TE polarized plane wave (Fig. 2(a)), the polarization in which the electric field (E) is polarized parallel to the interface, the three phase matched boundary conditions reduce to

$$E_o + E_{or} = E_{ot} \tag{10}$$

$$(E_o/Z_1)\cos\theta_1 - (E_{or}/Z_1)\cos\theta_1 = (E_{ot}/Z_2)\cos\theta_2 \tag{11}$$

$$(E_o^2/Z_1)\cos\theta_1 - (E_{or}^2/Z_2)\cos\theta_1 = (E_{ot}^2/Z_2)\cos\theta_2 \tag{12}$$

where Z_i is the characteristic impedance of the bulk medium i for $i = 1$ and $i = 2$. The characteristic impedance is $Z_i \triangleq |\vec{E}_i|/|\vec{H}_i| = \sqrt{\mu_i\mu_{ref}/\epsilon_i\epsilon_{ref}}$ where ϵ_i and μ_i are the relative permittivity and relative permeability of region i. By using any two of these three boundary conditions (see (10)–(12)), the reflectivity and transmissivity of the electric field can be calculated in terms of the reflected and transmitted angles and the characteristic impedances of the two dielectrics as

$$r_E^{TE} = \left(\frac{E_{or}}{E_o}\right)_{TE} = \frac{Z_2\cos\theta_1 - Z_1\cos\theta_2}{Z_2\cos\theta_1 + Z_1\cos\theta_2} \tag{13}$$

$$t_E^{TE} = \left(\frac{E_{ot}}{E_o}\right)_{TE} = \frac{2Z_2\cos\theta_1}{Z_2\cos\theta_1 + Z_1\cos\theta_2}. \tag{14}$$

As was the case for the wavevector, it is convenient to rewrite these equations in terms of quantities normalized to a reference region. This normalization is performed through the use of an amplitude refractive index defined as

$$n_{am}^{TE} \triangleq Z_{ref}/Z = \sqrt{\epsilon_r/\mu_r} \tag{15}$$

where the vacuum was used as a dispersionless reference region.

Using this expression for the amplitude refractive index (see (15)) the equations for the reflectivity and transmissivity can be rewritten in terms of the amplitude refractive indexes as

$$r_E^{TE} = \left(\frac{E_{or}}{E_o}\right)_{TE} = \frac{n_{am,1}^{TE}\cos\theta_1 - n_{am,2}^{TE}\cos\theta_2}{n_{am,1}^{TE}\cos\theta_1 + n_{am,2}^{TE}\cos\theta_2} \tag{16}$$

$$t_E^{TE} = \left(\frac{E_{ot}}{E_o}\right)_{TE} = \frac{2n_{am,1}^{TE}\cos\theta_1}{n_{am,1}^{TE}\cos\theta_1 + n_{am,2}^{TE}\cos\theta_2}. \tag{17}$$

Since these expressions for the reflectivity and transmissivity (see (16)–(17)) contain ratios of the amplitude refractive indexes, the reference dependence is removed. By using Maxwell's curl equations the expressions for the reflectivity and transmissivity of the magnetic field can be calculated in terms of the reflectivity and transmissivity of the electric field as

$$r_H^{\text{TE}} = \left(\frac{H_{or}}{H_o}\right)_{\text{TE}} = r_E^{\text{TE}} \tag{18}$$

$$t_H^{\text{TE}} = \left(\frac{H_{ot}}{H_o}\right)_{\text{TE}} = \frac{Z_1}{Z_2} t_E^{\text{TE}} = \frac{n_{am,2}^{\text{TE}}}{n_{am,1}^{\text{TE}}} t_E^{\text{TE}}. \tag{19}$$

Equations (16)–(19) are the generalized Fresnel equations for the reflectivity and transmissivity of a TE polarized plane wave. These equations require the definition of an amplitude refractive index that in general differs from the phase refractive index. Most lossless dielectric materials, however, have a relative permeability (μ_r) of unity. In this case of nonmagnetic dielectrics, the amplitude and phase refractive indexes are equal (as can be seen from (3) and (15)). Thus the distinction between the amplitude and phase refractive indexes is usually ignored. This is why the Fresnel equations are often written in terms of the phase refractive indexes in optics texts [29], [30]. It is important to note, however, that in general one must use the phase refractive index for phase matching, and a differing amplitude refractive index for calculation of the reflectivity and transmissivity of a dielectric interface.

2) TM Polarization: For a TM polarized plane wave shown in Fig. 2(b), the polarization in which the magnetic field (H) is parallel to the interface, the phase matched boundary conditions reduce to

$$(H_o/Y_1)\cos\theta_1 - (H_{or}/Y_1)\cos\theta_1 = (H_{ot}/Y_2)\cos\theta_2 \tag{20}$$

$$H_o + H_{or} = H_{ot} \tag{21}$$

$$(H_o^2/Y_1)\cos\theta_1 - (H_{or}^2/Y_1)\cos\theta_1 = (H_{ot}^2/Y_2)\cos\theta_2 \tag{22}$$

where Y_i is the characteristic admittance of the bulk medium i for $i = 1$ and $i = 2$. The characteristic admittance is defined as the ratio of the magnetic field amplitude to the electric field amplitude and is the reciprocal of the characteristic impedance, yielding $Y_i \triangleq |\vec{H}_i|/|\vec{E}_i| = \sqrt{\epsilon_i \epsilon_{\text{ref}}/\mu_i \mu_{\text{ref}}} = 1/Z_i$. By combining any two of the above three phase matched boundary conditions, the equations for the reflectivity and transmissivity of the magnetic field can be expressed as a function of the angles of propagation and the dielectric admittances:

$$r_H^{\text{TM}} = \left(\frac{H_{or}}{H_o}\right)_{\text{TM}} = \frac{Y_2\cos\theta_1 - Y_1\cos\theta_2}{Y_2\cos\theta_1 + Y_1\cos\theta_2} \tag{23}$$

$$t_H^{\text{TM}} = \left(\frac{H_{ot}}{H_o}\right)_{\text{TM}} = \frac{2Y_2\cos\theta_1}{Y_2\cos\theta_1 + Y_1\cos\theta_2}. \tag{24}$$

As was performed for TE polarization, the reflectivity and transmissivity of the interface can be rewritten in terms of normalized admittances through the use of an amplitude refractive index. The TM amplitude refractive index is defined in an analogous manner to the TE amplitude refractive index as

$$n_{am}^{\text{TM}} = Y_{\text{ref}}/Y = \sqrt{\mu_r/\epsilon_r} = 1/n_{am}^{TE} \tag{25}$$

where the vacuum is chosen as the reference region.

Using this definition for the TM amplitude refractive index (see (25)), the equations for the reflectivity and transmissivity of the magnetic field can be written in terms of the amplitude refractive indexes as

$$r_H^{\text{TM}} = \left(\frac{H_{or}}{H_o}\right)_{\text{TM}} = \frac{n_{am,1}^{\text{TM}}\cos\theta_1 - n_{am,2}^{\text{TM}}\cos\theta_2}{n_{am,1}^{\text{TM}}\cos\theta_1 + n_{am,2}^{\text{TM}}\cos\theta_2} \tag{26}$$

$$t_H^{\text{TM}} = \left(\frac{H_{ot}}{H_o}\right)_{\text{TM}} = \frac{2n_{am,1}^{\text{TM}}\cos\theta_1}{n_{am,1}^{\text{TM}}\cos\theta_1 + n_{am,2}^{\text{TM}}\cos\theta_2}. \tag{27}$$

As was the case for TE polarization, the equations for the reflectivity and transmissivity of the electric field can be obtained using Maxwell's curl equations, and are

$$r_E^{\text{TM}} = \left(\frac{E_{or}}{E_o}\right)_{\text{TM}} = r_H^{\text{TM}} \tag{28}$$

$$t_E^{\text{TM}} = \left(\frac{E_{ot}}{E_o}\right)_{\text{TM}} = \frac{Y_1}{Y_2} t_H^{\text{TM}} = \frac{n_{am,2}^{\text{TM}}}{n_{am,1}^{\text{TM}}} t_H^{\text{TM}}. \tag{29}$$

Equations (26)–(29) are the generalized Fresnel equations for the reflectivity and transmissivity of TM polarized light. The amplitude refractive index in these equations is the reciprocal of the amplitude refractive index for TE polarization. In an analogous manner to TE polarization, there is a special case, $\epsilon_r = 1$, in which the TM amplitude refractive index and the phase refractive index are identical. In this case, the phase refractive index can be used to calculate the reflectivity (transmissivity) at the interface. Although this case is not common for lossless dielectric materials, and thus not generally used in optics, it is important to note that there is nothing "special" about TE polarization that allows the amplitude refractive index to be identical to the phase refractive index. It just happens that most lossless dielectric materials have a relative permeability of unity, leading to identical TE amplitude and phase refractive indexes. For general dielectrics, three separate refractive indexes are required in order to use the unified results given in this paper: one for phase matching, one for TE reflectivity (transmissivity), and one for TM reflectivity (transmissivity). These refractive indexes are summarized in Table 1.

Table 1 Phase and Amplitude Refractive Indexes for Electromagnetic and Electron Waves

Index	Symbol	Electromagnetic Wave		Electron Wave
		TE	TM	EW
Phase	n_{ph}	$\sqrt{\mu_r\epsilon_r}$	$\sqrt{\mu_r\epsilon_r}$	$\sqrt{m_r^*(KE)_r}$
Amp.	n_{am}	$\sqrt{\epsilon_r/\mu_r}$	$\sqrt{\mu_r/\epsilon_r}$	$\sqrt{(KE)_r/m_r^*}$

3) Duality between TE and TM:

The reflectivity and transmissivity results for TE and TM polarized light are summarized in Table 2. The reflectivity and transmissivity for the electric (magnetic) field of a TE (TM) polarized wave are the same as those for the magnetic (electric) field of a TM (TE) polarized wave, where the TE amplitude refractive index (n_{am}^{TE}) is used for TE polarization and the TM amplitude refractive index (n_{am}^{TM}) is used for TM polarization. The similarity between the TE and TM reflectivity (transmissivity) results can be clarified by considering the polarization directions for both cases. For TE polarized light the electric field is parallel to the interface (tangential) and the magnetic field has a component normal to the interface (nontangential). For TM polarized light, the magnetic field is parallel to the interface (tangential) and the electric field has a component normal to the interface (nontangential). Thus there is one equation for the reflectivity (transmissivity) of the tangential field component (E for TE and H for TM) and another equation for the reflectivity (transmissivity) of the nontangential field component (H for TE and E for TM).

The duality between the reflectivity and transmissivity of TE and TM polarized light could alternatively be derived through the application of Babinet's principle [31] which states that if $\vec{E}_{a,n}$ and $\vec{H}_{a,n}$ are solutions to Maxwell's wave equation where $n = i, r, t$ for incident, reflected, and transmitted waves respectively, then the fields $\vec{E}_{b,n} = \mp Z_n \vec{H}_{a,n}$ and $\vec{H}_{b,n} = \pm Y_n \vec{E}_{a,n}$ are also solutions to Maxwell's equations. If field a describes TE polarization and satisfies the boundary conditions, the application of Babinet's transformation shows that field b describes TM polarization and also satisfies the boundary conditions. If the transformations are applied to the boundary conditions for TE polarization (field a) given in (10)–(12), the resultant equations are identical to the phase matched boundary conditions for TM polarization (field b) given in (20)–(22). Thus the reflectivity (transmissivity) for TM polarized light could be calculated through the application of Babinet's transformation to the boundary conditions for the dual TE problem. The fact that the equations describing TE and TM polarizations have the same functional form is a manifestation of this duality principle and is required by Maxwell's equations.

B. Electron Wave Amplitude Refractive Index

The directions of propagation of the reflected and transmitted EW's from a semiconductor interface (Fig. 3) were calculated by using phase matching considerations. The relative amplitudes of the reflected and transmitted EW's can be calculated from the phase matched boundary conditions, as they were in the electromagnetic case. The reflectivity and transmissivity of the EW amplitude can be calculated by considering any two of the following three boundary conditions: continuity of the EW amplitude across the boundary, continuity of the transmitted component of the gradient of the EW amplitude, and conservation of the transmitted component of the probability current, $\vec{J} \cdot \hat{z}$, where the probability current is defined as $J = \hbar/2jm^*[\nabla\psi^*\psi - \psi^*\nabla\psi]$ [32]. The analogy between the continuity of the wavefunction (gradient of the wavefunction) and the electromagnetic boundary conditions matching the tangential field component (nontangential field component) were developed in Section III. The third boundary condition, the conservation of probability current across the interface, is analogous to the conservation of power flow across the boundary in electromagnetics, since both are expressions of the conservation of the transmitted wave intensity.

In order to calculate the reflectivity (transmissivity) of the EW, a characteristic amplitude constant, X, will be defined in the same manner as was the characteristic impedance for TE polarization and the characteristic admittance for TM polarization, as

$$X = \frac{|\psi|}{|\nabla\psi|/m^*} = \sqrt{\frac{\hbar^2 m^*}{2(KE)}}. \tag{30}$$

This characteristic amplitude constant is analogous to the characteristic impedance for TE polarization, in which case $|E|$ is analogous ($\sim$) to $|\dot{\psi}|$ and $|H| \sim (1/m^*)|\nabla\psi|$, and to the characteristic admittance for TM polarization, in which case $|H| \sim |\psi|$ and $|E| \sim (1/m^*)|\nabla\psi|$. This characteristic amplitude constant has the same form as the characteristic impedance defined in a transmission line description of resonant tunneling processes in semiconductors (where $|E| \sim |\dot{\psi}|$) [33]. Using the characteristic amplitude constant, the equations for the reflectivity and transmissivity of the material interface can be calculated as

$$r_\psi^{EW} = \left(\frac{\psi_{or}}{\psi_o}\right) = \frac{X_2\cos\theta_1 - X_1\cos\theta_2}{X_2\cos\theta_1 + X_1\cos\theta_2} \tag{31}$$

$$t_\psi^{EW} = \left(\frac{\psi_{ot}}{\psi_o}\right) = \frac{2X_2\cos\theta_1}{X_2\cos\theta_1 + X_1\cos\theta_2}. \tag{32}$$

By inspection of the above equations, it is apparent that the reflectivity (transmissivity) of an EW incident upon a potential barrier have the same form as the equations describing the reflectivity (transmissivity) of the electric field for TE polarization [r_E^{TE}, (13)] and the reflectivity (transmissivity) of the magnetic field for TM polarization [r_H^{TM}, (23)]. Thus the reflectivity (transmissivity) of the EW is analogous to the reflectivity (transmissivity) of the tangential component of the EMW. As would be expected, the equations describing the reflectivity (transmissivity) of the gradient of the EW amplitude have the same form as the equations describing the reflectivity (transmissivity) of the nontangential component of the EMW (r_H^{TE} and r_E^{TM}). That is,

$$r_{\nabla\psi/m^*}^{EW} = \left(\frac{|\nabla\psi_r|/m_1^*}{|\nabla\psi_o|/m_1^*}\right) = r_\psi^{EW} \tag{33}$$

$$t_{\nabla\psi/m^*}^{EW} = \left(\frac{|\nabla\psi_t|/m_2^*}{|\nabla\psi_o|/m_1^*}\right) = \frac{X_1}{X_2} t_\psi^{EW}. \tag{34}$$

The analogy between the reflectivity (transmissivity) of the EW amplitude and the reflectivity (transmissivity) of

Table 2 Reflectivity and Transmissivity Expressions for Electromagnetic Waves (TE and TM) and Electron Waves

Quantity	Electromagnetic		Electron	Expression
	TE	TM	EW	
Reflectivity	r_E^{TE}	r_H^{TM}	r_ψ^{EW}	$\frac{n_{am,1}\cos\theta_1 - n_{am,2}\cos\theta_2}{n_{am,1}\cos\theta_1 + n_{am,2}\cos\theta_2}$
Reflectivity	r_H^{TE}	r_E^{TM}	$r_{\nabla\psi/m^*}^{EW}$	$\frac{n_{am,1}\cos\theta_1 - n_{am,2}\cos\theta_2}{n_{am,1}\cos\theta_1 + n_{am,2}\cos\theta_2}$
Transmissivity	t_E^{TE}	t_H^{TM}	t_ψ^{EW}	$\frac{2n_{am,1}\cos\theta_1}{n_{am,1}\cos\theta_1 + n_{am,2}\cos\theta_2}$
Transmissivity	t_H^{TE}	t_E^{TM}	$t_{\nabla\psi/m^*}^{EW}$	$\frac{2n_{am,2}\cos\theta_1}{n_{am,1}\cos\theta_1 + n_{am,2}\cos\theta_2}$

the tangential component of the EMW can be understood as follows. The EW boundary conditions describing the EW continuity at the boundary are scalar equations. The EMW boundary conditions describing the continuity of the tangential field component have the same form as the EW scalar equations, since the field is tangential to the interface. Therefore, the EW amplitude reflectivity (transmissivity) equation has the same form as the tangential EMW component reflectivity (transmissivity) equation. The gradient of the EW amplitude, on the other hand, is a vector that points in the direction of propagation of the EW. Thus the boundary condition describing the continuity of the transmitted component of the gradient of the EW amplitude are vector equations that require resolution of the gradient in the direction normal to the interface. The EMW boundary conditions for the nontangential field require a resolution of the field component in the direction tangential to the interface. Therefore, the reflectivity (transmissivity) of the gradient of the EW amplitude has the same form as the reflectivity (transmissivity) of the nontangential EMW component.

These analogies show that there is no inherent analogy between one of the EMW field amplitudes (E or H) and the EW amplitude. For bulk propagation, the EW amplitude is analogous to either E or H. For propagation past an interface, the EW amplitude is analogous to the tangential component of the electromagnetic field.

By defining the EW amplitude refractive index, the equations for the EW reflectivity and transmissivity can be expressed in terms of normalized quantities as were the EMW equations. The amplitude refractive index is defined as the ratio of the characteristic amplitude constant of a reference medium to the characteristic amplitude constant of the medium of propagation [(15) and (25)],

$$n_{am}^{EW} \triangleq X_{ref}/X = \sqrt{(KE)_r/m_r^*} \tag{35}$$

where the characteristic amplitude constant of the reference region is found through (30).

With this expression for the amplitude refractive index the reflectivity and transmissivity of the EW amplitude can be expressed as

$$r_\psi^{EW} = \left(\frac{\psi_{or}}{\psi_o}\right) = \frac{n_{am,1}^{EW}\cos\theta_1 - n_{am,2}^{EW}\cos\theta_2}{n_{am,1}^{EW}\cos\theta_1 + n_{am,2}^{EW}\cos\theta_2}, \tag{36}$$

$$t_\psi^{EW} = \left(\frac{\psi_{ot}}{\psi_o}\right) = \frac{2n_{am,1}^{EW}\cos\theta_1}{n_{am,1}^{EW}\cos\theta_1 + n_{am,2}^{EW}\cos\theta_2}. \tag{37}$$

Through the definition of the EW amplitude refractive index, the expression for the reflectivity and transmissivity at a semiconductor material boundary are identical to the expression for the reflectivity and transmissivity of the tangential component of the electromagnetic field. A general set of equations that can be used to describe the reflectivity and transmissivity for TE polarization, TM polarization, and EW's is given in Table 2. As is the case in electromagnetics, there is a special case in which the electron wave phase refractive index is equal to the electron wave amplitude refractive index. For EW's this occurs when the effective masses are equal on the two sides of the boundary. This constant effective mass case is analogous to the nonmagnetic dielectric case ($\mu_r = 1$) for TE polarization and the $\epsilon_r = 1$ case for TM polarization. In many material systems (such as $Ga_{1-x}Al_xAs$), however, the effective mass can change by more than 50% across a material interface. In these material systems, the dependence of the effective mass in the amplitude refractive index is important, requiring the use of the EW amplitude refractive index in the reflectivity (transmissivity) expressions for general dielectrics. For this reason, it is instructive to analyze the reflection (transmission) properties of general dielectric interfaces. This analysis is performed in the next two sections, and the results are applied to the $Ga_{1-x}Al_xAs$ material system in Section VII.

V. Total Internal Reflection

In Section III, phase matching considerations were used to calculate an expression for the refracted angle for both an EMW incident upon a boundary between dielectrics and an EW incident upon a boundary between semiconductor materials, yielding $n_{ph,1}\sin\theta_1 = n_{ph,2}\sin\theta_2$ (see (8)). This phase matching condition cannot be satisfied if

$$n_{ph,1} > n_{ph,2} \quad \text{and} \quad \theta_1 > \theta_c = \sin^{-1}(n_{ph,2}/n_{ph,1}), \tag{38}$$

where θ_c is referred to as the critical angle. When the phase matching condition is not satisfied, there is no transmitted wave. This condition corresponds to total internal reflection (TIR). In order to have a real critical angle, the parameters of the materials adjoining the interface must satisfy the first

part of (38). In order to have TIR, the incident angle must satisfy the second part of (38).

For optical nonmagnetic dielectric interfaces, (38), shows that TIR can occur if $\epsilon_1 > \epsilon_2$ where the critical angle is given as $\theta_c = \sin^{-1}(\sqrt{\epsilon_2/\epsilon_1})$. For general dielectrics and semiconductor interfaces, the range of material combinations that allow a critical angle is shown as the shaded region in Fig. 4, where $\Omega = \mu_1/\mu_2$ and $\Gamma = \epsilon_1/\epsilon_2$ for EMW's, and $\Omega = m_1^*/m_2^*$ and $\Gamma = (KE)_1/(KE)_2$ for electron waves. The hyperbola $\Omega\Gamma = 1$ ($n_{ph,1} = n_{ph,2}$) represents the onset of TIR, where the critical angle (θ_c) is equal to 90 deg. For material combinations below this curve ($\Omega\Gamma < 1$), the phase refractive index in region 2 is larger than the phase refractive index in region 1 and total internal reflection will not occur for any angle of incidence. For material combinations above this curve ($\Omega\Gamma > 1$), there is a real critical angle for the interface. A given critical angle θ_c is represented on the graph by the hyperbola $\Omega\Gamma = 1/\sin^2\theta_c$. As the product $\Omega\Gamma$ is increased from unity, the value of the critical angle decreases, approaching normal incidence as the product $\Omega\Gamma$ approaches infinity. Plots of the material combinations that yield a constant critical angle are shown for $\theta_c = 90$, 66.5, 45, and 22.5 deg.

The above conditions for TIR reduce to the standard expressions for the nonmagnetic dielectric case in which $\mu_1 = \mu_2 = 1$. This nonmagnetic dielectric condition is represented in Fig. 4 by the line $\Omega = 1$. Considering only the line $\Omega = 1$ gives the condition for a critical angle as $\Gamma > 1$, which reduces to, $\epsilon_1 > \epsilon_2$, the familiar nonmagnetic dielectric condition for TIR. In the electron wave case, the line $\Omega = 1$ corresponds to the effective masses being equal, $m_1^* = m_2^*$, in which case the condition for having total internal reflection is $(KE)_1 > (KE)_2$.

Since a given critical angle is represented by the curve $\Omega\Gamma = 1/\sin^2\theta_c$, there is an infinite set of relative material combinations that can be used to achieve a given critical angle. In electromagnetics, it is generally not possible to obtain lossless dielectrics with arbitrary permittivity and permeability. Thus it is difficult to use regions in Fig. 4 other than the line $\Omega = 1$. In this case, the critical angle is limited to the intersection of the line $\Omega = 1$ and the curve of constant critical angle. In semiconductor materials, since the kinetic energy and effective mass often differ on the two sides of an interface, there is more flexibility in the design of TIR devices such as EW waveguides [34]. This effective mass dependence on the critical angle is manifested in the $Ga_{1-x}Al_xAs$ material system in which TIR can occur from a potential drop due to the effective mass difference on the two sides of the boundary. The critical angle results discussed in this section are applied to the $Ga_{1-x}Al_xAs$ material system in Section VII.

VI. Brewster Angle

In electromagnetics, the Brewster angle is defined as the angle of incidence that produces zero reflectivity at the interface between two dielectrics. At this angle, the incident wave is totally transmitted. By solving the equation

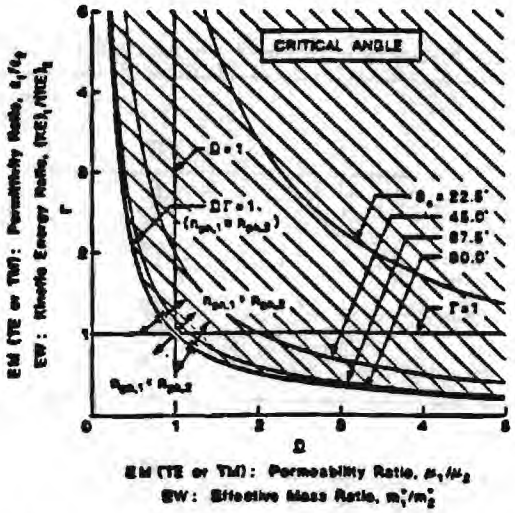

Fig. 4. The shaded region shows the range of material parameters (for the materials adjoining an interface) that allow for a real critical angle. This graph is valid for both general dielectric interfaces [$\Omega = \mu_1/\mu_2$ and $\Gamma = \epsilon_1/\epsilon_2$] and semiconductor interfaces [$\Omega = m_1^*/m_2^*$ and $\Gamma = (KE)_1/(KE)_2$]. Contour plots show the range of material parameters that results in a given critical angle for $\theta_c = 90$, 66.5, 45, and 22.5 *deg*. This graph shows that for general dielectric and semiconductor interfaces, there is an infinite set of material combinations that results in a given critical angle. For nonmagnetic dielectrics ($\mu_r = 1$), the shaded regions reduce to the familiar condition for a critical angle, $\epsilon_1 > \epsilon_2$.

for zero reflectivity (for either an EMW incident upon a boundary between two dielectrics or an EW incident upon an interface between semiconductor materials) the equation for the Brewster, θ_B, is found to be given as

$$\theta_B = \sin^{-1}\left(\sqrt{(1-\Lambda/\Upsilon)/(1-\Lambda^2)}\right) \qquad (39)$$

where Λ and Υ are functions of the material parameters. Since the amplitude refractive indexes differ for TE polarization, TM polarization, and electron waves, the definitions of Λ and Υ also differ. For TE polarization, $\Lambda = \mu_1/\mu_2$ and $\Upsilon = \epsilon_1/\epsilon_2$; for TM polarization, $\Lambda = \epsilon_1/\epsilon_2$ and $\Upsilon = \mu_1/\mu_2$; and for electron waves, $\Lambda = m_1^*/m_2^*$ and $\Upsilon = (KE)_1/(KE)_2$. In order for the interface to have a real Brewster angle, the argument of the square root in (39) must lie between 0 and 1. The ranges of material parameters that yield a real θ_B are shown as the shaded regions in Fig. 5. The material combinations that lie in these regions have a Brewster angle given by (39). These regions are bounded by the curve $\Lambda\Upsilon = 1$, which is the condition $n_{ph,1} = n_{ph,2}$, and by the curve $\Lambda = \Upsilon$, which is the condition $n_{am,1} = n_{am,2}$. The material combinations that lie along the boundary curve $\Lambda\Upsilon = 1$ do not have a Brewster angle. For the material combinations along this curve, the reflectivity is a constant and is not a function of the angle of the incident wave! The material combinations that lie on the line $\Lambda = \Upsilon$ have a Brewster angle at normal incidence. In other words, there is no reflected wave at normal incidence for these material combinations! For the material parameters in between these two boundary curves the Brewster angle is given by (39). Contour plots of

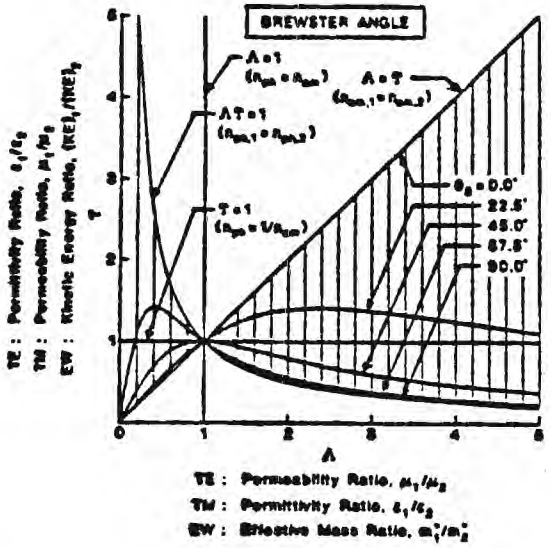

Fig. 5. The shaded region shows the range of material parameters (for the materials adjoining an interface) that allow for a real Brewster angle. This graph is valid for both electromagnetic waves (TE and TM), and electron waves. Contour plots show the range of material parameters that results in a given Brewster angle for θ_B = 90, 66.5, 45, 22.5, and 0 *deg*. Along the boundary curve $\Lambda\Upsilon = 1$ there is no Brewster angle; along the boundary curve $\Lambda = \Upsilon$ the Brewster angle occurs at normal incidence. For general dielectrics, a Brewster angle can occur for TE polarization, TM polarization, both polarizations, or neither polarization. Likewise, a Brewster angle may or may not occur at a semiconductor interface, depending on the material parameters.

material combinations for five constant Brewster angles (0, 22.5, 45, 66.5, and 90 deg) are shown in Fig. 5. For small Brewster angles, the material combinations stay close to the line $\Lambda = \Upsilon$, for small values of Υ, but approach the curve $\Lambda\Upsilon = 1$, as Υ approaches infinity. As the value of the Brewster angle is increased, the material combinations move away from the line $\Lambda = \Upsilon$ and toward the curve $\Lambda\Upsilon = 1$ at a faster rate. As the Brewster angle approaches grazing incidence, the material parameters rise sharply for small values of Υ and rapidly approach the curve $\Lambda\Upsilon = 1$. It should be noted that all Brewster angles pass through the point $\Lambda = \Upsilon = 1$. At this point, the two materials are the same and there is no interface; thus all of the incident wave is transmitted for every angle of incidence.

All of the above results are valid for both an EMW incident upon an interface between two general dielectrics and an EW incident upon a boundary between two semiconductor materials. In addition, the results are valid for both TE and TM polarizations in the electromagnetic case. Thus for general dielectric, there are ranges of material parameters that allow for a Brewster angle for TE polarization as well as for TM polarization. This result might seem to contradict the common optical understanding that a Brewster angle always occurs for TM polarization, and never occurs for TE polarization. This contradiction can be resolved by considering the case for nonmagnetic dielectric materials ($\mu_1 = \mu_2$), in which the graph in Fig. 5 is reduced to the line $\Lambda = 1$ (for TE polarization). It is apparent that this line does not intersect either region that allows for a Brewster angle. Thus there is no TE Brewster angle for nonmagnetic dielectric materials. The restriction to nonmagnetic dielectric materials reduces the TM polarization graph to the line $\Upsilon = 1$. This line is completely contained in the regions that have a Brewster angle. Thus there is a TM Brewster angle for all combinations of nonmagnetic dielectric materials. In general, however, one, both, or neither of the polarizations can have a Brewster angle. For most material combinations, either the TE polarized wave or the TM polarized wave will have a Brewster angle. For those material combinations that lie along the line $\Lambda\Upsilon = 1$, neither of the polarizations will have a Brewster angle; the reflectivity is independent of angle. For those material combinations that lie along the curve $\Lambda = \Upsilon$, both polarizations will have a Brewster angle at normal incidence (TE and TM polarization are identical at normal incidence). For all other material combinations, either one or the other of the polarizations will have a Brewster angle.

For material interfaces in which the effective mass is the same on the two sides of the boundary, no Brewster angle will occur. This result can be obtained directly from Fig. 5. The constant effective mass case ($m_1^* = m_2^*$) reduces Fig. 5 to the line $\Lambda = 1$. It is apparent from the graph that this line does not pass through the regions that have a Brewster angle. This condition is analogous to the nonmagnetic dielectric case ($\mu_r = 1$) for TE polarization and the $\epsilon_r = 1$ case for TM polarization. Thus an effective mass difference (across the interface) is required for an EW to have a Brewster angle. These results are applied to the $Ga_{1-x}Al_xAs$ material system in the next section where it is shown that all interfaces created in this material system will have a Brewster angle.

VII. Electron Wave Reflection and Refraction in $Ga_{1-x}Al_xAs$

The results that were derived for the reflectivity and transmissivity of an EW at a material interface can be directly applied to heterostructures in the $Ga_{1-x}Al_xAs$ material system. By inserting the appropriate expressions for the kinetic energy and effective mass into the expressions defining the phase and amplitude refractive indexes (see Tables 1 and 2) the reflectivity characteristics of a $Ga_{1-x1}Al_{x1}As/Ga_{1-x2}Al_{x2}As$ interface can be analyzed as a function of EW energy. For this material system, the potential energy and effective mass are a function of total electron energy ($\mathcal{E}$) and aluminum composition (x). It is instructive to analyze the ranges of EW energies and boundary compositions that allow for TIR (critical angle, θ_c) and zero reflectivity (Brewster angle, θ_B). The reflectivity of the boundary will be considered for two cases: $x_1 < x_2$ which is a potential rise shown in Fig. 6 and $x_1 > x_2$ which is a potential drop shown in Fig. 7.

For interfaces constructed using the $Ga_{1-x}Al_xAs$ material system, the range of usable compositions that maintain direct gap semiconductors is given as $0 \leq x_i \leq 0.45$. The electron kinetic energy and effective mass for electrons in

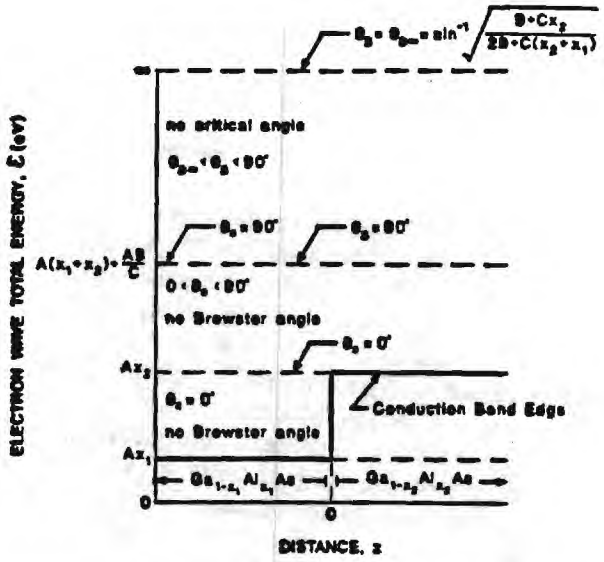

Fig. 6. Ranges of electron energies (Γ point) that allow for a critical and/or a Brewster angle at a semiconductor interface in the $Ga_{1-x}Al_xAs$ material system with $x_1 < x_2$. The electron wave is incident upon the interface from the left ($z < 0$). For electron waves with energies below Ax_2, all electrons will be totally internally reflected because $\theta_c = 0$. For electron waves with energies below $A(x_1+x_2)+AB/C$, there will be a nonzero critical angle, but no Brewster angle. For electron waves with energies above this critical energy, there will be no critical angle but there will be a Brewster angle. The asymptotic value of the Brewster angle is shown on the figure.

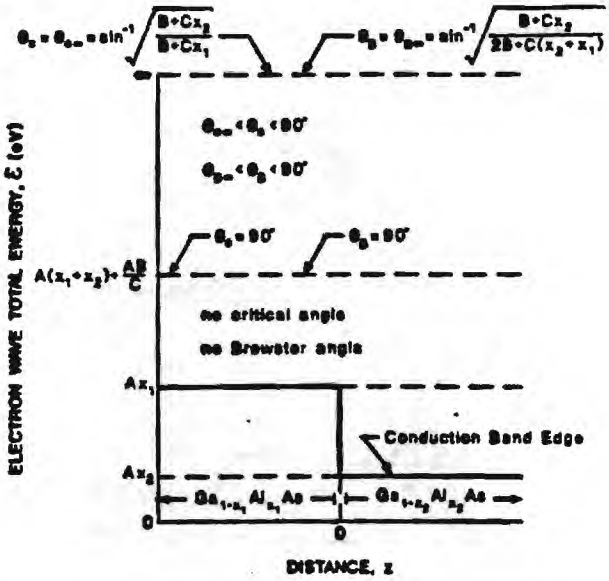

Fig. 7. Ranges of electron energies (Γ point) that allow for a critical and/or a Brewster angle at a semiconductor interface in the $Ga_{1-x}Al_xAs$ material system with $x_1 > x_2$. The electron wave is incident upon the interface from the left ($z < 0$). For electron waves with energies below $A(x_1 + x_2) + AB/C$, there is no critical angle or Brewster angle. For electron waves with energies above this critical energy, there will be both a critical angle and a Brewster angle. The asymptotic values of the Brewster and critical angle are shown on the figure.

the Γ valley in each of the two regions are given as [35]

$$(KE)_i = \mathcal{E} - Ax_i, \quad m_i^* = m_o(B+Cx_i), \quad i = 1,2 \tag{40}$$

where A, B, and C are constants, m_o is the free electron mass, and the bottom of the conduction band in pure GaAs is used as the zero of total energy. For $Ga_{1-x}Al_xAs$, $A = 0.77314$ eV (assuming a 62% conduction band offset [35]–[38]), $B = 0.067$, and $C = 0.083$ [35]. By using (40) for the kinetic energy and effective mass, the existence of both a critical angle and a Brewster angle can be investigated as a function of compositions (x_1 and x_2) and total electron energy ($\mathcal{E}$).

For this material system, the ratio of effective masses in the two regions is limited by the range of usable compositions given above. For interfaces with $x_1 < x_2$, the range of effective mass ratios (Ω for TIR and Υ for Brewster angle) is limited to the region $B/(B+0.45C) \leq m_1^*/m_2^* \leq 1$. For interfaces with $x_1 > x_2$, the range of effective mass ratios is limited to the region $1 \leq m_1^*/m_2^* \leq (B + 0.45C)/B$. These regions are shown graphically as the dotted regions of Fig. 8. In the case of the potential rise ($x_1 < x_2$), when $(KE)_2$ is equal to zero, the ratio of kinetic energies (Γ for TIR and Λ for Brewster angle) is equal to infinity. As the kinetic energy in the output region is increased, the ratio of kinetic energies decreases, approaching unity as $(KE)_2$ approaches infinity. The compositional difference of the rise gives the effective mass ratio (see (40)), fixing the ordinate of the graph. The energy dependence of the critical and Brewster angles is given as a vertical line at this ordinate. The points of intersection between the curves of constant critical (Brewster) angle and this line give the values of the EW kinetic energy that yield a given critical (Brewster) angle for the chosen compositional difference. An example line is shown in Fig. 8, where $x_1 = 0$ and $x_2 = 0.3$. The kinetic energy dependence of the critical and Brewster angle of a potential drop behaves in a similar manner to the potential rise. When $(KE)_1$ is equal to zero, the ratio of kinetic energies is equal to zero. As the kinetic energy in the input region increases, the ratio of kinetic energies increases, approaching unity as $(KE)_1$ approaches infinity. Again, the compositional difference fixes the ordinate on the graph. The ratio of kinetic energies for a given critical (Brewster) angle is given by the intersection of the curves of constant critical (Brewster) angle with a vertical line at the ordinate fixed by the effective mass ratio. A sample line is shown in Fig. 8 for a potential drop of $x_1 = 0.3$ and $x_2 = 0.0$. These energy dependencies of the critical and Brewster angle can be used to show the regions of EW input energies that allow a critical angle and/or a Brewster angle. These regions are discussed as follows.

For the potential rise (Fig. 6), if the electron energy in region 1 is less than the size of the potential rise, i.e., if $(KE)_1 < A(x_2 - x_1)$, then the EW will experience TIR from the potential barrier for all angles of incidence. For these electron energies, the critical angle θ_c occurs at normal incidence ($\theta_c = 0$). As $(KE)_1$ is increased past $A(x_2 - x_1)$, the EW will be partially transmitted at normal

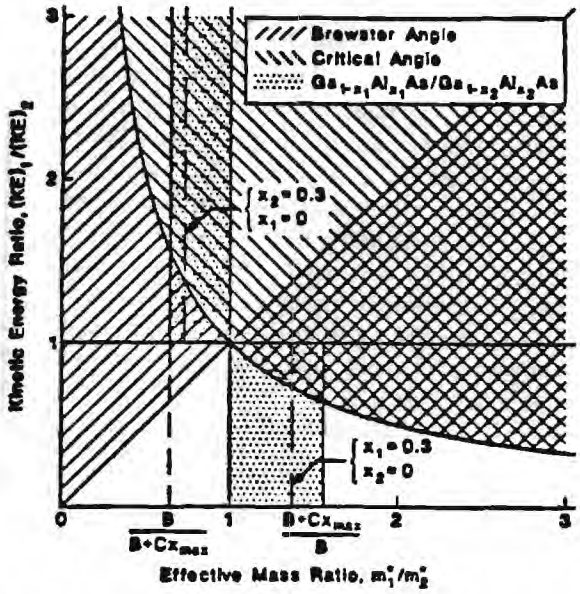

Fig. 8. Range of material parameters that are possible for direct gap interfaces in the $Ga_{1-x}Al_xAs$ material system. The dotted regions show the allowed effective mass and kinetic energy differences for this material system. The left rectangle is for interfaces with $x_2 > x_1$ and the right rectangle is for interfaces with $x_1 > x_2$. The intersection of these regions with the regions for a critical and Brewster angle can be used to calculate the results shown in Figs. 6 and 7. The effective mass difference of the interface reduces the rectangle to a vertical line, where the abscissa of the line is fixed by the kinetic energy. The intersection of the constant critical (Brewster) angle curves with this line, gives the value of the critical (Brewster) angle for each energy at the interface. Two example lines are shown.

incidence, but it will achieve TIR for all incident angles (θ_1) greater than the critical angle given by

$$\theta_c = \sin^{-1}\sqrt{\frac{(\mathcal{E}-Ax_2)(B+Cx_2)}{(\mathcal{E}-Ax_1)(B+Cx_1)}}. \tag{41}$$

As $(KE)_1$ is further increased, the critical angle increases from normal incidence, until the critical angle reaches grazing incidence at the electron energy $\mathcal{E}_c = A(x_1+x_2)+AB/C$. For all electron energies larger than $\mathcal{E}_c$, the EW will not experience TIR for any angle of incidence. At these energies, a fraction of the EW amplitude will be transmitted for all angles of incidence. The critical energy $\mathcal{E}_c$ is the energy at which the EW phase refractive indexes are equal on the two sides of the boundary ($n_{ph,1} = n_{ph,2}$). For EW's with energies less than this critical value, $n_{ph,1} > n_{ph,2}$ and TIR can occur. For EW's with energies greater than $\mathcal{E}_c$, $n_{ph,1} < n_{ph,2}$ and TIR can no longer occur. For EW's with energies equal to $\mathcal{E}_c$, the incident, reflected, and transmitted angles are all equal since the phase refractive indexes are equal on the two sides of the boundary.

The energy dependence of the Brewster angle for the potential rise of Fig. 6 follows a reciprocal behavior of the critical angle. For EW energies below the critical energy $\mathcal{E}_c$, there is no Brewster angle. As the EW energy is increased an infinitesimal amount above $\mathcal{E}_c$, a Brewster angle occurs at grazing incidence. For all EW energies above $\mathcal{E}_c$, there will be a Brewster angle given by

$$\theta_B = \sin^{-1}\sqrt{\frac{1-(\mathcal{E}-Ax_2)(B+Cx_1)/(\mathcal{E}-Ax_1)(B+Cx_2)}{1-(B+Cx_1)^2/(B+Cx_2)^2}}. \tag{42}$$

As the EW energy is further increased above $\mathcal{E}_c$, the Brewster angle decreases asymptotically to the value $\theta_{B\infty} = \sin^{-1}\sqrt{(B+Cx_2)/(2B+C(x_1+x_2))}$ as the energy approaches infinity. Thus for electron energies below the critical value $\mathcal{E}_c$, a fraction of the electron probability current will always be reflected. For electron energies above the critical value $\mathcal{E}_c$, there is an angle of incidence for each electron energy for which the electron probability current will be totally transmitted. As the EW energy approaches infinity, the angle of incidence that allows for total transmission asymptotically approaches the value $\theta_{B\infty}$. It is interesting to note that the asymptotic value of the Brewster angle is not normal incidence. This is because the reflectivity at normal incidence does not go to zero for high energies due to the effective mass difference. At high EW energies, the kinetic energy difference becomes negligible but the effective mass difference remains.

The energy dependence of the critical angle and the Brewster angle for a potential drop (Fig. 7) are similar to the results discussed above for the potential rise. In fact, these results predict a region of EW energies for which an EW can be totally internally reflected from a potential drop. This TIR occurs for energies at which the relative difference in effective masses is larger than the relative change in kinetic energies. Thus TIR will occur at a potential drop for electron energies whose input kinetic energy is significantly larger than the magnitude of the potential drop. The onset of TIR for a potential drop occurs at the same critical energy ($\mathcal{E}_c$) at which the TIR disappeared for the potential rise. For electron energies below $\mathcal{E}_c$, there is no critical angle. At these energies, all electron waves will be partially transmitted past the interface. As the electron energy is increased infinitesimally above $\mathcal{E}_c$, TIR occurs at grazing incidence. As the energy is further increased above $\mathcal{E}_c$, the critical angle asymptotically approaches the value $\theta_{c\infty} = \sin^{-1}\sqrt{(B+Cx_2)/(B+Cx_1)}$.

The Brewster angle behavior of the potential drop is the same as the Brewster angle behavior for the potential rise. For angles less than $\mathcal{E}_c$, there is no Brewster angle. For all EW's with energies above $\mathcal{E}_c$, there is a Brewster angle that is given by (42). In fact, the value of the Brewster angle for the potential drop is the refracted angle for an EW incident at the Brewster angle of the reciprocal potential rise. As the EW energy approaches infinity, the asymptotic value of the Brewster angle is again given by $\theta_{B\infty}$.

The energy dependence of the critical and Brewster angles for both the potential rise and the potential drop are summarized graphically on Figs. 6 and 7. These figures emphasize that fact that both a critical angle and a Brewster angle will exist for all interfaces in this material system. In

addition, these figures illustrate the important role of the effective mass in EW propagation in semiconductors. Merely viewing the band (potential energy) diagrams does not give complete information about the quantum reflectivity of a material interface between two semiconductors.

VIII. Summary and Discussion

A comprehensive set of analogies have been presented between electron wave propagation in semiconductors and electromagnetic propagation in general dielectrics. It has been shown that separate phase and amplitude refractive indexes are required for both cases. The phase refractive index is required for describing phase effects such as phase matching and total internal reflection, and the amplitude refractive index is required for describing amplitude effects such as the reflectivity of a material interface. For the electron wave, the phase (amplitude) refractive index is proportional to the square root of the product (ratio) of the kinetic energy and the effective mass of the medium of propagation. For the EMW, the phase (amplitude) refractive indexes is proportional to the square root of the product (ratio) of the permittivity and permeability of the medium of propagation.

By considering the phase matching and amplitude conditions of the electromagnetic boundary conditions, the reflection and refraction of an EMW incident upon an interface between two general dielectrics has been analyzed. It has been shown that one set of equations can be used to calculate the angles and the amplitudes of the reflected and transmitted waves for both TE and TM polarizations through the definition of different amplitude refractive indexes for each polarization. In addition, by applying the analogies discussed above, it has been demonstrated that the same set of expressions can be used to describe electron wave reflection and refraction at an interface between semiconductor materials through the definition of electron wave phase and amplitude refractive indexes. The behavior of the phase matching and reflectivity expressions have been determined as a function of material parameters. Through this analysis, it has been shown that for general dielectrics there are an infinite set of material parameters that produce a given critical angle. In addition, it has been shown that for general dielectrics a Brewster angle can occur for TE polarization, TM polarization, both TE and TM polarization, or neither TE nor TM polarization depending on the material parameters.

Using analogies between the electromagnetic and electron wave refractive indexes, the critical angle and Brewster angle for a semiconductor material interface have also been determined as a function of kinetic energy and effective mass of the electron wave on the two sides of the material interface. Analogous to the electromagnetic case, it has been shown that for general material systems (with arbitrary kinetic energy and effective mass), there are an infinite number of material compositions that produce a given critical angle. In addition, it has been shown that an electron wave can encounter a Brewster angle if the effective mass differs on the two sides of the boundary. For general material systems, this Brewster angle is a function of the energy of the electron wave and can occur at normal incidence for appropriate material combinations. These results for electron wave propagation have been applied to interfaces in the $Ga_{1-x}Al_xAs$ material system to determine the reflectivity of an interface as a function of electron energy and material composition. By applying this analysis, it has been shown that electron waves in the Γ band in this material system can be totally internally reflected from both a potential rise and a potential drop. In addition, it has been shown that a Brewster angle will exist for all interfaces in this material system. It should be noted that the Brewster angle calculated here for Γ band electrons in $Ga_{1-x}Al_xAs$ occurs at energies above the L band satellite minima. The analysis method, however, also applies to other material systems whose range of energies for Brewster angles may fall above or below those of any minima, depending on the material system parameters.

The present formalism can be used to analyze electron wave optical structures, such as the impressive experimental devices of Sivan *et al.* [17] and Spector *et al.* [18]–[19]. The phase matching relationships of the present work (in the limiting case of a constant effective mass throughout the device) reduce to the same expressions that they used to explain successfully the results of these electron geometrical optics experiments. In their work, a complete ray tracing analysis was performed, using the electron wave phase indexes of refraction, to predict the device response. In order to demonstrate the procedure of applying the present formalism to the analysis of electron wave optical devices, the electron wave prism switch [19] is treated. The results of this analysis are shown in Fig. 9. In this device, constructed in the two-dimensional electron gas configuration, an incident electron wave is refracted by a potential energy prism and is switched to collector A, B, or C. The potential energy prism is created by applying a gate voltage to the electrode labeled n_{ph1}^{EW}. The electron wave inside the prism (index n_{ph1}^{EW}) is incident upon the prism surface at angle θ_1 and is refracted into the output region (index n_{ph2}^{EW}) at angle θ_2. By using the current-voltage and electron density data given in [19], the index ratios ($n_{ph2}^{EW}/n_{ph1}^{EW}$) that switch the electron into collectors A, B, and C are calculated to be 1.4, 1.1, and 1.0, respectively. These index ratios would result in angles of refraction (θ_2) of 38 deg, 52 deg, and 67 deg, for collectors A, B, and C, respectively. From the geometry of the device, the ranges of incident angles that can be accepted by each collector are approximately 30 to 39 deg for collector A, 46 to 53 deg for collector B, and 60 to 68 deg for collector C. Thus the calculated angles of refraction are consistent with these angular ranges. In the limit of an index ratio of $n_{ph2}^{EW}/n_{ph1}^{EW} = \infty$, the electron wave would be refracted normal to the prism surface. For an index ratio of $n_{ph2}^{EW}/n_{ph1}^{EW} = 0.92$, the electron wave would be refracted parallel to the prism surface (onset of total internal reflection). For this index ratio, the angle of incidence θ_1 (= 67 deg) is equal to the critical angle as given by (38). The

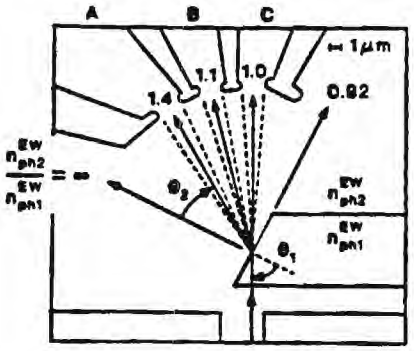

Fig. 9. Phase matching analysis of the electron wave prism switch of [19]. The electron wave inside the prism (index n_{ph1}^{EW}) is incident upon the prism surface at angle θ_1 and is refracted into the output region (index n_{ph2}^{EW}) at angle θ_2. By using the electron density and voltage-current data given in [19], the index ratios ($n_{ph2}^{EW}/n_{ph1}^{EW}$) that switch the electron into collectors A, B, and C are calculated to be 1.4, 1.1, and 1.0, respectively. These index ratios would result in angles of refraction (θ_2) of 38 deg, 52 deg, and 67 deg, for collectors A, B, and C, respectively. These angles are consistent with the given geometry of the device.

application of the present single-ray approach to the analysis of the electron wave prism switch [19], demonstrates the utility of the analogies between EMW propagation and EW propagation. In addition to analyzing phase effects (refraction angles), the present formalism can be used to extend these results to include amplitude effects such as reflectivity and transmissivity at boundaries. Furthermore, the present methods can be used to include simultaneously both phase and amplitude effects, incorporating important quantum interference physical optics effects [7]–[16] so as to calculate the total reflectance and transmittance of multiple-boundary, multiple-layer, and multiple-component electron optical devices.

Even though parabolic band, direct gap $Ga_{1-x}Al_xAs$ has been treated in this work, it should be emphasized that the methods can be applied to other material systems. It is conceptually straightforward to include nonparabolicity effects (often represented as $E(1 + \alpha E + \beta E^2 + \ldots) = \hbar^2|\bar{k}^{EW}|^2/2m^*$) in the analysis. Similarly, anisotropic effects can be incorporated through the use of a tensor effective mass and potential energy. This anisotropic case could be used if the lowest energy band consisted of ellipsoidal X minima energy surfaces (e.g., Si, AlAs, etc.) or ellipsoidal L minima energy surfaces (e.g., Ge) rather than the spherical Γ minimum energy surface associated with direct gap $Ga_{1-x}Al_xAs$.

Although the form of the potential energy has been taken to be $V = Ax$, since this linear relationship applies to direct gap $Ga_{1-x}Al_xAs$ and numerous other material systems, the analysis presented can be straightforwardly extended to general potentials given as $V = f(x)$. For example, for indirect gap $Ga_{1-x}Al_xAs$ ($0.45 \leq x \leq 1$) the potential $V = 1.900 + 0.125x + 0.193x^2$ [35], [36] can be used to calculate the phase and amplitude refractive indexes, from which the reflectivity (transmissivity) characteristics can be calculated.

The analysis presented in this paper is based on the single-band effective-mass equation. Such an analysis is valid for conduction electrons in type I superlattices constructed from semiconductors such as $Ga_{1-x}Al_xAs$ [40]. For the conduction of holes in the valence band of type I superlattices ($Ga_{1-x}Al_xAs$ [21]), the conduction of electrons in material systems with zero-field spin splitting in the conduction band (such as $Ga_{1-x}In_xAs$ [39]), or the conduction of electrons in type II superlattices [40], a multiband effective mass equation is required. In this case, the effective mass equation is an N-dimensional matrix equation rather than a scalar equation. The electron-wave amplitude ψ for single-band bulk propagation (the case treated in this paper) is analogous to either the electric or the magnetic field. For propagation across an interface, ψ is analogous to the component of the electromagnetic field that is normal to the plane of incidence. In the case of the two-band effective mass equation (lack of spin degeneracy), the resulting electromagnetic analogy differs from that treated in this paper. Bulk propagation in the two-band case is analogous to EMW propagation in an anisotropic media. The two bands represent a two-sheeted wavevector surface, analogous to the two-sheeted wavevector surface used to describe electromagnetic propagation in anisotropic materials [30]. In the electromagnetic case, the direction of the electric field polarization determines the wave decomposition into the two wavevector surfaces. In the electron wave case, the orientation of the electron spinor determines the decomposition of the electron wave into the two bands [21], [39]. In this manner, the electron spin is analogous to the electromagnetic field polarization. However, the electron wave eigen-solutions for the two-band model (spinors) are two-dimensional. Thus the two-band model describes a two-dimensional wavevector surface as opposed to the three-dimensional wavevector surface in electromagnetic optics [30]. In the N-band case, the N bands describe an N-sheeted wavevector surface in direct extension to the standard two-sheeted surface in anisotropic optics. The orientation of the N-dimensional vector describing the electron wave amplitude determines the wave decomposition into the wavevector surfaces. These analogies allow the description of multiband transport in terms of EMW propagation in anisotropic crystals.

An important result of this work is the demonstration that the analogies from the optics of nonmagnetic dielectrics are not applicable to electron wave propagation in semiconductors due to kinetic energy and effective mass differences across the interface. The optical expressions must first be generalized to include nonmagnetic dielectrics and then the results can be applied to the design of ballistic electron devices.

If the effective mass difference across the interface were not included in this analysis, many of the results would differ dramatically. By including the effective mass difference across a boundary, it was shown that an electron wave could be totally internally reflected from a potential drop. In addition, the existence of an electron wave Brewster angle is dependent upon the inclusion of the effective mass

dependence. In fact, when the effective mass is included in the analysis, the reflectivity of an interface for an arbitrary angle of incidence does not go to zero as the energy of the electron wave goes to infinity. Thus there is always a component of the electron wave that is reflected due to the effective mass difference on the two sides of the interface. These reflections will be eliminated if the electron waves are incident at the Brewster angle. For these material systems that have effective mass changes, the existence of an electron wave Brewster angle could become useful in the design of antireflection interfaces in ballistic electron devices [41]. As was discussed in Section I, recent experiments have demonstrated the importance of including these effective mass effects [24]–[26].

With the comprehensive set of quantitative analogies presented in this work, it is clear that a wide variety of electron wave optical devices are possible using electron wave propagation and that these devices can be designed starting with existing optical designs.

Using the results of the present formalism, electron wave optical components can be constructed including a wide variety of electron interference filters [27], [28] that have high-pass, low-pass, band-pass (narrow-band or wide-band), or notch (narrow-band and wide-band) characteristics. Impedance transformers (antireflection coatings) to reduce unwanted electron reflections at boundaries can be designed [41]. These could be used, for example, in the electron flow from the GaAs base of a bipolar junction transistor to the $Ga_{1-x}Al_xAs$ collector where $Ga_{1-x}Al_xAs$ is used to increase the breakdown voltage in the high electric field collector. One-dimensional periodic structures (diffraction gratings) can be designed to diffract electron waves [42]–[44], allowing a variety of beam-splitting and transistor-like switching functions to be performed.

In addition, nearly monoenergetic electron emitters can be designed that are voltage tunable [28], [46]. Electron emitters can be incorporated as hot electron injectors in the design of electroluminescent devices [46]–[47], photodetectors [46], and fast ballistic transistors [46]. Negative resistivity devices can also be designed utilizing linearly varying period (chirped) superlattices [48], [49] or Fabry–Perot emitter/filter structures [28], [45], [50]. All of these devices could be used in the construction of ultrahigh speed switches and high-frequency oscillators.

The quantitative analogies presented here may be used in the design of slab waveguides (quantum wells with a two-dimensional electron gas) [34] and channel waveguides (quantum wires with a one-dimensional electron gas). Electron waveguides must be used in nanometer-scale high-speed integrated circuits. They are also required in future electron guided-wave integrated circuits for implementing high-speed integrated switches, modulators, and logic devices for computers and communications. Such guided wave circuitry could also perform "optical-like" parallel data processing, in a manner analogous to present-day electromagnetic optical data processing which is done with guided-wave integrated optical circuits (with a wavelength approximately 100 times smaller than the wavelength in the electromagnetic optical devices). In addition, the interface to conventional digital electronic circuitry could be contained within the same semiconductor chip, thus greatly simplifying the "optics-electronics" interface.

References

[1] L. Esaki and R. Tsu, "Superlattice and negative differential conductivity in semiconductors," *IBM J. Res. Dev.*, vol. 14, pp. 61–65, Jan. 1970.

[2] A. F. J. Levi, J. R. Hayes, P. M. Platzman, and W. Wiegman, "Injected-hot-electron transport in GaAs," *Phys. Rev. Lett.*, vol. 55, pp. 2071–2073, Nov. 1985.

[3] M. Heiblum, M. I. Nathan, D. C. Thomas, and C. M. Knoedler, "Direct observation of ballistic transport in GaAs," *Phys. Rev. Lett.*, vol. 55, pp. 2200–2203, Nov. 1985.

[4] J. Spector, H. L. Stormer, K. W. Baldwin, L. N. Pfeiffer, and K. W. West, "Ballistic electron transport beyond 100 μm in 2D electron systems," *Surface Sci.*, vol. 228, pp. 283–285, 1990.

[5] S. Washburn and R. A. Webb, "Aharonov–Bohm effect in normal metal quantum coherence and transport," *Adv. Phys.*, vol. 35, pp. 375–422, July–Aug. 1986.

[6] T. K. Gaylord and K. F. Brennan, "Electron wave optics in semiconductors," *J. Appl. Phys.*, vol. 65, pp. 814–820, Jan. 1989.

[7] T. K. Gaylord, E. N. Glytsis, G. N. Henderson, K. P. Martin, D. B. Walker, D. W. Wilson, and K. F. Brennan, "Quantum interference effects in semiconductors: A bibliography," *Proc. IEEE*, vol. 79, pp. 1159–1180, Aug. 1991.

[8] L. L. Chang, L. Esaki, and R. Tsu, "Resonant tunneling in semiconductor double barriers," *Appl. Phys. Lett.*, vol. 24, pp. 593–595, June 1974.

[9] T. C. L. G. Sollner, W. D. Goodhue, P. E. Tannenwald, C. D. Parker, and D. D. Peck, "Resonant tunneling through quantum wells at frequencies up to 2.5 THz," *Appl. Phys. Lett.*, vol. 43, pp. 588–590, Sept. 1983.

[10] T. Nakagawa, H. Imamoto, T. Kojima, and K. Ohta, "Observation of resonant tunneling in AlGaAs/GaAs triple barrier diodes," *Appl. Phys. Lett.*, vol. 49, pp. 73–75, July 1986.

[11] C. J. Summers, K. F. Brennan, A. Torabi, and H. M. Harris, "Resonant tunneling and negative differential resistance in a variably spaced superlattice energy filter," *Appl. Phys. Lett.*, vol. 52, pp. 132–134, Jan. 1988.

[12] S. Sen, F. Capasso, A. C. Gossard, R. A. Spah, A. L. Hutchinson, and S. N. G. Chu, "Observation of resonant tunneling through a compositionally graded parabolic quantum well," *Appl. Phys. Lett.*, vol. 51, pp. 1428–1430, Nov. 1987.

[13] M. Heiblum, M. V. Fishetti, W. P. Dumke, D. J. Frank, I. M. Anderson, C. M. Knoedler, and L. Osterling, "Electron interference in quantum wells: observation of bound and resonant states," *Phys. Rev. Lett.*, vol. 58, pp. 816–819, Feb. 1987.

[14] R. C. Potter and A. A. Lakhani, "Observation of electron quantum interference effects due to virtual states in a double-barrier heterostructure at room temperature," *Appl. Phys. Lett.*, vol. 52, pp. 1349–1351, Apr. 1988.

[15] J. R. Hayes, P. England, and J. P. Harbison, "Quantum interference effects in GaAs/ GaAlAs bulk potential barriers," *Appl. Phys. Lett.*, vol. 52, pp. 1578–1580, May 1988.

[16] F. Beltram, F. Capasso, A. L. Hutchinson, and R. J. Malik, "Injection in a continuum miniband: Observation of negative transconductance in a superlattice-base transistor," *Appl. Phys. Lett.*, vol. 55, pp. 1534–1536, Oct. 1989.

[17] U. Sivan, M. Heiblum, C. P. Umbach, and H. Shtrikman, "Electrostatic electron lens in the ballistic regime," *Phys. Rev. B*, vol. 41, pp. 7937–7940, Apr. 1990.

[18] J. Spector, H. L. Stormer, K. W. Baldwin, L. N. Pfeiffer, and K. W. West, "Electron focusing in two-dimensional systems by means of an electrostatic lens," *Appl. Phys. Lett.*, vol. 56, pp. 1290–1292, Mar. 1990.

[19] J. Spector, H. L. Stormer, K. W. Baldwin, L. N. Pfeiffer, and K. W. West, "Refractive switch for two-dimensional electrons," *Appl. Phys. Lett.*, vol. 56, pp. 2433–2435, June 1990.

[20] W. van Haeringen and D. Lenstra, Eds., *Analogies in Optics and Micro Electronics*. Dordrecht, The Netherlands: Kluwer Academic, 1990.

[21] S. Datta, *Quantum Phenomena*. Reading, MA: Addison Wesley, 1989, chap. 1.

[22] M. Lundstrom, and S. Datta, "Physical device simulation in a shrinking world," *IEEE Circuits Dev.*, vol. 6, pp. 32–37, July 1990.
[23] D. Lenstra and W. van Haeringen, "Playing with electrons and photons in rings," in *Analogies in Optics and Micro Electronics*, W. van Haeringen and D. Lenstra, Eds., Dordrecht, The Netherlands: Kluwer Academic, 1990.
[24] H. Ohno, E. E. Mendez, and W. I. Wang, "Effects of carrier mass differences on the current–voltage characteristics of resonant tunneling structures," *Appl. Phys. Lett.*, vol. 56, pp. 1793–1795, Apr. 1990.
[25] W. J. Kaiser and L. D. Bell, "Direct investigation of subsurface interface electronic structure by Ballistic-Electron-Emission Microscopy," *Phys. Rev. Lett.*, vol. 60, pp. 1406–1409, Apr. 1988.
[26] L. D. Bell and W. J. Kaiser, "Observation of interface band structure by Ballistic-Electron-Emission Microscopy," *Phys. Rev. Lett.*, vol. 61, pp. 2368–2370, Nov. 1988.
[27] T. K. Gaylord, E. N. Glytsis, and K. F. Brennan, "Semiconductor superlattice interference filter design," *J. Appl. Phys.*, vol. 65, pp. 2535–2540, Mar. 1989.
[28] E. N. Glytsis, T. K. Gaylord, and K. F. Brennan, "Semiconductor biased superlattice tunable electron interference filter/emitter," *J. Appl. Phys*, vol. 65, pp. 1494–1497, Aug. 1989.
[29] E. Hecht, *Optics*. Reading, MA: Addison Wesley, 1987, chap. 3–4.
[30] M. Born and E. Wolf, *Principles of Optics*. Oxford, U.K.: Pergamon, 1980, chap. 1.
[31] R. E. Collin, *Field Theory of Guided Waves*. New York: McGraw-Hill, 1960, chap. 1.
[32] E. Merzbacher, *Quantum Mechanics*. New York: Wiley, 1970, chap. 4.
[33] A. N. Khondker, M. R. Kahn, A. F. M. Anwar, "Transmission line analogy of resonance tunneling phenomena: the generalized impedance concept," *J. Appl. Phys.*, vol. 63, pp. 5191–5193, May 1988.
[34] T. K. Gaylord, E. N. Glytsis, and K. F. Brennan, "Semiconductor electron-wave slab waveguides," *J. Appl. Phys.*, vol. 66, pp. 1483–1485, Aug. 1989.
[35] S. Adachi, "GaAs, AlAs, and $Al_xGa_{1-x}As$: Material parameters for use in research and device applications," *J. Appl. Phys.*, vol. 58, pp. R1–R29, Aug. 1985.
[36] H. C. Casey and M. B. Panish, *Heterostructure Lasers*. New York: Academic, 1978, section 4.2.
[37] R. C. Miller, D. A. Kleinman, and A. C. Gossard, "Energy-gap and effective masses for GaAs-$Al_xGa_{1-x}As$ quantum wells," *Phys. Rev. B*, vol. 29, pp. 7085–7087, Mar. 15, 1984.
[38] G. Ji, D. Huang, U. K. Reddy, H. Unlu, T. S. Henderson, and H. Morkoc, "Determination of band offsets in AlGaAs/GaAs and InGaAs/GaAs multiple quantum wells," *J. Vac. Sci. Tech.*, vol. B5, pp. 1346–1352, Sept.–Oct. 1987.
[39] S. Datta and B. Das, "Electronic analog of the electro-optic modulator," *Appl. Phys. Lett.*, vol. 56, pp. 665–667, Feb. 1990.
[40] M. Altarelli, "Band structure, impurities, and excitons in superlattices," in *Hetero-junctions and Semiconductor Superlattices*, G. Allan *et al.* Eds., New York: Springer-Verlag, 1986, pp. 12–37.
[41] T. K. Gaylord, E. N. Glytsis, and K. F. Brennan, "Electron-wave quarter-wavelength quantum well impedance transformers between differing energy-gap semiconductors," *J. Appl. Phys.*, vol. 67, pp. 2623–2630, Mar. 1990.
[42] K. Furuya, "Novel high-speed transistor using electron-wave diffraction," *J. Appl. Phys.*, vol. 62, pp. 1492–1494, Aug. 1987.
[43] K. Furuya and K. Kurishima, "Theoretical properties of electron wave diffraction due to a transversally periodic structure in semiconductors," *IEEE J. Quantum Electron.*, vol. 24, pp. 1652–1658, Aug. 1988.
[44] G. N. Henderson, E. N. Glytsis, and T. K. Gaylord, "Electron wave diffraction by semiconductor gratings Rigorous analysis and design parameters," *Appl. Phys. Lett.*, vol. 59, pp. 440–442, July 1991.
[45] E. N. Glytsis, T. K. Gaylord, and K. F. Brennan, "Theory and design of semiconductor electron wave interference filter/emitter," *J. Appl. Phys.*, vol. 65, pp. 6158–6167, Dec. 1989.
[46] C. J. Summers and K. F. Brennan, "Variably spaced superlattice energy filter, a new device design concept for high-energy electron injection," *Appl. Phys. Lett.*, vol. 48, pp. 806–808, Mar. 1986.
[47] K. F. Brennan and C. J. Summers, "The variably spaced superlattice electroluminescent display: A new high efficiency electroluminescence scheme," *J. Appl. Phys.*, vol. 61, pp. 5410–5418, June 1987.
[48] T. Nakagawa, H. Imamoto, T. Sakamoto, T. Kojima, K. Ohta, and N. J. Kawai, "Observation of negative differential resistance in CHIRP superlattices," *Electron. Lett.*, vol. 21, pp. 882–884, Sept. 1985.
[49] T. Nakagawa, N. J. Kawai, and K. Ohta, "Design principles for CHIRP superlattice devices," *Sup. Micro.*, vol. 1, no. 2, pp. 187–192, 1985.
[50] E. N. Glytsis, T. K. Gaylord, and K. F. Brennan, "Ballistic current–voltage characteristics of semiconductor superlattice electron-wave quantum-interference filter/emitter negative differential resistance devices," *J. Appl. Phys.*, vol. 69, pp. 3920–3933, Oct. 1991.

Gregory N. Henderson (Student Member, IEEE), for a photograph and biography please see page 1180 of the August 1991 issue.

Thomas K. Gaylord (Fellow, IEEE), for a photograph and biography please see page 1180 of the August 1991 issue.

Elias N. Glytsis (Senior Member, IEEE), for a photograph and biography please see page 1180 of the August 1991 issue.

Ballistic current-voltage characteristics of semiconductor superlattice electron-wave quantum-interference filter/emitter negative differential resistance devices

Elias N. Glytsis, Thomas K. Gaylord, and Kevin F. Brennan
School of Electrical Engineering and Microelectronics Research Center, Georgia Institute of Technology, Atlanta, Georgia 30332

(Received 2 October 1990; accepted for publication 27 June 1991)

The transmission and current-voltage characteristics of $Ga_{1-x}Al_xAs$ superlattice electron-wave quantum-interference filter/emitter negative differential resistance devices are analyzed with and without the self-consistency requirement. The analysis neglects the scattering effects within the superlattice since it is assumed that it is very thin (less than the electron coherence length). Thus, the calculated characteristics correspond to the ballistic component of the current. For the non-self-consistent calculation the single-band effective-mass time-independent Schroedinger equation is solved. For the self-consistent calculation, the Schroedinger and Poisson equations are solved iteratively until a self-consistent electron potential energy and electron density are obtained. It is shown that suitably designed electron-wave quantum-interference filter/emitters can exhibit strong negative differential resistance in the current-voltage characteristics, similar to those of resonant tunneling diodes. For low-to-moderate (2–30 meV) Fermi energies in the conduction band of $Ga_{1-x}Al_xAs$ (Si doping concentration less or equal to 2×10^{18} cm^{-3}) and temperatures near 30 K (in the ballistic transport regime), it is shown that space-charge effects are relatively small and result in a slight shift of the current-voltage and transmission characteristics toward higher bias voltages. In a fashion similar to that occurring in resonant tunneling diodes, the self-consistent field in electron-wave filter/emitter negative differential resistance devices partially screens the positive applied bias. Designs of $Ga_{1-x}Al_xAs$ resonant devices with current peak-to-valley ratios of ~ 50 as well as nonresonant (not exhibiting negative differential resistance) devices are analyzed. The corresponding electron charge density distributions are also presented. Superlattice electron-wave filter/emitter negative differential resistance devices can be used as high-speed switches, oscillators, and as monoenergetic emitters in electroluminescent devices and photodetectors.

I. INTRODUCTION

Nanostructure devices like multiple quantum wells and superlattices have been rapidly developed due to recent advances of microfabrication technology, particularly metalorganic chemical vapor deposition (MOCVD) and molecular-beam epitaxy (MBE). These fabrication technologies have been refined to the point where single monolayers can be grown with precise compositional control.[1] At these spatial dimensions, quantization effects largely dominate device characteristics, making further reduction in their sizes undesirable in some applications, thereby limiting the ultimate speed of the devices. However, quantum interference effects may also potentially be used in an advantageous way in novel devices. Quantum-mechanical interference effects have been experimentally observed for electron energies below the potential energy barriers in double-barrier and multibarrier resonant tunneling devices[2–6] and for electron energies above the barriers in single- and double-barrier structures.[7–9] With further improvements in the quality of the materials grown, ballistic transport has also been experimentally observed.[10,11] That is, electrons travel through the device without being scattered by deviations from crystalline perfection. Even with the addition of elastic scattering, the electrons exhibit clear quantum-mechanical plane-wave behavior.[12,13] These coherent waves maintain their phase throughout the device and thus can interfere, reflect, refract, and diffract in a manner analogous to the electromagnetic plane waves in dielectric media. Impressive experimental evidence of optical-like electron behavior in GaAs semiconductors has recently been reported.[14,15]

Quantitative analogies between quantum-mechanical electron waves in semiconductor materials and electromagnetic optical waves in dielectrics have already been developed.[16] With these analogies, existing electromagnetic optical analysis and design techniques can be used for the analysis and design of novel semiconductor quantum-wave devices. Possible devices include narrow-band superlattice interference filters[17,18] and filter/emitters[19,20] which can exhibit very narrow electron kinetic energy passbands and can be integrated into solid-state devices for potential use as monoenergetic emitters for electroluminescent devices,[21,22] photodetectors,[21,23] and subpicosecond ballistic transistors.[11,21] Beyond improving the speed of existing devices, however, the totally new concept of *guided electron-wave integrated circuits* has been proposed.[24,25] This

 0021-8979/91/073920-14$03.00

potentially next generation of integrated circuits could be comprised by many semiconductor quantum electron-wave devices interconnected by electron waveguides.[24–29]

Semiconductor superlattice interference filter and filter/emitter designs can be visualized from the optical interference filters counterparts but their designs cannot be simple copies of thin-film optical designs due to the constraints that are imposed by the ultrasmall dimensions, the usable composition range, and the applied bias voltage. The design of such quantum interference filters and filter/emitters has been presented in Refs. 17–20. In the present work the current-voltage (I-V) characteristics of these filter/emitters are calculated self-consistently. It is shown that these devices can exhibit negative differential resistivity similar to that occurring in resonant tunneling diodes. In addition, space-charge effects due to electron localization that have been shown to be very important in semiconductor device analysis and design are quantified for these structures. Several analytical techniques have been used and can be classified into two major categories: the classical approaches that include the solution of the nonlinear Poisson equation using Boltzmann or Fermi–Dirac statistics for the electron and hole concentrations,[30–35] and the quantum-mechanical approaches in which both the Schroedinger and Poisson equations are solved self-consistently through an iterative algorithm until a self-consistent electrostatic potential and electron density are achieved.[35–47] Most of these analyses have been applied to the resonant tunneling diodes[37,39–41,44] in which the space-charge effects have been shown to be significant. In this paper, for the first time, a complete quantum-mechanical-self-consistent analysis of the semiconductor superlattice filter/emitter is presented. These devices inherently differ from the resonant tunneling diodes in that they are designed to operate at electron energies above all barriers and wells of the semiconductor superlattice. Thus, electron localization is purely due to the quantum-mechanical interference mechanism.

In this work, the effects of the self-consistent potential on quantum-interference filter/emitter negative differential resistance devices are isolated and analyzed. The details of the model used are described in Sec. II. Several example cases are presented in Sec. III for the GaAs/$Ga_{1-x}Al_xAs$ alloy system. Resonant (exhibiting negative differential resistance) and nonresonant (not exhibiting negative differential resistance) filter/emitter devices are analyzed. The effects of the Fermi energy (doping) and temperature on the filter/emitter transmittance and current-voltage characteristics are included. Electron densities in the superlattice are also presented for resonant and nonresonant filter/emitters. It is found that the space-charge effects on the transmission and I-V characteristics of the filter/emitter devices can be significant for relatively high Fermi energies (above 30 meV) and generally lead to shifting of the device characteristics toward higher bias voltages. Finally, in Sec. IV, a summary and some discussion are presented.

II. MODEL DESCRIPTION

A voltage-biased semiconductor superlattice can serve simultaneously as an electron-wave interference filter and electron emitter. The theory and the design of such electron-wave filter/emitters have been presented in Refs. 19 and 20 using a non-self-consistent (linear electrostatic potential) model. The present self-consistent model is similar to the one used for the resonant tunneling devices.[36–45] The model formulation is based on the following given conditions:

(a) The semiconductor superlattice consists of an intrinsic region where quantum-mechanical analysis applies. Thus, the length of the device is smaller than the electron coherence length. Experimental measurements in ballistic hot-electron devices[10,11,14,15,48,49] (on GaAs/GaAlAs and InGaAs/InAlAs structures) indicate that the electron coherence length lies roughly between 10 and 100 nm. Of course, the electron coherence length depends strongly on the temperature (electron coherence length of the order of several micrometers was recently reported at very low temperatures[14,15]) and it is a statistical quantity. Therefore, the experimental data suggest that a measurable fraction of the electrons will exhibit coherent behavior within the filter/emitter. The transport of electrons through the filter/emitter negative differential resistance device is assumed to be strictly collisionless.

(b) For the filter/emitter region, the one-electron single-band effective mass time-independent Schroedinger equation is used. This is a valid approximation for electron energies near the Γ point in accordance with the filter/emitter design requirements.[20] The boundary conditions used at the heterojunction interfaces of the filter/emitter region (intrinsic region) are the continuity of the envelope wave function, ψ, and the continuity of the normal component of the probability current density or equivalently the continuity of the envelope wave function first derivative weighted by the inverse effective mass, $(1/m^*)\psi'$ (where ψ' denotes a first derivative). These two boundary conditions work sufficiently well for the III-V semiconductor family as long as the same band edge is considered on both sides of the discontinuity[50] (the conduction-band direct-gap minimum for the electron-wave filter/emitters).

(c) The applied voltage bias appears across the filter/emitter region. The voltage drop in the contacts is assumed negligible.

(d) The contact regions outside the filter/emitter are treated as having constant Fermi energy levels and equilibrium Fermi–Dirac statistics apply.

The electron potential energy of the electron-wave filter/emitter negative differential resistance device with an applied bias voltage is shown in Fig. 1. In this figure the electrostatic potential energy is assumed to be linear which is the first estimate used in order to start the iterative solution of the Schroedinger and Poisson equations. The filter/emitter consists of M layers, where M is an odd integer. The center layer is the resonant layer while the surrounding layers are quarter electron-wavelength layers (for the design pass energy of the filter/emitter).[19,20] When the design voltage is applied, electrons in a narrow energy

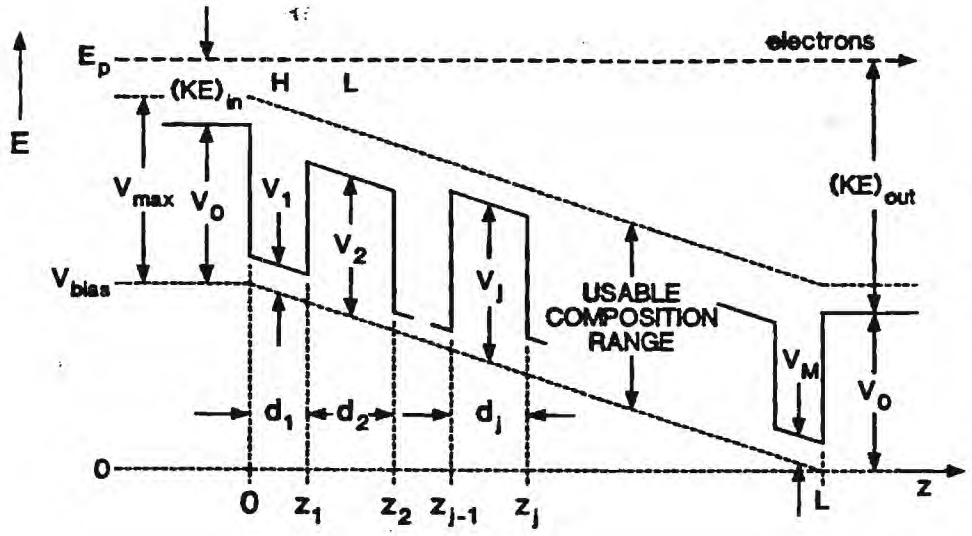

FIG. 1. Schematic representation of a biased semiconductor superlattice electron-wave interference resonance filter/emitter. At the design potential energy bias, V_{bias}, and input kinetic energy, KE_{in}, the layers have a thickness of a quarter (or a half for the resonant central layer) of an electron wavelength as measured in that layer. In this figure a linear (non-self-consistent) electrostatic potential is assumed.

band around the prespecified pass energy, E_p (Fig. 1), traverse the filter/emitter and are emitted with an output kinetic energy KE_{out}. The applied bias potential energy is denoted by V_{bias}, while the potential energies of the different layers are denoted by V_j and their effective masses by m_j^* ($j=1,2,...,M$). For the solution of the self-consistent problem the filter/emitter region is divided into N subregions of equal width Δz as shown in Fig. 2. The potential energy of each subregion i ($i=1,2,...,N$) is $V_i' = [V(z_{i-1}') + V(z_i')]/2$, where $V(z)$ is the electrostatic potential energy (which is one of the unknowns of the self-consistent problem). An alternative to the stair-step approximation[51] would be a piecewise linear potential energy approximation.[20,52] In the limit of large N both approximations converge to the same solution. The one-electron envelope wave function in the ith subregion is denoted by ψ_i, while the change in the conduction-band edge, v_i, and the effective mass, m_i^*, are the change in the conduction-band edge and the effective mass of the region j ($j=1,2,...,M$) to which the subregion i belongs. Thus, the

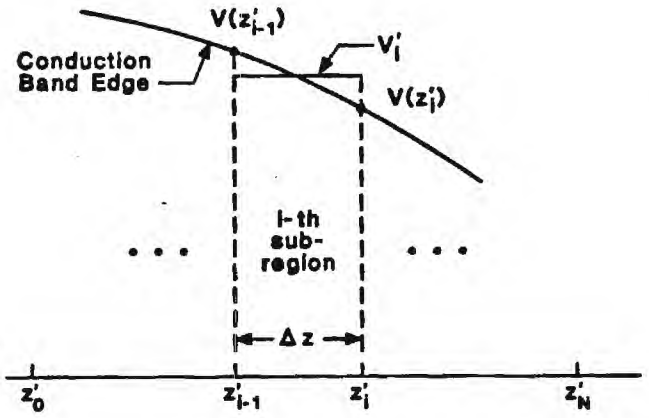

FIG. 2. Part of the resonant filter/emitter region between points z_{i-1}' and z_i' where the stair-step representation is used for the self-consistent potential $V(z)$.

one-electron envelope function time-independent Schroedinger equation for the ith subregion can be written

$$\frac{\hbar^2}{2m_i^*}\frac{d^2\psi_i}{dz^2} + (E - V_i' - v_i)\psi_i = 0, \quad z_{i-1}' < z < z_i', \tag{1}$$

where $\hbar$ is Planck's constant divided by 2π and E is the total electron energy. In order to solve Eq. (1), knowledge of the electrostatic potential energy $V(z)$ is required. Assuming that $V(z)$ is known, the solution for ψ_i can be written in the form

$$\psi_i(z) = C_i \exp[+jk_i(z - z_{i-1}')] + D_i \exp[-jk_i(z - z_{i-1}')] \tag{2}$$

for $z_{i-1}' < z < z_i'$ and with the electron wave vector $k_i = [2m_i^*(E - V_i' - v_i)/\hbar^2]^{1/2}$. The coefficients C_i and D_i of each subregion i can be found from the boundary conditions for the envelope wave functions and assuming that $\psi_0(z) = \exp(jk_0 z) + r_e \exp(-jk_0 z)$ and $\psi_{N+1}(z) = t_e \exp[jk_{N+1}(z - z_N')]$, where r_e and t_e are the amplitude reflection and transmission coefficients of the wave function. Using a transfer matrix approach,[51] r_e and t_e can be calculated first, and then all C_i and D_i can be computed recursively. Thus, once the overall transmission and reflection coefficients are found, the steady-state wavefunction $\psi(z) = \psi_l(z)$ for $z_{l-1}' < z < z_l'$ ($l=1,2,...,N$) can be determined at each incident energy E over the full range of interest.

After the wave function $\psi(z)$ is known throughout the entire structure, the electron density, $n(z)$, can be calculated by $n(z) = \langle \psi(z)\psi^*(z) \rangle$, where $\langle\ \rangle$ denotes summation (or equivalently integration) over all energies.[36] Furthermore, assuming Fermi–Dirac statistics the previous equation becomes

$$n(z) = \langle \psi(z)\psi^*(z) f(E,E_f) \rangle, \tag{3}$$

where $f(E,E_f)$ is the Fermi distribution function and E_f is the Fermi energy level. The distribution function is taken as being in equilibrium, in spite of the fact that a current

flows through the filter/emitter when a bias voltage is applied. However, the distribution function $f(E,E_f) = 1/\{1 + \exp[(E - E_f)/k_BT]\}$, where k_B is Boltzmann's constant and T is the absolute temperature, is reasonably accurate since the xy system is essentially decoupled from the quantization direction z, and can be considered in a quasi-equilibrium state.[37–43] Evaluation of Eq. (3) yields to the following approximate expression for $n(z)$:

$$n(z) \simeq \frac{k_BT(m_0^*)^{3/2}}{2\sqrt{2}\pi^2\hbar^3} \times \int_0^\infty |\psi(z)|^2 \ln[1 + \exp(E_f - E_z)/k_BT] \frac{dE_z}{\sqrt{E_z}}, \quad (4)$$

where E_z is the longitudinal component of the energy E. For the above computation, parabolic band structure and independence of $|\psi(z)|^2$ on the transverse energy component (momentum) were assumed. None of the two previous assumptions is strictly valid, but for low energies near the bottom of the conduction band (Γ valley) these are very good approximations and they greatly simplify the computational procedure for the evaluation of the electron density.[37–43] In addition, Eq. (4) accounts for only the left-to-right incident electrons. In order to be strictly correct, the electrons impinging from right to left should also be taken into account,[39–41] and the total electron density should be the sum of these two streams of electrons. However, the right-to-left incident stream of electrons has a negligible effect on the current density of the device for the design values of the applied voltage and temperature. The charge density corresponding to the spatial electron distributions given by Eq. (4) can be calculated by $-en(z)$ (where e is the electron charge) and then substituted into the one-dimensional Poisson equation,

$$\frac{d}{dz}\left(\epsilon_0\epsilon_r(z)\frac{d\phi}{dz}\right) = -en(z), \quad (5)$$

where ϵ_0 is the permittivity of free space, ϵ_r is the relative permittivity along the device, and $\phi(z)$ is the electrostatic potential. Defining the electrostatic potential energy as before by $V(z) = -e\phi(z)$, Eq. (5)can be written as

$$\frac{d^2V(z)}{dz^2} \simeq -\frac{e^2n(z)}{\epsilon_0\epsilon_r}, \quad (6)$$

where ϵ_r is the relative permittivity of GaAs (assumed constant throughout the filter/emitter for simplicity). Solving Eq. (6) numerically, using the method of finite differences, the electrostatic potential energy $V(z)$ can be found and used in the Schroedinger equation [Eq. (1)].

The computation algorithm starts with the solution of Eq.(1) assuming linear electrostatic potential energy (Fig. 1). After computation of the wave function, the electron density can be calculated from Eq. (4). Then Eq. (6) can be solved for a new estimate of the electrostatic potential energy $V(z)$. This procedure is iterated until convergence of the electrostatic potential energy $V(z)$ is obtained. Then, the current density, J, can be calculated at each applied bias using the equation[51,53]

$$J \simeq \frac{em_0^*k_BT}{2\pi^2\hbar^3}\int_0^\infty T(E_z) \times \ln\left(\frac{1+\exp[(E_f-E_z)/k_BT]}{1+\exp[(E_f-E_z-V_{bias})/k_BT]}\right) dE_z, \quad (7)$$

where $T(E_z)$ is the transmission coefficient of the device, calculated using the self-consistent electrostatic potential, and is given by

$$T(E_z) = \left(\frac{(E-V_0)/m_{M+1}^*}{(E-V_0-V_{bias})/m_0^*}\right)^{1/2} |t_e|^2. \quad (8)$$

For the derivation of Eq. (7), parabolic band structure and independence of $T(E_z)$ on transverse energy component were assumed, similar to the assumptions for the validity of Eq. (4). In the following section several results of resonant (exhibiting negative differential resistance) and nonresonant (not exhibiting negative differential resistance) devices in the $Ga_{1-x}Al_xAs$ alloy family are presented.

III. RESULTS OF THE CALCULATIONS FOR $Ga_{1-x}Al_xAs$ ALLOYS

A practical material system to be used in fabricating electron-wave interference devices is $Ga_{1-x}Al_xAs$. For this material system the maximum allowable composition in aluminum is $x_{max} = 0.45$ in order to avoid the direct/indirect band-gap transition. The electron potential energy of the jth layer is given by $V_j = Ax_j$ ($A = 0.773$ eV),using the ~60/40 rule conduction-to-valence band-edge discontinuity,[54,55] and its effective mass is given by $m_j^* = (B + Cx_j)m_0$ ($B = 0.067$, $C = 0.083$), where m_0 is the free-electron mass. The ⟨100⟩ monolayer thickness for any usable composition remains the same and equals 0.2827 nm (lattice-matched material system). Two resonant and one nonresonant example designs will be presented. These designs will take into account the minimization of the inter-valley scattering (Γ-L band transition) according to the analysis presented in Ref. 20. The two resonant devices will be referred to as resonant filter/emitters A and B respectively.

A. Resonant filter/emitter A design criteria

Resonant filter/emitter A was designed with the algorithm of Ref. 20 for a bias potential energy $V_{bias} = 0.10$ eV and an output kinetic energy at resonance $KE_{out} = 0.13$ eV, assuming a Fermi energy level at the input region of 30 meV (measured from the bottom of the conduction band). In order to reduce intervalley transitions for the applied resonance bias and kinetic energy, the maximum allowable aluminum composition had to be reduced[20] to 0.2, which was also selected to be the input and output region compositions (Fig. 1). The operating temperature was assumed to be 25 K. The characteristics of the nine-layer ($M = 9$) resonant filter/emitter A (exact design) are given in Table I. In this table, the thickness of each layer in

TABLE I. Design parameters of an electron-wave interference resonant filter/emitter consisting of nine layers surrounded by $Ga_{0.8}Al_{0.2}As$ and designed to emit 0.13-eV electrons for the exact design and 0.125-eV electrons for the constrained-composition design when biased at 0.10 eV.

	Resonant filter/emitter A design							
	Exact design				Constrained-composition design			
Layer No. j	Number monolayers thick	Aluminum composition x_j	Unbiased electron potential energy V_j (eV)	Normalized effective mass m_j^*/m_0	Number monolayers thick	Aluminum composition x_j	Unbiased electron potential energy V_j (eV)	Normalized effective mass m_j^*/m_0
1	10	0.0249	0.0193	0.0691	10	0.00	0.0000	0.0670
2	12	0.1225	0.0947	0.0772	12	0.13	0.1005	0.0778
3	10	0.0630	0.0487	0.0722	10	0.07	0.0541	0.0728
4	12	0.1557	0.1204	0.0799	12	0.13	0.1005	0.0778
5	18	0.0402	0.0311	0.0703	18	0.00	0.0000	0.0670
6	11	0.1712	0.1324	0.0812	11	0.20	0.1546	0.0836
7	9	0.0855	0.0661	0.0741	9	0.07	0.0541	0.0728
8	10	0.1622	0.1254	0.0805	10	0.20	0.1546	0.0836
9	8	0.0142	0.0109	0.0682	8	0.00	0.0000	0.0670

monolayers, the aluminum composition x_j, the unbiased electron potential energy V_j, and the normalized effective mass m_j^*/m_0 are given. The total thickness of the filter/emitter A is 100 monolayers (28.3 nm), which is within the electron coherence length [assumption (a) of Sec. II] at 25 K. An alternate design which takes into account the practical constraint of having a finite number of composition levels is also shown in Table I (constrained-composition design). This version of resonant filter/emitter A restricts the aluminum compositions to four distinct levels (0.0, 0.07, 0.13, and 0.20 as is required by typical MBE fabrication systems). The transmission characteristics (calculated using a non-self-consistent analysis) of these exact and constrained-composition designs are shown in Fig. 3(a) as functions of the output kinetic energy KE_{out} (Fig. 1) for an applied bias potential energy of 0.10 eV (resonance design value). The constrained-composition design has its peak electron transmission at $KE_{out} = 0.125$ eV instead of the 0.13-eV design value due to the four distinct aluminum composition levels. Interestingly, the transmission (transmission of 99.8% at 0.125 eV) peak of the constrained-composition design is larger than the peak of the exact design (transmission of 94.4% at 0.13 eV). This is due to the more symmetric configuration of the constrained composition design. However, the exact design remains the optimal design for $KE_{out} = 0.13$ eV and for $V_{bias} = 0.10$ eV.

B. Resonant filter/emitter B design criteria

Resonant filter/emitter B was designed using the same procedure[19] as resonant filter/emitter A. The Fermi energy level of resonant filter/emitter B was calculated to be $E_f = 2.26$ meV using a donor concentration of $N_D = 2 \times 10^{18}$ cm^{-3}, a donor ionization energy of 5.8 meV (for silicon dopant), and an operating temperature of 25 K. The calculational procedure was based on the numerical solution of the charge neutrality equation at flat-band equilibrium using Fermi–Dirac statistics.[56] This is a conservative calculation which does not take into account the

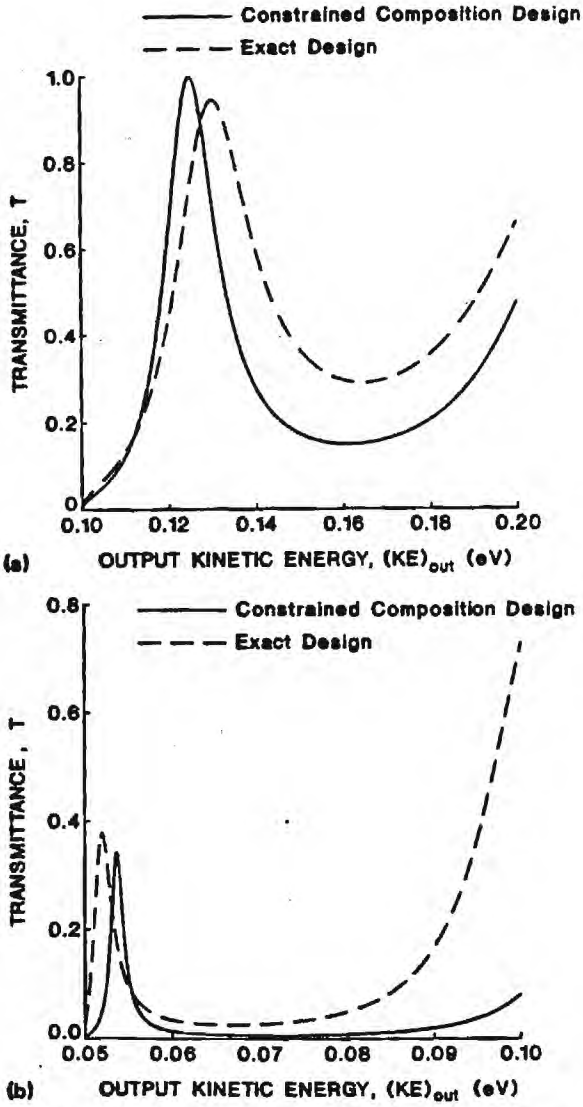

FIG. 3. Electron transmission characteristics of the nine-layer resonant filter/emitters as a function of the output kinetic energy for an applied bias potential energy of V_{bias}. The characteristics of the exact design (dashed line) and of the constrained composition design (solid line) are shown. (a) Resonant filter/emitter A for $V_{bias} = 0.10$ eV and (b) resonant filter/emitter B for $V_{bias} = 0.05$ eV.

TABLE II. Design parameters of an electron-wave interference resonant filter/emitter consisting of nine layers surrounded by $Ga_{0.8}Al_{0.2}As$ and designed to emit 0.0520-eV electrons for the exact design and 0.0536-eV electrons for the constrained-composition design when biased at 0.05 eV.

	Resonant filter/emitter B design							
	Exact design				Constrained-composition design			
Layer No. j	Number monolayers thick	Aluminum composition x_j	Unbiased electron potential energy V_j (eV)	Normalized effective mass m_j^*/m_0	Number monolayers thick	Aluminum composition x_j	Unbiased electron potential energy V_j (eV)	Normalized effective mass m_j^*/m_0
1	11	0.0226	0.0175	0.0689	11	0.00	0.0000	0.0670
2	21	0.1702	0.1316	0.0811	21	0.20	0.1546	0.0836
3	11	0.0419	0.0324	0.0705	11	0.07	0.0541	0.0728
4	20	0.1814	0.1402	0.0821	20	0.20	0.1546	0.0836
5	20	0.0140	0.0109	0.0682	21	0.00	0.0000	0.0670
6	17	0.1819	0.1407	0.0821	17	0.20	0.1546	0.0836
7	10	0.0348	0.0269	0.0699	10	0.07	0.0541	0.0728
8	16	0.1866	0.1443	0.0825	16	0.20	0.1546	0.0836
9	10	0.0513	0.0397	0.0712	10	0.00	0.0000	0.0670

broadening of the donor ionization energies and the band tailing due to the heavy doping.[57] To restrict intervalley scattering, the maximum allowable aluminum composition was chosen again to be 0.2, which is also equal to the compositions of the input and output regions. In this design, due to the lower Fermi energy level, the design bias potential energy had to be chosen lower than previously and was selected to be 0.05 eV. The output kinetic energy of resonant filter/emitter B at its resonance was selected to be 0.052 eV in order to be near the Fermi level of the input region. The design characteristics of the nine-layer ($M = 9$) resonant filter/emitter B (exact design) are shown in Table II. For this design the total thickness of the filter/emitter is 136 monolayers (38.4 nm), which is again within the electron coherence length at 25 K. The thickness of resonant filter/emitter B is larger than that of resonant filter/emitter A due to the lower resonance energy and applied voltage bias. A constrained-composition design is also included in Table II with three only-aluminum composition levels (the 0.13 composition level is not necessary in this case). In this constrained-composition design the center layer thickness was increased by 1 monolayer (21 instead of 20) to shift the transmission peak closer to the design transmission peak and at lower output kinetic energies (which is desirable due to the low Fermi energy level). The transmission characteristics of the exact and the constrained composition designs are shown in Fig. 3(b) as a function of the output kinetic energy for a bias potential energy of 0.05 eV (non-self-consistent calculation). For both of the resonant filter/emitter B designs the peak transmissions are smaller than those of resonant filter/emitter A (37.9% for the exact design and 34.4% for the constrained-composition design) for the corresponding design energy and bias potential. The smaller peak transmission is due to the lower input kinetic energies and applied resonant bias voltages. In the remainder of this paper, the constrained-composition designs for both resonant filter/emitters A and B will be analyzed, since these designs are practical from a fabrication point of view.

C. Self-consistent and non-self-consistent analyses

Using the algorithm presented in Sec. II, constrained-composition resonant filter/emitters A and B were analyzed with both the non-self-consistent (linear electrostatic potential) and the self-consistent approach. The stair-step representation used for the self-consistent computation consisted of steps of monolayer thickness, i.e., $\Delta z = 0.2827$ nm and $N = 100$ for resonant filter/emitter A and $N = 137$ for resonant filter/emitter B. Comparing the stair-step results with those of the exact analysis (using Airy and complimentary Airy functions[20,52] for non-self-consistent potential) excellent agreement was found (error was smaller than $\pm 10^{-5}$ for the wave-function amplitude). Thus, the above selection of Δz was also considered more than adequate for the self-consistent analysis.

The electron potential energy across the filter/emitter is shown as a function of the longitudinal distance (z) for the non-self-consistent (linear) and the self-consistent electrostatic potential in Figs. 4(a) (resonant filter/emitter A for $V_{bias} = 0.10$ eV) and 4(b) (resonant filter/emitter B for $V_{bias} = 0.05$ eV). It is observed that the difference between the self-consistent and the linear potential is larger for resonant filter/emitter A (with a Fermi energy $E_f = 30$ meV) than for filter/emitter B (with a Fermi energy $E_f = 2.26$ meV). This difference is at least an order of magnitude smaller for resonant filter/emitter B. The difference between the self-consistent and the linear electrostatic potential energy, $\Delta V = V_{SC}(z) - V_L(z)$ [where $V_{SC}(z)$ and $V_L(z)$ are the self-consistent and linear electrostatic potential energies], is shown in Figs. 5(a) (resonant filter/emitter A for $V_{bias} = 0.10$ eV) and 5(b) (resonant filter/emitter B for $V_{bias} = 0.05$ eV). Since resonant filter/emitter A has more carriers available and a larger transmission peak at the resonant energy, stronger electron localization is expected, which raises the potential energy profile for the transmitted electrons higher than that of filter/emitter B.

The wave-function square amplitude, $|\psi(z)|^2$, as function of the longitudinal (z) direction, is shown for both the

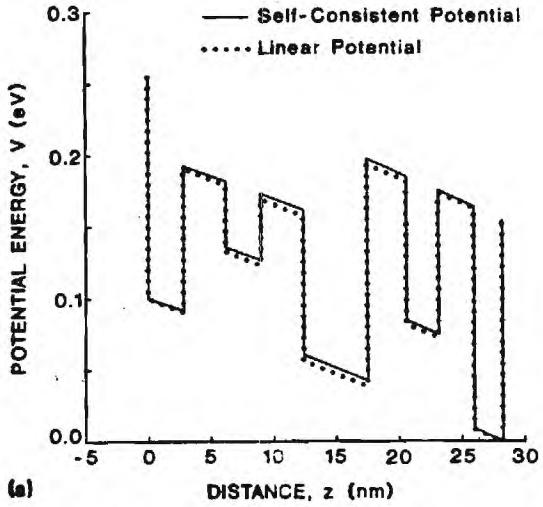

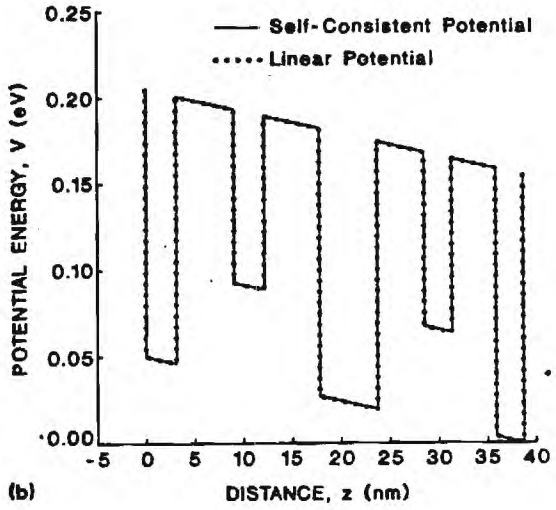

FIG. 4. Electron potential energy profile along the filter/emitter region. Both the self-consistent (solid line) and the non-self-consistent (dotted line) potential energy profiles are shown. (a) Resonant filter/emitter A for $V_{bias} = 0.10$ eV and (b) resonant filter/emitter B for $V_{bias} = 0.05$ eV.

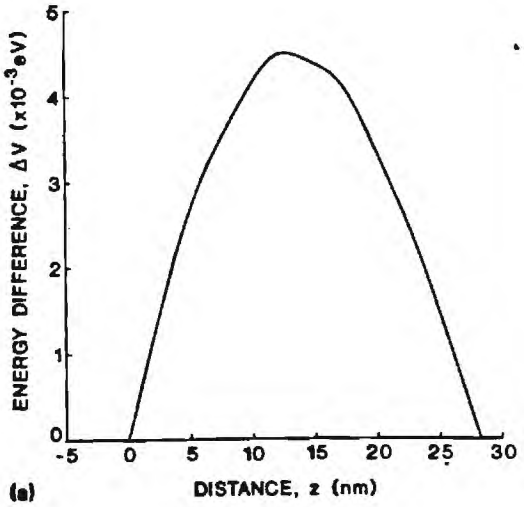

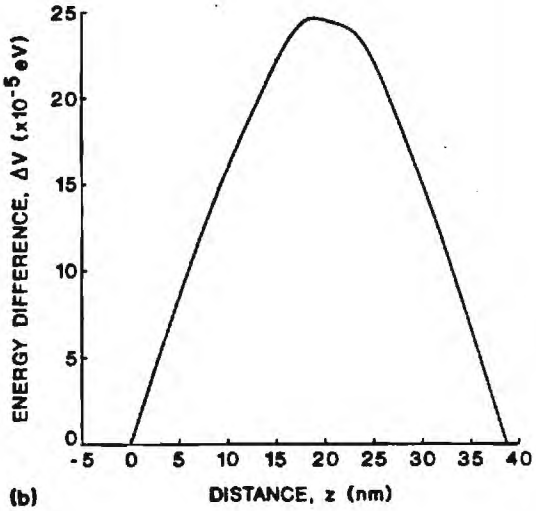

FIG. 5. Difference ΔV between the self-consistent and the linear electrostatic potential energy along the filter/emitter region. (a) Resonant filter/emitter A for $V_{bias} = 0.10$ eV and (b) resonant filter/emitter B for $V_{bias} = 0.05$ eV.

non-self-consistent and the self-consistent approaches in Figs. 6(a) (resonant filter/emitter A) and 6(b) (resonant filter/emitter B). In both cases the square amplitude of the wave function was calculated at the resonant energy of the non-self-consistent design. Consequently for resonant filter/emitter A the wavefunction was computed for $KE_{out} = 0.0125$ eV (or total electron energy $E = V_0 + KE_{out} = 0.28$ eV) and $V_{bias} = 0.10$ eV, while for filter/emitter B it is computed for $KE_{out} = 0.0536$ eV (or $E = 0.21$ eV) and $V_{bias} = 0.05$ eV. From Fig. 6(a) it is observed that the square of the wave-function amplitude peaks at the boundaries between layers of differing compositions. In addition, the highest peaks appear at the boundaries of the central (resonant) layer. The square of the wave-function amplitude is not exactly symmetric around the central (resonant) layer due to the asymmetry of the filter/emitter in layer thicknesses. For the self-consistent calculation it can be seen from Figs. 6(a) and 6(b) that the wave functions corresponding to the self-consistent potentials have lower and slightly shifted peaks [Fig. 6(a)] since the self-consistent electrostatic potential is expected to shift the filter/emitter characteristics to higher applied voltages. The self-consistent effect is more pronounced in the case of resonant filter/emitter A since for this design a higher Fermi energy level ($E_f = 30$ meV) was assumed, and consequently the screening effect was stronger. Comparing the square of the wave-function amplitudes of these filter/emitters with those of resonant tunneling diodes,[43] a fundamental difference is observed. The peaks of the square of the wave-function amplitude in the resonant tunneling diodes occur inside the well region (resonant layer), while in the resonant filter/emitter cases the peaks occur at the boundaries of the central (resonant) layer with the surrounding layers. Thus, electron localization is expected near and at the interfaces between differing aluminum composition layers and especially near the interfaces of the central layer. This may be due to higher electron velocities inside the well regions than inside the barrier regions, re-

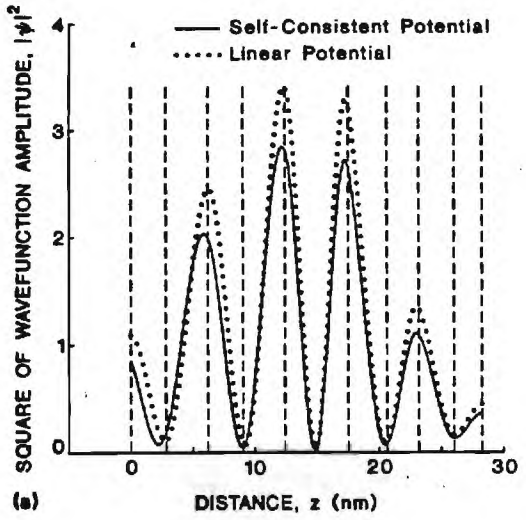

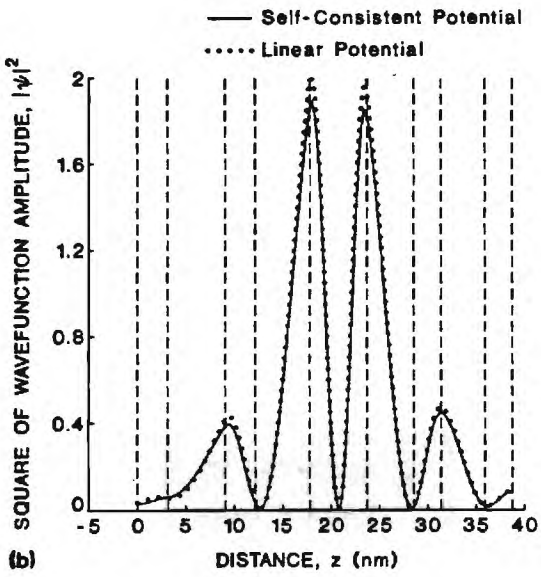

FIG. 6. Square of the wave-function amplitude, $|\psi(z)|^2$, along the filter/emitter region. Both the self-consistent (solid line) and the non-self-consistent wave function (dotted line) are shown. The dashed lines represent boundaries between different aluminum composition layers of the filter/emitter. (a) Resonant filter/emitter A for $V_{bias} = 0.10$ eV and (b) resonant filter/emitter B for $V_{bias} = 0.05$ eV.

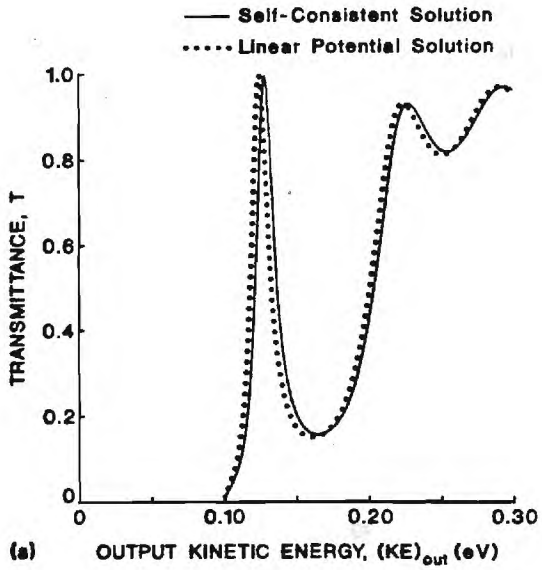

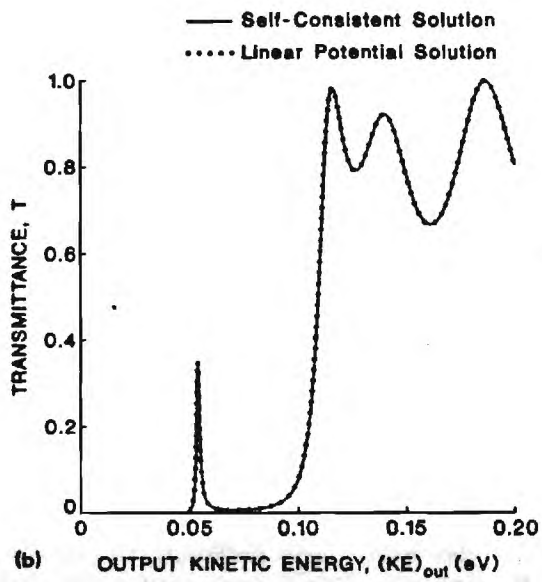

FIG. 7. Electron transmission characteristics of the nine-layer filter/emitters as a function of the output kinetic energy for an applied bias potential energy of V_{bias}. The characteristics of the non-self-consistent (dotted line) and of the self-consistent electron potential energy (solid line) are shown. (a) Resonant filter/emitter A for $V_{bias} = 0.10$ eV and (b) resonant filter/emitter B for $V_{bias} = 0.05$ eV.

sulting in an electron localization near the interfaces between the differing electron velocity regions.

The electron-wave transmission characteristics of the resonant filter/emitters can be calculated using Eqs. (1), (2),and (8) for both the non-self-consistent and the self-consistent electrostatic potential. The results of the calculation are shown in Figs. 7(a) (resonant filter/emitter A for $V_{bias} = 0.10$ eV) and 7(b) (resonant filter/emitter B for $V_{bias} = 0.05$ eV). In both self-consistent electrostatic potential cases there is a slightshift of the transmittance curve toward higher output kinetic energies (or equivalently input kinetic energies) from its corresponding linear electrostatic potential case. This was expected due to the increased electron potential energy. The effect is again more pronounced for resonant filter/emitter A due to its higher Fermi energy.

The electron density, $n(z)$, can be calculated from Eq. (4) using the self-consistent electrostatic potential. The electron densities of the two resonant filter/emitters are shown in Figs. 8(a) (resonant filter/emitter A for $V_{bias} = 0.10$ eV) and 8(b) (resonant filter/emitter B for $V_{bias} = 0.05$ eV) as functions of the longitudinal distance (z). Comparisons of Figs. 6 and 8 reveal some similarity between the $|\psi(z)|^2$ and $n(z)$. This is expected since $n(z)$ is an energy average over all electrons using Fermi–Dirac statistics [Eq. (3)], and to this average, electrons with energies near the resonant energy (Figs. 6) mainly contribute.

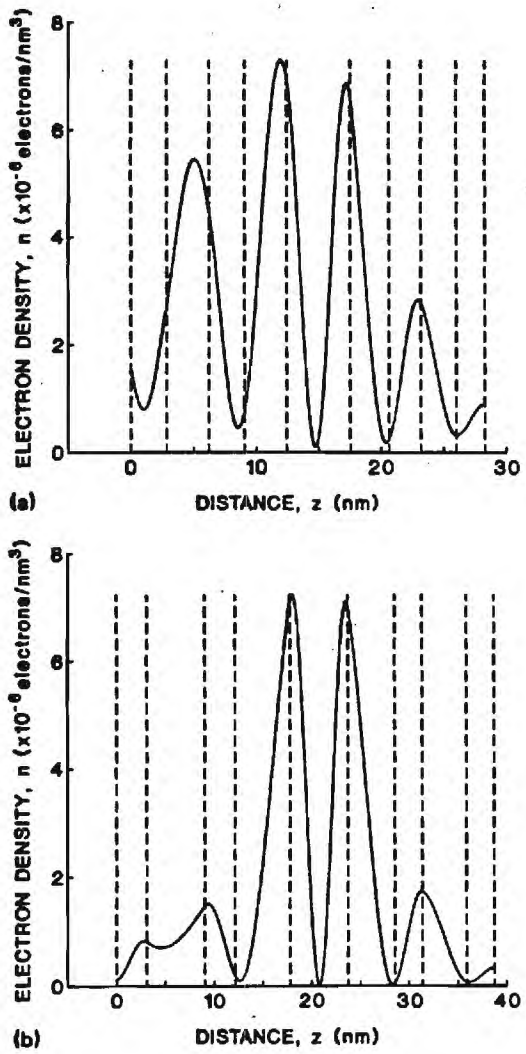

FIG. 8. Electron density distribution along the filter/emitter region using the self-consistent electron potential energy profile. The dashed lines represent boundaries between different aluminum composition layers of the filter/emitter. (a) Resonant filter/emitter A for $V_{bias} = 0.10$ eV and $KE_{out} = 0.125$ eV (resonant values) and (b) resonant filter/emitter B for $V_{bias} = 0.05$ eV and $KE_{out} = 0.0536$ eV.

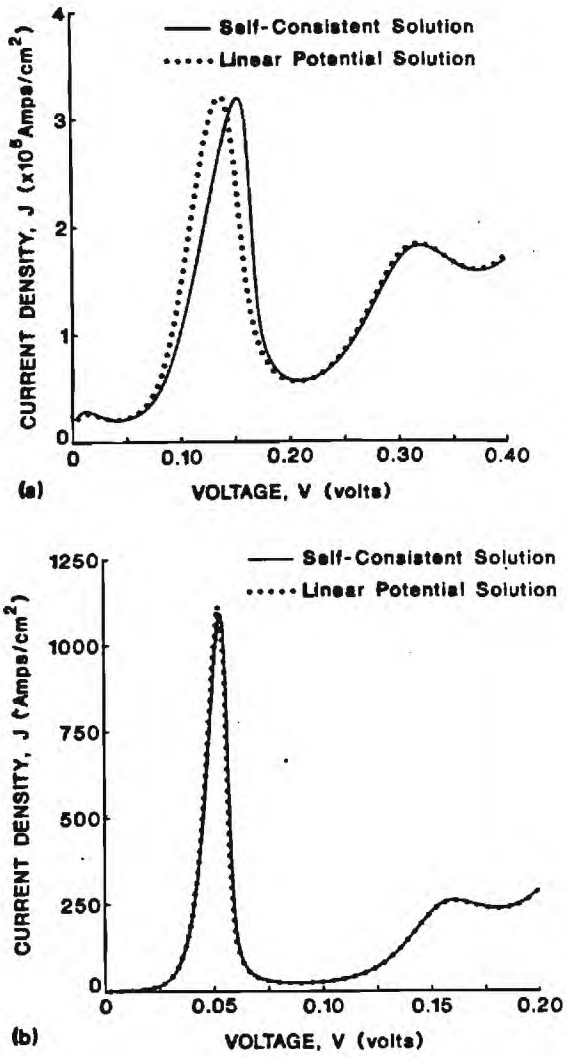

FIG. 9. Current-voltage characteristics of the filter/emitters using the self-consistent (solid line) and the non-self-consistent electron potential energy profile (dotted line). (a) Resonant filter/emitter A and (b) resonant filter/emitter B.

Finally the current-voltage characteristics of the resonant filter/emitters can be calculated using Eq. (7) with either a linear or a self-consistent electrostatic potential. The *I-V* characteristics of resonant filter/emitters A and B are shown in Figs. 9(a) and 9(b), respectively. The effect of the self-consistent electrostatic potential is again stronger for resonant filter/emitter A. In both cases the self-consistent characteristics are shifted (in the case of resonant filter/emitter B this shift is small) to higher applied bias voltages. This is in agreement with the *I-V* characteristics of the resonant tunneling diodes.[37–43] From the *I-V* characteristics a negative differential resistivity (NDR) is clearly observed. For resonant filter/emitter A the peak-to-valley ratio is 5.74 (with peak current density $J = 3.22 \times 10^6$ A/cm^2 at 0.155 V) for the self-consistent calculation, and 5.78 for the non-self-consistent calculation (with peak current density $J = 3.20 \times 10^6$ A/cm^2 at 0.135 V). For resonant filter/emitter B the peak-to-valley ratio is 46.1 (with peak current density $J = 1.09 \times 10^3$ A/cm^2 at ~0.0525 V) for the self-consistent calculation, and 47.2(with peak current density $J = 1.11 \times 10^3$ A/cm^2 at 0.0525 V) for the non-self-consistent calculation. It is observed that filter/emitter B has about three orders of magnitude smaller current density even if its Fermi energy is only one order of magnitude smaller than that of resonant filter/emitter A. However, resonant filter/emitter B exhibits an order of magnitude larger peak-to-valley ratio. All the above calculations were performed for $T = 25$ K and for a relative dielectric permittivity of GaAs of 13.18.

D. Effects of temperature variation

The temperature dependence of resonant filter/emitter B current-voltage characteristics is shown in Fig. 10 for $T = 25$, 35, and 50 K. The Fermi energy levels were computed[56] as described previously for resonant filter/emitter B and are $E_f = 2.26$, 3.63, and 5.26 meV, respectively. The self-consistent as well as the non-self-consistent *I-V* characteristics are shown for the three selected temperatures. For higher temperatures the electron coherence

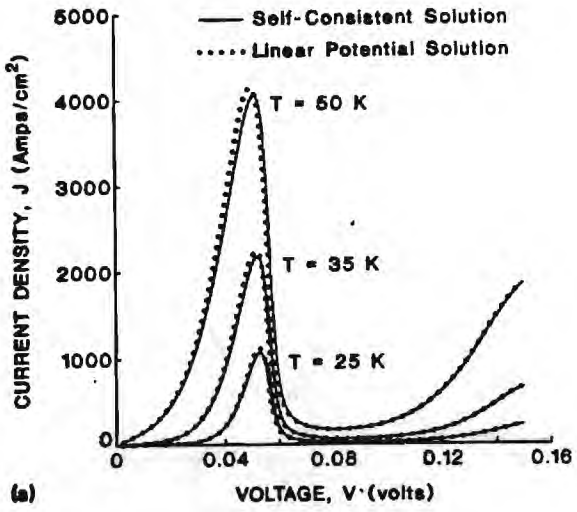

FIG. 10. Temperature dependence of the I-V characteristics of resonant filter/emitter B for $T = 25$, 35, and 50 K. Both self-consistent (solid lines) and non-self-consistent (dotted lines) characteristics are included.

TABLE III. Design parameters of an electron-wave interference nonresonant filter/emitter consisting of nine layers surrounded by $Ga_{0.8}Al_{0.2}As$ and designed to emit 0.0536-eV electrons for the constrained-composition design when biased at 0.05 eV.

Nonresonant filter/emitter C design				
	Constrained-composition design			
Layer No. j	Number monolayers thick	Aluminum composition x_j	Unbiased electron potential energy V_j (eV)	Normalized effective mass m_j^*/m_0
1	11	0.00	0.0000	0.0670
2	21	0.20	0.1546	0.0836
3	11	0.07	0.0541	0.0728
4	20	0.20	0.1546	0.0836
5	10	0.00	0.0000	0.0670
6	17	0.20	0.1546	0.0836
7	10	0.07	0.0541	0.0728
8	16	0.20	0.1546	0.0836
9	10	0.00	0.0000	0.0670

length is expected to be smaller than the dimensions of the filter/emitter, thus significantly degrading the quantum interference behavior of the device due to scattering mechanisms.

E. Analysis of nonresonant filter/emitters

The two resonant filter/emitters A and B described previously have been designed to exhibit electron transmission peaks for a specified input (or output) kinetic energy and applied bias potential. A question that now arises is how a nonresonant filter/emitter would perform. In order to answer this question, resonant filter/emitter B is redesigned so that the central layer is a quarter-electron wavelength layer instead of a half-electron wavelength layer. The resulting nonresonant filter/emitter C (Table III) has a 10-monolayer-thick central layer (instead of a 21-monolayer-thick central layer for the resonant filter/emitter B). Consequently, the nonresonant filter/emitter C is not expected to exhibit any negative differential resistance behavior. The rest of the layers of nonresonant filter/emitter C have the characteristics shown in Table II for the resonant filter/emitter B. The electron potential energy profile of the nonresonant filter/emitter C is shown in Fig. 11(a) for both the non-self-consistent and self-consistent computation. The difference ΔV between the self-consistent and the linear electrostatic potential energy is shown in Fig. 11(b). It is observed that this difference is approximately two orders of magnitude smaller than that of the resonant filter/emitter B. Thus, the space-charge effects are much less significant in the nonresonant design. The square of the wave-function amplitude, $|\psi(z)|^2$, for an output kinetic energy of 0.0536 eV (resonant energy of the resonant filter/emitter B) and for an applied bias potential energy of 0.05 eV (resonant bias potential energy of the resonant filter/emitter B) is shown in Fig. 11(c). Comparing Fig. 11(c)with Fig. 6(b) a significant difference can be observed. In the nonresonant filter/emitter C the wave-function square amplitude drops fast along the longitudinal direction of the device, revealing very small electron localization inside the nonresonant filter/emitter. The difference between the self-consistent and the non-self-consistent calculation is insignificant for the nonresonant device. The electron transmission characteristics of the nonresonant filter/emitter C are presented in Fig. 11(d) for $V_{bias} = 0.05$ eV. No peak in the transmission is observed between 0.05 and 0.08 eV as was expected [compare with Fig. 7(b) for the resonant filter/emitter B]. The electron density distribution, $n(z)$, is shown in Fig. 11(e). This distribution resembles the $|\psi(z)|^2$ distribution since for all the electron energies near the Fermi level the filter/emitter exhibits the same nonresonant electron transmission response. Finally, the I-V characteristics of the nonresonant filter/emitter C are shown in Fig. 11(f). No negative differential resistance is observed in this case as was expected [compare with Fig. 9(b) of the resonant filter/emitter B]. In addition, the current density is much smaller (2–3 orders of magnitude) for voltages up to 0.10 V since most of the incident electrons are reflected due to the nonresonant behavior of the filter/emitter. All the computations for the nonresonant filter/emitter C were performed again for a temperature of 25 K.

IV. DISCUSSION AND SUMMARY

In all the example cases presented for both the resonant and the nonresonant filter/emitters, the step size Δz of the stair-step approximation was selected to be one monolayer. Smaller step sizes (fraction of a monolayer) have also been tested but the final results were almost unaffected (observed changes were smaller than $\pm 10^{-6}$). Therefore, the 1-monolayer thickness was retained for savings and efficiency of computer time. The number of energy points (in momentum space) for the integral computation [Eqs. (4) and (7)] was varied between 400 and 1000 points depending on the electron transmission characteristics of

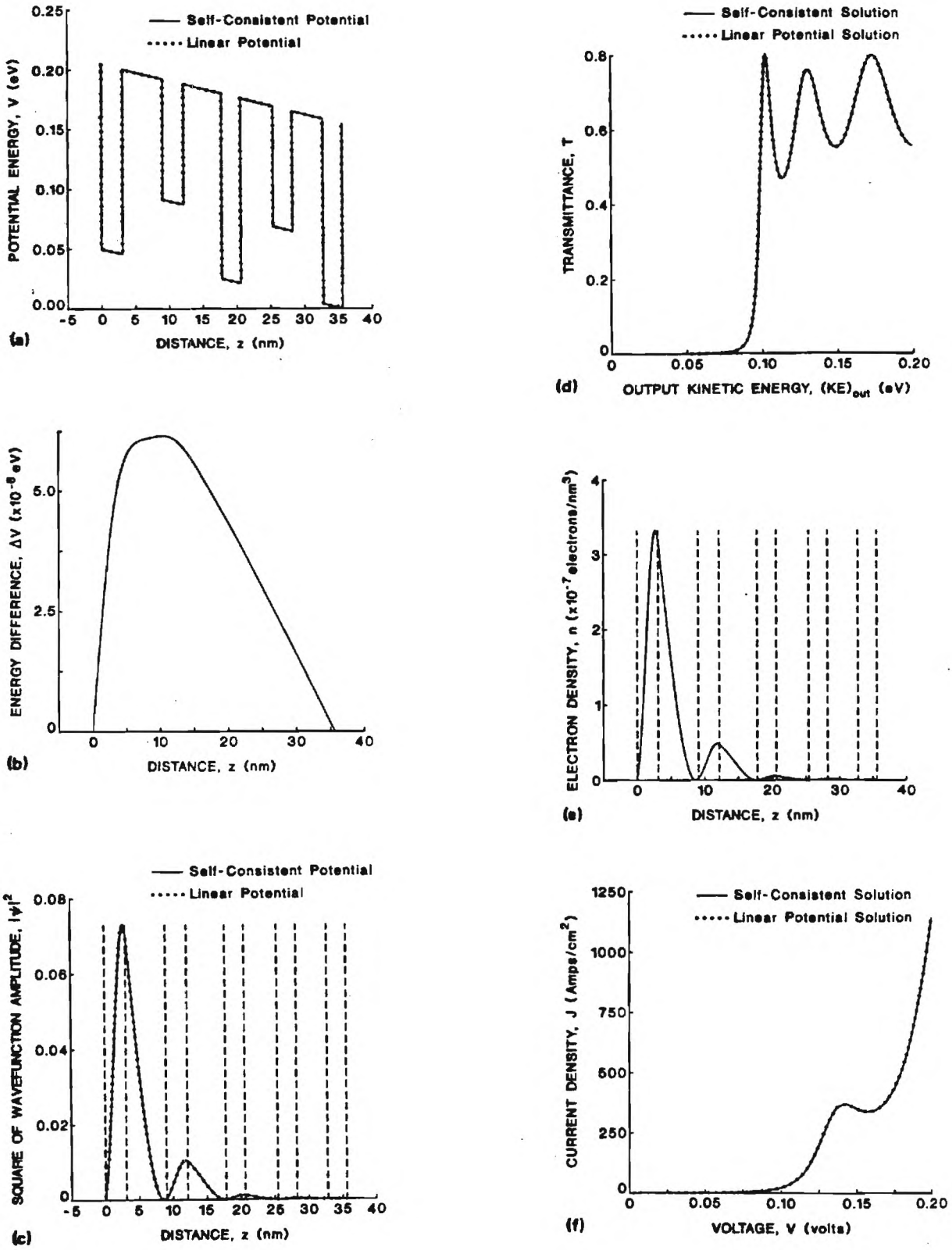

FIG. 11. Characteristics of the nonresonant filter/emitter C. (a) The electron potential energy profile; self-consistent potential (solid line) and non-self-consistent (dotted line) potential energy profile along the filter/emitter region for $V_{bias} = 0.05$ eV. (b) The difference ΔV between the self-consistent and non-self-consistent (linear) electron potential energy profiles along the filter/emitter region for $V_{bias} = 0.05$ eV. (c) The square of the wave-function amplitude distribution for $V_{bias} = 0.05$ eV and $KE_{out} = 0.0536$ eV. The dashed lines represent boundaries between the layers of differing aluminum composition of the filter/emitter. (d) The electron transmission characteristics for both the self-consistent (solid line) and the non-self-consistent (dotted line) electron potential energy profile for $V_{bias} = 0.05$ eV. (e) The self-consistent electron density distribution along the nonresonant filter/emitter for $V_{bias} = 0.05$ eV. The dashed lines represent boundaries between different aluminum composition layers of the filter/emitter. (f) Current-voltage characteristics of the nonresonant filter/emitter using the self-consistent (solid line) and the non-self-consistent (dotted line) electron potential energy profile.

the filter/emitter. For example, resonant filter/emitter B needed more energy points than resonant filter/emitter A due to its sharper energy (momentum) space characteristics. Convergence of the algorithm was obtained within 3–25 iterations for resonant filter/emitter A, and 2–6 iterations for resonant filter/emitter B. The convergence criterion selected was that the maximum absolute difference of the electrostatic potential energy between two successive iterations should be less than a preselected value. This value for the examples presented was set equal to 10^{-4}. All computations were performed in a CDC-Cyber 855 or 990 mainframe computer with CPU times varying between 400 and 45 000 s, with the most time-consuming cases being the *I-V* characteristics computations (using 80 voltage values).

In the analysis presented in this paper, only states corresponding to propagating electrons are considered. In actual devices, it is possible for electrons injected from the contacts to scatter inelastically into lower-energy states that could be bound states for the superlattice structure. However, due to the low temperature, the small longitudinal dimensions (compared to the electron coherence length), and the absence of doping, inelastic scattering can be neglected and only the ballistic component of the current considered. Thus, in a ballistic analysis like the one presented in this paper, the link between propagating and bound states has been removed. However, the contribution of the bound (localized) states could be significant in a self-consistent solution since the electrostatic potential would be altered by the bound electrons. For this reason the exact eigenstates of the bound electrons were calculated for both filter/emitters A and B. The bound electronic state energies can be determined exactly, under the effective mass approximation, through the solution of the appropriate eigenvalue equation for the superlattice. Using this approach for the unbiased filter/emitter A the following four eigenstates were found: $E_0 = 0.0530$, $E_1 = 0.0812$, $E_2 = 0.1053$, and $E_3 = 0.1304$ eV, where all energies are measured from the bottom of the conduction band of GaAs. However, under the design operation bias of 0.10 V the number of bound eigenstates of the superlattice reduces to two: $E_0 = 0.1006$ and $E_1 = 0.1143$ eV. In order to determine the resonant strength of these localized states the electron transmissivity was computed over the total range of energies. It was found that under the design bias voltage the contribution of the eigenenergy $E_0 = 0.1006$ eV eigenstate was very small (transmissivity of less than 0.7%) and of the eigenenergy $E_1 = 0.1143$ eV was not observable. The small transmissivity reveals that the localized eigenwave functions cannot be efficiently excited, thus making the electron localization in these states very small and consequently of negligible effect on the electrostatic potential distribution and the self-consistent solution presented for filter/emitter A. Similarly, for the unbiased filter/emitter B the following five eigenstates were calculated: $E_0 = 0.0519$, $E_1 = 0.0925$, $E_2 = 0.0973$, $E_3 = 0.1259$, and $E_4 = 0.1353$ eV. Under the designed operation bias of 0.05 V, the number of bound eigenstates reduces to four: $E_0 = 0.0749$, $E_1 = 0.1001$, $E_2 = 0.1396$, and $E_3 = 0.1457$ eV. Again using the electron transmissivity calculation method, the maximum transmissivity was found for the $E_3 = 0.1457$ eV eigenstate and was less than 7%. The excitations of the remainder of the localized eigenenergies were negligible. Again this reveals that these localized states can not be efficiently excited to produce any significant localized space-charge effects due to the bound states. Thus the presented self-consistent calculations are not altered. Similar results were also calculated for the nonresonant filter/emitter C. More detailed information about the calculation of the bound eigenstates and their resonant strengths will be presented in a future publication.[58] If strong localized states exist in designed filter/emitter devices, then the electron density of Eq. (4) would be replaced by

$$n(z) = n_{\text{prop}}(z) + \sum_i n_{\text{bound},i}(z), \tag{9}$$

where $n_{\text{prop}}(z)$ is given by Eq. (4) and $n_{\text{bound},i}(z)$ (ith bound state contribution) for sufficiently long times approaches[43]

$$n_{\text{bound},i}(z) \simeq \frac{m^*(z) k_B T}{\hbar^2 \pi} |\psi_i(z)|^2 \times \ln\{1 + \exp[(E_f - E_i)/k_B T]\}, \tag{10}$$

where E_i and $\psi_i(z)$ are the bound eigenenergy and the corresponding eigenwave function, and $m^*(z) = m_j$ when z is within the jth layer. The above expression is approximate in that it uses Fermi–Dirac statistics inside the superlattice, and these are valid only under equilibrium. However, in cases where the bound states can be strongly excited, Eq. (9) can give more accurate results than Eq. (4). A remedy in the case of strong localized states would be the inclusion of a depletion region on the collector side so as to prevent electrons from being backscattered into the structure. The presence of a sizable electric field produced within the depletion region would serve to redirect the carrier's momentum in the forward direction after a possible scattering, thus greatly reducing backscattered injection. This is similar to the action of the collector in a junction transistor biased in the active mode.[59] Of course, bound states in the structure can be eliminated altogether by selecting GaAs to be the material of the output region. This does not affect the design of the filter/emitter. In this case the bound states cannot exist in the superlattice.

The analysis presented describes a purely quantum-mechanical transport and is valid for distances that are less than the electron coherence length. In all the examples analyzed, it was assumed that the semiconductor materials had parabolic bandstructure. This was a good approximation since both filter/emitters have been designed to resonate at low electron energies. However, for sufficiently high applied bias voltages, the electron energies exceed the parabolic band-structure regime, and the band structure is more appropriately treated as nonparabolic. Furthermore, the band structure may vary with the direction of the electron-wave propagation (anisotropy). Both of these effects can be incorporated by using an energy-dependent aniso-

tropic effective mass. In the latter case the solutions of the Schroedinger equation have to be modified but the remainder of the analysis is still valid. The anisotropic case could be used when the lowest-energy band consisted of ellipsoidal X minima energy surfaces (Si, AlAs, etc.) or ellipsoidal L minima energy surfaces (Ge) rather than the spherical Γ minimum energy surface associated with the direct gap $Ga_{1-x}Al_xAs$.

Finally, in the analysis and the examples presented, the effect of the space-charge field due to the contact-filter/emitter junctions was not taken into account. The present analysis has focused on the filter/emitter region design and function. The impinging electrons (from the left-hand side of Fig. 1) were assumed to originate from the quasi-equilibrium contact regions and are incident on the filter/emitter. The self-consistent potential will not be significantly altered by the contacts in shape or relative magnitude. However, the contacts will cause an elevation of the electron potential energy profile of the whole filter/emitter structure due to the inevitable alignment of the Fermi energy levels at equilibrium. For this reason a specialized transit region between the contacts and the filter/emitter will be required for the designed operation of the device. The design and fabrication of this specialized region and its effect in the function of the filter/emitter is under investigation.

In summary, for the first time to our knowledge, the transmission and the current-voltage characteristics of electron-wave quantum-interference resonant filter/emitters were studied using a non-self-consistent and a self-consistent analysis. It was shown that the resonant filter/emitters can exhibit negative differential resistivity similar to that in resonant tunneling diodes. Several example designs on $Ga_{1-x}Al_xAs$ alloys were presented including both resonant and nonresonant filter/emitters. For low temperatures (in the ballistic transport regime) it was shown that the effect of the space-charge fields is insignificant for nonresonant filter/emitters, while it can be quite significant for resonant filter/emitters at high Fermi energy levels. The I-V characteristics of the resonant filter/emitters are shifted to higher applied voltages due to the screening effect of the electron localization. However, the peak-to-valley ratios remained almost the same as those from the non-self-consistent computation. Importantly, in contrast to resonant tunneling diodes the valley current is lower and remains low over a larger voltage range ("flat valley"). The square of the wave-function amplitude distributions, electron potential energy profiles, and electron density profiles were also presented. Semiconductor superlattice electron-wave quantum-interference resonant filter/emitters have potential use as high-speed switches and oscillators and as monoenergetic emitters in electroluminescent devices and photodetectors.

This research was supported in part by a grant from the Joint Services Electronics Program under contract No. DAAL-03-90-C-0004. One of us (K.F.B.) was supported in part by a Presidential Young Investigator award from the National Science Foundation and another (E.N.G.) by a Research Initiation award from the National Science Foundation.

[1] L. Esaki and R. Tsu, IBM J. Res. Dev. **13**, 61 (1970).
[2] L. L. Chang, L. Esaki, and R. Tsu, Appl. Phys. Lett. **24**, 593 (1974).
[3] T. C. L. G. Sollner, W. D. Goodhue, P. E. Tannenwald, C. D. Parker, and D. D. Peck, Appl. Phys. Lett. **43**, 588 (1983).
[4] T. Nakagawa, H. Imamoto, T. Kojima, and K. Ohta, Appl. Phys. Lett. **49**, 73 (1986).
[5] C. J. Summers, K. F. Brennan, A. Torabi, and H. M. Harris, Appl. Phys. Lett. **52**, 132 (1988).
[6] S. Sen, F. Capasso, A. C. Gossard, R. A. Spah, A. L. Hutchinson, and S. N. G. Chu, Appl. Phys. Lett. **51**, 1428 (1987).
[7] M. Heiblum, M. V. Fischetti, W. P. Dumke, D. J. Frank, I. M. Anderson, and C. M. Knoedler, Phys. Rev. Lett. **58**, 816 (1987).
[8] R. C. Potter and A. A. Lakhani, Appl. Phys. Lett. **52**, 1349 (1988).
[9] J. R. Hayes, P. England, and J. P. Harbison, Appl. Phys. Lett. **52**, 1578 (1988).
[10] A. F. J. Levi, J. R. Hayes, P. M. Platzman, and W. Wiegmann, Phys. Rev. Lett. **55**, 2071 (1985).
[11] M. Heiblum, M. I. Nathan, D. C. Thomas, and C. M. Knoedler, Phys. Rev. Lett. **55**, 2200 (1985).
[12] S. Washburn and R. A. Webb, Adv. Phys. **35**, 375 (1986).
[13] Y. Imry, in *Directions in Condensed Matter Physics*, edited by G. Grinstein and G. Mazenko (World Scientific, Singapore, 1986), pp. 101–163.
[14] J. Spector, H. L. Stormer, K. W. Baldwin, L. N. Pfeiffer, and K. W. West, Appl. Phys. Lett. **56**, 1290 (1990).
[15] J. Spector, H. L. Stormer, K. W. Baldwin, L. N. Pfeiffer, and K. W. West, Appl. Phys. Lett. **56**, 2433 (1990).
[16] T. K. Gaylord and K. F. Brennan, J. Appl. Phys. **65**, 814 (1989).
[17] T. K. Gaylord and K. F. Brennan, Appl. Phys. Lett. **53**, 2047 (1988).
[18] T. K. Gaylord, E. N. Glytsis, and K. F. Brennan, J. Appl. Phys. **65**, 2535 (1989).
[19] E. N. Glytsis, T. K. Gaylord, and K. F. Brennan, J. Appl. Phys. **66**, 1494 (1989).
[20] E. N. Glytsis, T. K. Gaylord, and K. F. Brennan, J. Appl. Phys. **66**, 6158 (1989).
[21] C. J. Summers and K. F. Brennan, Appl. Phys. Lett. **48**, 806 (1986).
[22] K. F. Brennan and C. J. Summers, J. Appl. Phys. **61**, 5410 (1987).
[23] K. F. Brennan and C. J. Summers, IEEE J. Quantum Electron. **QE-23**, 320 (1987).
[24] T. K. Gaylord, E. N. Glytsis, and K. F. Brennan, J. Appl. Phys. **66**, 1483 (1989).
[25] T. K. Gaylord, E. N. Glytsis, and K. F. Brennan, J. Appl. Phys. **66**, 1842 (1989).
[26] G. Nimtz and P. Marquardt, Appl. Phys. A **47**, 317 (1988).
[27] A. Szafer and A. D. Stone, Phys. Rev. Lett. **62**, 300 (1989).
[28] S. Datta, M. R. Melloch, S. Bandyopadhyay, R. Noren, M. Vaziri, M. Miller, and R. Reinfenberger, Phys. Rev. Lett. **55**, 2344 (1985).
[29] H. R. Frohne, M. J. McLennan, and S. Datta, J. Appl. Phys. **66**, 2699 (1989).
[30] D. J. BenDaniel and C. B. Duke, Phys. Rev. **152**, 683 (1966).
[31] J. L. Blue and C. L. Wilson, IEEE Trans. Electron Devices **30**, 1056 (1983).
[32] M. S. Lundstrom and R. J. Schuelke, IEEE Trans. Electron Devices **30**, 1151 (1983).
[33] I. D. Mayergoyz, J. Appl. Phys. **59**, 195 (1986).
[34] C. M. Snowden, *Semiconductor Device Modelling* (Peregrinus, London, 1988).
[35] S. Selberherr, *Analysis and Simulation of Semiconductor Devices* (Springer, New York, 1984).
[36] S. Datta, *Quantum Phenomena*, Vol. VIII in *Modular Series on Solid-State Devices* (Addison-Wesley, Reading, MA, 1989).
[37] H. Ohnishi, T. Inata, S. Muto, N. Yokoyama, and A. Shibatomi, Appl. Phys. Lett. **49**, 1248 (1986).
[38] H. Ohnishi, N. Yokoyama, and A. Shibatomi, IEEE Trans. Electron Devices **36**, 2335 (1989).
[39] M. Cahay, M. McLennan, S. Datta, and M. S. Lundstrom, Appl. Phys. Lett. **50**, 612 (1987).
[40] M. Cahay, M. A. Osman, H. L. Grubin, and M. McLennan, in *Nanostructure Physics and Fabrication* (Academic, New York, 1989), pp. 495–499.
[41] M. Cahay, M. McLennan, S. Datta, and M. S. Lundstrom, in *Funda-*

mental Research on the Numerical Modelling of Semiconductor Devices and Processes, edited by J. J. H. Miller (Boole, Dublin, 1987), pp. 53–57.
[42] W. Pötz, Superlattices and Microstructures 6, 187 (1989).
[43] K. F. Brennan, J. Appl. Phys. 62, 2392 (1987).
[44] C. M. Wu and E. S. Yang, Solid-State Electron. 22, 241 (1979).
[45] H. L. Berkowitz and R. A. Lux, J. Vac. Sci. Technol. B 5, 967 (1987).
[46] N. C. Kluksdahl, A. M. Kriman, and D. K. Ferry, Phys. Rev. B 39, 7720 (1989).
[47] R. K. Mains, J. P. Sun, and G. I. Haddad, Appl. Phys. Lett. 55, 371 (1989).
[48] K. Imamura, S. Muto, N. Yokoyama, M. Sasa, H. Ohnishi, S. Hiyamizu, and H. Nishi, Surf. Sci. 174, 481 (1986).
[49] K. Seo, M. Heiblum, C. M. Knoedler, J. E. Oh, J. Pamulapati, and P. Bhattacharya, IEEE Electron. Device Lett. 2, 73 (1989).
[50] M. Altarelli, in *Heterojunctions and Semiconductor Superlattices*, edited by G. Allan, G. Bastard, N. Boccra, M. Lannoo, and M. Voos (Springer, New York, 1986), pp. 12–37.
[51] M. O. Vassell, J. Lee, and H. F. Lockwood, J. Appl. Phys. 54, 5206 (1983).
[52] K. F. Brennan and C. J. Summers, J. Appl. Phys. 61, 614 (1986).
[53] R. Tsu and L. Esaki, Appl. Phys. Lett. 22, 562 (1973).
[54] H. C. Casey and M. B. Panish, *Heterostructure Lasers Part A. Fundamental Principles* (Academic, New York, 1978), Chap. 4.
[55] R. C. Miller, D. A. Kleinman, and A. C. Gossard, Phys. Rev. B 29, 7085 (1984).
[56] T. K. Gaylord and J. N. Linxwiler, Jr., Am. J. Phys. 44, 353 (1976).
[57] R. F. Pierret, *Advanced Semiconductor Fundamentals*, Vol. VI in *Modular Series on Solid-State Devices* (Addison-Wesley, Reading, MA, 1987).
[58] E. N. Glytsis, T. K. Gaylord, and K. F. Brennan, J. Appl. Phys. (to be published).
[59] B. G. Streetman, *Solid State Electronic Devices*, 3rd ed. (Prentice Hall, Englewood Cliffs, NJ, 1990), p. 235.

Quantum Interference Effects In Semiconductors: A Bibliography

THOMAS K. GAYLORD, FELLOW, IEEE, ELIAS N. GLYTSIS, MEMBER, IEEE, GREGORY N. HENDERSON, STUDENT MEMBER, IEEE, KEVIN P. MARTIN, DAVID B. WALKER, DANIEL W. WILSON, STUDENT MEMBER, IEEE, AND KEVIN F. BRENNAN, SENIOR MEMBER, IEEE

Refinements in growth techniques such as molecular beam epitaxy (MBE) have produced materials with ballistic (collisionless) electron transport lengths of over a micron. Coupled with nanolithography it is now possible to fabricate structures with both lateral and vertical dimensions on the order of the deBroglie wavelength of a ballistic electron. In these structures quantum interference effects can dominate the electronic behavior. In view of the rapidly expanding interest and activity in this area, the following bibliography has been compiled as an introduction and study guide to this field. The papers listed describe the extensive theoretical and experimental results that have been obtained on quantum interference effects as well as discuss possible application areas. Works of a fundamental nature concerning phenomena that are basic to all semiconductor behavior have not been included. Articles on the properties and band structure of semiconductors, which are essential to a complete understanding of quantum interference effects, have not been included. Conference papers, though frequently very important, have not been included to conserve space. The papers are listed alphabetically according to the first author's surname. As in the compilation of any bibliography, numerous valuable and pertinent articles have probably been inadvertently omitted.

I. BIBLIOGRAPHY

[1] R. J. Aggarwal, M. A. Reed, W. R. Frensley, Y. C. Kao, and J. H. Luscombe, "Tunneling spectroscopic study of finite superlattices," *Appl. Phys. Lett.*, vol. 57, pp. 707–709, Aug. 13, 1990.

[2] Y. Aharonov and D. Bohm, "Significance of electromagnetic potentials in the quantum theory," *Phys. Rev.*, vol. 115, pp. 485–491, Aug. 1, 1959.

[3] D. Ahn, "Theory of polar-optical-phonon scattering in a semiconductor quantum wire," *J. Appl. Phys.*, vol. 69, pp. 3596–3600, Mar. 15, 1991.

[4] A. Aishima and Y. Fukushima, "Negative resistance in a finite superlattice owing to quantum mechanical reflection," *J. Appl. Phys.*, vol. 61, pp. 249–256, Jan. 1, 1987.

Manuscript received January 16, 1991; revised July 8, 1991. This work was supported in part by a grant from the Joint Services Electronics Program under Contract DAAL-03-90-C-0004. G. N. Henderson was supported by an Office of Naval Research Graduate Research Fellowship and E. N. Glytsis was supported by a Research Initiation Award ECS-8909971 from the National Science Foundation. K. P. Martin was supported by the National Science Foundation under Grant ECS-8922512.

The authors are with the School of Electrical Engineering and Microelectronics Research Center, Georgia Institute of Technology, Atlanta, GA 30332.

IEEE Log Number 9101226.

[5] G. Allan, G. Bastard, N. Boccara, M. Lannoo, and M. Voos, Eds., *Heterojunctions and Semiconductor Superlattices*. Berlin, Germany: Springer-Verlag, 1986.

[6] D. R. Allee, S. Y. Chou, J. S. Harris, and R. F. W. Pease, "Engineering lateral quantum interference devices using electron beam lithography and molecular beam epitaxy," *J. Vac. Sci. Technol. B*, vol. 7, pp. 2015–2019, Nov./Dec. 1989.

[7] D. R. Allee, S. Y. Chou, J. S. Harris, and R. F. W. Pease, "Resonant tunneling of 1-dimensional electrons across an array of 3-dimensionally confined potential wells," *Superlattices Microstructures*, vol. 7, pp. 131–134, 1990.

[8] S. J. Allen, R. Bhat, G. Brozak, E. A. Andrada e Silva, F. DeRosa, L. T. Florez, P. Grabbe, J. P. Harbison, D. M. Hwang, M. Koza, P. F. Miceli, S. A. Schwarz, L. J. Sham, and M. C. Tamargo, "Vertical transport, tunnelling cyclotron resonance, and saturated mini-band transport in semiconductor superlattices," *Electronic Properties of Multilayers and Low-Dimensional Semiconductor Structures*, J. M. Chamberlain, L. Eaves, and J. C. Portal, Eds. London, U.K.: Plenum Press, 1989, pp. 117–132.

[9] M. Altarelli, "Band structure, impurities and excitons in superlattices," in *Heterostructures and Semiconductor Superlattices*, G. Allan, G. Bastard, N. Boccara, M. Lannoo, and M. Voos, Eds. Berlin, Germany: Springer-Verlag, 1986, pp. 12–37.

[10] B. L. Al'tshuler and A. G. Aronov, "Magnetoresistance of thin films and of wires in a longitudinal magnetic field," *JETP Lett.*, vol. 33, pp. 499–501, May 1981.

[11] B. L. Al'tshuler, "Fluctuations in the extrinsic conductivity of disordered conductors," *JETP Lett.*, vol. 41, pp. 648–651, June 25, 1985.

[12] B. L. Al'tshuler, A. G. Aronov, and D. E. Khmelnitsky, "Effects of electron-electron collisions with small energy transfers on quantum localisation," *J. Phys. C: Solid State Phys.*, vol. 15, pp. 7367–7386, Dec. 1982.

[13] B. L. Al'tshuler, A. G. Aronov, and B. Z. Spivac, "The Aaronov-Bohm effect in disordered conductors," *JETP Lett.*, vol. 33, pp. 94–97, Jan. 20, 1981.

[14] B. L. Al'tshuler, A. G. Aronov, B. Z. Spivak, D. Yu. Sharvin, and Yu. V. Sharvin, "Observation of the Aaronov–Bohm effect in hollow metal cylinders," *JETP Lett.*, vol. 35, pp. 588–591, June 5, 1982.

[15] B. L. Al'tshuler and P. A. Lee, "Disordered electronic systems," *Phys. Today*, vol. 41, pp. 36–44, Dec. 1988.

[16] E. S. Alves, L. Eaves, M. Henini, O. H. Hughes, M. L. Leadbeater, F. W. Sheard, G. A. Toombs, G. Hill, and M. A. Pate, "Observation of intrinsic bistability in resonant tunnelling devices," *Elec. Lett.*, vol. 24, pp. 1190–1191, Sept. 1, 1988.

[17] E. S. Alves, M. L. Leadbeater, L. Eaves, M. Henini, O. H. Hughes, A. Celeste, J. C. Portal, G. Hill, and M. A. Pate, "Hybrid magneto-electric states in resonant tunnelling structures," *Superlattices Microstructures*, vol. 5, pp. 527–530, 1989.

0018-9219/91/0800-1159$01.00

[18] F. Ancilotto. "Quantum tunneling of electrons through a double barrier in a transverse magnetic field," *J. Phys. C - Sol. St. Phys.* vol. 21. pp. 4657–4662. 1988.
[19] M. G. Ancona. "Asymptotic structure of the density-gradient theory of quantum structure," in *Computational Electronics*. K. Hess. J. P. Leburton. and U. Ravaioli. Eds. Norwell. MA: Kluwer. 1991. pp. 255–258.
[20] P. W. Anderson. D. J. Thouless. E. Abrahams. and D. S. Fisher. "New method for scaling theory of localization," *Phys. Rev. B*. vol. 22. pp. 3519–3526. Oct. 15. 1980.
[21] T. Ando and S. Mori. "Effective-mass theory of semiconductor heterojunctions and superlattices." *Surface Sci.*. vol. 113. pp. 124–130. Jan. 1982.
[22] T. Ando. A. B. Fowler. and F. Stern. "Electronic properties of two-dimensional systems." *Rev. of Modern Phys.*. vol. 54. pp. 438–621. Apr. 1982.
[23] W. Andreoni and R. Car. "Similarity of (Ga. Al. As) alloys and ultrathin heterostructures: Electronic properties from the empirical pseudopotential method." *Phys. Rev. B* . vol. 21. pp. 3334–3344. Apr. 15. 1988.
[24] A. F. M. Anwar. A. N. Khondker. and M. R. Khan. "Calculation of the traversal time in resonant tunneling devices." *J. Appl. Phys.*. vol. 65. pp. 2761–2765. Apr. 1. 1989.
[25] Y. Arakawa. A. Larsson. J. Paslaski. and A. Yariv. "Active Q switching in a GaAs/AlGaAs multiquantum well laser with an intracavity monolithic loss modulator." *Appl. Phys. Lett.*. vol. 48. pp. 561–563. Mar. 1986.
[26] Y. Arakawa. K. Vahala. and A. Yariv. "Quantum noise and dynamics in quantum well and quantum wire lasers." *Appl. Phys. Lett.*. vol. 45. pp. 950–952. Nov. 1. 1984.
[27] Y. Arakawa. K. Vahala. and A. Yariv. "Dynamic and spectral properties of semiconductor lasers with quantum-well and quantum-wire effects." *Surface Sci.*. vol. 174. pp. 155–162. Aug. 1986.
[28] Y. Arakawa. K. Vahala. and A. Yariv. "Reduction of the spectral linewidth of semiconductor lasers with quantum wire effects-Spectral properties of GaAlAs double heterostructure lasers in high magnetic fields." *Appl. Phys. Lett.*. vol. 48. pp. 384–386. Feb. 10. 1986.
[29] Y. Arakawa and A. Yariv. "Quantum well lasers-gain. spectra. dynamics." *IEEE J. Quantum Electron.*. vol. 22. pp. 1887–1899. Sept. 1986.
[30] Y. Arakawa. T. Sogawa. M. Nishioka. M. Tanaka. and H. Sakaki. "Picosecond pulse generation (<1.8 ps) in a quantum well laser by a gain switching method." *Appl. Phys. Lett.*. vol. 26. pp. 1295–1297. Oct. 26. 1987.
[31] D. Arnold and K. Hess. "The effect of reflecting contacts on high field transport." *Solid-State Electron* . vol. 31. no. 3/4. pp. 593–594. 1988.
[32] D. Arnold. K. Hess. T. Higman. J. J. Coleman. and G. J. Iafrate. "Dynamics of heterostructure hot-electron diodes." *J. Appl. Phys.*. vol. 66. pp. 1423–1427. Aug. 1. 1989.
[33] D. Arnold. K. Hess. and G. J. Iafrate. "Electron transport in heterostructure hot-electron diodes." *Appl. Phys. Lett.*. vol. 53. pp. 373–375. Aug. 1. 1988.
[34] H. E. G. Arnot. M. Watt. C. M. Sotomayor-Torres. R. Glew. R. Cusco. J. Bates. and S. P. Beaumont. "Photoluminescence of overgrown GaAs-GaAlAs quantum dots." *Superlattices Microstructures*. vol. 5. pp. 459–463. 1989.
[35] M. Artaki and K. Hess. "Transient and steady-state electron transport in GaAs/$Al_xGa_{1-x}As$ heterojunctions at low temperatures: The effects of electron-electron interations." *Phys. Rev. B*. vol. 37. pp. 2933–2945. Feb. 15. 1988.
[36] M. Asada. "Intraband relaxation time in quantum-well lasers." *IEEE J. Quantum Electron.*. vol. 25. pp. 2019–2026. Sept. 1989.
[37] D. E. Aspnes. "Modulation spectroscopy/electric field effects on the dielectric function of semiconductors" in *Handbook on Semiconductors*. T. S. Moss. Ed. Holland. The Netherlands: North-Holland. 1980. pp. 109–154.
[38] Y. Avishai and Y. B. Band. "Quantum electronic conductance of terminal junction." *Phys. Rev. Lett.*. vol. 62. pp. 2527–2530. May 22. 1989.
[39] Y. Avishai and Y. B. Band. "Electronic conductance of an orifice in a magnetic field." *Phys. Rev. B*. vol. 40. pp. 3429–3432. Aug. 15. 1989.
[40] Y. Avishai and B. Horovitz. "Phase transition of the Ahronov-Bohm perodicity in metallic cylinders." *Phys. Rev. B*. vol. 35. pp. 423–426. Jan. 1. 1987.
[41] M. Ya. Azbel. "Quantum particle in one-dimensional potentials with incommensurate periods." *Phys. Rev. Lett.*. vol. 43. pp. 1954–1957. Dec. 24. 1979.
[42] M. Ya. Azbel. "Quantum delta-dimensional Landauer formula." *J. Phys. C: Solid State Phys.*. vol. 14. pp. L225–L230. 1981.
[43] M. Ya. Azbel. "Resonance tunnelling and localization spectroscopy." *Solid State Commun.*. vol. 45. pp. 527–530. Feb. 1983.
[44] P. F. Bagwell. "Solution of Dyson's equation in a quasi-1D wire." *J. Phys.: Condens. Matter*. vol. 2. pp. 1–9. 1990.
[45] P. F. Bagwell. "Evanescent modes and scattering in quasi-one-dimensional wires." *Phys. Rev. B.*. vol. 41. pp. 10354–10371. May 15. 1990.
[46] P. F. Bagwell. D. A. Antoniadis. and T. P. Orlando. "Quantum mechanical nonstationary transport phenomena in nanostructured silicon inversion layers." *VLSI Electronics: Microstructure Science*. vol. 18. ch. 8. pp. 305–355. 1989.
[47] P. F. Bagwell. T. P. E. Broekaert. T. P. Orlando. and C. G. Fonstad. "Resonant tunneling diodes and transistors with a one. two. and three dimensional electron emitter."*J. Appl. Phys.* 1991.
[48] P. F. Bagwell and T. P. Orlando. "Landauer's conductance formula and its generalization to finite voltages." *Phys. Rev. B*. vol. 40. pp. 1456–1464. July 15. 1989.
[49] P. F. Bagwell and T. P. Orlando. "Broadened conductivity tensor and density of states for a superlattice potential in one. two. and three dimensions." *Phys. Rev. B*. vol. 40. pp. 3735–3748. Aug. 15. 1989.
[50] T. B. Bahder. C. A. Morrison. and J. D. Bruno. "Resonant level lifetime in GaAs AlGaAs double-barrier structures." *Appl. Phys. Lett.*. vol. 51. pp. 1089–1090. Oct. 5. 1987.
[51] B. H. Bairamov. R. A. Evarestov. I. P. Ipatova. Yu. E. Kitaev. A. Yu. Maslov. M. Delaney. T. A. Grant. M. V. Klein. D. Levi. J. Klem. and H. Morkoc. "Inelastic light scattering in GaAs-AlAs superlattices." *Superlattices Microstructures*. vol. 6. no. 2. pp. 227–231. 1989.
[52] V. I. Balykin and V. S. Letokhov. "Deep focusing of an atomic beam in the Angstrom region by laser radiation. " *Sov. Phys. JETP*. vol. 67. pp. 78–83. Jan. 1988.
[53] V. I. Balykin and V. S. Letokhov. "Laser optics of neutral atomic beams." *Phys. Today*. vol. 42. pp. 23–28. Apr. 1989.
[54] K. M. S. Bandara. D. D. Coon. Byungsung O. Y. F. Lin. and M. H. Francombe. "Exchange interactions in quantum well subbands." *Appl. Phys. Lett.*. vol. 53. pp. 1931–1933. Nov. 14. 1988.
[55] K. M. S. V. Bandara. D. D. Coon. and H. Zhao. "Resonant tunneling time delay and quantum well sheet density." *J. Appl. Phys.*. vol. 66. pp. 1227–1230. Aug. 1. 1989.
[56] H. Bando. T. Nakagawa. H. Tokumoto. K. Ohta. and K. Kajimura. "Resonant magnetotunneling in AlGaAs GaAs triple barrier diodes." *Japan. J. Appl. Phys.*. vol. 26. pp. DO14–DO15. 1987.
[57] S. Bandyopadhyay. "Quantum phase coherent effects in the photo-luminescence spectra of disordered mesoscopic structures." in *Nanostructure Physics and Fabrication*. M. A. Reed and W. P. Kirk. Eds. San Diego. CA: Academic. 1989. pp. 117–121.
[58] S. Bandyopadhyay. G. H. Bernstein. and W. Porod. "Quantum devices based on phase coherent lateral quantum transport." in *Nanostructure Physics and Fabrication*. M. A. Reed and W. P. Kirk. Eds. San Diego. CA: Academic. 1989. pp. 183–188.
[59] S. Bandyopadhyay and M. Cahay. "The generalized scattering matrix approach: An efficient technique for modeling quantum transport in relatively large and heavily doped structures." in *Computational Electronics* . K. Hess. J. P. Leburton. and U. Ravaioli. Eds. Norwell. MA: Kluwer Academic. 1991. pp. 223–226.
[60] S. Bandyopadhyay and W. Porod. "Performance of electrostatic Aharonov-Bohm interferometers in the diffusive regime. *Appl .Phys. Lett.*. vol. 53. pp. 2323–2325. Dec. 5. 1988.
[61] I. Bar-Joseph. G. Sucha. D. A. B. Miller. D. S. Chemla. B. I. Miller. and U. Koren. "Self-electro-optic effect device and modulation converter with InGaAs/InP multiple quantum wells." *Appl. Phys. Lett.*. vol. 52. pp. 51–53. Jan. 1. 1988.
[62] H. U. Baranger. "Transport in electron waveguides: Filtering and bend resistances. " in *Computational Electronic*. K. Hess. J. P. Leburton. and U. Ravaioli. Eds. Norwell. MA: Kluwer Academic. 1991. pp. 201–206.

[63] H. U. Baranger, J. Pelouard, J. Pone, and R. Castagne, "Ballistic peaks in the distribution function from intervalley transfer in a submicron structure," *Appl. Phys. Lett.*, vol. 51, pp. 1708–1710, Nov. 23, 1987.

[64] H. U. Baranger and A. D. Stone, "Quenching of the Hall resistance in ballistic microstructures: A collimation effect," *Phys. Rev. Lett.*, vol. 63, pp. 414–417, July 24, 1989.

[65] J. R. Barker, "Theory of quantum transport in lateral nanostructures," in *Nanostructure Physics and Fabrication*, M. A. Reed and W. P. Kirk, Eds. San Diego, CA: Academic, 1989, pp. 253–262.

[66] J. B. Barner and S. T. Ruggiero, "Observation of the incremental charging of Ag particles by single electrons," *Phys. Rev. Lett.*, vol. 59, pp. 807–810, Aug. 17, 1987.

[67] G. Bastard, "Superlattice band structure in the envelope-function approximation," *Phys. Rev. B*, vol. 24, pp. 5693–5697, Nov. 15, 1981.

[68] G. Bastard, J. A. Brum, and R. Ferreira, "Electronic states in semiconductor heterostructures," in *Solid State Physics*, vol. 44, H. Ehrenreich and D. Turnbull, Eds. Boston, MA: Academic, 1991, pp. 229–415.

[69] R. T. Bate, "The future of microstructure technology — The industry view," *Superlattices Microstructures*, vol. 2, pp. 9–11, Jan. 1986.

[70] P. E. Batson, K. L. Kavanagh, J. M. Woodall, and J. W. Mayer, "Electron-energy-loss scattering near a single misfit dislocation at the GaAs/GaInAs interface," *Phys. Rev. Lett.*, vol. 57, pp. 2729–2732, Nov. 24, 1986.

[71] A. I. Baz', "Lifetime of intermediate states," *Sov. J. Nuc. Phys.*, vol. 4, pp. 182–188, Feb. 1967.

[72] G. Bauer, F. Kuchar, and H. Heinrich, (Eds.), *Two-dimensional Systems, Heterostructures, and Superlattices (Solid-state Sciences)*, vol. 53. Berlin, Germany: Springer-Verlag, 1984.

[73] G. Bauer, F. Kuchar, and H. Heinrich, Eds., *Two-dimensional Systems, Physics, and New Devices Solid-state Sciences*, vol. 67. Berlin, Germany: Springer-Verlag, 1986.

[74] S. P. Beaumont, "Fabrication and overgrowth of quantum wires and dots for optoelectronic applications," in *Nanostructure Physics and Fabrication*, M. A. Reed and W. P. Kirk, Eds. San Diego, CA: Academic, 1989, pp. 67–76.

[75] C. W. J. Beenakker and H. van Houten, "Magnetotransport and nonadditivity of point-contact resistances in series," *Phys. Rev. B.*, vol. 39, pp. 10445–10448, May 15, 1989.

[76] C. W. J. Beenakker and H. van Houten, "Billiard model of a ballistic multiprobe conductor," *Phys. Rev. Lett.*, vol. 63, pp. 1857–1860, Oct. 23, 1989.

[77] C. W. J. Beenakker and H. van Houten, "Semi-classical theory of magnetoresistance anomalies in ballistic multi-probe conductors," *Electronic Properties of Multilayers and Low Dimensional Semiconductor Structures*, J. M. Chamberlain, L. Eaves, and J. C. Portal, Eds. London, U.K.: Plenum, 1989, pp. 75–94.

[78] C. W. J. Beenakker and H. van Houten, "Quantum transport in semiconductor nanostructures," in *Solid State Physics*, vol. 44, H. Ehrenreich and D. Turnbull, Eds. Boston, MA: Academic, 1991, pp. 1–228.

[79] L. D. Bell, M. H. Hecht, W. J. Kaiser, and L. C. Davis, "Direct spectroscopy of electron and hole scattering," *Phys. Rev. Lett.*, vol. 64, pp. 2679–2682, May 28, 1990.

[80] L. D. Bell and W. J. Kaiser, "Observation of interface band structure by ballistic-electron-emission microscopy," *Phys. Rev. Lett.*, vol. 61, pp. 2368–2371, Nov. 14, 1988.

[81] L. D. Bell and W. J. Kaiser, "Scanning tunneling microscopy methods for spectroscopic imaging of subsurface interfaces," *Scanning Microscopy*, vol. 2, pp. 1231–1236, 1988.

[82] L. D. Bell, W. J. Kaiser, M. H. Hecht, and F. J. Grunthaner, "Direct control and characterization of a Schottky barrier by scanning tunneling microscopy," *Appl. Phys. Lett.*, vol. 52, pp. 278–280, Jan. 1988.

[83] T. E. Bell, "The quest for ballistic action," *IEEE Spectrum*, vol. 23, pp. 36–38, Feb. 1986.

[84] F. Beltram, F. Capasso, A. L. Hutchinson, and R. J. Malik, "Injection in a continuum miniband: Observation of negative transconductance in a superlattice-base transistor," *Appl. Phys. Lett.*, vol. 55, pp. 1534–1536, Oct. 9, 1989.

[85] F. Beltram, F. Capasso, D. L. Sivco, A. L. Hutchinson, S. N. G. Chu, and A. Y. Cho, "Scattering-controlled transmission resonances and negative differential conductance by field-induced localization in superlattices," *Phys. Rev. Lett.*, vol. 64, pp. 3167–3170, June 25, 1990.

[86] S. Ben Amor, L. Dmowski, J. C. Portal, J. P. Praseuth, and L. Goldstein, "Two-dimensional electron gas at $Ga_{0.47}In_{0.53}As/(Al_xGa_{1-x})_{0.48}In_{0.52}As$ interface," *Appl. Phys. Lett.*, vol. 53, pp. 479–481, Aug. 8, 1988.

[87] S. Ben Amor, K. P. Martin, J. J. L. Rascol, R. J. Higgins, R. C. Potter, A. A. Lakhani, and H. Hier, "Magnetotransport studies of charge accumulation in an AlInAs/GaInAs tunneling structure," *Appl. Phys. Lett.*, vol. 54, pp. 1908–1910, May 8, 1989.

[88] S. Ben Amor, K. P. Martin, J. J. L. Rascol, R. J. Higgins, R. C. Potter, A. A. Lakhani, and H. Hier, "Magneto-electric states in wide-well double barrier tunneling structures," *Surface Sci.*, vol. 228, pp. 378–381, Apr. 1990.

[89] S. Ben Amor, K. P. Martin, J. J. L. Rascol, R. J. Higgins, A. Torabi, H. M. Harris, and C. J. Summers, "Transverse magnetic field dependence of the current-voltage characteristics of double-barrier quantum well tunneling structures," *Appl. Phys. Lett.*, vol. 53, pp. 2540–2542, Dec. 19, 1988.

[90] S. Ben Amor, J. J. L. Rascol, K. P. Martin, R. J. Higgins, R. C. Potter, and H. Hier, "Transverse magnetic field studies in $Al_{1-x}In_xAs/Ga_{1-x}In_xAs$ quantum-well tunneling structures," *Phys. Rev. B*, vol. 41, pp. 7860–7863, Apr. 15, 1990.

[91] D. J. BenDaniel and C. B. Duke, "Space-charge effects of electron tunneling," *Phys. Rev.*, vol. 152, pp. 683–692, Dec. 9, 1966.

[92] S. Bending, C. Zhang, K. von Klitzing, E. Marclay, P. Gueret, and H. P. Meier, "Quasiclassical behavior of ballistic electrons in a perpendicular magnetic field," *Phys. Rev. B*, vol. 39, pp. 12981–12984, June 15, 1989.

[93] A. D. Benoit, S. Washburn, C. P. Umbach, R. B. Laibowitz, and R. A. Webb, "Asymmetry in the magnetoconductance of metal wires and loops," *Phys. Rev. Lett.*, vol. 57, pp. 1765–1768, Oct. 6, 1986.

[94] G. Benyuan, C. Coluzza, and M. Mangiantini, "The effect of scattering centers on resonant tunneling in double barrier heterostructures," *Superlattices Microstructures*, vol. 6, no. 2, pp. 153–156, 1989.

[95] R. Beresford, L. F. Luo, K. F. Longenbach, and W. I. Wang, "Resonant interband tunneling device with multiple negative differential resistance regions," *IEEE Electron Device Lett.*, vol. 11, pp. 110–113, Mar. 1990.

[96] S. Berger, H. A. Huggins, A. E. White, K. T. Short, and D. Loretto, "A new technique to produce single crystal epitaxial nanostructures," in *Nanostructure Physics and Fabrication*, M. A. Reed and W. P. Kirk, Eds. San Diego, CA: Academic, 1989, pp. 401–405.

[97] K. F. Berggren, T. J. Thornton, D. J. Newson, and M. Pepper, "Magnetic depopulation of 1D subbands in a narrow 2D electron gas in a GaAs:AlGaAs heterojunction," *Appl. Rev. Lett.*, vol. 57, pp. 1769–1772, Oct. 6, 1986.

[98] G. Bernstein and D. K. Ferry, "Negative differential conductivity in lateral surface superlattices," *J. Vac. Sci. Technol. B*, vol. 5, pp. 964–966, July/Aug. 1987.

[99] G. Bernstein and D. K. Ferry, "Observation of negative differential conductivity in a FET with structured gate," *Z. Phys. B*, vol. 67, pp. 449–452, 1987.

[100] G. H. Bernstein and A. Kriman, "Novel electron-diffraction transistor," *Proc. SPIE*, vol. 1284, pp. 91–100, 1990.

[101] G. H. Bernstein and A. Kriman, "Electron diffraction transistors," in *Proc. IEEE/Cornell Conf. on Advanced Concepts in High Speed Semiconductor Devices and Circuits*, pp. 246–254, Aug. 1989.

[102] R. Bertoncini, A. M. Kriman, and D. K. Ferry, "Field/scattering interaction quantization in high-field quantum transport," in *Nanostructure Physics and Fabrication*, M. A. Reed and W. P. Kirk, Eds. San Diego, CA: Academic, 1989, pp. 213–217.

[103] R. Bhandari, "Classical light waves and spinors," in *Analogies in Optics and Micro-Electronics*, W. van Haeringen and D. Lenstra, Eds. Dordrecht: Kluwer Academic Publishers, 1990, pp. 69–82.

[104] S. Bhobe, W. Porod, S. Bandyopadhyay, and D. J. Kirkner, "Tailoring transport properties by wavefunction engineering in quantum wells and its device applications," in *Nanostructure Physics and Fabrication*, M. A. Reed and W. P. Kirk, Eds. San Diego, CA: Academic, 1989, pp. 201–206.

[105] M. L. Biermann and C. R. Stroud, "Wave packets in a semiconductor superlattice," *Appl. Phys. Lett.*, vol. 58, pp. 2279–2281

1991.
[106] J. Bleuse, G. Bastard, and P. Voisin, "Electric-field-induced localization and oscillatory electro-optical properties of semiconductor superlattices," *Phys. Rev. Lett.*, vol. 60, pp. 220–223, Jan. 18, 1988.
[107] P. Blood, E. D. Fletcher, and C. T. Foxon, "Short-period (AlAs)(GaAs) superlattice lasers grown by molecular beam epitaxy," *Appl. Phys. Lett.*, vol. 53, pp. 299–301, July 25, 1988.
[108] A. R. Bonnefoi, R. T. Collins, T. C. McGill, R. D. Burnham, and F. A. Ponce, "Resonant tunneling in GaAs/AlAs heterostructures grown by metalorganic chemical vapor deposition," *Appl. Phys. Lett.*, vol. 46, pp. 285–287, Feb. 1, 1985.
[109] M. Botton and A. Ron, "Stimulated emission by ballistic electrons in semiconducting superlattices," *Appl. Phys. Lett.*, vol. 5, pp. 418–420, Jan. 30, 1989.
[110] A. Botula and K. L. Wang, "Improved small-signal analysis of the quantum-well injection transit time diode," *IEEE Trans. Electron Devices*, vol. 37, pp. 58–66, Jan. 1990.
[111] G. D. Boyd, D. A. B. Miller, D. S. Chemla, S. L. McCall, A. C. Gossard, and J. H. English, "Multiple quantum well reflection modulator," *Appl. Phys. Lett.*, vol. 50, pp. 1119–1121, Apr. 27, 1987.
[112] K. F. Brennan, "Self-consistent analysis of resonant tunneling in a two-barrier-one-well microstructure," *J. Appl. Phys.*, vol. 62, pp. 2392–2400, Sept. 15, 1987.
[113] K. F. Brennan and C. J. Summers, "Theory of resonant tunneling in a variably spaced multiquantum well structure: An Airy function approach," *J. Appl. Phys.*, vol. 61, pp. 614–623, Jan. 15, 1987.
[114] K. F. Brennan and Y. Wang, "Analysis of the two-dimensional dark currents in quantum well devices," *Appl. Phys. Lett.*, vol. 57, pp. 1337–1339, Sept. 24, 1990.
[115] L. Brey, G. Platero, and C. Tejedor, "Generalized transfer Hamiltonian for the study of resonant tunneling," *Phys. Rev. B*, vol. 38, pp. 10507–10511, Nov. 15, 1988.
[116] S. Briggs and J. P. Leburton, "Size effects in multisubband quantum wire structures," *Phys. Rev. B*, vol. 38, pp. 8163–8170, Oct. 15, 1988.
[117] T. P. E. Broekaert, W. Lee, and C. G. Fonstad, "Pseudomorphic $In_{0.53}Ga_{0.47}As$/AlAs/InAs resonant tunneling diodes with peak-to-valley ratios of 30 at room temperature," *Appl. Phys. Lett.*, vol. 53, pp. 1545–1547, Oct. 17, 1988.
[118] E. R. Brown, T. C. L. G. Sollner, C. D. Parker, W. D. Goodhue, and C. L. Chen, "Oscillations up to 420 GHz in GaAs/AlAs resonant tunneling diodes," *Appl. Phys. Lett.*, vol. 55, pp. 1777–1779, Oct. 23, 1989.
[119] G. Brozak, E. A. de Andrada e Silva, L. J. Sham, F. DeRosa, P. Miceli, S. A. Schwarz, J. P. Harbison, L. T. Florez, and S. J. Allen, "Tunneling cyclotron resonance and the renormalized effective mass in semiconductor barriers," *Phys. Rev. Lett.*, vol. 64, pp. 471–474, Jan. 22, 1990.
[120] G. Brozak, M. Helm, F. DeRosa, C. H. Perry, M. Koza, R. Bhat, and S. J. Allen, Jr., "Thermal saturation of band transport in a superlattice," *Phys. Rev. Lett.*, vol. 64, pp. 3163–3166, June 25, 1990.
[121] F. A. Buot and K. L. Jensen, "A distribution-function approach in the many-body quantum transport theory of quantum-based devices," in *Computational Electronics*, K. Hess, J. P. Leburton, and U. Ravaioli, Eds. Norwell, MA: Kluwer Academic, 1991, pp. 219–222.
[122] M. Buttiker, "Small normal-metal loop coupled to an electron reservoir," *Phys. Rev. B*, vol. 32, pp. 1846–1849, Aug. 1, 1985.
[123] M. Buttiker, "Role of quantum coherence in series resistors," *Phys. Rev. B*, vol. 33, pp. 3020–3026, Mar. 1, 1986.
[124] M. Buttiker, "Four-terminal phase-coherent conductance," *Phys. Rev. Lett.*, vol. 57, pp. 1761–1764, Oct. 6, 1986.
[125] M. Buttiker, "Voltage fluctuations in small conductors," *Phys. Rev. B*, vol. 35, pp. 4123–4126, Mar. 15, 1987.
[126] M. Buttiker, "Coherent and sequential tunneling in series barriers," *IBM J. Res. Develop.*, vol. 32, pp. 63–75, Jan. 1988.
[127] M. Buttiker, "Symmetry of electrical conduction," *IBM J. Res. Develop.*, vol. 32, pp. 317–334, May 1988.
[128] M. Buttiker, "When is the Hall resistance quantized?" in *Nanostructure Physics and Fabrication*, M. A. Reed and W. P. Kirk, Eds. San Diego, CA: Academic, 1989, pp. 319–329.
[129] M. Buttiker, "Transmission, reflection and the resistance of small conductors," *Electronic Properties of Multilayers and Low Dimensional Semiconductor Structures*, J. M. Chamberlain, L. Eaves, and J. C. Portal, Eds. London, U.K.: Plenum, 1989, pp. 51–73.
[130] M. Buttiker, "Traversal, reflection and dwell time for quantum tunneling," *Electronic Properties of Multilayers and Low Dimensional Semiconductor Structures*, J. M. Chamberlain, L. Eaves, and J. C. Portal, Eds. London, U.K: Plenum, 1989, pp. 297–315.
[131] M. Buttiker, "Phase-sensitive voltage measurements," in *Analogies in Optics and Micro-Electronics*, W. van Haeringen and D. Lenstra, Eds. Dordrecht: Kluwer Academic, 1990, pp. 185–202.
[132] M. Buttiker, Y. Imry, and M. Ya. Azbel, "Quantum oscillations in one-dimensional normal-metal rings," *Phys. Rev. A*, vol. 30, pp. 1982–1989, Oct. 19, 1984.
[133] M. Buttiker, Y. Imry, and R. Landauer, "Josephson behavior in small normal one-dimensional rings," *Phys. Lett. A*, vol. 96, pp. 365–367, July 18, 1983.
[134] M. Buttiker, Y. Imry, R. Landauer, and S. Pinhas, "Generalized many-channel conductance formula with application to small rings," *Phys. Rev. B*, vol. 31, pp. 6207–6215, May 15, 1985.
[135] M. Buttiker and R. Landauer, "Comment on 'The quantum mechanical tunnelling time problem—revisited'," *J. Phys. C*, vol. 21, pp. 6207–6213, Dec. 1988.
[136] G. Bylinsky, "A quantum leap in electronics," *Fortune*, vol. 119, pp. 113–120, Jan. 30, 1989.
[137] M. Cahay, S. Bandyopadhyay, and H. L. Grubin, "Doubled frequency of the conductance minima in electrostatic Aharonov-Bohm oscillations in one-dimensional rings," in *Nanostructure Physics and Fabrication*, M. A. Reed and W. P. Kirk, Eds. San Diego, CA: Academic, 1989, pp. 407–411.
[138] M. Cahay, P. Marzolf, and S. Bandyopadhyay, "Numerical study of the higher order moments of conductance fluctuations in mesoscopic structures, " in *Computational Electronics*, K. Hess, J. P. Leburton, and U. Ravaioli, Eds. Norwell, MA: Kluwer Academic, 1991, pp. 263–266.
[139] M. Cahay, M. McLennan, and S. Datta, "Conductance of an array of elastic scatterers: A scattering-matrix approach," *Phys. Rev. B*, vol. 37, pp. 10125–10136, June 15, 1988.
[140] M. Cahay, M. McLennan, S. Datta, and M. S. Lundstrom, "Importance of space-charge effect in resonant tunneling devices," *Appl. Phys. Lett.*, vol. 50, pp. 612–614, Mar. 9, 1987.
[141] M. Cahay, M. A. Osman, H. L. Grubin, and M. McLennan, "Space-charge effects in compositional and effective-mass superlattices," in *Nanostructure Physics and Fabrication*, M. A. Reed and W. P. Kirk, Eds. San Diego, CA: Academic, 1989, pp. 495–499.
[142] W. Cai, T. F. Zheng, P. Hu, B. Yudanin, and M. Lax, "Model of phonon-associated electron tunneling through a semicondutor double barrier," *Phys. Rev. Lett.*, vol. 63, pp. 418–421, July 24, 1989.
[143] D. Calecki, J. F. Palmier, and A. Chomette, "Hopping conduction in multiquantum well structures," *J. Phys. C: Solid State*, vol. 17, pp. 5017–5030, 1984.
[144] F. Capasso, Ed., *Physics of Quantum Electron Devices (Springer Series in Electronics and Photonics)*. Berlin, Germany: Springer-Verlag, 1990.
[145] F. Capasso and S. Datta, "Quantum electron devices," *Phys. Today*, vol. 43, pp. 74–82, Feb. 1990.
[146] F. Capasso and R. A. Kiehl, "Resonant tunneling transistor with quantum well base and high-energy injection: A new negative differential resistance device," *J. Appl. Phys.*, vol. 58, pp. 1366–1368, Aug. 1, 1985.
[147] F. Capasso, K. Mohammed, and A. Y. Cho, "Sequential resonant tunneling through a multiquantum well superlattice," *Appl. Phys. Lett.*, vol, 48, pp. 478–480, Feb. 17, 1986.
[148] F. Capasso, K. Mohammed, and A. Y. Cho, "Resonant tunneling through double barriers, perpendicular quantum transport phenomena in superlattices, and their device applications," *IEEE J. Quantum Electron.*, vol. 22, pp. 1853–1869, Sept. 1986.
[149] F. Capasso, K. Mohammed, A. Y. Cho, R. Hull, and A. L. Hutchinson, "Effective mass filtering: Giant quantum amplification of the photo-current in a semiconductor superlattice," *Appl. Phys. Lett.*, vol. 47, pp. 420–422, Aug. 15, 1985.
[150] F. Capasso, K. Mohammed, A. Y. Cho, R. Hull, and A. L. Hutchinson, "New quantum photoconductivity and large photocurrent gain by effective-mass filtering in a forward-biased superlattice p-n junction," *Phys. Rev. Lett.*, vol. 55, pp. 1152–1155, Sept. 2, 1985.

[151] F. Capasso, S. Sen, F. Beltram, and A. Y. Cho, "Resonant tunnelling superlattice devices, Physics and circuits in *Physics of Quantum Electron Devices*, F. Capasso, Ed. Berlin, Germany: Springer-Verlag, 1990, pp. 181–252.

[152] F. Capasso, S. Sen, F. Beltram, L. M. Lunardi, A. S. Vengurlekar, P. R. Smith, N. J. Shah, R. J. Malik, and A. Y. Cho, "Quantum functional devices: Resonant-tunneling transistors, circuits with reduced complexity, and multiple-valued logic," *IEEE Trans. Electron Devices*, vol. 36, pp. 2065–2082, Oct. 1989.

[153] F. Capasso, S. Sen, A. C. Gossard, A. L. Hutchinson, and J. H. English, "Quantum-well resonant tunneling bipolar transistor operating at room temperature," *IEEE Electron Device Lett.*, vol. EDL-7, pp. 573–576, Oct. 1986.

[154] F. Capasso, S. Sen, L. M. Lunardi, and A. Y. Cho, "Quantum transistors and circuits break through the barriers," *Circuits and Devices*, vol. 7, pp. 18–25, May 1991.

[155] J. P. Carton, J. L. Pichard, and N. Zanon, "Many-channel conductance of d-dimensional pure and randomly layered materials," *J. Phys. C: Solid State Phys.*, vol. 19, pp. 4041–4054, 1986.

[156] A. Celeste, L. A. Cury, J. C. Portal, M. Allovon, D. K. Maude, L. Eaves, M. Davies, M. Heath, and M. Maldonado, "AlAs and InAs mode LO phonon emission assisted tunneling in (InGa)As/(AlIn)As double barrier structures," *Solid-State Electron.*, vol. 32, pp. 1191–1195, Dec. 1989.

[157] J. M. Chamberlain, L. Eaves, and J. C. Porta eds., *Electroni Properties of Multilayers and Low Dimensional Semiconductor Structures*. London, U.K.: Plenum, 1989.

[158] V. Chandrasekhar, M. J. Rooks, S. Wind, and D. E. Prober, "Observation of Aharonov-Bohm electron interfence effects with periods h/e and h/2e in individual micron-size, normal-metal rings," *Phys. Rev. Lett.*, vol. 55, pp. 1610–1613, Oct. 7, 1985.

[159] A. M. Chang, G. Timp, T. Y. Chang, J. E. Cunningham, B. Chelluri, P. M. Mankiewich, R. E. Behringer, and R. E. Howard, "Magneto-quantum transport in a quasi-one-dimensional GaAs-$Al_xGa_{1-x}As$ ring," *Surface Sci.*, vol. 196, pp. 46–51, Mar. 1988.

[160] A. M. Chang, G. Timp, R. E. Howard, R. E. Behringer, P. M. Mankiewich, J. E. Cunningham, T. Y. Chang, and B. Chelluri, "Quantum transport in quasi-one-dimensiona GaAs-$Al_xGa_{1-x}As$ heterostructure devices, *Superlattices Microstructures*, vol. 4, pp. 515–520, 1988.

[161] A. M. Chang, K. Owusu-Sekyere, and T. Y. Chang, "Observation of phase-shift locking of the Aharonov-Bohm effect in doubly connected GaAs-$Al_xGa_{1-x}As$ heterostructure devices," *Solid State Commun.*, vol. 67, pp. 1027–1030, Sept. 1988.

[162] L. L. Chang, L. Esaki, and R. Tsu, "Resonant tunneling in semiconductor double barriers," *Appl. Phys. Lett.*, vol. 24, pp. 593–595, June 15, 1974.

[163] D. S. Chemla, "Degenerate four-wave mixing in room-temperature GaAs/GaAlAs multiple quantum well structures," *Appl. Phys. Lett.*, vol. 42, pp. 925–927, June 1, 1983.

[164] D. S. Chemla, D. A. B. Miller, and S. Schmitt-Rink, "Generation of ultrashort electrical pulses through screening by virtual populations in biased quantum wells," *Phys. Rev. Lett.*, vol. 59, pp. 1018–1021, Aug. 31, 1987.

[165] J. F. Chen, L. Yang, and A. Y. Cho, "Investigation of the influence of the well and barrier thicknesses in GaSb/AlSb/GaSb/AlSb/InAs double-barrier interband tunneling structures," *IEEE Electron Device Lett.*, vol. 11, pp. 532–534, Nov. 1990.

[166] R. Y. Chiao, "Berry's phases in optics," in *Analogies in Optics and Micro-Electronics*, W. van Haeringen and D. Lenstra, Eds. Dordrecht: Kluwer Academic, 1990, pp. 151–162.

[167] K. K. Choi, L. Fotiadis, P. G. Newman, and G. J. Iafrate, "Thermally stimulated hot-electron spectroscopy," *Appl. Phys. Lett.*, vol. 57, pp. 76–78, July 2, 1990.

[168] K. K. Choi, B. F. Levine, C. G. Bethea, J. Walker, and R. J. Malik, "Photoexcited coherent tunneling in a double-barrier superlattice," *Phys. Rev. Lett.*, vol. 59, pp. 2459–2462, Nov. 23, 1987.

[169] K. K. Choi, P. G. Newman, P. A. Folkes, and G. J. Iafrate, "Self-consistent resonant states and phase coherence in a wide double-barrier structure," *Appl. Phys. Lett.*, vol. 54, pp. 359–361, Jan. 23, 1989.

[170] K. K. Choi, P. G. Newman, P. A. Folkes, and G. J. Iafrate, "Electron tunneling in single- and double-barrier structures," *Phys. Rev. B*, vol. 40, pp. 8006–8009, Oct. 15, 1989.

[171] K. K. Choi, D. C. Tsui, and K. Alavi, "Experimental determination of the edge depletion width of the two-dimensional electron gas in GaAs/$Al_xGa_{1-x}As$," *Appl. Phys. Lett.*, vol. 50, pp. 110–112, Jan. 12, 1987.

[172] K. K. Choi, D. C. Tsui, and S. C. Palmateer, "Size effects on electron-electron interactions in GaAs-$Al_xGa_{1-x}As$ heterostructures," *Phys. Rev. B*, vol. 32, pp. 5540–5542, Oct. 15, 1985.

[173] S. Y. Chou, D. R. Allee, R. F. W. Pease, and J. S. Harris, "Observation of electron resonant tunneling in a lateral dual-gate resonant tunneling field-effect transistor," *Appl. Phys. Lett.*, vol. 55, pp. 176–178, July 10, 1989.

[174] S. Y. Chou, D. R. Allee, R. F. W. Pease, and J. S. Harris, "Quantum interference devices fabricated using molecular-beam epitaxy and ultra-high-resolution electron-beam lithography," *IEEE Trans. Electron Devices*, vol. 36, pp. 2617–2618, Nov. 1989.

[175] S. Y. Chou, D. A. Antoniadis, and H. I. Smith, "Observation of electron velocity overshoot in sub-100-nm-channel MOSFET's in silicon," *IEEE Electron Device Lett.*, vol. EDL-6, pp. 665–667, Dec. 12, 1985.

[176] S. Y. Chou, D. A. Antoniadis, and H. I. Smith, "Application of the Shubnikov-de Hass oscillations in the characterization of Si MOSFET's and GaAs MODFET's," *IEEE Trans. Electron Devices*, vol. ED-34, pp. 883–889, Apr. 1987.

[177] S. Y. Chou, D. A. Antoniadis, H. I. Smith, and M. A. Kastner, "Conductance fiucuations in ultra-short-channel Si MOSFETs", *Solid State Commun.*, vol. 61, pp. 571–572, Mar. 1987.

[178] S. Y. Chou and J. S. Harris, "Room-temperature observation of resonant tunneling through an AlGaAs/GaAs quasiparabolic quantum well grown by molecular beam epitaxy," *Appl. Phys. Lett.*, vol. 52, pp. 1422–1424, Apr. 25, 1988.

[179] S. Y. Chou, J. S. Harris, and R. F. W. Pease, "Lateral resonant tunneling field-effect transistor," *Appl. Phys. Lett.*, vol. 52, pp. 1982–1984, June 6, 1988.

[180] S. Y. Chou, H. I. Smith, and D. A. Antoniadis, "X-ray lithography for sub-100-nm-channel-length transistors using masks fabricated with conventional photolithography, anisotropic etching, and oblique shadowing," *J. Vac. Sci. Technol. B*, vol. 3, pp. 1587–1589, Nov./Dec. 1985.

[181] S. Y. Chou, E. Wolak, J. S. Harris, and R. F. W. Pease, "A lateral resonant tunneling FET," *Superlattices Microstructures*, vol. 4, pp. 181–186, 1988.

[182] C. S. Chu and R. S. Sorbello, "Effect of impurities on the quantized conductance of narrow channels," *Phys. Rev. B*, vol. 40, pp. 5941–5949, Sept. 15, 1989.

[183] F. Claro, F. Vivanco, and M. Pacheco, "Resonant tunneling: Relation between the transmission coefficient and a measurable quantity," *Surface Sci.*, vol. 228, pp. 486–488, 1990.

[184] A. Cohn and M. Rabinowitz, "Classical tunneling," *Int. J. Theor. Phys.*, vol. 29, no. 3, pp. 215–223, 1990.

[185] D. A. Collins, D. H. Chow, and T. C. McGill, "Experimental observation of large room-temperature current gains in a Stark effect transistor," *Appl. Phys. Lett.*, vol. 58, pp. 1673–1675, Apr. 15, 1991.

[186] L. A. Collins and A. L. Merts, "Model calculations for an atom interacting with an intense, time-dependent electric field," vol. 37, pp. 2415–2431, Apr. 1, 1988.

[187] S. Collins, D. Lowe, and J. R. Barker, "The quantum mechanical tunnelling time problem–revisited," *J. Phys. C*, vol. 20, pp. 6213–6232, Dec. 1987.

[188] S. Collins, D. Lowe, and J. R. Barker, "A dynamic analysis of resonant tunnelling," *J. Phys. C*, vol. 20, pp. 6233–6243, Dec. 1987.

[189] D. D. Coon and H. C. Liu, "Tunneling currents and two-body effects in quantum well and superlattice structures," *Appl. Phys. Lett.*, vol. 47, pp. 172–174, July 15, 1985.

[190] D. D. Coon and H. C. Liu, "Frequency limit of double barrier resonant tunneling oscillators," *Appl. Phys. Lett.*, vol. 49, pp. 94–96, July 14, 1986.

[191] D. D. Coon and E. Sorar, "Design of superlattice termination layers," *Appl. Phys. Lett.*, vol. 56, pp. 1790–1792, Apr. 30, 1990.

[192] E. Corcoran, "A thin line," *Scientif. Amer.*, vol. 263, pp. 98–100, Aug. 1990.

[193] E. Corcoran, "Electron switches," *Scientif. Amer.*, vol. 263, pp. 169–170, Sept. 1990.

[194] L. A. Cury, A. Celeste, and J. C. Portal, "Resonant-tunneling effects in a parabolic quantum well obtained by application of crossed magnetic and electric fields in a semiconductor quantum barrier," *Phys. Rev. B* , vol. 39, pp. 8760–8763, Apr. 15, 1989.

[195] G. Danan, B. Etienne, F. Mollot, R. Planel, A. M. Jean-Louis, F. Alexandre, B. Jusserans, G. Le Roux, J. Y. Marzin, H. Savary, and B. Sermage, "Optical evidence of the direct-to-indirect-gap transition in GaAs-AlAs short-period superlattices," *Phys. Rev. B* vol. 35, pp. 6207–6212, Apr. 15, 1987.

[196] G. Danan, J. S. Weiner, A. Pinczuk, J. Valladares, L. N. Pfeiffer, and K. West, "Optical investigation of a one-dimensional electron gas," in *Nanostructure Physics and Fabrication* , M. A. Reed and W. P. Kirk, Eds. San Diego, CA: Academic, 1989, pp. 113–116.

[197] B. Darling, "Multisubband electron transport in GaAs-$Al_xGa_{1-x}As$ quantum wells," *IEEE J. Quantum Electron.*, vol. 24, pp. 1628–1640, Aug. 1988.

[198] A. K. Das, M. L. Glasser, and S. H. Payne, "On a two-dimensional electron gas modulated by a periodic potential", *J. Phys. C* , vol. 21, pp. 357–366, Jan. 1988.

[199] S. Datta, "Quantum interference devices in *Physics of Quantum Electron Devices*, F. Capasso, Ed. Berlin, Germany: Springer-Verlag, 1990, pp. 321–352.

[200] S. Datta, *Quantum Phenomena* , vol. 8 in *Modular Series on Solid State Devices* , R. F. Pierret and G. W. Neudeck, Eds. Reading, MA: Addison-Wesley, 1989.

[201] S. Datta, "Quantum devices," *Superlattices Microstructures* , vol. 6, no. 1, pp. 83–93, 1989.

[202] S. Datta, "Steady-state quantum kinetic equation," *Phys. Rev. B* , vol. 40, pp. 5830–5833, Sept. 15, 1989.

[203] S. Datta, "Keldysh formalism and the Landauer-Buttiker approach," in *Physics of Low-Dimensional Semiconductor Structures* , P. N. Butcher, N. H. March, and M. P. Tosi, Eds. London, U.K.: Plenum, 1991.

[204] S. Datta and S. Bandyopadhyay, "Aharonov-Bohm effect in semiconductor microstructures," *Phys. Rev. Lett.*, vol. 58, pp. 717–720, Feb. 16, 1987.

[205] S. Datta, M. Cahay, and M. McLennan, "Scatter-matrix approach to quantum transport," *Phys. Rev. B* , vol. 36, pp. 5655–5658, Oct. 1, 1987.

[206] S. Datta and B. Das, "Electronic analog of the electro-optic modulator," *Appl. Phys. Lett.*, vol. 56, pp. 665–667, Feb. 12, 1990.

[207] S. Datta and M. J. McLennan, "Quantum transport with dissipation: Linear and non-linear response," in *Nanostructure Physics and Fabrication* , M. A. Reed and W. P. Kirk, Eds. San Diego, CA: Academic, 1989, pp. 241–251.

[208] S. Datta and M. J. McLennan, "Quantum transport in ultrasmall electronic devices," *Rep. Prog. Phys.*, vol. 53, pp. 1003–1048, Aug. 1990.

[209] S. Datta, M. R. Melloch, S. Bandyopadhyay, and M. S. Lundstrom, "Proposed structure for large quantum interference effects," *Appl. Phys. Lett.*, vol. 48, pp. 487–489, Feb. 17, 1986.

[210] S. Datta, M. R. Melloch, S. Bandyopadhyay, R. Noren, M. Vaziri, M. Miller, and R. Reifenberger, "Novel interference effects between parallel quantum wells," *Phys. Rev. Lett.*, vol. 55, pp. 2344–2347, Nov. 18, 1985.

[211] J. H. Davies, "Electronic states in narrow semiconducting wires near threshold," *Semicond. Sci. Technol.*, vol. 3, pp. 995–1009, Oct. 1988.

[212] J. H. Davies, "Analytic self-consistent calculations for inhomogeneous two-dimensional electron gases," in *Nanostructure Physics and Fabrication* , M. A. Reed and W. P. Kirk, Eds. San Diego, CA: Academic, 1989, pp. 107–111.

[213] R. A. Davies, M. J. Kelley, and T. M. Kerr, "Tunneling between two strongly coupled superlattices," *Phys. Rev. Lett.*, vol. 55, pp. 1114–1116, Sept. 2, 1985.

[214] R. A. Davies, M. J. Kelley, and T. M. Kerr, "Room-temperature oscillations in a superlattice structure," *Electron. Lett.*, vol. 22, pp. 131–133, Jan. 30, 1986.

[215] R. A. Davies, M. J. Kelley, and T. M. Kerr, "Consequence of layer thickness fluctuations on superlattice miniband structures," *Appl. Phys. Lett.*, vol. 53, pp. 2641–2643, Dec. 26, 1988.

[216] C. C. Dean and M. Pepper, "One-dimensional electron localisation and conduction by electron-electron scattering in narrow silicon MOSFETs," *J. Phys. C* , vol. 17, pp. 5663–5676, 1984.

[217] J. A. del Alamo and C. C. Eugster, "Quantum field-effect directional coupler," *Appl. Phys. Lett.*, vol. 56, pp. 78–80, Jan. 1, 1990.

[218] M. H. Degani, "Stark ladders in strongly coupled GaAs–AlAs superlattices," *Appl. Phys. Lett.*, vol. 59, pp. 57–59, July 1, 1991.

[219] C. Delalande and M. Voos, "Optical processes in semiconductor quantum wells," *Surface Sci.*, vol. 174, pp. 111–119, 1986.

[220] B. Deveaud, J. Shah, T. C. Damen, B. Lambert, A. Chomette, and A. Regreny, "Optical studies of perpendicular transport in semiconductor superlattices," *IEEE J. Quantum Electron.*, vol. 24, pp. 1641–1651, Aug. 1988.

[221] K. Diff, "Charge transport in resonant tunneling double-barrier diodes," Ph.D. dissertation, Temple University, Philadelphia, PA, Aug. 1989.

[222] K. Diff, K. F. Brennan, T. K. Gaylord, and E. N. Glytsis, "Wavepacket propagation in semiconductor superlattice interference filters," (Abstract) *Bull. Am. Phys. Soc.*, vol. 35, p. 825, Mar. 1990.

[223] K. Diff, G. Neofotistos, H. Guo, and J. D. Gunton, "Resonant tunneling in double-barrier diodes," in *Nanostructure Physics and Fabrication* , M. A. Reed and W. P. Kirk, Ed. San Diego, CA: Academic, 1989, pp. 285–290.

[224] D. J. Di Maria, M. V. Fischetti, J. Batey, L. Dori, E. Tierney, and J. Stasiak, "Direct observation of ballistic electrons in silicon dioxide," *Phys. Rev. Lett.*, vol. 57, pp. 3213–3216, Dec. 22, 1986.

[225] R. B. Dingle, "Some magnetic properties of metals I. General introduction and properties of large systems of electrons," *Proc. Roy. Soc. A* , London, vol. 211, pp. 500–516, 1952.

[226] R. Dingle, "Confined carrier quantum states in ultrathin semiconductor heterostructures," *Festkorperprobleme XV* , H.J. Queisser, Ed. New York: Pergamon, 1975, pp. 21–48.

[227] R. Dingle, W. Wiegmann, and C. H. Henry, "Quantum states of confined carriers in very thin $Al_xGa_{1-x}As$-GaAs-Al_xGa_{1-x} as heterostructures," *Phys. Rev. Lett.*, vol. 33, pp. 827–830, Sept. 30, 1974.

[228] A. V. Dmitriev, "On the determination of the resonant tunnelling time," *J. Phys. - Condens. Mat.*, vol. 1, pp. 7033–7036, 1989.

[229] W. Dobbelaere, D. Huang, M. S. Unlu, and H. Morkoc, "Al-GaAs/GaAs multiple quantum well reflection modulators grown on Si substrates," *Appl. Phys. Lett.*, vol. 53, pp. 94–96, July 1988.

[230] G. H. Dohler, "Semiconductor device," U. S. Patent 3 882 533 assigned to Max-Planck-Gesellschaft zur Forderung der Wissenschaften, May 6, 1975.

[231] G. H. Dohler, G. Fasol, T. S. Low, J. N. Miller, and K. Ploog, "Observation of tunable room temperature photoluminescence in GaAs doping superlattices," *Solid State Commun.*, vol. 57, pp. 563–566, Feb. 1986.

[232] G. H. Dohler, R. Tsu, and L. Esaki, "A new mechanism for negative differential conductivity in superlattices," *Solid State Commun.*, vol. 17, pp. 317–320, Aug. 1, 1975.

[233] K. Douglas, N. A. Clark, and K. J. Rothschild, "Nanometer molecular lithography," *Appl. Phys. Lett.*, vol. 48, pp. 676–678, Mar. 10, 1986.

[234] T. J. Drummond, P. L. Gourley, and T. E. Zipperian, "Quantum-tailored solid-state devices," *IEEE Spectrum* , vol. 25, pp. 33–37, June 1988.

[235] J. Dryzek and A. Czapla, "Quantum size effect in optical spectra of thin metallic films," *Phys. Rev. Lett.*, vol. 58, pp. 721–724, Feb. 16, 1987.

[236] T. Duffield, R. Bhat, M. Koza, F. DeRosa, K. M. Rush, and S. J. Allen, "Barrier-bound resonances in semiconductor superlattices in strong magnetic fields," *Phys. Rev. Lett.*, vol. 59, pp. 2693–2696, Dec. 7, 1987.

[237] L. F. Eastman, "Ballistic electrons in compound semiconductors," *IEEE Spectrum* , vol. 23, pp. 42–45, Feb. 1986.

[238] L. Eaves, "Introduction to resonant tunnelling in semiconductor heterostuctures," *Electronic Properties of Multilayers and Low Dimensional Semiconductor Structures* , J. M. Chamberlain, L. Eaves, and J. C. Portal, Eds. London, U.K.: Plenum, 1989, pp. 243–256.

[239] L. Eaves, "Charge build up and intrinsic bistability in resonant tunneling," in *Analogies in Optics and Micro-Electronics* , W. van Haeringen and D. Lenstra, Eds. Dordrecht: Kluwer Academic, 1990, pp. 227–242.

[240] L. Eaves, P. S. S. Guimaraes, B. R. Snell, F. W. Sheard, D. C. Taylor, G. A. Toombs, J. C. Portal, L. Dmowski, K. E. Singer, G. Hill, and M. A. Pate, "Tunneling and hot electron effects in single barrier (AlGa)As/GaAs heterostructure devices," *Superlattices Microstructures* , vol. 2, pp. 49–55, Jan. 1986.

[241] L. Eaves, F. W. Sheard, and G. A. Toombs, "The investigation of single and double barrier (resonant tunnelling heterostructures using high magneti fields in *Physics of Quantum Electron Devices* , F. Capasso, Ed. Berlin, Germany: Springer-Verlag, 1990, pp. 107–146.

[242] L. Eaves, D. C. Taylor, J. C. Portal, and L. Dmowski, "Quantum tunneling of electrons through III-V heterostructure barriers," in *Two Dimensional Systems, Physics, and New Devices* , (*Solid State Physics* , vol. 67), 1986, pp. 96–106.

[243] J. P. Eisenstein, L. N. Pfeiffer, and K. W. West, "Field-induced resonant tunneling between parallel two-dimensional electron systems," *Appl. Phys. Lett.*, vol. 58, pp. 1497–1499, Apr. 8, 1991.

[244] P. England, J. E. Golub, L. T. Florez, and J. P. Harbison, "Optical switching in a resonant tunneling structure," *Appl. Phys. Lett.*, vol. 58, pp. 887–889, Mar. 4, 1991.

[245] P. England, J. R. Hayes, E. Colas, and M. Helm, "Hot-electron spectroscopy of Bloch electrons in high-order minibands in semi-conductor superlattices," *Phys. Rev. Lett.*, vol. 63, pp. 1708–1711, Oct. 16, 1989.

[246] P. England, J. R. Hayes, J. P. Harbison, D. M. Hwang, and L. T. Florez, "Tunneling measurement of the density of states of a superlattice," *Appl. Phys. Lett.*, vol. 53, pp. 391–393, Aug. 1, 1988

[247] P. England, J. R. Hayes, M. Helm, J. P. Harbison, L. T. Florez, and S. J. Allen, Jr., "Resonant tunneling in crossed electric and magnetic fields," *Appl. Phys. Lett.*, vol. 54, pp. 1469–1471, Apr. 10, 1989.

[248] J. C. Englund, C. C. Sung, and Y. Q. Li, "Model of optical bistability in the quantum well self-electro-optic-effect device," *J. Opt. Soc. Amer. B* , vol. 4, pp. 1083–1086, July 1987.

[249] H. L. Engquist and P. W. Anderson, "Definition and measurement of the electrical and thermal resistances," *Phys. Rev. B* , vol. 24, pp. 1151–1154, July 15, 1981.

[250] O. Entin-Wohlman, C. Hartzstein, and Y. Imry, "Quantum oscillations in the magnetotransport of a finite two-dimensional Anderson model," *Phys. Rev. B* , vol. 34, pp. 921–926, July 15, 1986.

[251] R. Eppenga, M. F. H. Schuurmans, and S. Colak, "New $k \cdot p$ theory for $GaAs/Ga_{1-x}Al_xAs$-type quantum wells," *Phys. Rev. B*, vol. 36, pp. 1554–1564, July 15, 1987.

[252] P. Erdos and Z. Domanski, "Density of states of electrons and electromagnetic waves in one-dimensional random media," in *Analogies in Optics and Micro-Electronics* , W. van Haeringen and D. Lenstra, Eds. Dordrecht: Kluwer Academic, 1990, pp. 49–68.

[253] L. Esaki, "A bird's-eye view on the evolution of semiconductor superlattices and quantum wells," *IEEE J. Quantum Electron.*, vol. 22, pp. 1611–1624, Sept. 9, 1986.

[254] L. Esaki, "The evolution of semiconductor quantum structures in reduced dimensionality - Do-it-yourself quantum mechanics," *Electronic Properties of Multilayers and Low Dimensional Semiconductor Structures* , J. M. Chamberlain, L. Eaves, and J. C. Portal, Eds. London, U.K: Plenum, 1989, pp. 1–24.

[255] L. Esaki and L. L. Chang, "New transport phenomenon in a semiconductor 'superlattice'," *Phys. Rev. Lett.*, vol. 33, pp. 495–498, Aug. 19, 1974.

[256] L. Esaki and R. Tsu, "Superlattice and negative differential conductivity in semiconductors," *IBM J. Res. Develop.*, vol. 14, pp. 61–65, Jan. 1970.

[257] C. C. Eugster, J. A. del Alamo, P. A. Belk, and M. J. Rooks, "Criteria for the observation of one-dimensional transport in split-gate field-effect quantum wires," *Appl. Phys. Lett.*, vol. 58, June 24, 1991.

[258] J. P. Falck and E. H. Hauge, "Larmor clock reexamined," *Phys. Rev. B*, vol. 38, pp. 3287–3297, Aug. 15, 1988.

[259] F. F. Fang and W. E. Howard, "Negative field-effect mobility on (100) Si surfaces, *Phys. Rev. Lett.*, vol. 16, pp. 797–799, May 2, 1966.

[260] C. S. Feigerle, D. T. Pierce, A. Seiler, and R. J. Celotta, "Intense source of monochromatic electrons: Photoemission from GaAs," *Appl. Phys. Lett.*, vol. 44, pp. 866–868, May 1, 1984.

[261] F. E. Fernandez and C. M. Falco, "Multilayers for soft x-ray optics," *IEEE J. Quantum Electron.*, vol. 24, pp. 1758–1762, Aug. 1988.

[262] D. K. Ferry, "Theory of resonant tunneling and surface superlattices" in *Physics of Quantum Electron Devices* , F. Capasso, Ed. Berlin, Germany: Springer-Verlag, 1990, pp. 77–105.

[263] D. K. Ferry, G. Bernstein, R. Puechner, J. Ma, A. M. Kriman, R. Mezenner, W. P. Liu, G. N. Maracas, and R. Chamberlin, "Magnetoconductance in lateral surface superlattices," *Surface Sci.*, vol. 228, pp. 520–523, Apr. 1990.

[264] H. A. Fertig and S. Das Sarma, "Elastic scattering in resonant tunneling systems," *Phys. Rev. B* , vol. 40, pp. 7410–7412, Oct. 1, 1989.

[265] D. S. Fisher and P. A. Lee, "Relation between conductivity and transmission matrix," *Phys. Rev. B* , vol. 23, pp. 6851–6854, June 15, 1981.

[266] F. Flam, "Single electron transistor explained," *Science* , vol. 252, p. 215, Apr. 12, 1991.

[267] C. Foden and K. W. H. Stevens, "Tunneling times and a quantum clock," *IBM J. Res. Develop.*, vol. 32, pp. 99–102, Jan. 1988.

[268] C. J. B. Ford, "The low-field Hall effect in quasi-ballistic wires," in *Nanostructure Physics and Fabrication* , M. A. Reed and W. P. Kirk, Ed. San Diego, CA: Academic, 1989, pp. 389–394.

[269] C. J. B. Ford and H. Ahmed, "Fabrication of GaAs heterojunction ring structures," *Microelectron. Engr.*, vol. 6, pp. 169–174, 1987.

[270] C. J. B. Ford, T. J. Thornton, R. Newbury, M. Pepper, and H. Ahmed, "Transport in GaAs heterojunction ring structures," *Superlattices Microstructures* , vol. 4, pp. 541–544, 1988.

[271] C. J. B. Ford, T. J. Thornton, R. Newbury, M. Pepper, H. Ahmed, D. C. Peacock, D. A. Ritchie, J. E. F. Frost, and G. A. C. Jones, "Electrostatically defined heterojunction rings and the Aharonov-Bohm effect," *Appl. Phys. Lett.*, vol. 54, pp. 21–23, Jan. 2, 1989.

[272] K. Forrest and P. H. E. Meijer, "Tunneling calculations for $GaAs$-$Al_xGa_{1-x}As$ graded band-gap sawtooth superlattices," *IEEE J. Quantum Electron.*, vol. 26, pp. 1067–1074, June 1990.

[273] A. B. Fowler, "Semiconductor interferometer," U. S. Patent 4 550 330 assigned to International Business Machines Corp., Oct. 29, 1985.

[274] A. B. Fowler, A. Hartstein, and R. A. Webb, "Conductance in restricted-dimensionality accumulation layers," *Phys. Rev. Lett.* vol. 48, pp. 196–199, Jan. 18, 1982.

[275] A. B. Fowler and W. E. Howard, "Planar superlattice structure," *IBM Tech. Disclosure Bull.*, vol. 12, pp. 2237–2237a, May 1970.

[276] A. B. Fowler and G. L. Timp, "Electron tuned quantum well device," U. S. Patent 4 942 437 assigned to International Business Machines Corp., July 17, 1990.

[277] E. Fradkin, E. Dagotto, and D. Boyanovsky, "Physical realization of the parity anomaly in condensed matter physics," *Phys. Rev. Lett.*, vol. 57, pp. 2967–2970, Dec. 8, 1986.

[278] W. R. Frensley, "Simulation of resonant-tunneling heterostructure devices," *J. Vac. Sci. Technol. B* , vol. 3, pp. 1261–1266, July/Aug. 1985.

[279] W. R. Frensley, "Transient response of a tunneling device obtained from the Wigner function," *Phys. Rev. Lett.*, vol. 57, pp. 2853–2856, Dec. 1, 1986.

[280] W. R. Frensley, "Wigner-function model of a resonant-tunneling semiconductor device," *Phys. Rev. B* , vol. 36, pp. 1570–1580, July 15, 1987.

[281] W. R. Frensley, "Ballistic transport filter and device," U. S. Patent 4 866 488 assigned to Texas Instruments Inc., Sept. 12, 1989.

[282] W. R. Frensley, "Quantum kinetic theory of nanoelectronic devices," in *Nanostructure Physics and Fabrication* , M. A. Reed and W. P. Kirk, Ed. San Diego, CA: Academic, 1989, pp. 231–240.

[283] W. R. Frensley, "Quantum kinetic theory of tunneling devices," in *Computational Electronics*, K. Hess, J. P. Leburton, and U. Ravaioli, Eds. Norwell, MA: Kluwer Academic, 1991, pp. 195–200.

[284] W. R. Frensley, M. A. Reed, and A. Seabaugh, "Is resonant tunneling transistor a reality?", *Phys. Today*, vol. 43, p. 132, Sept. 1990.

[285] I. J. Fritz, P. L. Gourley, and L. R. Dawson, "Critical layer thickness in $In_{0.2}Ga_{0.8}As/GaAs$ single strained quantum well structures," *Appl. Phys. Lett.*, vol. 13, pp. 1004–1006, Sept. 28,

1987.
[286] H. R. Frohne, M. J. McLennan, and S. Datta, "An efficient method for the anaylsis of electron waveguides," *J. Appl. Phys.*, vol. 66, pp. 2699–2705, Sept. 15, 1989.
[287] K. Fujiwara, N. Tsukada, and T. Nakayama, "Observation of free excitons in room-temperature photoluminescence of GaAs/AlGaAs single quantum wells," *Appl. Phys. Lett.*, vol. 53, pp. 675–677, Aug. 22, 1988.
[288] T. Furuta, K. Hirakawa, J. Yoshino, and H. Sakaki, "Splitting of photoluminescence spectra and negative differential resistance caused by the electric field induced resonant coupling of qunatized levels in GaAs-AlGaAs multi-quantum well structures," *Japan. J. Appl. Phys.*, vol. 25, pp. L151–L154, Feb. 1986.
[289] K. Furuya, "Novel high-speed transistor using electron-wave diffraction," *J. Appl. Phys* , vol. 62, pp. 1492–1494, Aug. 15, 1987.
[290] K. Furuya, "Possibility of high-speed device on electron wave principle, *J. Cryst. Growth* , vol. 98, pp. 234–242, Nov. 1989.
[291] K. Furuya and K. Kurishima, "Theoretical properties of electron wave diffraction due to a transversally periodic structure in semiconductors," *IEEE J. Quantum Electron.*, vol. 24, pp. 1652–1658, Aug. 1988.
[292] K. Furuya and K. Kurishima, "Electron wave diffraction by nanometer grating and its application for high-speed transistors," *J. Vac. Sci. Technol. B*, vol. 6, pp. 1845–1848, Nov.–Dec. 1988.
[293] K. Furuya, K. Kurishima, and S. Samadi, "Theoretical characteristics of electron diffraction transistor," *Trans. Inst. Electron. and Commun. Eng. Japan.*, vol. E72, pp. 307–309, Apr. 1989.
[294] K. Furuya, K. Kurishima, and T. Yamamoto, "Proposal of electron diffraction transistor," *Trans. Inst. Electron. and Commun. Eng. Japan E*, vol. 71, pp. 286–288, Apr. 1988.
[295] G. Galecki and G. Nimtz, "Electron quantum valve device—a new type of FIR-detector," *Infrared Phys.*, vol. 312, pp. 85–88, 1991.
[296] H. Gamo, "Electron waves in semiconductor heterojunctions," (Abstract) *Bull. Am. Phys. Soc.*, vol. 35, p. 211, Mar. 1990.
[297] P. Gavrilovic, J. M. Brown, R. W. Kaliski, N. Holonyak, Jr., K. Hess, M. J. Ludowise, W. T. Dietze, and C. R. Lewis, "Resonant tunneling in a $GaAs_{1-x}P_x$-GaAs strained-layer quantum-well heterostructure," *Solid State Commun.*, vol. 52, pp. 237–239, Oct. 1984.
[298] T. K. Gaylord and K. F. Brennan, "Semiconductor superlattice electron wave interference filters," *Appl. Phys. Lett.*, vol. 53, pp. 2047–2049, Nov. 21, 1988.
[299] T. K. Gaylord and K. F. Brennan, "Electron wave optics in semiconductors," *J. Appl. Phys.*, vol. 65, pp. 814–820, Jan. 15, 1989.
[300] T. K. Gaylord, K. F. Brennan, and E. N. Glytsis, "Semiconductor quantum well electron and hole waveguides," U. S. Patent 4 970 563 assigned to Georgia Tech Research Corp., Nov. 13, 1990.
[301] T. K. Gaylord, K. F. Brennan, and E. N. Glytsis, "Solid state quantum mechanical electron and hole wave devices," U. S. Patent 4 985 737 assigned to Georgia Tech Research Corp., Jan. 15, 1991.
[302] T. K. Gaylord, E. N. Glytsis, and K. F. Brennan, "Semiconductor superlattice interference filter design," *J. Appl. Phys.*, vol. 65, pp. 2535–2540, Mar. 15, 1989.
[303] T. K. Gaylord, E. N. Glytsis, and K. F. Brennan, "Semiconductor electron wave slab waveguides," *J. Appl. Phys.* (Commun.), vol. 66, pp. 1483–1485, Aug. 1, 1989.
[304] T. K. Gaylord, E. N. Glytsis, and K. F. Brennan, "Semiconductor quantum wells as electron slab waveguides," *J. Appl. Phys.*, vol. 66, pp. 1842–1848, Aug. 15, 1989.
[305] T. K. Gaylord, E. N. Glytsis, and K. F. Brennan, "Electron-wave quarter-wavelength quantum well impedance transformers between differing energy-gap semiconductors," *J. Appl. Phys.*, vol. 67, pp. 2623–2630, Mar. 1, 1990.
[306] T. K. Gaylord, E. N. Glytsis, and K. F. Brennan, "Semiconductor biased superlattice tunable interference filter/emitter," U. S. Patent 4 987 458 assigned to Georgia Tech. Research Corp., Jan. 22, 1991.
[307] Y. Gefen, Y. Imry, and M. Ya. Azbel, "Quantum oscillations and the Aharonov-Bohm effect for parallel resistors," *Phys. Rev. Lett.*, vol. 52, pp. 129–132, Jan. 9, 1984.
[308] B. Y. Gelfand, S. Schmitt-Rink, and A. F. J. Levi, "Tunneling in the presence of phonons: A solvable model," *Phys. Rev. Lett.*, vol. 62, pp. 1683–1686, Apr. 3, 1989.
[309] J. Genoe, C. V. Hoof, W. V. Roy, J. H. Smet, K. Fobelets, R. P. Mertens, and G. Borghs, "Capacitances in double-barrier tunneling structures," *IEEE Trans. Electron Devices*, vol. 38, pp. 2006–2012, Sept. 1991.
[310] J. M. Gerard and J. Y. Marzin, "High quality ultrathin InAs/GaAs quantum wells grown by standard and low-temperature modulated-fluxes molecular beam epitaxy," *Appl. Phys. Lett.*, vol. 53, pp. 568–570, Aug. 15, 1988.
[311] R. R. Gerhardts, D. Weiss, and K. von Klitzing, "Novel magnetoresistance oscillations in a periodically modulated two-dimensional electron gas," *Phys. Rev. Lett.*, vol. 62, pp. 1173–1176, Mar. 6, 1989.
[312] J. M. Gering, D. A. Crim, D. G. Morgan, P. D. Coleman, W. Kopp, and H. Morkoc, "A small-signal equivalent-circuit model for GaAs-$Al_xGa_{1-x}As$ resonant tunneling heterostructures at microwave frequencies," *J. Appl. Phys.*, vol. 61, pp. 271–276, Jan. 1, 1987.
[313] E. Gerjuoy and D. D. Coon, "Analytic S-matrix considerations and time delay in resonant tunneling," *Superlattices Microstructures* , vol. 5, no. 3, pp. 305–315, 1989.
[314] A. K. Ghatak, I. C. Goyal, and R. L. Gallawa, "Mean lifetime calculations of quantum well structures: A rigorous analysis," *IEEE J. Quantum Electron.*, vol. 26, pp. 305–310, Feb. 1990.
[315] A. K. Ghatak, K. Thyagarajan, and M. R. Shenoy, "A novel numerical technique for solving the one-dimensional Schroedinger equation using matrix approach—Application to quantum well structures," *IEEE J. Quantum Electron.*, vol. 24, pp. 1524–1531, Aug. 1988.
[316] M. Gijs, C. Van Haesendonck, and Y. Bruynseraede, "Resistance oscillations and electron localization in cylindrical Mg films," *Phys. Rev. Lett.*, vol. 52, pp. 2069–2072, June 4, 1984.
[317] L. I. Glazman and A. V. Khaetskii, "Nonlinear quantum conductance of a point contact," *JETP Lett.*, vol. 48, pp. 591–595, Nov. 1988.
[318] L. I. Glazman and A. V. Khaetskii, "Nonlinear quantum conductance of a lateral microconstraint in a heterostructure," *Europhys. Lett.*, vol. 9, no. 3, pp. 263–267, June 1, 1989.
[319] E. N. Glytsis, T. K. Gaylord, and K. F. Brennan, "Semiconductor biased superlattice tunable electron interference filter/emitter," *J. Appl. Phys.*, vol. 65, pp. 1494–1497, Aug. 1, 1989.
[320] E. N. Glytsis, T. K. Gaylord, and K. F. Brennan, "Theory and design of semiconductor electron-wave interference filters/emitters," *J. Appl. Phys.*, vol. 65, pp. 6158–6167, Dec. 15, 1989.
[321] E. N. Glytsis, T. K. Gaylord, and K. F. Brennan, "Ballistic current-voltage characteristics of semiconductor superlattice electron-wave quantum-interference filter/emitter negative differential resistance devices," *J. Appl. Phys.*, vol. 69, Oct. 1, 1991.
[322] A. Goldberg, H. M. Schey, and J. C. Schwartz, "Computer-generated motion pictures of one-dimensional quantum-mechanical transmission and reflection phenomena," *Amer. J. Phys.*, vol. 35, pp. 177–186, Mar. 1967.
[323] V. J. Goldman, D. C. Tsui, and J. E. Cunningham, "Resonant tunneling in magnetic fields: Evidence for space-charge buildup," *Phys. Rev. B* , vol. 35, pp. 9387–9390, June 15, 1987.
[324] R. Golub, S. Felber, R. Gahler, and E. Gutsmiedl, "A modest proposal concerning tunneling times," *Phys. Lett. A* , vol. 148, pp. 27–30, Aug. 6, 1990.
[325] C. E. T. Goncalves da Silva and E. E. Mendez, "Resonant tunneling via Landau levels in GaAs-$Ga_{1-x}Al_xAs$ heterostructures," *Phys. Rev. B* , vol. 38, pp. 3994–3997, Aug. 15, 1988.
[326] K. W. Goossen, G. D. Boyd, J. E. Cunningham, W. Y. Jan, D. A. B. Miller, D. S. Chemla, and R. M. Lum, "GaAs-AlGaAs multiquantum well reflection modulators grown on GaAs and silicon substrates," *IEEE Photonics Technology Lett.*, vol. 1, pp. 304–306, Oct. 1989.
[327] A. C. Gossard, "Growth of microstructures by molecular beam epitaxy," *IEEE J. Quantum Electron.*, vol. 22, pp. 1649–1655, Sept. 1986.
[328] T. R. Govindan, H. L. Grubin, and F. J. de Jong, "Density matrix coordinate representation numerical studies of quantum well and barrier devices," in *Computational Electronics* , K. Hess, J. P. Leburton, and U. Ravaioli, Eds. Norwell, MA: Kluwer Academic, 1991, pp. 215–218.
[329] Z. S. Gribnikov, "Negative differential conductivity in a mul-

tilayer heterostructure," *Soviet Phys. - Semicon.*, vol. 6, pp. 1204–1205, Jan. 1973.
[330] A. A. Grinberg, "Thermionic emission in heterosystems with different effective electronic masses," *Phys. Rev. B* , vol. 33, pp. 7256–7258, May 15, 1986.
[331] A. A. Grinberg and A. Katalsky, "Theory of the quantum well emission transistor," *J. Appl. Phys.*, vol. 65, pp. 821–825, Jan. 15, 1989.
[332] P. Gueret, "Dynamic polarization effects in tunneling," *Electronic Properties of Multilayers and Low Dimensional Semiconductor Structures*, J. M. Chamberlain, L. Eaves, and J. C. Portal Eds. London, U.K.: Plenum, 1989, pp. 317–329.
[333] P. Gueret, C. Rossel, W. Schlup, and H. P. Meier, "Investigations on resonant tunneling in III-V heterostructures: Comparisons between experimental data and model calculations," *J. Appl. Phys.*, vol. 66, pp. 4312–4316, Nov. 1, 1989.
[334] A. H. Guerrero, "Exchange energy interactions in quantum well heterostructures," in *Computational Electronics* , K. Hess, J. P. Leburton, and U. Ravaioli, Eds. Norwell, MA: Kluwer Academic, 1991, pp. 251–254.
[335] H. Guo, K. Diff, G. Neofotistos, and J. D. Gunton, "Time-dependent investigation of the resonant tunneling in a double-barrier quantum well," *Appl. Phys. Lett.*, vol. 53, pp. 131–133, July 11, 1988.
[336] W. Hansen, T. P. Smith, III, J. A. Brum, J. M. Hong, K. Y. Lee, C. M. Knoedler, D. P. Kern, and L. L. Chang, "Magnetic effects in quantum dots," in *Nanostructure Physics and Fabrication* , M. A. Reed and W. P. Kirk, Eds. San Diego, CA: Academic, 1989, pp. 97–105.
[337] G. Harbeke, "Quantized transport: A countered query," *Phys. Today* , vol. 43, pp. 111–112, Jan. 1990.
[338] H. K. Harbury and W. Porod, "Numerical study of electronic states in a quantum wire at crossing heterointerfaces," in *Computational Electronics* , K. Hess, J. P. Leburton, and U. Ravaioli, Eds. Norwell, MA: Kluwer Academic, 1991, pp. 243–246.
[339] H. Harbury and W. Porod, "A proposed quantum wire structure: An 'accumulation wire' at crossing heterointerfaces," *J. Vac. Sci. Technol. B* , vol. 8, pp. 923–928, July-Aug. 1990.
[340] P. G. Harper, "Single band motion of conduction electrons in a uniform magnetic field," *Proc. Phys. Soc. Lond. A* , vol. 68, pp. 874–878, 1955.
[341] P. G. Harper, "The general motion of conduction electrons in a uniform magnetic field, with applications to the diamagnetism of metals," *Proc. Phys. Soc. Lond. A* , vol. 68, pp. 879–892, 1955.
[342] J. P. Harrang, R. J. Higgins, R. K. Goodall, P. R. Jay, M. Laviron, and P. Delecluse, "Quantum and classical mobility determination of the dominant scattering mechanisms in the two-dimensional electron gas of an AlGaAs/GaAs heterojunction," *Phys. Rev. B* , vol. 32, pp. 8126–8135, Dec. 15, 1985.
[343] A. Harwit, J. S. Harris, and A. Kapitulnik, "Calculated quasi-eigenstates and quasi-eigenenergies of quantum well superlattices in an applied electric field," *J. Appl. Phys.*, vol. 60, pp. 3211–3213, Nov. 1, 1986.
[344] I. Hase, K. Taira, H. Kawai, T. Watanabe, K. Kaneko, N. and Watanabe, "Strained GaInAs-base hot electron transistor," *Electron. Lett.*, vol. 24, pp. 279–280, Mar. 3, 1988.
[345] M. Hashemi, J. Ramdani, B. T. McDermott, K. Reid, and S. M. Bedair, "Atomic layer epitaxy of planar-doped structures for nonalloyed contacts and field-effect transistor," *Appl. Phys. Lett.*, vol. 56, pp. 964–966, Mar. 5, 1990
[346] E. H. Hauge, J. P. Falck, and T. A. Fjeldly, "Transmission and reflection times for scattering of wave packets off tunneling barriers," *Phys. Rev. B* , vol. 36, pp. 4203–4214, Sept. 15, 1987.
[347] E. H. Hauge and J. A. Stovneng, "Tunneling times: A critical review," *Rev. Mod. Phys.*, vol. 61, pp. 917–936, Oct. 1989.
[348] J. R. Hayes, P. England, and J. P. Harbison, "Quantum interference effects in GaAs/GaAlAs bulk potential barriers," *Appl. Phys. Lett.*, vol. 52, pp. 1578–1580, May 9, 1988.
[349] J. R. Hayes and A. F. J. Levi, "Dynamics of extreme nonequilibrium electron transport in GaAs," *IEEE J. Quantum Electron.*, vol. 22, pp. 1744–1752, Sept. 1986.
[350] L. X. He, K. P. Martin, R. J. Higgins, J. S. Brooks, P. R. Jay, and P. Delescluse, "Quantized Hall effect in gated AlGaAs/GaAs heterostructures: Localization as a function of number density and magnetic field," *Solid State Commun.*, vol. 59, pp. 691–695, Sept. 1986.
[351] S. He and S. D. Sarma, "Quantum conduction in narrow constrictions," *Phys. Rev. B*, vol. 40, pp. 3379–3382, Aug. 15, 1989.
[352] M. H. Hecht, L. D. Bell, and W. J. Kaiser, "Ballistic-electron-emission microscopy of subsurface defects at the Au-GaAs(100) interface," *Appl. Surface Sci.*, vol. 41/42, pp. 17–24, 1989.
[353] M. H. Hecht, L. D. Bell, W. J. Kaiser, and F. J. Grunthaner, "Ballistic-electron-emission microscopy investigation of Schottky barrier interface formation," *Appl. Phys. Lett.*, vol. 55, pp. 780–782, Aug. 21, 1989.
[354] M. Heiblum, "Tunneling hot electron transfer amplifiers (theta): Amplifiers operating up to the infrared," *Solid-State Electron.*, vol. 24, pp. 343–366, 1981.
[355] M. Heiblum, "Ballistic electrons and holes observed in a semiconductor," *Opt. News*, vol. 14, pp. 13–16, Oct. 1988.
[356] M. Heiblum, "Ballistic transport in the vertical and horizontal domanins," in *Nanostructure Physics and Fabrication*, M. A. Reed and W. P. Kirk, Eds. San Diego, CA: Academic, 1989, pp. 229–230.
[357] M. Heiblum, "Ballistic electron transport in the plane," *Electronic Properties of Multilayers and Low Dimensional Semiconductor Structures*, J. M. Chamberlain, L. Eaves, and J. C. Portal, Eds. London, U.K.: Plenum, 1989, pp. 421–423.
[358] M. Heiblum, I. M. Anderson, and C. M. Knoedler, "DC performance of ballistic tunneling hot-electron transfer amplifiers," *Appl. Phys. Lett.*, vol. 49, pp. 207–209, July 28, 1986.
[359] M. Heiblum, E. Calleja, I. M. Anderson, W. P. Dumke, C. M. Knoedler, and L. Osterling, "Evidence of hot-electron transfer into an upper valley in GaAs," *Phys. Rev. Lett.*, vol. 56, pp. 2854–2857, June 30, 1986.
[360] M. Heiblum and L. F. Eastman, "Ballistic electrons in semiconductors", *Scientif. Amer.*, vol. 256, pp. 102–110, Feb. 1987.
[361] M. Heiblum and M. V. Fischetti, "Ballisti electron transport in hot electron transistors in *Physics of Quantum Electron Devices* , F. Capasso, Ed. Berlin, Germany: Springer-Verlag, 1990, pp. 271–320.
[362] M. Heiblum, M. V. Fischetti, W. P. Dumke, D. J. Frank, I. M. Anderson, C. M. Knoedler, and L. Osterling, "Electron interference effects in quantum wells: Observation of bound and resonant states," *Phys. Rev. Lett.*, vol. 58, pp. 816–819, Feb. 23, 1987.
[363] M. Heiblum, M. I. Nathan, D. C. Thomas, and C. M. Knoedler, "Direct observation of ballistic transport in GaAs," *Phys. Rev. Lett.*, vol. 55, pp. 2200–2203, Nov. 11, 1985.
[364] M. Heiblum, K. Seo, H. P. Meier, and T. W. Hickmott, "Observation of ballistic holes," *Phys. Rev. Lett.*, vol. 60, pp. 828–831, Feb. 29, 1988.
[365] M. Heiblum, K. Seo, H. P. Meier, and T. W. Hickmott, "First observation of ballistic holes in a p-type THETA device," (Abstract) *IEEE Trans. Electron Devices* , vol. 35, p. 2428, Dec. 1988.
[366] M. Heiblum, D. C. Thomas, C. M. Knoedler, and M. I. Nathan, "Tunneling hot electron transfer amplifiers (theta): Ballistic GaAs devices with current gain," *Surface Sci.*, vol. 174, pp. 478–480, Aug. 1986.
[367] H. Heinrich, G. Bauer, and F. Kuchar (eds.), *Physics and Technology of Submicron Structures (Solid-state Sciences)* , vol. 83. Berlin, Germany: Springer-Verlag, 1988.
[368] P. Helgesen, T. G. Finstad, and K. Johannessen, "Sequential resonant and nonresonant tunneling in GaAs/AlGaAs multiple quantum wells," *J. Appl. Phys.*, vol. 69, pp. 2689–2691, Feb. 15, 1991.
[369] M. Helm, E. Colas, J. R. Hayes, B. Van der Gaag, and L. M. Schiavone, and D. M. Hwang, "Anisotropic transport in a modulation-doped GaAs quantum well microstructured by growth on a submicron grating," *Appl. Phys. Lett.*, vol. 58, pp. 1320–1322, Mar. 25, 1991.
[370] M. Helm, F. M. Peters, P. England, and E. Colas, "Resonant tunneling in a transverse magnetic field: Transition from the electric to the magnetic quantum limit," *Phys. Rev. B* , vol. 39, pp. 3427–3430, Feb. 15, 1989.
[371] G. N. Henderson, T. K. Gaylord, and E. N. Glytsis, "Ballistic electron transport in semiconductor heterostructures and its analogies in electromagnetic propagation in general dielectrics," *Proc. IEEE* , vol. 79, Nov. 1991.
[372] G. N. Henderson, E. N. Glytsis, and T. K. Gaylord, "Electron wave diffraction by semiconductor gratings: Rigorous analysis and design parameters," *Appl. Phys. Lett.*, vol. 59, pp. 440–442,

July 22, 1991.
[373] M. Henini, M. L. Leadbeater, E. S. Alves, L. Eaves, O. H. Hughes, G. Hill, and M. A. Pate, "The effects of conduction band anisotropy on hybrid magneto-electric states in resonant tunneling devices," *Surface Sci.*, vol. 228, pp. 433–436, Apr. 1990.
[374] D. C. Herbert, "Structured-base hot-electron transistors: 1. Scattering rates," *Semicond. Sci. Technol.*, vol. 3, pp. 101–110, Feb. 1988.
[375] C. Herring and M. H. Nichols, "Thermionic emission," *Rev. Mod. Phys.*, vol. 21, pp. 185–270, Apr. 1949.
[376] K. Hess, "Supercomputer images of electron device physics," *Phys. Today* , vol. 43, pp. 34–42, Feb. 1990.
[377] K. Hess and G. J. Iafrate, "Theory and applications of near ballistic transport in semiconductors", *Proc. IEEE* , vol. 76, pp. 519–532, May 1988.
[378] K. Hess, H. Morkoc, H. Shichijo, and B. G. Streetman, "Negative differential resistance through real-space electron transfer," *Appl. Phys. Lett.*, vol. 35, pp. 469–471, Sept. 15, 1979.
[379] T. W. Hickmott, P. M. Solomon, R. Fischer, and H. Morkoc, "Resonant Fowler-Nordheim tunneling in n⁺GaAs-undoped $Al_xGa_{1-x}As$-n⁺GaAs capacitors," *Appl. Phys. Lett.*, vol. 44, pp. 90–92, Jan. 1, 1984.
[380] T. Hiramoto, T. Odagiri, K. Hirakawa, Y. Iye, and T. Ikoma, "Anomalous drain conductance in quasi-one-dimensional AlGaAs/GaAs quantum wire transistors fabricated by focused ion beam implantation," in *Nanostructure Physics and Fabrication* , M. A. Reed and W. P. Kirk, Eds. San Diego, CA: Academic, 1989, pp. 175–182.
[381] Y. Hirayama and T. Saku, "Conductance characteristics of ballistic one-dimensional channels controlled by a gate electrode," *Appl. Phys. Lett.*, vol. 54, pp. 2556–2558, June 19, 1989.
[382] Y. Hirayama, T. Saku, S. Tarucha, and Y. Horikoshi, "Ballistic electron transport in macroscopic four-terminal square structures with high mobility," Appl. Phys. Lett., vol. 58, pp. 2672–2674, June 10, 1991.
[383] F. Hirler, J. Smoliner, E. Gornik, and G. Weimann, "Energy levels in quantum wires studied by tunneling and magnetotransport experiments," *Appl. Phys. Lett.*, vol. 57, pp. 261–263, July 16, 1990.
[384] D. R. Hofstadter, "Energy levels and wave functions of Bloch electrons in rational and irrational magnetic fields," *Phys. Rev. B* , vol. 14, pp. 2239–2249, Sept. 15, 1976.
[385] K. Hong and D. Pavlidis, "Self-consistent analysis of lattice-matched and pseudomorphic quantum-well emission transistors," *J. Appl. Phys.*, vol. 69, pp. 2662–2666, Feb. 15, 1991.
[386] R. E. Howard, L. D. Jackel, and W. J. Skocpol, "Nanostructures: Fabrication and applications," *Microelectron. Engr.*, vol. 3, pp. 3–16, 1985.
[387] R. E. Howard, L. D. Jackel, P. M. Mankiewich, and W. J. Skocpol, "Electrons in silicon microstructures," *Science* , vol. 231, pp. 346–349, Jan. 24, 1986.
[388] B. Y. K. Hu, J. W. Wilkins, and S. K. Sarker, "Quantum transport equation approach to nonequilibrium screening," in *Nanostructure Physics and Fabrication* , M. A. Reed and W. P. Kirk, Eds. San Diego, CA: Academic, 1989, pp. 273–277.
[389] G. Y. Hu and R. F. O'Connell, "1/f noise in two-dimensional meso-scopic systems from a generalized quantum Langevin equation approach," in *Nanostructure Physics and Fabrication* , M. A. Reed and W. P. Kirk, Ed. San Diego, CA: Academic, 1989, pp. 501–505.
[390] C. I. Huang, M. J. Paulus, C. A. Bozada, S. C. Dudley, K. R. Evans, C. E. Stutz, R. L. Jones, and M. E. Cheney, "AlGaAs/GaAs double barrier diodes with high peak-to-valley current ratio," *Appl. Phys. Lett.*, vol. 51, pp. 121–123, July 13, 1987.
[391] P. Huang, D. S. Pan, and N. C. Luhmann, "A new method of determination of the I-V characteristics of negative differential conductive devices by microwave reflection coefficient measurements,"*IEEE Electron. Device Lett.*, vol. 11, pp. 570–572, Dec. 1990.
[392] Z. H. Huang, P. H. Cutler, T. E. Feuchtwang, R. H. Good, E. Kazes, H. Q. Nguyen and S. K. Park, "Spin precession and phase delay tunneling times," *J. de Physique C* , vol. 6, pp. 17–22, Nov. 1988.
[393] Z. H. Huang, P. H. Cutler, T. E. Feuchtwang, R. H. Good, E. Kazes, H. Q. Nguyen, and S. K. Park, "Computer simulation of a wave packet tunneling through a square barrier," *IEEE Trans. Electron Devices* , vol. 36, pp. 2665–2670, Nov. 1989.
[394] Z. H. Huang, P. H. Cutler, T. E. Feuchtwang, E. Kazes, H. Q. Nguyen, and T. E. Sullivan, "Model studies of tunneling time," *J. Vac. Sci. Technol. A* , vol. 8, pp. 186–191, Jan. 1990.
[395] M. Hundhausen, T. Ichiguchi, and Y. Shiraki, "Magnetoresistance of multiple electron gas wires at the AlGaAs/GaAs heterointerface," *Appl. Phys. Lett.*, vol. 53, pp. 110–112, July 11, 1988.
[396] D. C. Hutchings, "Transfer matrix approach to the analysis of an arbitrary quantum well structure in an electric field," *Appl. Phys. Lett.*, vol. 55, pp. 1082–1084, Sept. 11, 1989.
[397] K. M. Hutchings, A. D. C. Grassie, M. Lakrimi, and J. Bird, "The fabrication of sub-micron width mesas in $GaAs/Ga_{1-x}Al_xAs$ heterojunction material," *Solid-State Technol.*, vol. 31, pp. 1057–1059, Oct. 1988.
[398] G. J. Iafrate, J. B. Krieger, and Y. Li, "Quantum transport and dynamics for Bloch electrons in electric fields," in*Electronic Properties of Multilayers and Low Dimensional Semiconductor Structures*, J. M. Chamberlain, L. Eaves, and J. C. Portal, Eds., London, U.K.: Plenum, 1989, pp. 211–228.
[399] G. J. Iafrate, J. B. Krieger, and Y. Li, "Many-body effects and density functional formalism in nanoelectronics," in *Computational Electronics*, K. Hess, J. P. Leburton, and U. Ravaioli, Eds. Norwell, MA: Kluwer Academic, 1991, pp. 183–188.
[400] G. J. Iafrate, H. R. Wittmann, M. A. Stroscio, and L. Cooper, "Perspective on the future of microstructure technology," *Superlattices Microstructures*, vol. 2, pp. 5–7, 1986.
[401] K. Iga, H. Uenohara, and F. Koyama, "Electron reflectance of multiquantum barrier (MQB)," *Electron. Lett.*, vol. 22, pp. 1008–1010, Sept. 11, 1986.
[402] J. Ihm, "Effects of the layer thickness on the electronic character in GaAs-AlAs superlattices," *Appl. Phys. Lett.*, vol. 50, pp. 1068–1070, Apr. 20, 1987.
[403] K. Imamura, S. Muto, N. Yokoyama, M. Sasa, H. Ohnishi, S. Hiyamizu, and H. Nishi, "Characterization of GaAs/AlGaAs hot electron transistors using magnetic field effects on launched-electron transport," *Surface Sci.*, vol. 174, pp. 481–486, 1986.
[404] Y. Imry, "Active transmission channels and universal conductance fluctuations," *Europhys. Lett.*, vol. 1, pp. 249–256, Mar. 1, 1986.
[405] Y. Imry, "The physics of mesoscopic systems," in *Directions in Condensed Matter Physics* , G. Grinstein and E. Mazenko, Eds. Singapore, China: World Scientific, 1986, pp. 101–163.
[406] Y. Imry, "Theoretical considerations of some new effects in narrow wires," in *Nanostructure Physics and Fabrication* , M. A. Reed and W. P. Kirk, Eds. San Diego, CA: Academic, 1989, pp. 379–388.
[407] Y. Imry and R. A. Webb, "Quantum interference and the Aharonov-Bohm effect," *Scientif. Amer.*, vol. 260, pp. 56–62, Apr. 1989.
[408] T. Inata, S. Muto, Y. Nakata, S. Sasa, T. Fujii, and S. Hiyamizu, "A pseudomorphic $In_{0.53}Ga_{0.47}As$/AlAs resonant tunneling barrier with a peak-to-valley current ratio of 14 at room temperature," *Japan. J. Appl. Phys.*, vol. 26, pp. L1332–L1334, Aug. 1987.
[409] K. Ishibashi, K. Nagata, K. Gamo, S. Namba, S. Ishida, K. Murase, M. Kawabe, and Y. Aoyagi, "Universal magneto-conductance flucuations in narrow n⁺GaAs wires," *Solid State Commun.*, vol. 61, pp. 385–389, Feb. 1987.
[410] K. Ishihara, S. Kinoshita, K. Furuya, Y. Miyamoto, K. Uesaka, and M. Miyauchi, "GaInAs/InP hot electron transistors grown by OMVPE," *Japan. J. Appl. Phys.*, vol. 26, pp. L911–L913, June 1987.
[411] K. Ismail, "The study of electron transport in field-effect-induced quantum wells on GaAs/GaAlAs," Ph.D. dissertation, Massachusetts Institute of Technology, Cambridge, MA, May 1989.
[412] K. Ismail, D. A. Antoniadis, and H. I. Smith, "One-dimensional subbands and mobility modulation in GaAs/AlGaAs quantum wires," *Appl. Phys. Lett.*, vol. 54, pp. 1130–1132, Mar. 20, 1989.
[413] K. Ismail, D. A. Antoniadis, H. I. Smith, C. T. Liu, K. Nakamura, and D. C. Tsui, "Lateral resonant tunneling in a double-barrier field-effect transistor," *Appl. Phys. Lett.*, vol. 55, pp. 589–591, Aug. 7, 1989.
[414] K. Ismail, D. A. Antoniadis, and H. I. Smith, "A lateral-surface-superlattice structure on GaAs/AlGaAs for far-infrared and magnetocapacitance measurements," *J. Vac. Sci. Technol. B.*, vol. 7, pp. 2000–2002, Nov./Dec. 1989.

[415] K. Ismail, W. Chu, D. A. Antoniadis, and H. I. Smith, "Surface-superlattice effects in a grating-gate GaAs/GaAlAs modulation doped field-effect transistor," *Appl. Phys. Lett.*, vol. 52, pp. 1071–1073, Mar. 28, 1988.

[416] K. Ismail, W. Chu, R. T. Tiberio, A. Yen, H. J. Lezec, M. I. Shepard, C. R. Musil, J. Melngailis, D. A. Antoniadis, and H. I. Smith, "Resonant tunneling across and mobility modulation along surface-structured quantum wells," *J. Vac. Sci. Technol.*, vol. 7, pp. 2025–2029, Nov./Dec. 1989.

[417] K. Ismail, W. Chu, A. Yen, D. A. Antoniadis, and H. I. Smith, "Negative transconductance and negative differential resistance in a grid-gate modulation-doped field-effect transistor," *Appl. Phys. Lett.*, vol. 54, pp. 460–462, Jan. 30, 1989.

[418] K. Ismail, T. P. Smith, W. T. Masselink, and H. I. Smith, "Magnetic flux commensurability in coupled quantum dots," *Appl. Phys. Lett.*, vol. 55, pp. 2766–2768, Dec. 25, 1990.

[419] C. Jacoboni, P. Lugli, R. Brunetti, and Reggiani, "A Monte Carlo technique for quantum transport in semiconductors," *Superlattices Microstructures*, vol. 2, pp. 209–212, 1986.

[420] F. C. Jain and K. K. Bhattacharjee, "Multiple quantum well optical modulator structures using surface acoustic wave induced Stark effect," *IEEE Photonics Tech. Lett.*, vol. 1, pp. 307–309, Oct. 1989.

[421] A. P. Jauho and M. Jonson, "Tunneling times in heterostructures," *Superlattices Microstructures*, vol. 6, no. 3, pp. 303–307, 1989.

[422] W. Jaworksi and D. M. Wardlaw, "Time delay in tunneling: Transmission and reflection time delays," *Phys. Rev. A*, vol. 37, pp. 2843–2854, Apr. 15, 1988.

[423] K. L. Jensen and F. A. Buot, "The inclusion of scattering in the simulation of quantum well devices," in *Computational Electronics*, K. Hess, J. P. Leburton, and U. Ravaioli, Eds. Norwell, MA: Kluwer Academic, 1991, pp. 239–242.

[424] J. L. Jewell, Y. H. Lee, S. L. McCall, J. P. Harbison, and L. T. Florez, "High finesse (Al,Ga)As interference filters grown by molecular beam epitaxy," *Appl. Phys. Lett.*, vol. 53, pp. 640–642, Aug. 22, 1988.

[425] G. Ji, D. Huang, U. K. Reddy, and H. Morkoc, "Determination of band offsets in AlGaAs/GaAs multiple quantum wells," *J. Vac. Sci. Technol. B*, vol. 5, pp. 1346–1352, Sept./Oct. 1987.

[426] B. Jogai and K. L. Wang, "Dependence of tunneling current on structural variations of superlattice devices," *Appl. Phys. Lett.*, vol. 46, pp. 167–168, Jan. 15, 1985.

[427] B. Jogai, K. L. Wang, and K. W. Brown, "Free-electron desity and transit time in a finite superlattice," *J. Appl. Phys*, vol. 59, pp. 2968–2970, Apr. 15, 1986.

[428] S. John, "Photon localization: The inhibition of electromagnetism in certain dielectrics," in *Analogies in Optics and Micro-Electronics*, W. van Haeringen and D. Lenstra, Eds. Dordrecht: Kluwer Academic, 1990, pp. 105–116.

[429] M. Jonson, "Quantum-mechanical resonant tunneling in the presence of a boson field," *Phys. Rev. B*, vol. 39, pp. 5924–5933, Mar. 15, 1989.

[430] M. Jonson and A. Grincwajg, "Effect of inelastic scattering on resonant and sequential tunneling in double barrier heterostructures," *Appl. Phys. Lett.*, vol. 51, pp. 1729–1731, Nov. 23, 1987.

[431] H. P. Joosten, H. J. M. F. Noteborn, and D. Lenstra, "Numerical study of coherent tunnelling in a double-barrier structure," *Thin Solid Films*, vol. 184, pp. 199–206, 1990.

[432] A. Kabasi, D. Chattopadhyay, and C. K. Sarkar, "The cooling rate of one-dimensional hot electrons in quantum well wires of polar semiconductors," *Solid-State Technol.*, vol. 3, pp. 1025–1028, Oct. 1988.

[433] W. J. Kaiser and L. D. Bell, "Direct investigation of subsurface interface electronic structure by ballistic-electron-emission microscopy," *Phy. Rev. Lett.*, vol. 60, pp. 1406–1409, Apr. 4, 1988.

[434] W. J. Kaiser and R. C. Jaklevic, "Reliable and versatile scanning tunneling microscope," *Rev. Sci. Intr.*, vol. 59, pp. 537–540, Apr. 1988.

[435] R. K. Kalia, W. Xue, and P. A. Lee, "Hopping magnetoconduction and the random structure in quasi one-dimensional inversion layers," *Phys. Rev. Lett.*, vol. 57, pp. 1615–1618, Sept. 29, 1986.

[436] V. Kalmeyer and R. B. Laughlin, "Differential conductance in three-dimensional resonant tunneling," *Phys. Rev. B*, vol. 35, pp. 9805–9808, June 15, 1987.

[437] S. C. Kan, S. Wu, S. Sanders, G. Griffel, and A. Yariv, "Optically controlled resonant tunneling in a double-barrier diode," *J. Appl. Phys.*, vol. 69, pp. 3384–3386, Mar. 1, 1991.

[438] S. B. Kaplan and A. Hartstein, "Magnetoconductance of pinched silicon accumulation layers," *Phys. Rev. B*, vol. 33, pp. 2909–2911, Feb. 15, 1986.

[439] R. Kapre, A. Madhukar, and S. Guha, "$In_{0.3}Ga_{0.7}As$ AlAs-based resonant tunneling diodes grown on prepatterned and nonpatterned GaAs (100) substrates," *IEEE Electron Device Lett.*, vol. 11, pp. 270–272, June 1990.

[440] R. M. Kapre, A. Madhukar, and S. Guha, "Highly strained GaAs/InGaAs resonant tunneling diodes with simultaneously high peak current densities and peak-to-valley ratios at room temperature," *Appl. Phys. Lett.*, vol. 58, pp. 2255–2257, May 20, 1991.

[441] A. Kastalsky, T. Duffield, S. J. Allen, and J. Harbison, "Photovoltaic detection of infrared light in a GaAs/AlGaAs superlattice," *Appl. Phys. Lett.*, vol. 52, pp. 1320–1322, Apr. 18, 1988.

[442] A. Kastalsky and S. Luryi, "Novel real-space hot-electron transfer devices," *IEEE Electron Device Lett.*, vol. 4, pp. 334–336, Sept. 1983.

[443] M. Kaveh, "What to expect from similarities between the Schrodinger and Maxwell equations," in *Analogies in Optics and Micro-Electronics*, W. van Haeringen and D. Lenstra, Eds. Dordrecht: Kluwer Academic, 1990, pp. 21–34.

[444] H. Kawai, K. Kaneko, and N. Watanabe, "Photoluminescence of AlGaAs/GaAs quantum wells grown by metalorganic chemical vapor deposition," *J. Appl. Phys.*, vol. 56, pp. 463–467, July 15, 1987.

[445] R. F. Kazarinov and R. A. Suris, "Possibility of the amplification of electromagnetic waves in a semiconductor with a superlattice," *Sov. Phys. Semicond.*, vol. 5, pp. 707–709, Oct. 1971.

[446] R. F. Kazarinov and R. A. Suris, "Electric and electromagnetic properties of semiconductors with a superlattice," *Sov. Phys. Semicond.*, vol. 6, pp. 120–131, July 1972.

[447] M. Keever, H. Shichijo, K. Hess, S. Banerjee, L. Witkowski, H. Morkoc, and B. G. Streetman, "Measurements of hot-electron conduction and real-space transfer in GaAs-$Al_xGa_{1-x}As$ heterojunction layers," *Appl. Phys. Lett.*, vol. 38, pp. 36–38, Jan. 1, 1981.

[448] V. P. Kesan, T. D. Linton, C. M. Maziar, D. P. Neikirk, P. A. Blakey, and B. G. Streetman, "Power optimized design of quantum well oscillators," *1987 IEEE International Electron Device Meeting Tech. Dig.*, pp. 62–65, Dec. 6–9, 1987.

[449] V. P. Kesan, A. Mortazawi, D. R. Miller, T. Itoh, B. G. Streetman, and D. P. Neikirk, "Microwave frequency operation of the quantum well injection transit time (QWITT) diode," *Electron. Lett.*, vol. 24, pp. 1473–1474, Nov. 24, 1988.

[450] V. P. Kesan, A. Mortazawi, D. R. Miller, V. K. Reddy, D. P. Neikirk, and T. Itoh, "Microwave and millimeter-wave QWITT diode oscillators," *IEEE Trans. Microwave Theory Tech.*, vol. 37, pp. 1933–1941, Dec. 1989.

[451] V. P. Kesan, D. P. Neikirk, P. A. Blakey, B. G. Streetman, and T. D. Linton, "Influence of transit time effects on the optimum design and maximum oscillation frequency of quantum well oscillators," *IEEE Trans. Electron Devices*, vol. 35, pp. 405–413, Apr. 1988.

[452] V. P. Kesan, D. P. Neikirk, B. G. Streetman, and P. A. Blakey, "A new transit time device using quantum well injection," *IEEE Electron. Device Lett.*, vol. 8, pp. 129–131, Apr. 1987.

[453] A. N. Khondker, M. R. Khan, and A. F. M. Anwar, "Transmission line analogy of resonance tunneling phenomena: The generalized impedance concept," *J. Appl. Phys.*, vol. 63, pp. 5191–5193, May 15, 1988.

[454] A. Khurana, "Ballistic electron transport through a narrow channel is quantized," *Phys. Today*, vol. 41, pp. 21–23, Nov. 1988.

[455] C. Kidner, I. Mehdi, J. R. East, and G. I. Haddad, "Power and stability limitations of resonant tunneling diodes," *IEEE Trans. Microwave Theory Tech.*, vol. 38, pp. 864–872, July 1990.

[456] I. Kim, T. K. Gustafson, and L. Thylen, "Analysis of quantum-confined structures using the beam propagation method," *Appl. Phys. Lett.*, vol. 57, pp. 285–287, July 16, 1990.

[457] K. Kim and K. Hess, "Electron transport in AlGaAs GaAs tunneling hot electron transfer amplifiers," *J. Appl. Phys.*, vol. 64, pp. 3057–3062, Sept. 15, 1988.

[458] K. Kim, K. Hess, and F. Capasso, "Monte Carlo study of electron heating and enhanced thermionic emission by hot phonons in heterolayers," *Appl. Phys. Lett.*, vol. 52, pp. 1167–1169, Apr. 4, 1988.

[459] W. B. Kinard, M. H. Weichold, G. F. Spencer, and W. P. Kirk, "Laterally confined resonant tunneling diode with adjustable quantum-dot cross-section," in *Nanostructure Physics and Fabrication* , M. A. Reed and W. P. Kirk, Ed. San Diego, CA: Academic, 1989, pp. 129–133.

[460] G. Kirczenow, "Theory of the conductance of ballistic quantum channels," *Solid State Commun.*, vol. 68, no. 8, pp. 715–718, Nov. 1988.

[461] G. Kirczenow, "Resonant conduction in ballistic quantum channels," *Phys. Rev. B* , vol. 39, pp. 10452–10455, May 15, 1989.

[462] G. Kirczenow, "Theory of electron injection into one-dimensional conductors," *J. Phys. Cond. Matter* , vol. 1, pp. 305–309, 1989.

[463] I. C. Kizilyalli and K. Hess, "Physics of real-space transfer transistors," *J. Appl. Phys* , vol. 65, pp. 2005–2013, Mar. 1, 1989.

[464] D. A. Kleinman and R. C. Miller,"Band-gap renormalization in semi-conductor quantum wells containing carriers," *Phys. Rev. B.*, vol. 32, pp. 2266–2272, Aug. 15, 1985.

[465] N. C. Kluksdahl, A. M. Kriman, D. K. Ferry, and C. Ringhofer, "Self-consistent study of the resonant-tunneling diode," *Phys. Rev. B* , vol. 39, pp. 7720–7735, Apr. 15, 1989.

[466] D. Y. K. Ko and J. C. Inkson, "Matrix method for tunneling in heterostructures: Resonant tunneling in multilayer systems," *Phys. Rev. B* , vol. 38, pp. 9945–9951, Nov. 15, 1988.

[467] E. Kobayashi, C. Hamaguchi, T. Matsuoka, and K. Taniguchi, "Monte Carlo study of hot-electron transport in an InGaAs/InAlAs single heterostructure," *IEEE Trans. Electron Devices* , vol. 36, pp. 2353–2360, Oct. 1989.

[468] T. E. Kopley, P. L. McEuen, and R. G. Wheeler, "Resonant tunneling through single electronic states and its suppression in a magnetic field," *Phys. Rev. Lett.*, vol. 61, pp. 1654–1657, Oct. 3, 1988.

[469] J. P. Kotthaus, "Transport properties and infrared excitations of laterally periodic nanostructures," in *Nanostructure Physics and Fabrication* , M. A. Reed and W. P. Kirk, Ed. San Diego, CA: Academic, 1989, pp. 67–76.

[470] L. P. Kouwenhoven, B. J. van Wees, C. J. P. M. Harmans, J. G. Williamson, H. van Houten, C. W. J. Beenakker, C. T. Foxon, and J. J. Harris, "Nonlinear conductance of quantum point contacts," *Phys. Rev. B* , vol. 39, pp. 8040–8043, Apr. 15, 1989.

[471] D. Kowal, U. Sivan, O. Entin-Wohlman, and Y. Imry, "Transmission through multiply-connected wire systems," *Phys. Rev. B* , vol. 42, pp. 9009–9018, Nov. 15, 1990.

[472] J. B. Krieger, and G. J. Iafrate, "Dynamics of a Bloch electron in a uniform electric field; Bloch oscillations," *Physica B* , vol. 134, pp. 228–232, Nov. 1985.

[473] A. M. Kriman, G. H. Bernstein, B. S. Haukness, and D. K. Ferry, "Analysis of electron diffraction in a novel field-effect transistor" *Superlattices Microstructures* , vol. 6, pp. 381–385, 1989.

[474] A. M. Kriman, B. S. Haukness, and D. K. Ferry, "Electron waveguide transmission resonance at a defect," *Proc. SPIE* , vol. 1284, pp. 82–90, 1990.

[475] S. Krishnamurthy, M. A. Berding, A. Sher, and A. B. Chen, "Ballistic transport in semiconductor alloys," *J. Appl. Phys.*, vol. 63, pp. 4540–4547, May 1, 1988.

[476] H. Kroemer, W. Y. Chien, J. S. Harris, and D. D. Edwall, "Measurement of isotype heterojunction barriers by C-V profiling," *Appl. Phys. Lett.*, vol. 36, pp. 295–297, Feb. 15, 1980.

[477] H. Kroemer and Q. G. Zhu, "On the interface connection rules for effective-mass wave functions at an abrupt heterojunction between two semiconductors with different effective mass," *J. Vac. Sci. Technol.*, vol. 21, pp. 551–553, July/Aug. 1982.

[478] A. Kumar, and P. F. Bagwell, "Resonant tunneling in a multichannel wire," *Solid State Commun.*, vol. 75, pp. 949–953, Sept. 1990.

[479] T. H. Kuo, H. C. Lin, R. C. Potter, and D. Shupe, "A novel A/D converter using resonant tunneling diodes," *IEEE J. Solid-State Circuits* , vol. 26, pp. 145–149, Feb. 1991.

[480] K. Kurishima, K. Furuya, and S. Samadi, "Theoretical study of electron wave diffraction caused by transverse potential grating – effect of incident angle," *IEEE J. Quantum Electron.*, vol. 25, pp. 2350–2356, Nov. 1989.

[481] M. Kuzuhara, K. Kim, D. Arnold, and K. Hess, "Ballistic electron transport across collector barriers in AlGaAs/GaAs hot-electron transistors," *Appl. Phys. Lett.*, vol. 52, pp. 1252–1254, Apr. 11, 1988.

[482] M. Kuzuhara, K. Kim, and K. Hess, "Transient stimulation of AlGaAs/ GaAs/AlGaAs and AlGaAs/InGaAs/AlGaAs hot-electron transistors," *IEEE Trans. Electron. Devices* , vol. 36, pp. 118–123, Jan. 1989.

[483] C. S. Kyono, V. P. Kesan, D. P. Neikirk, C. M. Maziar, and B. G. Streetman, "Dependence of apparent barrier height on barrier thickness for perpendicular transport in AlAs/GaAs single-barrier structures grown by molecular beam epitaxy," *Appl. Phys. Lett.*, vol. 54, pp. 549–551, Feb. 6, 1989.

[484] M. La Brecque, "Circuits and devices a molecule wide," *Mosaic* , vol. 20, pp. 16–27, Spring 1989.

[485] M. La Brecque, "Devices that assemble themselves," *Mosaic* , vol. 20, pp. 28–33, Spring 1989.

[486] B. Laikhtman, U. Sivan, A. Yacoby, C. P. Umbach, M. Heiblum, J. A. Kash, and H. Shtrikman, "Long mean free path of hot electrons selectively injected to higher subbands," *Phys. Rev. Lett.*, vol. 65, pp. 2181–2184, Oct. 22, 1990.

[487] R. Landauer, "Spatial variation of currents and fields due to localized scatterers in metallic conduction," *IBM J. Res. Develop.*, vol. 1, pp. 223–231, July 1957.

[488] R. Landauer, "Electrical resistance of disordered one-dimesional lattices," *Philos. Mag.*, vol. 21, pp. 863–867, 1970.

[489] R. Landauer, "Can a length of perfect conductor have a resistance?" *Phys. Lett. A* , vol. 85, pp. 91–93, Sept. 14, 1981.

[490] R. Landauer, "Electrical transport in open and closed systems," *Z. Phys. B - Condens. Mat.*, vol. 68, pp. 217–228, 1987.

[491] R. Landauer, "Can we switch by control of quantum mechanical transmission?" *Phys. Today* , vol. 42, pp. 119–121, Oct. 1989.

[492] R. Landauer, "Conductance determined by transmission: Probes and quantised constriction resistance," *J. Phys.: Cond. Matter* , vol. 1, pp. 8099–8110, 1989.

[493] R. Landauer, "Nanostructure physics: Fashion or depth?" in *Nanostructure Physics and Fabrication* , M. A. Reed and W. P. Kirk, Eds. San Diego, CA: Academic, 1989, pp. 17–30.

[494] R. Landauer, "Electrons as guided waves in laboratory structures: Strengths and problems," in *Analogies in Optics and Micro-Electronics* , W. van Haeringen and D. Lenstra, Eds. Dordrecht: Kluwer Academic, 1990, pp. 243–258.

[495] R. Landauer and M. Buttiker, "Resistance of small metallic loops," *Phys. Rev. Lett.*, vol. 54, pp. 2049–2052, May 6, 1985.

[496] R. Landauer and M. Buttiker, "Diffusive traversal time: Effective area in magnetically induced interference," *Phys. Rev. B* , vol. 36, pp. 6255–6260, Oct. 15, 1987.

[497] R. Lang and K. Nishi, "Electronic state localization in semiconductor superlattices," *Appl. Phys. Lett.*, vol. 45, pp. 98–100, July 1, 1984.

[498] D. C. Langreth and E. Abrahams, "Derivation of the Landauer conductance formula," *Phys. Rev. B*, vol. 24, pp. 2978–2984, Sept. 15, 1981.

[499] A. I. Larkin and D. E. Khmel'nitskii, "Mesoscopic fluctuations of current-voltage characteristics," *Sov. Phys. JETP*, vol. 64, pp. 1075–1077, Nov. 1986.

[500] A. Larsson, S. I. Borenstain, B. Jonsson, A. I. Andersson, J. Westin, and T. G. Andersson, "Photon-assisted resonant tunneling through variably spaced superlattice energy filters," *Appl. Phys. Lett.*, vol. 58, pp. 1297–1298, Mar. 25, 1991.

[501] R. B. Laughlin, "The relationship between high-temperature superconductivity and the fractional quantum Hall effect," *Science*, vol. 242, pp. 525–533, Oct. 28, 1988.

[502] S. E. Laux, D. J. Frank, and F. Stern, "Quasi-one-dimensional electron states in a split-gate GaAs/AlGaAs heterostructure," *Surface Sci.*, vol. 196, pp. 101–106, Mar. 1988.

[503] H. Q. Le, J. J. Zayhowski, and W. D. Goodhue, "Stark effect in $Al_xGa_{1-x}As/GaAs$ coupled quantum wells," *Appl. Phys. Lett.*, vol. 50, pp. 1518–1520, May 25, 1987.

[504] M. L. Leadbeater, E. S. Alves, L. Eaves, M. Henini, O. H. Hughes, A. Celeste, J. C. Portal, G. Hill, and M. A. Pate, "Magnetic field studies of elastic scattering and optic-phonon emission in resonant-tunneling devices," *Phys. Rev. B.*, vol. 39, pp. 3438–3441, Feb. 15, 1989.

[505] M. L. Leadbeater, E. S. Alves, L. Eaves, M. Henini, O. H. Hughes, F. W. Sheard, and G. A. Toombs, "Charge build-up and intrinsic bistability in an asymetric resonant tunneling

structure," *Semicond. Sci. Technol.*, vol. 3, pp. 1060–1062, Oct. 1988.

[506] M. L. Leadbeater, E. S. Alves, L. Eaves, M. Henini, O. H. Hughes, F. W. Sheard, and G. A. Toombs, "High magnetic field studies of intrinsic bistability, electron thermalization and ballistic effects in resonant tunneling devices," in *Nanostructure Physics and Fabrication*, M. A. Reed and W. P. Kirk, Eds. San Diego, CA: Academic, 1989, pp. 263–272.

[507] M. L. Leadbeater, L. Eaves, P. E. Simmonds, G. A. Toombs, F. W. Sheard, P. A. Claxton, G. Hill, and M. A. Pate, "Magnetic field studies of negative differential conductivity in double barrier resonant tunneling structures based on n⁺InP/(InGa)As," *Solid-State Electron.*, vol. 31, pp. 707–710, 1988.

[508] C. R. Leavens and G. C. Aers, "Dwell time and phase times for transmission and reflection," *Phys. Rev. B*, vol. 39, pp. 1202–1206, Jan. 15, 1989.

[509] J. A. Lebens, R. H. Silsbee, and S. L. Wright, "Tunneling and transverse wave vector conservation in GaAs/AlGaAs heterostructures," *Appl. Phys. Lett.*, vol. 51, pp. 840–842, Sept. 14, 1987.

[510] P. A. Lee, "Universal conductance fluctuations in disordered metals," *Physica A*, vol. 140, pp. 169–174, 1986.

[511] Y. Lee, M. J. McLennan, and S. Datta, "Anomalous R_{xx} in the quantum Hall regime due to impurity-bound states," *Phys. Rev. B*, vol. 44, 1991.

[512] A. J. Leggett, "Quantum and classical concepts at the one-electron level," in *Nanostructure Physics and Fabrication*, M. A. Reed and W. P. Kirk, Eds. San Diego, CA: Academic, 1989, pp. 31–42.

[513] D. Lenstra, L. P. J. Kamp, and W. van Haeringen, "Mode conversion, Bloch oscillations and Zener tunneling with light by means of the Sagnac effect," *Opt. Commun.*, vol. 60, pp. 339–344, Dec. 15, 1986.

[514] D. Lenstra and R. T. M. Smokers, "Theory of nonlinear quantum tunneling resistance in one-dimensional disordered systems," *Phys. Rev. B*, vol. 38, pp. 6452–6460, Oct. 1, 1988.

[515] D. Lenstra and W. van Haeringen, "Elastic scattering in a normal-metal loop causing resistive electronic behavior," *Phys. Rev. Lett.*, vol. 57, pp. 1623–1626, Sept. 29, 1986.

[516] D. Lenstra and W. van Haeringen, "Playing with electrons and photons in rings," in *Analogies in Optics and Micro-Electronics*, W. van Haeringen and D. Lenstra, Eds. Dordrecht: Kluwer Academic, 1990, pp. 3–20.

[517] D. Lenstra, W. van Haeringen, and R. T. M. Smokers, "Carrier dynamics in a ring, Landauer resistance and localization in a periodic system," *Physica A*, vol. 162, pp. 405–413, 1990.

[518] C. S. Lent, "The resonant hot electron transfer amplifier: A continuum resonance device," *Superlattices Microstructures*, vol. 3, pp. 387–389, July 1987.

[519] C. S. Lent, "Calculation of transport through ballistic quantum structures," in *Computational Electronics*, K. Hess, J. P. Leburton, and U. Ravaioli, Eds. Norwell, MA: Kluwer Academic, 1991, pp. 259–262.

[520] C. S. Lent and M. Leng, "Bloch states of electrons in a corrugated quantum channel in a magnetic field," *Appl. Phys. Lett.*, vol. 58, pp. 1650–1652, Apr. 15, 1991.

[521] C. S. Lent, S. Sivaprakasam, and D. J. Kirkner, "Calculation of ballistic transport in two-dimensional quantum structures using the finite element method," in *Nanostructure Physics and Fabrication*, M. A. Reed and W. P. Kirk, Eds. San Diego, CA: Academic, 1989, pp. 279–284.

[522] C. S. Lent, S. Sivaprakasam, and L. Liang, "Electron quantum waveguides: Cavities, constrictions, and bends," *Proc. SPIE*, vol. 1284, pp. 31–38, 1990.

[523] J. Leo and A. H. MacDonald, "Disorder-assisted tunneling through a double-barrier structure," *Phys. Rev. Lett.*, vol. 64, pp. 817–820, Feb. 19, 1990.

[524] X. Letartre, D. Stievenard, and E. Barbier, "Accurate determination of the conduction-band offset of a single quantum well using deep level transient spectroscopy," *Appl. Phys. Lett.*, vol. 58, pp. 1047–1049, Mar. 11, 1991.

[525] A. F. J. Levi, "Scaling 'ballistic' heterojunction bipolar transistors," *Electron. Lett.*, vol. 24, pp. 1273–1275, Sept. 29, 1988.

[526] A. F. J. Levi, J. R. Hayes and R. Bhat, "'Ballistic' injection devices in semiconductors," *Appl. Phys. Lett.*, vol. 48, pp. 1609–1611, June 9, 1986.

[527] A. F. J. Levi, J. R. Hayes, P. M. Platzman, and W. Wiegmann, "Injected-hot-electron transport in GaAs," *Phys. Rev. Lett.*, vol. 55, pp. 2071–2073, Nov. 4, 1985.

[528] A. F. J. Levi and S. Schmitt-Rink, "Nonequilibrium electron dynamics in small semiconductor structures," in *Nanostructure Physics and Fabrication*, M. A. Reed and W. P. Kirk, Eds. San Diego, CA: Academic, 1989, pp. 221–228.

[529] A. F. J. Levi, R. J. Spah, and J. H. English, "Electron transport dynamics in quantized intrinsic GaAs," *Phys. Rev. B*, vol. 36, pp. 9402–9405, Dec. 15, 1987.

[530] B. F. Levine, C. G. Bethea, K. K. Choi, J. Walker, and R. J. Malik, "Bound-to-extended state absorption GaAs superlattice transport infrared detectors," *J. Appl. Phys.*, vol. 64, pp. 1591–1593, Aug. 1, 1988.

[531] B. F. Levine, C. G. Bethea, G. Hasnain, J. Walker, and R. J. Malik, "GaAs/AlGaAs quantum-well, long-wavelength infrared (LWIR) detector with a detectivity comparable to HgCdTe," *Electron. Lett.*, vol. 24, pp. 747–749, June 9, 1988.

[532] B. F. Levine, C. G. Bethea, G. Hasnain, J. Walker, R. J. Malik, and J. M. Vandenberg, "Coherent enhancement of the hot-electron mean free path by superlattice transmission resonances," *Phys. Rev. Lett.*, vol. 63, pp. 899–902, Aug. 21, 1989.

[533] B. F. Levine, K. K. Choi, C. G. Bethea, J. Walker and R. J. Malik, "New 10μm infrared detector using intersubband absorption in resonant tunneling GaAlAs superlattices," *Appl. Phys. Lett.* vol. 50, pp. 1092–1094, Apr. 20, 1987.

[534] B. F. Levine, K. K. Choi, C. G. Bethea, J. Walker, and R. J. Malik, "High field hot electron transport through $Al_xGa_{1-x}As$ multiquantum well superlattices," *Solid-State Electron.*, vol. 31, pp. 583–587, Mar.-Apr. 1988.

[535] B. F. Levine, G. Hasnain, C. G. Bethea, and N. Chand, "Broadband 8–12μm high-sensitivity GaAs quantum well infrared photodetector," *Appl. Phys. Lett.*, vol. 54, pp. 2704–2706, June 26, 1989.

[536] Q. Li and C. M. Soukoulis, "Half-flux-quantum magnetoresistance oscillations in disordered metal rings," *Phys. Rev. Lett.*, vol. 57, pp. 3105–3108, Dec. 15, 1986.

[537] D. Lippens, E. Barbier, and P. Mounaix, "Fabrication of high-performance $Al_xGa_{1-x}As/In_yGa_{1-y}As/GaAs$ resonant tunneling diodes using a microwave-compatible technology," *IEEE Electron Device Lett.*, vol. 12, pp. 114–116, Mar. 1991.

[538] J. Lin and L. C. Chiu, "Quantum calculations of ballistic transport," *Appl. Phys. Lett.*, vol. 10, pp. 919–921, Mar. 6, 1989.

[539] R. K. Littleton and R. E. Camley, "Investigation of localization in a 10-well superlattice," *J. Appl. Phys.*, vol. 59, pp. 2817–2820, Apr. 15, 1986.

[540] C. T. Liu, D. C. Tsui, M. Shayegan, K. Ismail, D. A. antoniadis, and H. I. smith, "Guiding-center-drift resonance of two-dimensional electrons in a grid-gate superlattice potential," *Appl. Phys. Lett.*, vol. 58, pp. 2945–2947, June 24, 1991.

[541] H. C. Liu, "Tunneling time through heterojunction double barrier diodes," *Superlattices Microstructures*, vol. 3, pp. 379–382, July 1987.

[542] H. C. Liu, "Quantum inductance in resonant tunneling," *J. Appl. Phys.*, vol. 69, pp. 2705–2707, Feb. 15, 1991.

[543] H. C. Liu and G. C. Aers, "Theory of the vertical transport through one, two, and three dimensionally confined quantum wells," *Solid State Commun.*, vol. 67, no. 12, pp. 1131–1133, Sept. 1988.

[544] H. C. Liu and G. C. Aers, "Resonant tunneling through one-, two-, and three-dimensionally confined quantum wells," *J. Appl. Phys.*, vol. 65, pp. 4908–4914, June 15, 1989.

[545] Y. Z. Liu, R. J. Anderson, R. A. Milano, and M. J. Cohen, "Effect of heterojunction spike on the quantum efficiency of an AlGaAs/GaAs heterojunction charge coupled device," vol. 40, pp. 967–969, June 1, 1982.

[546] G. Lommer, F. Malcher, and U. Rossler, "Electron states in $GaAs/Ga_{1-x}Al_xAs$ heterostructures: Subband Landau-levels," *Superlattices Microstructures*, vol. 2, pp. 273–278, 1986.

[547] A. P. Long, P. H. Beton, and M. J. Kelly, "Hot-electron transport in heavily doped GaAs," *Semicond. Sci. Technol.*, vol. 1, pp. 63–70, July 1986.

[548] S. S. Lu, K. Lee, M. I. Nathan, and S. L. Wright, "Resonant indirect Fowler-Nordheim tunneling in $Al_{0.8}Ga_{0.2}As$ barrier," *Appl. Phys. Lett.*, vol. 58, pp. 266–268, Jan. 21, 1991.

[549] W. W. Lui and J. Frey, "A simplified method for quantum size effect analysis in sub-micron devices including Fermi-Dirac statistics," in *Nanostructure Physics and Fabrication*, M. A. Reed and W. P. Kirk, Eds. San Diego, CA: Academic, 1989,

pp. 291–295.
[550] M. Lundstrom and S. Datta, "Physical device simulation in a shrinking world," *Circuits and Devices*, vol. 6, pp. 32–37, July 1990.
[551] S. Luryi, "Frequency limit of double-barrier resonant-tunneling oscillators," *Appl. Phys. Lett.*, vol. 47, pp. 490–492, Sept. 1, 1985.
[552] S. Luryi and F. Capasso, "Resonant tunneling of two-dimensional electrons through a quantum wire: A negative transconductance device," *Appl. Phys. Lett.*, vol. 47, pp. 1347–1349, Dec. 15, 1985.
[553] S. Luryi, A. Kastalsky, A. C. Gossard, and R. H. Hendel, "Charge injection transistor based on real-space hot-electron transfer," *IEEE Trans. Electron Device Lett.*, vol. 31, pp. 832–839, June 1984.
[554] I. W. Lyo and P. Avouris, "Negative differential resistance on the atomic scale: Implications for atomic scale devices," *Science*, vol. 245, pp. 1369–1371, Sept. 22, 1989.
[555] S. K. Lyo, "Electron-electron scattering and mobilities in semiconductors and quantum wells," *Phys. Rev. B*, vol. 34, pp. 7129–7134, Nov. 15, 1986.
[556] A. H. MacDonald and G. W. Bryant, "Strong-magnetic-field states of the pure electron plasma," *Phys. Rev. Lett.*, vol. 58, pp. 515–518, Feb. 2, 1987.
[557] S. Maeda, "Activities of the research and development association for future electron devices," *Proc. IEEE*, vol. 77, pp. 1420–1429, Sept. 1989
[558] C. Mailhot and D. L. Smith, "Effects of compressive uniaxial stress on the electronic structure of GaAs-$Ga_{1-x}Al_xAs$ quantum wells," *Phys. Rev. B*, vol. 36, pp. 2942–2945, Oct. 15, 1987.
[559] S. J. Manion, L. D. Bell, W. J. Kaiser, P. D. Maker, and R. E. Muller, "Lateral tunneling through voltage-controlled barriers," *Appl. Phys. Lett.*, vol. 59, pp. 213–215, July 8, 1991.
[560] P. M. Mankiewich, R. E. Behringer, R. E. Howard, A. M. Chang, T. Y. Chang, B. Chelluri, J. Cunningham, and G. Timp, "Observation of Aharonov-Bohm effect in quasi-one-dimensiona GaAs AlGaAs rings," *J. Vac. Sci. Technol. B*, vol. 6, pp. 131–133, Jan./Feb. 1988.
[561] P. M. Mankiewich, R. E. Howard, L. D. Jackel, W. J. Skocpol, and D. M. Tennant, "Nanometer metal-oxide-semiconductor field-effect transistors: A flexible tool for studying inversion layer physics," *J. Vac. Sci. Technol. B*, vol. 4, pp. 380–382, Jan. Feb. 1986.
[562] K. P. Martin, "Comment on 'Proposal of novel electron wave coupled devices'," Appl. Phys. Lett., vol. 59, p. 375, July 15, 1991.
[563] K. P. Martin, S. Ben Amor, J. J. L. Rascol, R. J. Higgins, R. C. Potter, and H. Hier, "Trajectory domains in a wide-well double-barrier tunneling structure in crossed electric and magnetic fields," *Appl. Phys. Lett.*, vol. 56, pp. 1772–1774, Apr. 30, 1990.
[564] P. J. Martin, B. G. Oldaker, A. H. Miklich, and D. E. Pritchard, "Bragg scattering of atoms from a standing light wave," *Phys. Rev. Lett.*, vol. 60, pp. 515–518, Feb. 8, 1988.
[565] T. G. Matheson, "Tunneling and lifetime effects in tipped silicon inversion layers," Ph.D. dissertation, University of Oregon, Eugene, Dec. 1980.
[566] T. G. Matheson and R. J. Higgins, "Tunneling in tilted Si inversion layers," *Phys. Rev. B*, vol. 25, pp. 2633–2644, Feb. 15, 1982.
[567] H. Mathieu, P. Lefebvre, J. Allegre, B. Gil, and A. Regreny, "Differential spectroscopy of GaAs-$Ga_{1-x}Al_xAs$ quantum wells: An unambiguous identification of light-hole and heavy-hole states," *Phys. Rev. B*, vol. 36, pp. 6581–6584, Oct. 15, 1987.
[568] M. J. McLennan, Y. Lee, and S. Datta, "Voltage drop in mesoscopic systems: A numerical study using a quantum kinetic equation," *Phys. Rev. B*, vol. 43, June 15, 1991.
[569] M. J. McLennan, Y. Lee, R. K. Lake, G. Neofotistos, and S. Datta, "Dissipative quantum transport in electron waveguides," in *Computational Electronics*, K. Hess, J. P. Leburton, and U. Ravaioli, Eds. Norwell, MA: Kluwer Academic, 1991, pp. 247–250.
[570] I. Mehdi and G. I. Haddad, "InP based resonant tunneling diodes for millimeter-wave power generation," in *Nanostructure Physics and Fabrication*, M. A. Reed and W. P. Kirk, Eds. San Diego, CA: Academic, 1989, pp. 207–211.
[571] U. Meirav, M. A. Kastner, M. Heiblum, and S. J. Wind, "One-dimensional electron gas in GaAs: Periodic conductance oscillations as a function of density," *Phys. Rev. B.*, vol. 40, pp. 5871–5874, Sept. 15, 1989.
[572] U. Meirav, M. A. Kastner, and S. J. Wind, "Single-electron charging and periodic conductance resonances in GaAs nanostructures," *Phys. Rev. Lett.*, vol. 65, pp. 771–774, Aug. 6, 1990
[573] E. E. Mendez, F. Agullo-Rueda, and J. M. Hong, "Temperature dependence of the electronic coherence of GaAs-GaAlAs superlattices," *Appl. Phys. Lett.*, vol. 56, pp. 2545–2547, June 18, 1990.
[574] E. E. Mendez, E. Calleja, C. E. T. Goncalves da Silva, L. L. Chang, and W. I. Wang, "Observation by resonant tunneling of high-energy states in GaAs-$Ga_{1-x}Al_xAs$ quantum wells," *Phys. Rev. B*, vol. 33, pp. 7368–7370, May 15, 1986.
[575] E. E. Mendez, E. Calleja, and W. I. Wang, "Tunneling through indirect-gap semiconductor barriers," *Phys. Rev. B*, vol. 34, pp. 6026–6029, Oct. 15, 1986.
[576] E. E. Mendez, E. Calleja, and W. I. Wang, "Inelastic tunneling in AlAs-GaAs-AlAs heterostructures," *Appl. Phys. Lett.*, vol. 53, pp. 977–979, Sept. 12, 1988.
[577] E. E. Mendez, L. Esaki, and W. I. Wang, "Resonant magnetotunneling in GaAlAs-GaAs-GaAlAs heterostructures," *Phys. Rev. B*, vol. 33, pp. 2893–2896, Feb. 15, 1986.
[578] E. E. Mendez, W. I. Wang, E. Calleja, and C. E. T. Goncalves de Silva, "Resonant tunneling via X-point states in AlAs-GaAs-AlAs hetero-structures," *Appl. Phys. Lett.*, vol. 50, pp. 1263–1265, May 4, 1987.
[579] E. E. Mendez, W. I. Wang, B. Ricco, and L. Esaki, "Resonant tunneling of holes in AlAs-GaAs-AlAs heterostructures," *Appl. Phys. Lett.*, vol. 47, pp. 415–417, Aug. 15, 1985.
[580] R. Merlin, "Structural and elctronic properties of nonperiodic superlattices," *IEEE J. Quantum Electron.*, vol. 24, pp. 1791–1798, Aug. 1988.
[581] A. Miller, R. J. Manning, P. K. Milsom, D. C. Hutchings, D. W. Crust, and K. Woodbridge, "Transient grating studies of excitonic optical nonlinearities in GaAs AlGaAs multiple-quantum-well structures," *J. Opt. Soc. Amer. B*, vol. 6, pp. 567–578, Apr. 1989.
[582] D. A. B. Miller, D. S. Chemla, T. C. Damen, A. C. Gossard, W. Wiegmann, T. H. Wood, and C. A. Burrus, "Novel hybrid optically bistable switch: The quantum well self-electro-optic effect device," *Appl. Phys. Lett.*, vol. 45, pp. 13–15, July 1, 1984.
[583] D. A. B. Miller, D. S. Chemla, T. C. Damen, T. H. Wood, C. A Burrus, A. C. Gossard, and W. Wiegmann, "Optical-level shifter and self-linearized optical modulator using a quantum-well self-electro-optic effect device," *Opt. Lett.*, vol. 9, pp. 567–569, Dec. 1984.
[584] D. A. B. Miller, J. E. Henry, A. C. Gossard, and J. H. English, "Integrated quantum well self-electro-optic effect device: 2 x 2 array of optically bistable switches," *Appl. Phys. Lett.*, vol. 49, pp. 821–823, Sept. 29, 1986.
[585] D. C. Miller, R. K. Lake, S. Datta, M. S. Lundstrom, M. R. Melloch, and R. Reifenberger, "Modulation of the conductance of T-shaped electron waveguide structures with a remote gate," in *Nanostructure Physics and Fabrication*, M. A. Reed and W. P. Kirk, Eds. San Diego, CA: Academic, 1989, pp. 165–174.
[586] D. R. Miller and D. P. Neikirk, "Simulation of intervalley mixing in double-barrier diodes using the lattice Wigner function," *Appl. Phys. Lett.*, vol. 58, pp. 2803–2805, June 17, 1991.
[587] R. C. Miller, A. C. Gossard, D. A. Kleinman, and O. Munteanu, "Parabolic quantum wells with the GaAs-$Al_xGa_{1-x}As$ system," *Phys. Rev. B*, vol. 29, pp. 3740–3743, Mar. 15, 1984.
[588] F. P. Milliken, S. Washburn, C. P. Umbach, R. B. Laibowitz, and R. A. Webb, "Effect of partial coherence on Aharonov–Bohm oscillations in metal loops," *Phys. Rev. B*, vol. 36, pp. 4465–4468, Sept. 15, 1987.
[589] A. S. Moffat, "Engineering at the lower limits of size," *Mosaic*, vol. 21, pp. 30–40, 1990.
[590] L. W. Molenkamp, A. A. M. Staring, C. W. J. Beenakker, R. Eppenga, C. E. Timmering, J. G. Williamson, C. J. P. M. Harmans, and C. T. Foxon, "Electron-beam collimation with a quantum point contact," *Phys. Rev. B*, vol. 41, pp. 1274–1277, Jan. 15, 1990.
[591] T. Mori, H. Ohnishi, K. Imamura, S. Muto, and N. Yokoyama, "Resonant tunneling hot-electron transistor with current gain of 5," *Appl. Phys. Lett.*, vol. 49, pp. 1779–1780, Dec. 29, 1986.
[592] R. A. Morrow and K. R. Brownstein, "Model effective-mass Hamiltonians for abrupt heterojunctions and the associated

wave-function-matching conditions," *Phys. Rev. B*, vol. 30, pp. 678–680, July 15, 1984.
[593] S. Munnix and D. Bimberg, "Simulation of electron beam induced current at GaAs/AlGaAs heterojunctions under forward bias," *Appl. Phys. Lett.*, vol. 51, pp. 2121–2123, Dec. 21, 1987.
[594] R. Nagarajan, T. Kamiya, and A. Kurobe, "Band filling in GaAs/ AlGaAs multiquantum well lasers and its effect on the threshold current," *IEEE J. Quantum Electron.*, vol. 25, pp. 1161–1169, June 1989.
[595] G. A. Nagy and M. Szilagyi, *Introduction to the Theory of Space-Charge Optics* . New York: Halsted-Wiley, 1974.
[596] T. Nakagawa, H. Imamoto, T. Sakamoto, T. Kojima, K. Ohta, and N. J. Kawai, "Observation of negative differential resistance in CHIRP superlattices," *Electron. Lett.*, vol. 21, pp. 882–884, Sept. 12, 1985.
[597] T. Nakagawa, H. Imamoto, T. Kojima, and K. Ohta, "Observation of resonant tunneling in AlGaAs/GaAs triple barrier diodes," *Appl. Phys. Lett.*, vol. 49, pp. 73–75, July 14, 1986.
[598] T. Nakagawa, T. Fujita, Y. Matsumoto, T. Kojima, and K. Ohta, "Resonant tunneling of holes in AlAs/GaAs triple barrier diodes," *Appl. Phys. Lett.*, vol. 50, pp. 974–976, Apr. 13, 1987.
[599] T. Nakagawa, N. J. Kawai, and K. Ohta, "Design principles for CHIRP superlattice devices," *Superlattices Microstructures* , vol. 1, pp. 187–192, 1985.
[600] T. Nakamura, M. Ikeda, S. Muto, and I. Umebu, "Characterization of interfacial atomic steps in GaAs/AlAs superlattices by transmission electron microscopy," *Appl. Phys. Lett.*, vol. 53, pp. 379–381, Aug. 1, 1988.
[601] K. Nakamura, A. Shimizu, M. Koshiba, and K. Hayata, "Finite-element analysis of quantum wells of semiconductors with arbitrary potential profiles," *IEEE J. Quantum Electron.*, vol. 25, pp. 889–895, May 1989.
[602] Y. Nakata, M. Asada, and Y. Suematsu, "Novel triode device using metal-insulator superlattice proposed for high-speed response," *Electron. Lett.*, vol. 22, pp. 58–59, Jan. 2, 1986.
[603] M. I. Nathan and M. Heiblum, "A gallium arsenide ballistic transistor?" *IEEE Spectrum* , vol. 23, pp. 45–47, Feb. 1986.
[604] J. Nayyer, Y. Suematsu, and K. Shimomura, "Analysis of reflection-type optical switches with intersecting waveguides," *J. Lightwave Technol.*, vol. 6, pp. 1146–1152, June 1988.
[605] G. Neofotistos, K. Diff, and J. D. Gunton, "Time-dependent modeling of resonant tunneling structures using the 3-dimensional Schrodinger equation: Investigation of the intrinsic time characteristics of a zero-dimensional semiconductor nanostructure," in *Nanostructure Physics and Fabrication* , M. A. Reed and W. P. Kirk, Eds. San Diego, CA: Academic, 1989, pp. 135–139.
[606] G. Neofotistos, H. Guo, K. Diff, and J. D. Gunton, "Resonant tunneling in double-barrier parabolic well structures," *IEEE Trans. Electron Devices* , vol. 36, pp. 745–749, Apr. 1989.
[607] G. Neofotistos, R. Lake, and S. Datta, "Inelastic-scattering effects on single-barrier tunneling," *Phys. Rev. B* , vol. 43, pp. 2442–2445, Jan. 15, 1991.
[608] G. Nimtz and P. Marquardt, "The electron cut-off wavelength transistor," *Appl. Phys. A* , vol. 47, pp. 317–318, Dec. 1988.
[609] J. A. Nixon, J. H. Davies, and J. R. Barker, "Fluctuations in submicron semiconducting devices caused by the random positions of dopants," in *Nanostructure Physics and Fabrication* , M. A. Reed and W. P. Kirk, Eds. San Diego, CA: Academic, 1989, pp. 123–127.
[610] S. Noda, K. Kojima, K. Mitsunaga, K. Kyuma, K. Hamanaka, and T. Nakayama, "Ridge waveguide AlGaAs/GaAs distributed feedback lasers with multiple quantum well structure," *Appl. Phys. Lett.*, vol. 48, pp. 1767–1769, June 30, 1986.
[611] D. D. Norwood, H. E. Swoboda, M. D. Dawson, A. L. Smirl, D. R. Andersen, and T. C. Hasenberg, "Room-temperature short-period transient grating measurement of perpendicular transport in GaAs/AlGaAs multiple quantum wells," *Appl. Phys. Lett.*, vol. 59, pp. 219–221, July 8, 1991.
[612] H. J. M. F. Noteborn, H. P. Joosten, and D. Lenstra, "Self-consistent study of coherent tunneling through a double barrier structure," *Phys. Scrip. T* , vol. 33, pp. 219–226, 1990.
[613] R. N. Nottenburg, A. F. J. Levi, B. Jalali, D. Sivco, D. A. Humphrey, and A. Y. Cho, "Nonequilibrium electron transport in heterostructure bipolar transistors probed by magnetic field," *Appl. Phys. Lett.*, vol. 56, pp. 2660–2662, June 25, 1990.
[614] T. Odagaki and H. Aoyama, "Hyperinflation in periodic and quasiperiodic chains," *Phys. Rev. Lett.*, vol. 61, pp. 775–778, Aug. 15, 1988.
[615] A. A. Odintsov, "Single electron transport in a two-dimensional electron gas system with modulated barriers: A possible dc current standard," *Appl. Phys. Lett.*, vol.58, pp. 2695–2697, June 10, 1991.
[616] H. Ohnishi, T. Inata, S. Muto, N. Yokoyama, and A. Shibatomi, "Self-consistent analysis of resonant tunneling devices," *Appl. Phys. Lett.*, vol. 49, pp. 1248–1250, Nov. 10, 1986.
[617] H. Ohnishi, N. Yokoyama, and A. Shibatomi, "Modeling electron transport in InGaAs-based resonant-tunneling hot-electron transistors," *IEEE Trans. Electron Devices* , vol. 63, pp. 2335–2339, Oct. 1989.
[618] H. Ohno, E. E. Mendez, J. A. Brum, J. M. Hong, F. Agullo-Rueda, L. L. Chang, and L. Esaki, "Observation of 'Tamm States' in superlattices," *Phys. Rev. Lett.*, vol. 64, pp. 2555–2558, May 21, 1990.
[619] H. Ohno, E. E. Mendez, and W. I. Wang, "Effects of carrier mass differences on the current-voltage characteristics of resonant tunneling structures," *Appl. Phys. Lett.*, vol. 56, pp. 1793–1795, Apr. 30, 1990.
[620] K. K. Ohta, S. T. Nakagawa, Y. N. Kawai, K. T. Kojima, and T. M. Kawashima, "Semiconductor device," U. S. Patent 4 620 206 assigned to Agency of Industrial Science and Technology, Oct. 28, 1986.
[621] G. R. Olbright, T. E. Zipperian, J. Klem, and G. R. Hadley, "Optical switching in N x N arrays of individually addressable electroabsorption modulators based on Wannier-Stark carrier localization in GaAs/GaAlAs superlattices," *J. Opt. Soc. Amer. B* , vol. 8, pp. 346–354, Feb. 1991.
[622] U. Olin, "Model for optical bistability in GaAs/AlGaAs Fabry-Perot etalons including diffraction, carrier diffusion, and heat conduction," *J. Opt. Soc. Am. B*, vol. 7, pp. 35–42, Jan. 1990.
[623] T. P. Orlando, P. F. Bagwell, R. A. Ghanbari, and K. Ismail, "Quantum device modeling with the convolution method," in *Electronic Properties of Multilayers and Low Dimensional Semiconductor Structures*, J. M. Chamberlain, L. Eaves, and J. C. Portal Eds. London, U.K.: Plenum, 1989, pp. 191–210.
[624] A. Palevski, M. Heiblum, C. P. Umbach, C. M. Knoedler, A. N. Broers, and R. H. Koch, "Lateral tunneling, ballistic transport, and spectroscopy in a two-dimensional electron gas," *Phys. Rev. Lett.*, vol. 62, pp. 1776–1779, Apr. 10, 1989.
[625] J. F. Palmier, "Electrical transport perpendicular to layers in superlattices," in *Heterojunction and Semiconductor Superlattices*, G. Allan, G. Bastard, N. Boccara, M. Lannoo, and M. Voos, Eds. Berlin, Germany: Springer-Verlag, 1988, pp. 127–145.
[626] J. F. Palmier, H. Le Person, C. Minot, A. Chomette, A. Regreny, and D. Calecki, "Hopping mobility in semiconductor superlattices," *Superlattices Microstructures*, vol. 1, no. 1, pp. 67–72, 1985.
[627] B. Pannetier, J. Chaussy, R. Rammal, and P. Gandit, "Magnetic flux quantization in the weak-localization regime of a nonsuperconducting metal," *Phys. Rev. Lett.*, vol. 53, pp. 718–721, Aug. 13, 1984.
[628] M. C. Payne, "Electrostatic and electrochemical potentials in quantum transport," *J. Phys.: Cond. Matt.*, vol. 1, pp. 4931–4938, 1989.
[629] P. M. Petroff, "Carrier confinement t one and zer degrees of freedom in *Physics of Quantum Electron Deviees*, F. Capasso, Ed. Berlin, Germany: Springer-Verlag, 1990, pp. 353–366.
[630] P. M. Petroff, A. C. Gossard, R. A. Logan, and W. Weigmann, "Toward quantum well wires: Fabrication and optical properties," *Appl. Phys. Lett.*, vol. 41, pp. 635–638, Oct. 1, 1982.
[631] V. Pevzner and K. Hess, "Quantum ray tracing: A new approach to quantum transport in mesoscopic systems," in *Computational Electronics*, K. Hess, J. P. Leburton, and U. Ravaioli, Eds. Norwell, MA: Kluwer Academic, 1991, pp. 227–230.
[632] D. T. Pierce, R. J. Celotta, G. C. Wang, W. N. Unertl, A. Galejs, C. E. Kuyatt, and S. R. Mielczarek, "GaAs spin polarized electron source," *Rev. Sci. Instr.*, vol. 51, pp. 478–499, Apr. 1980.
[633] G. Platero, P. A. Schulz, L. Brey, and C. Tejedor, "Quantum transmission channels for magnetotunneling in semiconductor microstructures," *Surface Sci.*, vol. 228, pp. 291–295, Apr. 1990.
[634] R. Pool, "A small, small, very small diode," *Science*, vol. 246, pg. 1251, Dec. 8, 1989.
[635] R. Pool, "A prism for electrons," *Science*, vol. 248, pg. 1606, June 29, 1990.

[636] R. Pool, "A transistor that works electron by electron," *Science*, vol. 249, pg. 629, Aug. 10, 1990.
[637] R. C. Potter and A. A. Lakhani, "Observation of electron quantum interference effects due to virtual states in a double-barrier heterostructure at room temperature," *Appl. Phys. Lett.*, vol. 52, pp. 1349–1351, Apr. 18, 1988.
[638] W. Potz, "Self-consistent treatment of resonant-tunneling structures," *Superlattices Microstructures*, vol. 6, no.2, pp. 187–192, 1989.
[639] P. J. Price, "Calculation of electron propagation in heterostructures," *Superlattices Microstructures*, vol. 2, pp. 213–217, 1986.
[640] P. J. Price, "Resonant tunneling properties of heterostructures," *Superlattices Microstructures*, vol. 2, no. 6, pp. 593–596, 1986.
[641] P. J. Price, "Theory of resonant tunneling in heterostructures," *Phys. Rev. B*, vol. 38, pp. 1994–1998, July 15, 1988.
[642] P. J. Price, "Simple theory of double-barrier tunneling," *IEEE Trans. Electron Devices*, vol. 36, pp. 2340–2343, Oct. 1989.
[643] D. E. Pritchard, "Atom gratings and guides," *Opt. News*, vol. 14, pp. 7–8, Dec. 1988.
[644] D. E. Prober, "Quantum transport in microstructures," *Microelectron. Eng.*, vol. 5, pp. 203–216, 1986.
[645] A. Pruisken and Z. Wang, "Mesoscopic conductance fluctuations in disordered metals," in *Nanostructure Physics and Fabrication*, M. A. Reed and W. P. Kirk, Eds. San Diego, CA: Academic, 1989, pp. 413–417.
[646] C. F. Quate, "Vacuum tunneling: a new technique for microscopy," *Phys. Today*, vol. 39, pp. 26–33, Aug. 1986.
[647] L. Q. Qian and B. W. Wessels, "Scanning tunneling optical spectroscopy of semiconductors," *Appl. Phys. Lett.*, vol. 58, pp. 1295–1296, Mar. 25, 1991.
[648] L. Q. Qian and B. W. Wessels, "Scanning tunneling optical spectroscopy of semiconductor quantum well structures," *Appl. Phys. Lett.*, vol 58, pp. 2538–2539, June 3, 1991.
[649] D. C. Radulescu, G. W. Wicks, W. J. Schaff, A. R. Calawa, and L. F. Eastman, "Anisotropic transport in modulation doped quantum well structures," *J. Appl. Phys.*, vol. 61, pp. 2301–2306, Mar. 15, 1987.
[650] J. J. L. Rascol, K. P. Martin, S. Ben Amor, R. J. Higgins, A. Celeste, J. C. Portal, A. Torabi, H. M. Harris, and C. J. Summers, "Magneto-spectral analysis of tunneling processes in a double-quantum-well tunneling structure," *Phys. Rev. B*, vol. 41, pp. 3733–3737, Feb. 15, 1990.
[651] J. J. L. Rascol, K. P. Martin, R. E. Carnahan, R. J. Higgins, L. Cury, J. C. Portal, B. G. Park, E. Wolak, K. L. Lear, and J. S. Harris, "Influence of ballistic electrons on the device characteristics of vertically integrated resonant tunneling diodes," *Appl. Phys. Lett.*, vol. 58, pp. 1482–1484, Apr. 8, 1991.
[652] J. J. L. Rascol, K. P. Martin, R. E. Carnahan, R. J. Higgins, L. Cury, J. C. Portal, B. G. Park, E. Wolak, K. L. Lear, and J. S. Harris, "Influence of ballistic electrons on the device characteristics of vertically integrated resonant tunneling diodes," *Superlattices Microstructures*, vol. 9, 1991.
[653] A. Rauh, G. H. Wannier, and G. Obermair, "Bloch electrons in irrational magnetic fields," *Phys. Stat. Sol.*, vol. 63, pp. 215–229, 1974.
[654] U. Ravaioli, M. A. Osman, W. Potz, N. Kluksdahl, and D. K. Ferry, "Investigation of ballistic transport through resonant-tunneling quantum wells using Wigner function approach," *Physica B*, vol. 134, pp. 36–40, 1985.
[655] R. C. Reddick, R. J. Warmack, D. W. Chilcott, S. L. Sharp, and T. L. Ferrell, "Photon scanning tunneling microscopy," *Rev. Sci. Instr.*, vol. 61, pp. 3669–3677, Dec. 1990.
[656] U. K. Reddy, G. I. Haddad, I. Mehdi, and R. K. Mains, "Fabrication and room temperature operation of a resonant tunneling transistor with a pseudomorphic InGaAs base," in *Nanostructure Physics and Fabrication*, M. A. Reed and W. P. Kirk, Eds. San Diego, CA: Academic, 1989, pp. 189–193.
[657] M. A. Reed, "Quantum semiconductor devices," *1986 Symp. VLSI Technol. Papers. Digest of Technical Papers*, pp. 1–4, 1986.
[658] M. A. Reed, R. T. Bate, K. Bradshaw, W. M. Duncan, W. R. Frensley, J. W. Lee, and H. D. Shih, "Spatial quantization in GaAs-AlGaAs multiple quantum dots," *J. Vac. Sci. Technol. B*, vol. 4, pp. 358–360, Jan./Feb. 1986.
[659] M. A. Reed, W. R. Frensley, W. M. Duncan, R. J. Matyi, A. C. Seabaugh, and H. L. Tsai, "Quantitative resonant tunneling spectroscopy: Current-voltage characteristics of precisely characterized resonant tunneling diodes," *Appl. Phys. Lett.*, vol. 54, pp. 1256–1258, Mar. 27, 1989.
[660] M. A. Reed, W. R. Frensley, R. J. Matyi, J. N. Randall, and A. C. Seabaugh, "Realization of a three-terminal resonant tunneling device: The bipolar quantum resonant tunneling transistor," *Appl. Phys. Lett.*, vol. 54, pp. 1034–1036, Mar. 13, 1989.
[661] M. A. Reed and J. W. Lee, "Resonant tunneling in a GaAs/AlGaAs barrier/InGaAs quantum well heterostructure," *Appl. Phys. Lett.*, vol. 50, pp. 845–847, Mar. 30, 1987.
[662] M. A. Reed, J. W. Lee, and H. L. Tsai, "Resonant tunneling through a double GaAs/AlAs superlattice barrier, single quantum well heterostructure," *Appl. Phys. Lett.*, vol. 49, pp. 158–160, July 21, 1986.
[663] M. A. Reed, J. N. Randall, R. J. Aggarwal, R. J. Matyi, T. M. Moore, and A. E. Wetsel, "Observation of discrete electronic states in a zero-dimensional semiconductor nanostructure," *Phys. Rev. Lett.*, vol. 60, pp. 535–537, Feb. 8, 1988.
[664] L. Reggiani and V. Kozlov, "Population inversion in superconducting quantum wells under ballistic conditions," in *Nanostructure Physics and Fabrication*, M. A. Reed and W. P. Kirk, Eds. San Diego, CA: Academic, 1989, pp. 479–483.
[665] L. F. Register, U. Ravaioli, and K. Hess, "Transient response in mesoscopic devices," in *Computational Electronics*, K. Hess, J. P. Leburton, and U. Ravaioli, Eds. Norwell, MA: Kluwer Academic, 1991, pp. 235–238.
[666] E. A. Rezek, N. Holonyak, Jr., B. A. Vojak, and H. Shichijo, "Tunnel injection into the confined-particle states of an $In_{1-x}Ga_xP_{1-z}As_z$ well in InP," *Appl. Phys. Lett.*, vol. 31, pp. 703–705, Nov. 15, 1977.
[667] S. S. Rhee, J. S. Park, R. P. G. Karunasiri, Q. Ye, and K. L. Wang, "Resonant tunneling through a $Si/Ge_xSi_{1-x}/Si$ heterostructure on GeSi buffer layer," *Appl. Phys. Lett.*, vol. 53, pp. 204–206, July 18, 1988.
[668] B. Ricco and M. Ya. Azbel, "Physics of resonant tunneling. The one-dimensional double-barrier case," *Phys. Rev. B*, vol. 29, pp. 1970–1981, Feb. 15, 1984.
[669] F. A. Riddoch and B. K. Ridley, "On the scattering of electrons by polar optical phonons in quasi-2D quantum wells," *J. Phys. C*, vol. 16, pp. 6971–6982, Dec. 30, 1983.
[670] C. Ringhofer, "Numerical methods for the simulation of quantum devices using the Wigner function approach," in *Computational Electronics*, K. Hess, J. P. Leburton, and U. Ravaioli, Eds. Norwell, MA: Kluwer Academic, 1991, pp. 207–214.
[671] M. L. Roukes and O. L. Alerhand, "Mesoscopic junctions, random scattering, and strange repellers," *Phys. Rev. Lett.*, vol. 65, pp. 1651–1654, Sept. 24, 1990.
[672] M. L. Roukes, A. Scherer, S. J. Allen, Jr., H. G. Craighead, R. M. Ruthen, E. D. Beebe, and J. P. Harbison, "Quenching of the Hall effect in a one-dimensional wire," *Phys. Rev. Lett.*, vol. 59, pp. 3011–3014, Dec. 28, 1987.
[673] M. L. Roukes, A. Scherer, and B. P. Van der Gaag, "Are transport anomalies in 'electron waveguides' classical?" *Phys. Rev. Lett.*, vol. 64, pp. 1154–1157, Mar. 5, 1990.
[674] M. L. Roukes, T. J. Thornton, A. Scherer, and B. P. Van der Gaag, "Electron-boundary scattering in quantum wires," *Electronic Properties of Multilayers and Low-Dimensional Semiconductor Structures*, J. M. Chamberlain, L. Eaves, and J. C. Portal, Eds. London, U.K.: Plenum, 1989, pp. 95–116.
[675] J. M. Ryan, J. Han, A. M. Kriman, D. K. Ferry, and P. Newman, "Overshoot saturation in ultra-short channel FETs due to minimum acceleration lengths," in *Nanostructure Physics and Fabrication*, M. A. Reed and W. P. Kirk, Eds. San Diego, CA: Academic, 1989, pp. 195–199.
[676] A. Rydberg, H. Gronqvist, and E. Kollberg, "Millimeter- and submillimeter-wave multipliers using quantum-barrier-varactor (QBV) diodes," *IEEE Electron Device Lett.*, vol. 11, pp. 373–375, Sept. 1990.
[677] A. Sachrajda, D. Landheer, R. Boulet, J. Stalica, and T. Moore, "Evidence for an inhomogeneity size effect in micron size GaAs/AlGaAs constrictions," in *Nanostructure Physics and Fabrication*, M. A. Reed and W. P. Kirk, Eds. San Diego, CA: Academic, 1989, pp. 395–399.
[678] V. Sankaran and J. Singh, "Coherent tunneling of mixed state hole wave packets in coupled quantum well structures," *Appl. Phys. Lett.*, vol. 58, pp. 1509–1511, Apr. 8, 1991.
[679] H. Sakaki, "High mobility effect of electrons in ultrafine semiconductor wire structures," *J. Vac. Sci. Technol.*, vol. 19, pp. 148–149, Jul./Aug. 1981.
[680] H. Sakaki, H. Kurata, and M. Yamanishi, "Novel quantum-well

optical bistability device with excellent on/off ratio and high speed capability," *Electron. Lett.*, vol. 24, pp. 1–2, Jan. 7, 1988.
[681] H. Sakaki, T. Matsusue, and M. Tscuchiya, "Resonant tunneling in quantum heterostructures: Electron transport, dynamics, and device applications," *IEEE J. Quantum Electron.*, vol. 25, pp. 2498–2504, Dec. 1989.
[682] R. Sakamoto, K. Akai, and M. Inoue, "Real Space transfer and hot-electron transport properties in III-V semiconductor hetero- structures," *IEEE Trans. Electron Devices* , vol. 36, pp. 2344–2352, Oct. 1989.
[683] P. Santhanam, S. Wind, and D. E. Prober, "One-dimensional electron localization and superconducting fluctuations in narrow aluminum wires," *Phys. Rev. Lett.*, vol. 53, pp. 1179–1182, Sept. 17, 1984
[684] A. Sasaki, "Effective-mass superlattice," *Phys. Rev. B* , vol. 30, pp. 7016–7020, Dec. 15, 1984.
[685] A. Sasaki, "Strained-layer effective-mass superlattices," *Surface Sci.*, vol. 174, pp. 624–629, Aug. 1986.
[686] H. J. Schellnhuber and G. M. Obermair, "First-principles calculation of diamagnetic band structure," *Phys. Rev. Lett.*, vol. 45, pp. 276–279, July 28, 1980.
[687] H. J. Schellnhuber, G. M. Obermair, and A. Rauh, "First-principles calculation of diamagnetic band structure. II. Spectrum and wave functions," *Phys. Rev. B* , vol. 23, pp. 5191–5202, May 15, 1981.
[688] G. Scher, M. Smith, and M. Baranger, "Numerical calculations in elementary quantum mechanics using Feynman path integrals," *Ann. Phys.*, vol. 130, pp. 290–306, 1980.
[689] H. Schmid, S. A. Rishton, D. P. Kern, S. Washburn, R. A. Webb, A. Kleinsasser, T. H. P. Chang, and A. Fowler, "Fabrication of quantum devices in metals and semiconductors," *J. Vac. Sci. Technol. B* , vol. 6, pp. 122–126, Jan./Feb. 1988.
[690] E. F. Schubert, J. E. Cunningham, and W. T. Tsang, "Perpendicular electronic transport in doping superlattices," *Appl. Phys. Lett.*, vol. 51, pp. 817–819, Sep. 14, 1987.
[691] J. N. Schulman and Y. C. Chang, "Band mixing in semiconductor superlattices," *Phys. Rev. B* , vol. 31, pp. 2056–2068, Feb. 15, 1986.
[692] J. N. Schulman and T. C. McGill, "Complex band structure and superlattice electronic states," *Phys. Rev. B* , vol. 23, pp. 4149–4155, Apr. 15, 1981.
[693] P. A. Schulz and C. Tejedor, "Resonant tunneling through Landau levels in quantum wells in the presence of inelastic-scattering broadening," *Phys. Rev. B.*, vol. 41, pp. 3053–3059, Feb. 15, 1990.
[694] C. Schwartz, "Feasibility of tunable infrared detectors using metal-insulator-metal structures," *J. Appl. Phys.*, vol. 61, pp. 777–780, Jan. 15, 1987.
[695] C. Schwartz, "Efficient technique for calculating the bound and virtual energy spectrum of semiconductor structures," *Appl. Phys. Lett.*, vol. 50, pp. 457–459, Feb. 23, 1987. C. Schwartz, "Reflection properties of pseudorandom multilayers," *Appl. Opt.*, vol. 27, pp. 1232–1234, Apr. 1, 1988.
[696] C. Schwartz, "Effective mass effects in triangular quantum wells achieved from compositional grading," *IEEE J. Quantum Electron.*, vol. 24, pp. 1712–1715, Aug. 1988.
[697] C. Schwartz and L. F. DeSandre, "New calculational technique for multilayer stacks," *Appl. Opt.*, vol. 26, pp. 3140–3144, Aug. 1, 1987.
[698] J. H. F. Scott-Thomas, M. A. Kastner, D. A. Antoniadis, H. I. Smith, and S. Field, "Si metal-oxide semiconductor field effect transistor with 70-nm slotted gates for study of quasi-one-dimensional quantum transport," *J. Vac. Sci. Technol. B*, vol. 6, pp. 1841–1844, Nov./Dec. 1988.
[699] J. H. F. Scott-Thomas, S. B. Field, M. A. Kastner, H. I. Smith, and D. A. Antoniadis, "Conductance oscillations periodic in the density of a one-dimensional electron gas," *Phys. Rev. Lett.*, vol. 62, pp. 583–586, Jan. 30, 1990.
[700] A. C. Seabaugh, W. R. Frensley, J. N. Randall, M. A. Reed, D. L. Farrington, and R. J. Matyi, "Psuedomorphic bipolar quantum resonant-tunneling transistor," *IEEE Trans. Electron Devices*, vol. 36, pp. 2328–2334, Oct. 1989.
[701] A. Seilmeier, H. J. Hubner, G. Abstreiter, G. Weimann, and W. Schlapp, "Intersubband relaxation in GaAs-$Al_xGa_{1-x}As$ quantum well structures observed directly by an infrared bleaching technique," *Phys. Rev. Lett.*, vol. 59, pp. 1345–1348, Sept. 21, 1987.
[702] S. Sen, F. Capasso, A. C. Gossard, R. A. Spah, A. L. Hutchinson, and S. N. G. Chu, "Observation of resonant tunneling through a compositionally graded parabolic quantum well," *Appl. Phys. Lett.*, vol. 51, pp. 1428–1430, Nov. 2, 1987.
[703] K. Seo, M. Heiblum, C. M. Knoedler, W. P. Hong, and P. Bhattacharya, "Pseudomorphic InGaAs base ballistic hot-electron device," *Appl. Phys. Lett.*, vol. 53, pp. 1946–1948, Nov. 14, 1988.
[704] K. Seo, M. Heiblum, C. M. Knoedler, J. E. Oh, J. Pamulapati, and P. Bhattacharya, "High-gain pseudomorphic InGaAs base ballistic hot-electron device," *IEEE Electron Device Lett.*, vol. 10, pp. 73–75, Feb. 1989.
[705] B. O. Seraphin and N. Bottka, "Band-structure analysis from electro-reflectance studies," *Phys. Rev.*, vol. 145, pp. 628–636, May 13, 1969.
[706] J. Shah, "Hot carriers in quasi-2-D polar semiconductors," *IEEE J. Quantum Electron.*, vol. 22, pp. 1728–1743, Sept. 1986.
[707] B. Shapiro, "Quantum conduction on a Cayley Tree," *Phys. Rev. Lett.*, vol. 50, pp. 747–750, Mar. 7, 1983.
[708] D. Yu. Sharvin and Yu. V. Sharvin, "Magnetic-flux quantization in a cylindrical film of a normal metal," *JETP Lett.*, vol. 34, pp. 272–275, Sept. 5, 1981.
[709] T. J. Shewchuk, P. C. Chapin, P. D. Coleman, W. Kopp, R. Fischer, and H. Morkoc, "Resonant tunneling oscillations in a GaAs-$Al_xGa_{1-x}As$ heterostructure at room temperature," *Appl. Phys. Lett.*, vol. 46, pp. 508–510, Mar. 1, 1985.
[710] T. J. Shewchuk, J. M. Gering, P. C. Chapin, P. D. Coleman, W. Kopp, C. K. Peng, and H. Morkoc, "Stable and unstable current-voltage measurements of a resonant tunneling heterostructure oscillator," *Appl. Phys. Lett.*, vol. 47, pp. 986–988, Nov. 1, 1985.
[711] M. S. Shur and L. F. Eastman, "Ballistic transport in semiconductor at low temperatures for low-power high-speed logic," *IEEE Trans. Electron Devices* , vol. ED-26, pp. 1677–1683, Nov. 1979.
[712] J. A. Simmons, D. C. Tsui, and G. Weimann, "Quantum interference effects in high-mobility mesoscopic GaAs $Al_xGa_{1-x}As$ heterostructures," *Surface Sci.*, vol. 196, pp. 81–88, Mar. 1988.
[713] J. G. Simmons, "Generalized formula for the electric tunnel effect between similar electrodes separated by a thin insulating film," *J. Appl. Phys.*, vol. 34, pp. 1793–1803, June 1963.
[714] J. Singleton, R. J. Nicholas, N. J. Pulsford, N. R. Couch, and M. J. Kelly, "Quasi-bound states in an asymetric GaAs-AlAs superlattice," *J. De Physique* , vol. 48, pp. C5435–C5437, Nov. 1987.
[715] U. Sivan, M. Heiblum, and C. P. Umbach, "Hot ballistic transport and phonon emission in a two-dimensional electron gas," *Phys. Rev. Lett.*, vol. 63, pp. 992–995, Aug. 28, 1989.
[716] U. Sivan, M. Heiblum, C. P. Umbach, and H. Shtrikman, "Electrostatic electron lens in the ballistic regime," *Phys. Rev. B* , vol. 41, pp. 7937–7940, Apr. 15, 1990.
[717] W. J. Skocpol, "Quantum effects in quasi-one-dimensiona MOSFETs in *Physics of Quantum Electron Devices* , F. Capasso, Ed. Berlin, Germany: Springer-Verlag, 1990, pp. 367–399.
[718] W. J. Skocpol, L. D. Jackel, R. E. Howard, P. M. Mankiewich, and D. M. Tennant, "Quantum transport in narrow MOSFET channels," *Surface Sci.*, vol. 170, pp. 1–13, April 1986.
[719] W. J. Skocpol, L. D. Jackel, E. L. Hu, R. E. Howard, and L. A. Fetter, "One-dimensional localization and interaction effects in narro (0.1-micrometers) silicon inversion layers," *Phys. Rev. Lett.*, vol. 49, pp. 951–955, Sept. 27, 1982.
[720] W. J. Skocpol, P. M. Mankiewich, R. E. Howard, L. D. Jackel, D. M. Tennant, and A. D. Stone, "Nonlocal potential measurements of quantum conductors," *Phys. Rev. Lett.*, vol. 58, pp. 2347–2350, June 1, 1987.
[721] W. J. Skocpol, P. M. Mankiewich, R. E. Howard, L. D. Jackel, D. M. Tennant, and A. D. Stone, "Universal conductance fluctuations in silicon inversion-layer nanostructures," *Phys. Rev. Lett.*, vol. 56, pp. 2865–2868, June 30, 1988.
[722] F. T. Smith, "Lifetime matrix in collision theory," *Phys. Rev.* , vol. 118, pp. 349–356, Apr. 1, 1960.
[723] C. G. Smith, M. Pepper, H. Ahmed, J. E. F. Frost, D. G. Hasko, D. C. Peacock, D. A. Ritchie, and G. A. C. Jones, "Quantum ballistic transport through a zero-dimensional structure," *Superlattices Microstructures* , vol. 5, pp. 599–602, 1989.
[724] C. G. Smith, M. Pepper, H. Ahmed, J. E. F. Frost, D. G. Hasko, D. C. Peacock, D. A. Ritchie, and G. A. C. Jones, "The transition from one- to zero-dimensional ballistic transport," *J. Phys. C* , vol. 21, pp. L893–L898, Feb. 1988.

[725] H. I. Smith, K. Ismail, W. Chu, A. Yen, C. Ku, M. L. Schattenburg, and D. A. Antoniadis, "Fabrication of quantum-effect electronic devices using x-ray nanolithography," in *Nanostructure Physics and Fabrication* , M. A. Reed and W. P. Kirk, Eds. San Diego, CA: Academic, 1989, pp. 57–65.

[726] T. P. Smith, H. Arnot, J. M. Hong, C. M. Knoedler, S. E. Laux, and H. Schmid, "Capacitance oscillations in one-dimensional electron systems," *Phys. Rev. Lett.*, vol. 59, pp. 2802–2805, Dec. 14, 1987.

[727] D. Sokolovski and L. M. Baskin, "Traversal time in quantum scattering," *Phys. Rev. A* , vol. 36, pp. 4604–4611, Nov. 15, 1987.

[728] T. C. L. G. Sollner, E. R. Brown, W. D. Goodhue, and H. Q. Le, "Observation of millimeter-wave oscillations from resonant tunneling diodes and some theoretical considerations of ultimate frequency limits," *Appl. Phys. Lett.*, vol. 50, pp. 332–334, Feb. 9, 1987.

[729] T. C. L. G. Sollner, E. R. Brown, W. D. Goodhue, and H. Q. Le, "Microwave and millimeter-wave resonant-tunnelling devices in *Physics of Quantum Electron Devices*, F. Capasso, Ed. Berlin, Germany: Springer-Verlag, 1990, pp. 147–180.

[730] T. C. L. G. Sollner, E. R. Brown, C. D. Parker, and W. G. Goodhue, "High-frequency applications of resonant-tunnelling devices," *Electronic Properties of Multilayers and Low Dimensional Semiconductor Structures* , J. M. Chamberlain, L. Eaves, and J. C. Portal, Eds. London, U.K.: Plenum, 1989, pp. 283–296.

[731] T. C. L. G. Sollner, W. D. Goodhue, P. E. Tannenwald, C. D. Parker, and D. D. Peck, "Resonant tunneling through quantum wells at frequencies up to 2.5 THz," *Appl. Phys. Lett.*, vol. 43, pp. 588–590, Sept. 15, 1983.

[732] T. C. L. G. Sollner, P. E. Tannenwald, D. D. Peck, and W. D. Goodhue, "Quantum well oscillators," *Appl. Phys. Lett.*, vol. 45, pp. 1319–1321, Dec. 15, 1984.

[733] P. M. Solomon, S. L. Wright, and C. Lanza, "Perpendicular transport across (Al,Ga)As and the Γ to X transition," *Superlattices Microstructures* , vol. 2, no. 6, pp. 521–525, 1986.

[734] F. Sols, M. Macucci, U. Ravaioli, and K. Hess, "On the possibility of transistor action based on quantum interference phenomena," *Appl. Phys. Lett.*, vol. 54, pp. 350–352, Jan. 23, 1989.

[735] F. Sols, M. Macucci, U. Ravaioli, and K. Hess, "Criteria for transistor action based on quantum interference phenomena," in *Nanostructure Physics and Fabrication* , M. A. Reed and W. P. Kirk, Eds. San Diego, CA: Academic, 1989, pp. 157–164.

[736] F. Sols, M. Macucci, U. Ravaioli, and K. Hess, "Theory for a quantum modulated transistor," *J. Appl. Phys.* , vol. 66, pp. 3892–3906, Oct. 15, 1989.

[737] J. J. Song, Y. S. Yoon, A. Fedotowsky, Y. B. Kim, J. N. Schulman, C. W. Tu, D. Huang, and H. Morkoc, "Barrier-width dependence of optical transitions involving unconfined energy states in GaAs-$Al_xGa_{1-x}As$ superlattices," *Phys. Rev. B* , vol. 34, pp. 8958–8962, Dec. 15, 1986.

[738] J. J. Song, Y. S. Yoon, P. S. Jung, A. Fedotowsky, J. N. Schulman, C. W. Tu, J. M. Brown, D. Huang, and H. Morkoc, "Above barrier doublets in GaAs/$Al_xGa_{1-x}As$ superlattices," *Appl. Phys. Lett.*, vol. 50, pp. 1269–1271, May 4, 1987.

[739] R. Sooryakumar, A. Pinczuk, A. C. Gossard, D. S. Chemla, and L. J. Sham, "Tuning of the valence-band structure of GaAs quantum wells by uniaxial stress," *Phys. Rev. Lett.*, vol. 58, pp. 1150–1153, Mar. 16, 1987.

[740] J. Spector, H. L. Stormer, K. W. Baldwin, L. N. Pfeiffer, and K. W. West, "Electron focusing in two-dimensional systems by means of an electrostatic lens," *Appl. Phys. Lett.*, vol. 56, pp. 1290–1292, Mar. 26, 1990.

[741] J. Spector, H. L. Stormer, K. W. Baldwin, L. N. Pfeiffer, and K. W. West, "Control of ballistic electrons in macroscopic two-dimensional electron systems," *Appl. Phys. Lett.*, vol. 56, pp. 967–969, Mar. 5, 1990.

[742] J. Spector, H. L. Stormer, K. W. Baldwin, L. N. Pfeiffer, and K. W. West, "Ballistic electron transport beyond 100μm in 2D electron systems," *Surf. Sci.*, vol. 228, pp. 283–285, 1990.

[743] J. Spector, H. L. Stormer, K. W. Baldwin, L. N. Pfeiffer, and K. W. West, "Refractive switch for two-dimensional electrons," *Appl. Phys. Lett.*, vol. 56, pp. 2433–2435, June 11, 1990.

[744] J. Spector, H. L. Stormer, K. W. Baldwin, L. N. Pfeiffer, and K. W. West, "Noninteracting beams of ballistic two-dimensional electrons," *Appl. Phys. Lett.*, vol. 58, pp. 263–265, Jan. 21, 1991.

[745] C. J. Stanton, D. W. Bailey, and K. Hess, "Monte Carlo modeling of femtosecond relaxation processes in AlGaAs/GaAs quantum wells," *IEEE J. Quantum Electron.*, vol. 24, pp. 1614–1627, Aug. 1988.

[746] F. Stern, "Electronic structure of laterally restriced systems" in *Interfaces, Quantum Wells, and Superlattices* , C. R. Leavens and R. Taylor, Eds. New York: Plenum, 1987, pp. 127–142.

[747] F. Stern, "Electrons in heterojunctions," in *Heterostructures and Semiconductor Superlattices* , G. Allan, G. Bastard, N. Boccara, M. Lannoo, and M. Voos, Eds. Berlin, Germany: Springer-Verlag, 1986, pp. 38–47.

[748] M. D. Stiles and D. R. Hamann, "Ballistic electron transmission through interfaces," *Phys. Rev. B* , vol. 38, pp. 2021–2037, July 15, 1988.

[749] A. D. Stone, "Magnetoresistance fluctuations in mesoscopic wires and rings," *Phys. Rev. Lett.*, vol. 54, pp. 2692–2695, June 24, 1985.

[750] A. D. Stone, M. Y. Azbel, and P. A. Lee, "Localization and quantum-mechanical resonant tunneling in the presence of a time-dependent potential," *Phys. Rev. B* , vol. 31, pp. 1707–1714, Feb. 15, 1985.

[751] A. D. Stone and P. A. Lee, "Effect of inelastic processes on resonant tunneling in one dimension," *Phys. Rev. Lett.*, vol. 54, pp. 1196–1199, Mar. 18, 1985.

[752] A. D. Stone and A. Szafer, "What is measured when you measure a resistance? - The Landauer formula revisited," *IBM J. Res. Develop.*, vol. 32, pp. 384–413, May 1988.

[753] A. D. Stone, A. Szafer, and H. U. Baranger, "New theoretical results on ballistic quantum transport: Quenching of the Hall resistance and quantized contact resistance," in *Nanostructure Physics and Fabrication* , M. A. Reed and W. P. Kirk, Eds. San Diego, CA: Academic, 1989, pp. 369–378.

[754] H. L. Stormer, L. N. Pfeiffer, K. W. Baldwin, K. W. West, and J. Spector, "Atomically precise superlattice potential imposed on a two-dimensional electron gas," *Appl. Phys. Lett.*, vol. 58, pp. 726–728, Feb. 18, 1991.

[755] J. A. Stovneng and E. H. Hauge, "Tunneling times and the Buttiker-Landauer model," in *Nanostructure Physics and Fabrication* , M. A. Reed and W. P. Kirk, Eds. San Diego, CA: Academic, 1989, pp. 303–310.

[756] P. Streda, "Quantised Hall effect in a two-dimensional periodic potential," *J. Phys. C* , vol. 15, pp. 1299–1303, Feb. 1982.

[757] M. A. Stroscio, "Quantum-based electronic devices," *Superlattices Microstructures*, vol. 2, pp. 45–47, 1986.

[758] S. Subramaniam, S. Bandyopadhyay, and W. Porod, "Analysis of the device performance of quantum interference transistors utilizing ultrasmall semiconductor T-structures," *J. Appl. Phys.*, vol. 68, pp. 4861–4870, Nov. 1, 1990.

[759] H. Sugawara, J. N. Schulman, and H. Sakaki, "Subband structures and wave functions of electrons in quantum wires and in-plane superlattices consisting of grid-inserted quantum-well structures," *J. Appl. Phys.*, vol. 69, pp. 2722–2724, Feb. 15, 1991.

[760] A. R. Sugg and J. P. C. Leburton, "Modeling of modulation-doped multiple-quantum-well structures in applied electric fields using the transfer-matrix technique," *IEEE J. Quantum Electron.*, vol. 27, pp. 224–231, Feb. 1991.

[761] M. Sumetskii, "Photon-assisted resonant tunneling through a double quantum well structure: Nanometer infrared detector," *Phys. Lett. A*, vol. 153, pp. 149–154, Feb. 25, 1991.

[762] C. J. Summers and K. F. Brennan, "Variably spaced superlattice energy filter, a new device design concept for high-energy electron injection," *Appl. Phys. Lett.*, vol. 48, pp. 806–808, Mar. 24, 1986.

[763] C. J. Summers, K. F. Brennan, H. D. Rogers, and B. K. Wagner, "The variably spaced superlattice energy filter," *Superlattices Microstructures*, vol. 3, no. 2, pp. 147–152, 1987.

[764] C. J. Summers, K. F. Brennan, A. Torabi, H. M. Harris, and J. Comas, "Resonant tunneling studies of variably spaced multiple quantum well structures in the AlGaAs system," *J. de Physique*, vol. 48, pp. C5457–C5461, Nov. 1987.

[765] C. J. Summers, K. F. Brennan, A. Torabi, and H. M. Harris, "Resonant tunneling and negative differential resistance in a variably spaced superlattice energy filter," *Appl. Phys. Lett.*, vol. 52, pp. 132–134, Jan. 11, 1988.

[766] M. Sweeny and J. Xu, "On photon-assisted tunneling in quan-

tum well structures," *IEEE J. Quantum Electron.*, vol. 25, pp. 885–888, May 1989.
[767] A. Szafer and A. D. Stone, "Theory of quantum conduction through a constriction," *Phys. Rev. Lett.*, vol. 62, pp. 300–303, Jan. 16, 1989.
[768] S. Tarucha, Y. Hirayama, and Y. Tokura, "Subband mixing effect in double-barrier diodes with a restricted lateral dimension," *Appl. Phys. Lett.*, vol. 58, pp. 1623–1625, Apr. 15, 1991.
[769] S. Tarucha and K. Ploog, "Sequential resonant tunneling characteristics of AlAs/GaAs multiple-quantum-well structures," *Phys. Rev. B*, vol. 38, pp. 4198–4204, Aug. 15, 1988.
[770] S. Tarucha, K. Ploog, and K. von Klitzing, "Resonance-induced quenching of luminescence and reduction of tunneling time in $Al_xGa_{1-x}As$/GaAs multiple quantum well structures," *Phys. Rev. B.*, vol. 36, pp. 4558–4561, Sept. 15, 1987.
[771] Z. Tesanovic, M. V. Jaric, and S. Maekawa, "Quantum transport and surface scattering," *Phys. Rev. Lett.*, vol. 57, pp. 2760–2763, Nov. 24, 1986.
[772] S. Thoms, I. McIntyre, S. P. Beaumont, M. Al-Mudares, R. Cheung, and C. D. W. Wilkinson, "Fabrication of quantum wires in GaAs/AlGaAs heterolayers," *J. Vac. Sci. Technol. B*, vol. 6, pp. 127–130, Jan./Feb. 1988.
[773] T. J. Thornton, M. Pepper, H. Ahmed, D. Andrews, and G. J. Davies, "Electron transport across depleted region of a fine-gate GaAs:AlGaAs heterojunction FET," *Electron. Lett.*, vol. 22, pp. 247–249, Feb. 27, 1986.
[774] T. J. Thornton, M. Pepper, H. Ahmed, D. Andrews, and G. J. Davies, "One-dimensional conduction in the 2D electron gas of a GaAs-AlGaAs heterojunction," *Phys. Rev. Lett.*, vol. 56, pp. 1198–1201, Mar. 17, 1986.
[775] D. J. Thouless, M. Kohmoto, M. P. Nightingale, and M. den Nijs, "Quantized Hall conductance in a two-dimensional periodic potential," *Phys. Rev. Lett.*, vol. 49, pp. 405–408, Aug. 9, 1982.
[776] D. J. Thouless and Q. Niu, "Wavefunction scaling in a quasi-periodic potential," *J. Phys. A*, vol. 16, pp. 1911–1919, June 1983.
[777] G. Timp, H. U. Baranger, P. deVegvar, J. E. Cunningham, R. E. Howard, R. Behringer, and P. M. Mankiewich, "Propagation around a bend in a multichannel electron waveguide," *Phys. Rev. Lett.*, vol. 60, pp. 2081–2084, May 16, 1988.
[778] G. Timp, R. Behringer, S. Sampere, J. E. Cunningham, and R. E. Howard, "When isn't the conductance of an electron waveguide quantized?" in *Nanostructure Physics and Fabrication*, M. A. Reed and W. P. Kirk, Eds. San Diego, CA: Academic, 1989, pp. 331–345.
[779] G. Timp, A. M. Chang, J. E. Cunningham, T. Y. Chang, P. Mankiewich, R. Behringer, and R. E. Howard, "Observation of the Aharonov-Bohm effect for $\omega_c\tau > 1$," *Phys. Rev. Lett.*, vol. 58, pp. 2814- 2817, June 29, 1987.
[780] G. Timp, A. M. Chang, P. DeVegvar, R. E. Howard, R. Behringer, J. E. Cunningham, and P. Mankiewich, "Quantum transport in one-dimensional GaAs/AlGaAs microstructures," *Surface Sci.*, vol. 196, pp. 68–78, Mar. 1988.
[781] G. Timp, A. M. Chang, P. Mankiewich, R. Behringer, J. E. Cunningham, T. Y. Chang, and R. E. Howard, "Quantum transport in an electron-wave guide," *Phys. Rev. Lett.*, vol. 59, pp. 732–735, Aug. 10, 1987.
[782] D. Z. Y. Ting, E. T. Yu, D. A. Collins, D. H. Chow, and T. C. McGill, "Modeling InAs/GaSb/AlSb interband tunnel structures," in *Computational Electronics*, K. Hess, J. P. Leburton, and U. Ravaioli, Eds. Norwell, MA: Kluwer Academic, 1991, pp. 189–194.
[783] R. L. Tober, J. Pamulapati, P. K. Bhattacharya, and J. E. Oh, "Piezoreflectance characterization of resonant tunneling and modulation-doped heterostructures," *J. Electron. Matls.*, vol. 18, pp. 379–384, May 1989.
[784] R. L. Tober, J. Pamulapati, J. E. Oh, and P. K. Bhattacharya "Piezoreflectance characterization of double-barrier resonant tunneling structures," *Appl. Phys. Lett.*, vol. 53, pp. 883–885, Sept. 5, 1988.
[785] R. L. Tober, A. L. Smirl, T. F. Boggess, and J. N. Schulman, "Piezoreflectance as a supplement to photoreflectance for nondestructive characterization of $GaAs/Al_xGa_{1-x}As$ multiple quantum wells," *J. Appl. Phys.*, vol. 64, pp. 4678–4682, Nov. 1, 1988.
[786] Y. Tokura and K. Tsubaki, "Conductivity due to quantum interference in a proposed washboard transistor," *Appl. Phys. Lett.*, vol. 51, pp. 1807–1808, Nov. 30, 1987.
[787] M. Tomizawa, T. Furuta, K. Yokoyama, and A. Yoshii, "Modeling for electron transport in AlGaAs/GaAs/AlGaAs double-heterojunction structures," *IEEE Trans. Electron Devices*, vol. 36, pp. 2380–2385, Nov. 1989.
[788] A. Tonomura, "Electron holography: A new view of the microscopic," *Phys. Today*, vol. 43, pp. 22–29, Apr. 1990.
[789] G. A. Toombs and F. W. Sheard, "The background to resonant tunnelling theory," *Electronic Properties of Multilayers and Low Dimensional Semiconductor Structures*, J. M. Chamberlain, L. Eaves, and J. C. Portal, Eds. London, U.K.: Plenum, 1989, pp. 257–282.
[790] W. T. Tsang, "Extremely low threshold (AlGa)As modified multiquantum well heterostructure lasers grown by molecular-beam epitaxy," *Appl. Phys. Lett.*, vol. 39, pp. 786–788, Nov. 15, 1981.
[791] W. T. Tsang, T. H. Chiu, and J. E. Cunningham, "Observations on intensity oscillations in reflection high-energy electron diffraction during chemical beam epitaxy," *Appl. Phys. Lett.*, vol. 50, pp. 1376–1378, May 11, 1987.
[792] R. Tsu, L. L. Chang, G. A. Sai-Halasz, and L. Esaki, "Effects of quantum states on the photocurrent in a 'superlattice'," *Phys. Rev. B*, vol. 34, pp. 1509–1512, June 16, 1975.
[793] R. Tsu and G. Dohler, "Hopping conduction in a 'superlattice'," *Phys. Rev. B*, vol. 12, pp. 680–686, July 15, 1975.
[794] R. Tsu and L. Esaki, "Tunneling in a finite superlattice," *Appl. Phys. Lett.*, vol. 22, pp. 562–564, June 1, 1973.
[795] K. Tsubaki, T. Honda, H. Saito, and T. Fukui, "Electron wave interference device with fractional layer superlattices," *Appl. Phys. Lett.*, vol. 58, pp. 376–378, Jan. 28, 1991.
[796] K. Tsubaki and Y. Tokura, "Coherence length in quantum interference devices having periodic potential," *Appl. Phys. Lett.*, vol. 53, pp. 859–861, Sept. 5, 1988.
[797] H. Tsuchiya, M. Ogawa, and T. Miyoshi, "Simulation of quantum transport in quantum devices with spatially varying effective mass," *IEEE Trans. Electron Devices*, vol. 38, pp. 1246–1252, June 1991.
[798] M. Tsuchiya, J. M. Gaines, R. H. Yan, R. J. Simes, L. A. Coldren, and P. M. Petroff, "Optical anisotropy in a quantum-well-wire array with two-dimensional quantum confinement," *Phys. Rev. Lett.*, vol. 62, pp. 466–469, Jan. 23, 1989.
[799] M. Tsuchiya, T. Matsusue, and H. Sakaki, "Tunneling escape rate of electrons from quantum well in double-barrier heterostructures," *Phys. Rev. Lett.*, vol. 59, pp. 2356–2359, Nov. 16, 1987.
[800] M. Tsuchiya, P. M. Petroff, and L. A. Coldren, "Use of tilted-superlattices for quantum-well-wire lasers," (Abstract) *IEEE Trans. Electron Devices*, vol. 36, pp. 2612–2613, Nov. 1989.
[801] M. Tsuchiya and H. Sakaki, "Precise control of resonant tunneling current in AlAs/GaAs/AlAs double barrier diodes with atomically-controlled barrier widths," *Japan. J. Appl. Phys.*, vol. 25, pp. L185–L187, Mar. 1986.
[802] M. Tsuchiya and H. Sakaki, "Dependence of resonant tunneling current on well widths in AlAs/GaAs/AlAs double barrier diode structures," *Appl. Phys. Lett.*, vol. 49, pp. 88–90, July 14, 1986.
[803] M. Tsuchiya and H. Sakaki, "Dependence of resonant tunneling current on Al mole fractions in $Al_xGa_{1-x}As$-GaAs-$Al_xGa_{1-x}As$ double barrier structures," *Appl. Phys. Lett.*, vol. 50, pp. 1503–1505, May 25, 1987.
[804] M. Tsuchiya, H. Sakaki, and J. Yoshino, "Room temperature observation of differential negative resistance in an AlAs/GaAs/AlAs resonant tunneling diode," *Japan. J. Appl. Phys.*, vol. 24, pp. L466–L468, June 1985.
[805] N. Tsukada, A. D. Wieck, and K. Ploog, "Proposal of novel electron wave coupled devices," *Appl. Phys. Lett.*, vol. 56, pp. 2527–2529, June 18, 1990.
[806] S. E. Ulloa, Y. C. Lee, and B. S. Mendoza, "Interlevel plasmons in quasi-one-dimensional structures," in *Nanostructure Physics and Fabrication*, M. A. Reed and W. P. Kirk, Eds. San Diego, CA: Academic, 1989, pp. 141–145.
[807] C. P. Umbach, P. Santhanam, C. van Haesendonck, and R. A. Webb, "Nonlocal electrical properties in mesoscopic devices," *Appl. Phys. Lett.*, vol. 50, pp. 1289–1291, May 4, 1987.
[808] C. P. Umbach, S. Washburn, R. B. Laibowitz, and R. A. Webb, "Magnetoresistance of small, quasi-one-dimensional, normal-metal rings and lines," *Phys. Rev. B*, vol. 30, pp. 4048–4051, Oct. 1, 1984.
[809] M. P. van Albada, A. Lagendijk, and M. B. van der Mark,

"Towards observation of Anderson localization of light," in *Analogies in Optics and Micro-Electronics*, W. van Haeringen and D. Lenstra, Eds. Dordrecht: Kluwer Academic, 1990, pp. 85–104.

[810] D. van der Marel, "Theory of the quantum ballistic transport in constrictions and quantum resonance devices," in *Nanostructure Physics and Fabrication*, M. A. Reed and W. P. Kirk, Eds. San Diego, CA: Academic, 1989, pp. 149–156.

[811] D. van der Marel and E. G. Haanappel, "Model calculations of the quantum ballistic transport in two-dimensional constriction-type microstructures," *Phys. Rev. B*, vol. 39, pp. 7811–7820, Apr. 15, 1989.

[812] C. Van Haesendonck, "Aharonov-Bohm oscillations and non-local electronic conduction," in *Analogies in Optics and Micro-Electronics*, W. van Haeringen and D. Lenstra, Eds. Dordrecht: Kluwer Academic, 1990, pp. 165–184.

[813] H. van Houten and C. W. J. Beenakker, "Electron beams and waveguide modes: Aspects of quantum ballistic transport," in *Nanostructure Physics and Fabrication*, M. A. Reed and W. P. Kirk, Eds. San Diego, CA: Academic, 1989, pp. 347–359.

[814] H. van Houten and C. W. J. Beenakker, "Quantum point contacts and coherent electron focusing," in *Analogies in Optics and Micro-Electronics*, W. van Haeringen and D. Lenstra, Eds. Dordrecht: Kluwer Academic, 1990, pp. 203–226.

[815] H. van Houten, B. J. van Wees, M. G. J. Heijman, and L. P. Andre, "Submicron conducting channels defined by shallow mesa etch in GaAs-AlGaAs heterojunctions," *Appl. Phys. Lett.*, vol. 49, pp. 1781–1783, Dec. 29, 1986.

[816] H. van Houten, B. J. van Wees, J. E. Mooij, C. W. J. Beenakker, J. G. Williamson, and C. T. Foxon, "Coherent electron focusing in a two-dimensional electron gas," *Europhys. Lett.*, vol. 5, pp. 721–725, Apr. 15, 1990.

[817] M. A. van Hove, W. H. Weinberg, and C. M. Chan, *Low-Energy Electron Diffraction* (Springer Series in Surface Sciences, vol. 6). Berlin, Germany: Springer, 1986.

[818] B. J. van Wees, L. P. Kouwenhoven, E. M. M. Willems, and C. J. P. M. Harmans, "Quantum ballistic transport in high magnetic fields," in *Nanostructure Physics and Fabrication*, M. A. Reed and W. P. Kirk, Eds. San Diego, CA: Academic, 1989, pp. 361–368.

[819] B. J. van Wees, H. van Houton, C. W. J. Beenakker, J. G. Williamson, L. P. Kouwenhoven, D. van der Marel, and C. T. Foxon, "Quantized conductance of point contacts in a two-dimensional electron gas," *Phys. Rev. Lett.*, vol. 60, pp. 848–850, Feb. 29, 1988.

[820] M. O. Vassell, J. Lee, and H. F. Lockwood, "Multibarrier tunneling in$Ga_{1-x}Al_xAs$ heterostructures," *J. Appl. Phys.*, vol. 54, pp. 5206–5213, Sept. 1983.

[821] A. S. Vengurlekar, F. Capasso, A. L. Hutchinson, and W. T. Tsang, "Miniband conduction of minority electrons and negative transconductance by quantum reflection in a superlattice transistor," *Appl. Phys. Lett.*, vol. 56, pp. 262–264, Jan. 15, 1990.

[822] B. A. Vojak, W. D. Laidig, N. Holonyak, M. D. Camras, J. J. Coleman, and P. D. Dapkus, "High-energy (visible-red) stimulated emission in GaAs," *J. Appl. Phys.*, vol. 52, pp. 621–626, Feb. 1981.

[823] K. Wakita, Y. Yoshikuni, M. Nakao, Y. Kawamura, and H. Asahi, "Observation of low chirp modulation in long wavelength InGaAs/InAlAs multiple-quantum-well optical modulators," *Japan. J. Appl. Phys.*, vol. 26, pp. L1629–L1631, Oct. 1987.

[824] S. B. Waltman and W. J. Kaiser, "An electron tunneling sensor," *Sensors and Actuators*, vol. 19, pp. 201–210, 1989.

[825] K. L. Wang and P. Yuh, "Theory and applications of band-aligned superlattices," *IEEE J. Quantum Electron.*, vol. 25, pp. 12–19, Jan. 1989.

[826] R. L. Wang, Y. K. Su, Y. H. Wang, and K. F. Yarn, "Negative differential resistance of a delta-doping-induced double-barrier quantum-well diode at room temperature," *IEEE Electron Device Lett.*, vol. 11, pp. 428–430, Oct. 1990.

[827] S. Y. Wang and S. H. Lin, "High speed III-V electrooptic waveguide modulators at $\lambda = 1.3$ micrometers," *J. Lightwave Technol.*, vol. 6, pp. 758–771, June 1988.

[828] G. H. Wannier, "A result not dependent on rationality for Bloch electrons in a magnetic field," *Phys. Stat. Sol.*, vol. 88, pp. 757–765, 1978.

[829] A. C. Warren, "Surface superlattices and quasi-one-dimensional conduction in silicon inversion layers," Ph.D. dissertation, Massachusetts Institute of Technology, Cambridge, June 1985.

[830] A. C. Warren, D. A. Antoniadis, H. I. Smith, and J. Melngailis, "Surface superlattice formation in silicon inversion layers using 0.2-μm period grating-gate electrodes," *IEEE Electron Device Lett.*, vol. EDL-6, pp. 294–296, June 1985.

[831] A. C. Warren, I. Plotnik, E. H. Anderson, M. L. Schattenburg, D. A. Antoniadis, and H. I. Smith, "Fabrication of sub-100nm linewidth periodic structures for study of quantum effects from interference and confinement in Si inversion layers," *J. Vac. Sci. Technol. B*, vol. 4, pp. 365–368, Jan./Feb. 1986.

[832] A. C. Warren, D. A. Antoniadis, and H. I. Smith, "Quasi one-dimensional conduction in multiple, parallel inversion lines," *Phys. Rev. Lett.*, vol. 56, pp. 1858–1861, Apr. 28, 1986.

[833] S. Washburn, H. Schmid, D. Kern, and R. A. Webb, "Normal-metal Aharonov-Bohm effect in the presence of a transverse electric field," *Phys. Rev. Lett.*, vol. 59, pp. 1791–1794, Oct. 19, 1987.

[834] S. Washburn, C. P. Umbach, R. B. Laibowitz, and R. A. Webb, "Temperature dependence of the normal-metal Aharonov-Bohm effect," *Phys. Rev. B*, vol. 32, pp. 4789–4792, Oct. 1, 1985.

[835] S. Washburn and R. A. Webb, "Aharonov-Bohm effect in normal metal quantum coherence and transport," *Adv. in Phys.*, vol. 35, pp. 375–422, July-Aug. 1986.

[836] M. Watt, H. E. G. Arnot, C. M. Sotomayor-Torres, and S. P. Beaumont, "Surface phonon studies of nanostructures," in *Nanostructure Physics and Fabrication*, M. A. Reed and W. P. Kirk, Eds. San Diego, CA: Academic, 1989, pp. 89–96.

[837] M. Watt, C. M. Sotomayor-Torres, R. Cheung, C. D. W. Wilkinson, H. E. G. Arnot, and S. P. Beaumont, "Raman scattering of reactive-ion etched GaAs," *J. Mod. Opt.*, vol. 35, pp. 365–370, Mar. 1988.

[838] R. A. Webb, "Quantum interference effects in condensed matter physics," in *Nanostructure Physics and Fabrication*, M. A. Reed and W. P. Kirk, Eds. San Diego, CA: Academic, 1989, pp. 43–54.

[839] R. A. Webb and S. Washburn, "Quantum interference fluctuations in disordered metals," *Phys. Today*, vol. 41, pp. 46–53, Dec. 1988.

[840] R. A. Webb, S. Washburn, C. P. Umbach, R. B. Laibowitz, "Observation of h/e Aharonov-Bohm oscillations in normal-metal rings," *Phys. Rev. Lett.*, vol. 54, pp. 2696–2699, June 24, 1985.

[841] T. Weil and B. Vinter, "Equivalence between resonant tunneling and sequential tunneling in double-barrier diodes," *Appl. Phys. Lett.*, vol. 50, pp. 1281–1283, May 4, 1987.

[842] J. S. Weiner, A. C. Gossard, J. H. English, D. A. B. Miller, D. S. Chemla, and C. A. Burrus, "Low-voltage modulator and self-biased self-electro-optic-effect device," *Electron. Lett.*, vol. 23, pp. 75–77, Jan. 18, 1987.

[843] J. S. Weiner, D. A. B. Miller, D. S. Chemla, T. C. Damen, C. A. Burrus, T. H. Wood, A. C. Gossard, and W. Wiegmann, "Strong polarization-sensitive electroabsorption in GaAs/AlGaAs quantum well waveguides," *Appl. Phys. Lett.*, vol. 47, pp. 1148–1150, Dec. 1, 1985.

[844] J. S. Weiner, H. F. Hess, R. B. Robinson, T. R. Hayes, D. L. Sivco, A. Y. Cho, and M. Ranade, " Electronic properties of semiconductor nanostructures probed by scanning tunneling microscopy," *Appl. Phys. Lett.*, vol 58, pp. 2402–2404, May 27, 1991.

[845] C. Weisbuch and B. Vinter, *Quantum Semiconductor Structures*. San Diego, CA: Academic, 1991.

[846] A. Weisshaar, J. Lary, S. M. Goodnick, and V. K. Tripathi, "Negative differential resistance in a resonant quantum wire structure," *IEEE Electron Device Lett.*, vol. 12, pp. 2–4, Jan. 1991.

[847] D. A. Wharam, M. Pepper, H. Ahmed, J. E. F. Frost, D. G. Hasco, D. C. Peacock, D. A. Ritchie, and G. A. C. Jones, "Addition of the one-dimensional quantised ballistic resistance," *J. Phys. C: Solid State Phys.*, vol. 21, pp. L887–L891, Feb. 1988.

[848] D. A. Wharam, T. J. Thornton, R. Newbury, M. Pepper, H. Ahmed, J. E. F. Frost, D. G. Hasko, D. C. Peacock, D. A. Ritchie, and G. A. C. Jones, "One-dimensional transport and the quantisation of the ballistic resistance," *J. Phys. C: Solid State Phys.*, vol. 21, pp. L209–L214, 1988.

[849] R. G. Wheeler, K. K. Choi, A. Goel, R. Wisnieff, and D. E. Prober, "Localization and electron-electron interaction effects in submicron-width inversion layers," *Phys. Rev. Lett.*, vol. 49, pp. 1674–1677, Nov. 29, 1982.

[850] A. E. White, R. C. Dynes, and J. P. Garno, "Corrections to the one-dimensional density of states: Observation of a Coulomb gap?" *Phys. Rev. Lett.*, vol. 56, pp. 532–535, Feb. 3, 1986.

[851] H. K. Wickramasinghe, "Scanned-probe microscopes," *Scientific Amer.*, vol. 261, pp. 98–105, Oct. 1989.

[852] E. P. Wigner and L. Eisenbud, "Higher angular momenta and long range interaction in resonance reactions," *Phys. Rev.*, vol. 72, pp. 29–41, July 1, 1947.

[853] D. W. Wilson, E. N. Glytsis, and T. K. Gaylord, "Quantum well, voltage-induced quantum well, and quantum barrier electron waveguides: Mode characteristics and maximum current," *Appl. Phys. Lett.*, vol. 59, Oct. 7, 1991.

[854] N. S. Wingreen, K. W. Jacobsen, and J. W. Wilkins, "Resonant tunneling with electron-phonon interaction: An exactly solvable model," *Phys. Rev. Lett.*, vol. 61, pp. 1396–1399, Sept. 19, 1988.

[855] R. W. Winkler, J. P. Kotthaus, and K. Ploog, "Landau-band conductivity in a two-dimensional electron system modulated by an artificial one-dimensional superlattice potential," *Phys. Rev. Lett.*, vol. 62, pp. 1177–1180, Mar. 6, 1989.

[856] J. P. Woerdman and R. J. C. Spreeuw, "Optical level crossings," in *Analogies in Optics and Micro-Electronics*, W. van Haeringen and D. Lenstra, Eds. Dordrecht: Kluwer Academic, 1990, pp. 135–150.

[857] E. Wolak, B. G. Park, K. L. Lear, and J. S. Harris, "Variation of the spacer layer between two resonant tunneling diodes," *Appl. Phys. Lett.*, vol. 55, pp. 1871–1873, Oct. 30, 1989.

[858] E. Wolak, K. Shepard, S. Y. Chou, and J. S. Harris, "Elastic scattering in resonant tunneling devices with one degree of freedom," *Superlattices Microstructures*, vol. 5, pp. 251–253, 1989.

[859] D. L. Wolford, T. F. Keuch, and J. A. Bradley, M. A. Gell, D. Ninno, and M. Jaros, "Pressure dependence of GaAs/$Al_xGa_{1-x}As$ quantum-well bound states: The determination of valence-band offsets," *J. Vac. Sci. Technol. B*, vol. 4, pp. 1043–1050, July/Aug. 1986.

[860] K. B. Wong, M. Jaros, M. A. Gell, and D. Ninno, "Confined electron states in GaAs-$Ga_{1-x}Al_xAs$ ($0.2 \leq x \leq 1.0$) superlattices," *J. Phys. C*, vol. 19, pp. 53–65, Jan. 10, 1986.

[861] T. H. Wood, "Multiple quantum well (MQW) waveguide modulators," *J. Lightwave Technol.*, vol. 6, pp. 743–757, June 1988.

[862] T. K. Woodward, T. C. McGill, and R. D. Burnham, "Experimental realization of a resonant tunneling transistor," *Appl. Phys. Lett.*, vol. 50, pp. 451–453, Feb. 23, 1987.

[863] C. M. Wu and E. S. Yang, "Carrier transport across heterojunction interfaces," *Solid-State Electron.*, vol. 22, pp. 241–248, Mar. 1979.

[864] J. C. Wu, M. N. Wybourne, W. Yindeepol, A. Weisshaar, and S. M. Goodnick, "Interference phenomenon due to a double bend in a quantum wire," *Appl. Phys. Lett.*, vol. 59, pp. 102–104, July 1, 1991.

[865] J. S. Wu, K. H. Chang, C. P. Lee, C. Y. Chang, D. G. Liu, and D. C. Liou, "Quantum effect in the accumulation layer on field-induced photoluminescence of double-barrier resonant tunneling structures," *Appl. Phys. Lett.*, vol. 59, pp. 87–89, July 1, 1991.

[866] J. S. Wu, C. Y. Chang, C. P. Lee, Y. H. Wang II, F. Wai, "Origin of the enhancement of negative differential resistance at low temperatures in double-barrier resonant tunneling structures," *IEEE Electron Device Lett.*, vol.10, pp. 301–303, July 1989.

[867] R. Wyatt and W. J. Devlin, "10kHz linewidth 1.5 μm InGaAsP external cavity laser with 55 nm tuning range," *Electron. Lett.*, vol. 19, pp. 110–112, Feb. 3, 1983.

[868] D. X. Xu, G. D. shen, M. Willander, G. V. Hansson, J. F. Luy, and F. Schaffler, "Variations of resonant tunneling properties with temperature in strained $Si_{1-x}Ge_x$/Si double-barrier structures," *Appl. Phys. Lett.*, vol. 58, pp. 2500–2502, June 3, 1991.

[869] W. Xue and P. A. Lee, "Two-dimensional resonant tunneling," *Phys. Rev. B*, vol. 38, pp. 3913–3917, Aug. 15, 1988.

[870] E. Yablonovitch, "The chemistry of solid-state electronics," *Science*, vol. 246, pp. 347–351, Oct. 20, 1989.

[871] E. Yablonovitch, "Photonic band structure," in *Analogies in Optics and Micro-Electronics*, W. van Haeringen and D. Lenstra, Eds. Dordrecht: Kluwer Academic, 1990, pp. 117–134.

[872] M. C. Yalabik, G. Neofotistos, K. Diff, H. Guo, and J. D. Gunton, "Quantum mechanical simulation of charge transport in very small semiconductor structures," *IEEE Trans. Electron Devices*, vol. 36, pp. 1009–1014, June 1989.

[873] M. Yamanishi, "Ultrafast modulation of quantum states by virtual charge polarization in biased quantum well structures," *Superlattices Microstructures*, vol. 6, pp. 403–408, 1989.

[874] R. H. Yan, R. J. Simes, and L. A. Coldren, "Analysis and design of surface-normal Fabry-Perot electrooptic modulators," *IEEE J. Quantum Electron.*, vol. 25, pp. 2272–2280, Nov. 1989.

[875] C. H. Yang, M. J. Yang, and Y. C. Kao, "Magnetotunneling spectroscopy in a double-barrier heterostructure: Observation of incoherent resonant-tunneling processes," *Phys. Rev. B.*, vol. 40, pp. 6272–6276, Sept. 15, 1989.

[876] R. Q. Yang, and J. M. Xu, "Analysis of guided electron waves in coupled quantum wells," *Phys. Rev. B*, vol. 43, pp. 1699–1706, Jan. 15, 1991.

[877] R. Q. Yang, and J. M. Xu, "Population inversion through resonant interband tunneling," *Appl. Phys. Lett.*, vol. 59, pp. 181–182, July 8, 1991.

[878] R. Q. Yang, and J. M. Xu, "Energy-dependent electron wave coupling between two asymmetrical quantum well waveguides," *Appl. Phys. Lett.*, vol. 59, pp. 315–317, July 15, 1991.

[879] A. Yariv, C. Lindsey, and U. Sivan, "Approximate analytic solution for electronic wave functions and energies in coupled quantum wells", *J. Appl. Phys.*, vol. 58, pp. 3669–3672, Nov. 1, 1985.

[880] N. Yokoyama, K. Imamura, S. Muto, S. Hiyamizu, and H. Nishi, "A new functional, resonant-tunneling hot electron transistor (RHET)," *Japan. J. Appl. Phys.*, vol. 24, pp. L853–L854, Nov.1985.

[881] N. Yokoyama, S. Muto, H. Ohnishi, K. Imamura, T. Mori, and T. Inata, "Resonant-tunnelling hot electron transistors (RHET) in *Physics of Quantum Electron Devices*, F. Capasso, Ed. Berlin, Germany: Springer-Verlag, 1990, pp. 253–269.

[882] J. F. Young, B. M. Wood, and S. Charbonneau, "Optical probes of resonant tunneling structures," *Electronic Properties of Multilayers and Low Dimensional Semiconductor Structures*, J. M. Chamberlain, L. Eaves, and J. C. Portal, Eds. London, U.K.: Plenum, 1989, pp. 331–350.

[883] P. F. Yuh and K. L. Wang, "One-dimensional transport in quantum well wire—high electron mobility transistor," *Appl. Phys. Lett.*, vol. 49, pp. 1738–1740, Dec. 22, 1986.

[884] P. F. Yuh and K. L. Wang, "Large Stark effects for transitions from local states to global states in quantum well structures," *IEEE J. Quantum Electron.*, vol. 25, pp. 1671–1676, July 1989.

[885] P. F. Yuh and K. L. Wang, "Novel infrared band-aligned superlattice laser," *Appl. Phys. Lett.*, vol. 51, pp. 1404–1406, Nov. 2, 1987.

[886] P. F. Yuh and K. L. Wang, "Formalism of the Kronig-Penney model for superlattices of variable basis," *Phys. Rev. B* , vol. 38, pp. 13307–13315, Dec. 1988.

[887] A. Zaslavsky, V. J. Goldman, D. C. Tsui, and J. E. Cunningham, "Resonant tunneling and intrinsic bistability in asymmetric double-barrier heterostructures," *Appl. Phys. Lett.*, vol. 53, pp. 1408–1410, Oct. 10, 1988.

[888] A. Zaslavsky, D. C. Tsui, M. Santos, and M. Shayegan, "Magnetotunneling in double-barrier heterostructures," *Phys. Rev. B.*, vol. 40, pp. 9829–9833, Nov. 15, 1989.

[889] A. Zaslavsky, D. C. Tsui, M. Santos, and M. Shayegan, "Resonant tunneling of two-dimensional electrons into one-dimensional subbands of a quantum wire," *Appl. Phys. Lett.*, vol. 58, pp. 1440–1442, Apr. 1, 1991.

[890] J. Zhang and W. Potz, "On transport in heterostructures within the independent-particle picture," in *Computational Electronics* , K. Hess, J. P. Leburton, and U. Ravaioli, Eds. Norwell, MA: Kluwer Academic, 1991, pp. 231–234.

[891] B. Zimmerman, E. Marclay, M. Ilegems, and P. Gueret, "Self-consistent calculations of tunneling currents in n^+-GaAs/i-$Al_xGa_{1-x}As$/n^+-GaAs structures and comparison with measurements," *J. Appl. Phys.*, vol. 64, pp. 3581–3588, Oct. 1, 1988.

[892] J. E. Zucker, T. L. Hendrickson, and C. A. Burrus, "Electro-optic phase modulation in GaAs/AlGaAs quantum well waveguides," *Appl. Phys. Lett.*, vol. 52, pp. 945–947, Mar. 21, 1988.

[893] J. E. Zucker, T. L. Hendrickson, and C. A. Burrus, "Low voltage phase modulation in GaAs/AlGaAs quantum well optical waveguides," *Electron. Lett.*, vol. 24, pp. 112–113, Jan. 21, 1988.

Thomas K. Gaylord (Fellow, IEEE) received the B.S. degree in physics and the M.S. degree in electrical engineering from the University of Missouri-Rolla, Columbia. He received the Ph.D. degree in electrical engineering from Rice University, Houston, TX.

Presently he is with the Georgia Institute of Technology, Atlanta, where he is now Regents' Professor and Julius Brown Chair Professor of Electrical Engineering. He is the author of some 180 technical journal publications in the areas of solid state holography, semiconductors, grating diffraction, and optical computing.

Dr. Gaylord is a Fellow of the Optical Society of America. He is also the recipient of seven Sigma Xi research awards, the "Curtis W. McGraw Research Award" from the American Society for Engineering Education, the IEEE Centennial Medal, the "Georgia Tech Outstanding Teacher" award, and the "Georgia Tech Outstanding Doctoral Advisor" award. He received an honorary "Professional Degree of Electrical Engineer" from the University of Missouri-Rolla in 1985 and the "Engineer of the Year" award from Georgia Society of Professional Engineers in 1988.

Elias N. Glytsis (Member, IEEE) received the B.S. degree in electrical engineering and the M.Sc. degree from the National Technical University of Athens, Greece in 1982. He received the M.S. and Ph.D. degrees in electrical engineering from the Georgia Institute of Technology, Atlanta, in 1984 and 1987.

Since January 1988 he has been with the School of Electrical Engineering of Georgia Institute of Technology as an Assistant Professor. His current research interests are in electromagnetic theory of grating diffraction, optical computing, integrated-optics, thin films, electro-optic and optoelectronic devices, semiconductor quantum electron-wave devices, and effects of geomagnetic fields on power systems. He has published over 30 journal and conference publications and has been co-guest editor of a special issue of the Optical Society of America on grating diffraction.

Gregory N. Henderson (Student Member, IEEE) received the B.S.E.E. degree from Texas Tech University, Lubbock, in 1989 and the M.S. degree in electrical engineering from the Georgia Institute of Technology, Atlanta, in 1991. Currently, he is pursuing the Ph.D. degree in electrical engineering at the Georgia Institute of Technology with the support of an Office of Naval Research Graduate Research Fellowship.

His research interests include analysis, design, and experimental characterization of ballistic electron transport in semiconductor nanostructures. He has also worked in the development of optical computing processors using photorefractive materials.

Mr. Henderson is a member of the Optical Society of America, Sigma Xi, Eta Kappa Nu, and Tau Beta Pi.

Kevin P. Martin received the B.S., M.S., and Ph.D. degrees in physics from the Ohio State University, Columbus.

Presently, he is a senior research scientist in the Microelectronics Research Center at the Georgia Institute of Technology, Atlanta. His research interests include transport and defect properties in III-V semiconductors materials and devices. Most recently, his activities have looked at transport mechanisms in semiconductor quantum well devices. This includes tunneling processes under ideal (without scattering) and nonideal (with energy-momentum relaxation effects) conditions.

Dr. Martin is a member of the American Physical Society.

David B. Walker received the B.S.E.E. degree from Purdue University, West Lafayette, IN, in 1982.

After graduation, he went to work at the Polaroid Corporation as an electronics design engineer. He was recognized as the Outstanding Engineer of the Year at Polaroid in 1985. In 1990 he came to Georgia Institute of Technology, Atlanta, where, as a President's Fellow, he is pursuing the Ph.D. degree in electrical engineering. His current research interests include ballistic electron transport devices and optical information processing.

Mr. Walker received the Col. Oscar P. Cleaver Award as the outstanding graduate student in 1991.

Daniel W. Wilson (Student Member, IEEE) was born in Rapid City, SD, on January 9, 1965. He received the B.S. degree in electrical engineering from Iowa State University, Ames, in 1988, and the M.S. degree in electrical engineering from Georgia Institute of Technology, Atlanta, in 1989. Presently, he is working towards the Ph.D. degree at Georgia Institute of Technology in the areas of electron waveguides and optical waveguides.

His research interests include electron wave optics and quantum phenomena in semiconductors, integrated optics, and nonlinear optics.

Mr. Wilson is a member of the Optical Society of America, Tau Beta Pi, and Eta Kappa Nu.

Kevin F. Brennan (Senior Member, IEEE) was born in Elizabeth, NJ, on October 18, 1956. He received the B.S. degree in physics from the Massachusetts Institute of Technology, Cambridge, in 1978 and the M.S. degree in physics and the Ph.D. degree in electrical engineering from the University of Illinois at Urbana-Champaign, in 1984.

He is currently an Associate Professor with the School of Electrical Engineering at the Georgia Institute of Technology, Atlanta. His current research interests include modeling of avalanche photodiodes, high-field effects in compound semiconductors, and transport in submicrometer Si and GaAs devices.

Quantum well, voltage-induced quantum well, and quantum barrier electron waveguides: Mode characteristics and maximum current

Daniel W. Wilson, Elias N. Glytsis, and Thomas K. Gaylord
Department of Electrical Engineering and Microelectronics Research Center, Georgia Institute of Technology, Atlanta, Georgia 30332

(Received 18 April 1991; accepted for publication 22 July 1991)

It is shown that finite-potential heterostructure wells, homostructure voltage-induced wells, and heterostructure barriers can act as waveguides for ballistic electrons and that waveguiding is described by a single dispersion relation and can occur at energies above all band edges. The guided mode cutoffs, electron velocity, effective mass, density of states, and ballistic current density (applicable to 2D electron gases) are presented. The maximum ballistic guided current flowing in a given direction for a 10 monolayer $Ga_{0.75}Al_{0.25}As/GaAs/Ga_{0.9}Al_{0.1}As$ waveguide is found to be 2.3 mA per μm of waveguide width–allowing considerably greater currents than in single-mode quantum wires.

Recent experiments have demonstrated micron-length ballistic (collisionless) electron transport and ballistic electron refraction in two-dimensional electron gas (2DEG) structures.[1,2] In these devices, the quantum well at the 2DEG interface acts as a slab waveguide for electron waves. Other experiments have demonstrated that "one-dimensional (1D) wires" defined in GaAs-GaAlAs heterostructures can act as channel electron waveguides.[4] In most analyses of 2D and 1D electron waveguides, it has been assumed that the waveguide has hard-wall boundaries (infinite potential),[4,5] or that the confining potential does not couple the transverse and longitudinal electron wave vector components.[6–8] While the hard-wall boundary may be reasonable for the gate-voltage defined sidewalls of one-dimensional wires, it is not valid for the boundaries formed by a heterostructure. The assumption that the transverse and longitudinal wave vector components are independent leads to a parabolic energy dispersion relation that does not give proper electron wave phase matching at the boundary.[9,10] In this letter, 2D electron waveguides are analyzed without any of the above assumptions.

We first consider a ballistic electron wave with energy E incident at an angle θ_1 on a single potential energy step which can be either a rise ($V_1 < V_2$) or a drop ($V_1 > V_2$). The effective masses are taken to vary in the same manner as the potential energies, i.e., $m_1^* < m_2^*$ for $V_1 < V_2$ and vice versa. This holds explicitly for the $Ga_{1-x}Al_xAs$ system, in which the conduction band potential energy $V = Ax$ and the effective mass $m^* = m_0(Bx + C)$, where $A = 0.7731$ eV, $B = 0.067$, $C = 0.083$, and m_0 is the free electron mass. The time-independent Schrödinger equation for the envelope wave function ψ in the effective mass approximation is $(-\hbar^2/2m_j^*)\nabla^2\psi(\mathbf{r}) + V_j\psi(\mathbf{r}) = E\psi(\mathbf{r})$, where j is the region index ($j = 1,2$). The boundary conditions are that ψ and $(1/m^*)(\partial\psi/\partial x)$ must be continuous. Snell's law for ballistic electrons is $k_1 \sin\theta_1 = k_2 \sin\theta_2$, where $k_j = \sqrt{(2m_j^*/\hbar^2)(E - V_j)}$ ($j = 1,2$).[9] The onset of total internal reflection (TIR) ($\theta_2 = 90°$) occurs at the critical angle $\theta_{1cr} = \sin^{-1}(k_2/k_1)$.[11] TIR can occur below the critical energy $E_{cr} = (m_2^*V_2 - m_1^*V_1)/(m_2^* - m_1^*)$ for a potential rise and above the critical energy for a potential drop. The existence of TIR for a potential drop requires differing effective masses. When TIR occurs, the wave function in region 2 decays as $\exp(-\gamma_2 x)$, and the electron wave in region 1 experiences a phase shift $\phi = -2\tan^{-1}[(m_1^*/m_2^*)(\gamma_2/k_{1x})]$, where $\gamma_2 = \sqrt{\beta^2 - k_2^2}$, $k_{1x} = \sqrt{k_1^2 - \beta^2}$, and the wave vector components are k_{1x} (transverse) and β (longitudinal).

The two-dimensional (slab) electron waveguide is shown in Fig. 1 and is composed of a cover, film, and substrate with potential energies V_c, V_f, and V_s, and effective masses m_c^*, m_f^*, and m_s^*, respectively. The potential energy diagrams for the three electron waveguide configurations are shown as insets in Fig. 2. They are the heterostructure well ($V_f < V_s < V_c, m_f^* < m_s^* < m_c^*$), the homostructure voltage-induced well ($V_f < V_s < V_c, m_f^* = m_s^* = m_c^*$), and the heterostructure barrier ($V_f > V_s > V_c, m_f^* > m_s^* > m_c^*$). The guiding region in all cases is the film which has thickness d, and the cover and substrate are taken to be infinitely thick. Both wells and barriers can act as electron waveguides since TIR can occur for both a potential rise and a potential drop. The heterostructure well and barrier may be formed by MBE growth, and the homostructure voltage-induced well may be formed by the gate-defined sidewalls of one-dimensional wires.

An electron injected into the film can be guided by TIR if its zigzag angle θ is greater than both the film-cover and film-substrate critical angles. However, only those electrons that constructively interfere with themselves as they reflect from the cover and substrate boundaries will be guided over significant distances. This requires that the sum of the phase shifts on TIR from the cover and substrate plus the phase shift incurred due to round-trip transverse propagation through the film must equal a multiple of 2π. Thus the dispersion equation is $2k_{fx}d + \phi_c + \phi_s = 2\nu\pi$, $\nu = 0,1,2,...$, where k_{fx} is the transverse propagation constant in the film, and ϕ_c and

 0003-6951/91/401855-03$02.00

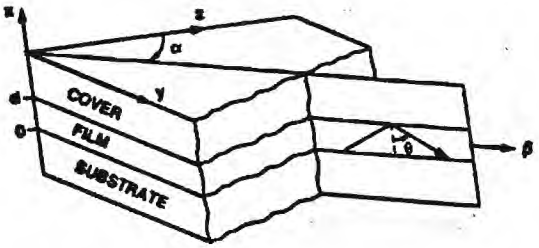

FIG. 1. Slab electron waveguide composed of a cover, film, and substrate. The guided mode has propagation vector β and zig–zag angle θ.

ϕ_s are the phase shifts on TIR from the cover and substrate respectively.[11] Thus

$$k_{fx}d - \tan^{-1}\left(\frac{m_f^*\gamma_s}{m_s^*k_{fx}}\right) - \tan^{-1}\left(\frac{m_f^*\gamma_c}{m_c^*k_{fx}}\right) = \nu\pi, \quad (1)$$

where $\gamma_{c,s} = \sqrt{\beta^2 - k_{c,s}^2}$, $k_{fx} = \sqrt{k_f^2 - \beta^2}$, and $\nu = 0,1,2,\ldots$.[10] This equation is valid for all three types of electron waveguides. Electron waves that satisfy Eq. (1) are guided modes and have wave functions of the form $\psi_\nu(\mathbf{r}) = \psi_\nu(x)\exp(i\beta\cdot\mathbf{r}_\parallel)$, where the mode propagation vector $\boldsymbol{\beta} = \beta_y\hat{y} + \beta_z\hat{z}$ and $\mathbf{r}_\parallel = y\hat{y} + z\hat{z}$. The transverse wave functions of the guided modes will be evanescent in the cover and substrate, and oscillatory in the film. Note that separation of the wave function into transverse and longitudinal parts does not lead to independent wave vector components.

Cutoff of the guided modes occurs when: $\beta = 0$ or $\gamma_s = 0$. When β decreases to zero, the electron no longer propagates down the waveguide, it merely reflects back and forth between the cover and the substrate. When γ_s decreases to zero, the wave function is no longer evanescent, and the electron is refracted into the substrate. The condition $\gamma_s = 0$ is sufficient for guided mode cutoff since $\gamma_s < \gamma_c$ by definition. Equations for the cutoff energies $E_{\beta=0}$ and $E_{\gamma_s=0}$ can be found by substituting $\beta = 0$ and $\gamma_s = 0$ into Eq. (1).[10] Equation (1) and the cutoff equations can be numerically solved to yield the E vs β dispersion curve and the cutoff energies of each guided mode M_ν. These results are shown in Fig. 2. The $Ga_{1-x}Al_xAs$ compositions of Fig. 2 were used for consistency among the three waveguide types. The heterostructure well [Fig. 2(a)] has both a $\beta = 0$ (lower energy) cutoff *and* a $\gamma_s = 0$ (upper energy) cutoff. The voltage-induced well [Fig. 2(b)] has only a $\beta = 0$ (lower energy) cutoff, and the heterostructure barrier [Fig. 2(c)] has only a $\gamma_s = 0$ (lower energy) cutoff. Clearly, waveguiding can occur at energies above the band edges of all three regions (c,f,s). Further, all of the dispersion curves are nonparabolic [Eq. (1)]. This is in contrast to the commonly used parabolic subband approximation, $E(\beta) = E_{\beta=0} + \hbar^2\beta^2/(2m_f^*)$. From Eq. (1), the dispersion curves are parabolic only in the limit of infinite confinement ($V_c = \infty, V_s = \infty$).

The guided electron velocity v_β is the group velocity of an electron wave packet, $v_\beta = (1/\hbar)(\partial E/\partial\beta)$. By differentiating Eq. (1), it can be shown that $v_\beta = P_c v_c + P_f v_f + P_s v_s$ where P_j is the probability of finding the electron in region j, and $v_j = \hbar\beta/m_j^*$ is the velocity an electron would have in *bulk* material like that of region j ($j = c,f,s$). Example velocity curves for the $\nu = 1$ mode in each of the three waveguide types are plotted in Fig. 3(a). Note that at the $\gamma_s = 0$ cutoff, $v_\beta = v_s$. By differentiating the velocity expression, the guided mode effective mass $1/m_\beta^* = (1/\hbar^2)(\partial^2 E/\partial\beta^2)$ is obtained. From Fig. 3(b), it is seen that m_β^* can differ significantly from m_f^*, and that the guided electron can become infinitely "heavy" when $\partial^2 E/\partial\beta^2 = 0$ (usually near the $\gamma_s = 0$ cutoff). The guided mode density of states per unit area $g_\beta(E)$ was derived by applying periodic (Born–von Karman) boundary conditions to the guided mode wave function. This yields the

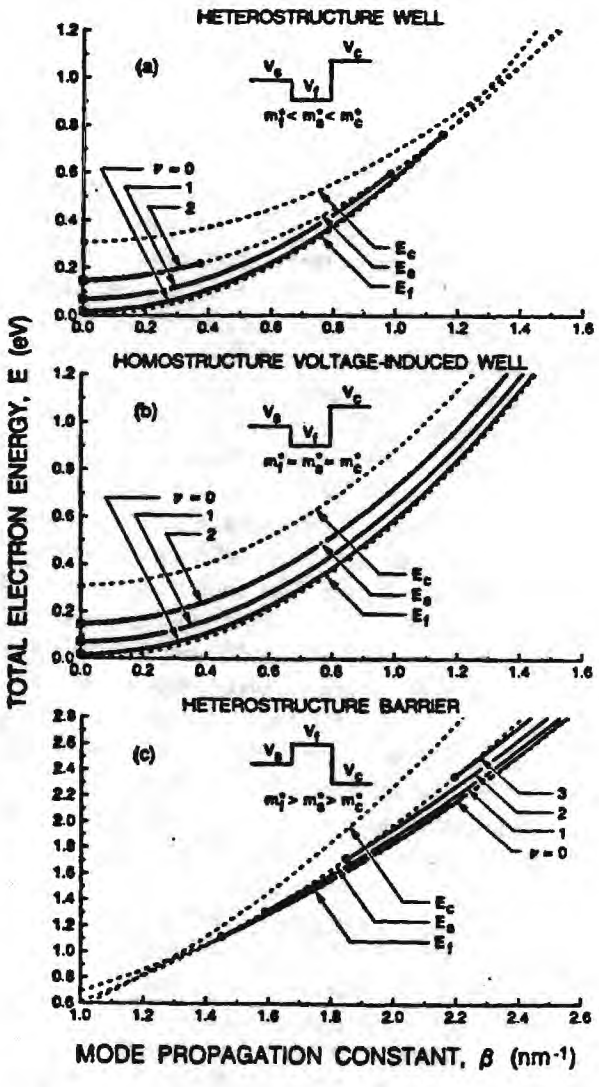

FIG. 2. Dispersion curves for $Ga_{1-x}Al_xAs$ electron waveguides wi $d = 50$ monolayers. (a) Heterostructure well with $x_c = 0.4$, $x_f = 0$, ar $x_s = 0.2$. (b) Homostructure voltage-induced well with $x_c = x_f = x_s =$ but V_c, V_f, and V_s the same as in (a). (c) Heterostructure barrier wi $x_c = 0, x_f = 0.4$, and $x_s = 0.2$. In (a) and (b) only three modes propaga whereas in (c) an infinite number of modes propagate (only four a shown). The dashed curves are the free electron dispersion curves $= \hbar^2\beta^2/(2m_j^*) + V_j$ ($j = c,f,s$). Solid squares indicate $\beta = 0$ cutoffs; sol circles indicate $\gamma_s = 0$ cutoffs.

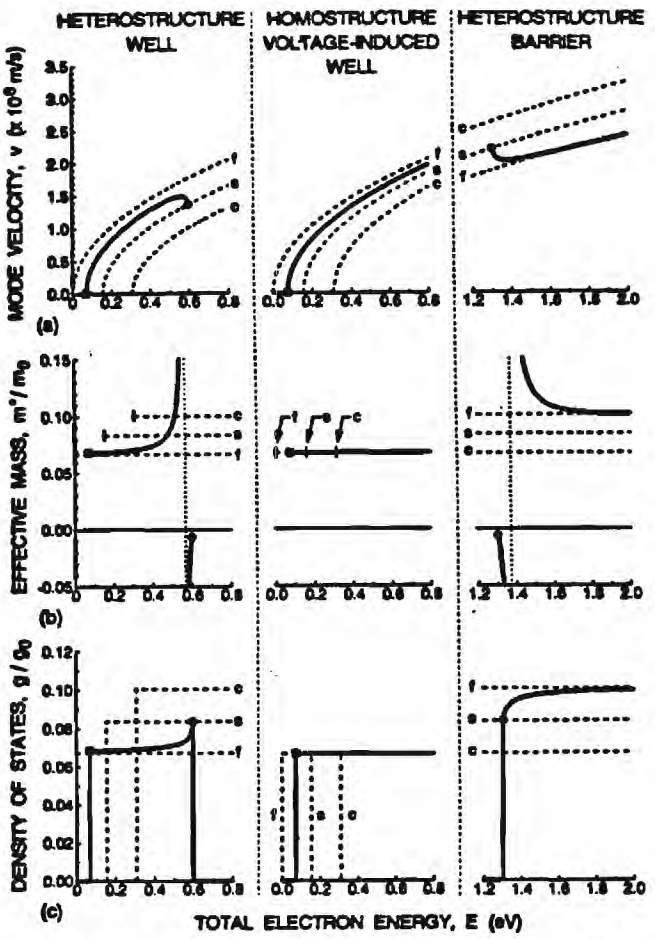

FIG. 3. (a) Guided mode velocity, (b) normalized guided mode effective mass, and (c) normalized guided mode density of states $[g_0 = m_0/(\pi\hbar^2)]$ for the $\nu = 1$ mode in the waveguides of Fig. 2. In (a) the dashed curves are the electron velocity in a bulk region j, $v_j = \sqrt{2(E - V_j)/m_j^*}$. In (b) the dashed curves are the effective masses m_j^*, and in (c) the dashed curves are the nonballistic 2DEG density of states for region. Solid squares and circles have the same meaning as in Fig. 2.

density of states between mode propagation angles α and $\alpha + d\alpha$, $g_\beta(E)d\alpha = \beta(E)d\alpha/[2\pi^2(\partial E/\partial\beta)]$, and the density of states over all α, $g_\beta(E) = \beta(E)/[\pi(\partial E/\partial\beta)]$, where the spin degeneracy of 2 has been included. The guided mode density of states $g_\beta(E)$ and the nonballistic 2DEG density of states $g_{2D}(E) = m^*/(\pi\hbar^2)$ are compared in Fig. 3(c).

The ballistic guided current density flowing in a given direction $(+z)$ can be obtained by integrating over all occupied states the product of the charge, the $+z$ component of the velocity, and the density of states. Thus, the ballistic guided current density is

$$J_z = \frac{-e}{2\pi^2\hbar}\sum_{\nu=0}^{\nu_{\max}}\int_0^\infty\int_{-\pi}^{\pi}\beta_\nu(E)\cos(\alpha)f_{\rm bal}(E,\alpha)\,dE\,d\alpha, \tag{2}$$

where $f_{\rm bal}(E,\alpha)$ is the distribution of ballistic electrons in energy and angle. The ballistic electron injector determines $f_{\rm bal}(E,\alpha)$ in much the same way a light source determines the wavelength- and angle-dependent distribution of photons launched into an optical waveguide. Equation (2) is valid for all three types of electron waveguides. As an example, we calculate the maximum current density for a single-mode 10 monolayer ($d = 2.8267$ nm) $Ga_{0.75}Al_{0.25}As/GaAs/Ga_{0.9}Al_{0.1}As$ heterostructure well waveguide. For this waveguide, $E_{\beta=0} = 0.0743$ eV and $E_{\gamma_z=0} = 0.2885$ eV (below the L-valley minima in GaAs to avoid intervalley scattering) which yields a mode propagation energy range $\Delta E = 0.2142$ eV. For maximum current, all the allowed modes propagating in the forward direction, would be filled, i.e., $f_{\rm bal}(E,\alpha) = 1$ for $E_{\beta=0} < E < E_{\gamma_z=0}$, $-\pi/2 < \alpha < \pi/2$, and $f_{\rm bal}(E,\alpha) = 0$ for all other E, α. This case yields $|J_z^{\max}| \simeq 2.3$ mA per μm of waveguide width. This value can be roughly compared to that predicted by the known maximum current in a single-vertical-mode (subband) hard-wall 1D wire of width W, $I_{\rm 1D}^{\max} = Ne\Delta E/(\pi\hbar)$,[12] where $N = 2W/\lambda$ is the number of lateral modes. For the comparison, we choose an equivalent energy $E_{\rm eq} = 0.15$ eV (near middle of ΔE) which corresponds to a wavelength $\lambda_{\rm eq} \simeq 12.2$ nm. For $W = 1$ μm, then $N \simeq 163.5$ and $I_{\rm 1D}^{\max} \simeq 2.7$ mA which is in close agreement with $J_z^{\max}$. The sizeable value of $J_z^{\max}$ makes it feasible to interconnect multiple ballistic electron devices with a single slab waveguide, as opposed to using multiple low-current-capacity 1D quantum wires.

Electron waveguides are potentially useful in high-speed electronic circuitry. They could also be a central component in future integrated electron guided-wave circuits similar to present-day integrated optical circuits. This research was sponsored by the Joint Services Electronics Program under Grant No. DAAL-03-90-C-0004 and by the National Science Foundation Grant No. ECS-9111866. One of us (E.N.G.) was supported by a Research Initiation Award from the National Science Foundation.

[1] J. Spector, H. L. Stormer, K. W. Baldwin, L. N. Pfeiffer, and K. W. West, Appl. Phys. Lett. 56, 1290, 2433 (1990); 58, 263 (1991).
[2] U. Sivan, M. Heiblum, C. P. Umbach, and H. Shtrikman, Phys. Rev. B 41, 7937 (1990).
[3] G. Timp, A. M. Chang, P. Mankiewich, R. Behringer, J. E. Cunningham, T. Y. Chang, and R. E. Howard, Phys. Rev. Lett. 59, 732 (1987).
[4] H. R. Frohne, M. J. McLennan, and S. Datta, J. Appl. Phys. 66, 2699 (1989).
[5] C. S. Chu and R. S. Sorbello, Phys. Rev. B 40, 5941 (1989).
[6] S. Datta, M. Cahay, and M. McLennan, Phys. Rev. B 36, 5655 (1987).
[7] G. Kirczenow, Phys. Rev. B 39, 10452 (1989).
[8] P. F. Bagwell, Phys. Rev. B 41, 10354 (1990).
[9] T. K. Gaylord and K. F. Brennan, J. Appl. Phys. 65, 814 (1989).
[10] T. K. Gaylord, E. N. Glytsis, and K. F. Brennan, J. Appl. Phys. 66, 1842 (1989).
[11] Analogous to analyses of dielectric slab waveguides; e.g., D. Marcuse, *Theory of Dielectric Optical Waveguides* (Academic, New York, 1974); H. Kogelnik, in *Integrated Optics*, edited by T. Tamir (Springer, Berlin, 1975).
[12] M. C. Payne, J. Phys. Condens. Matter 1, 4931 (1989).

Solid State Communications, Vol. 80, No. 8, pp. 591-596, 1991.
Printed in Great Britain.

0038-1098/91$3.00+.00
Pergamon Press plc

BALLISTIC ELECTRON EMISSION TESTING OF SEMICONDUCTOR HETEROSTRUCTURES

Gregory N. Henderson,* Thomas K. Gaylord,* Elias N. Glytsis,* and Phillip N. First,**
Microelectronics Research Center, Georgia Institute of Technology, Atlanta, Georgia 30332

and William J. Kaiser
Jet Propulsion Laboratory, California Institute of Technology, Pasadena, California 91109

(Received 11 July 1991 by R. H. Silsbee)
(In Revised Form September 19, 1991, by R.H. Silsbee)

In ballistic electron emission microscopy (BEEM) and spectroscopy, ballistic electrons are injected into a sample using a scanning tunneling microscope to probe the electrical properties of buried interfaces. In this communication, a method is proposed that uses the BEEM technique to observe the electron wave optical properties of semiconductor heterostructures. This method provides a three-terminal configuration for characterizing electron wave devices that overcomes many of the limitations encountered in other two- and three-terminal measurement techniques. Specifically, the method provides an injector, which is well isolated from the heterostructure, that injects a collimated beam of ballistic carriers with a precisely controlled energy distribution. These carriers accurately probe the quantum transmittance of a voltage-tunable electron wave interference structure, which can be designed with a light doping to minimize impurity and electron-electron scattering. A general procedure is presented for analyzing this experimental configuration based on a combination of the models used to describe BEEM and ballistic electron transport in semiconductors. Using this procedure, BEEM testing of an electron wave energy filter is modeled and clear quantum interference effects are predicted. This BEEM configuration should allow for the precise characterization of a wide range of ballistic electron transport effects such as quantum reflections from interfaces and electron wave interference effects, phenomena that are presently of wide interest.

Due to recent advances in nanostructure fabrication techniques such as molecular beam epitaxy and nanolithography, electron wave interference effects have been observed in semiconductor heterostructures for electron energies below the barriers in resonant tunneling structures [1-3] and for energies above the barriers in semiconductor heterostructures [2-7]. In all of these experiments, a degenerately doped emitter region was used as the source of ballistic electrons. The ballistic electrons were injected by tunneling through a barrier or by being emitted above a barrier. Interference effects were manifested as peaks in the current-voltage and conductance-voltage characteristics. Two of these structures [4,6] used a three-terminal configuration in order to tune the interference resonances without changing the distribution of injected electrons.

In spite of impressive experimental results that have been achieved in these electron wave interference experiments, all of these configurations suffer from three common limitations. First, since electron wave interference effects are dominant only at low temperatures (due to phonon scattering), the emitter must be degenerately doped in order to provide sufficient carriers. This degenerate doping causes increased impurity and electron-electron scattering, which have been shown to be the principal mechanisms that destroy quantum interference effects at low temperatures [8]. Also, as a consequence of heavy emitter doping, there is generally large band bending induced between the emitter and the interference structure [4]. This band bending alters the quantum transmittance of the structure, making quantitative modeling difficult. Second, it is difficult to make a third contact to the base region of the structure. The contact must be extremely small, on the order of 50-100 nm, and requires degenerate doping of the base layer [4,6], thus greatly increasing the

* and School of Electrical Engineering
** and School of Physics

scattering. Third, collimation of the injected electrons has been limited in previous designs because the devices have relied on potential-induced acceleration as the collimating mechanism. Since bias voltages are constrained to be less than the threshold voltage for intervalley scattering ($\approx 1\,V$), the degree of collimation is limited. A poorly collimated input distribution smears out the interference resonances, further obscuring the locations and amplitudes of the interference peaks.

In this communication it is proposed to use ballistic electron emission microscopy (BEEM) and spectroscopy as a diagnostic measurement technique for semiconductor electron wave heterostructures that can overcome the above limitations. This complements the previous uses of BEEM for studying buried interfaces [9,10] and scattering in the base electrode [11]. In the BEEM configuration ballistic electrons are injected with precise energy control from a scanning tunneling microscope (STM) into a metal base. These electrons propagate ballistically through the base (approximately 10-20 nm) to probe a base-semiconductor interface. By monitoring the number of electrons transmitted across the interface as a function of tip-base voltage, the electrical characteristics of the interface, such as the barrier height, can be determined. The method presented in the present communication is an extension of conventional BEEM where a multilayer electron wave structure is placed directly below the base-semiconductor interface, as is shown in Fig. 1. By monitoring the number of electrons that are transmitted through the structure as a function of tip-base voltage, the quantum transmittance of the structure can be determined. Interference resonances will appear as peaks in the conductance-voltage curves in a manner similar to other quantum interference measurements [1-7].

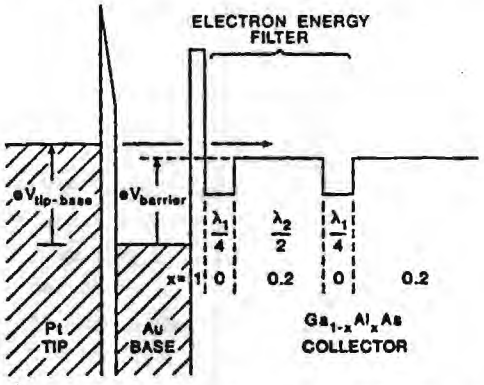

Fig. 1 - Energy band configuration in BEEM testing of a quantum electron wave interference structure, where the semiconductor structure is directly below the gold base. Ballistic electrons injected from the STM tip are used to probe the quantum transmittance of the structure. The structure shown is an electron energy filter which is designed to transmit at 53 meV above the Γ conduction band minimum in the output region. At this energy, the barrier and wells are quarter- and half-wavelength layers, respectively.

The BEEM diagnostic measurement technique described here is not restricted by the first two limitations of past quantum interference measurement methods. The first limitation, the degenerate doping of the semiconductor structure, is removed since the carriers are generated by the STM. This significantly reduces the impurity and electron-electron scattering, thus enhancing the quantum interference effects. A light doping (around $10^{16}\,cm^{-3}$) of the structure can be used to control the band bending imposed by the Fermi level pinning at the base-semiconductor interface. If the device is made sufficiently thinner than the depletion width, there will be minimal band bending through the structure; the Fermi level will be pinned near midgap throughout. The second limitation, the difficulty of providing a base contact, is removed because the base is exposed and thus easily accessible in this configuration. Changing the base-collector voltage will allow precise tuning of the resonance energies, without affecting the energy of injection. The third limitation, poor collimation of the injected distribution, can be improved in the BEEM technique. Of the electrons incident at the base-semiconductor interface, only those within a few degrees of normal incidence are transmitted into the semiconductor, due to the small critical angle of the base-semiconductor interface [10,12]. The electrons within this small angular range are, however, refracted into the semiconductor into a broad distribution from 0 to 90 deg. This distribution is collimated in the forward direction due to the nonlinearity of the refraction process [12] and the high reflectivity for those electrons incident near the critical angle in the base [12]. If one assumes the worst case condition in which the electrons in the base are uniformly distributed in solid angle between normal incidence and the critical angle, then the normalized distribution in the semiconductor is given as $g(\theta_2) = [1 - r^2(\theta_2)]cos\theta_2$, where θ_2 is the angle of refraction (measured from the interface normal) inside the semiconductor, and r is the reflectivity of the base-semiconductor interface for a given incident energy. This distribution is shown in Fig. 2 for an interface between gold and $Ga_{0.8}Al_{0.2}As$ with an energy of incidence of 100 meV above the conduction band in the $Ga_{0.8}Al_{0.2}As$. Although the electrons tunnel through the $AlAs$ layer and then directly enter the first $GaAs$ layer of the three-layer filter, the input distribution is

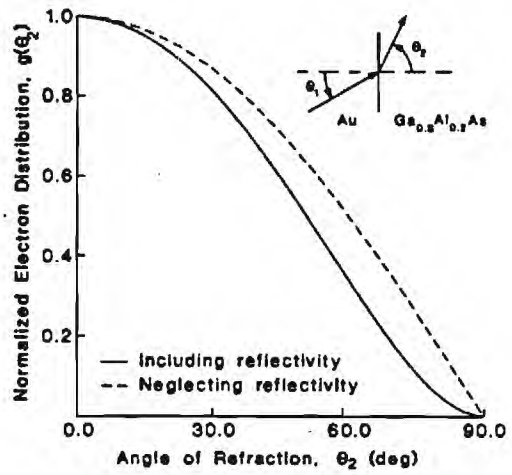

Fig. 2 - Distribution of electrons injected from a gold base into a $Ga_{0.8}Al_{0.2}As$ semiconductor. The distribution is plotted with respect to the angle of refraction (measured from the interface normal) in the semiconductor (θ_2) for a kinetic energy of $100\,meV$ in the $Ga_{0.8}Al_{0.2}As$. The solid line is the distribution that includes the quantum reflectivity at the interface, the dashed line is the approximate distribution $cos\theta_2$ that results from neglecting the quantum reflectivity.

calculated in $Ga_{0.8}Al_{0.2}As$ (rather than $GaAs$) since the output reference region is $Ga_{0.8}Al_{0.2}As$. The input distribution could equally well be calculated in $GaAs$ (or any other material) but the device response would remain unchanged. The shape of the injected distribution, however, is very insensitive to the energy of injection and the composition of aluminum in the energy range of 0 to $1\,eV$ and the aluminum composition range of 0 to 0.45. The distribution could be further collimated in the forward direction if a base metal were used that had a band minimum close to the top of the Schottky barrier $V_{barrier}$ (Fig. 1), thus reducing the angle of refraction θ_2 [12].

The use of an STM injector provides significant advantages beyond the removal of the above limitations. At low temperatures, the energy of the injected electrons can be accurately controlled (within a few meV) by the tip-base voltage of the STM [13], while the injection current is independently set by adjusting the tip-base separation. Feedback control of the this separation holds the injected current at a fixed value, automatically normalizing the collector current to the injected current [10]. These features allow for a precise characterization of the transmittance of the heterostructure, decoupling it from the injector response.

The collector current I_c of the structure can be calculated by integrating the product of the electron transmittance of the heterostructure $[T_e(E_z, E_t) = 1 - r^2(E_z, E_t)]$ and the injected electron distribution over the tip energies $E = E_z + E_t$, where E_z is the energy associated with the component of the momentum normal to the interface, and E_t is the energy associated with the component of the momentum tangential to the interface. The electrons in the base are propagating at an angle $\theta_1 = arctan(\sqrt{E_t/(E_z - V_1)})$ (measured from the interface normal) which are then refracted into θ_2 in the output region, where V_1 is the potential energy of the electrons in the base [12]. The integral of the collector current can be evaluated numerically as a function of tip-base voltage $V_{tip-base}$ to calculate the current-voltage characteristic of the structure. By inserting $T_e(E_z, E_t)$ into the collector current expression developed in Ref. [10], one achieves an expression for the collector current I_c normalized to the tip current I_t,

$$I_c/I_t = \frac{R\int_{E_{min}}^{\infty} D(E_z)\int_0^{E_{max}} T_e(E_z, E_t) f(E) dE_t dE_z}{\int_0^{\infty} D(E_z)\int_0^{\infty} [f(E) - f(E + eV_{tip-base})] dE_t dE_z}, \quad (1)$$

where $f(E)$ is the Fermi-Dirac distribution, E is the electron energy in the tip, $D(E_z)$ is the tunneling probability, R is an energy-independent scattering term in the base, E_{min} is the minimum normal energy that can be transmitted to the collector due to the Schottky barrier $V_{barrier}$ (Fig. 1), and E_{max} is the maximum energy (for a given E_z) that can be transmitted to the collector due to total internal reflection at the base-semiconductor interface [10]. The electron transmittance of the structure can be calculated using any of the methods employed to describe quantum transport such as the chain matrix extension of the envelope function approximation [14] or the Wigner function approach [15].

In order to demonstrate the utility of this method, an electron wave interference filter was designed for Γ minimum electrons in $Ga_{1-z}Al_zAs$ (Fig. 1) using the design method presented in Ref. [16]. This device is analogous to a thin-film Fabry-Perot filter in optics, where, at the design energy, the center layer is a half-wavelength resonant layer and the two adjacent layers are quarter-wavelength reflectors. The filter in Fig. 1 was designed to be resonant for a normal incidence (i.e. $E_t = 0$) kinetic energy (KE) of $53\,meV$ above the conduction band minimum in the output region, $Ga_{0.8}Al_{0.2}As$. The resonant layer was

designed as a barrier surrounded by two wells (as opposed to the equivalent well surrounded by two barriers) in order to ensure that the resultant effects are due to interference above the barriers and not due to resonant tunneling through the barriers. The electron transmittance of this structure was calculated using the chain matrix extension of the envelope approximation [14]. The transmittance of the filter is shown in Fig. 3 for both normal incidence ($\theta_2 = 0.0\,deg$) and an incidence of $\theta_2 = 30.0\,deg$. At the design kinetic energy, $KE = 53\,meV$, the normal-incidence transmittance of the device peaks at 80%, as is shown in Fig. 3. The transmittance at resonance is not unity due to reflections from the base-semiconductor boundary. As the angle of incidence is increased, the resonant peak shifts to higher energies (shorter wavelengths). The transmittance at $\theta_2 = 30.0\,deg$ peaks at $70\,meV$ which is consistent with the expected shift for this angle, as calculated from thin-film optics principles [12,17]. As the energy of injection is varied from the resonance energy, the transmittance drops. The full-width-at-half-maximum (FWHM) of the resonance peak is $16.6\,meV$.

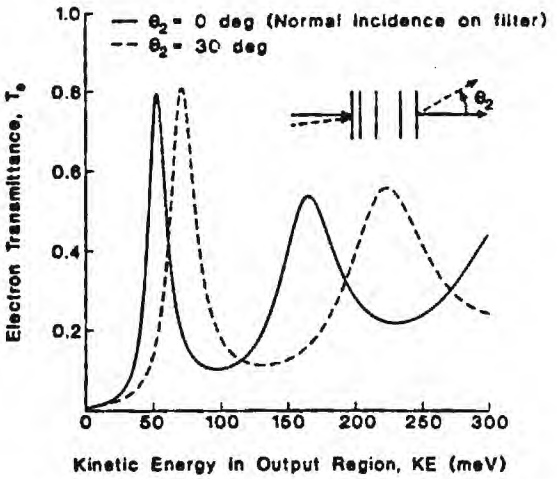

Fig. 3 - Quantum transmittance of the three-layer electron energy filter shown in Fig. 1 as measured in the $Ga_{0.8}Al_{0.2}As$ output region. At normal incidence, the filter transmittance peaks at $KE = 53\,meV$, with a transmittance of 80% and a FWHM of $14.6\,meV$. As the angle of incidence is changed, the transmittance peaks at higher energies, resulting in a peak at $KE = 70\,meV$ for $\theta_2 = 30.0\,deg$. The transmittance at resonance is not unity due to reflections from the base-semiconductor interface.

By substituting the complete filter transmittance (for all angles of incidence) into Eq. (1), the current-voltage, conductance-voltage, and differential-conductance-voltage characteristics of the filter can be calculated. These results are shown in Figs. 4a, 4b, and 4c respectively for temperatures of $4.2\,K$ and $77\,K$. The two peaks in the differential-conductance characteristic correspond to the two peaks in the transmittance T_e shown in Fig. 3. This similarity can be seen in Fig. 4c where the transmittance has been superimposed on the differential-conductance curves. In the experiment, it is likely that the amplitude of the second peak will be significantly reduced since the electrons can start entering the L minima in $Ga_{0.8}Al_{0.2}As$ at $V_{tip-base} - V_{barrier} = 0.16\,V$. The characteristics below this voltage, however, should closely resemble Fig. 4. It should be noted that each differential-conductance peak occurs a voltage for which the Fermi energy in the tip is slightly above the energy of that transmittance peaks. This shift is a complicated function of the power-law dependence of the collector current near the threshold $V_{tip-base} = V_{barrier}$ [10], the distribution of injected electrons $g(\theta_2)$, and the transmittance of the filter. This shift is consistent, however, with the electromagnetic case in which the transmittance of an interference filter peaks at an energy that is displaced from the normal incidence resonant energy when illuminated by a distributed source [17]. For the first peak this shift amounts to $2\,meV$ above the resonance energy, corresponding to a tip-base voltage of $V_{tip-base} - V_{barrier} = 55\,meV$. The FWHM of the conductance peaks can be approximated as a sum of the width of the transmittance peak and the width of the derivative of the Fermi-Dirac distribution ($\approx 2k_BT$). For the first peak, this estimate gives a FWHM of $17.3\,meV$ at $4.2\,K$ and $31.2\,meV$ at $77\,K$, which can be compared with the simulation values of $14.8\,meV$ and $29.9\,meV$, respectively.

It has been demonstrated analytically that the primary effect of the application of a base-collector voltage to this filter structure is a linear shift of the resonance energy [18]. Thus, tuning of the base-collector voltage will shift the resonance peak in the conductance-voltage characteristic of the device. This tunability of the resonance should allow for great flexibility in the characterization of electron wave interference effects.

The analysis used to achieve the results of Fig. 4 were based on an ideal experimental configuration with no background noise current, no scattering at the base semiconductor boundary, and no scattering in the device, the three mechanisms that are most likely to reduce the magnitude of the interference peaks. Since the steps in the $d(Ic/It)/dV$ curve shown in Fig. 4

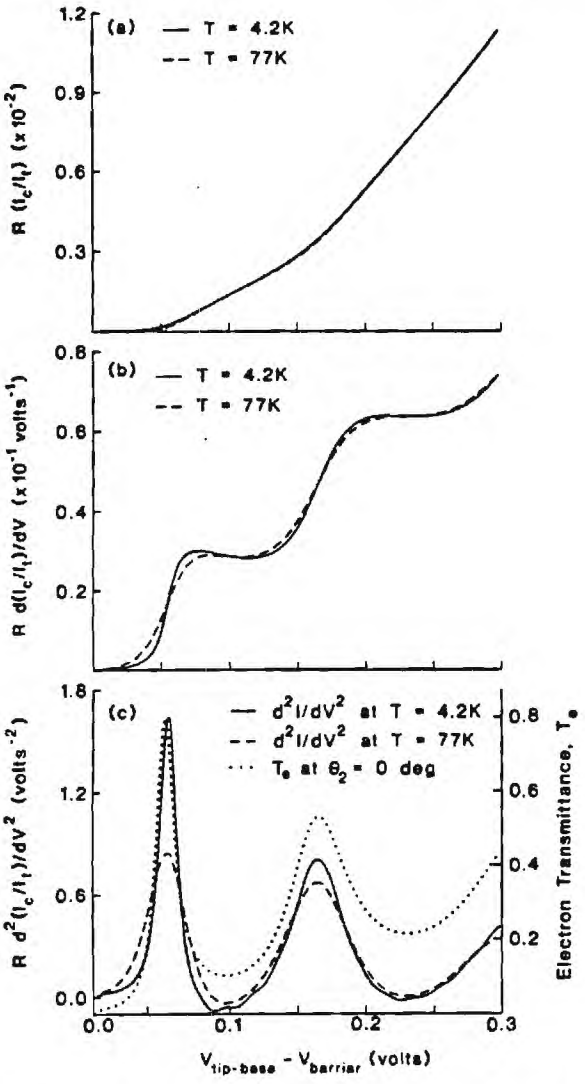

Fig. 4 - Current-voltage (a), conductance-voltage (b), and differential-conductance-voltage (c) characteristics of the interference filter of Fig. 1. The peaks in the differential-conductance-voltage characteristic (c) correspond to the two peaks in the transmittance shown in Fig. 3. The differential conductance peaks occur at energies slightly higher than the transmittance peaks as discussed in the text. The first peak occurs at $V_{tip-base} - V_{barrier} = 55\,meV$, with a FWHM of $17.3\,meV$ at $4.2\,K$ and a FWHM of $31.2\,meV$ at $77\,K$. The second peak lies above the L minima in the output region and is therefore likely to have a significantly reduced amplitude.

are an order magnitude larger than previously resolved dI/dV steps [10], it is likely that the signal peaks will be significantly larger than the background noise current fluctuations. The accurate agreement between the momentum-conservation theory and BEEM spectra for *GaAs* [10] indicate that the component of the current that scatters at the base-semiconductor interface will be small compared to the momentum conserving current. However, if there is significant scattering at the base-semiconductor interface, the primary effect is to change the distribution of electrons ($g(\theta_1, E)$) injected into the semiconductor. Simulations that incorporate various injected distributions show similar behavior to the results shown in Fig. 4. The locations and amplitudes of the interference peaks shift, but the interference resonances are still resolvable. The final contributor to the noise current is scattering in the interference structure. Since the structure is significantly thinner ($\approx 200\,nm$) and more lightly doped ($\approx 10^{18}\,cm^{-3}$) than previous structures used to demonstrate quantum interference effects ($\approx$ 800 to $1000\,nm$), it is likely that this component of the noise current will not significantly degrade the interference measurements.

The modeling of this simple ballistic electron interference filter clearly demonstrates the potential BEEM holds as a diagnostic tool for quantum structures. This method could be used in the precise analysis and characterization of other quantum interference structures such as resonant tunneling diodes [19], multilayer energy filters [16,18], impedance transformers [20], and quantum interference transistors [21]. In addition, this method could be used to investigate many other quantum transport effects that are presently of great interest. For instance, the technique could be used to analyze the quantum mechanical reflection and transmission past a single interface, demonstrating such effects as the dependence on effective mass differences across the interface and the existence of a Brewster angle [12,22]. Additionally, the method could be used to characterize the reflectance and resonance effects occurring in quarter- and half-wavelength material layers [4-6,16,18]. A complete understanding and characterization of these fundamental effects is extremely important in the design of future electron guided wave integrated circuits [12].

In conclusion, a method has been proposed that uses ballistic electron emission microscopy and spectroscopy to test and characterize quantum electron wave heterostructures. The BEEM technique provides a three-terminal testing configuration that overcomes many of the limitations of other two- and three-terminal testing configurations. A simulation of the use of this technique has been performed for an electron wave interference filter and the quantum interference

effects are shown to be clearly observable. This method can be used to characterize a variety of ballistic transport effects such as quantum reflections from material interfaces and electron wave interference effects. In addition, the method could be combined with other quantum transport measurement techniques such as magneto-transport [23] and optical [24] techniques in order analyze a wide range of quantum structures. In the future, the technique could be expanded to two-probe and multi-probe configurations in order to analyze complex ballistic transport effects such as propagation in electron waveguides [25] and ballistic electron diffraction from gratings [26].

Acknowledgements - This research was supported in part by grant no. DAAL-03-90-C-0004 from the Joint Services Electronics Program and by grant no ECS-9111866 from the National Science Foundation. One of us (G.N.H.) was supported by an office of Naval Research Graduate Research Fellowship, and one of us (E.N.G.) was supported by a Research Initiation Award from the National Science Foundation. The authors gratefully acknowledge the original suggestion of C. A. Kukkonen of the Jet Propulsion Laboratories that led to the present work.

References

[1] R. Tsu and L. Esaki, *Appl. Phys. Lett.* **22**, 562 (1973).

[2] S. Sen, F. Capasso, A. C. Gossard, R. A. Spah, A. L. Hutchinson, and S. N. G. Chu, *Appl. Phys. Lett.* **51**, 1428 (1987).

[3] S. Y. Chou and J. S. Harris, *Appl. Phys. Lett.* **52**, 1422 (1988).

[4] M. Heiblum, M. V. Fischetti, W. P. Dumke, D. J. Frank, I. M. Anderson, and C. M. Knoedler and L. Osterling, *Phys. Rev. Lett.* **58**, 816 (1987).

[5] R. C. Potter, and A. A. Lakhani, *Appl. Phys. Lett.* **52**, 1349 (1988).

[6] J. R. Hayes, P. England, and J. P. Harbison, *Appl. Phys. Lett.* **52**, 1578 (1988).

[7] F. Beltram, F. Capasso, A. L. Hutchinson, and R. J. Malik, *Appl. Phys. Lett.* **55**, 1534 (1989).

[8] S. Washburn and R. A. Webb, *Adv. in Phys.* **35**, 375 (1986).

[9] W. J. Kaiser and L. D. Bell, *Phys. Rev. Lett.* **60**, 1406 (1988).

[10] L. D. Bell and W. J. Kaiser, *Phys. Rev. Lett.* **61**, 2368 (1988).

[11] L. D. Bell, M. H. Hecht, W. J. Kaiser, and L. C. Davis, *Phys. Rev. Lett.* **64**, 2679 (1990).

[12] G. N. Henderson, T. K. Gaylord, and E. N. Glytsis, *Proc. IEEE* **79**, (Nov. 1991). (accepted)

[13] H. F. Hess, R. B. Robinson, R. C. Dynes, J. M. Valles, and J. V. Waszczak, *J. Vac. Sci. Technol. A* **8**, 450 (1990).

[14] T. K. Gaylord and K. F. Brennan, *J. Appl. Phys.* **65**, 814 (1989).

[15] W. R. Frensley, *Phys, Rev. Lett.* **57**, 2853 (1986).

[16] T. K. Gaylord, E. N. Glytsis, and K. F. Brennan, *J. Appl. Phys.* **65**, 2535 (1989).

[17] H. A. Macleod, *Thin Film Optical Filters.* (McGraw Hill, New York, 1989), Chpt. 7.

[18] E. N. Glytsis, T. K. Gaylord, and K. F. Brennan, *J. Appl. Phys.* **66**, 1494 (1989).

[19] M. A. Reed, W. R. Frensley, W. M. Duncan, R. J. Matyi, A. C. Seabaugh, and H. L. Tsai, *Appl. Phys. Lett.* **54**, 1256 (1989).

[20] T. K. Gaylord, E. N. Glytsis, and K. F. Brennan, *J. Appl. Phys.* **67**, 2623 (1990).

[21] S. Datta, *Super. and Micro.* **6**, 83 (1989).

[22] H. Ohno, E. E. Mendez, and W. I. Wang, *Appl. Phys. Lett.* **56**, 1793 (1990).

[23] G. Landwehr, in *Electronic Properties of Multilayer and Low-Dimensional Semiconductor Strucutres*, J. M. Chamberlain, L. Eaves, and J.-C. Portal Eds. (Plenum Press, New York, 1989), pg. 33.

[24] B. Deveaud, in *Electronic Properties of Multilayer and Low-Dimensional Semiconductor Strucutres*, J. M. Chamberlain, L. Eaves, and J.-C. Portal Eds. (Plenum Press, New York, 1989), pg. 399.

[25] T. K. Gaylord, E. N. Glytsis, and K. F. Brennan, *J. Appl. Phys.* **66**, 1483 (1989).

[26] G. N. Henderson, E. N. Glytsis, and T. K. Gaylord, *Appl. Phys. Lett.* **59**, 440 (1991).

Electromagnetic analogies to general-Hamiltonian effective-mass electron wave propagation in semiconductors with spatially varying effective mass and potential energy

Gregory N. Henderson, Thomas K. Gaylord, and Elias N. Glytsis
School of Electrical Engineering and Microelectronics Research Center, Georgia Institute of Technology, Atlanta, Georgia 30332

(Received 1 October 1991; revised manuscript received 10 December 1991)

It is shown that exact, quantitative electromagnetic analogies exist for *all* forms of the general Hamiltonian [R. A. Morrow and K. R. Brownstein, Phys. Rev. B 30, 678 (1984)], which applies to single-band effective-mass electron wave propagation in semiconductors. It is further shown that these analogies are valid for propagation in the bulk, propagation past abrupt interfaces between materials, and propagation within one- and two-dimensionally inhomogeneous materials. These results indicate that the correct form of the single-band effective-mass Hamiltonian can be determined through appropriate wave-function-amplitude-sensitive experiments. Wave-function-phase-sensitive experiments (such as the measurement of electron wave refraction directions) are not adequate to specify completely the Hamiltonian. The present analogies suggest many wave-function-amplitude-sensitive experiments that can be used to determine the correct form of the Hamiltonian. The results of the present analysis are broadly applicable to general effective-mass propagation, unlike other recent work that has treated specific cases.

Recent advances in nanostructure growth and fabrication techniques (such as molecular-beam epitaxy and nanolithography) have led to the development of semiconductor devices in which the device response is dominated by ballistic-electron (phase-coherent) transport.[1-5] Such ballistic electrons have been reflected and refracted,[1] focused,[2,3] and interfered[4,5] in a manner analogous to electromagnetic waves in dielectrics. Based on these results, it has been shown analytically, that under the effective-mass approximation, exact, quantitative analogies can be drawn between ballistic (collisionless) electron transport in semiconductors and electromagnetic wave propagation in dielectrics.[6]

These previous analogies were developed both for propagation in the bulk and for propagation past abrupt interfaces between materials.[6] In developing these analogies, the electron wave boundary conditions at an abrupt interface between dissimilar semiconductors were assumed to be the conservation of the electron wave amplitude ψ and the conservation of the product of the inverse effective mass and the normal component of the gradient of the electron wave amplitude, $\nabla\psi\cdot\hat{\mathbf{n}}/m$. The choice of these boundary conditions is equivalent to choosing the Hamiltonian H such that

$$H\psi=\frac{-\hbar^2}{2}\nabla\cdot\left[\frac{\nabla\psi}{m(\mathbf{r})}\right]+V(\mathbf{r})\psi=E\psi\ , \tag{1}$$

for electron wave propagation in a region of spatially varying effective mass $m(\mathbf{r})$ and spatially varying potential energy $V(\mathbf{r})$, where $\hbar$ is Planck's constant divided by 2π, and E is the total electron energy.[7] This Hamiltonian is probably the most widely used form of the effective-mass Hamiltonian.[7,8] There are, however, other Hermitian forms of the effective-mass Hamiltonian and each results in different boundary conditions.[9,10] von Roos[9] has suggested a Hermitian class of effective-mass Hamiltonian functions. Using this class of functions, Morrow and Brownstein[10] have shown that only those Hamiltonians that lie within a subset of this class of functions have physical meaning when considering the matching of the boundary conditions across an abrupt interface. There is, however, significant disagreement as to the exact form of the Hamiltonian within this class, based on consideration of a number of specific cases.[11-16] The purpose of the present paper, therefore, is to draw a set of exact, quantitative analogies between electromagnetic wave propagation in dielectrics and effective-mass electron wave propagation described by the complete class of Hamiltonians given by Morrow and Brownstein. These analogies will be drawn for propagation in the bulk, propagation past abrupt interfaces, and for propagation within one- and two-dimensionally inhomogeneous materials, and will be valid for whatever form of the general Hamiltonian is ultimately shown to be correct. In addition, these analogies present the specific types of experiments that can be performed to identify the correct form of the effective-mass Hamiltonian.

Morrow and Brownstein[10] demonstrated that, of the general class of Hamiltonians (H) suggest by von Roos,[9] only those that take the form

$$H\psi=\frac{-\hbar^2}{2}(m(\mathbf{r})^{\alpha}\nabla\cdot\{m(\mathbf{r})^{\beta}\nabla[m(\mathbf{r})^{\alpha}\psi]\})+V(\mathbf{r})\psi=E\psi \tag{2}$$

with the constraint

$$2\alpha+\beta=-1 \tag{3}$$

have physical meaning, when considering propagation past an abrupt interface between dissimilar semiconductors. Using comparisons of more exact theories and the effective-mass theory, many authors have attempted to

deduce the values of α and β, resulting in a wide range of values from $\alpha=-\frac{1}{2}$ and $\beta=0$ (Ref. 11) to $\alpha=0$ and $\beta=-1$ (Refs. 12–14). As Morrow suggests,[11] the determination of the correct values of α and β will doubtlessly depend on experiments. Galbraith and Duggan have used photoluminescence data to shown that $\alpha=0$ and $\beta=-1$ for GaAs/$Ga_{1-x}Ga_xAs$ quantum wells.[15] Similar results have recently been reported for GaAs/$Ga_{1-x}Al_xAs$ quantum wells by Mojahedie and Osinski.[16] However, these results are valid *only* for GaAs/$Ga_{1-x}Al_xAs$ heterostructures.[15] Since the determination of α and β is still an open problem in general, this paper will draw electromagnetic analogies to the general form of the Hamiltonian given in Eq. (2) for all values of α and β. The analogies that are drawn dictate the form experiments must take in order to determine the correct values of α and β.

For the Hamiltonian of Eq. (2), the boundary conditions for an electron wave at an interface are[10]

$$m^{\alpha}\psi \text{ continuous} \tag{4}$$

and

$$m^{\alpha+\beta}\nabla\psi\cdot\hat{\mathbf{n}} \text{ continuous} , \tag{5}$$

where $\hat{\mathbf{n}}$ is the unit vector normal to the interface. Analogously, the boundary conditions for an electromagnetic wave at an interface between two dielectrics require the continuity of the tangential component of the electric field ($\mathcal{E}$) and the continuity of the tangential component of the magnetic field ($\mathcal{H}$) across the interface. Based on this consideration, it is reasonable to look for analogies between $\Phi=m^{\alpha}\psi$ and either $\mathcal{E}$ or $\mathcal{H}$. In the previous work based on Eq. (1), it was demonstrated that ψ (not Φ) was analogous to $\mathcal{E}$ for TE polarization and to $\mathcal{H}$ for TM polarization.[6] The analogies of the present paper will be consistent with these analogies because Eq. (1) is the $\alpha=0$ special case of Eq. (2) for which $\Phi=\psi$.

For bulk propagation in a homogeneous medium, an exact analogy can be drawn between Φ and *both* $\mathcal{E}$ and $\mathcal{H}$. In this case, the Hamiltonian for the electron wave propagation [Eq. (2)] reduces to a Helmholtz equation of the form

$$\nabla^2\Phi=-k^2\Phi , \tag{6}$$

where $k^2=2m(E-V)/\hbar^2$. This wave equation [Eq. (6)] is exactly analogous to the Helmholtz equation for an electromagnetic wave propagating in a homogeneous dielectric of permittivity ϵ and permeability μ, where Φ is replaced by $\mathcal{E}$ for the electric-field equation and by $\mathcal{H}$ for the magnetic-field equation. In the electromagnetic case, $k^2=\omega^2\mu\epsilon$, where ω is the radian frequency of the wave. Since the electron wave Helmholtz equation has exactly the same form as both the electric-field Helmholtz equation and the magnetic-field Helmholtz equation, an exact analogy can be drawn between Φ and *both* $\mathcal{E}$ and $\mathcal{H}$. Using these analogies and the definitions given in Ref. 6, one can define a phase-refractive index for electron waves as

$$n_{\text{ph}}^{\text{EW}}=m_r^{1/2}(E-V)_r^{1/2} , \tag{7}$$

where $m_r=m/m_{\text{ref}}$ is the relative effective mass and $(E-V)_r=(E-V)/(E-V_{\text{ref}})$ is the relative kinetic energy, where m_{ref} and V_{ref} are the effective mass and potential energy in a reference region.[6] This electron wave phase-refractive index is analogous to the phase-refractive index for electromagnetic waves $n_{\text{ph}}^{\text{EM}}=\sqrt{\mu_r\epsilon_r}$, where μ_r is the relative permeability and ϵ_r is the relative permittivity of the dielectric. With these results, phase-propagation effects, such as interference, can be analyzed using standard electromagnetic results where $\mathcal{E}$ (or $\mathcal{H}$) is replaced by Φ and $n_{\text{ph}}^{\text{EM}}$ is replaced by $n_{\text{ph}}^{\text{EW}}$. These results are valid for all the Hamiltonians given in Eq. (2).

The above analogies can be extended to describe electron wave propagation past an abrupt interface between materials 1 and 2 with effective masses m_1 and m_2 and potential energies V_1 and V_2, respectively. When a plane wave [the eigensolution to Eq. (6)] is incident upon such an interface, part of the wave is reflected back into region 1 and part of the wave is transmitted (refracted) into region 2. The boundary conditions [Eqs. (4) and (5)] are used to calculate the directions of propagation and the amplitudes of the reflected and transmitted waves. By substituting $\Phi_1=\exp(j\mathbf{k}_{1,i}\cdot\mathbf{r})+r\exp(j\mathbf{k}_{1,r}\cdot\mathbf{r})$ and $\Phi_2=t\exp(j\mathbf{k}_2\cdot\mathbf{r})$ into the boundary conditions [Eqs. (4) and (5)], one finds that

$$\theta_i=\theta_r=\theta_1 , \tag{8}$$

$$n_{\text{ph},1}\sin\theta_1=n_{\text{ph},2}\sin\theta_2 , \tag{9}$$

$$r=\frac{n_{\text{amp},1}\cos\theta_1-n_{\text{amp},2}\cos\theta_2}{n_{\text{amp},1}\cos\theta_1+n_{\text{amp},2}\cos\theta_2} , \tag{10}$$

and

$$t=\frac{2n_{\text{amp},1}\cos\theta_1}{n_{\text{amp},1}\cos\theta_1+n_{\text{amp},2}\cos\theta_2} , \tag{11}$$

where the electron wave amplitude index of refraction is defined as

$$n_{\text{amp},l}^{\text{EW}}=m_{r,l}^{\beta+1/2}(E-V)_{r,l}^{1/2} \tag{12}$$

for region l. These expressions [Eqs. (8)–(11)] are *exactly* the same as the analogous electromagnetic expressions for the reflection and refraction of an electromagnetic wave from an interface between dielectrics 1 and 2 with relative permittivities $\epsilon_{r,1}$ and $\epsilon_{r,2}$ and relative permeabilities $\mu_{r,1}$ and $\mu_{r,2}$ respectively.[6] In the electromagnetic case, Eqs. (10) and (11) give the reflectivity and transmissivity of the electric field for TE polarization and of the magnetic field for TM polarization. Therefore, when considering propagation past an abrupt material interface, Φ is analogous to the electric field for TE polarization and to the magnetic field for TM polarization. In other words, Φ is analogous to the electromagnetic field quantity that is parallel to the interface.[6] In the electromagnetic case, the amplitude index of refraction for region l has one value for TE polarization, $n_{\text{amp},l}^{\text{TE}}=\epsilon_{r,l}^{1/2}/\mu_{r,l}^{1/2}$, and another value for TM polarization, $n_{\text{amp},l}^{\text{TM}}=\mu_{r,l}^{1/2}/\epsilon_{r,l}^{1/2}$.[6] Using the above results for the indices of refraction, one can construct a general set of analogies between electron wave propagation, TE-polarized electromagnetic wave propagation, and TM-

polarized electromagnetic wave propagation. This set of analogies is shown in Table I. These analogies, which have been developed for the general form of the effective-mass Hamiltonian given in Eq. (2), are valid for both propagation in the bulk and for propagation past abrupt interfaces between materials. In the case of an abrupt material interface, Eqs. (8)–(11) are valid for electron waves, TE-polarized electromagnetic waves, and TM-polarized electromagnetic waves, where the appropriate indices of refraction are used for each case.

Motivated by the results for abrupt interfaces, one can attempt to draw similar analogies for propagation within materials with general one- and two-dimensional inhomogeneities in effective mass and/or potential energy. Again, the analogy will be drawn between Φ and either $\mathcal{E}$ (for TE polarization) or $\mathcal{H}$ (for TM polarization), where the electromagnetic wave is propagating in a one- or two-dimensionally inhomogeneous dielectric. In this case, TE (TM) polarization is defined as the polarization in which the electric (magnetic) field is polarized normal to the plane containing the gradient of the inhomogeneity. In the case of such an inhomogeneity, the Hamiltonian for the electron wave [Eq. (2)] can be expanded as a wave equation for Φ.

$$\nabla^2\Phi-\left[\frac{\nabla m_r^{-\beta}(\mathbf{r})\cdot\nabla}{m_r^{-\beta}(\mathbf{r})}\right]\Phi+k_0^2 m_r(\mathbf{r})[E-V(\mathbf{r})]_r\Phi=0\,, \tag{13}$$

where $m_r(\mathbf{r})=m(\mathbf{r})/m_0$ is the varying relative effective mass, $[E-V(\mathbf{r})]_r=[E-V(\mathbf{r})]/(E-V)_0$ is the varying relative kinetic energy, m_0 is the average effective mass, $(E-V)_0$ is the average kinetic energy, and $k_0=[2m_0(E-V)_0/\hbar^2]^{1/2}$ is the average wave vector of propagation in the medium. This wave equation [Eq. (13)] is exactly analogous to the wave equation for TE propagation in a one- or two-dimensionally inhomogeneous dielectric,

$$\nabla^2\mathcal{E}-\left[\frac{\nabla\mu_r(\mathbf{r})\cdot\nabla}{\mu_r(\mathbf{r})}\right]\mathcal{E}+k_0^2\mu_r(\mathbf{r})\epsilon_r(\mathbf{r})\mathcal{E}=0\,, \tag{14}$$

where $\mu_r(\mathbf{r})=\mu(\mathbf{r})/\mu_0$ is the relative permeability modulation, $\epsilon_r(\mathbf{r})=\epsilon(\mathbf{r})/\epsilon_0$ is the relative permittivity modulation, μ_0 is the average permeability, ϵ_0 is the average permittivity, and $k_0=(\omega^2\mu_0\epsilon_0)^{1/2}$ is the average wave vector of propagation. By comparison of these wave equations [Eqs. (13) and (14)], one can see that the analogies between electron wave propagation within a one- or two-dimensionally inhomogeneous semiconductor and TE-polarized electromagnetic wave propagation within a one- or two-dimensionally inhomogeneous dielectric are the *same* analogies as those developed for propagation past abrupt material interfaces, which are shown in Table I. As one would expect, a similar analogy exists between electron wave propagation within a one- or two-dimensionally inhomogeneous semiconductor and TM-polarized electromagnetic wave propagation within a one- or two-dimensionally inhomogeneous dielectric,

$$\nabla^2\mathcal{H}-\left[\frac{\nabla\epsilon_r(\mathbf{r})\cdot\nabla}{\epsilon_r(\mathbf{r})}\right]\mathcal{H}+k_0^2\mu_r(\mathbf{r})\epsilon_r(\mathbf{r})\mathcal{H}=0\,, \tag{15}$$

where the analogies are again given in Table I. Thus, the analogies of Table I are valid for propagation in the bulk, propagation past abrupt material interfaces, and propagation within one- and two-dimensionally inhomogeneous semiconductors. For all of these cases, standard electromagnetic analysis techniques can be used to analyze electron wave effects such as interference, propagation, reflection, refraction, and diffraction, where the analogies of Table I are used.

At this point, one might wonder whether such exact analogies exists for general three-dimensional inhomogeneities. In this case, the analogies do not hold. For general three-dimensional inhomogeneities, decoupled TE and TM polarization cannot be defined. Therefore, one cannot write scalar wave equations [like Eqs. (14) and (15)] for the electric and the magnetic field, but must use the curl equations. Since the vector field quantities are coupled, no exact analogy can be drawn between the vector electromagnetic fields and the scalar electron wave amplitude.

In conclusion, this work has shown that exact, quantitative analogies exist for *all* forms of the general Hamiltonian of Morrow and Brownstein.[10] In addition, these analogies were developed for propagation in the bulk, propagation past abrupt interfaces between materials, and propagation within one- or two-dimensionally inhomogeneous materials. With these analogies, one can analyze a wide class of electron wave effects such as reflection and refraction,[1,2] interference,[4,5] and diffraction[17] using well-understood electromagnetic analysis methods.

An understanding of these electron wave optical effects in semiconductors has become of increasing importance in the past few years. Recent experiments have verified that the electron wave phase index of refraction is proportional to the product of the square root of the kinetic energy[1–3] and the square root of the effective mass.[18,19] It is likely that, in the near future, similar experiments will be performed to verify the dependence of the amplitude index of refraction on kinetic energy and effective mass. Since the form of the amplitude refractive index is linked to the form of the effective-mass Hamiltonian (through $n_{\text{amp}}\propto m^{\beta+1/2}$), experiments that establish the power dependence of the effective mass in the amplitude index of refraction can be used to identify the correct form of the effective-mass Hamiltonian. The recent experiments on transition energies in $GaAs/Ga_{1-x}Al_xAs$

TABLE I. Analogies between effective-mass electron wave propagation and electromagnetic wave propagation in general dielectrics. The previously established constraint $2\alpha+\beta=-1$ applies.

Electron wave	Electromagnetic wave	
EW	TE	TM
$m^{\alpha}\psi$	$\mathcal{E}$	$\mathcal{H}$
m	$\mu^{-1/\beta}$	$\epsilon^{-1/\beta}$
$(E-V)$	$\mu^{1+1/\beta}\epsilon$	$\epsilon^{1+1/\beta}\mu$

quantum wells[15,16] fit this category since the transition energies are strongly dependent on the reflectivity of the barriers (and thus strongly dependent on β).[15] Due to the exact analogies to electromagnetics, it is easy to conceive of other numerous experiments (such as measuring interface reflectivity) to establish this dependence. However, regardless of the results of such experiments, the exact, quantitative analogies established in this paper remain valid. In addition, if the correct form of the Hamiltonian (for material systems other than $GaAs/Ga_{1-x}Al_xAs$) is shown to be other than $\alpha=0$ and $\beta=-1$, the results of previous work based on this assumption (such as Refs. 6 and 17) can be simply modified using Table I, with the analysis methods remaining valid.

This research was supported in part by Grant No, DAAL-03-90-C-0004 from the Joint Services Electronics Program and by Grant No. ECS-9111866 from the National Science Foundation. One of us (G.N.H.) was supported in part by the Office of Naval Research, and one of us (E.N.G.) was supported in part by the National Science Foundation.

[1]J. Spector, H. L. Stormer, K. W. Baldwin, L. N. Pfeiffer, and K. W. West, Appl. Phys. Lett. **56**, 2433 (1990).

[2]J. Spector, H. L. Stormer, K. W. Baldwin, L. N. Pfeiffer, and K. W. West, Appl. Phys. Lett. **56**, 1290 (1990).

[3]U. Sivan, M. Heiblum, C. P. Umbach, and H. Shtrikman, Phys. Rev. B **41**, 7937 (1990).

[4]For a bibliography on quantum interference effects, see T. K. Gaylord, E. N. Glytsis, G. N. Henderson, K. P. Martin, D. B. Walker, D. W. Wilson, and K. F. Brennan, Proc. IEEE **79**, 1159 (1991).

[5]See, for example, M. Heiblum, M. V. Fischetti, W. P. Dumke, D. J. Frank, I. M. Anderson, and C. M. Knoedler, Phys. Rev. Lett. **58**, 816 (1987).

[6]G. N. Henderson, T. K. Gaylord, and E. N. Glytsis, Proc. IEEE **79**, 1643 (1991).

[7]M. Altarelli, *Heterostructures and Semiconductors Superlattices* (Springer-Verlag, 1986), p. 12.

[8]S. Datta, *Quantum Phenomena* (Addison Wesley, Reading, MA, 1989), Chap. 6.

[9]O. von Roos, Phys. Rev. B **27**, 7547 (1983).

[10]R. A. Morrow and K. R. Brownstein, Phys. Rev. B **30**, 678 (1984).

[11]R. A. Morrow, Phys. Rev. B **35**, 8074 (1987).

[12]G. T. Einevoll and P. C. Hemmer, J. Phys. C **21**, L1193 (1988).

[13]R. A. Morrow, Phys. Rev. B **36**, 4836 (1987).

[14]G. T. Einevoll, P. C. Hemmer, and J. Thomsen, Phys. Rev. B **42**, 3485 (1990).

[15]I. Galbraith and G. Duggan, Phys. Rev. B **38**, 10057 (1988).

[16]M. Mojahedie and M. Osinski, Opt. Soc. Am. Annu. Meet. Tech. Dig. Ser. **17**, 113 (1991).

[17]G. N. Henderson, E. N. Glytsis, and T. K. Gaylord, Appl. Phys. Lett. **59**, 440 (1991).

[18]H. Ohno, E. E. Mendez, and W. I. Wang, Appl. Phys. Lett. **56**, 1793 (1990).

[19]L. D. Bell and W. J. Kaiser, Phys. Rev. Lett. **61**, 2368 (1988).